UNIVERSITÉ DE STRASBOURG

ÉCOLE DOCTORALE DES SCIENCES DE LA VIE ET DE LA SANTE
Institut de génétique et de biologie moléculaire et cellulaire IGBMC
Unistra- Inserm U1258 / CNRS UMR-7104

THÈSE présentée par :

Alexandra JIMENEZ ARMIJO

Soutenue le : **12 septembre 2023**

Pour obtenir le grade de : **Docteur de l'Université de Strasbourg**

Discipline : Sciences de la vie et de la santé

Spécialité : Aspects moléculaires et cellulaires de la biologie

ROGDI- une nouvelle protéine avec un motif leucine-zipper-régulant le développement neurologique et orofacial

THÈSE dirigée par :

[Mme BLOCH-ZUPAN Agnès]	Professeur des Universités, Université de Strasbourg

RAPPORTEURS :

[Mme BABAJKO Sylvie]	Directeur de recherches, Centre de Recherche des Cordeliers, Paris
[M MITSIADIS Thimios]	Professeur, University of Zurich, UZH Institut für Orale Biologe

---

AUTRES MEMBRES DU JURY :

[M BOHM Johan]	Directeur de recherches, IGBMC, Strasbourg
[Mme TORRES Maria Angélica]	Professeur, Université du Chili, Santiago, Chili

UNIVERSITÉ DE STRASBOURG

DOCTORAL SCHOOL OF LIFE AND HEALTH SCIENCES
The Institute of Genetics and Molecular and Cellular Biology IGBMC
Unistra- Inserm U1258 / CNRS UMR-7104

THESIS presented by:

Alexandra JIMENEZ ARMIJO

Defended on: **September 12, 2023**

To obtained the grade of: **Doctor of University of Strasbourg**

Area: Life and health sciences

Specialty: Molecular and Cellular Aspects of Biology

ROGDI- a novel protein with a leucine zipper domain- dually regulating neurological and orofacial development

THESIS directed by:

[Ms. BLOCH-ZUPAN Agnès] Professor, University of Strasbourg

REPORTERS:

[Ms. BABAJKO Sylvie] Research Director, Centre de Recherche des Cordeliers, Paris

[Mr. MITSIADIS Thimios] Professor, University of Zurich, UZH Institut für Orale Biologe

---

OTHER JURY MEMBERS:

[Mr. BOHM Johan] Research Director, IGBMC, Strasbourg

[Ms. TORRES Maria Angélica] Professor, University of Chile, Santiago, Chile

Remerciements

Je tiens à exprimer ma gratitude au Dr Sylvie Babajko, au Dr Thimios Mitsiadis, au Dr Johann Böhm et au Dr María Angélica Torres pour avoir accepté d'être membres du jury de cette thèse de doctorat. Je leur suis reconnaissante et très honorée de leur participation.

Je remercie sincèrement les Drs Sylvie Babajko, Thimios Mitsiadis et Johann Böhm, membres de mon comité de suivi de thèse pendant ces quatre années, pour avoir consacré leur temps et leurs compétences à l'évaluation et à l'appréciation de mon travail de doctorat. Leurs observations précises, leurs critiques bienveillantes et leurs recommandations judicieuses ont considérablement influencé le résultat final de ce travail.

Merci au Dr María Angélica Torres, qui m'a soutenue et encouragée à poursuivre dans le domaine de la recherche. Elle m'a fait bénéficier de son aide constante, même à distance. Elle m'a fait confiance et m'a donné l'opportunité de travailler dans l'enseignement et de progresser dans ma carrière professionnelle.

Je tiens à adresser mes sincères remerciements à ma directrice de thèse, le Pr Agnès Bloch-Zupan, pour son soutien constant et sa direction essentielle tout au long de la réalisation de ces travaux. J'apprécie sa confiance en mes compétences et le fait qu'elle m'ait donné l'opportunité d'élargir mes connaissances en matière de recherche, d'enseignement et dans le domaine de l'odontologie. Ses conseils et ses critiques franches m'ont permis d'améliorer la qualité de ma recherche et d'aiguiser mes capacités d'analyse. Je tiens également à la remercier d'avoir été compréhensive et patiente pendant les parties difficiles de ce travail de recherche, et d'avoir été présente lorsque j'avais besoin d'elle.

Merci au Dr Karen Niederreither, mon superviseur lors de mon master, qui a toujours pris le temps de discuter avec moi et m'a apporté une contribution précieuse qui a permis d'améliorer considérablement cette thèse. Je suis reconnaissante pour les échanges enrichissants que nous avons eus au cours de ce projet. Karen a su « challenger » mes idées, me poussant à explorer de nouvelles perspectives et à faire preuve d'esprit critique. Ses conseils ont été d'une valeur inestimable dans ma vie professionnelle et personnelle.

Au Dr Virginie Laugel-Haushalter pour son assistance comme superviseur pendant mes premières années de doctorat, pour m'avoir fait bénéficier de son expertise du modèle de souris, de la génétique expérimentale et des diverses approches méthodologiques. Son aide et ses conseils ont ainsi parfaitement complémenté ceux de ma directrice de thèse.

Au Dr Isaac Maximiliano Bugueno pour son accueil à Strasbourg lors de mon arrivée, et pour son assistance et ses conseils techniques au cours du projet.

Au Dr Magali Hernandez, pour son expertise dans le domaine du développement du cerveau et sa gentille amitié.

Je tiens également à remercier l'ensemble du groupe de recherche dirigé par le Dr Yann Hérault pour son soutien, particulièrement :

Le Dr Yann Hérault pour sa générosité à partager ses connaissances et ses idées, ce qui a grandement enrichi mon expérience.

Le Dr Maria Victoria Hinckelmann pour son aide et son soutien dans les domaines de la biologie moléculaire et de la génétique des souris.

Le Dr Marion Pellen pour son soutien en biologie moléculaire et son aide dans la langue française.

Claire Chevalier, pour son soutien dans la manipulation des souris et le bien-être des animaux.

Maria Tarruella, qui a rendu mes journées au laboratoire beaucoup plus agréables.

Le Dr Véronique Brault, le Dr Michel Roux, Arnaud Duchon, Marie-Christine Fischer, Valérie Hérault, Pauline Stephan, Victorine Artot, Jean-Baptiste Oswald, et Jeremy Jehl pour leur soutien en biologie et pour avoir partagé des moments conviviaux pendant mon doctorat.

Je suis reconnaissante à l'équipe du Dr Pascal Dollé, qui a été à l'origine de ce projet. Le Dr Pascal Dollé, qui a consacré du temps à l'orientation de mon projet, pour son soutien et ses conseils critiques. Les ingénieures de l'équipe, Brigitte Schuhbaur et Valérie Fraulob, pour leur conseils et apprentissage des techniques et leur assistance au laboratoire.

Au Pr Ariane Berdal pour avoir partagé ses connaissances sur la vitamine D et l'histologie dentaire.

Au Dr Gilles Laverny pour m'avoir donné l'opportunité d'en apprendre plus sur le récepteur de la vitamine D et pour nous avoir fourni les souris *VDR-null* et *VDRgem*. Pour son soutien constant et son aide dans l'analyse des données.

Au Dr Gergö Gogl pour ses conseils en protéomique et son aide dans l'interprétation des données.

À Yvan De Feraudy et au Dr Jocelyn Laporte pour leur aide dans les analyses musculaires.

Merci à Mohammed Selloum pour son soutien dans l'élevage de souris, le phénotypage et son implication dans le projet *Phenomin*.

Fabrice Riet pour son implication dans le projet *Phenomin* et l'analyse des résultats des tests de comportement.

Le personnel de l'animalerie de l'ICS, en particulier Sophie Brignon et Milan Herrmann pour avoir pris soin de la lignée *Rogdi*.

Les Drs Olivia Wendling et Hugues Jacobs, ainsi que Bruno Weber pour leur expertise en matière d'analyse histologique.

Je remercie le Dr Matthieu Jung et le Dr Christelle Thibault-Carpentier de la plateforme IGBMC-GenomEast pour leur soutien dans l'analyse du séquençage de l'ARN.

Les Drs Yves Lutz et Elvire Guiot du Centre d'imagerie de l'IGBMC pour leur assistance dans l'imagerie microscopique.

Le Dr Naji Karhouf pour son aide dans l'imagerie par microscopie électronique à balayage.

Je remercie Mme Marzena Kawczynski pour son aide et son soutien permanents dans la gestion des données des patients.

J'apprécie la participation et le soutien inestimable des patients et de leurs familles.

Je tiens également à remercier le soutien financier de l'Agence nationale pour la recherche et le développement (ANID, programme de bourses : Doctorado Becas Chile).

Jose Tomas Ahumada, pour sa merveilleuse amitié qui dure depuis des années. Pour ses encouragements et son soutien tout au long des parties difficiles et satisfaisantes de cette aventure.

À Natalia, Carolina, Nicolas, Matias, Angelina, Carla, Mariela, Vicente, Alvaro et tous ceux qui ont fait partie de ma vie au cours de ce processus. Pour leur soutien émotionnel, leur écoute et leurs paroles de réconfort au moment où j'en avais le plus besoin.

À ma mère, pour ses sacrifices qui m'ont permis de me concentrer sur mon éducation et de suivre mes aspirations. Je lui serai toujours reconnaissante de m'avoir soutenue pendant mes études.

À ma sœur Antonia, pour avoir été tout simplement elle-même et pour avoir toujours été disponible au bout du fil.

À la douceur de ma vie et compagne à quatre pattes, Dulce, je suis éternellement reconnaissante pour l'amour et la compagnie qu'elle apporte à mes journées.

Je suis profondément reconnaissante à tous ceux qui ont participé à ce chemin. Pour leurs conseils, leur soutien et leurs encouragements. Sans leur aide dans la recherche et dans ma vie personnelle, ce travail n'aurait pas été possible.

Acknowledgements

I want to express my gratitude to Dr. Sylvie Babajko, Dr. Thimios Mitsiadis, Dr. Johann Böhm, and Dr. María Angélica Torres for agreeing to serve as jury members for this PhD thesis committee. I am grateful and honored by their participation.

I am deeply grateful to Dr. Sylvie Babajko, Dr. Thimios Mitsiadis and Dr. Johann Böhm for serving on my follow-up thesis committee during these 4 years and for devoting their time and skills to evaluating and assessing my work. Their accurate observations, kind critiques, and considerate recommendations significantly influenced this work's final result.

To Dr. María Angélica Torres, who gave me her support and encouragement to pursue in the research field. I appreciate her constant help, even from a distance. For trusting me and giving me the opportunity to teach and advance in my professional career.

I would like to express my sincere gratitude to my thesis director, Prof. Agnès Bloch-Zupan, for her constant support and outstanding direction throughout the completion of this thesis. Agnès, I appreciate her confidence in my abilities and am thankful for giving me the opportunity to expand my knowledge in research, teaching, and dentistry. Her constant feedback and frank criticism were helpful in improving my research and sharpening my analytical abilities. I also want to thank her for being understanding and patient during the difficult parts of this research and for being there when I needed her.

To Dr. Karen Niederreither, my master's supervisor who has always made time for me, and provided valuable contribution that significantly improved the quality of this thesis. I am grateful for the motivating discussions we had during the course of this project. Dr. Niederreither consistently challenged my ideas, pushing me to explore new perspectives and think critically. Her advices have been invaluable in my professional and personal life.

To Dr. Virginie Laugel-Haushalter for her assistance as supervisor during my first years of PhD, thus providing invaluable help thanks to her expertise in the field of mouse genetics and various experimental approaches. Her help and advice perfectly complemented those of my thesis director.

To Dr. Isaac Maximiliano Bugueno for welcoming in Strasbourg when I arrived, and for his assistance and technical advice throughout the project.

To Dr. Magali Hernandez, for her expertise in brain development and her kind friendship.

I would also like to acknowledge the support of the entire research team led by Dr. Yann Hérault, particularly:

Dr. Yann Hérault for his generosity in sharing knowledge and ideas, which greatly enriched my experience.

Dr. Maria Victoria Hinckelmann for all of her assistance and support in the fields of molecular biology and mouse genetics.

Dr. Marion Pellen for support in molecular biology and her help in French language.

Claire Chevalier, for her support in mouse manipulation and animal welfare.

Maria Tarruella, who made my days in the lab so much more enjoyable.

Dr. Véronique Brault, Dr. Michel Roux, Arnaud Duchon, Marie-Christine Fischer, Valérie Hérault, Pauline Stephan, Victorine Artot, Jean-Baptiste Oswald, and Jeremy Jehl for support and advice, and for sharing nice moments during my PhD work.

I am thankful to the team of Dr. Pascal Dollé, in which the project started. To Dr. Pascal Dollé, for giving up his time for project guidance, for his support, and critical advice. To Brigitte Schuhbaur and Valérie Fraulob for their technical support and laboratory assistance.

Prof. Ariane Berdal for sharing her knowledge in vitamin D signaling and tooth histology.

Dr. Gilles Laverny for giving me the opportunity to learn more about vitamin D and for providing the *VDR-null* and *VDR$_{gem}$* mice. For his constantly support and help with data analysis.

Dr. Gergö Gogl for his advice in proteomics and help in interpreting results.

Yvan De Feraudy and Dr. Jocelyn Laporte for their help in muscle analyses.

Mohammed Selloum for his support in mouse breeding, phenotyping and involvement in the *Phenomin* project.

Fabrice Riet for his involvement in the *Phenomin* project and analysis of behavioral tests results.

Members of the ICS mouse facility, especially Sophie Brignon and Milan Herrmann, for taking care of the *Rogdi* line.

Dr. Olivia Wendling, Dr. Hugues Jacobs and Bruno Weber for providing their expertise in histological analysis.

I thank Dr. Matthieu Jung and Dr. Christelle Thibault-Carpentier from the IGBMC GenomEast platform for their support in RNA sequencing analysis.

Drs. Yves Lutz and Elvire Guiot from the IGBMC Imaging Center for their assistance in microscopy imaging.

Dr. Naji Karhouf for his support in scanning electron microscopy imaging.

I thank Mrs. Marzena Kawczynski for her ongoing assistance and support in managing patient’s data.

I appreciate the patients and families' participation and priceless support.

I would like to thank to the financial support of the National Agency for Research and Development (ANID, Scholarship Program: Doctorado Becas Chile).

Jose Tomas Ahumada, for his wonderful friendship that has lasted over the years, even from dental school. For his encouragement and support throughout both the difficult and satisfying parts of this venture.

To Natalia, Carolina, Nicolas, Matias, Angelina, Carla, Mariela, Vicente, Alvaro and everyone who has been part of my life during this journey. For their emotional support, lending a listening ear and offering words of encouragement when I needed it the most.

To my mother, for her sacrifices that allowed me to concentrate on my education and follow my aspirations. I will always be grateful to her for supporting my education.

To my sister Antonia, for simply being herself and for always being just a phone call away.

To the sweetness of my life, my “furry” companion Dulce, I am forever grateful for the love and happiness she brings to my days.

I am deeply grateful to everyone who was part of this journey. For their guidance, support, and encouragement. Without their helpful advice in research and in my personal life, this work would not have been possible.

Table of Contents

List of Tables

List of Figures

Introduction

This doctoral thesis will first present the context of rare diseases and their association with dental anomalies. It will then examine dental development and the main pathways involved, focusing in particular on enamel formation.

1. Rare diseases

A disease is defined as rare when it affects less than one in 2,000 people. More than 7,000 rare diseases have been described, with new rare diseases being identified every week. 80% of rare diseases have a genetic origin. Rare diseases affect 3 to 4 million people in France and nearly 30 million in Europe [14]. In Chile, it is estimated that those affected by some of these diseases could reach 1.5 million people [15]. For many rare diseases, due to a deficit in both medical and scientific knowledge, many patients are not diagnosed, and their disease remains unidentified. A careful examination of the oral cavity may provide invaluable information for an earlier, faster and more accurate diagnosis of rare diseases [16,17].

France has maintained its position as a global leader in the field of rare diseases since 2004, thanks to three subsequent national strategy plans. The construction of 23 health networks, supported by 387 reference centers and 1,800 competence centers, provides comprehensive care as close to patients as possible in the battle against rare diseases [18].

The Reference Center for Rare Oral and Dental Diseases (CRMR O-Rares) (2018-2022) has a coordinating site (Strasbourg – Hôpitaux Universitaires de Strasbourg), a constituent site (Paris - Hôpital Rothschild) and 16 competence centers located throughout France (Angoulême, Besançon, Bordeaux, Dijon, Lyon, Marseille, Montpellier, Nancy, Nantes, Paris APHP Henri Mondor Créteil, Paris APHP Pitié Salpétrière, Reims, Rennes, Rouen, Toulouse, and Tours), whose mission is to provide care and follow-up for patients as close to their home city. This coordinated reference center network helps to diagnose rare diseases, implement therapies, and organize patient care. Hence all components of this Rare Oral and Dental Diseases (CRMR O-Rares) reference center network coordinate local care and allow better identification of affected patients. They are involved in research programs and facilitate development and progression of knowledge.

To better understand these disorders, CRMR O-Rares research incorporates clinical, preclinical, bioinformatics, genetic and biological approaches, including developmental approaches. In the same line of translational research that characterizes our center, new projects are continuously being established.

The investigation of oral and dental defects from a phenotypic, genotypic and fundamental perspective is one of the main objectives. In order to present high-performance diagnostic tools and novel therapy methods, multidisciplinary scientific and clinical teams have been brought together under the auspices of two international programs (European Union in the framework of the INTERREG IV and V Upper Rhine program RARENET), directed by Pr. Agnès Bloch-Zupan.

Thanks to these programs, the team has built and validated a high-throughput sequencing method gene panel which can be used to identify uncommon, rare, and orphan oral disorders [19,20]. The study of phenotypes at the molecular and physiological levels has generated

encouraging novel findings. To date, numerous new rare disease target genes have been discovered, with published findings improving disease understanding [21–25].

In partnership with the Mouse Clinical Institute (Institut Clinique de la Souris-ICS), under the INTERREG IV, V and *Phenomin* projects, it has been possible to generate novel mouse models of uncommon disorders with an inactivation of the genes *Smoc2* and *Rogdi*.

These models have helped in phenotypic exploration, notably using imaging techniques such as Micro-CT and scanning electron microscopy. They have also facilitated the understanding of developmental and pathophysiological mechanisms that can be employed to develop innovative therapeutics (i.e., maxillary bone regeneration and implant osseointegration).

2. **Orodental anomalies**

Dental and oral anomalies, as dysmorphology traits and clues, are critical to the early detection of rare genetic diseases. Hence, dental defects (such as enamel alterations) are quite useful to identify several rare diseases, especially when assessed in combination with extraoral clinical diagnosis. Over 950 rare disorders have oral and dental development defects. Most often, a wide range of gene mutations produce these rare/orphan disorders.

Dental abnormalities are defined as changes to one or more primary or permanent teeth's outward appearance, internal structure, or topography. The etiology (or original causes) of these dental malformations is often genetically determined or sometimes acquired. Dental anomalies can affect the number of teeth, tooth size or shape, tooth location or position, overall dental growth, or other components of dental structure (see Table 1 below). Hence overall, dental defects can either be isolated or included as a symptom of an overall syndrome [16].

Timing is a crucial factor in tooth development. When a process is disrupted during dental development it may indeed have a dramatic effect(s). Obvious variations in tooth morphology and structure occur in different species. To date, rodent models have been critical in our elucidation of the underlying molecular mechanisms dictating dental morphogenesis [26].

A table of the definition of patient dental anomalies and how they can be classified is presented below:

Table 1 Dental anomalies and oral warning signs. Adapted from [1].

Type of Anomaly	Clinical Signs	Anomalies observed
Number anomalies		
Reduced number	Anodontia	Absence of all dental elements
	Oligodontia	More than 5 missing teeth = 6 and above
	Hypodontia	From 1 to 5 missing teeth
Increased number	Supplementary teeth	The tooth repeats the shape and function of an adjacent tooth
	Supernumerary teeth	Elements are atypical, smaller and rudimentary. They are classified into: -Mesiodens: between the two upper central incisors -Paramolar: in the molar region -Distomolar: behind the third molar
Location anomalies	Ectopia	The element is located near the usual site, in a vestibular, lingual or palatal position
	Transposition	Two contiguous teeth reciprocally invert their position
	Heterotopia	Element located far from the usual position. If the position is outside the oral cavity it is defined as migration.
Position anomalies	Version	Inclination of a tooth towards the buccal or palatal side, forward (mesioversion) or backward (distortion)
	Inversion	Inverted tooth position (root versus alveolar ridge and crown versus basal bone portion). It is constantly accompanied by inclusion.
	Rotation	The element rotates along its longitudinal axis
	Intrusion	The tooth crown is on a lower plane than the occlusal plane
	Extrusion	The coronal margin is located higher than the occlusal plane
Volume anomalies	Gigantism	Macrodontia
	Dwarfism	Microdontia
	Taurodontism	Tooth with wide crown, short roots, extended pulp chamber

Type of Anomaly	Clinical Signs	Anomalies observed
Shape anomalies	Crown anomalies	Accessory cusps, conical or tuberculate shape of the crown
	Roots anomalies	Anomalies in number, shape and size
	Endodontic anomalies	Anomalies in number, shape and size of the root canal morphology
Developmental anomalies	Enamel pearl	Small hard rounded excrescence, located near the enamel-cement junction.
	Fusion	Fusion of two teeth. Coalescence anomaly: due to close contact between germs; it can affect crowns and roots or only the crowns
	Concrescence	Two teeth are joined along the root surfaces by cementum. Coalescence anomaly
	Invaginated tooth	It is due to an infolding of enamel into dentine. There are two forms, coronal and radicular, with the coronal one being more common.
Structural anomalies	Enamel anomalies	Quantitative and/or qualitative enamel defect affecting some or all teeth. Amelogenesis imperfecta: abnormal formation of the enamel, unrelated to any systemic or generalized conditions. Autosomal dominant or autosomal recessive or x-linked pattern. It affects both deciduous and permanent.
	Dentin anomalies	Dentinogenesis imperfecta: brown teeth, crowns shrunk due to enamel flaking not supported by intact dentin. Autosomal dominant. It affects both deciduous and permanent.

3. **Odontogenesis**

To understand dental anomalies, it is necessary to focus on dental development and disturbances. Teeth develop as an ectodermal organ. Other examples of ectodermal structures include hair follicles, mammary glands, and nails. All ectodermally-derived organs have a similar development (Figure 1). An ectodermal epithelial placode invades the underlying mesenchyme. In this process a variety of diffusible communication signals direct ectoderm to invade underlying ectomesenchyme, and coordinate this complex remodeling process. Odontogenesis or tooth development indeed offers a great model for understanding the molecular principles of organogenesis. Mammalian teeth develop through a number of distinct morphological stages that call for sequential and reciprocal interactions between the oral epithelium and ectomesenchyme generated from the neural crest [26,27].

In humans, primary dentition begins about 6 weeks in utero, gradually erupting between the ages of 6 months and 2.5 years, with development often being finished by 3 years. The primary dentition is then replaced by the permanent dentition. For the permanent dentition, eruption starts around age 6 and is finished by ages 18 to 25 [28].

Tooth development is a complex process that involves precise and time-dependent orchestration of multiple genetic, molecular, and cellular interactions [29]. It is characterized by several successive stages: dental lamina formation, placode stage, bud stage, cap stage, bell stage. This is followed by terminal cytodifferentiation of odontoblasts and ameloblasts. Root formation occurs, and the tooth eruptions ensue. Odontogenesis begins with the formation of the dental lamina. This lamina results from interactions between the epithelium (the oral ectoderm) and the underlying ectomesenchyme. Ectomesenchyme derives from the migrating cephalic neural crest cells [30]. These cells induce the formation of the dental mesenchyme, dental pulp, odontoblasts, dentin matrix, cementum, periodontium [31,32]. The odontogenic epithelium continues to enter into the underlying mesenchyme. The base of the bud flattens as it moves from the bud stage to the cap stage, where it bends into a cap form, with edges known as "cervical loops". A capsule is formed when the surrounding mesenchyme condenses during the transition from bud to cap stage.

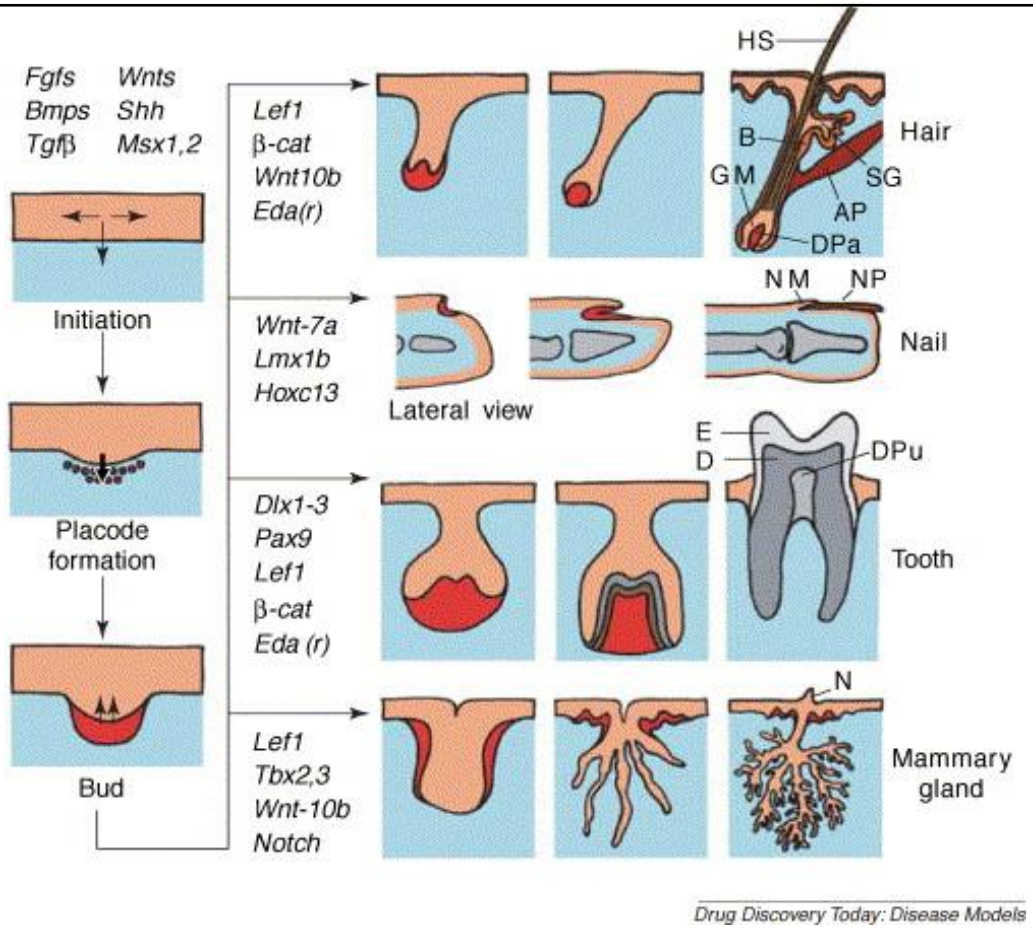

Figure 1. Embryonic development of epidermal appendages. Ectodermal placode formation is initiated by signals from the embryonic ectoderm (pink) to the underlying mesenchyme (blue). Epithelial placodes appear and subsequently grow into the surrounding mesenchyme. These early developmental events are similar in all ectodermal organs. At later stages, epithelial buds undergo different morphogenetic configurations, resulting in the formation of more specialized structures. Some genes, including *Fgfs* and *Bmps*, are involved in the early development of all appendages, whereas others are only important for the development of certain epidermal derivatives, for example *Lef1*, *Eda* and *Edar*, as indicated. Abbreviations: AP, arrector pili muscle; β-cat, β-catenin; B, bulge; D, dentin; DPa, dermal papilla; DPu, dental pulp; E, enamel; GM, germinal matrix; HS, hair shaft; N, nipple; NM, nail matrix; NP, nail plate; SG, sebaceous gland. From reference [3,33]

The cervical loops eventually deepen, curve toward one another with a bell-shape, given the name to the following stage. The inner enamel epithelium (IEE), is located between the cervical loops and develops into the primary enamel knot, which is a signaling center (see Figure 2) [4].

The primary enamel knot is a complex transitory structure involved in cusp formation that contains cells in contact with the basement membrane, internal round cells, and peripheral cells grouped concentrically. At the end of the cap stage this structure undergoes apoptosis, but within the molars some cells of the enamel knot will form the secondary enamel knots- which participate in cusp formation [12]. In the bell stage, the dental papilla is gradually defined by the enamel organ. Cusps begin to develop and the size of the crown increases.

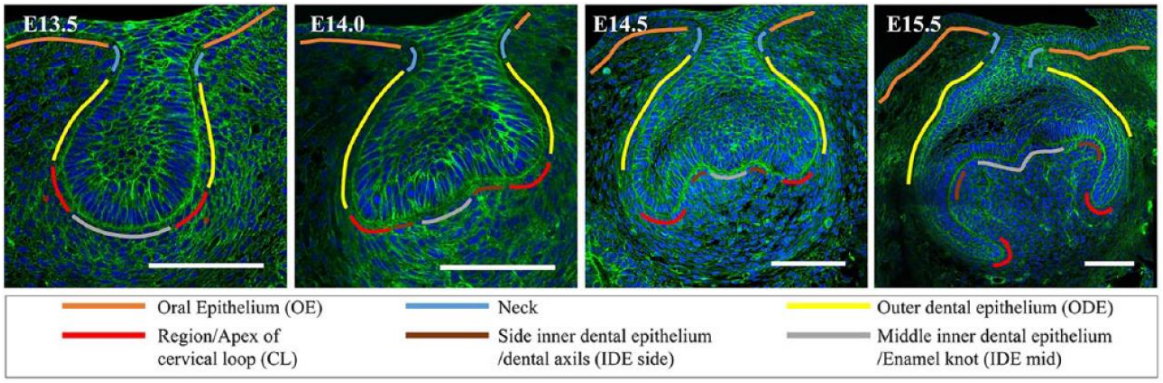

Figure 2. Molar tooth germs show dynamic shape change from bud to cap to bell stage. Confocal images of frontally sliced tooth germs at the indicated stages were stained with phalloidin (green) for F-actin and DAPI (4',6-diamidino-2-phenylindole; blue) for nuclei. Scale bar = 100 µm. From reference [4].

Ameloblasts and odontoblasts are defined as the differentiated cells that will create the mineralized tissues of the tooth crown. Prior to cell differentiation, at the bell stage, ameloblasts differentiate from the IEE and odontoblasts from the neighboring dental papillary cells. Both cell types (ameloblasts and odontoblasts) develop specific phenotypes in a process termed cytodifferentiation [4,6,12]. Odontoblasts first produce a thin layer of pre-dentin, which is mainly composed of collagen. Pre-dentin will provide a signal to pre-ameloblasts inducing them to differentiate into secretory ameloblasts. The basal lamina degrades when the pre-ameloblasts go through terminal differentiation, and during the transition stage, when an atypical basal lamina is produced [9]. Secretory ameloblasts will then start to secrete enamel matrix proteins (EMP). Odontoblasts and ameloblasts will continue secreting dentin and enamel, respectively. While enamel is secreted until it reaches the required thickness, dentin continues to form throughout life [12].

The development of the root starts once the crown is fully formed and enamel covers the future cementoenamel junction (CEJ). A double layer of cells known as Hertwig's epithelial root sheath (HERS) develops when cells of the inner and outer enamel epithelium grow from the cervical loop. Between the dental follicle and the dental pulp, this sheath of epithelial cells wraps around the dental pulp, enclosing all but the basal part of the pulp. The inner epithelial cells of HERS will determine the size, shape and number of tooth roots guiding the differentiation of the ectomesenchymal cells of the pulp into odontoblasts. Odontoblasts will then secrete the dentin of the root [6,34]. After that, for the following three weeks, as the root grows, the portion of HERS continuously fragments. This causes a direct contact between the newly formed dentin and dental follicle cells that will differentiate into cementoblasts (cells that will form the cementum) (Figure 3) [34,35]. The tooth starts to erupt after 1/2 to 2/3 of root formation, normally in an axial direction [6].

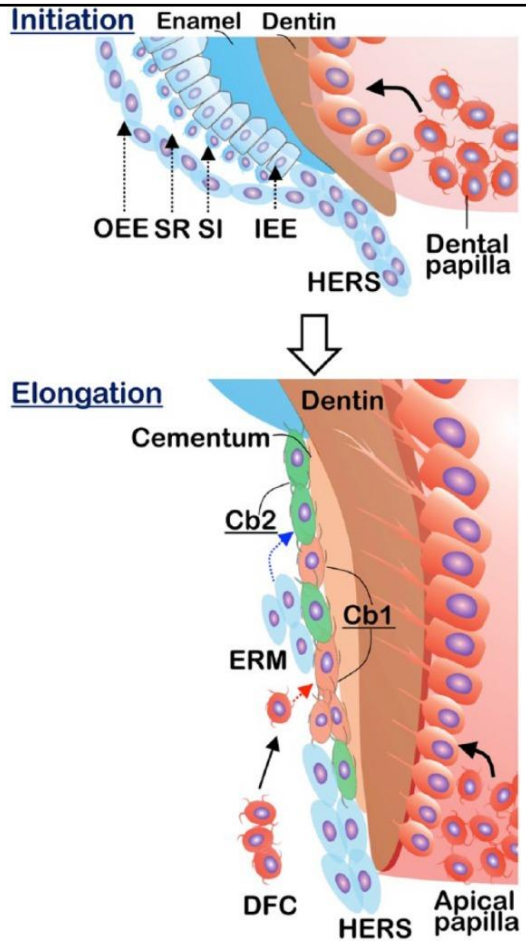

Figure 3. Diagram showing root morphogenesis in 2 stages: root initiation and root elongation. HERS is formed by fusion of outer enamel epithelium (OEE) and inner enamel epithelium (IEE), which marks the initiation of root formation. The odontoblasts derived from the dental papilla (apical papilla at root elongation stage) form dentin, whereas there are 2 stem cell niches giving rise to cementoblasts (Cb), including the dental follicle (dashed red arrow) and HERS (dashed blue arrow). Some HERS cells eventually become epithelial rests of Malassez (ERM). DFC, dental follicle cell; HERS, Hertwig's epithelial root sheath; SI, stratum intermedium; SR, stellate reticulum. From reference [5].

4. Genes and signaling pathways involved in tooth development

During embryonic tooth development and subsequent tissue proliferation, numerous interactions take place. The contact between the epithelium and the mesenchyme, is a crucial stage [36]. Epithelio-mesenchymal interactions require a messenger system between both structures separated by the basement membrane. This includes direct cell-cell communication, matrix vesicles, ions, extracellular matrix molecules, growth and transcription factors, among others. Most genes are associated with central tooth development regulations and signaling pathway interactions between cells and tissues [37].

Bone morphogenetic protein 4 (*Bmp4*) and fibroblast growth factor 8 (*Fgf8*) are the first signals during tooth development. The expression of these molecules in the oral ectoderm will cause the underlying mesenchyme to respond with differential expression of divergent homeobox genes (*Barx1*, *Dlx2*, *Msx1* and *Msx2*) [38].

The conserved wingless-type MMTV integration site (Wnt), bone morphogenetic protein (BMP), fibroblast growth factor (FGF), and sonic hedgehog (Shh) pathways are significant molecular regulators of odontogenesis, starting to act early at the stage of formation of the dental lamina (see Figure 4). During tooth formation, these factors work together to establish which developmental pathway a particular cell population will undertake. These same signaling factors also signal in stem cell populations [12]. The basis for tooth development is the stable and accurate expression of many, including all of the aforementioned signaling molecules. Hence the differential and spatial restriction of Wnt/FGF/Shh levels (either the up-regulation or down-regulation of many of these signaling pathways) may elicit a range of dental anomalies [39].

The earliest known markers of tooth initiation include *Wnt10b*, Shh expression, pituitary homeobox 2 (*Pitx2*) and *Fgf8* [12]. Shh plays crucial roles in mammalian development. Shh is expressed predominantly in the dental epithelium marking the initial stages of tooth formation. Shh signaling controls the development of a variety of dental components, including enamel, dentin, cementum, and other soft tissues [40].

Canonical Wnt and Shh signaling in particular seem to be essential for odontogenesis, as disruption of any of these pathways results in either defective tooth development or supernumerary teeth [12]. Supernumerary teeth or dental agenesis are linked to mutations in the intracellular WNT antagonists *AXIN2* and *APC*. In both the primary and permanent dentition, variation in tooth number is a typical developmental defect in humans. These differences are frequently isolated, non-syndromic malformations, or characteristics of developmental syndromes [41].

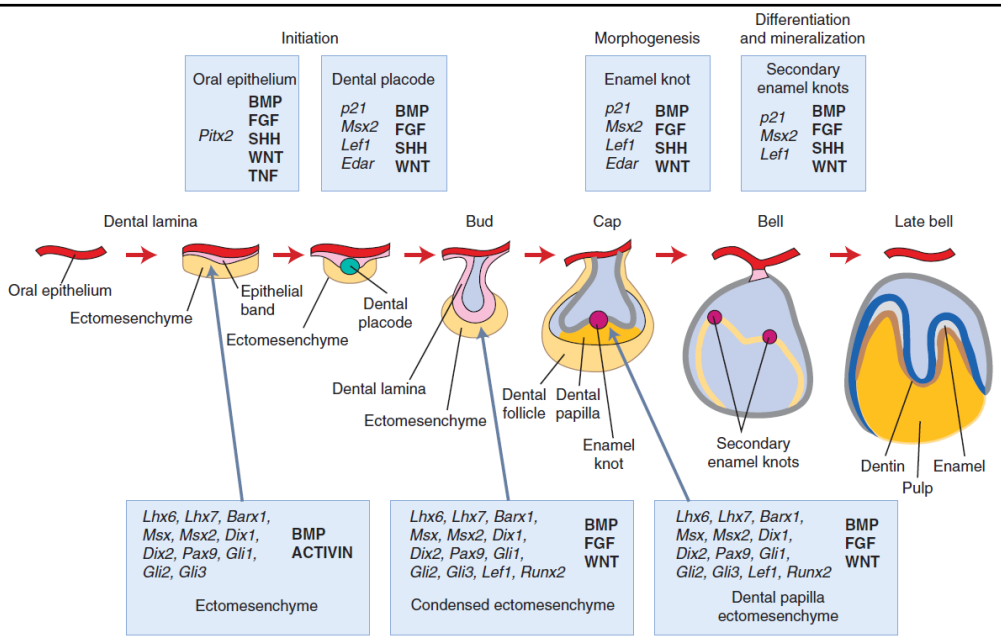

Figure 4. Molecular signaling during tooth crown development. Expression of transcription factor-coding genes (all these genes, except *Edar* and *p21*, code for transcription factors) [italics] and signaling molecules [bold]. From reference [6].

5. Amelogenesis

Dental enamel is the hardest and most mineralized structure in our body (having a 98% mineral content). Enamel has a unique composition (making it the hardest body tissue-type), which is reflected in the unique process by which it is formed. Enamel formation (also known as amelogenesis) is a strictly controlled stepwise process [42]. This process involves the formation of various epithelium-derived cell types, including the inner enamel epithelium (IEE) and the outer enamel epithelium (OEE). These cells converge at the cervical loop, a niche for dental epithelial stem cells, providing a constant source of enamel-forming cells until the enamel crown is fully formed. In rodent incisors, the stem cell niche in the cervical loop is retained for life, enabling continuous growth of long teeth [43].

Ameloblasts originate from the IEE. They transform from pre-ameloblasts to post-mitotic cells and then into differentiated ameloblasts. Dental cells differentiate into odontoblasts and ameloblasts at the end of the late bell stage and continuing during crown formation. Odontoblasts at these stages secrete the dentin matrix (having a 70% mineral content, 20% of organic matrix and 10% of water) [44]. During amelogenesis, the ameloblast cell type continuously secretes a highly organized extracellular organic matrix while slowly moving away from the dentinal surface until the desired thickness of the matrix is achieved. In mammals, enamel formation can be divided into pre-secretion, secretion, and maturation stages [42].

Throughout the secretory and maturation stages, the enamel organ's cells go through morphological changes. Secretory ameloblasts, the stratum intermedium, the stellate reticulum, and the single-layer OEE are all clearly identifiable at the secretory stage [43,44].

Secretory ameloblasts are post-mitotic cells with a unique process known as the Tomes' process. Tomes' process is a structural component of ameloblasts, located on their secretory side. It is essential for the secretion of the enamel matrix proteins into the extracellular matrix. Secretory ameloblasts produce and secrete a protein-rich scaffold. Enamel proteins must be secreted and then removed during enamel maturation (i.e. mineralization). Hence, enamel matrix protein (EMP) secretion is required to direct the generation of the highly ordered, therefore very strong mineralized composition of the enamel structure [7]. During the secretion stage, ameloblasts secrete a number of enamel matrix proteins (EMPs). These EMPs include amelogenin (AMEL), ameloblastin (AMBN), and enamelin (ENAM) (Figure 5). These proteins can be classified as structural proteins. This is because their secretion is essential in determining the proper microstructure of the enamel [7].

Secretory ameloblasts change their morphology into maturation-stage ameloblasts, losing the Tomes' process and shrinking in height by roughly 50%. Ameloblasts at this stage have an enlarged nucleus that appears more central when compared to secretory ameloblasts. The most recognizable alteration at this stage is the cyclic transformation of ruffle-ended (RE) ameloblasts into smooth-ended (SE) ameloblasts. This ruffle to smooth (RE to SE) ameloblast modulation is required for the maintenance of pH homeostasis in the mineralizing enamel matrix microenvironment (Figure 5) [44]. The other three epithelial cell populations from the secretory stage (stratum intermedium, stellate reticulum, and OEE) reorganize to become the papillary layer (PL) cells, rich in blood vasculature [43]. PL cells participate in ion transport from the blood to the ameloblasts [11,45].

During the maturation stage, both the deposition of hydroxyapatite and matrix turnover, require controlled pH regulatory mechanisms. This pH regulation is mediated by a number of ion transporters [46]. Enamel formation during the maturation-stage of amelogenesis involves mineral deposition, crystal growth, protease activation, and the degradation of the internalized organic matrix. Every one of these events in enamel maturation requires the tight control of extracellular pH, including the bicarbonate concentration. To recapitulate, any pH alteration could have pronounced effects during enamel maturation. Maintenance of pH homeostasis of the mineralizing enamel matrix environment is essential for modulation and for completion of enamel mineralization. A continued acidification of pH during enamel maturation inhibits enamel mineralization and eventually become toxic to cells [8,47].

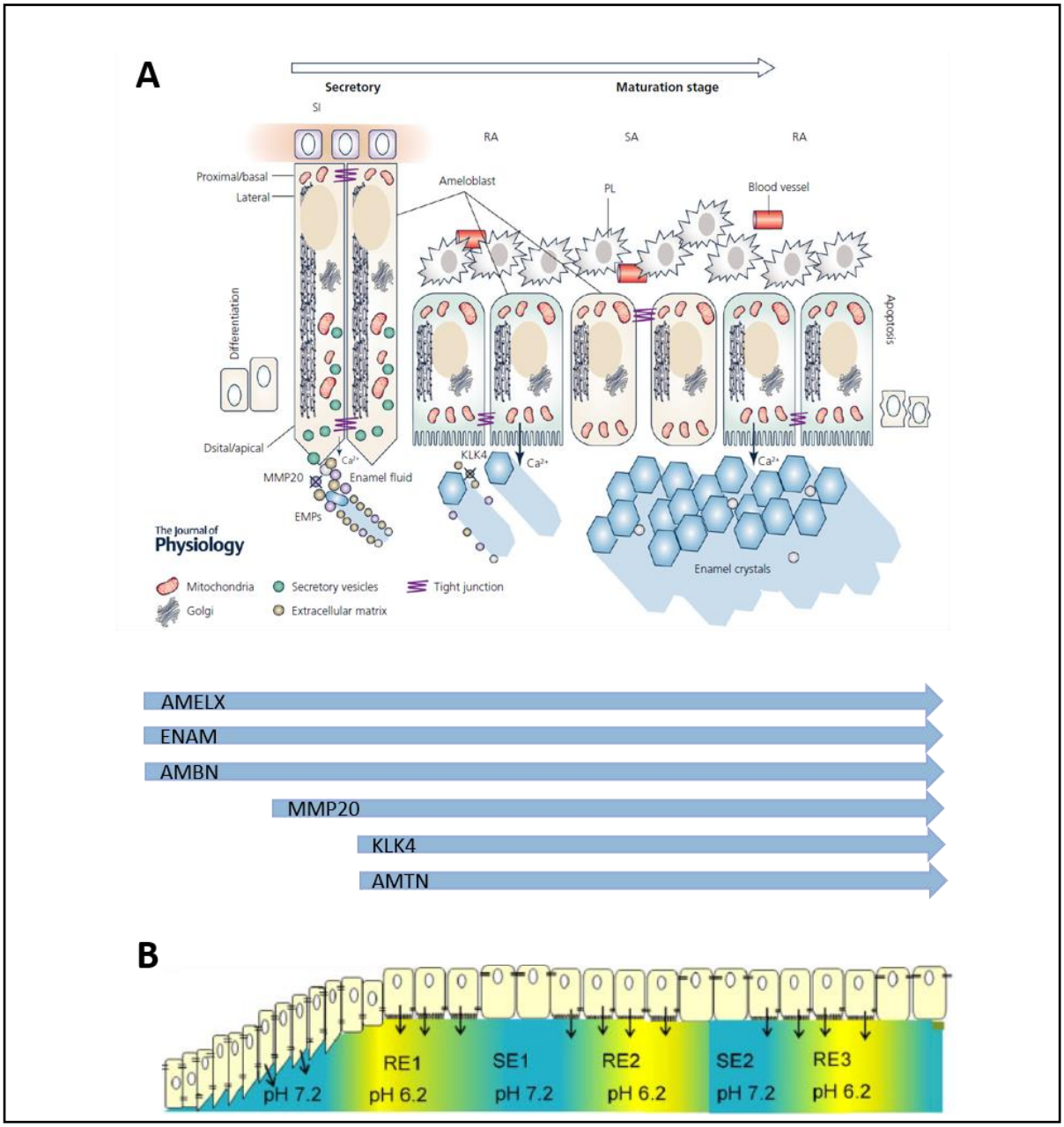

Figure 5. Histological changes in amelogenesis and ameloblast modulation. (A) The histological development of enamel crystals goes hand in hand with changes in ameloblast morphology. Undifferentiated epithelial cells receive signals to transform into secretory ameloblast cells of some 75 μm tall and ~5 μm in diameter with a specialized distal cell process (Tomes' process) which plays an important role in matrix exocytosis. These same cells will retransform into shorter cells (~35 μm tall) during maturation devoid of the Tomes' process. At the maturation stage, ameloblasts undergo cyclical changes from a cell with a distal ruffled border, the ruffled-ameloblast (RA), to a cell with a smooth distal border, the smooth-ameloblast (SA). Tight junctions are found at the basal and apical pole of secretory ameloblasts. The apical or distal pole is closest to the enamel crystals. In RA cells, tight junctions are found only at the apical pole but in SA cells they are located at the basal pole. Organellar distribution differs in cells at each stage. SI = stratum intermedium, PL = papillary layer, EMPs = enamel matrix proteins. AMELX, ENAM, and AMBN are secreted since early stages of amelogenesis. MMP20 and KLK4 are the main proteases in AMELX processing. AMTN is secreted during the transition to the maturation stage as KLK4. During maturation, the ameloblast, at its distal pole, becomes ruffle ended (RE), while the enamel is slightly acid. Later the RE ameloblast loses its ruffled border and turns into a smooth-ended (SE) cell in contact with pH-neutral enamel, after which it becomes RE again. This periodic change moves in a wavelike manner from the apical end toward the incisal end and is called *modulation* or *pH cycling*. (B) illustrates the changes in pH of enamel during modulation. Figure adapted from [7,8].

Enamel formation needs Ca^{2+}, but crystal growth also requires an extracellular pH cycling. Modulation involves near pH-neutral (in SE cells) enamel and acidic pH (in RE cells). pH is important to allow optimized enzyme function [8]. In maturation stage, enzymes like matrix metalloproteinase 20 (MMP20) and KLK4 (a calcium-dependent peptidase) cleave newly secreted EMPs into various derivative fragments [29,48]. This allows for full mineralization, defined as increasing both the width and thickness of enamel hydroxyapatite crystal deposition.

6. **Proteins critical to the amelogenesis process**

Amelogenesis requires the synthesis of many different proteins. Three of them are key structural proteins needed to develop enamel: amelogenin, ameloblastin, and enamelin (Figure 6). The production of these proteins is followed by their degradation by metalloproteinases, and the final mineralization of the organic matrix until enamel maturation, resulting in a highly mineralized tissue [49].

Amelogenin (AMELX, X standing for "X-linked") is the most abundant protein (90%) of enamel matrix proteins (EMP). Its expression in the pre-secretory and secretory stages leads to enamel formation assembling into nanospheres that regulate crystal arrangement adsorbing apatite [7,44]. Amelogenin has also been found in the dentin mantle, showing that there is structural continuity between enamel and dentin [49]. Ameloblastin represents about 5% of EMP helping to separate rod and interrod enamel. The less expressed protein is enamelin playing a role in crystal elongation [44].

During the pre-secretory stage, inactive enamelysin (also known as MMP20) is located inside the ameloblast. Enamelysin quantities increase, whereas amelogenin levels are reduced during the secretory stage [49]. *Amtn* and *Klk4* are both expressed in the ameloblast lineage starting in the transition stage between secretory and maturation ameloblasts. Both *Amtn* and *Klk4* are necessary for proper dental enamel maturation [50]. Kallikrein 4 (KLK4), a serine

protease, that takes the place of MMP20, helps in extracellular matrix degradation [51]. AMTN plays a crucial role in the aprismatic enamel development, influencing biomineralization by promoting hydroxyapatite mineralization [52].

To mineralize enamel, ameloblasts must transport Ca^{2+} and HPO_4^{2-} (Pi) into the enamel space using transmembrane transporter molecules, including members of sodium-calcium exchanger family (solute carrier 8A/SLC8A) and sodium-potassium-calcium exchangers (NCKX/SLC24A family) [45]. Slc26a1 is actively involved in maturation-stage amelogenesis, mediated pH regulation process, and is significantly up-regulated at the mRNA level at this stage [53,54]. *Cftr, Car6, and Car12* are all significantly up-regulated at the onset of the maturation stage of amelogenesis when compared to the secretory stage (Figure 6). Carbonic anhydrases (CA) catalyze the reversible conversion of CO_2 to bicarbonate (HCO^-_3) [47,55]. Mice null for *Cftr* have enamel defects, *Cftr* expression increased significantly during the rat enamel maturation stage versus the earlier secretory stage [56]. It has been described that Wdr72 is also involved in vesicular trafficking and membrane turnover in ameloblasts, especially during endocytosis [57]. WDR72 is a member of the WD40-repeat protein family, and its predicted protein structure is similar to proteins that regulate membrane deformation [57].

Additionally, during amelogenesis, there must be a direct contact between the ameloblasts and the secreted extracellular matrix. For these interactions, integrins (ITGB6), laminins (LAMA3 and LAMB3), collagens (COL17A1), and organelles like desmosomes and hemidesmosomes are all required (Figure 6) [9].

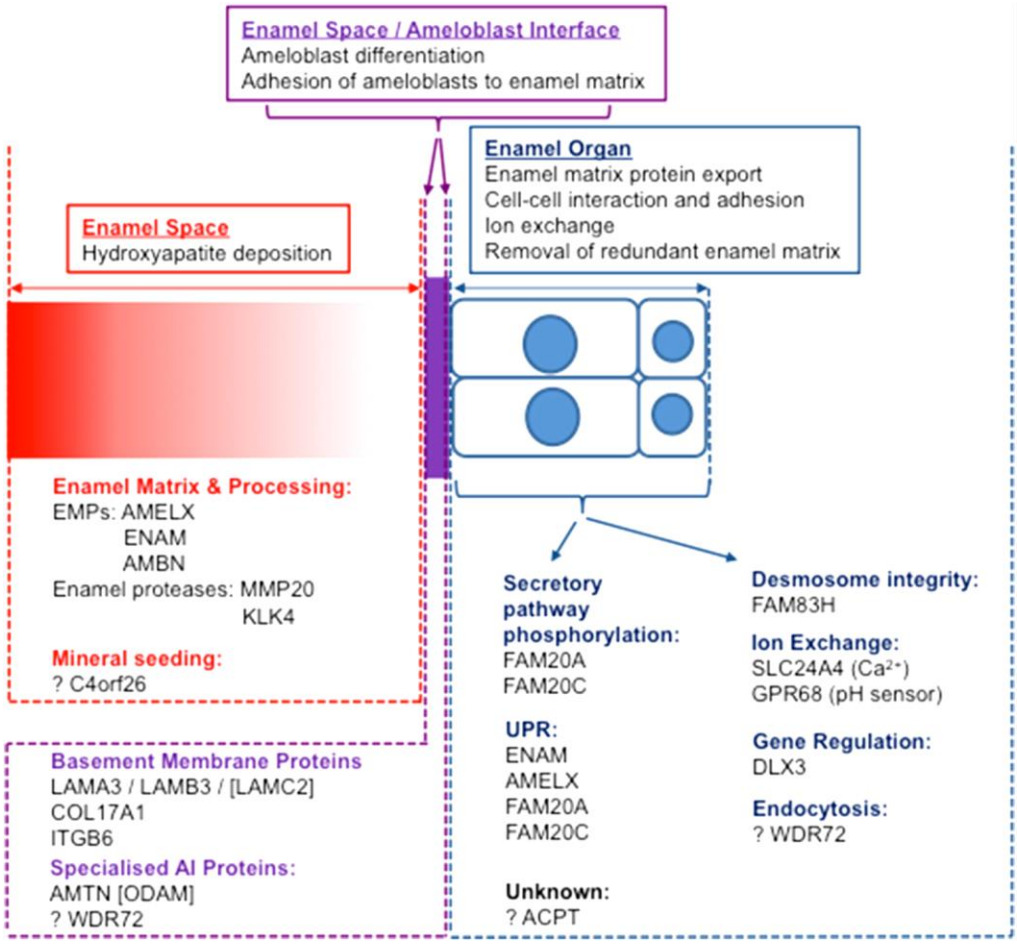

Figure 6. The three "compartments" involved in amelogenesis: the enamel space (extracellular matrix; red), the enamel organ (ameloblast cell layer and supporting cells; blue) and the interface between the two (purple). Known AI proteins are grouped according to functions within compartments. Those with no causative mutations for AI identified are designated by square brackets. From reference [9].

7. pH cycling and V-ATPase function in amelogenesis

During the maturation stage, deposition of hydroxyapatite and matrix turnover requires controlled pH regulatory mechanisms. This regulation is mediated by a variety of ion transporters [46]. As mentioned above, ameloblasts undergo a morphological change during this stage, cycling between ruffle- and smooth-ended forms. These changes serve to secrete calcium and phosphate, neutralize protons released during the growth of hydroxyapatite crystals, and to reabsorb and degrade AMEL (that has been broken down by MMP-20 and KLK4 – see Figure 7) [10]. It has been reported that the dysregulation of genes involved in pH control often produces severe amelogenesis *imperfecta* (AI)-like phenotypes. Hence, pH alterations can lead to deficits in enamel structure, including compositional anomalies (such as hypocalcification or hypomaturation) [54]. Enamel formation during maturation-stage amelogenesis involves mineral deposition, crystal growth, protease activities, and the degradation of the internalized organic matrix, all of which require tight control of extracellular pH and bicarbonate concentration. Extracellular pH and bicarbonate level alterations can have pronounced effects on enamel development. Maintenance of pH homeostasis of the

mineralizing enamel matrix environment is essential for the modulation and completion of enamel mineralization. Hence, enamel pH needs to periodically alternate between 6.0 and 7.2 [58]. A continued acidification of enamel pH may inhibit mineralization, and eventually be toxic to cells [8,47]. By releasing a HCO_3^- rich intercellular fluid onto the enamel surface, ameloblasts move from the RA phase to the SA phase. These cyclic alterations allow ameloblasts to develop an acidic zone on the enamel surface during the ruffle-ended phase. This is followed by a rapid elevation of pH of the enamel surface [11].

Ion transporters are extremely important to mineralize enamel, mediating the pH regulation process. Nbce1, Ae2, CFTR and carbonic anhydrases such as Car2, Car3, Car6, and Car12 have been found expressed in ameloblasts (Figure 8) [10,11,47]. NBCe1 is found at the basal pole of secretory ameloblasts, allowing for the movement of bicarbonate from the papillary layer cells and/or blood circulation into ameloblasts. AE2 and CFTR are found at the apical side of ameloblasts, allowing for the movement of bicarbonate from ameloblasts to the enamel matrix. In the case of carbonic anhydrases (CA), they catalyze the reversible conversion of CO_2 to bicarbonate (HCO_3^-) [47,55,59,60].

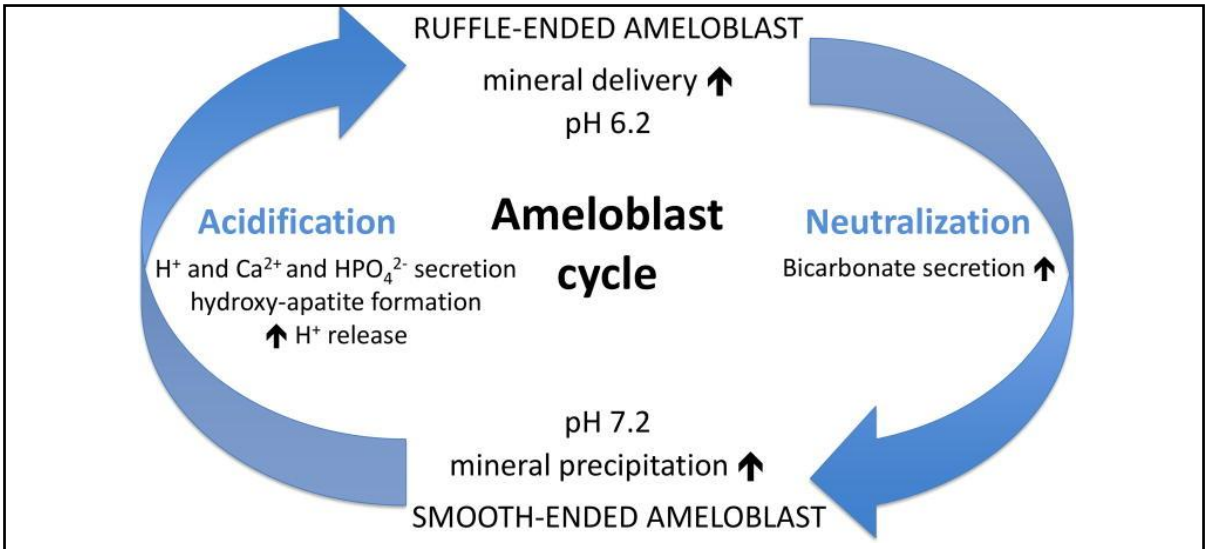

Figure 7. pH cycle in the luminal surface of ameloblasts during the maturation phase of amelogenesis. Cells cycle between smooth-ended and ruffle-ended stages multiple times. This cycling is accompanied by luminal pH changes between approximately 6.2 and 7.2. The primary driver of acidification is the release of protons liberated during hydroxyl-apatite formation. Acidification is counterbalanced then by the buffering effect of bicarbonate. From reference [10].

Vacuolar H^+-ATPase (V-ATPase) has also been found at the maturation stage of amelogenesis in the ruffle border of ruffle-ended ameloblasts (RA) and in intracellular vesicles in the smooth-ended ameloblasts (Figure 8) [11]. V-ATPases are highly conserved proton pumps consisting of a cytosolic V1 subcomplex with at least 8 subunits (A-H). V-ATPases contains the sites of ATP hydrolysis, attached to an integral membrane Vo subcomplex with at least 5 subunits (a, c, c", d and c) that forms the transmembrane proton pore. There are different V-ATPases isoforms depending on the cell type and tissue. In the case of the "*a"* subunit, required for proton translocation, there are four isoforms - *a1, a2, a3,* and *a4*. The *a1* isoform of V-ATPases is more common in neurons, while *a4* is enriched in renal intercalated and

epididymal clear cells. Despite being ubiquitously expressed, *a3* isoform V-ATPases have expression levels at least 100 times higher in osteoclasts than in all other cell types [61–63].

V-ATPase is essential for acidification of endosomes, lysosomes, and the trans-Golgi network, as well as for acid secretion by osteoclasts, kidney intercalated cells, and some tumor cells [64,65]. In contrast to the conventional osteoclast-type plasma membrane associated proton pump, which acidifies the extracellular environment, the V-ATPase in the apical pole of ameloblasts appears to have an intracellular acidification role [65].

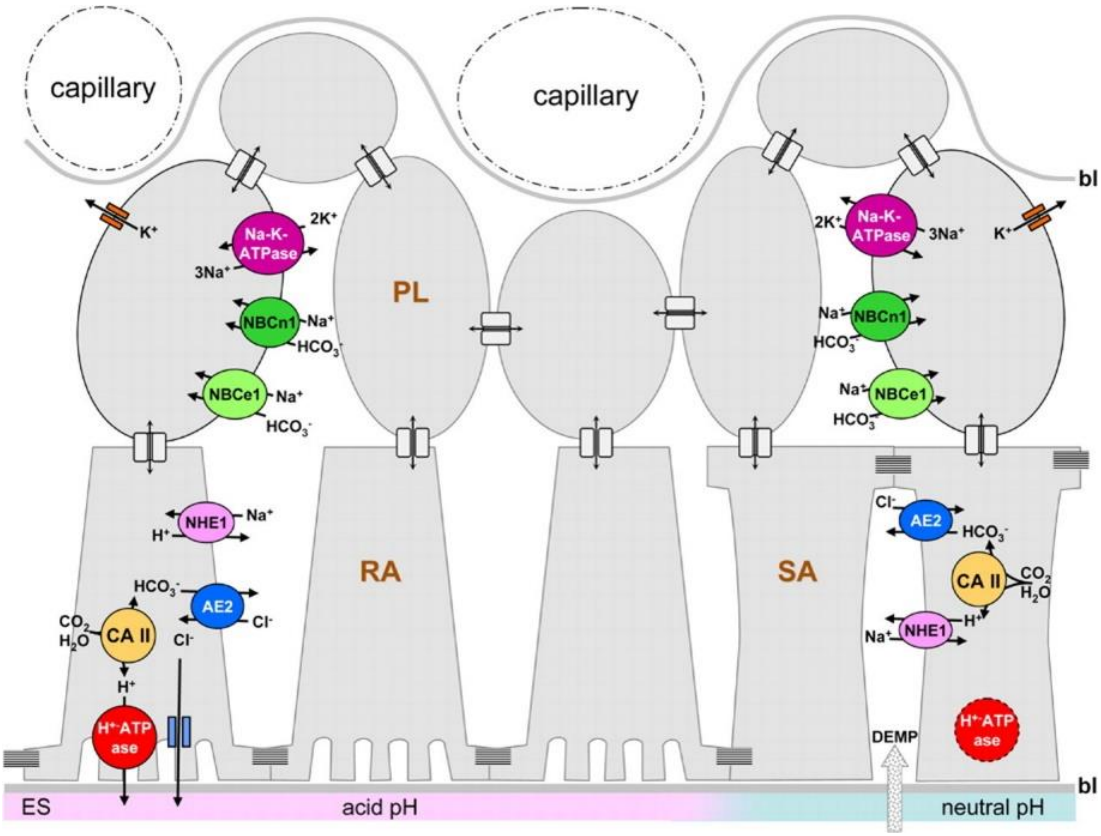

Figure 8. Diagrammatic model of the enamel organ during maturation stage of amelogenesis stating the localization of ion transporters (colored circles). The ameloblasts cyclically change between ruffle-ended ameloblasts (RA) and smooth-ended ameloblasts (SA). The present model assumes that ameloblasts and papillary cells (PL) act as a functional syncytium allowing free diffusion of ions via the numerous connected gap junctions. Furthermore, it suggests that carbonic anhydrase (CA II or other isoforms) together with vacuolar H^+-ATPase, AE2, and a Cl^- channel (possibly CFTR) are key players in the acidification of the enamel surface compartment (ES) in the RA stage. In SA cells, internalization of the H^+-ATPase from the distal cell surface membrane precludes this acidification and the intercellular spaces between SA cells open toward the enamel surface. This allows acidified, decomposed enamel matrix proteins (DEMP) to escape from the bulk enamel and let the HCO_3^--containing intercellular fluid neutralize the enamel surface. bl, Basal lamina. From reference [11].

ATP6V1A encodes for the A subunit that belongs to the cytosolic V1 complex. It has been described that variants encountered in *ATP6V1A* gene show amelogenesis *imperfecta*/enamel dysplasia at a rate of 42% [66]. A similar phenotype has been found in patients with autosomal recessive osteopetrosis (OMIM #259700), caused by variants in the *TCIRG1* gene, which encodes for the *a3* subunit of the V1 complex. Autosomal recessive osteopetrosis patients display abnormal dentition and enamel dysplasia. A mouse model for

osteopetrosis with a point mutation in the V-ATPase *a3* subunit showed abnormalities in tooth development, with a delay in enamel mineralization. Enamel was thinner and mineralization was significantly reduced [67].

While control of acid/base homeostasis and ion transport are essential for the development of healthy enamel, mineral transport to the enamel is also required for proper crystal growth [47]. Blood Ca^{2+} levels, enamel matrix proteins, and mineralization-regulating substances like amelogenins and Mg^{2+} affect how quickly ameloblasts transfer Ca^{2+}. When the majority of amelogenins and Mg^{2+} have been eliminated, mineral accretion is at its peak during mid- and late maturity [8].

8. **Amelogenesis *imperfecta* and its management**

Amelogenesis *imperfecta* (AI) is a heterogeneous group of different diseases affecting enamel formation. Amelogenesis *imperfecta* can be inherited in an autosomal dominant, autosomal recessive, or X-linked mode [68,69]. AI can present as an isolated disease or coexist with other abnormalities and symptoms as part of syndromic disorders [44]. The variety of enamel defects seen in individuals with AI are categorized according to the thickness, hardness, and smoothness of the damaged enamel. It is thought that variations in these characteristics reflect disturbances during amelogenesis. Problems during secretory stage lead to a pathologically thin or hypoplastic enamel, as a result of poor appositional growth and related crystal elongation defects. Disturbances during the maturation stage of amelogenesis result in pathologically soft (hypomaturation) enamel of normal thickness, due to a failure in the degradation of the EMP. In the case of a severe failure in mineralization with an enamel of normal thickness, the AI is classified as hypocalcified.

Factors such as age, associated medical conditions, AI type and severity, socio-economic status, have to be considered in treatment planning. Patients main demands are in pain management and aesthetics. These patients suffer from reduced quality of life, social integration difficulties, and loss of self-esteem. Oral hygiene and rigorous follow-up are recommended. Hypomineralized enamel shows progressive alteration with time because of its softness and post-eruptive enamel breakdown.

AI is a rare inherited enamel disease, which explains the difficulties of evidence-based clinical recommendation. This makes AI treatment challenging. Prevention, restorative, including prosthodontic dentistry must be done to maintain oral function and growth. Enamel must be restored to prevent tooth loss and allowing oral hygiene maintenance. Composite veneers in adolescents and young adults with severe forms of AI show excellent success rates and longevity with few adverse events. Treatment alternatives can also include minimally invasive dentistry, with the objective of maintaining tooth vitality. The goal is to achieve therapeutic solutions during the entire patient's life. Genetic and biological knowledge of AI physiopathology can be very helpful in treatment plan decision [69,70].

In France, a National Protocol for Diagnosis and Care (PNDS) for amelogenesis *imperfecta* has been developed as a guideline for good practice [71]. The PNDS is designed to improve the diagnosis, care, and follow-up of people with rare diseases. The aim of this protocol is to explain, to the involved health professionals, the current optimal diagnostic and therapeutic

management and care pathway of a patient with amelogenesis *imperfecta* based on scientific evidence.

Specific rare disease reference centers such as the reference center for rare oral and dental diseases O-Rares in Strasbourg (Centre de Référence des Maladies Rares Orales et Dentaires, Pôle de Médecine et Chirurgie Bucco-dentaire, Hôpitaux Universitaires de Strasbourg) provide advice and capitalize expertise contributing to the improvement of AI patient management, as well as developing research programs to enhance knowledge about the origins and molecular pathogenesis of these rare diseases.

9. **Mouse models mimicking rare orodental diseases**

Odontogenesis in the mouse begins on the 11th day of embryonic development (E11), mirroring analogous stages of tooth development in human (see Figure 9). The continuous growth and eruption of the rodent incisor (not found in humans) makes rodents a useful model system for researching how cells proliferate, migrate, differentiate, and deposit mineral matrix throughout dental development (Orsini et al., 2015). In addition, our ability to mutate or modulate gene expression in mouse and other rodents allows us to better understand how genetics can affect dental development. Hence, it is important to understand the distinctions between mouse and human to better apply this information.

The human dentition differs to that of the mouse in several aspects. In human, the dental formula is diphyodontia (primary and permanent dentition) and is composed of four types of teeth (incisors, canines, premolars and molars). For the mouse, the dental formula is monophyodontia (one set of teeth) with the two types of teeth (incisors and molars) separated by an edentulous space called diastema. The incisors of the mouse are characterized by an asymmetrical development. In mouse, enamel is present only on the labial side [38]. Despite these differences, the mouse is an excellent model for studying dental development and anomalies. Indeed, genetic ablation or "knockout" mice have been generated mimicking human rare diseases and associated orodental abnormalities [67,72–76].

Our research team work has a focus on rare diseases through human genetics and generating mouse models that mimick the disease. This serves to better understand the role of the affected proteins, elucidate novel gene targets, and to potentially develop therapeutic strategies for patient treatment. For instance, the *Ltbp3*$^{-/-}$ mouse model shows a similar phenotype to Verloes-Bourguignon syndrome caused by *LTBP3* variants. *Ltbp3*$^{-/-}$ mutant mice display craniofacial anomalies and amelogenesis *imperfecta* [72]. Another human rare disease is caused by mutations or altered expression of the *SMOC2* gene. *Smoc2* $^{-/-}$ mutant mice exhibit oligodontia, microdontia, tooth root deficits, alveolar bone hypoplasia, and a variety of skeletal abnormalities . Smoc2-GFP reporter expression in mouse shows that Smoc2 dynamically labels a variety of dental and bone progenitors. *Smoc2*$^{-/-}$ mutants dysplay an alteration in the structure of enamel prisms, with a reduced crystal compaction, smaller teeth, and reduced alveolar ossification [73].

During my research we have investigated a new gene, *ROGDI*. Interestingly, *ROGDI* regulates both neurological and orofacial development. In humans *ROGDI* variants result in

Kohlschütter-Tönz syndrome. Here, affected patients display epilepsy, intellectual disability, psychomotor regression, along with amelogenesis *imperfecta*.

The pathophysiology and role of Rogdi can be investigated using the *Rogdi*$^{-/-}$ mouse model. A manuscript describing the murine *Rogdi*$^{-/-}$ knockout phenotype, comparing it to the clinical symptoms observed in patients, is reported on page 160.

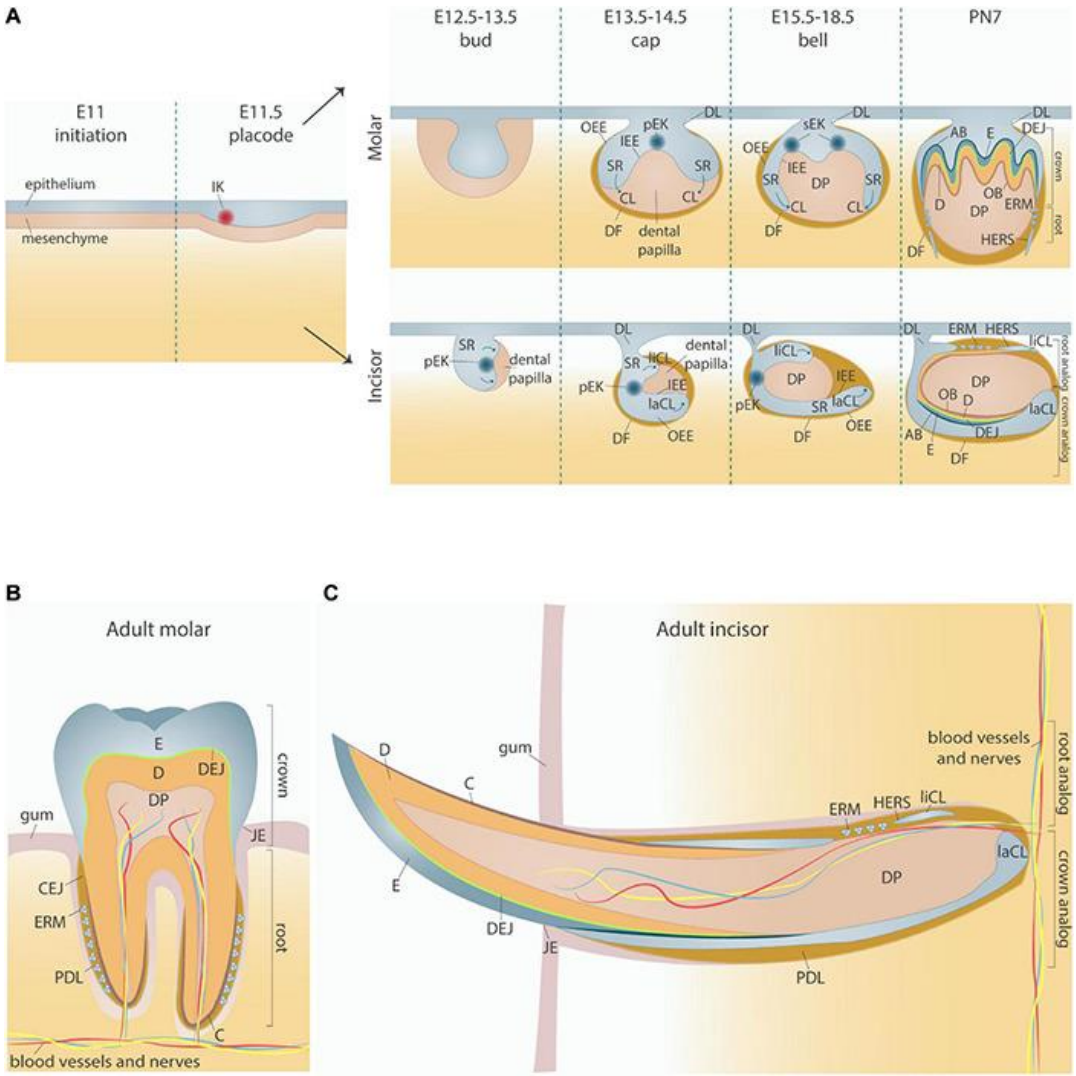

Figure 9. Overview of mouse tooth development. (A) Embryonic stages of mouse tooth development, with divergent morphology of molar and incisor tooth germs. (B, C) Schematic of fully formed adult molar (B) and incisor (C). AB, ameloblasts; C, cementum; CEJ, cemento-enamel junction; CL, cervical loop; D, dentin; DEJ, dentino-enamel junction; DF, dental follicle; DL, dental lamina; DP, dental pulp; E, enamel; E11-18.5, embryonic days; ERM, epithelial cells rests of Malassez; HERS, Hertwig's epithelial root sheath; IEE, inner enamel epithelium; IK, initiation knot; JE, junctional epithelium; laCL, labial cervical loop; liCL, lingual cervical loop; pEK, primary enamel knot; PDL, periodontal ligament; PN7, postnatal day 7; OB, odontoblasts; OEE, outer enamel epithelium; SR, stellate reticulum. From reference [12].

Objectives

This thesis focuses on rare orodental diseases, specifically in amelogenesis imperfecta and enamel phenotypes encountered in rare human diseases, whether isolated or syndromic, and in mouse models developing these diseases.

The objectives of this Ph.D. thesis are to analyze a *Rogdi*$^{-/-}$ mouse mutant to understand the role of ROGDI during development and the pathophysiology behind its inactivation in Kohlschütter-Tönz syndrome (KTS). Identifying the role of ROGDI will facilitate understanding of the phenotype encountered in this disease, particularly the dental and neurological symptoms. Our goal is to apply a variety of approaches (including mouse genetic modeling) for improving our understanding of this disease, and thus the management of patients affected with this syndrome.

The **first chapter** provides an overview of rare orodental diseases and the clinical research correlating phenotype and genetics.

Amelogenesis imperfecta (AI) is the main focus of this thesis. AI is a heterogeneous group of diseases where there is a disruption of the development of enamel. We show an evolution in the classification of the AI phenotypes, using next generation sequencing to classify this group of diseases at the molecular level and not only at the clinical level (**article #1**). The classification used until nowadays was described by Witkop in 1988, dividing AI into 4 types according to the nature of the enamel defects and the mode of transmission (Type I hypoplastic, Type II hypomature, Type III hypomineralized, and Type IV hypomature/hypoplastic with taurodontism). There currently exist more than 70 genes known to cause disease. At the Reference Center for Rare Oral and Dental Diseases (O-Rares, Strasbourg), patients exhibiting AI were enrolled and evaluated using the D4/phenodent protocol (www.phenodent.org). Using a specialized next generation sequencing (NGS) panel called GenoDENT, families provided written informed consents for phenotyping as well as molecular analysis and diagnosis. With this study was possible to clarify the molecular basis of the Witkop's AI classification.

A case report of "A novel homozygous variant in *GJA1* causing a Hallermann-Streiff/Oculodentodigital Dysplasia overlapping Phenotype: a clinical report" is presented (**article #2**). Here, thanks to whole-exome sequencing (WES) it was possible to identify a homozygous variant in the *GJA1* gene affecting the second extracellular loop of the CX43 protein causing clinical features of both Hallermann-Streiff (HSS, OMIM 234100) and Oculodentodigital Dysplasia (ODDD, OMIM 164200) syndromes. CX43 protein allows the cell-to-cell exchange of ions and small molecules. During enamel development, CX43 is involved in the transport of ions from the papillary layer into the ameloblasts.

AI can be isolated or associated to a syndrome. In the case of KTS linked to *ROGDI* variants, patients present the hypomineralization type of AI, in which enamel is less mineralized, porous, rough, and brown stained in both primary and permanent teeth. This type of AI is associated with problems during the maturation stage of amelogenesis [77].

The most significant clinical traits of this disease are highlighted in the section titled **Kohlschütter-Tönz syndrome** of this text.

Signals guiding craniofacial development are also used in establishing sensory, motor, and cognitive function. Such widespread cranio-oro-facial phenotypes are often due to alterations

in key DNA transcriptional factors or members of the DNA repair process. Our laboratory combines patient-based clinical screens with the strength of the IGBMC/Institute Clinique de la Souris (ICS) in creating and analyzing equivalent mouse models.

The **second chapter** addresses studies using mouse models as a tool for translational research in orodental disorders.

Numerous genetically altered mice used as models for rare diseases replicate the craniofacial and dental anomalies, found in humans. This enables a deeper examination of the effects of the underlying molecular dysfunctions. We identify, treat, and perform genomic screenings of patients with unusual dental craniofacial defects to identify candidate genes. Additionally, there are rodent models available that have defective dentine, enamel, and other dental tissues in addition to gene mutations for which no human disease has yet been described. They offer proof that these genes play a role in tooth development and identify prospective new candidate genes in humans (**article #3**).

The principal subject of this PhD work is the investigation of a novel leucine zipper domain-containing protein of unknown function, ROGDI. Patients with an autosomal recessive mutation in this gene exhibit Kohlschütter-Tönz Syndrome, displaying epilepsy, severe psychomotor regression, and amelogenesis imperfecta symptoms. Using the approach of gene targeting we have generated an equivalent mouse model for this disease (**article #4**). The article details the work carried out on a *Rogdi* gene-inactivated (*Rogdi*$^{-/-}$) mouse model summarizing the phenotype encountered in KTS using behavioral, morphological, and molecular approaches. To understand neurodegenerative and enamel deficits, comparative genomic studies were conducted. Whole genome RNA-sequencing, combined with bioinformatic approaches helped to uncover a *Rogdi* transcriptional network. Behavioral tests as well as *in situ hybridization*, immunohistochemistry, Micro-CT, and SEM analysis showed that *Rogdi*$^{-/-}$ mice displayed a similar phenotype compared to KTS patients. The phenotypic correlations between the mouse model and human, and the identification of Rogdi role will hopefully help researchers and clinicians understand the combination of dental and neurological symptoms and improve patient healthcare and management.

We have also worked in collaboration with Dr. Gilles Lavery (team of Daniel Metzger - IGBMC - Functional Genomics and Cancer) whose interest is the pathophysiological role of vitamin D signaling, to understand the role of this receptor in tooth development. The **article #5** of this PhD work describes two vitamin D receptor mouse models (*VDR-null* and *VDR*$_{gem}$) presenting tooth and alveolar bone defects.

Results

Chapter 1: Rare orodental diseases

1. Amelogenesis *imperfecta*: Next-generation sequencing sheds light on Witkop's classification.

Amelogenesis imperfecta (AI) refers to a group of rare genetic diseases that affect the formation, structure, and clinical appearance of enamel, either as isolated trait, or in association with other symptoms. The prevalence of AI varies from 1/700 to 1/14000. This disease can be inherited in an autosomal dominant, autosomal recessive or X-linked manner. Primary and permanent teeth are concerned with almost the same severity [68,69]. Enamel may be modified in its width, microstructure, or mineralization degree. Thus, clinical symptomatology goes from light discoloration to disintegration/break- down of the enamel of the entire tooth. AI can be classified into different sub-types (hypoplastic [quantitative defects], hypomineralized, and hypomature [qualitative defects]) based on the nature of the enamel defect, i.e., thickness, hardness, and/or color. Witkop, in 1988, considered reclassifying these AI considering the type of enamel flaws and the mode of transmission [78]. Type I hypoplastic, Type II hypomature, Type III hypomineralized, and Type IV hypomature/hypoplastic with taurodontism were the four basic types of AI, each of which had subtypes. [79]) have remarked on this classification and suggested including molecular data. Since then, more genes have been found, and currently, more than 70 genes have been associated to AI.

We used next-generation sequencing (NGS) to investigate a heterogeneous group of AI patients in an effort to identify the disease's genetic cause and enhance diagnosis and treatment. A cohort of 115 patients exhibiting isolated (73%) or syndromic (27%) AI were enrolled and evaluated. The NGS panel called GenoDENT, which investigates 567 genes at once, was used for molecular analysis. Results were correlated with the patient's phenotype to arrive at a final diagnosis. In both isolated and syndromic AI, the most common AI is the hypoplastic type, followed by hypomature and hypomineralized type.

47 newly reported class 4 or 5 variations, out of the 151 sequenced variants, are included in this article. For isolated AI, the genotypes linked to *MMP20* and *FAM83H* were the most commonly found. The most frequently mutated genes found in syndromic AI in this study were *FAM20A* (enamel-kidney syndrome), *LTBP3* (Verloes Bourguignon syndrome) and *ROGDI* (Kohlschütter-Tönz syndrome).

frontiers | Frontiers in Physiology

TYPE Original Research
PUBLISHED 09 May 2023
DOI 10.3389/fphys.2023.1130175

Check for updates

OPEN ACCESS

EDITED BY
Frédéric Lézot,
Institut National de la Santé et de la Recherche Médicale (INSERM), France

REVIEWED BY
Olivier Duverger,
National Institute of Dental and Craniofacial Research (NIH), United States
Tim Wright,
University of North Carolina at Chapel Hill, United States

*CORRESPONDENCE
Agnes Bloch-Zupan,
agnes.bloch-zupan@unistra.fr

†These authors contributed equally to this work and share first authorship

SPECIALTY SECTION
This article was submitted to Craniofacial Biology and Dental Research, a section of the journal Frontiers in Physiology

RECEIVED 22 December 2022
ACCEPTED 06 March 2023
PUBLISHED 09 May 2023

CITATION
Bloch-Zupan A, Rey T, Jimenez-Armijo A, Kawczynski M, Kharouf N, O-Rare consortium, Dure-Molla MdL, Noirrit E, Hernandez M, Joseph-Beaudin C, Lopez S, Tardieu C, Thivichon-Prince B, ERN Cranio Consortium, Dostalova T, Macek M Jr, International Consortium, Alloussi ME, Qebibo L, Morkmued S, Pungchanchaikul P, Orellana BU, Manière M-C, Gérard B, Bugueno IM and Laugel-Haushalter V (2023), *Amelogenesis imperfecta*: Next-generation sequencing sheds light on Witkop's classification.
Front. Physiol. 14:1130175.
doi: 10.3389/fphys.2023.1130175

COPYRIGHT
© 2023 Bloch-Zupan, Rey, Jimenez-Armijo, Kawczynski, Kharouf, O-Rare consortium, Dure-Molla, Noirrit, Hernandez, Joseph-Beaudin, Lopez, Tardieu, Thivichon-Prince, ERN Cranio Consortium, Dostalova, Macek, International Consortium, Alloussi, Qebibo, Morkmued, Pungchanchaikul, Orellana, Manière, Gérard, Bugueno and Laugel-Haushalter. This is an open-access article distributed under the terms of the Creative Commons Attribution License (CC BY). The use, distribution or reproduction in other forums is permitted, provided the original author(s) and the copyright owner(s) are credited and that the original publication in this journal is cited, in accordance with accepted academic practice. No use, distribution or reproduction is permitted which does not comply with these terms.

Amelogenesis imperfecta: Next-generation sequencing sheds light on Witkop's classification

Agnes Bloch-Zupan[1,2,3,4,5*†], Tristan Rey[4,6†], Alexandra Jimenez-Armijo[4†], Marzena Kawczynski[3], Naji Kharouf[7], O-Rare consortium, Muriel de La Dure-Molla[8], Emmanuelle Noirrit[9], Magali Hernandez[10], Clara Joseph-Beaudin[11], Serena Lopez[12], Corinne Tardieu[13], Béatrice Thivichon-Prince[14], ERN Cranio Consortium, Tatjana Dostalova[15], Milan Macek Jr[15], International Consortium, Mustapha El Alloussi[16], Leila Qebibo[17], Supawich Morkmued[18], Patimaporn Pungchanchaikul[18], Blanca Urzúa Orellana[19], Marie-Cécile Manière[1,3], Bénédicte Gérard[6], Isaac Maximiliano Bugueno[1,3,4] and Virginie Laugel-Haushalter[1,4,6]

[1]Université de Strasbourg, Faculté de Chirurgie Dentaire, Strasbourg, France, [2]Université de Strasbourg, Institut d'études avancées (USIAS), Strasbourg, France, [3]Hôpitaux Universitaires de Strasbourg (HUS), Pôle de Médecine et Chirurgie Bucco-dentaires, Hôpital Civil, Centre de référence des maladies rares orales et dentaires, O-Rares, Filiére Santé Maladies rares TETE COU, European Reference Network ERN CRANIO, Strasbourg, France, [4]Université de Strasbourg, Institut de Génétique et de Biologie Moléculaire et Cellulaire (IGBMC), IN-SERM U1258, CNRS- UMR7104, Illkirch, France, [5]Eastman Dental Institute, University College London, London, United Kingdom, [6]Hôpitaux Universitaires de Strasbourg, Laboratoires de diagnostic génétique, Institut de Génétique Médicale d'Alsace, Strasbourg, France, [7]Université de Strasbourg, Laboratoire de Biomatériaux et Bioingénierie, Inserm UMR_S 1121, Strasbourg, France, [8]Rothschild Hospital, Public Assistance-Paris Hospitals (AP-HP), Reference Center for Rare Oral and Den-tal Diseases (O-Rares), Paris, France, [9]Centre Hospitalier Universitaire (CHU) Rangueil, Toulouse, Competence Center for Rare Oral and Den-tal Diseases, Toulouse, France, [10]Centre Hospitalier Régional Universitaire de Nancy, Université de Lorraine, Competence Center for Rare Oral and Dental Diseases, Nancy, France, [11]Centre Hospitalier Universitaire de Nice, Competence Center for Rare Oral and Dental Diseases, Nice, France, [12]Centre Hospitalier Universitaire de Nantes, Competence Center for Rare Oral and Dental Diseases, Nantes, France , [13]APHM, Hôpitaux Universitaires de Marseille, Hôpital Timone, Competence Center for Rare Oral and Dental Diseases, Marseille, France, [14]Centre Hospitalier Universitaire de Lyon, Competence Center for Rare Oral and Dental Diseases, Lyon, France, [15]Department of Stomatology (TD) and Department of Biology and Medical Genetics (MM) Charles University 2nd Faculty of Medicine and Motol University Hospital, Prague, Czechia, [16]Faculty of Dentistry, International University of Rabat, CReSS Centre de recherche en Sciences de la Santé, Rabat, Morocco, [17]Unité de génétique médicale et d'oncogénétique, CHU Hassan II, Fes, Morocco, [18]Faculty of Dentistry, Khon Kaen University, Khon Kaen, Thailand, [19]Instituto de Investigación en Ciencias Odontológicas, Facultad de Odontología, Universidad de Chile, Santiago, Chile

Amelogenesis imperfecta (AI) is a heterogeneous group of genetic rare diseases disrupting enamel development (Smith et al., Front Physiol, 2017a, 8, 333). The clinical enamel phenotypes can be described as hypoplastic, hypomineralized or hypomature and serve as a basis, together with the mode of inheritance, to Witkop's classification (Witkop, J Oral Pathol, 1988, 17, 547–553). AI can be described in isolation or associated with others symptoms in syndromes. Its occurrence was estimated to range from 1/700 to 1/14,000. More than 70 genes have currently been identified as causative.

Objectives: We analyzed using next-generation sequencing (NGS) a heterogeneous cohort of AI patients in order to determine the molecular etiology of AI and to improve diagnosis and disease management.

Methods: Individuals presenting with so called "isolated" or syndromic AI were enrolled and examined at the Reference Centre for Rare Oral and Dental Diseases (O-Rares) using D4/phenodent protocol (www.phenodent.org). Families gave written informed consents for both phenotyping and molecular analysis and diagnosis using a dedicated NGS panel named GenoDENT. This panel explores currently simultaneously 567 genes. The study is registered under NCT01746121 and NCT02397824 (https://clinicaltrials.gov/).

Results: GenoDENT obtained a 60% diagnostic rate. We reported genetics results for 221 persons divided between 115 AI index cases and their 106 associated relatives from a total of 111 families. From this index cohort, 73% were diagnosed with non-syndromic amelogenesis imperfecta and 27% with syndromic amelogenesis imperfecta. Each individual was classified according to the AI phenotype. Type I hypoplastic AI represented 61 individuals (53%), Type II hypomature AI affected 31 individuals (27%), Type III hypomineralized AI was diagnosed in 18 individuals (16%) and Type IV hypoplastic-hypomature AI with taurodontism concerned 5 individuals (4%). We validated the genetic diagnosis, with class 4 (likely pathogenic) or class 5 (pathogenic) variants, for 81% of the cohort, and identified candidate variants (variant of uncertain significance or VUS) for 19% of index cases. Among the 151 sequenced variants, 47 are newly reported and classified as class 4 or 5. The most frequently discovered genotypes were associated with *MMP20* and *FAM83H* for isolated AI. *FAM20A* and *LTBP3* genes were the most frequent genes identified for syndromic AI. Patients negative to the panel were resolved with exome sequencing elucidating for example the gene involved ie *ACP4* or digenic inheritance.

Conclusion: NGS GenoDENT panel is a validated and cost-efficient technique offering new perspectives to understand underlying molecular mechanisms of AI. Discovering variants in genes involved in syndromic AI (*CNNM4, WDR72, FAM20A* . . .) transformed patient overall care. Unravelling the genetic basis of AI sheds light on Witkop's AI classification.

KEYWORDS

enamel, amelogenesis imperfecta, genetics, rare diseases, NGS, next-generation sequencing

Introduction

Enamel is the only mineralized structure of the body with an ectodermal origin. It has extraordinary mechanical and chemical properties. It is strongest and hardest material in the body and acts as an efficient barrier against environmental assaults whether mechanical, chemical, or physical. Enamel is incapable of regeneration or repair as ameloblasts, the specialized post-mitotic ectoderm-derived cells that produce the enamel matrix, disappear when the teeth erupt within the oral cavity. Normally, these ameloblasts produce proteins (enamelin, amelogenin, ameloblastin . . .) in the secretory phase, mineralize this matrix and then mature it, in the maturation phase, by removing almost all the scaffold proteins *via* enzymes (KLK4, MMP20) to allow hydroxyapatite-crystal growth towards 96%–98% mineral content.

Amelogenesis imperfecta (AI) is a heterogeneous group of rare inherited diseases affecting amelogenesis, i.e. the enamel developmental process, in both primary and permanent dentitions and may be evident as an isolated trait or associated to other symptoms in syndromes. Amelogenesis imperfecta may manifest in different forms based on the phenotypic nature of the observed enamel defect, divided in three categories: hypoplastic (quantitative defect i.e. thinner enamel, pitted or striae enamel, enamel agenesis), hypomineralized (softer rough colored undermineralized enamel) or -hypomature (relatively hard but colored not translucent enamel). In 1988, Witkop (Witkop, 1988) proposed a revised classification of amelogenesis imperfecta considering the nature of the enamel defects as well the mode of inheritance (Table 1) and dividing AI into 4 classes (Type I hypoplastic, Type II hypomaturation, Type III hypocalcified, Type IV hypomaturation/hypoplastic with taurodontism). This classification was challenged by other authors cited in (Crawford et al., 2007) who proposed to add molecular data. More than 70 genes have been associated to "isolated" or "syndromic" AI. These genes encode a wide array of potential activities in amelogenesis, from enamel matrix

TABLE 1 Witkop's classification of amelogenesis imperfecta phenotypes and associated mode of inheritance (Witkop and Sauk, 1976; Witkop 1988) and current knowledge about corresponding associated genes.

TYPE	Class	Phenotype	Mode of inheritance	Phenotype OMIM number #	Genes
I -HYPOPLASTIC	IA	HYPOPLASTIC, PITTED	AD	104530	*LAMA3, LAMB3, LAMC2, COL7A1, COL17A1, ITGB6/4*
				616221	
	IB	HYPOPLASTIC, LOCAL	AD	104500	*ENAM*
	IC	HYPOPLASTIC, LOCAL	AR	204650	*ENAM*
				617297	*ACP4?*
	ID	HYPOPLASTIC, SMOOTH	AD	620104	*SP6?*
	IE	HYPOPLASTIC, SMOOTH	XLD	301200	*AMELX, ARHGAP6, HCCS?*
	IF	HYPOPLASTIC, ROUGH	AD	616270	*AMBN*
	IG	ENAMEL AGENESIS	AR	204690	*FAM20A*
	IH		AR	616221	*ITGB6*
	IJ		AR	617297	*ACP4 = ACPT*
	IK		AD	620104	*SP6*
II -HYPOMATURATION	IIA	HYPOMATURATION, PIGMENTED	AR	204700	*KLK4, MMP20, WDR72, ODAPH = C4orf26, SLC24A4, GPR68*
				612529	
				613211	
				614832	
				615887	
				617217	
	IIB	HYPOMATURATION	XLR	301200	*AMELX?*
	IIC	SNOW CAPPED TEETH	XL	301200	*AMELX—ARHGAP6*
	IID	SNOW CAPPED TEETH	AD	?	?
III -HYPOCALCIFIED	IIIA		AD	130900	*FAM83H (AD), AMTN (AD)*
				617607	
	IIIB		AR	618386	*RELT (AR) (IIIC?)*
IV -HYPOMATURATION-HYPOPLASTIC WITH TAURODONTISM	IVA	HYPOMATURATION-HYPOPLASTIC WITH TAURODONTISM	AD	104510	*DLX3*
	IVB	HYPOPLASTIC-HYPOMATURATION	AD	104510	*DLX3*
		WITH TAURODONTISM			
V -SYNDROMIC AI					*TSC1, FAM20A, DLX3, LTBP3, CNNM4, ROGDI, SLC13A5, SLC10A7, GALNS, AIRE, ORAI1, STIM1, PORCN, PEX1, PEX6, PEX26, CLDN16, CLDN19, FAM20C, SLC4A4, ATP6V1A ...*

Bold values correspond to the original Witkop's classification.

proteins, to intracellular vesicle trafficking, to ameloblast attachment to the matrix or neighbor cells, to ion transport, to mineralization, to matrix-protein degradation. Critically, the syndromic manifestations of AI and other defects have proven to be an efficient strategy for elucidating the processes of odontogenesis providing better identification into new genes/proteins and their role in the physiopathology of enamel defects as well as the recognition of

new clinical entities. Furthermore, some of these identified genes are involved in both syndromic and non-syndromic rare diseases.

In this paper, we propose to revise Witkop's classification in the light of recent progress in genetics and genomics. The next-generation sequencing panel GenoDENT (Prasad et al., 2016a; Rey et al., 2019) and exome sequencing (WES) (Laugel-Haushalter et al., 2019) have improved understanding and recognition of AI and associated syndromes. We report in this paper individuals with pathogenic variants in known genes involved in AI but also individuals with variants in new candidate genes and individuals presenting variants of uncertain significance (VUS) in known genes. It is our hope that the clinical pictures provided with the proposed classification will assist clinicians in AI recognition. By combining clinical and genetic diagnosis we expect to reveal previously undiscovered rare diseases with a broader clinical spectrum thus improving our diagnoses and management. This strategy would emphasize the role of dentists in the new era of personalized medicine.

Material and methods

Individual's phenotypes

Individuals were enrolled and examined in the Reference Center (CRMR) for rare oral and dental diseases or in one of the 16 affiliated Competence Centers (CCMR) of the French O-Rares network, Filière TETECOU) or by their treating practitioners from France and other countries (ex. the ERN CRANIO). They were recruited between 2009 and 2021. When possible, parents and relatives were also included in the study.

Oral phenotype was documented using the D[4]/phenodent registry protocol, a Diagnosing Dental Defects Database [see www.phenodent.org, for assessment form], which is approved by CNIL (French National commission for informatics and liberty, number 908416). This clinical study is registered at https://clinicaltrials.gov: NCT01746121 and NCT02397824, and with the MESR (French Ministry of Higher Education and Research) Bioethics Commission as a biological collection "Orodental Manifestations of Rare Diseases" DC-2012-1,677 within DC-2012-1,002 and was acknowledged by the CPP (person protection committee) Est IV 11 December 2012.

The individuals presenting AI and the non-affected family members gave written informed consents in accordance with the Declaration of Helsinki, both for the D[4]/phenodent registry and for genetic analyses performed on salivary samples (Oragene® DNA OG-250, OG_650 commercial kits (DNA Genotek Inc., Ottawa, Ont, Canada). Genomic DNA was extracted according to the manufacturer's protocol included in the biological collection.

The terminology used to describe dental and enamel abnormalities has been detailed in (de La Dure-Molla et al., 2019).

Individuals' biological samples were sent to the reference center of Strasbourg, France for genetical analysis.

Individual's genotypes

Next-generation sequencing panel genodent

The GenoDENT panel has been evolving through times from its first published version (Prasad et al., 2016a). The last updated version 6.0 explores 567 genes (Supplementary Table S1).

The GenoDENT panel interrogates two categories of genes: a diagnostic panel (248 genes known as responsible for rare diseases with orodental expression in human) and a discovery panel (319 candidate genes reported as being involved in tooth development or orodental anomalies in animal models for example).

Probe design was performed on the Agilent SureDesign portal (https://erray.chem.agilent.com/suredesign, Agilent, United States) in order to capture, by complementarity, the exonic sequence as well as 25 bases of their flanking intronic sequences. Libraries were prepared with the Agilent SureSelect QXT protocol and sequenced on a NextSeq 550 (Illumina, San Diego, United States). GenoDENT is implemented in a diagnostic setting and its results are directly available for the individual medical file and genetic counselling. Variants are classified according to the American College of Medical Genetics (ACMG) classification (Richards et al., 2015; Harrison et al., 2019). Upon identification of variants of class 4 (probably pathogenic) or 5 (pathogenic), extended familial segregation is performed *via* Sanger sequencing; a detailed report is written and sent to the geneticist. A variant of uncertain significance (VUS) or class 3 should not be used in clinical decision-making. Class 2 are likely benign polymorphisms.

Whole exome sequencing

Trio whole Exome Sequencing (WES) was performed on trio for individuals 7.10, 7.11, 9.1, 9.2, 9.3, 17.1, 17.2, 17.3, 17.4, 18.3, 18.8, 18.10, and 24.2 by Integragen (Evry, France, 2014). Exons of DNA samples were captured using in-solution enrichment methodology (SureSelect Human All Exon Kits, Agilent, Massy, France) with the company's biotinylated oligonucleotide probe library (Agilent Human All Exon v5+UTR 75 Mb Kit) and sequenced with an Illumina HISEQ 2000 (Illumina, San Diego, United States) as paired-end 75 bp reads, resulting in an average coverage of 80X.

Bioinformatics analysis

STARK (Stellar Tools from raw sequencing data Analysis to variant RanKing) is a bioinformatics pipeline based on the GATK recommendations used to process the NGS data (DePristo et al., 2011). Annotation and ranking of SNV/indel were performed by VaRank (Geoffroy et al., 2015) in combination with the Alamut Batch software (Interactive Biosoftware, Rouen, France). Variant effect on the nearest splice site was predicted using MaxEntScan (Yeo and Burge, 2004), NNSplice (Reese et al., 1997) and Splice Site Finder (Shapiro and Senapathy, 1987).Very stringent criteria were applied to filter out non-pathogenic variants: 1) variants represented with an allele frequency of more than 1% in public variation databases including the 1,000 Genomes ('The 1000 Genomes Project Consortium et al., 2015), the GnomAD database (Exome Aggregation Consortium et al., 2016) or our internal exome database, 2) variants in 5′ or 3′ UTR, 3) variants with intronic

10.3389/fphys.2023.1130175

TABLE 2 Variations found in individuals presenting with syndromic amelogenesis imperfecta.

Patient number	Diagnosis/AI	Gene	Variant and location	Zygosity	Mode of inheritance	Rank	Effect of the mutation	Consistent with the known disease phenotype	Family segregation	Status
17.1 (female)	Hypoplastic, short stature	***LTBP3*** ***Chr11(GRCh37):*** ***NM_001130144.3***	c.421C>T; p.(Gln141*) Exon 2 Huckert M et al. (2015)	compound heterozygous	AR	4	non-sense	Yes	S(A,C)	exome
			c.1531 + 1G>T; p.? Intron 8 Huckert M et al. (2015)		AR	4	splice		S(A,C)	
17.2 (female)	Hypoplastic, short stature	***LTBP3*** ***Chr11(GRCh37):*** ***NM_001130144.3***	c.2071_2084del; p.(Tyr691Leufs*95) Exon 14 Huckert M et al. (2015)	homozygous	AR	4	frameshift	Yes	S(A,C) S(U,R) MoFa(U,C)	exome
17.3 (male)	Hypoplastic, short stature	***LTBP3*** ***Chr11(GRCh37):*** ***NM_001130144.3***	c.2216del; p.(Gly739Alafs*7) Exon 15 Huckert M et al. (2015)	homozygous	AR	4	frameshift	Yes	MoFa(U,C)	exome
17.4 (male)	Hypoplastic, short stature	***LTBP3*** ***Chr11(GRCh37):*** ***NM_001130144.3***	c.2356del; p.(Val786Trpfs*82) Exon 17 Huckert M et al. (2015)	homozygous	AR	4	frameshift	Yes	MoFa(U,C) 3S(A,C)	exome
17.5 (female)	Hypoplastic, short stature	***LTBP3*** ***Chr11(GRCh37):*** ***NM_001130144.3***	c.3087del; p.(Asn1030Thrfs*47) Exon 22	homozygous	AR	4	frameshift	Yes	MoFa(U,C)	panel
17.6 (female)	Hypoplastic, short stature	***LTBP3*** ***Chr11(GRCh37):*** ***NM_001130144.3***	c.3629-2A>G; p.? Intron 26	homozygous	AR	4	splice	Yes	MoFa(U,C)	panel
Patient number	**Diagnosis/AI**	**Gene**	**Variant and location**	**Zygosity**		**Rank**	**Effect of the mutation**	**Consistent with the known disease phenotype**	**Family segregation**	**Status**
18.1 (female)	Hypoplastic AI, nephrocalcinosis	***FAM20A*** *Chr17(GRCh37):* *NM_017565.4*	c.34_35del; p.(Leu12Alafs*67) Exon 1 Cho et al. (2012)	compound heterozygous	AR	5	frameshift	Yes	S(A,C)	panel
			c.610del; p.(Ala204Profs*12) Exon 3		AR	4	frameshift		S(A,C)	
18.2 (male)	Hypoplastic AI, nephrocalcinosis	***FAM20A*** *Chr17(GRCh37):* *NM_017565.4*	c.53_54delinsAG; p.(Leu18Arg) Exon 1	putative compound heterozygous	AR	3	missense	Yes	NA	panel
			c.976_978del; p.(Glu326del) Exon 7		AR	3	deletion		NA	
18.3 (male)	Hypoplastic AI, nephrocalcinosis	***FAM20A*** *Chr17(GRCh37):* *NM_017565.4*	c.217C>T; p.(Arg73*) Exon 1 Jaureguiberry et al. (2012)	compound heterozygous	AR	4	non-sense	Yes	Fa(U,C) S(A,C)	exome
			c.727C>T; p.(Arg243*) Exon 5 Jaureguiberry et al. (2012)		AR	4	non-sense		Mo(U,C) S(A,C)	

(Continued on following page)

10.3389/fphys.2023.1130175

TABLE 2 (*Continued*) Variations found in individuals presenting with syndromic amelogenesis imperfecta.

Patient number	Diagnosis/AI	Gene	Variant and location	Zygosity	Mode of inheritance	Rank	Effect of the mutation	Consistent with the known disease phenotype	Family segregation	Status
18.4 (female)	Hypoplastic AI, nephrocalcinosis	***FAM20A*** *Chr17(GRCh37): NM_017565.4*	c.406C>T; p.(Arg136*) Exon 2 O'Sullivan et al. (2011)	homozygous	AR	5	non-sense	Yes	NA	panel
18.5 (male)	Hypoplastic AI, nephrocalcinosis	***FAM20A*** *Chr17(GRCh37): NM_017565.4*	c.915_918del; p.(Phe305Leufs*76) Exon 6 Jaureguiberry et al. (2012)	compound heterozygous	AR	4	frameshift	Yes	Fa(U,C)	panel
			c.928 + 2T>C; p.? Intron 6		AR	4	splice		Mo(U,C)	
18.6 (male)	Hypoplastic AI, nephrocalcinosis	***FAM20A*** *Chr17(GRCh37): NM_017565.4*	c.915_918del; p.(Phe305Leufs*76) Exon 6 Jaureguiberry et al. (2012)	compound heterozygous	AR	4	frameshift	Yes	S(A,C) Mo(U,C)	panel
		FAM20A *Chr17(GRCh37): NM_017565.4*	c.1301 + 5G>A; p.? Intron 9		AR	3	splice	Yes	S(A,C) Fa(U,C)	panel
18.7 (female)	Hypoplastic AI, nephrocalcinosis	***FAM20A*** *Chr17(GRCh37): NM_017565.4*	c.1106_1107delAG; p.(Glu369Glyfs*10) Exon 7 Prasad et al. (2016a)	homozygous	AR	4	frameshift	Yes	NA	panel
18.8 (female)	Hypoplastic AI, nephrocalcinosis	***FAM20A*** *Chr17(GRCh37): NM_017565.4*	c.1361 + 1G>A; p.? Intron 10	homozygous	AR	4	splice	Yes	NA	exome
18.9 (female)	Hypoplastic AI, nephrocalcinosis	***FAM20A*** *Chr17(GRCh37): NM_017565.4*	c.1369A>T; p.(Lys457*) Exon 11 Jaureguiberry et al. (2012)	homozygous	AR	4	non-sense	Yes	S(A,C)	panel
18.10 (female)	Hypoplastic AI, nephrocalcinosis	***FAM20A*** *Chr17(GRCh37): NM_017565.4*	c.1369A>T; p.(Lys457*) Exon 11 Jaureguiberry et al. (2012)	homozygous	AR	4	non-sense	Yes	MoFa(U,C)	exome
Patient number	**Diagnosis/AI**	**Gene**	**Variant and location**	**Zygosity**		**Rank**	**Effect of the mutation**	**Consistent with the known disease phenotype**	**Family segregation**	**Status**
19.1 (male)	Hypoplastic, pits, mucopolysaccharidosis IV	**GALNS Chr16(GRCh37): NM_000512.5**	c.121-31T>C; p.? Intron 1 Prasad et al. (2016b)	compound heterozygous	AR	3	splice	Yes	Mo(U,C)	panel
			c.953C>G; p.(Thr312Ser) Exon 9 Yamada et al. (1998)		AR	5	missense		Fa(U,C)	
19.2 (female)	Hypoplastic, pits, mucopolysaccharidosis IV	***GALNS Chr16(GRCh37): NM_000512.5***	c.1156C>T; p.(Arg386Cys) Exon 11 Ogawa et al. (1995)	heterozygous	AR	5	missense	Yes	Mo(U,R) Fa(U,R)	panel
			c.1558T>C; p.(Trp520Arg) Exon 14 Zanetti et al. (2021)	heterozygous	AR	2	missense		M(U,Chom)	

(Continued on following page)

TABLE 2 (*Continued*) Variations found in individuals presenting with syndromic amelogenesis imperfecta.

Patient number	Diagnosis/AI	Gene	Variant and location	Zygosity	Mode of inheritance	Rank	Effect of the mutation	Consistent with the known disease phenotype	Family segregation	Status
Patient number	**Diagnosis/AI**	**Gene**	**Variant and location**	**Zygosity**		**Rank**	**Effect of the mutation**	**Consistent with the known disease phenotype**	**Family segregation**	**Status**
20.1 (female)	Hypoplastic, banding pattern, Lyonisation, Microphthalmia with linear skin defects (MLS) syndrome	***AMELX-ARHGAP6 ChrX(GRCh37): g.125958-12725766del***	ChrX(GRCh37):g.125958-12725766del Many genes including AMELX	heterozygous	XL	4	deletion	Yes	NA	panel
Patient number	**Diagnosis/AI**	**Gene**	**Variant and location**	**Zygosity**		**Rank**	**Effect of the mutation**	**Consistent with the known disease phenotype**	**Family segregation**	**Status**
21.1 (male)	Hypoplastic, Smith Magenis syndrome	***RAI1***	arr[GRCh37] 17p11.2(17280004_20239827)x1 Many genes including RAI1	heterozygous	AD	4	deletion	-	NA	panel
Patient number	**Diagnosis/AI**	**Gene**	**Variant and location**	**Zygosity**		**Rank**	**Effect of the mutation**	**Consistent with the known disease phenotype**	**Family segregation**	**Status**
22.1 (male)	Hypoplastic, Loeys-Dietz syndrome	***TGFBR2* Chr4(GRCh37): NM_003242.6**	c.1561T>C; p.(Trp521Arg) Exon 7 Mátyás et al. (2006)	heterozygous	AD	5	missense	Yes	Fa(U,R) Mo(A,NA)	panel
Patient number	**Diagnosis/AI**	**Gene**	**Variant and location**	**Zygosity**		**Rank**	**Effect of the mutation**	**Consistent with the known disease phenotype**	**Family segregation**	**Status**
23.1 (female)	Hypoplastic, Kohlschutter-Tonz like syndrome	***SLC13A5* Chr17(GRCh37): NM_177550.5**	c.203C>A; p.(Pro68Gln) Exon 2 Schossig et al. (2017)	compound heterozygous	AR	4	missense	Yes	S(A,C)	panel
			c.434C>A; p.(Thr145Lys) Exon 4 Schossig et al. (2017)		AR	4	missense		S(A,C)	
Patient number	**Diagnosis/AI**	**Gene**	**Variant and location**	**Zygosity**		**Rank**	**Effect of the mutation**	**Consistent with the known disease phenotype**	**Family segregation**	**Status**
24.1 (female)	Hypomature, Kohlschutter Tonz syndrome	***ROGDI Chr16(GRCh37): NM_024589.3***	c.46 + 37_46-30del; p.? Intron 1 Tucci et al. (2013)	compound heterozygous	AR	4	deletion	Yes	Mo(U,C)	Insbruck
			c.507del; p.(Glu170Argfs*72) Exon 7 Tucci et al. (2013)		AR	4	deletion		Fa(U,C)	
24.2 (female)	Hypomature, Kohlschutter Tonz syndrome	***ROGDI Chr16(GRCh37): NM_024589.3***	c.117 + 1G>T; p.? Intron 2 Huckert et al. (2014)	homozygous	AR	4	splice	Yes	NA	panel

(Continued on following page)

10.3389/fphys.2023.1130175

TABLE 2 (*Continued*) Variations found in individuals presenting with syndromic amelogenesis imperfecta.

Patient number	Diagnosis/AI	Gene	Variant and location	Zygosity	Mode of inheritance	Rank	Effect of the mutation	Consistent with the known disease phenotype	Family segregation	Status
24.3 (female)	Hypomature, Kohlschutter Tonz syndrome	*ROGDI Chr16(GRCh37): NM_024589.2*	c.366dup; p.(Ala123Serfs*19) Exon 6 Tucci et al. (2013)	compound heterozygous	AR	4	frameshift	Yes	Mo(U,C)	panel
			c.402C>G; p.(Tyr134*) Exon 6 Aswath al. (2018)		AR	4	non-sense		Fa(U,C)	
Patient number	Diagnosis/AI	Gene	Variant and location	Zygosity		Rank	Effect of the mutation	Consistent with the known disease phenotype	Family segregation	Status
25.1 (male)	Hypomature/ Hypomineralized, short stature, intra uterine growth retardation, skeletal dysplasia, submucosal cleft palate	*SLC10A7 Chr4(GRCh37): NM_001300842.3*	c.269T>G; p.(Leu90Arg) Exon 3	homozygous	AR	3	missense	Yes	MoFa(U,C)	panel
25.2 (female)	Hypomature/ Hypomineralized, short stature, intra-uterine growth retardation, skeletal dysplasia	*SLC10A7 Chr4(GRCh37): NM_001300842.3*	c.908C>T; p.(Pro303Leu) Exon 11 Laugel Haushalter et al. (2019)	homozygous	AR	4	missense	Yes	MoFa3S(U,C)	exome
Patient number	Diagnosis/AI	Gene	Variant and location	Zygosity		Rank	Effect of the mutation	Consistent with the known disease phenotype	Family segregation	Status
26.1 (female)	Hypomineralized, Jalili syndrome	*CNNM4 Chr2(GRCh37): NM_020184.4*	c.586T>C; p.(Ser196Pro) Exon 1 Parry et al. (2009)	homozygous	AR	4	missense	Yes	S(A,C) Mo(U,C)	panel
26.2 (male)	Hypomineralized, Jalili syndrome	*CNNM4 Chr2(GRCh37): NM_020184.4*	c.1495G>A; p.(Val499Met) Exon 2 Prasad MK et al. (2016b)	homozygous	AR	4	missense	Yes	NA	panel
Patient number	Diagnosis/AI	Gene	Variant and location	Zygosity		Rank	Effect of the mutation	Consistent with the known disease phenotype	Family segregation	Status
27.1 (female)	Hypoplastic, Trichodentosseus syndrome	*DLX3 Chr17(GRCh37): NM_005220.3*	c.561_562del; p.(Tyr188Glnfs*13) Exon 3 Dong et al. (2005)	heterozygous	AD	4	frameshift	Yes	MoS(A,C)	panel
27.2 (male)	Hypoplastic, Trichodentosseus syndrome	*DLX3 Chr17(GRCh37): NM_005220.3*	c.561_562del; p.(Tyr188Glnfs*13) Exon 3 Dong et al. (2005)	heterozygous	AD	4	frameshift	Yes	Fa(A,C)	panel

Variations found in 11 different genes in 31 individuals presenting with syndromic amelogenesis imperfecta. Forty-two variants were found, 7 variants are of uncertain significance.

Variants known before the panel implementation are reported in grey, variants previously reported by the team are represented in salmon, variants published thanks to the panel are represented in blue or green, variants reported for the first time are highlighted in green. Familial segregation is also reported when available and reported in this format: Family member code (Phenotype code, Genotype code). Fa: father; Mo: mother; S: sibling; D: daughter; So: son; Co: cousin; A: affected; U: unaffected; NA: not available; C: carrier; R: reference genotype.

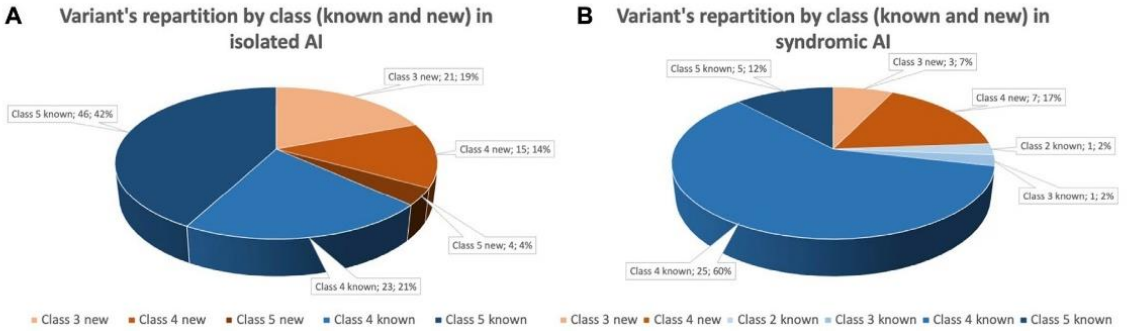

FIGURE 1
Identified variants within the cohort grouped by pathogenic class and novelty. Variant were classified following ACMG recommendations. **(A)** Variant's repartition by pathogenic class and novelty for individual affected by isolated AI. Forty variants (37%) are newly identified variants (orange gradient), 69 (63%) variants are already reported in literature (blue gradient). Among variants reported, 50 (46%) are pathogenic (class 5), 38 (35%) are likely pathogenic (class 4) and 21 (19%) are of uncertain significance. **(B)**. Variant's repartition by pathogenic class and novelty for individual affected by syndromic AI. Seven variants (24%) are newly identified variants (orange gradient), 32 variants (76%) are already reported in literature (blue gradient). Among variants reported, 5 (12%) are pathogenic (class 5), 32 (77%) are likely pathogenic (class 4), 4 (9%) are of uncertain significance (class 3) and 1 (2%) is probably begin (class 2).

locations and no prediction of local splice effect, and 4) synonymous variants without pathogenic prediction of local splice effect. Annotations of structural variations (SV) were performed by AnnotSV (Geoffroy et al., 2018).

Sanger sequencing and segregation

Primers' design was done using the Amplifix v1.5.4 software. Primers were then ordered from Eurofin MWG (Supplementary Table S2). The amplicons' sizes were checked by electrophoresis on the Caliper LabChip GX (Life science). After enzymatic purification with the Illustra™ Exoprostar™ kit (Sigma Aldrich) to remove dNTPs and salts, the PCR product was used to perform a sequence reaction with the BigDye™ Terminator v1.1 Cycle Sequencing Kit (Applied Biosystems, Thermofisher Scientific). The BigDye Xterminator™ Purification Kit (Applied Biosystems by Thermofisher Scientific) was used to purified product. This purified product was then loaded on the 3,500 Series Genetic Analyzers (Applied Biosystems, Thermofisher Scientific) sequencer. Final sequence data were analyzed with SEQUENCE Pilot (JSI medical systems).

Results

We report genetic results for 221 individuals divided between 115 amelogenesis imperfecta (AI) index cases (71 females and 44 males) and 106 relatives from 111 families. Among index cases, 73% were diagnosed with non-syndromic AI and 27% with syndromic AI. Clinical phenotype was assessed according to Witkop's classification and repartition for index's phenotype is: Type I hypoplastic AI (61 individuals, 53%), Type II hypomature AI (31 individuals, 27%), Type III hypomineralized AI (18 individuals 16%) and Type IV hypoplastic-hypomature with taurodontism AI (5 individuals, 4%).

Genetic variants were analyzed using NGS GenoDENT panel and following the ACMG recommendations (Richards et al., 2015; Harrison et al., 2019). Pathogenic variant (class 5) or likely pathogenic variant (class 4) were identified for 81% of the reported index individuals. Non-conclusive variants of uncertain significance (VUS) (class 3) represented the remaining 19%.

Among the 151 sequenced variants identified for indexes, 47 are newly reported and classified as class 4 or 5 (Table 2; Supplementary Table S3).

More specifically for isolated AI individuals, 109 variants are described with 40 newly reported (four class 5, 15 class 4 and 21 VUS) and 69 already reported (46 class 5 and 23 class 4). For syndromic AI, 42 variants are listed with ten newly reported (7 class 4, 3 VUS) and 32 already reported (5 class 5, 25 class 4, 1 class 2 and 1 VUS) (Figure 1). For some individuals two variants have been reported in the case of an autosomal recessive (AR) disorder and heterozygous compound variants (23 isolated AI individuals and 10 syndromic). VUS have been identified in different situations: nine times as solo heterozygous variant, two times as homozygous variant, four times as two heterozygous VUS and seven times as heterozygous associated with a pathogenic variant.

The most frequently discovered genotypes were associated with *MMP20*, *FAM83H* and then *AMELX* and *ENAM* variants for isolated AI (Figure 2). We didn't find any variant in *GPR68*, *STIM1*, *RELT*, *ITGB6/4*, *AMTN* and *SP6 genes*. In individuals presenting syndromic AI we reported variants in *LTBP3*, *FAM20A* and *GALNS*, *SLC13A5*, *DLX3*, *RAI1*, *TGFBR2*, *CNNM4*, *SLC10A7*, *ROGDI* (Figure 3) but didn't find any variant in *TP63*, *TSC1-2*, *AIRE*, *CLDN16*, *CLDN19*, *ORAI1*, *STIM1*, *RELT*, *PEX26*, *PEX1*, *PEX6*, *PORCN* and *MSX2*.

Familial segregation, with Sanger sequencing, of variants previously identified in index cases was performed on

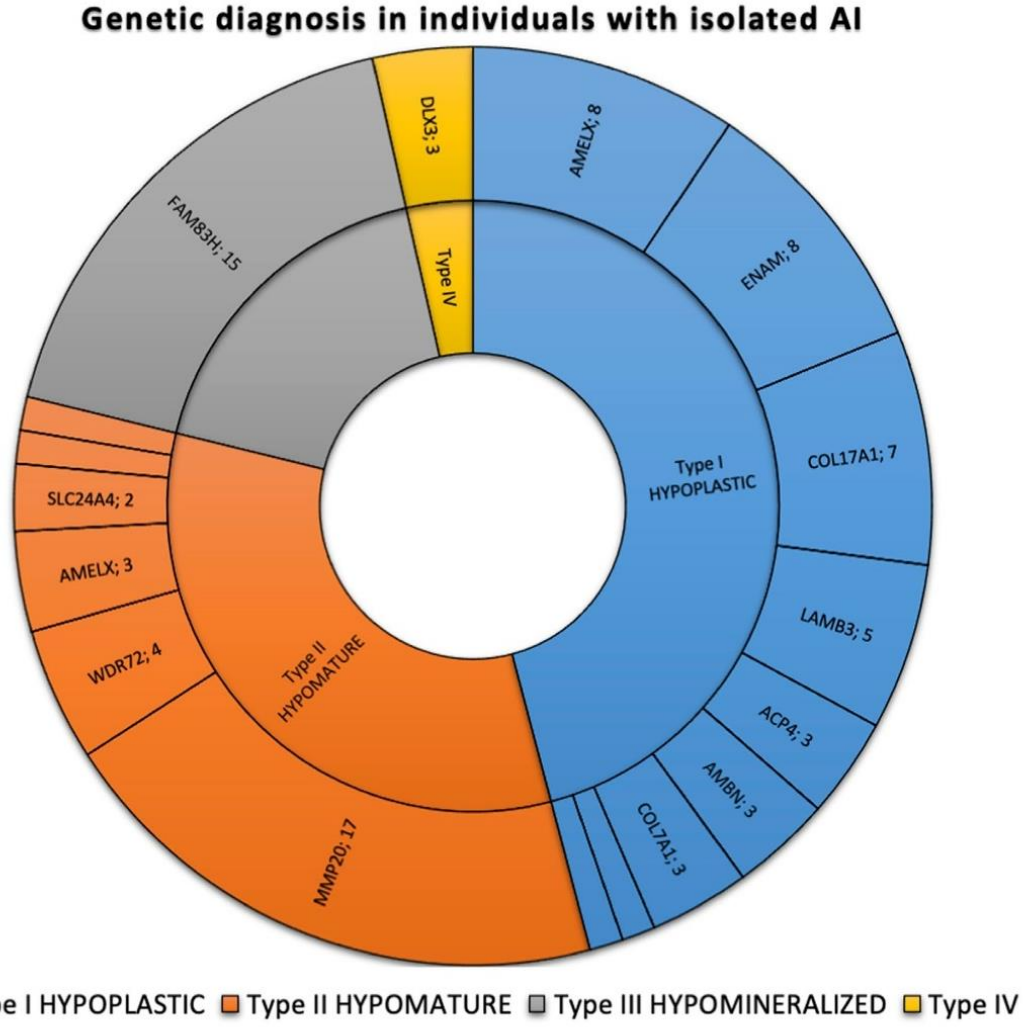

FIGURE 2
Phenotypic and genetic diagnosis in 86 individuals with isolated AI. Number of patients per main type of AI and per gene. Type I hypoplastic AI represents 39 individuals (45.3%) in blue associated with 9 different genes (*AMELX, ENAM, COL17A1, LAMB3, ACP4, AMBN, COL7A1, LAMA3, LAMC2*). Type II hypomature AI represents 28 individuals (32.6%) in orange associated with 6 different genes (*MMP20, WDR72, AMELX, SLC24A4, KLK4*). Type III hypomineralized AI represents 16 individuals (18.6%) in grey associated with 2 different genes (*FAM83H, WDR72*). Type IV hypoplastic-hypomature with taurodontism AI represents 3 individuals (3.5%) in yellow in 1 gene (*DLX3*).

106 individuals. Among them, 33 affected individuals were carrier of the familial variant, 35 non-affected individuals were carrier of one of the two familial variants in the context of a recessive pathology, 31 non-affected individuals did not carry the familial variant. Phenotype/genotype correlation was not conclusive for 7 individuals mostly because sufficient phenotypic information was not available.

Through this deliberate yet targeted strategy, we were able to identify pathogenic variants in known genes involved in AI as expected. In addition, we identified variants in candidate genes previously unreported in AI as well as individuals presenting novel VUS in known genes. As it is nearly impossible in the field of rare disease to create an exhaustive repertoire of pathological variants, we present the findings of this study following (Witkop, 1988) classification, gene by gene linking phenotypic clinical description with the associated genotype.

Additionally, working with this panel of variants, with annotated gene functions, and with the genotype/phenotype associations described in the cited literature, we aim to refine the clinical classification on the basis of Witkop's classification to integrate the current understanding of AI in the context of genetic data, with an initial segregation of phenotypes as "isolated" or "syndromic". Listed below are the proposed categories and sub-categories under this novel "GenoDENT" classification.

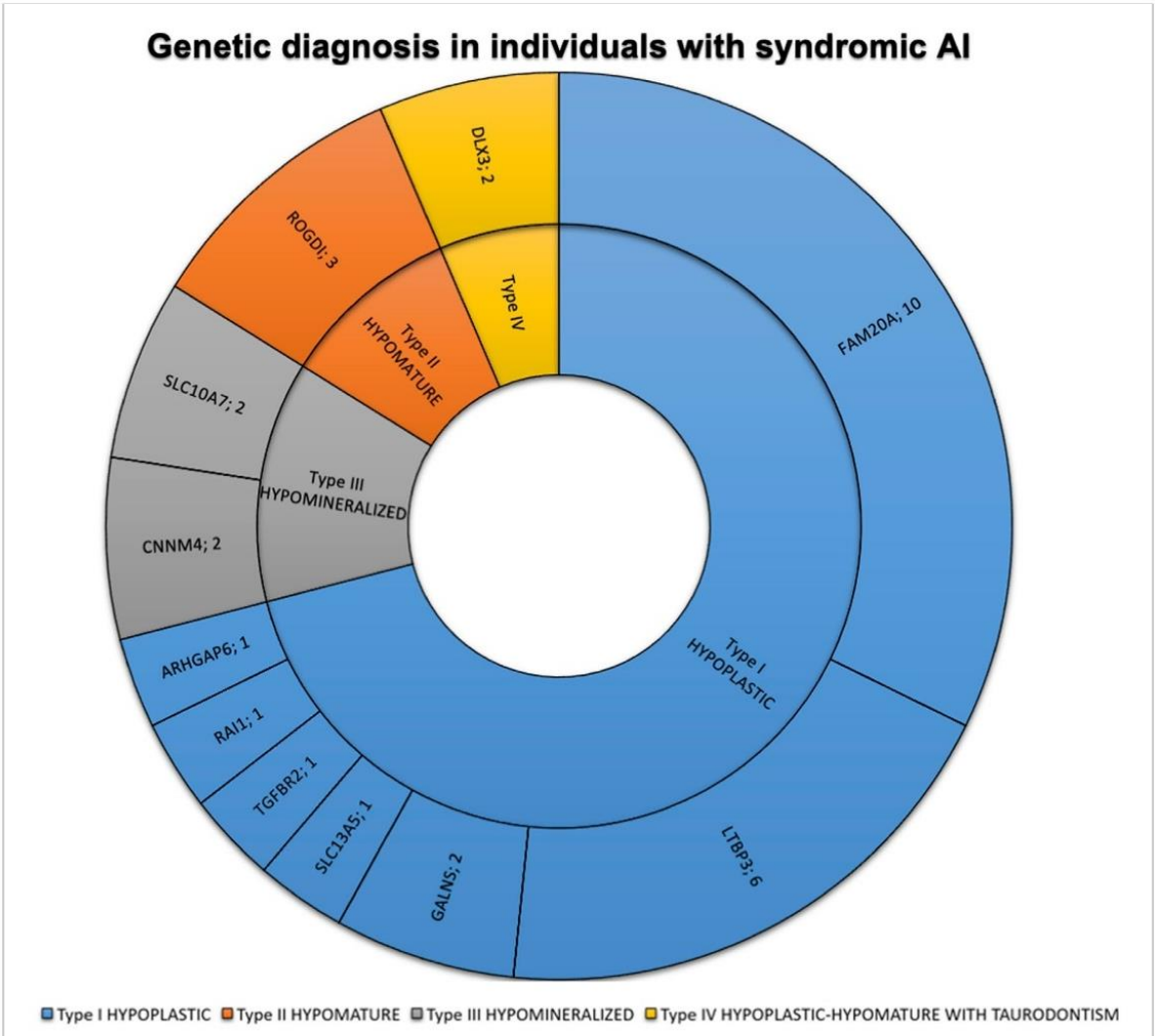

FIGURE 3
Phenotypic and genetic diagnosis in 31 individuals with syndromic AI. Number of patients per main type of AI and per gene. Type I hypoplastic AI represents 22 individuals (71%) in blue associated with 7 different genes (*FAM20A, LTBP3, GALNS, ARHGAP6, RAI1, SLC13A5, TGFBR2*). Type II hypomature AI represents 3 individuals (9.7%) in orange associated with 1 gene (*ROGDI*). Type III hypomineralized AI represents 4 individuals (12.9%) in grey associated with 2 different genes (*CNNM4, SLC10A7*). Type IV hypoplastic-hypomature with taurodontism AI represents 2 individuals (6.5%) in yellow in 1 gene (*DLX3*).

"ISOLATED" AMELOGENESIS IMPERFECTA

AI can occur with or without associated syndromic conditions. These following proposed classes of AI expand on Witkop's classification to describe non-syndromic AI diseases at a genetic level.

Type I—Hypoplastic

Hypoplastic AI describes quantitative enamel defects such as localized hypoplasia, generalized hypoplasia, enamel pits, enamel striae, groove defects, thin but mineralized enamel, or in extreme cases, the complete absence of enamel. Anomalies observed in hypoplastic AI, result from failure during the enamel matrix secretory stage (Wang et al., 2015). Four forms of hypoplastic AI—the pitted, local, smooth and rough forms - are autosomal dominant (type IA, IB, ID and IF), three are autosomal recessive (type IC, IG and IJ), and one is X-linked (type IE) (Witkop and Sauk, 1976).

Type IA—Hypoplastic, pitted, autosomal dominant *COL17A1, COL7A1, LAMA3, LAMB3* (#104530), *LAMC2, ITGB6* (#616221)

Enamel may display pits on the labial or buccal surfaces often arranged in rows and columns. Often these pits are obvious as they

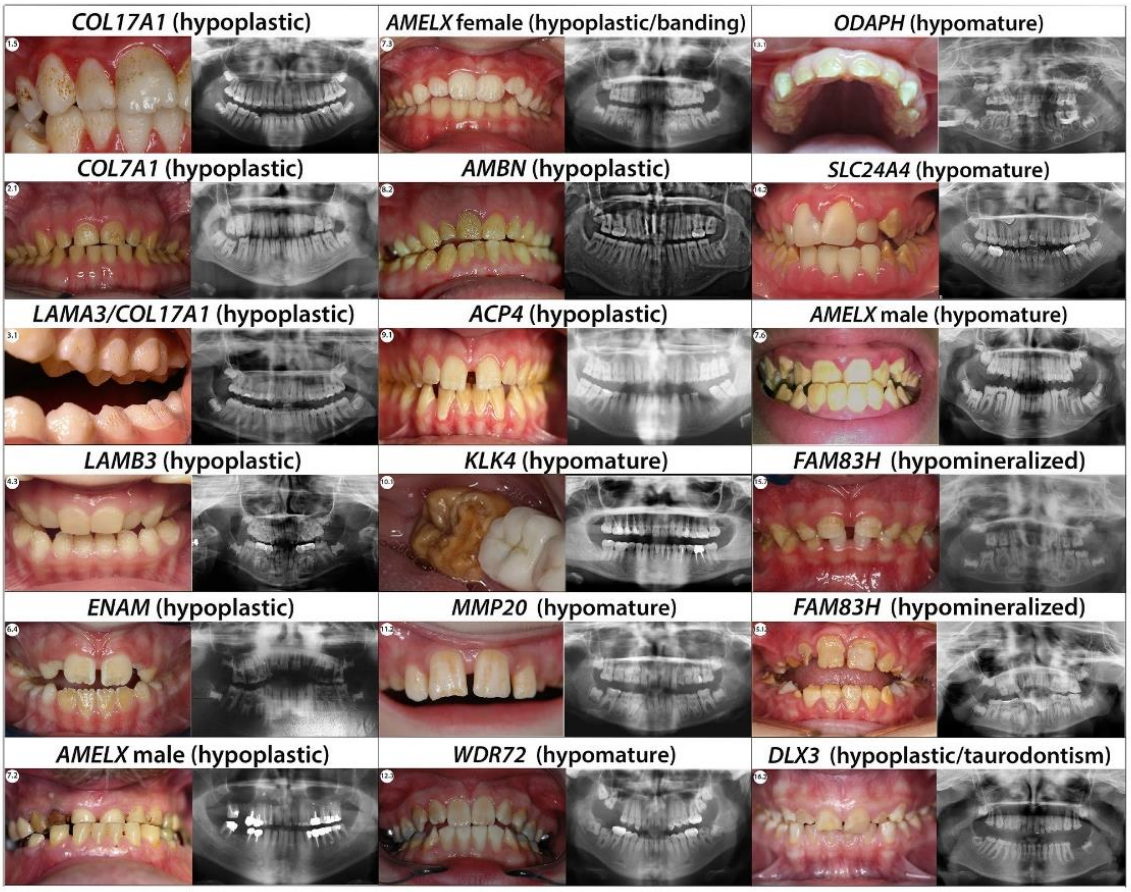

FIGURE 4
Phenotype/Genotype correlation for isolated AI. Typical phenotype/genotype correlation observed in patients presenting with isolated Amelogenesis imperfecta (intraoral pictures and radiographs). Patients who are carrier of *AMELX* mutations can present with different types of AI. Indeed, the phenotype can be either hypoplastic (severe with almost no enamel in male and with a lyonization banding pattern in female) or hypomature depending on the mutation's localisation. When the mutations occur in a MMP20 cleavage site the *AMELX* related AI observed is a X-linked hypomature AI.

are colored by extrinsic stains that can be removed by professional cleaning.

The genes implicated in this subtype of AI encode proteins of the extracellular matrix, important for the attachment of the ameloblast cells to their matrix, structural component of hemidesmosomes *COL17A1*, anchoring fibril to the basement membrane *COL7A1*, laminin constituting chains *LAMA3*, *LAMB3*, *LAMC2*, integrins adhesion receptors that function in signaling from the extracellular matrix to the cell *ITGB6* (a receptor for the laminins). *COL7A1* gene encodes the alpha-1 chain of type VII collagen (Burgeson et al., 1985). *COL17A1* encodes the homotrimer type XVII collagen (COL17). *LAMA3*, *LAMB3*, *LAMC2* genes encode laminin α3, laminin β3, and laminin γ2, respectively, forming together the heterotrimer laminin-332 (LM-332).

Both LM-332 and COL17 are crucial in ameloblast differentiation and enamel formation, mutations of which result in enamel defects consisting of hypoplasia, pitting, roughness, thinning or furrowing of enamel (Yuen et al., 2012).

These same genes, under an autosomal recessive inheritance transmission are responsible for various forms of epidermolysis bullosa (EB: Non-Herlitz junctional epidermolysis bullosa (nH-JEB) *COL17A1*; recessive dystrophic epidermolysis bullosa (RDEB) *COL7A1;* junctional EB (JEB) LAMA3, *LAMB3*, *LAMC2*) (Masunaga, 2006). In EB, the phenotype synopsis includes nails dystrophy, skin hyperhidrosis and hyperkeratosis, blistering of skin and mucosa, eye defects, hair anomalies with alopecia or loss of eyelashes and an abnormal dentition with extensive enamel hypoplasia, focal pitting, and discoloration.

COL17A1

In our current study, we found six individuals (1.1–1.6) presenting with, hypoplastic pitted AI. The enamel appears

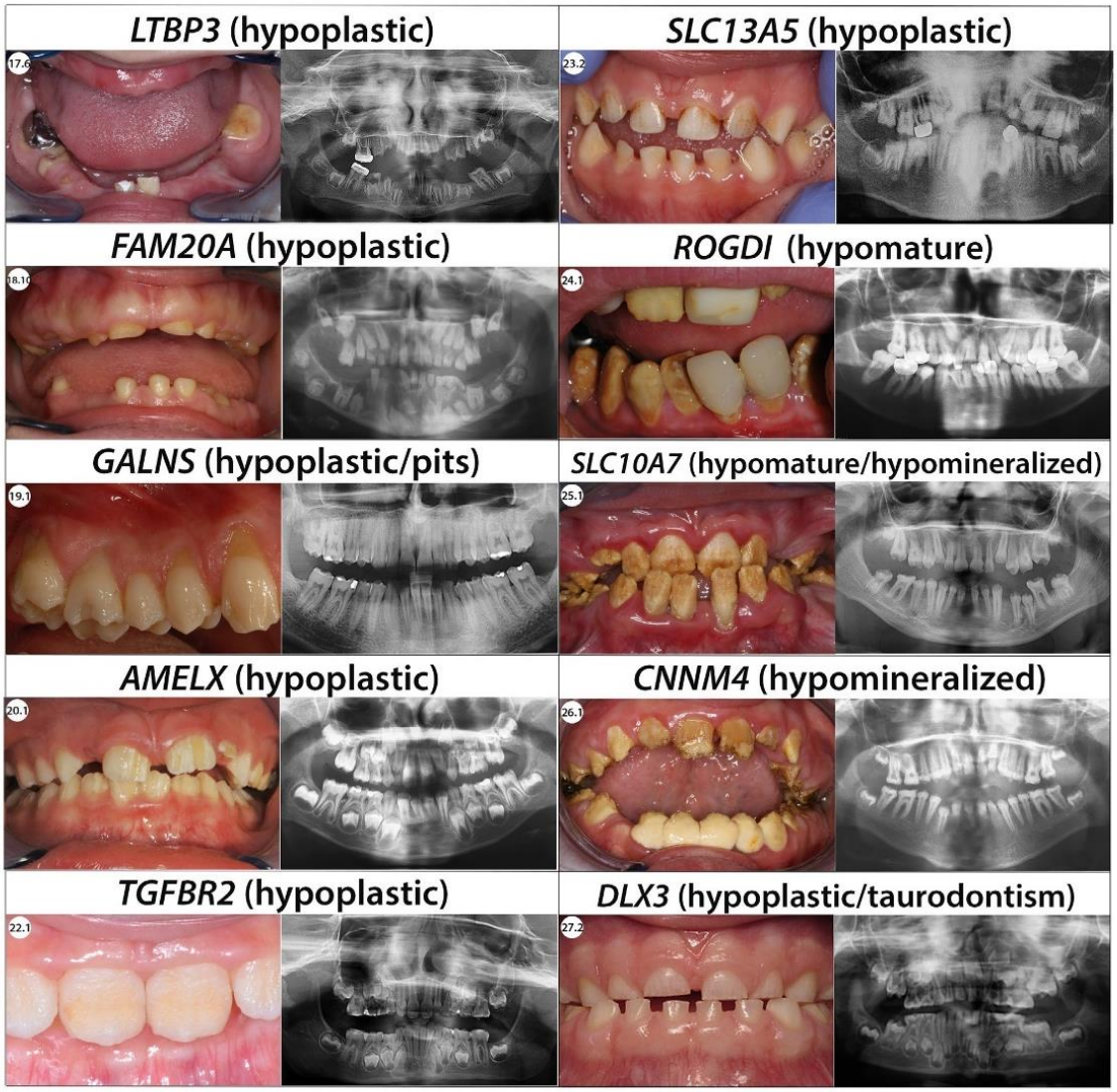

FIGURE 5
Phenotype/Genotype correlation for syndromic AI.

pitted, rough, of normal hardness and presents yellow-brown extrinsic stains. Radiographs show normal enamel opacity (Figure 4; Supplementary Figure S1A).

We identified heterozygous loss of function variants in *COL17A1* gene in each of them (Supplementary Table S3; Supplementary Figure S2A). In individuals 1.2, 1.5, and 1.6 the heterozygous variants we identified were originally described as pathogenic in EB individuals. The heterozygous variant found in individual 1.2 was also found in her affected sister and daughters (Supplementary Figure S3.1). The heterozygous variant found in individual 1.6 was also detected in his mother but the parents' phenotype was not known (Supplementary Figure S3.2). Individuals 1.1, 1.3 and 1.4 and their variants were already described in an autosomal dominant mode by our team in (Prasad et al., 2016b). Heterozygous variants in *COL17A1* gene, historically discovered in EB families, were reported in the literature as responsible for enamel defects and an AI phenotype in heterozygous carriers, including parents non-affected with EB (McGrath et al., 1996; Prasad et al., 2016a; b).

COL7A1

We report three individuals (2.1, 2.2 and 2.3) presenting with an hypoplastic pitted AI phenotype with thin enamel and yellow

discoloration (Figure 4; Supplementary Figure S1B). Panoramic X-rays show thinner enamel. We found in these 3 individuals *COL7A1* heterozygous variants not previously described (Supplementary Table S3; Supplementary Figure S1B, S2B).

Individual 2.1 has an intronic heterozygous variant (NM_000094.4:c.2440 + 3A>C) in intron 19. This variant is predicted to have an impact on the splicing site possibly leading to an, in phase, exon 18 skipping. Exon 18 codes for a Fibronectin type III domain involved in interactions with integrins. A variant implicating a similar splice site defect has been described in an individual presenting epidermolysis bullosa with enamel defects (c.2440 + 1G>T) (Vahidnezhad et al., 2017).

Individual 2.2 and 2.3 both carry a heterozygous missense variant NM_000094.4:c.3605G>A; p.(Arg1202His) and NM_000094.4:c.3785T>C; p.(Met1262Thr) located respectively in the Von Willebrand factor type A and Collagen triple helix repeat protein domains. No other missense variant was described in the Von Willebrand domain, but other missense variants have been described as pathogenic in the Collagen triple helix domain (Yenamandra et al., 2018). Individual 2.2 has an affected sibling carrying the same variant. Individual 2.3 inherited his variant from his affected mother (Supplementary Figures S3.3, S3.4).

All these variants were, so far, classified as VUS and further investigations would be needed to determine their impacts on the phenotype.

Variants in this gene were only previously reported in individuals with epidermolysis bullosa in autosomal dominant or recessive conditions.

LAMA3

We report one individual (3.1) presenting severe hypoplastic AI carrying a mutation in *LAMA3*. A digenic inheritance with variants in both in *COL17A1*, and *LAMA3* has been previously described (Prasad et al., 2016a) (Supplementary Table S3; Supplementary Figure S2C). The heterozygous variant, transmitted by her affected mother, in *COL17A1* NM_000494.4:c.1141 + 1G>A is a pathogenic variant altering the splicing site in exon 14. The individual also carries an heterozygous variant in *LAMA3* not inherited from her mother NM_000227.6:c.1650_1659del; p.(Ile550Metfs*46). We hypothesize this additional mutation could explain the phenotype severity gradient between 3.1 and her mother. Indeed, both are presenting hypoplastic AI but in 3.1 the phenotype is more severe, and the pits are numerous and clearly visible (Figure 4; Supplementary Figure S1C).

LAMB3

Each of the individuals reported in this publication (4.1, 4.2, 4.3, 4.4 and 4.5) carrying mutations in *LAMB3* present with hypoplastic AI with an irregular pitted and thinner enamel and no sign of epidermolysis bullosa (Figure 4; Supplementary Figure S1C).

Among the pathogenic variants reported in this gene, bi-allelic loss of function variants was described in patients with severe EB and AI. Dominant heterozygous frameshift variations were reported in patients with isolated AI: all those variations were located in the last two exons of *LAMB3* gene. For these published patients, a dominant negative effect was proposed by Smith (Smith et al., 2019). In our cohort, two patients have such 3′end variations: patients 4.4 and 4.5, NM_000228.3: c.2926del; p.(Val976Trpfs*54) and c.3305del; p.(Gly1102Valfs*7) (Supplementary Figure S3.5; Supplementary Figure S2D).

We also report in our cohort, three patients with isolated AI and a non-sense mutation located before the 3′end of the gene (4.1, 4.2 and 4.3) 4.1 and 4.3 were reported in (Prasad et al., 2016a) and reanalyzed in the context of this publication. Revisiting these data showed that 4.1 also presented a non-sense mutation in position 42 (c.124C>T; p.(Arg42*)); we also detected a new missense variant c.3490C>T; p.(Arg1164Cys) which is predicted to be deleterious by SIFT (v6.2.0) and Polyphen-2. Familial segregation showed that those two variations affected both alleles in this patient (Supplementary Figure S3.6).

Patient 4.2 has one premature stop codon in position 635 and on the second allele, a splice variation was detected, c.1288 + 1G>T (Supplementary Figure S3.7). This variation was previously reported by Kiritsi et al. (2015) and the authors confirmed the impact of the splice variant by mRNA study: the variation induced an in-frame skipping of exon 11 and was predicted to produce an incomplete protein p.(Ser378_Arg430delinsCys). According to (Kiritsi et al., 2015), the patient presented with AI and a mild form of EB with favorable evolution.

The clinical synopsis of *LAMB3*-related AR epidermolysis bullosa, junctional 1A intermediate includes enamel hypoplasia, enamel pitting and corneal erosion, corneal scarring besides skin, hair and nails defects. Notably, individual 4.2 has a history of recurrent corneal ulcers and might therefore present a mild form of EB.

Patient 4.3 has a stop mutation in position 635. A splice variation was also detected in this patient c.944-14C>G but mRNA analysis could not be performed and familial segregation was not possible.

The first two cases (4.1 and 4.2) could thus be compatible with a recessive form of AI: those patients combined one null allele and a possible hypomorphic second allele. An AR clinical continuum may go from severe EB/AI in patients with biallelic null variations to mild EB/AI or isolated AI in patients with one null mutation occurring with a hypomorphic allele.

LAMC2

A 4-year-old individual (5.1) displayed a hypoplastic/hypomature AI phenotype. The primary dentition showed thin white opaque enamel (Supplementary Figure S1C).

We found a heterozygous *LAMC2* variant NM_005562.3: c.493C>T; p.(Arg165Cys) with an allele frequency of 0.2% in GnomAD, predicted deleterious by SIFT (v4.0.3) and PolyPhen-2 and located in the Laminin EGF domain (Supplementary Table S3; Supplementary Figure S2E). Heterozygous variants in this gene have not previously been associated with AI in human but this gene is known to be involved in enamel formation defects in mice (Wazen et al., 2016) and the patient's phenotype is similar to the one observed in mice. The allele is inherited from her mother but her phenotype was not available (Supplementary Figure S3.8).

ITGB6

Individuals with AR variants in integrin-β6 (*ITGB6*), have been described as affected with hypoplastic pitted and hypomineralized

AI. Enamel is less dense, presents disorganized prisms, and severe pitting in the coronal side of tooth with pigmentations (Poulter et al., 2014a; Wang S.-K. et al., 2014; Seymen et al., 2015a). Though this established phenotype infers a Type 1A classification, no *ITGB6* pathogenic variants were found in our cohort.

Type IB—hypoplastic local, autosomal dominant, #104500

Whereas other genes with this mode of inheritance may yet to be discovered, our survey of the literature and our cohort currently suggest that this classification is composed only for mutations of *ENAM*.

ENAM

ENAM encodes enamelin, the largest enamel matrix protein, composed of 1,142 amino acid. It is a secretory protein with a 39 amino acid signal peptide. During amelogenesis, the protein is found among the developing crystallites in the enamel rods and interrods (Daubert et al., 2016). Its presence is necessary for correct prism morphogenesis, contributing to thicker enamel (Shore et al., 2010). Variants in ENAM cause hypoplastic AI (Mårdh et al., 2002; Kim et al., 2005a), in which defective enamel is thin or absent, with horizontal row of pits, linear depressions, or one large hypoplastic area. These defects appear most prominent on the buccal surfaces of the teeth involving the middle third of the enamel.

Non-sense variants disrupting the enamelin domain, splice variants, small deletions and insertions and one big insertion have been described to be causative of Amelogenesis imperfecta (Hu and Yamakoshi, 2003).

We identified in our cohort eight individuals with hypoplastic AI manifest as thin, rough enamel in permanent teeth, columns of pits, and linear depressions in enamel. Hypoplastic enamel is clearly identified in panoramic X-Rays especially visible on unerupted teeth (Figure 4; Supplementary Figure S1D).

We detected *ENAM* heterozygous variants in each of these individuals (Supplementary Table S3; Supplementary Figure S2F). Three new, never reported, variants are described in this paper. Individual 6.1 presented a missense heterozygous variant in exon 3 NM_031889.3:c.101T>C; p.(Leu34Pro) (Supplementary Table S3). Missense variants in the N-terminal domain have previously been described, reportedly negatively impacting ameloblast secretory pathway leading to endothelial reticulum (ER) stress and an activated unfolded protein response (Brookes et al., 2017). With this proposed mechanism, a functional analysis could improve identification of the VUS towards pathogenic.

For individual 6.3, we detected a heterozygous 1bp duplication on a splice site NM_031889.3:c.588 + 1 dup; p.(Asn197Glufs*25). This variant was also detected in her affected sister and father (Supplementary Figure S3.9). The variant occurred at the same position than the already described deletion c.588+1delG; p.(Asn197Ilefs*81) found in individuals 6.4, 6.5, 6.6 (Supplementary Figure S3.10) and 6.7 (Supplementary Figure S3.11). Interestingly in 6.3 the phenotype seemed slightly different to the one observed in the four individuals carrying the deletion with an hypoplastic but also hypomature whitish enamel. Individual 6.3 also presented agenesis of 16, 26, 36, 46 but no further variant explaining the missing teeth was identified.

Individual 6.8, his affected sister, and their mother were all heterozygous for a non-sense mutation in exon 9 NM_031889.3: c.664C>T; p.(Gln222*) (Supplementary Figure S3.12).

Truncating variants earlier and later in the protein were already described in this gene and found to be causative of hypoplastic amelogenesis imperfecta (Ozdemir et al., 2005a; Seymen et al., 2014a).

Type IC -hypoplastic local, autosomal recessive, #204650

ENAM mutations also currently comprise the entire classification of type 1C, though further genes may await discovery.

ENAM

The phenotype is more severe than in local hypoplastic autosomal dominant AI and has also been linked to *ENAM* variants but in a recessive mode of inheritance (2 alleles affected). This leads to the conclusion that *ENAM* variants associated phenotype is dosage dependent. Indeed, Ozdemir et al., 2005a, Hart et al., 2003 described families for which carriers of only one *ENAM* variant were less affected presenting only localized enamel pitting, whereas family members with compound heterozygous or homozygous *ENAM* variants presented severe hypoplastic AI. Lindemeyer et al., 2010 also described the case of a nine-year-old boy with homozygous variants in *ENAM* and severe hypoplastic AI and smooth teeth.

We did not detect any cases AR mode of inheritance associated with *ENAM* in our cohort.

Type ID - Hypoplastic, smooth, autosomal dominant

This type of AI shows crowns with a yellow to brown color. The enamel tends to be thin in some teeth and absent in others. The tooth surfaces are smooth to uneven and sensitive to temperature changes and touch. Radiographs reveal a lack of enamel.

As the texture of the crowns is smooth, the attrition is apparent on the occlusal surfaces (Burzynski et al., 1973). No gene has previously been associated to this category, but here we propose *SP6* as the first possible gene classified in this type of AI based on our literature survey.

SP6

SP6 encodes a transcription factor expressed during amelogenesis and involved in regulating proliferation and differentiation of ameloblasts (Nakamura et al., 2004; 2008; Utami et al., 2011; Muto et al., 2012; Ruspita et al., 2020). Autosomal dominant pathogenic variants have been published in two unrelated families in association with severe hypoplastic AI (Smith et al., 2020; Kim et al., 2021b). Interestingly in the two families, the same amino acid (Ala273) was modified. No variant in this gene was evident in our cohort.

Type IE—hypoplastic, smooth, x-linked dominant, #301200

The surface of the enamel can vary, showing smooth, rough, pitted, or local defects (Witkop, 1988). Due to random X chromosome inactivation in female (Lyonisation effect), differences exist in phenotypic expression between affected males and heterozygous females. Affected males (XY) have only a very thin, smooth enamel, which appears nearly homogeneous. Females (XX) present a milder phenotype with a banding pattern featuring hypoplastic enamel rough/pitted, vertically ridged and normal enamel. Radiographically, thinner enamel contrasts normally from dentin.

AMELX

AMELX, Amelogenin X-linked, has been identified as the gene involved in this AI. The gene resides in intron 1 of *ARHGAP6* in the opposite orientation (Iwase et al., 2007). Amelogenins are highly conserved proteins secreted by ameloblasts that constitute 90% of the enamel organic matrix. As the proteins are digested and removed in maturation phase, mineral crystals grow in well-organized prism patterns (Gibson et al., 2001).

Genotype-phenotype correlation revealed that variants in the N-terminal (Lagerström et al., 1991; Kim et al., 2004) and C-terminal parts (Greene et al., 2002) of AMELX cause hypoplastic AI.

In our cohort, we identified five females (7.1, 7.3, 7.4, 7.8 and 7.11) presenting the typical hypoplastic AI banding pattern (Figure 4; Supplementary Figure S1E).

We identified heterozygous variation in *AMELX* in each of these individuals (Supplementary Table S3; Supplementary Figure S2G). Female individuals 7.1 to 7.3 were carrying a non-sense *AMELX* variant NM_182680.1:c.11G>A; p.(Trp4*) firstly reported by (Hart et al., 2002b). Individual 7.4 carried a newly reported variant NM_182680.1(*AMELX*):c.47C>A; p.(Ala16Asp) predicted damaging by SIFT (v6.2.0) and Polyphen-2 and inherited by her affected father (Supplementary Figure S3.13). Individuals 7.5 to 7.7 were presenting already reported missense variant. Individuals 7.8 to 7.11 were carrying frameshift variant originally reported by (Lench and Winter, 1995).

Male individual 7.9 is the cousin of 7.8 female and carried the same variant (Supplementary Figure S3.14). He presented the characteristic female lyonisation banding pattern thus requiring further understanding and clarification. His karyotype revealed XXY aneuploidy, the most common disorder of sex chromosomes in humans, with a prevalence of one in 500 males. This finding explained the lyonisation pattern in a male and was consistent with his associated behavioral disorder.

Individual 7.11 is the mother of 7.10 male. The mother presented the typical female hypoplastic banding pattern. The boy showed a severe hypoplastic AI with almost no enamel associated with delayed dental eruption and behavioral issues. As the boy's phenotype presented as syndromic, this family was directly sequenced by whole exome sequencing. We identified a pathogenic 1bp deletion leading to a premature stop codon c.541del; p.(Leu181Cysfs*8), a mutation previously reported (Kindelan et al., 2000) in both the mother and the boy (Supplementary Figure S3.15). This variation clearly explained the AI phenotype but no other variation was discovered as possibly explaining behavioral issues presented by this boy.

Male individuals 7.5, 7.6 and 7.7 presented a different hypomature amelogenesis imperfecta phenotype with a smooth yellow opaque enamel (Supplementary Figure S1E). Individuals 7.6 and 7.7 carry a c.208C>A; p.(Pro70Thr) variant first described by Collier et al., 1997 (Supplementary Figures S3.16, S3.17). Functional analyses showed that this variant is reducing the interactions between amelogenin and the MMP20, metalloproteinase degrading amelogenin in the maturation phase (Tanimoto et al., 2008). Therefore, depending on the patho-physiological mechanism, *AMELX* might also be the gene involved in the hypomature form of AI type IIC (snow-capped teeth X-linked) or eventually IIB (hypomaturation X-linked). This would be discussed further in these mentioned categories.

Individual 7.7 also had a frequently reported heterozygous variant in *WNT10* gene (c.682T>A; p.(Phe228Ile), explaining the 12, 15, 22, 28 agenesis.

Type IF—amelogenesis imperfecta, hypoplastic, autosomal recessive #616270

Hypoplastic enamel in the primary and permanent dentitions, showing a rough and discolored appearance is the hallmark of this AI. The enamel may be absent, pitted, or thinner. We currently list only *AMBN* as the causative gene defect in this class.

AMBN

AMBN gene (4q13.3), containing 13 exons was discovered as the causative gene for non-syndromic autosomal recessive amelogenesis imperfecta (Toyosawa et al., 2000). It encodes ameloblastin (AMBN, also named "amelin" or "sheathlin"), the second most abundant enamel matrix protein, critical to amelogenesis (Lu et al., 2018).

Four cases have been reported so far in the literature with AMBN variants associated with non-syndromic AI (Poulter et al., 2014b; Lu et al., 2018; Liang et al., 2019).

In our cohort we identified three individuals with a hypoplastic amelogenesis imperfecta combined with recessive variants in *AMBN* (Supplementary Table S3; Figure 4; Supplementary Figures S1F, S2H). Individuals 8.1, and 8.2 presented compounds heterozygous variants never described before. 8.1 displayed a splice variant in intron 1 NM_016519.6:c.15 + 1G>A and a non-sense variant in exon 8 c.577G>T; p.(Gly193*) (Supplementary Figure S3.18). 8.2 was carrying a non-sense variant in exon 5 NM_016519.6:c.209C>G; p.(Ser70*) and a splice variant in intron 7 c.571-1G>C. The non-sense mutation hadn't previously been described, however Poulter et al. (2014b) described a large deletion resulting in the loss of exon 6. Individual 8.3 was already described in (Prasad et al., 2016a). We detected a homozygous splice variant in intron 6 never described before NM_016519.6:c.532-1G>C. This is the first splicing variant described in this gene.

Type IG—enamel agenesis, autosomal recessive enamel-renal syndrome (ERS), #204690

Commonly described as an isolated AI, enamel agenesis may be observed concomitantly with other orodental and/or systemic features such as nephrocalcinosis in Enamel Renal Syndrome (ERS, MIM#204690), or gingival hyperplasia in Amelogenesis Imperfecta and Gingival Fibromatosis Syndrome (AIGFS, MIM#614253 moved to MIM#204690) (O'Sullivan et al., 2011).

FAM20A

These conditions are allelic, and are now considered as a spectrum of ERS and due to recessive variants in *FAM20A* gene (17q24.2; 11 exons (Nalbant et al., 2005; Jaureguiberry et al., 2012). FAM20A is a secreted glycoprotein, Golgi Associated Secretory Pathway Pseudokinase and its intact signal sequence is required for secretion. Various human tissues reveal high transcript levels in lung and liver and intermediate levels in thymus and ovary (Nalbant et al., 2005).

The clinical phenotype is highly distinctive and when recognized leads to the clinical diagnosis and the subsequent exploration *via* ultrasound of the presence of renal calcifications.

The diagnostic criteria of ERS are based on oral findings, including clinical (severe enamel hypoplasia, delayed or absent tooth eruption, gingival hyperplasia) and radiographic signs (non-erupting teeth, pulp calcifications and hyperplastic dental follicle) (de la Dure-Molla et al., 2014). Associated focal ectopic calcification features, along with the presence of renal abnormalities are also pathognomonic of ERS (Torres et al., 2018). Dental defects are present since the primary dentition, with no declared tooth pain or sensitivity (Dourado et al., 2019). Nephrocalcinosis (NC) and other kidney disorders have been included as frequent findings, especially in the early adulthood (Dellow et al., 1998; Martelli-Júnior et al., 2011). In that sense, it is speculated that even those individuals with oral characteristics showing no renal defects, but with biallelic *FAM20A* variants, will eventually develop NC (Dourado et al., 2019) and should be tested for and followed for NC and other renal defects.

As the phenotype was initially described as isolated AI, it appears in "isolated" AI in the original classification. However, as nephrocalcinosis is observed in these patients, it should be reclassified as syndromic AI. Therefore, data concerning patients with *FAM20A* variations will be discussed in the syndromic section (Table 2, Supplementary Figures S1M, S2R, S3.39, S3.40, S3.41, S3.42).

Type IJ—amelogenesis imperfecta, autosomal recessive, #617297

In this type of AI, the enamel is thin with irregular surface and teeth appears yellow.

ACP4

This phenotype is associated with recessive homozygous or compound heterozygous variants in *ACP4* gene encoding testicular acid phosphatase (Seymen et al., 2016; Smith C. E. et al., 2017). All variants reported so far were localized in the histidine phosphatase domain. This domain contains conserved Histidine residues that are phosphorylated during the catalytic activity of the protein and other residues that are forming a phosphate pocket and interact with the phospho group of substrates before, during and after its transfer to the Histidine residue. Variants were reported mostly in exon 4 and 7 and only one was reported in exon 3 (Seymen et al., 2016; Smith C. E. et al., 2017).

We found three unrelated families (individuals 9.1, 9.2 and 9.3) with hypoplastic amelogenesis imperfecta, with thin enamel with irregular surface, and a yellowish color. X-rays showed a thinner enamel of normal density, long teeth, and slim roots (Figure 4; Supplementary Figure S1G).

These families were previously negative on the GenoDENT panel first version (Prasad et al., 2016a), and were further investigated by whole exome sequencing analysis. We found compound heterozygous variants in the *ACP4* gene (Supplementary Table S3; Supplementary Figure S2I). Indeed *ACP4*, discovered in 2016 (Seymen et al., 2016), was not on the first version of GenoDENT but was added at version 0.4. Individual 9.1 had a previously reported missense variant in exon 4 NM_033068.3:c.331C>T; p.(Arg111Cys) and a splice variant in intron 6 c.645 + 1G>A; p.? which was predicted to lead to an in frame exon 6 skipping. This is the first case reported incidence of a splice variant of *ACP4*. Individual 9.2 had an already described missense variant in exon 4 NM_033068.3:c.428C>T; p.(Thr143Met) and a second variant not yet reported in exon 7, in the histidine phosphatase domain c.736G>A, p.(Val246Met). This variant is predicted damaging by SIFT (v6.2.0) and Polyphen-2. Individual 9.3 had 2 new missense variants, the first one is in exon 6, NM_033068.3:c.626T>C; p.(Leu209Pro) is in the domain but the second one is in the exon 11, in cytoplasmic domain c.1199C>A; p.(Ala400Asp). No variants were reported in the cytoplasmic part of the protein. Our results are generally consistent with previously described variants, but also suggest that the cytoplasmic region of the protein, as well as the extracellular region could have a role in amelogenesis.

Individual 9.3 also had agenesis of teeth 18, and 28, consistent with one of the most frequent variant found in *WNT10A* gene NM_025216.3:c.682T>A; p.(Phe228Ile).

Type II—Hypomaturation

Hypomature amelogenesis imperfecta relates to a qualitative rather than a quantitative (hypoplastic) enamel defect. Enamel maturation begins when final enamel thickness has been reached and concentrates on proteolytic degradation and removal of secreted matrix proteins as well as on hydroxyapatite crystal growth (Robinson, 2014). Enamel might be less translucid, opaque (snow-capped), pigmented but rather hard and protective. Two forms of hypomature amelogenesis imperfecta - the pigmented and the snow-capped are autosomal dominant (type IIA and IIC) and two are X-linked (type IIB and IID) (Witkop and Sauk, 1976).

Type IIA—hypomaturation, pigmented, autosomal recessive, A1 #204700 *KLK4*; A2 # 612529 *MMP20*; A3 # 613211 *WDR72*; A4 # 614832 *ODAPH*; A5 # 615887 *SLC24A4*; A6 # 617217 *GPR68*

This type of AI is characterized by pigmented hypomature enamel. The overall volume of the teeth is preserved, but enamel is hypomineralized therefore not differentially contrasting from dentin on X-rays. Enamel is colored from white opaque to brown. It is prone to post-eruptive breakdown. These AI have been associated with homozygous or compound heterozygous variants in six genes: *KLK4, MMP20, WDR72, C4ORF26, SLC24A4,* and *GPR68*.

All individuals (Figure 4; Supplementary Figure S1H,I) we are reporting in this section present a hypomature AI phenotype. Radiographs showed a lack of contrast between enamel and dentin.

KLK4

*KLK4*encodes an enamel matrix protease requiring cleavage for its activation after secretion by ameloblasts. *KLK4* encodes a serine protease that, once activated during maturation stage, will degrade enamel proteins to allow the growth in width and thickness of enamel crystallites (Simmer et al., 2009).

Truncating variants in this gene have been previously described (Wang et al., 2013; Seymen et al., 2015b; Smith C. E. L. et al., 2017). In our cohort, individual 10.1 displayed pigmented hypomature, hypomineralized enamel. As a compound heterozygous, he is carrying a previously reported non-sense variant (Hart et al., 2004) associated with a new missense mutation in *KLK4* NM_004917.4: c.443G>T; p.(Cys148Phe) and c.458G>A; p.(Trp153*) (Supplementary Table S3; Supplementary Figure S2J and Supplementary Figure S3.19). The missense variant is affecting a highly conserved amino-acid and is predicted to be deleterious by SIFT and Polyphen-2. This is the first report of the putative pathogenic missense variants c.443G>T; p.(Cys148Phe) in this gene.

MMP20

MMP20 encodes a zinc-dependent endopeptidase activated during the secretion stage and continuing to be expressed by ameloblasts during the maturation stage. It supports enamel maturation by degrading the enamel protein matrix. As KLK4 and MMP20 seem to work in a collaborative manner, it is not surprising to note a similar dental phenotype in individuals with *KLK4* (Hart et al., 2004) or *MMP20* (Kim et al., 2005b) variants. We found 16 individuals (Supplementary Table S3; Supplementary Figure S2K) presenting with hypomature AI both in their primary and permanent dentitions; their phenotypes are similar to the ones described in the literature and associated with *MMP20* recessive inheritance (Kim et al., 2005b; Ozdemir et al., 2005b; Papagerakis et al., 2008; Lee et al., 2010; Gasse et al., 2013; 2017; Kim et al., 2017; 2020; Wang et al., 2020; Nikolopoulos et al., 2021).

Individuals 11.1, 11.2, 11.3 and 11.4 have compound heterozygous variants in *MMP20* gene (Supplementary Figures S3.20, 3.21, 3.22). All have in common the first variant NM_004771.4: c.103A>C; p.(Arg35 =). This pathogenic variant was firstly reported in Prasad et al., 2016a in individual V2.13. Its splicing impact was then functionally demonstrated by Kim et al., 2020. For individual 11.4 the second variant c.1362C>G; p.(Tyr454*) is novel and has been discovered thanks to GenoDENT panel. Other variants truncating the protein were already described in this gene (Papagerakis et al., 2008; Kim et al., 2017) but never so late in the protein. Indeed c.1362C>G; p.(Tyr454*) occurred in the last exon, inducing the truncation of the hemopoxin domain involved in binding inhibitors of metallopeptidases. It is also plausible that the domain may restrict cleavage site selection (Lee et al., 2010). We have tentatively classified this variant as probably damaging. We also report another new heterozygous pathogenic mutation found in individual 11.8 c.359dup; p.(Asn120Lysfs*9), along with a second variant on the other allele (Supplementary Figure S3.23) already reported c.954-2A>T (Kim et al., 2005b). This new variant was classified as probably damaging in light of later truncations being so described (Kim et al., 2017). The GenoDENT panel highlighted a compound heterozygous VUS in individual 11.11 c.530G>A; p.(Gly177Glu) associated to a known pathogenic variant (c.954-2A>T) (Kim et al., 2005b) (Supplementary Figure S3.24). This missense VUS creates an amino-acid substitution of the conserved Gly177 in the Matrixin protein domain, involved in the peptidase activity, and is likely predicted deleterious by SIFT (v4.0.3), VariantTaster (v2021) and PolyPhen-2. This VUS was not previously reported in the GnomAD database.

Individuals 11.12 and 11.13 both have a heterozygous variant NM_004771.4:c.566T>C; p.(Leu189Pro) already reported by the team (Gasse et al., 2017) along with respectively c.910G>A; p.(Ala304Thr) described in (Lee et al., 2010) and a novel variant in individual 11.3 reported c.1126C>T; p.(Gln376*). Due to the lack of parental DNA, we could not confirm the relative position of the variant in individual 11.13. It would however lead to the loss of almost all the hemopoxin domain, so, we classified this variant as probably damaging. Individuals 11.14 to 11.17 are all homozygous for the pathogenic variant c.954-2A>T (Supplementary Figure S3.25).

WDR72

WDR72 is a transporter, it encodes a protein predicted to be an intracellular vesicle coat protein that is mostly expressed during maturation stage but also at secretory stage. The stronger expression has nevertheless been detected during maturation initiation (El-Sayed et al., 2009; Katsura et al., 2014). WDR72 has recently been confirmed as regulating vesicle trafficking in ameloblasts (Katsura et al., 2022) and being involved in distal renal tubular acidosis (Khandelwal et al., 2021).

We identified four individuals with hypomature AI (Figure 4).

New variants in *WDR72* were identified by GenoDENT (Supplementary Table S3; Supplementary Figure S2L) in individuals 12.1, 12.2 and 12.4. Individual 12.1 presented a homozygous deletion including a part of intron 1 and the beginning of exon 2 NM_182758.4:c.-13 + 989_7del. In individual 12.2, we detected, a non-sense mutation in exon 2 and a 10 bp deletion at the intron 9 splice site. Truncating variation are known to be pathogenic but no splice variants were previously described in this gene. Intriguingly, the 12.2 phenotype is more complex than in other reported individuals as this patient also presented with small teeth, tooth agenesis, mild deafness and nephrocalcinosis. The recent description of the role of WDR72 in kidney-associated diseases and the syndromic nature of the diseases

presented by 12.2 would demand possible future consideration of WDR72 in a class of syndromic AI. Individual 12.3 is compound heterozygous for two known pathogenic variants reported in (Prasad et al., 2016a). In individual 12.4 we detected two novel compound heterozygous 1 bp deletion in exon 15 c.2388del; p.(Lys796Asnfs*16) and c.2146del; p.(Ala716Profs*10), resulting in a frameshift and a premature stop codon a known mechanism in this disease (Supplementary Figure S3.26).

ODAPH

C4ORF26, named also ODAPH, odontogenesis associated phosphoprotein, function is not yet well defined. *ODAPH* encodes a proline rich protein expressed during the secretory and maturation stage, suggesting a possible role in hydroxyapatite crystallization (Parry et al., 2012). ODAPH is important to maintain the integrity of the atypical basal lamina at maturation stage (Ji et al., 2021). Our cohort included individual 13.1 with hypomature AI (Figure 4). This individual was previously described in (Prasad et al., 2016b). He carries a small homozygous deletion NM_178497.5:c.39_46del; p.(Cys14Glyfs*18) identified using the GenoDENT panel (Supplementary Table S3; Supplementary Figure S2M). The phenotype was consistent with previous individuals described with truncating variants in this gene (Parry et al., 2012).

SLC24A4

SLC24A4 is a potassium-dependent sodium/calcium exchanger expressed by maturation stage ameloblasts (Hu P. et al., 2012). It likely performs a role in calcium provision to the enamel during maturation (Wang S. et al., 2014). One large deletion encompassing intron 14 to exon 17 has been described (Seymen et al., 2014b) whereas Prasad et al., 2016a described a homozygous deletion including the last three exons (15,16 and 17) and Parry et al., 2013 a non-sense homozygous variant.

Two individuals (14.1 and 14.2) with hypomature AI (Figure 4) showed novel homozygous *SLC24A4* variants using our GenoDENT panel (Supplementary Table S3; Supplementary Figures S1I, S2N). Individual 14.1 was already described in (Prasad et al., 2016a) with a homozygous deletion including the 3 last exon (15,16 and 17) of the *SLC24A4* gene NM_153646.4:c.(1,537 + 1_1538-1)_*67. Individual 14.2 and her affected sister carried a homozygous variant affecting a splice site with strong exon skipping predictions c.1716 + 5G>A (Supplementary Figure S3.27). No splice variant has previously been reported so we have classified this variant as a VUS pending functional analysis.

GPR68

GPR68 is a proton-sensing protein present during all stages of amelogenesis. It has been suggested that the protein acts as a pH sensor directing ameloblasts to switch between the ruffle ended and smooth ended conformations during the maturation stage (Parry et al., 2016b).

pH-Sensing G-protein-Coupled Receptor (GPR68) has been showed to be implied in ameloblast (Ludwig et al., 2003; 2003; Tomura et al., 2008; Frick et al., 2009) and odontoblast (Yang et al., 2006; Pereverzev et al., 2008) function. First human pathogenic variants were reported in (Parry et al., 2016b) associated with hypomaturation AI in three families (#617217). The clinical phenotype showed an enamel of apparent normal thickness but poorly mineralized, with brown discoloration. Weaker enamel tended to be prematurely lost secondary to attrition or masticatory stress, especially in the posterior teeth. Only few other cases, were additionally published, associated with the same type of AI (Seymen et al., 2021; Spedicati et al., 2021). No variants in this gene were found in our cohort.

Type IIB—hypomaturation, x-linked recessive

No gene has been clearly implicated in this category but we hypothesize that such phenotypes may be due to *AMELX* defects. Indeed, when *AMELX* mutations occur at specific MMP20 cleavage sites, the resulting phenotype is impaired matrix degradation and hypomature enamel. Thus, this category reasonably includes male individuals 7.5, 7.6 and 7.7 presenting a hypomature phenotype (Suplementary Figure 1E).

Type IIC—snow capped teeth, X-linked

In this form, both primary and permanent dentitions were affected. In males, primary teeth were opaque ground-glass white, and secondary teeth were mottled yellow-brown and white. Enamel had normal thickness, moderately soft, and did not contrast from dentin on x-ray. The teeth chipped and abraded more easily than normal teeth, but the loss of enamel was not as rapid as in the hypocalcified form (Rathi et al., 2014). Because of the appearance of the teeth in this form, referred to as snow-capped in its most marked form, confusion with fluorosis sometimes occurs (Rao and Witkop, 1971).

AMELX

Complete deletion of *AMELX* has been associated to this phenotype (Hu J. C.-C. et al., 2012).

We did not find this phenotype among our cohort.

Type IID—snow capped teeth, autosomal dominant

As with Type IIC, the phenotype is that of snow-capped appearance, except the X-linkage can be ruled out based on male: female incident rates. No gene has yet been implicated in this category. Although we identified individuals in our cohort with snow-capped teeth, we could not define a gene potentially responsible for this clinical entity.

Type III—hypomineralization

Hypocalcified amelogenesis imperfecta is characterized by an enamel of normal thickness but soft, porous and shedding easily from the dentin. The color of enamel can range from white to creamy yellow (Mendoza et al., 2007).

Enamel can be easily lost after eruption (post eruptive breakdown). These teeth are very sensitive even to physical contact with a toothbrush. Oral microbiome evolving in calculus is largely depositing on teeth resulting in severe gingivitis. Both autosomal dominant and autosomal recessive classifications are described related to three known genes in total.

Two categories are described: autosomal dominant (type IIIA associated to *FAM83H* variants and IIIB associated to *AMTN* variants) and - autosomal recessive (type IIIC associated to *RELT* variants).

We identified individuals with variants in *FAM83H* gene, we didn't detect any individual with *AMTN* or *RELT* variants in our cohort.

Type IIIA—amelogenesis imperfecta, hypomineralization type autosomal dominant #130900

To date, two genes are associated to the hypomineralized autosomal dominant inheritance subtype of AI.

FAM83H

Family with sequence similarity 83, member H (FAM83H), is an intracellular protein with ubiquitous expression (Lee et al., 2011). It reaches maximum expression in ameloblasts during the secretory stages. FAM83H regulates the organization of the keratin cytoskeleton and is involved in desmosome formation (Kuga et al., 2016). Variants identified in *FAM83H* cause autosomal dominant hypocalcified AI (Mendoza et al., 2007; Kim et al., 2008).

We report 15 individuals (15.1-15.15) presenting with hypocalcified amelogenesis imperfecta (Figure 4), affecting both primary and permanent dentitions with secondary loss of enamel, and colored teeth. Occlusal and incisal wear gave a conical form to the canines. There was no difference in radio-opacity between enamel and dentin.

The 15 individuals carried autosomal dominant variants in exon 5 (Supplementary Table S3; Supplementary Figures S1J, S2O, S3.28–3.37). This is consistent with previously reported variants as each of the variants identified to date have mapped to this largest and final exon of *FAM83H*. All of them except the one encountered in 15.13 are frameshift or non-sense variants, a mechanism already described as disease causing. Only three of those individuals had a novel variant: 15.1 NM_198488.5:c.930_939dup; p.(Val314Argfs*14), 15.6 c.1309_1311delinsTAG; p.(His437*) and 15.9 c.1375C>T; p.(Gln459*). Individual 15.4 c.1282C>T; p.(Gln428*) carries a variant previously described in (Prasad et al., 2016a). Individual 15.13 is the only one presenting a missense variant NM_198488.5:c.1498C>G; p.(Leu500Val). He also displays a variant in *WDR72* NM_182758.4:c.1283T>G; p.(Ile428Ser) (Supplementary Figure S3.36). The phenotype in this individual appears more severe possibly due to the compound effect of the two variants or to his more advanced age and accentuated tooth wear.

AMTN

Amelotin, encoded by *AMTN*, is a proline, leucine, threonine and glutamine rich protein binding to ODAM (odontogenic, ameloblast associated) and SCPPPQ1 (secretory calcium-binding phosphoproteins proline-glutamine rich 1) to form aggregates able to maintain the attachment between ameloblasts and the produced enamel during maturation stage (Holcroft and Ganss, 2011; Fouillen et al., 2017).

A large deletion in *AMTN* spanning exon 3–6 has been reported yet to cause hypomineralized AI (Smith et al., 2016). No variant in this gene was found among our cohort.

Type IIIB or IIIC-amelogenesis imperfecta, hypomineralization type autosomal recessive #618386

This type of AI is characterized by hypocalcified enamel in both primary and permanent dentitions. A normal or near-normal enamel volume can be found prior to tooth eruption. Post-eruptive changes are rapid and lead to enamel loss, enamel disintegrates from occlusal surfaces of the molars, leaving a ring of intact enamel remaining on the sides. Some people also have anterior open bite (Kim et al., 2019; Nikolopoulos et al., 2020). Homozygous frameshift, missense, and splice junction variants in *RELT* have been described in affected individuals (Kim et al., 2019).

RELT

The protein encoded by this gene is a member of the TNF-receptor superfamily able to activate the NF-kappaB pathway and selectively bind TNF receptor-associated factor 1 (TRAF1).

In mice, *Relt* is expressed in the odontoblast and ameloblast layers, specifically in secretory stage ameloblasts where there is ~20-fold higher expression than in maturation stage ameloblasts. It has been published that $Relt^{-/-}$ incisor enamel was of normal thickness but rough-surfaced and generally hypomineralized correlating with the phenotype found in humans. *RELT* was originally classified as causative of a new type of AI called type IIIC (#618386) but following Witkop's classification, as recessive hypocalcified hypoplastic AI, it could be classified in type IIIB.

We did not detect any individuals with *RELT* variants in our cohort.

Type IV—hypomaturation-hypoplastic with taurodontism #104510

Amelogenesis imperfecta, hypomaturation-hypoplastic type or hypoplastic-hypomature type, with taurodontism (AIHHT) is an autosomal dominant trait associated with enamel defects and enlarged pulp chambers (Dong et al., 2005). The difference between the two subtypes is slight and is based on the dominance of the hypomaturation *versus* the hypoplastic phenotype. So far, only one gene (*DLX3*) was associated to the hypomature-hypoplastic type IVA and no gene was described for the hypoplastic-hypomature type IVB.

Type IVA—hypomaturation-hypoplastic with taurodontism autosomal dominant #104510

For this phenotype, enamel thickness is supposed to be normal and hypomaturation is predominant over hypoplasia. Enamel appears as mottled yellow white to yellow brown with pits on the buccal surfaces. Taurodontism with large pulp chambers is observed on radiographs. Only one gene has thus far been proposed to cause this defect: *DLX3* (Wimalarathna et al., 2020).

DLX3

DLX3 is an important transcription factor involved in osteogenic differentiation (Sun et al., 2019). It is located on chromosome 17q21.3-q22, and contains 3 coding exons (Scherer et al., 1995; Price et al., 1998). *DLX3* plays a role in craniofacial development, and in the development of the ventral forebrain. DLX3 has three main domains: The N- and C-terminus transactivation domains, and a central sequence-specific DNA-binding distal-less-like homeodomain, encoded by exons 2 and 3. The homeodomain can interact directly with DNA in a sequence-specific way and regulates the expression of target genes throughout numerous developmental processes (Whitehouse et al., 2019). Only one missense variant had been described in *DLX3* gene for AI with taurodontism and attenuated tricho-dento-osseous syndrome in exon 2 by (Whitehouse et al., 2019).

Individuals 16.1 and 16.2 showed hypoplastic amelogenesis imperfecta with taurodontism (Figure 4), and enamel surface with striae (16.1), or thinner enamel (16.2). Taurodontism was really apparent on 16.2. 16.3 presented an hypomature/hypoplastic enamel and smaller 12, 22, as well as probable third molar agenesis. Dental agenesis could be linked to the additional variant discovered in *WNT10A* gene NM_025216.3:c.637G>A; p.(Gly213Ser). Dental radiographs confirmed the decreased thickness of enamel, and various degrees of molar taurodontism (Supplementary Figure S1K). In 16.1 we detected a heterozygous missense variant in exon 1 NM_005220.3:c.92C>G; p.(Thr31Ser) predicted possibly damaging by Polyphen-2 and localized in the distal-less-like homeobox protein domain. In individual 16.2 the heterozygous variant was located in exon 3 c.537C>A; p.(Asn179Lys) concerning a well conserved amino acid and predicted damaging by SIFT (v6.2.0) and Polyphen-2. Individual 16.3 carries the variant c.710A>G; p.(Tyr237Cys) (Supplementary Table S3; Supplementary Figure S2P). 16.1-16.3 did not present any bone nor hair additional phenotypes.

As this gene has also been linked to tricho-dento-osseus syndrome, we will describe further syndromic individuals linked to *DLX3*, in the coming syndromic section of this publication, illustrating therefore the tight and thin border between isolated and syndromic AI.

Type IVB—hypoplastic-hypomaturation with taurodontism, autosomal dominant

Enamel is thin with big hypoplastic areas. Hypoplasia is more pronounced than hypomaturation. Taurodontism with large pulp chambers is observed on X-Rays. No gene has ever been implicated with this phenotype (Wimalarathna et al., 2020). We suggest that types IVA and IVB might be a single subtype.

Syndromic amelogenesis imperfecta

Amelogenesis imperfecta can be found in isolation as previously described but also in association with extra-oral clinical signs (Supplementary Table S4). Recognition of AI subtype as well as associated symptoms could orientate clinical diagnosis, refine genetic diagnosis and contribute to improving patient care. After identification of the implicated gene, retro-phenotyping will also help assess and confirm overall clinical diagnosis.

In this paper we are discussing extra-oral key phenotypes for syndromes in which enamel defects are well characterized. Other genes associated to syndromes with insufficient characterization or minor enamel defects are classified by major extra oral clinical signs. To facilitate recognition of AI subtypes and further diagnosis we will describe and classify syndromic AI according to the 3 main defects categories, hypoplastic, hypomature and hypomineralized AI and their mode of inheritance (Figure 5; Table 2; Supplementary Table S4).

Syndromic hypoplastic AI

Hypoplastic AI is the hallmark of numerous syndromes. To date 22 genes have been associated to syndromes including hypoplastic AI in their clinical synopsis. Thirteen genes (*FAM20A*, *GALNS*, *TSC1*, *TSC2*, *TP63*, *MSX2*, *FAM20C*, *ARHGAP6*, *RAI1*, *PEX1*, *PEX2*, *PEX26*, *TGFBR2* and *ATP6V1A*) have been associated with clinical signs within the head and neck area, eleven with skin, nail and hair defects (*TSC1*, *TSC2*, *TP63*, *ARHGAP6*, *PORCN*, *TGFBR2*, *PEX1*, *PEX2*, *PEX26*, *ORAI1* and *STIM1*), three with immune deficit (*AIRE*, *ORAI1* and *STIM1*), seven with skeletal defects (*LTBP3*, *GALNS*, *TP63*, *MSX2*, *PORCN*, and *FAM20C*), five with neurological issues (*ATP6V1A*, *SLC13A5*, *PEX1*, *PEX2* and *PEX26*), two with cardiovascular defects (*LTBP3*, *TGFBR2*), and eight with genitourinary defects (*FAM20A* and *FAM20C*, *CLDN19*, *CLDN16*, *WDR72*, *TSC1*, *TSC2*, *RAI1*). It is therefore of importance to explore these potential associated phenotypes while taking medical history and examination.

Dental anomalies and short stature DASS #601216 Verloes Bourguignon syndrome, Platyspondyly with hypoplastic AI absent enamel—AR—*LTBP3*

DASS is characterized by short stature with brachyolmia as well as hypoplastic amelogenesis imperfecta with almost absent enamel (Huckert et al., 2015). Some individuals exhibit valvular and/or vascular defects, including mitral valve prolapse, aortic root dilation, and aortic as well as other arterial aneurysms and dissections (Dugan et al., 2015; Guo et al., 2018).

Associated tooth agenesis was described by (Noor et al., 2009; Dugan et al., 2015). Clinical oral examination showed also microstomia, tooth crowding, high arched palate. Teeth were small and had a yellowish color. Radiographic findings included thin enamel with reduced radiopacity, irregular alveolar bone level, and alveolar bone infectious lesions (Intarak et al., 2019).

LTBP3

DASS is an autosomal recessive disorder caused by homozygous or compound heterozygous variants in *LTBP3* gene (11q12) (Li et al., 1995; Huckert et al., 2015). *LTBP3* encodes latent transforming growth factor-beta-binding protein 3, modulating TGFbeta bioavailability in the extracellular matrix. Deleterious variants in *LTBP3* have also been associated with autosomal dominant Geleophysic dysplasia 3 (#617809). Ultrastructural enamel defects showed an absence of initial aprismatic enamel layer and an abnormal secretion of non-prismatic bulk enamel, suggesting LTBP3 plays a role in the life cycle of ameloblasts especially at the secretory stages with Tomes process formation (Huckert et al., 2015).

We identified *LTBP3* as the gene behind short stature and absent enamel (individuals 17.1–17.4) using exome sequencing (Huckert et al., 2015). GenoDENT panel was subsequently exanded with addition of this gene and we identified in 2 unrelated consanguineous families, additional individuals 17.5 and 17.6 with a similar phenotype and two new homozygous loss of function variants (Table 2; Supplementary Figures S1L, S2Q, S3.38). Teeth were small, spaced, and had a yellowish color. No enamel, impacted teeth, and irregular alveolar bone level were visible on panoramic radiographs. The first pathogenic variant (Individual 17.5) NM_001130144.3:c.3087del; p.(Asn1030Thrfs*47) was a one nucleotide deletion leading to a frameshift and a premature stop codon. The second variant (17.6) was an intronic mutation c.3629-2A>G which led to an aberrant exon 27 splice site. This would probably induce exon 27 skipping resulting in a 132 bp in phase deletion equivalent to a 44 amino acid deletion (position 1,211–1,254).

Mucopolysaccharidosis type IVA #25300—AR—*GALNS*

Mucopolysaccharidosis type IVA is characterized by intracellular accumulation of excessive glycosaminoglycans (GAGs): chondroitin-6-sulfate (C6S) and keratan sulfate (KS) mainly in bone, cartilage, and its extracellular matrix. GAG accumulation leads to unique skeletal dysplasia in MPS IVA individuals.

Most MPS IVA individuals usually look healthy at the neonatal period; however, bone abnormalities in the spine can be seen through X-rays even at birth in a severe form of individuals with MPS IVA. Skeletal symptoms are found later in childhood or adolescence. The most common symptoms include short stature, skeletal dysplasia, dental anomalies, and corneal clouding (Peracha et al., 2018; Akyol et al., 2019; Sawamoto et al., 2020). There is variable severity, but individuals with the severe phenotype usually do not survive past the second or third decade of life (Montaño et al., 2008).

Primary and permanent posterior teeth are described with concave buccal surfaces with pitting, pointed cusps, and concave occlusal surfaces. The enamel is hypoplastic with rough surface. The color varies from whitish-opaque to more yellowish-grey. Enamel surface is too weak to resist minor stress explaining the strong abrasion. The characteristic teeth color may be explained by the high porosity of enamel changing its optical properties (Rølling et al., 1999).

It is important to know that dental findings are found in MPS IVA, but not in MPS IVB. On radiographs, the enamel is thin but with normal radiodensity (Supplementary Figures S1N, S2S).

GALNS

Mucopolysaccharidosis type IVA (MPS IVA; Morquio syndrome A) is an autosomal recessive lysosomal storage disease caused by variants in the galactosamine-6-sulfate sulfatase gene (*GALNS*), located on chromosome 16q24.3. *GALNS* contains 14 exons and 13 introns (Sawamoto et al., 2020).

We report two individuals with compound heterozygous variations in the *GALNS* gene. Individual 19.1 was previously described by our team (Prasad et al., 2016a).

In individual 19.2, we found a missense variant NM_000512.5: c.1156C>T; p.(Arg386Cys) firstly described by (Ogawa et al., 1995), the second variant c.1558T>C; p.(Trp520Arg) was a class 2 variant so we cannot conclude that this variant is indeed involved in the individual phenotype as it is inherited by her homozygous unaffected mother (Table 2). Nevertheless, individual 19.2 presents the typical enzymatic deficiency and was given a confirmed MPS clinical diagnosis. So, either this class 2 variant contributes to the phenotype, or the individual is carrying another variant in this gene not detected by the panel such as a deep intronic variation. Such deep intronic variants have already been described in *GALNS* (Caciotti et al., 2018).

Autoimmune polyglandular syndrome type I #240300 autoimmune polyendocrine syndrome, type I, with or without Reversible Metaphyseal dysplasia—AD, AR—*AIRE*

Autoimmune polyglandular syndrome type I (APS-1) is a rare, autosomal recessive autoimmune disease.

The main symptom triad in APS-1 comprises chronic mucocutaneous candidiasis, adrenal insufficiency, and hypoparathyroidism. Various autoimmune diseases and ectodermal abnormalities are also commonly associated with the syndrome including enamel hypoplasia in permanent teeth (Suh et al., 2019). In addition to enamel defects in permanent teeth, hypoplastic pits and hypomature patches in deciduous teeth with underlying changes in the prismatic enamel ultrastructure are observed. The enamel looks severely hypoplastic throughout, except for the most cervical region. Deciduous teeth display opacities and yellowish cervical patches, suggestive of enamel hypomaturation. They are chalky with yellowish patches. The microstructure of the enamel prisms suggests an impaired mineralization, and prisms are clearly different. It was found that, in APS-1, auto-antibodies attack ameloblasts amongst other cells types, making it the first known disease of dental hard tissues with an auto-immune aetiology (Pavlic and Waltimo-Sirén, 2009).

AIRE

The disease has been associated to variations in the autoimmune regulator gene (*AIRE*) which consists of 14 exons (Nagamine et al., 1997) and is located on chromosome 21q22 (Aaltonen et al., 1997). AIRE protein is localized in the cell nucleus, where it forms distinct speckles (Björses et al., 1999). Analysis of its multidomain structure

reveals that human AIRE belongs to the group of proteins able to bind to chromatin and regulate the process of gene transcription (Perniola, 2018). No variant in this gene were found in our cohort.

Tuberous sclerosis # *605284*—AD—*TSC1-2*

Tuberous sclerosis complex (TSC) is characterized by frequent neuropsychiatric disorders including, in a variable way, intellectual disability, attention-deficit/hyperactivity disorders, autism spectrum disorders (ASD), psychiatric disorders and learning difficulties, seizures, the development of benign tumors, and oral manifestations. The most common oral manifestations are fibromas, gingival hyperplasia and enamel hypoplasia. Other less frequent oral findings are a high arched palate, bifid uvula, cleft lip and/or palate, delayed dental eruption and the presence of diastemas. Enamel hypoplasia is present in the permanent dentition of almost all individuals, and is associated with an increased risk of caries. This anomaly typically affects the vestibular surfaces of several teeth (Harutunian et al., 2011).

TSC1-TSC2

Individuals with TSC present variants of the *TSC1* and *TSC2* genes, which intervene in cell cycle regulation. The *TSC1* gene (9q34) encodes hamartin, a protein that interacts with tuberin (TSC2) to form a protein complex that inhibits signal transduction to the downstream effectors of the mammalian target of rapamycin (MTOR) (Inoki et al., 2002). The *TSC1* gene consists of 23 exons, of which the last 21 contain coding sequence and the second is alternatively spliced (Slegtenhorst et al., 1997).

The *TSC* gene on chromosome 16 was named *TSC2*. *TSC2* has 41 small exons spanning 45 kb of genomic DNA and encodes a 5.5-kb mRNA (van Bakel et al., 1997). No variants of *TSC1* or *TSC2* were identified in our cohort.

EEC syndrome-3 (EEC3) #604292 Rapp-Hodgkin syndrome #129400—AD—*TP63*

Ectrodactyly, ectodermal dysplasia, and cleft lip/palate syndrome 3 EEC3 (#604292 Maas et al., 1996; Celli et al., 1999; Rinne et al., 2006; Kosaki et al., 2008), ankyloblepharon-ectodermal defects, cleft lip/palate syndrome AEC (#106260), Rapp-Hodgkin (#129400), Acro dermatoungual lacrimal tooth syndrome ADULT (#103285), SHFM4 (#605289), Hay-Wells syndrome (#106260), and limb-mammary syndrome (#603543) are autosomal dominant allelic conditions due to mutations in the same gene, namely, *TP63* (15 exons, 3q28) (Yang et al., 1999) encoding tumor protein 63.

In EEC 3, ectodermal defects manifest as sparse and fine hair, dry skin, soft nails and decrease in sweet capacity (Sutton and van Bokhoven, 2010). (Sripathomsawat et al., 2011) also reported individuals with enamel hypoplasia and hypodontia.

Rapp-Hodgkin syndrome (RHS) is characterized by anhidrotic ectodermal dysplasia and cleft lip/palate. The face of the individuals is characteristic. They have narrow nose and small mouth, wiry, slow growing, and uncombable hair, sparse eyelashes and eyebrows, obstructed lacrimal puncta/epiphora, bilateral stenosis of external auditory canals, microsomia, hypodontia, cone-shaped incisors, enamel hypoplasia, and dystrophic nails (Kantaputra et al., 2003). The first individuals described in the literature were: a mother and her son and daughter (Rapp and Hodgkin, 1968) presenting with anhidrotic ectodermal dysplasia, cleft lip, and cleft palate and an unusually narrow and a small mouth.

TP63

TP63 plays an important role allowing cells to undergo apoptosis in response to DNA damage (Flores et al., 2002) and is involved in tumor and metastasis suppression (Su et al., 2010). Given its broad expression pattern, we suggest that *TP63* mutation affect the cell differentiation or fate of ameloblasts in development, though we await experimental evidence. Kantaputra et al., 2003 identified a heterozygous missense variant (S545P) in the *TP63* gene in a Thaï teenager presenting all the characteristics of the syndrome. No variant in this gene is reported in this publication.

Craniosynostosis 2 # 604757—AD—*MSX2*

Craniosynostosis is the premature fusion of calvarial sutures.

MSX2

The gene is located on chromosome 5q34-q35 (Jabs et al., 1993). (Hassan et al., 2004) showed that Msx2 regulates the expression of osteocalcin and therefore is implicated in the control of bone formation. This gene is reported for craniosynostosis in human. Two previous publications (Aïoub et al., 2007; Molla et al., 2010) reported that, in the targeted deletion mouse model *Msx2*$^{-/-}$, Msx2 was implicated in both isolated enamel dysplasia (regulating amelogenin, enamelin) and syndromic enamel dysplasia (through alterations in cell-cell junctions). To date one duplication of the entire gene *MSX2* has been reported in a syndromic (craniofacial, eye and limb anomalies) individual associated with hypoplastic AI (Plaisancié et al., 2015). No variant in this gene was identified in our cohort.

Raine syndrome # 259775—AR—*FAM20C*

Raine syndrome is an autosomal recessive disease characterized by neonatal osteosclerotic bone dysplasia with a poor prognosis and individuals who generally die within the first few weeks of life. The density of all bones is increased and it is especially evident for the skull. The face is dysmorphic with a narrow prominent forehead, proptosis, depressed nasal bridge, and midface hypoplasia. The periosteal bone formation is typical of the disease and extends along the diaphysis of long bones adjacent to areas of cellular soft tissue (Simpson et al., 2007; 2009).

The syndrome was firstly described *postmortem* by (Raine et al., 1989) on a female fetus presenting with microcephaly, exophthalmos, hypoplastic nose and midface, gum hyperplasia, cleft palate, low-set ears, osteosclerosis and hypoplastic lungs. Simpson et al., 2009 reported the first two unrelated individuals who survived during the childhood and showing typical features of the Raine syndrome. Hypoplastic amelogenesis imperfecta was observed in patients surviving childhood (Acevedo et al., 2015).

FAM20C

(Simpson et al., 2007) identified homozygous and compound heterozygous variants in *FAM20C* (7p22) in individuals with Raine syndrome. FAM20C is a Golgi associated secreted protein kinase, partnering with FAM20A, phosphorylating small integrin-binding ligand N-linked glycoproteins SIBLINGS, among other proteins, and playing a substancial role in osteogenesis and amelogenesis. No variant in this gene was identified in our cohort.

Focal dermal hypoplasia #305600—XLD—*PORCN*

Focal dermal hypoplasia (FDH) also named Golz or Golz-Gorlin syndrome is an X-linked dominant syndrome. FDH features include atrophy and linear pigmentation of the skin, herniation of fat through the dermal defects, and multiple papillomas of the mucous membranes or skin. In addition, digital anomalies consist of syndactyly, polydactyly, camptodactyly, and oligodactyly, ridged dysplastic nails, alopecia (scalp, eyebrow, and eyelashes). Ocular anomalies (coloboma of iris and choroid, strabismus, microphthalmia) have also been present in some cases. Intellectual disability occurs in some individuals. Striated trabecular bones (osteopathia striata) are a constant feature (Larrègue and Duterque, 1975; Happle and Lenz, 1977; Alsharif et al., 2018; Frisk et al., 2018). There is considerable diversity in the severity of the craniofacial and oral manifestations between individuals. The face is asymmetric, the nose displays hypoplastic alae and the philtrum looks flat in some cases. More severely affected individuals show thin lips with very little vermillion. Dental manifestations are the most commonly observed oral findings, presenting widely spaced teeth, including hypoplastic teeth, showing both hypoplasia and yellow brown hypomineralized areas of enamel. The developmental dental defects vary and include notching of the incisal edges of teeth and marked mamelons, localized hypoplastic vertical enamel groves, and hypodontia (Wright et al., 2016).

PORCN

Most of the individuals with FDH are female, with heterozygous or mosaic variants in the *PORCN* gene. Males (mosaic variants) account for 10% of affected individuals; heterozygous non-mosaic variants are lethal in males (Deidrick et al., 2016).

PORCN gene is located in chromosome Xp11.23, and contains 15 exons and spans about 12 kb. The first exon is non-coding (Caricasole et al., 2002). *PORCN* encodes and endoplasmic reticulum protein: the protein-serine O-palmitoleoyl transferase porcupine or porcupine O-acyltransferase. Although the exact function of the PORCN protein is uncertain, proteins in the porcupine (PORC) family are involved in WNT (wingless and int homologue) signaling pathway which is extremely important for embryonic development (Durmaz et al., 2018) including odontogenesis. No variant in this gene was identified in our cohort.

MLS syndrome with associated hypoplastic enamel X—ARHGAP6

Microphthalmia with linear skin defects (MLS) syndrome is an X-linked disorder that has been linked to different loci. One such condition includes associated AI in a hypoplastic form.

ARHGAP6

Because the Amelogenin gene (*AMELX*) is nested within intron 1 of *ARHGAP6*, partial deletions in *ARHGAP6* can completely remove *AMELX* giving a distinctive enamel phenotype resembling "snow-capped" teeth (Hu J. C.-C. et al., 2012). This phenotype was already described in isolated hypomature AI IIC section.

Ras homologue GTPase activation protein 6 (*ARHGAP6*), belongs to the Rho GTPase-activating protein (RhoGAP) family. *ARHGAP6* does not appear essential for normal enamel formation. Failed *ARHGAP6* expression did not appreciably alter the severity of enamel defects when *AMELX* was absent (Hu J. C.-C. et al., 2012).

We report one individual (20.1) carrying a 12 Mb deletion of the Xp22.2 region (Table 2). This region is including not only the *AMELX* gene but also the full *ARHGAP6* gene.

This female individual suffers from microphthalmia with linear skin defects (MLS) syndrome and associated hypoplastic enamel with a banding pattern characteristic of the female lyonisation effect (bands of normal enamel next to defective enamel; AI hypoplastic IE) (Supplementary Figure S1N).

Smith-Magenis syndrome # 182290—AD—*RAI1*

Smith-Magenis syndrome is an autosomal dominant disease which occurs mostly *de novo*. Clinical phenotype includes moderate intellectual deficiency with frequent behavioral issues (temper tantrums, nail yanking, insertion of foreign objects into body orifices, self-injurious behaviors), sleep disturbance, dysmorphic facial features. Affected patients can present with variable congenital anomalies (heart defects, structural renal anomalies, scoliosis) including oral anomalies like AI or dental agenesis (Vieira et al., 2012).

RAI1

The syndrome is in 90% of the cases due to a 3.7 Mb deletion in chromosome 17p11.2 encompassing the *RAI1* gene (Vieira et al., 2012).

We identified with the GenoDENT panel, in individual 21.1, a deletion in the 17p11.2 region leading to a possible diagnosis of Smith-Magenis syndrome with hypoplastic AI (Table 2). The exact size of the deletion was further characterized by array analysis. Individual 21.1 presented the classical 3.7 Mb deletion associated with the syndrome as well as classical associated phenotype including the hypoplastic enamel described by (Wright et al., 2015).

Loeys-Dietz syndrome 2 # 610168—AD—*TGFBR2*

Loeys-Dietz syndrome type 2 is characterized by micrognathia, retrognathia, hypertelorism, bifid uvula, cardiovascular anomalies, pectus deformity, joint laxity, scoliosis, hand and feet anomalies, skin texture and color anomalies and hypoplastic AI (Jani et al., 2020).

TGFBR2

Variants in *TGFBR2* have been associated with Loeys Dietz syndrome type 2. TGFBR2 codes for a transmembrane protein with a serine/threonine-kinase domain forming a heterodimeric complex with TGF-beta type I receptor, TGFBR1, binding TGF-beta, TGF-beta1, TGF-beta2 and TGF-beta3, ligands. This receptor/ligand complex phosphorylates proteins, which then enter the nucleus and regulate the transcription of genes related to cell proliferation, cell cycle arrest, wound healing, immunosuppression, and tumorigenesis.

Here we report an individual 22.1 with a heterozygous missense variant in the *TGFBR2* NM_003242.6:c.1561T>C; p.(Trp521Arg) (Table 2; Supplementary Figures S1O, S3.43) and diagnosed with

Loeys-Dietz syndrome including hypoplastic amelogenesis imperfecta. This variation was already reported by (Mátyás et al., 2006). The variant is most probably transmitted by the affected mother though we were not able to access the mother's DNA to confirm.

Developmental and epileptic encephalopathy 93 #618012—AD—*ATP6V1A*

Developmental and epileptic encephalopathy 93 is an autosomal dominant disorder with, among other features, delayed psychomotor and impaired intellectual developments, as well as early onset epilepsy. Additional clinical features like microcephaly and hypoplastic amelogenesis imperfecta were observed in epileptic encephalopathy (Guerrini et al., 2022).

ATP6V1A

This disorder has been associated with *ATP6V1A* (ATPase, H + Transporting, Lysosomal, 70-KD, V1 Subunit A). It codes for a component of vacuolar ATPase, a multimeric enzyme, an ATP-dependent protein pump function, which mediates acidification of eukaryotic intracellular organelles and is necessary to activate mTORC1 (Zoncu et al., 2011). No variant in this gene was found among our cohort.

Hypomagnesemia 3, renal # 248250—AR—*CLDN16*

Familial hypomagnesemia with hypercalciuria and nephrocalcinosis is an autosomal recessive progressive renal disorder with progressive loss of the renal function characterized by excessive urinary Ca^{2+} and Mg^{2+} excretion (Müller et al., 2006). Hypoplastic, hypomature amelogenesis imperfecta is also detected in some individuals (Bardet et al., 2016).

CLDN16

(Simon et al., 1999) identified homozygous and compound heterozygous variants in the *CLDN16* gene in ten individuals presenting renal hypomagnesemia. CLDN16 is localized on chromosome 3q28, and consists of 5 exons and encodes a protein of 305 AA with 4 transmembrane domains and intracellular N and C termini (Simon et al., 1999). *CLDN16* is required for cell division (Kittler et al., 2004), is selectively expressed at tight junctions of renal epithelial cells and plays a central role in the reabsorption of divalent cations (Kausalya et al., 2006). No variant in this gene was identified among our cohort.

Renal Hypomagnesemia-5 with ocular involvement # 248190—AR—*CLDN19*

Renal hypomagnesemia-5 with ocular involvement (HOMG5) is an autosomal recessive disorder characterized by severe renal magnesium wasting, progressive renal failure, nephrocalcinosis, and severe visual impairment (Konrad et al., 2006). Hypoplastic, hypomature amelogenesis imperfecta is also present in some individuals (Yamaguti et al., 2017).

CLD19

Konrad et al., 2006 found two different homozygous missense variants in the *CLDN19* gene in families with renal magnesium wasting, renal failure, and severe ocular involvement. Indeed, the syndrome is caused by homozygous or compound heterozygous variants in the claudin-19 gene on chromosome 3q28. Claudins, such as CLDN19, are transmembrane proteins found in tight junctions. Tight junctions form barriers that control the passage of ions and molecules across an epithelial sheet and the movement of proteins and lipids between apical and basolateral domains of epithelial cells (Lee et al., 2006). No variant in this gene was identified among our cohort.

Heimler syndrome #234580 and #616617—AR—*PEX1* and *PEX6*

Heimler syndrome-1 (HMLR1) is an autosomal recessive syndrome reported as the mildest form of the peroxisomal biogenesis disorder spectrum (PBD 1A (Zellweger)). This disease is characterized by sensorineural hearing loss, enamel hypoplasia of the permanent dentition and nail abnormalities with Beau lines (transverse ridges) of the toenails and white patches in the fingernails (leukonychia) (Heimler et al., 1991; Pollak et al., 2003), with or without retinal dystrophy (Ratbi et al., 2015; Mechaussier et al., 2020). In contrast to individuals with PBDs at the severe end of the clinical spectrum (neurologic dysfunction, craniofacial abnormalities, liver dysfunction, and biochemically absence of peroxisomes), Heimler affected individuals showed no identifiable dysmorphic or additional neurologic features.

PEX1

Ratbi et al. (2015) identified homozygous and compound heterozygous variants in the peroxisome biogenesis factor 1 gene (*PEX1*) in 4 families, including the family reported by (Heimler et al., 1991). Human PEX1 gene is located on chromosome 7q21, and is composed of 24 exons and encodes a 147-kD protein member of the AAA protein family (ATPases associated with diverse cellular activities). Those proteins participate in a broad range of cellular processes, as indicated by the designation AAA which comes from ATPases associated with diverse cellular activities and are specially required for peroxisomal matrix protein import (Portsteffen et al., 1997; Reuber et al., 1997). No variant in this gene was identified among our cohort.

PEX6

Another form of Heimler syndrome (HMLR2; #616617) is caused by a variant in the *PEX6* gene (601,498) located on chromosome 6p21, consisting of 17 exons and 16 introns, spanning about 14 kb (Zhang et al., 1999). No variant in this gene was identified among our cohort.

Peroxisome biogenesis disorder PBD 7A (Zellweger) #614872 7B #614873—AR—*PEX26*

It has been shown by (Neuhaus et al., 2017) that *PEX26* is responsible for Zellweger Syndrome. Patient carrying recessive variant present hypoplastic AI (Kim et al., 2021a). No variant in this gene is reported in this publication.

Developmental and epileptic encephalopathy 25, with AI #615905—AR—*SLC13A5*

Individuals with developmental and epileptic encephalopathy 25 present epileptic seizures since the first days of life in most of the cases, and a developmental outcome ranging from mild to severe

intellectual disability, plus variable combinations and degrees of ataxia, and in addition, teeth with hypoplastic enamel (Hardies et al., 2015). Several individuals have been reported suffering from early onset, regular and difficult to control seizures. In some cases, seizures could be controlled with conventional antiepileptic treatment but showed deterioration of gait which improved after usage of another antiepileptic medication.

Oral manifestations encompass delayed eruption of permanent teeth, small and cylindrical teeth with wide interdental spaces, and yellowish to brownish discolorations. Lower permanent incisors are described as sharp and thin; premolars and molars seem extremely worn. Clinically, the enamel of primary and permanent teeth is hypoplastic with a smooth, hard and pitted surface. Dental panoramic radiographs show a lack of enamel in both dentitions. Histologically, the enamel layer is very thin. No lines of Retzius or enamel prisms are visible and the surface presents small pits. These pits are a common sign for hypoplastic AI. The dentin presents a normal structure (Schossig et al., 2017).

SLC13A5

Developmental and epileptic encephalopathy 25 with amelogenesis imperfecta is a rare disease caused by variants in *SLC13A5* genes. *SLC13A5* is located in the chromosome 17p13-p12, and contains at least 12 exons (Inoue et al., 2002). *SLC13A5* encodes a high affinity sodium-dependent citrate transporter, which is mainly expressed in liver and brain. Neurons are considered incapable of *de novo* synthesis of tricarboxylic acid cycle intermediates; therefore, they rely on the uptake of intermediates, such as citrate, to maintain their energy status and neurotransmitter production (Hardies et al., 2015).

This epilepic encephalopathy was described as Kolschütter-Tönz like syndrome (KTS like) as the phenotype is similar to the one observed in individuals with variations in the *ROGDI* gene except for the enamel defects: AI is hypoplastic in patient with *SLC13A5* variations and hypomature in individuals with *ROGDI* mutations. Kolschütter-Tönz syndrome will be described later in the paper as individuals present a hypomature AI.

We report one individual 23.1 carrying a compound heterozygous missense variants affecting exons 2 and 4 NM_177550.5:c.203C>A; p.(Pro68Gln), c.434C>A; p.(Thr145Lys) showing a hypoplastic AI with thin opaque enamel (Table 2; Supplementary Figures S1O, S2T). The *SLC13A5* individual in our panel, is an individual described with *SLC13A5* variant discovered through GenoDENT panel after the identification of the gene by WES in another family of the Schossig et al., 2017 cohort (Schossig et al., 2017) with a phenotype described as Kohlschütter-Tonz like syndrome (KTS).

Syndromic hypomature AI

Hypomature AI is also manifest in syndromic conditions. Three genes have thus far been identified as causing syndromes with associated hypomature AI.

Immunodeficiency 9 # 612782—AR—*ORAI1*

Primary immunodeficiency-9 (IMD9) is a recessive disease characterized by early onset of recurrent infections due to defective T-cell activation. The individuals present congenital myopathy resulting in muscle weakness, and features of ectodermal dysplasia including a hypomature amelogenesis imperfecta with soft dental enamel (McCarl et al., 2009).

ORAI1

By analyzing individuals described by (Feske et al., 1996), (Feske, 2010) showed for the first time that individuals with this type of immune dysfunction were homozygous for a variant in the *ORAI1* gene. Indeed, the disease is caused by homozygous or compound heterozygous variants in *ORAI1* (610,277). This gene located on chromosome 12q24, encodes a subunit of the plasma membrane calcium channel CRAC essential for store-operated calcium entry (Vig et al., 2006) and the channel function. The gene is expressed in cells and organs involved in immunity ($CD4^+$ and $CD8^+$ T-cells, $CD19^+$ B-cells, and in a subset of cells in the thymus, spleen, and tonsils) but also in sarcolemma of muscle fibers, eccrine sweat glands, skin, vascular endothelium, hepatocytes, lung, and kidney (McCarl et al., 2009) and in ameloblast (Nurbaeva et al., 2015). No variant in this gene was identified among our cohort.

Immunodeficiency 10 # 612783—AR—*STIM1*

Immunodeficiency-10 is a primary autosomal recessive immunodeficiency, characterized by recurrent infections due to defective T- and NK-cell function. The individuals also have hypotonia, hypohidrosis and hypomature amelogenesis imperfecta. (Picard et al., 2009; Parry et al., 2016a) reported the disease for the first time in 3 siblings from central Europe who had recurrent infection due to defective T-cells, muscle hypotonia and enamel defects. They identified defects in cellular store-operated calcium entry, which is required for lymphocyte activation.

STIM1

Immunodeficiency 10 is due to a homozygous truncating variant in the *STIM1* gene (Picard et al., 2009; Parry et al., 2016a). STIM1 gene is located to chromosome 11p15.5 and contains 12 exons (Parker et al., 1996; Sabbioni et al., 1999). It encodes a 746 AA calcium sensor that conveys the calcium load of the endoplasmic reticulum to store-operated channels at the plasma membrane (Yuan et al., 2007) and mediate the gating of CRAC channels (McNally et al., 2012). ORAI1 and STIM1 are interacting as the ORAI1 membrane calcium channel is activated by the calcium sensor STIM1 when calcium reservoirs are depleted (Lacruz and Feske, 2015). AI, related to Immunodeficiency 10, is classified as hypomineralized on OMIM but due to recent publications we transfer it to hypomature AI section (Wang S. et al., 2014; Furukawa et al., 2017). No variant in this gene was identified among our cohort.

Kohlschütter-Tonz syndrome #226750—AR—*ROGDI*

This autosomal recessive syndrome was firstly described by (Kohlschütter et al., 1974) in a family of central Switzerland in which 5 brothers were affected but with no mention of the gene involved. Kohlschütter-Tonz syndrome (KTS) is characterized by severe global developmental delay, seizures, and AI affecting both primary and permanent teeth. The teeth present a yellow to brown discoloration. The most severely affected individuals have profound intellectual disability, never acquire speech, and

become bedridden early in life (Mory et al., 2012; Schossig et al., 2012).

ROGDI

(Schossig et al., 2012) reported for the first time the causative gene by identifying homozygous or compound heterozygous variants in ROGDI gene in 3 members of 3 unrelated families with KTS. ROGDI maps to chromosome 16p13.3., contains 11 exons and spans over 5.98 kb. It encodes a leucine-zipper protein with high expression in the human brain and spinal cord (Mory et al., 2012).

Both variants in *ROGDI* and *SLC13A5* cause epileptic encephalopathy and AI. Whereas *ROGDI* mutation manifests in an hypomature-hypomineralized AI with a rough colored dental surface and with seizure onset may be as late as age 3, individuals mutated for *SLC13A5* present hypoplastic AI, a smooth the dental surface sometimes with only mild discoloration and seizure onset is within the first days after birth.

Here we report three individuals with stop variants in *ROGDI* (24.1, 24.2, 24.3) (Table 2; Supplementary Figures S1P, S2U). Individuals 24.1 and 24.3 present compound heterozygous variants (Supplementary Figures S3.44) already described in the literature, while 27.2 has a homozygous variant found with our panel and previously published in (Huckert et al., 2014).

Syndromic hypomineralized AI

Two syndromic conditions associated with hypomineralized AI have been described.

Short stature, amelogenesis imperfecta, and skeletal dysplasia with scoliosis #618363—AR—*SLC10A7*

Affected individuals present with short stature, joints dislocation, advanced carpal ossification, abnormal vertebrae, hyperlordosis or kyphoscoliosis, small epiphyses and hypomineralized AI. Enamel has a yellow-brown appearance with a rough surface. Tooth crowns are short and widely spaced. Variable features include facial dysmorphism, moderate hearing impairment, and mildly impaired intellectual development. The phenotype severity is variable. Indeed, an individual with a milder phenotype was reported in (Laugel-Haushalter et al., 2019).

SLC10A7

This autosomal recessive syndrome was firstly described by (Dubail et al., 2018) in 6 unrelated individuals. It is due to variants in the *SLC10A7* gene encoding a calcium transporter.

The key phenotype to distinguish individuals with mutation in *SLC10A7*, within the wide spectrum of skeletal dysplasia, was the hypomineralized/hypomature enamel defects observed in all the individuals and the hypoplastic lower jaw.

Here we report 2 individuals with homozygous variants in *SLC10A7*. Individual 25.1 presents a novel homozygous variant in the gene. The variant identified by GenoDENT NGS panel affects exon 3 NM_001300842.3c.269T>G; p.(Leu90Arg) in which another homozygous variant was already described to be pathogenic (Ashikov et al., 2018). Individual 25.2 was already described in (Laugel-Haushalter et al., 2019, WES). She has a homozygous missense variant in the very last exon of the gene c.908C>T; p.(Pro303Leu) (Table 2; Supplementary Figure S3.45) and presents a mild phenotype of the disease but with the characteristic enamel defects (Supplementary Figures S1Q, S2V).

Jalili syndrome #217080—AR—*CNNM4*

The autosomal recessive syndrome was first described by (Jalili and Smith, 1988) in 29 individuals and is characterized by cone-rod dystrophy and AI. Nystagmus and photophobia are present from infancy or early childhood and progress with age. Enamel of primary and permanent teeth is hypomineralized (only 50% of mineralization), with a dark brown discoloration, and individuals are more susceptible to dental caries (Parry et al., 2009).

CNNM4

The disorder is caused by homozygous or compound heterozygous variants in *CNNM4* gene (607,805) sitting on chromosome 2q11.2. More than 24 different variants have been identified on individuals all around the world but the molecular mechanism of the disease remains unclear (Daneshmandpour et al., 2019). CNNM4 encodes a deduced 775 amino-acids protein. (Guo et al., 2005) hypothesized that the protein may have a role in metal ion transport and homeostasis. Indeed, (Yamazaki et al., 2013) showed in mice the role of Cnnm4 in Mg^{2+} transport. The protein is localized in keratocytes, in the retina, and in developing teeth specifically in ameloblasts (Parry et al., 2009; Polok et al., 2009).

Here we report two individuals with homozygous missense variants in this gene. In individual 26.1 we detected a homozygous missense variant, firstly described by (Parry et al., 2009): NM_020184.4:c.1495G>A; p.(Val499Met) (Table 2; Supplementary Figure S3.46). Other missense variants, were reported as pathogenic and causative of Jalili syndrome. Individual phenotype was consistent with the literature and described clinical synopsis. The "hypoplastic" enamel appearance of both primary and permanent teeth was due to extensive post-eruptive loss of soft enamel detaching easily from dentin. The teeth displayed yellow-brownish coloration with brown spots (Supplementary Figures S1R, S2W). Individual 26.2 has already been reported in (Prasad et al., 2016a) c.1495G>A; p.(Val499Met).

Syndromic hypoplastic/hypomature with taurodontism AI

One syndromic condition with hypoplastic/hypomature AI with taurodontism has been identified.

Tricho-dento-osseus syndrome #190320—AD—*DLX3*

Tricho-dento-osseous (TDO) syndrome is a rare autosomal dominant condition characterized by various dental and non-dental findings (Jagtap et al., 2019) (Duverger et al., 2017).

TDO emcompasses abnormal development of ectoderm derived structures. Patients presents with head and neck and skeletal phenotypes. Dysplastic nails, curly hair, abnormal density of bone, taurodontism, and hypoplastic amelogenesis imperfecta are common features of this disorder. The enamel appears extremely thin, with enlarged pulp chambers, and root furcations displaced apically. Mandibular prognathism, delayed teeth eruption, teeth discoloration, periapical abscesses, apically positioned furcation, shortened roots, other non-dental abnormalities are variably

present. Dental and non-dental features are variable even among affected individuals in the same family (Jain et al., 2017). The management of TDO individuals require a multidisciplinary approach involving both dentists and physicians. Periodic radiographic follow-up is required to prevent further complications such as osteomyelitis (Jagtap et al., 2019).

DLX3

TDO is caused by variants in a transcriptional regulator, Distal-less homeobox 3 gene, *DLX3*.

Here we describe two unrelated individuals, one girl (27.1) and one boy (27.2) presenting with tricho-dento-osseous syndrome (Supplementary Figure S1S). They are both carrying the same *DLX3* heterozygous frameshift variant in exon 3 NM_005220.3: c.561_562del; p.(Tyr188Glnfs*13) (Table 2; Supplementary Figures 3.47 and 3.48). This variant firstly described by (Dong et al., 2005) is altering the two amino-acids of the DNA-binding homeodomain and truncating the protein by 88 amino-acids.

Discussion

AI classification has always been evolving since the one proposed by (Weinmann et al., 1945). These early classifications were based mostly on detailed phenotypic observations (Darling, 1956; Witkop, 1957). Later it was recognized that the mode of inheritance was important to classified AI so, (Schulze, 1970) and (Witkop, 1971) proposed a classification encompassing the phenotype observation and the mode of inheritance. This classification system has been updated and improved since 1988 by (Witkop, 1988) and is currently the mostly frequently used classification demonstrating its extraordinary accuracy grounded on expert clinical skills. A classification based not only on the phenotype and the mode of inheritance but also on the genetic molecular defects was proposed since 1995 by (Aldred and Crawford, 1995), (Hart et al., 2002a) and (Aldred et al., 2003) but this was never fully achieved due to the lack of knowledge and technologies to complete both a clinical and a molecular diagnosis. In 2007 (Crawford et al., 2007) stated that laboratory genetic diagnosis was at that time only a research tool.

It is however now commonly accepted that the mode of inheritance and underlying genomic change are important to improve genetic counselling of affected individuals and their families.

Here we propose a Witkop's classification evolution including the phenotypical observations (hypoplastic, hypomature, hypomineralized and hypoplastic-hypomature with taurodontism), the mode of inheritance and the genetic diagnosis.

This is now possible as progresses in next-generation sequencing techniques, their availability and now reduced costs have opened the door to personalized oral medicine. GenoDENT NGS panel, exploring 567 genes involved in orodental development and diseases, was set up in research (Prasad et al., 2016a) and transferred in hospital diagnostic laboratories in 2019 (Rey et al., 2019). Its 60% diagnostic rate testify of its reliability and utility in the context of diagnosis, counselling and evolution of treatment options.

It took more than 10 years to gather an informative AI cohort (221 individuals from 111 families) with detailed clinical information (D[4]/phenodent).

Since the discovery of the first gene underlying an amelogenesis imperfecta from mapping of *AMELX* in 1989 (Lau et al., 1989) to its causative role in AI in 1990 (Lagerström et al., 1990; 1991); more than 70 genes have been discovered as important for amelogenesis and its defects. The most recent ones are *CLAUDIN 10* (Sewerin et al., 2022) and *ATP6V1A* (Guerrini et al., 2022). Knowledge is evolving fast on amelogenesis (Simmer et al., 2021) and enamel disturbances in rare diseases. (de La Dure-Molla et al., 2019) listed among 408 rare diseases with orodental manifestations, 105 conditions with enamel defects either isolated (21) or syndromic (84). In our cohort, 73% were diagnosed with non-syndromic amelogenesis imperfecta and 27% with syndromic amelogenesis imperfecta.

The boundaries between isolated and syndromic forms of AI are shrinking as novel information on genes, role of the proteins and associated symptoms and diseases are evolving. This was well illustrated by *FAM20A* and the recognition of enamel-renal syndrome (ERS); enamel-renal-gingival syndrome, hypoplastic amelogenesis imperfecta with nephrocalcinosis, amelogenesis imperfecta and gingival fibromatosis syndrome as allelic conditions and the subsequent transition from an isolated AI to a syndromic disease requiring a different holistic care. *WDR72* was identified in 2009 (El-Sayed et al., 2009). It was recently associated to distal renal tubular acidosis (Khandelwal et al., 2021) and this finding rapidly confirmed in 2019 that isolated *WDR72* associated hypomature AI was in fact a possible syndromic condition (Zhang et al., 2019). AI diagnosis should always bare in mind possible associated symptoms leading to a syndrome diagnosis.

AI clinical subtype recognition can be difficult as phenotype is evolving through time and might transform from a hypomineralized form to a visible "hypoplastic" form thanks to post-eruptive enamel breakdown. The terms hypocalfication and hypomaturation were used by Witkop (1988) before knowing the genes or mechanisms involved in amelogenesis and the pathogenesis of AI. It is now known from the timing of protein expression that these terms are not accurate and both the hypocalcified and hypomaturation phenotypes have as primary feature hypomineralization. *MMP20*, for example, is expressed during the secretory stage and continues to be expressed during the maturation stage yet is classified as hypomature AI and it is hypomineralized.

Clinically "hypocalcified" refers to softer enamel with post eruptive breakdown and "hypomature" to less mineralized but strong enough enamel preserving the teeth morphology therefore corresponding to a more advanced maturation process and the state of degradation of enamel matrix proteins.

The Witkop's classification terminology could be adjusted to use only names (I HYPOPLASIA, II HYPOMATURATION, III HYPOMINERALIZATION *versus* HYPOCALCIFICATION, IV HYPOMATURATION/HYPOPLASIA with TAURODONTISM) or only adjectives (hypoplastic, hypomature, hypomineralized, hypomature/hypoplastic). May be sections II and III of the classification should be united in a single hypomineralization section.

This paper gathers in the Supplementary Figures many clinical intraoral pictures and panoramic radiographs of genotype related amelogenesis imperfecta. This resource is meant to help clinicians improving their AI diagnosis and search for associated symptoms.

Dental anomalies and enamel defects are very precise key diagnostic clues (Boch-Zupan et al., 2012; de La Dure-Molla et al., 2019) helping, when recognized, to orientate a clinical diagnosis towards a broader genetic rare disease recognition. These AI phenotypes can be precise diagnostic signatures. Among them the clinical features linked to ERS (almost no enamel, impacted teeth, intrapulpal calcifications, root anomalies . . .) would immediately suggest a possible ERS and orientate the clinical team towards kidney investigations *via* ultrasound seeking nephrocalcinosis. In Heimler syndrome, the AI is only present in the permanent dentition and its recognition linked to seusorineural hearing loss could suggest the diagnosis.

Following genetic diagnosis, retro-phenotyping can also lead to the search and recognition of additional traits and the diagnosis of broader rare diseases. For example, the diagnosis of Jalili syndrome or amelogenesis imperfecta and dystrophy of the cones and rods of the retina was subsequently made in a 4-year-old boy who attended a rare disease competence center for enamel problems management. The genetic diagnosis pointed to the presence of autosomal bi–allelic recessive variants in the *CNNM4* gene with further confirmation of the presence of a retinal dystrophy. This transformed an isolated enamel restricted diagnosis to a broader rare disease identification.

Genotype recognition can change a clinical diagnosis: two patients with 2 different diagnoses: spondyloepiphyseal dysplasia and mucopolysaccharidosis type 4A (ORPHA: 309,297) were investigated for associated hypoplastic amelogenesis imperfecta (quantitative enamel defects). The results of the GenoDENT test showed variants in the *GALNS* gene responsible for mucopolysaccharidosis type 4A. The test changed the medical diagnosis for one of the patients. A revised diagnosis facilitates access to other treatments and care.

Phenotype/genotype identification can also lead to accurate information and genetic counselling, guide therapeutic management and facilitate the discovery of new genes and diseases.

Patients with negative results on the panel were further explored with exome sequencing and through international collaborations and larger cohort gathering new genes such as *LTBP3* (Huckert et al., 2015), *SLC13A5* (Schossig et al., 2017), *SLC10A7* (Laugel-Haushalter et al., 2019) were identified. Whole genome sequencing (WGS), as the PFMG 2025 initative (https://pfmg2025.aviesan.fr/en/; rare diseases with orodental manifestations https://pfmg2025.aviesan.fr/professionnels/preindications-et-mise-en-place/formes-syndromiques-de-maladies-rares-a-expression-bucco-dentaire/) could facilitate the discovery of the underlying genetic defects causing both non-syndromic and syndromic AI.

In this cohort we identified 151 variants. Among these, 124 were classified as likely pathogenic or pathogenic (class 4 or 5) and 47 were newly reported. It is interesting to notice that the most frequent genes identified in isolated AI were *AMELX* in hypoplastic, *MMP20* in hypomature and *FAM83H* in hypomineralized AI and *LTBP3* and *FAM20A* in syndromic conditions.

Our results allowed to provide for 81% of the index individuals a definitive genetic diagnosis, and for 19%, variants of unknown significance (VUS) were identified. Twenty-one new VUS were detected in patients with isolated AI and 3 new VUS in patients with syndromic AI.

However, for those uncertain variants, like new candidate genes, or for variants in different domains of the protein or with different possible physiopathological mechanisms, it could be difficult to confirm their pathogenicity and these variants are subsequently classified as variant of unknow significance (VUS).

To reclassify those variants and provide a clear genetic diagnostic it is important to develop reliable, easy to perform *in vitro* assays and functionally validate these variants. Furthermore, functional characterization will open new potential strategies for curative treatments.

Enamel defects have also been reported in others syndromes and the question remains to qualify them as amelogenesis imperfecta. For instance, genes associated with - skin, nails and hair defects among other symptoms are *ATR* (Tanaka et al., 2012), *CLDN1* (Feldmeyer et al., 2006), *COG6* (Shaheen et al., 2013), *FGF10, FGFR3, FGFR2* (Hollister et al., 1973), *HRAS* (Goodwin et al., 2014), *KRAS, NRAS, KRT14* (Tabata et al., 1996), *MBTPS2* (Martino et al., 1992); - with eye defects *NAA10*; - with skeletal anomalies *AKT1, B3GAT3, CYP27B1, CTSK, EVC1, EVC2, ERCC4, ERCC8, GJA1, GNAS, IDUA, IRX5, NDN, PTDSS1, SNORD116, RUNX2, TBCE, VDR*; - genito-urinary anomalies *HNF1B, VPS33B, VIPAR*; - intellectual disability *PSPA, GALC*; Usher syndrome *MYO7A, USH2A, PD2D7, ADGRV1, CLRN1*.

Amelogenesis is at the crossroad of many developmental processes and careful examination of the oral cavity of syndromic patients should be mandatory to deliver appropriate preventive care and follow up targeting oral health.

It is crucial that the team of health professionals involved in diagnosing and managing a possibly syndromic patient knows the value of an expert examination of the oral cavity and the importance of an acute diagnosis of these developmental defects assisting syndrome diagnosis (Bloch-Zupan et al., 2021). On the other hand, it is important that the dentist who can recognize abnormal teeth can convey the right information towards the medical team. Expert reference rare diseases reference centres can assist patients and their treating practitioners in diseases diagnosis and management according to evidence-based information.

Undergraduate, postgraduate and continuous education is important to ensure best management options for rare diseases patients.

Gathering data from large cohorts and pooling information from registries should also lead to a better understanding of the prevalence of AI as a whole or the various AI types and rare diseases. The prevalence stated in the literature from 1:700 to 1:14,000, according to the populations studied may not reflect reality. These data are of importance to facilitate financial undertaking and reimbursement by health authorities of comprehensive lifelong treatments.

Further actions are also needed to update International Classification of Diseases (ICD), The Systematized Nomenclature in Medicine (SNOMED), Orphanet and ontologies (HPO, Orphanet . . .) and to develop guidelines (https://www.has-sante.fr/jcms/p_3284538/fr/20amelogeneses-imparfaites) to ensure precision, personalized oral medicine and its dedication to treatment of individuals suffering from amelogenesis imperfecta.

Witkop's classification was and is still remarkable. It serves as a good basis to understand the nature of enamel defects and as a guide towards its revision as knowledge on genetics and pathophysiology is increasing. JT Wright (2023) in a recent paper discussed these issues and concluded upon the opportunity, thanks to advanced genetics, to "elaborating a more accurate and informative nosology for these conditions in order to improve communication between patients, families, clinicians and researchers".

The revised classification presented here, developed thanks to GenoDENT NGS panel, will hopefully provide a useful tool for accelerating genotype/phenotype causal relations and improved patient outcomes.

Data availability statement

The variants were submitted in ClinVar (https://www.ncbi.nlm.nih.gov/clinvar/), a freely available, public archive of human genetic variants and interpretations of their significance to disease, maintained at the National Institutes of Health (Landrum et al, 2018). Their accession numbers are: SCV003843192, SCV003843249, SCV003843250, SCV003843251, SCV003843254, SCV003843255, SCV003843256, SCV003843257, SCV003843258, SCV003843259, SCV003843870, SCV003843871, SCV003843872, SCV003843873, SCV003843875, SCV003843877, SCV003843878, SCV003843879, SCV003843881, SCV003843887, SCV003843888, SCV003843252, SCV003843247, SCV003843883, SCV003843886, SCV003842949, SCV003843193, SCV003842321, SCV003842323, SCV003842272, SCV003842271, SCV003842273, SCV003842270, SCV003842952, SCV003842312, SCV003842315, SCV003842322, SCV003842325, SCV003842326, SCV003842947, SCV003842948, SCV003842953, SCV003842954, SCV003842955, SCV003842957, SCV003843190, SCV003843191.

Ethics statement

The studies involving human participants were registered at https://clinicaltrials.gov: NCT01746121 and NCT02397824, and with the MESR (French Ministry of Higher Education and Research) Bioethics Commission as a biological collection "Orodental Manifestations of Rare Diseases" DC-2012-1,677 within DC-2012-1,002 and was acknowledged by the CPP (person protection committee) Est IV 11 December 2012. Written informed consent to participate in this study was provided by the participants' legal guardian/next of kin. Written informed consent was obtained from the individual(s), and minor(s)' legal guardian/next of kin, for the publication of any potentially identifiable images or data included in this article.

Author contributions

AB-Z, MK, AJ-A, IMB, M-CM, NK and all participating clinicians (O-Rares consortium: MLD-M, EN, MH, CJ-B, SL, CT, BT-P and other members; ERN Cranio and International consortia: TD, MM, MEA, LQ, SM, PP, NR, BUO and other members) enrolled participating individuals, collected the salivary samples and detailed the individuals' phenotype. TR, VLH, and BG identified the molecular basis of the disease through NGS assays. VL-H, TR, AJA, IMB, and AB-Z analysed the data and wrote the manuscript. AB-Z, TR, AJ-A, and VL-H designed the study and were involved from conception, funding seeking to drafting and critical review of the manuscript. All authors therefore contributed to conception, design, data acquisition, analysis, and interpretation, drafted and critically revised the manuscript. All authors gave final approval and agreed to be accountable for all aspects of the work. All authors gave final approval and agreed to be accountable for all aspects of the work.

Group members of Consortia

O-Rare Consortium

O-Rares Consortium: French Reference and Competence centers, healthcare network for rare oral and dental diseases CRMR/CCMR O-Rares, French Filière "TETECOU" and associated paediatric/genetic teams (Centres de Génétique et Centres de Référence Anomalies du Développement et Syndromes Malformatifs, Filière AnDDI Rares). Edouard Euvrard, Juliette Piard (Centre Hospitalier Universitaire de Besançon; Hôpital Jean Minjoz); Marie José Boileau, Elsa Garot, Didier Lacombe (CHU de Bordeaux—Hôpital Pellegrin); Victorin Ahossi, Laurence Faivre (CHU Dijon, Hôpital François Mitterrand); Caroline Delfosse (CHU de Lille); Klauss Dieterich, Service de génétique Hôpital Couple Enfant, Grenoble; Jean-Pierre Duprez, Jean-Jacques Morrier, Béatrice Thivichon-Prince, Béatrice Richard, Nathalie Guffon-Fouilhoux, Linda Pons, Massimiliano Rossi (Hospices Civils de Lyon, Groupement Centre, Pôle d'Activités Médicales d'Odontologie, Centre de soins Dentaires; Service de génétique, Centre de Référence Anomalies du Développement); Corinne Tardieu, Isabelle Blanchet (APHM, Hôpital de la Timone Enfants, Marseille); Dominique Droz, Magali Hernandez, Bruno Leheup (CHRU de Nancy—Hôpitaux de Brabois); Serena Lopez, Bertand Isidor (CHU de Nantes—Hôtel Dieu); Michèle Muller- Bolla, Clara Joseph-Beaudin (CHU de Nice); Muriel de La Dure Molla, Benjamin Fournier, Ariane Berdal (Hôpital Rothschild, APHP, Paris); Alain Verloes (AP-HP, Hôpital Robert Debré, Paris); Sandrine Marlin (AP-HP, Hôpital Necker Enfants Malades, Paris); Tiphaine Davit-Béal (AP-HP, Paris and CHU de Rennes); Marie Paule Gelle (CHU Reims, Hôpital Maison Blanche, Pôle: Odontologie); Bérénice Doray (CHU de la Réunion Site SUD (Terre Sainte)); Jean-Louis Sixou, Alinoe Lavillaurex, Sylvie Odent (CHU Rennes); Marine Lebrun (CHU Saint-Etienne); Agnès Bloch-Zupan, Isaac Maximiliano Bugueno, François Clauss, Jean-Christophe Dahlet, Jean-Luc Davideau, Olivier Etienne, Bruno Grollemund, Mathilde Huckert, Sophie Jung, Marzena Kawczynski, Adeline Loing, Marie-Cécile Manière, Prune Sadones, Marion Strub, Delphine Wagner, Yves Alembik, Salima El Chehadeh, Hélène Dollfus, Elise Schaefer, Sylvie Soskin, Anne De-Saint-Martin (Hôpitaux Universitaires de Strasbourg); Isabelle Bailleul-Forestier, Emmanuelle Noirrit, Frédéric Vaysse, Nicolas Chassaing (CHU de Toulouse—Hôpital Rangueil); Annick Toutain (CHU de Tours).

European reference network, ERN CRANIO, Consortium

Tatjana Dostalova, Milan Macek Jr, University Hospital Motol and 2nd Faculty of Medicine, Charles University, Prague, Czeck Republic.

International Consortium

Mustapha El Alloussi, Faculty of Dentistry, International University of Rabat,CReSS Centre de recherche en Sciences de la Santé, Morocco; Leeila Qebibo, Unité de génétique médicale et d'oncogénétique, CHU Hassan II, Fez, Morocco; Supawich Morkmued, Patimaporn Pungchanchaikul, Faculty of Dentistry, Khon Kaen University, Khon Kaen, Thailand; Nicole Revencu, Centre de Génétique humaine UCL Cliniques universitaires Saint-Luc, Bruxelles, Belgium; Blanca Urzúa Orellana, Instituto de Investigación en Ciencias Odontológicas, Facultad de Odontología, Universidad de Chile, Chile; Juliane Leonhardt Amar, Switzerland; Zouari Noura, Service de Pédiatrie, Hôpital universitaire Sahloul, Sousse Tunisie.

Funding

This work was financed by and contributed to the actions of the project No. 1.7 "RARENET: a trinational network for education, research and management of complex and rare disorders in the Upper Rhine" co-financed by the European Regional Development Fund (ERDF) of the European Union in the frame-work of the INTERREG V and previously INTERREG IV Upper Rhine program as well as to the ERN (Euro-pean reference network) CRANIO initiative. ABZ is a USIAS 2015 Fellow of the Institute of Advanced Studies (Institut d'Etudes Avancées) de l'Université de Strasbourg, France. This work was also supported by grants from the French Ministry of Health (National Program for Clinical Research, PHRC 2008 N°4266 Amelogenesis imperfecta), the University Hospital of Strasbourg (HUS, API, 2009–2012, "Development of the oral cavity: from gene to clinical phenotype in Human". This work of the Interdisciplinary Thematic Institute IMCBio, as part of the ITI 2021-2028 program of the University of Strasbourg, CNRS and Inserm, was supported by IdEx Unistra (ANR-10-IDEX-0002), and by SFRI-STRAT'US project (ANR 20-SFRI-0012) and EUR IMCBio (ANR-17-EURE-0023) under the framework of the French Investments for the Future Program. This study was possible thanks to the Projet EGENODENT financed by the Fonds d'Intervention Régionale (FIR) of the Agence Régionale de Santé Grand Est (2019-2022). We are grateful to funding provided by Filiére TETECOU and "Pierre Henri et ses amis" patient support groups. This work is the baseline of the HDH data challenge D-IA-GNO-DENT (2021-2023).

Acknowledgments

We are grateful to the families and individuals for their participation and invaluable contribution as well as to the patient support group: Amélogenèse France. We thank deeply health professionals contributing to patient's care (William BACON, Guy BASSONPIERRE, Jacques BELLEHSEN, Michèle BURGET, Emilie CHARPIOT, François CHARTON, Albert COSTI, Gabriel DOMINICI, Arnaud FROEHLY, Pierre HATTENBERGER, Guillaune HENGY, Clarisse HUCHON, Florence JOUANET, Véronique LAULY-SPIELMANN, Fabienne MACHWIRTH, Phillippe NEUMANN, Caroline RAYNAUD, Laurent RIGUET, Christine SCHINI, Jean-Marc SCHWEITZER, Pierre STOCKEL, Pierre WAHL). The computing resources for this work were provided by the BICS and BISTRO bioinformatics platforms in Strasbourg. We thank Patrick REILLY for critical reading and English language improvement of the manuscript

Conflict of interest

The authors declare that the research was conducted in the absence of any commercial or financial relationships that could be construed as a potential conflict of interest.

Publisher's note

All claims expressed in this article are solely those of the authors and do not necessarily represent those of their affiliated organizations, or those of the publisher, the editors and the reviewers. Any product that may be evaluated in this article, or claim that may be made by its manufacturer, is not guaranteed or endorsed by the publisher.

Supplementary material

The Supplementary Material for this article can be found online at: https://www.frontiersin.org/articles/10.3389/fphys.2023.1130175/full#supplementary-material

SUPPLEMENTARY FIGURE S1
Clinical intraoral photographs and panoramic radiographs detailing the phenotype of amelogenesis imperfecta patient for each associated genotype. Isolated AI: A COL17A1; B COL7A1; C LAMA3, LAMB3, LAMC2; D ENAM; E AMELX, F AMBN, G ACP4, H KLK4, MMP20; I WDR72, C4ORF26/ODAPH and SLC24A4; J FAM83H; K DLX3; Syndromic AI: L LTBP3; M FAM20A; N GALNS 2700 and ARHGAP6; O TGFBR2 and SLC13A5; P ROGDI; Q SLC10A7; R CNNM4; S DLX3. **Isolated AI. A *COL17A1*** Hypoplastic pitted amelogenesis imperfecta. Patients present pitted rough enamel with normal hardness. Some patients present a yellowish discoloration with brown extrinsic stains within the pits. Radiographs show normal density but sometimes thinner enamel. Patients 1.1, 1.3, and 1.4 were already described in Prasad et al., 2016 **B *COL7A1*** Hypoplastic amelogenesis imperfecta. Pitted, and thin enamel with yellow-brownish discoloration. Spaced teeth, and incisal and occlusal attrition reflect thinner enamel. **C *LAMA3, LAMB3 and LAMC2*** Hypoplastic amelogenesis imperfecta. Patient 3.1 presents a digenic mutation affecting both COL17A1 and LAMA3 genes. Enamel displays pits arranged in rows and columns. Comparing with COL17A1 mutations related phenotype, the enamel seems more pitted. Both primary and permanent dentition are affected. LAMB3 Patients 4.1 and 4.3 are 8-year-old. Enamel presents pits, and yellowish discoloration more pronounced in incisors. In the radiographs, enamel shows a normal density however unerupted teeth in 4.2, 4.3, 4.4 are clearly dysplastic. Patient 5.1 of 4-year-old, presents a mutation in LAMC2 showing a primary dentition with thin white enamel. Patient 3.1 and 4.1 were already described in Prasad et al. (2016). **D *ENAM*** Hypoplastic autosomal dominant amelogenesis imperfecta.

Thin enamel with white spots, and yellowish discoloration in some cases. In some cases, tooth size might be reduced, and teeth appear slim. Enamel pits, and linear depressions are visible. Patient 6.3 presents agenesis of 16, 26, 36, 46, and stainless-steel crowns covering primary lower molars, with an hypoplastic/hypomature AI. Hypoplastic enamel is visible also on non-erupted teeth in panoramic radiographs. **E *AMELX*** Hypoplastic amelogenesis imperfecta displaying in female individuals a banding pattern (Lyonisation effect) (patients 7.1, 7.3, 7.4, 7.8, 7.11), with vertically ridged teeth, alternating bands of normal and hypoplastic enamel mainly on incisors and spaced yellowish teeth smaller than normal. Male patients (7.2, 7.10) phenotype is more severe with almost no enamel. Patient 7.10 presents a delayed dental eruption. 7.9 is a male displaying a banding pattern AI phenotype similar to females. Further exploration established 7.9 with a XXY karyotype. Radiographs show a thinner with normal density enamel in patients 7.3, 7.6, 7.7, 7.7. In patients 7.2, 7.5, 7.10 there is no obvious contrast between enamel and dentin but enamel is very thin. Hypomature amelogenesis imperfecta (7.5, 7.6, 7.7): Patient 7.7 has agenesis of 12, 15, 22, 28 caused by an additional mutation in WNT10A gene. **F *AMBN*** Hypoplastic amelogenesis imperfecta. Affects both primary and permanent dentition. Patients present rough irregular pitted enamel. The enamel surface acquires a yellowish color with age. Patient 8.1 is 10- year-old, and presents an associated open bite. Individual 8.2 has an end-to-end bite. Patient 8.3 was already described in Prasad et al. (2016). He presents restorations on upper and lower incisors, and first molars. On radiographs, the enamel is almost absent. **G *ACP4*** Hypoplastic amelogenesis imperfecta. Thin enamel with irregular surface, and yellowish discoloration. Patient 9.2 has composite crowns on all her teeth, suggesting a generalized AI. Patient 9.3 presents agenesis of 18, 28 due to a mutation in WNT10A gene. X-rays show a thinner but normal density enamel, long teeth and slim roots. **H *KLK4 and MMP20*** Hypomature amelogenesis imperfecta. Patient 10.1 present a mutation in KLK4 gene showing molars with soft brown enamel, with a lack of radio-contrast between enamel and dentin. Opaque, smooth, and pigmented enamel with incisal and occlusal attrition in primary and permanent dentition is visible in patients with MMP20 variants. i.e., in patient 11.6 and 11.11 both dentition are affected. Thinner enamel than normal detaches easily from the dentin. Patient 11.2 was already published in Prasad et al. (2016) and presents taurodontism. Patients 11.5, 11.6, 11.9, 11.11, were published in Gasse et al. (2017). Patient 11.8 presents stainless steel crowns in molars with pronounced mammelons in permanent incisors. In X-rays, lack of contrast between enamel and dentin is clearly visible. I ***WDR72, C4ORF26/ODAPH, and SLC24A4*** Hypomature amelogenesis imperfecta. Yellow-brownish soft enamel with a mottled appearance that detaches easily from the dentin. Both primary and permanent teeth are affected. Radiographs show a lack of contrast between enamel and dentin. 12.1-4 (WDR72). 13.1 ODAPH. Individual 14.1 (SLC24A4) had primary molars with stainless steel crowns, and an agenesis of 45. Patient 14.2 presented an impacted 13, all permanent incisors were covered by composite veneers, and stainless-steel crowns protected the first lower molars, hypomature enamel is clearly present on other teeth. Radiographs show a lack of contrast between enamel and dentin. Patient 12.2, 13.1 and 14.1 were already published in Prasad et al., 2016. **J *FAM83H*** Hypomineralized amelogenesis imperfecta. Primary and permanent dentitions are affected with soft, colored enamel that detaches easily from the dentin (post eruptive breakdown). Spaced teeth with occlusal and incisal wear giving a conic form in canines are related to secondary enamel loss. Patients complain from high sensitivity. Patients 15.4, 15.6 present slight taurodontism as seen on x-ray. Patients 15.3, 15.5, 15.10 and 15.14 have stainless steel pediatric crowns on primary molars. 15.10, 15.12, 15.13, 15.14 present a clear open bite. Radiographs show no difference in radioopacity between enamel and dentin. **K *DLX3*** Hypoplastic—Hypomature amelogenesis imperfecta with taurodontism. 16.1 has a rough enamel surface, with white and brown spots. A stria as an hypoplastic defect is visible on lower incisal edges. Slight taurodontism is present. 16.2 showed very thin enamel and marked molar laurodontism. 37 is missing. Teeth colour is very "dentin" like as enamel is so thin. 16.3 presented with an hypoplastic clearly hypomature AI with taurodontism (16, 26, 36, 46 and even primary molars), white spots, and brown extrinsic stains. Dental radiographs show normal radiolucency of enamel even if thinner. **Syndromic AI L *LTBP3* (Verloes Bourguignon syndrome, Platyspondyly with AI)** Hypoplastic amelogenesis imperfecta. There is almost no enamel. Delayed teeth eruption. Large pulp chambers, Small, and spaced teeth, with a yellowish color. **M *FAM20A* (Enamel Renal Syndrome)** Hypoplastic amelogenesis imperfecta. There is almost no enamel. Eruption delay and microdontia, with spaced teeth, showing a yellow discoloration, and reduced enamel thickness affecting both dentitions. Patient 18.8 has a prosthetic rehabilitation on upper incisors. The radiographs analysis shows a delayed and impaired eruption of permanent dentition, ankylosed permanent teeth, hyperplasia of follicular sac, intrapulpal calcifications, root formation anomalies. Gingival hyperplasia is clearly visible. **N *GALNS* (Mucopolysaccharidosis type IV) and *ARHGAP6* (Linear skin defects with multiple congenital anomalies 1)** Hypoplastic amelogenesis imperfecta. Patients 19.1 and 19.2 affected with GALNS mutations have teeth with a rough thin enamel surface. On radiograph enamel is thin but with normal radioopacity. Female individual 20.1 has an AMELX deletion displaying a similar phenotype than the isolated form with a banding pattern of normal and hypoplastic enamel, she is affected by MLS syndrome. **O *TGFBR2* (Loeys-Dietz syndrome) and *SLC13A5* (Kohlschutter-Tonz like syndrome)** Hypoplastic amelogenesis imperfect. Patient 22.1 has a TGFBR2 mutation, teeth have a rough surface with pits, the enamel color is opaque yellowish. Panoramic radiograph shows normal enamel radiodensity. In patient 23.1 enamel is thin with opaque yellowish colour, and brown extrinsic stains. SLC13A5 mutation was already reported in Schossig et al. (2017). **P *ROGDI* (Kohlschutter-Tonz syndrome)** Hypomature amelogenesis imperfecta. Individuals present a yellow-brownish discoloration of enamel affecting both primary and permanent dentitions. Stainless steel crowns are covering the molars in patients 24.1 and 24.3. Patient 24.2 was published in Huckert et al., 2016. **Q *SLC10A7* (Short stature, amelogenesis imperfecta, and skeletal dysplasia with scoliosis)** Hypomature/Hypomineralized amelogenesis imperfecta affecting both the 2809 primary and permanent dentition with a yellowish enamel. Patient 25.2 presents stainless steel crowns on upper and lower molars and was already published in Laugel-Haushalter et al. (2019). The radiographs show similar density between dentin and enamel. **R *CNNM4* (Jalili Syndrome)** Hypomineralized amelogenesis imperfecta. 26.1 Extensive post eruptive breakdown and loss of enamel, yellow-brownish coloration with brown spots. High calculus accumulation on rough enamel surface clearly visible in lower incisors. 26.2 Primary dentition affected by AI, the enamel appears thin as it easily wears off from dentin. Stainless still crowns restorations in molars. **S *DLX3* (Tricho-Dento-Osseus syndrome)** Hypoplastic/hypomature? amelogenesis imperfecta with taurodontism. Patient 27.1 and 27.2 are affected by TDO syndrome. Dental radiographs show stronger radiolucency of thin enamel and taurodontism. Patient 27.2 is 6-year-old.

SUPPLEMENTARY FIGURE S2

Variants and corresponding protein domain. A gene is composed of exons represented by vertical lines and the initiation codon (ATG) and stop codon (TGA) are visualized by a black arrow. The variations detected in this study are symbolized by an arrow associated with the patient number in bold if homozygous. Green arrows correspond to variations never described before. Blue arrows correspond to variations already published by our team in Prasad et al. 2016. Orange arrows correspond to variations published by our team in collaborative studies. Gray arrows correspond to variations already known. Triangles symbolize splice variants, circle missenses variants, square nonsense variants, oval small deletion, rectangle small insertion, horizontal line bigger deletion. The shapes are coloured in blue when the individual is a male, in pink when the person is a female and purple for a male with suspected sex chromosome abnormalities. The corresponding protein domains are represented according to the PFAM database. The arrows indicate the localization of the detected variant with predictable protein impact. **A *COL17A1* variations and corresponding protein domain.** The gene transcript NM_000494.4 is made of 56 exons represented by vertical lines. **B *COL7A1* variations and corresponding protein domain.** The gene transcript NM_000094.4 is composed of 119 exons represented by vertical lines. **C *LAMA3* variations and corresponding protein domain. The** gene transcript NM_198129.4 is composed of 75 exons represented by vertical lines. **D *LAMB3* variations and corresponding protein domain.** The gene transcript NM_000228.3 is composed of 23 exons represented by vertical lines.**E *LAMC2* variations and corresponding protein domain.** The gene transcript NM_005562.3 is composed of 23 exons represented by vertical lines.**F *ENAM* variations and corresponding protein domain.** The gene transcript NM_031889.3 is composed of 9 exons represented by vertical lines. **G *AMELX* variations and corresponding protein domain.** The gene transcript NM_182680.1 is compoed of 7 exons represented by vertical lines. **H *AMBN* variations and corresponding protein domain** The gene transcript NM_016519.6 is composed of 13 exons represented by vertical lines.**I *ACP4* variations and corresponding protein domain.** The gene transcript NM_033068.3 is composed of 11 exons represented by vertical lines.**J *KLK4* variations and corresponding protein domain.** The gene transcript NM_004917.4 is composed of 5 exons represented by vertical lines. **K *MMP20* variations and corresponding protein domain.** The gene transcript NM_004771.4 is composed of 10 exons represented by vertical lines. **L *WDR72* variations and corresponding protein domain.** The gene transcript NM_182758.4 is composed of 20 exons represented by vertical lines. **M *ODAPH* variations**

and corresponding protein domain. The gene transcript NM_178497.5 is composed of 2 exons represented by vertical lines. **N *SLC24A4* variations and corresponding protein domain.** The gene transcript NM_153646.4 is composed of 17 exons represented by vertical lines.**O *FAM83H* variations and corresponding protein domain.** The gene transcript NM_198488.5 is composed of 5 exons represented by vertical lines.**P *DLX3* variations and corresponding protein domain.** The gene transcript NM_005220.3 is composed of 3 exons represented by vertical lines.**Q *LTBP3* variations and corresponding protein domain.** The gene transcript NM_001130144.3 is composedd of 28 exons represented by vertical lines.**R *FAM20A* variations and corresponding protein domain.** The gene transcript NM_017565.4 is composed of 11 exons represented by vertical lines.**S *GALNS* variations and corresponding protein domain.** The gene transcript NM_000512.5 is composed of 14 exons represented by vertical lines.**T *SLC13A5* variations and corresponding protein domain.** The gene transcript NM_177550.5 is composed of 12 exons represented by vertical lines.**U *ROGDI* variations and corresponding protein domain.** The gene transcript NM_024589.3 is composedd of 11 exons represented by vertical lines.**V *SLC10A7* variations and corresponding protein domain.** The gene transcript NM_001300842.3 is composed of 13 exons represented by vertical lines.**W *CNNM4* variations and corresponding protein domain.** The gene transcript NM_020184.4 is composed of 7 exons represented by vertical lines.

SUPPLEMENTARY FIGURE S3

Familial segregation of variants by Sanger sequencing (GRCh37). 1. Variant segregation in individual's 1.2 family. Individual 1.2 (I.1) is heterozygous for the variant NM_000494.4(*COL17A1*): c.1745-2A>C; p.?. Her affected sister and her two affected daughters are also heterozygous c.1745-2A>C. 2. Variant segregation in individual's 1.6 family. Individual 1.6 (II.1) is heterozygous for the variant NM_000494.4(*COL17A1*): c.3327del; p.(Pro1110Argfs*21). The variant is inherited from his mother. Phenotype of both parents was not available. 3. Variant segregation in individual's 2.2 family. Individual 2.2 (II.4) and her affected brothers (II.1 and II.3) are heterozygous for the variant NM_000094.4(*COL7A1*): c.3605G>A; p.(Arg1202His). Parental DNA were not available. 4. Variant segregation in individual's 2.3 family. Individual 2.3 (II.1) is heterozygous for the variant NM_000094.4(*COL7A1*): c.3785T>C; p.(Met1262Thr). The variant is inherited from his affected mother (I.2). Father (I.1) DNA and phenotype are not available. 5.Variant segregation in individual's 4.4 family. Individual 4.4 (II.1) is heterozygous for the variant NM_000228.3(*LAMB3*): c.2926del; p.(Val976Trpfs*54). The variant is inherited from his heterozygous father (I.1). 6. Variant segregation in individual's 4.1 family. Individual 4.1 (II.1) is compound heterozygous for the variant NM_000228.3(*LAMB3*): c.124C>T; p.(Arg42*) and c.3490C>T; p.(Arg1164Cys). 7. Variant segregation in individual's 4.2 family. Individual 4.2 (II.1) is compound heterozygous for the variant NM_000228.3(*LAMB3*): c.1288+1G>T; p.? and c.1903C>T; p.(Arg635*). 8. Variant segregation in individual's 5.1 family. Individual 5.1 (II.1) is heterozygous for the variant NM_005562.3(*LAMC2*): c.493C>T; p.(Arg165Cys). The variant is inherited from her mother (I.2). Parental phenotype is not available. 9. Variant segregation in individual's 6.3 family. Individual 6.3 (II.1), her affected sister (II.2) and affected father (I.1) are all heterozygous for the variant NM_031889.3(*ENAM*): c.588+1dup; p.?.10. Variant segregation in individual's 6.6 family. Individual 6.6 (II.1) is heterozygous for the variant NM_031889.3(*ENAM*): c.588+1del; p.?. Father (I.1) DNA and phenotype are unavailable (NA). 11. Variant segregation in individual's 6.1 family. Individual 6.1 (II.1), his affected sister (II.3) and mother (I.2) are heterozygous for the variant NM_031889.3(*ENAM*): c.588+1del; p.?. His second non -affected sister (II.2) and his father (I.1) do not carry the variant. 12. Variant segregation in individual's 6.8 family. Individual 6.8 (II.1), his affected sister (II.2) and mother (I.2) are heterozygous for the variant NM_031889.3(*ENAM*): c.664C>T; p.(Gln222*). His father does not carry the variant and his mother's phenotype is unavailable. 13. Variant segregation in individual's 7.4 family. Individual 7.4 (II.1) is heterozygous for the variant NM_182680.1(*AMELX*): c.47C>A; p.(Ala16Asp). The variant is inherited from her affected hemizygous father (I.1). 14. Variant segregation in individual's 7.8 family. Individual 7.8 (III.1) is heterozygous for the variant NM_182680.1(*AMELX*): c.473del; p.(Pro158Hisfs*31). The variant spread inside affected members of the family. The variant is heterozygous for females II.2 and II.3 and for male III.2 and hemizygous for 7.8's (III.1) grandfather (I.1). Individual 7.9 (III.2) is a male with a XXY karyotype explaining his heterozygous genotype. 15. Variant segregation in individual's 7.10 family. Individual 7.10 (II.1) is hemizygous for the variant NM_182680.1(*AMELX*): c.541del; p.(Leu181Cysfs*8). The variant is inherited from his affected heterozygous mother (I.2).16. Variant segregation in individual's 7.6 family. Individual 7.6 (II.1) and his brother (II.2) are hemizygous for the variant NM_182680.1(*AMELX*): c.208C>A; p.(Pro70Thr). Parental results are not available. 17. Variant segregation in individual's 7.7 family. Individual 7.7 (II.1) is hemizygous for the variant NM_182680.1(*AMELX*): c.208C>A; p.(Pro70Thr). The variant is inherited from mother (I.2) who are heterozygous as his sister (II.2). Their phenotypes are not available. 18. Variant segregation in individual's 8.1 family. Individual 8.1 (II.1) is heterozygous for the two variants NM_016519.6(*AMBN*): c.15+1G>A; p? and c.577G>T; p.(Gly193*). Her mother I.2 is heterozygous only for c.15+1G>A and her father (I.1) result are not available. 19. Reads visualization of individual 10.1 (II.1) highlighting two heterozygous compound variants NM_004917.4(*KLK4*) c.443G>T; p.(Cys148Phe) and c.458G>A; p.(Trp153*). Parental DNA was not available. 20. Variant segregation in individual's 11.1 family. Individual 11.1 (II.1) is heterozygous for the two variants NM_004771.4(*MMP20*): c.105A>C; p.(Arg35=) and c.389C>T; p.(Thr130Ile). The variant c.105A>C is inherited from his heterozygous mother (I.2) and the variant c.389C>T by his heterozygous father (I.1).21. Variant segregation in individual's 11.3 family. Individual 11.3 (II.1) and his sister (II.2) are compound heterozygous for the two variants NM_004771.4(*MMP20*): c.105A>C; p.(Arg35=) and c.954-2A>T; p.?. His mother (I.2) and brother (II.3) are heterozygous only for c.105A>C. His father (I.1) and second brother (II.1) are heterozygous only for c.954-2A>T.22. Variant segregation in individual's 11.4 family. Individual 11.4 (II.1) is compound heterozygous for the two variants NM_004771.4(*MMP20*): c.105A>C; p.(Arg35=) and c.1362C>G; p.(Tyr454*). The variant c.105A>C is inherited from his heterozygous mother (I.2) and the variant c.1362C>G from his heterozygous father (I.1).23. Variant segregation in individual's 11.8 family. Individual 11.8 (II.1) is compound heterozygous for the two variants NM_004771.4(*MMP20*): c.359dup; p.(Asn120Lysfs*9) and c.954-2A>T; p?. The variant c.359dup is inherited from his heterozygous father (I.1) and the variant c.954-2A>T from his heterozygous mother (I.2).24. Variant segregation in individual's 11.11 family. Individual 11.11 (II.1) is compound heterozygous for the two variants NM_004771.4(*MMP20*): c.530G>A; p.(Gly177Glu) and c.954-2A>T; p?. The variant c.530G>A is inherited from her heterozygous mother (I.2) and the variant c.954-2A>T from her heterozygous father (I.1).25. Variant segregation in individual's 11.15 family. Individual 11.15 (II.1) and her affected brother (II.2) are homozygous for NM_004771.4(*MMP20*): c.954-2A>T; p?. Their parents (I.1 and I.2) are heterozygous for c.954-2A>T.26. Reads visualization of individual 12.4 (II.1) with IGV using the paired-end sorting option highlighting two heterozygous compound variants NM_182758.4(*WDR72*): c.2146del; p.(Ala716Profs*10) and c.2388del ; p.(Lys796Asnfs*16). Arrow indicates informative read pairs for allelic relative position of the two variants. Parental DNA was not available.27. Variant segregation in individual's 14.2 family. Individual 14.2 (II.1) and her affected sister (II.2) are homozygous for the variant NM_153646.4(*SLC24A4*): c.1716+5G>A; p.?. Parents' DNA and phenotype are not available.28. Variant segregation in individual's 15.1 family. Individual 15.1 (II.1) is heterozygous for the variant NM_198488.5(*FAM83H*): c.930_939dup; p.(Val314Argfs*14). Her non-affected sister (II.2) do not carry the variant. Parents' DNA and phenotype are not available.29. Variant segregation in individual's 15.2 family. Individual 15.2 (II.1) is heterozygous de novo for the variant NM_198488.5(*FAM83H*): c.973C>T; p.(Arg325*). Her parents do not carry the variant and SNP filiation controls were verified.30. Variant segregation in individual's 15.6 family. Individual 15.6 (II.1) is heterozygous for the variant NM_198488.5(*FAM83H*):c.1309_1311delinsTAG; p.(His437*). This variant is inherited from her father (I.1) also heterozygous. 31Variant segregation in individual's 15.7 family. Individual 15.7 (II.1) is heterozygous de novo for the variant NM_198488.5(*FAM83H*): c.1374C>G; p.(Tyr458*). His parents do not carry the variant and SNP filiation controls were verified.32. Variant segregation in individual's 15.8 family. Individual 15.8 (II.1) is heterozygous de novo for the variant NM_198488.5(*FAM83H*): c.1374C>G; p.(Tyr458*). His parents do not carry the variant and SNP filiation controls were verified.33. Variant segregation in individual's 15.9 family. Individual 15.9 (II.1) is heterozygous for the variant NM_198488.5(*FAM83H*): c.1375C>T; p.(Gln459*). The variant is inherited from her father also heterozygous.34. Variant segregation in individual's 15.10 family. Individual 15.10 (II.1) is heterozygous de novo for the variant NM_198488.5(*FAM83H*): c.1379G>A; p.(Trp460*). Her parents do not carry the variant and SNP filiation controls were verified.35. Variant segregation in individual's 15.12 family. Individual 15.12 (II.1) and his brother (II.3) are heterozygous for the variant NM_198488.5(*FAM83H*): c.1387C>T; p.(Gln463*). Individual 16.12 (II.1) and his brother (II.3) are homozygous for the variant NM_182758.4(*WDR72*): c.1283T>G; p.(Ile428Ser). This variant is inherited from their mother (I.2) also heterozygous.36. Variant segregation in individual's 15.13 family. Individual 15.13 (II.1) and her brother (II.3) are heterozygous for the variant NM_198488.5(*FAM83H*): c.1498C>G; p.(Leu500Val). The variant *FAM83H*: c.1498C>G is not inherited from their mother and she is heterozygous for the *WDR72* c.1283T>G. Their father results are not available.37. Variant segregation in individual's 15.14 family. Individual 15.14 (II.1) is heterozygous for the variant NM_198488.5(*FAM83H*): c.1993C>T; p.(Gln665*). The variant is inherited from her

father (I.1).38. Variant segregation in individual's 17.6 family. Individual 17.6 (II.1) is homozygous for the variant NM_001130144.3(*LTBP3*): c.3629-2A>G; p?. Her parents (I.1 and I.2) are heterozygous for the variant.39. Variant segregation in individual's 18.3 family. Individual 18.3 (II.1) and his sister (II.2) are compound heterozygous for the variants NM_017565.4(*FAM20A*): c.217C>T; p.(Arg73*) and c.727C>T; p.(Arg243*). The mother (I.2) is heterozygous for the variant c.727C>T and the father (I.1) is heterozygous for the variant c.217C>T.40. Variant segregation in individual's 18.5 family. Individual 18.5 (II.1) is compound heterozygous for the variants NM_017565.4(*FAM20A*): c.915_918del; p.(Phe305Leufs*76) and c.928+2T>C; p?. Her mother (I.2) is heterozygous for c.928+2T>C and her father is heterozygous for c.915_918del.41. Variant segregation in individual's 18.6 family. Individual 18.6 (II.1) and his brother (II.2) are compound heterozygous for the variants NM_017565.4(*FAM20A*): c.915_918del; p.(Phe305Leufs*76) and c.1301+5G>A; p?. Their mother (I.2) is heterozygous for c.915_918del and their father is heterozygous for c.1301+5G>A.42. Variant segregation in individual's 18.9 family. Individual 18.9 (II.1) and his brother (II.2) are homozygous for the variant NM_017565.4(FAM20A): c.1369A>T; p.(Lys457*). Their mother (I.2) is heterozygous for c.1369A>T and their father's (I.1) result is not available.43. Variant segregation in individual's 22.1 family. Individual 22.1 (II.1) is heterozygous for the variant NM_003242.6(*TGFBR2*): c.1561T>C; p.(Trp521Arg). His father (I.1) do not carry the variant and his mother's (I.2) DNA is not available.44. Variant segregation in individual's 24.3 family. Individual 24.3 (II.1) is compound heterozygous for the variants NM_2024589.2(*ROGDI*): c.366dup; p.(Ala123Serfs*19) and c.366dup; p.(Tyr134*). The variant c.366dup is inherited from her mother (I.2) and the variant c.366dup from her father (I.1).45. Variant segregation in individual's 25.1 family. Individual 25.1 (II.1) is homozygous for the variant NM_001300842.3(*SLC10A7*): c.269T>G; p.(Leu90Arg). His mother (I.2) and father (I.1) are heterozygous for the variant.46. Variant segregation in individual's 26.1 family. Individual 26.1 (II.1) and her sister (II.2) are homozygous for the variant NM_2020184.1(*CNNM4*): c.586T>C; p.(Ser196Pro). Her mother (I.2) is heterozygous and her father's (I.1) DNA is not available.47. Variant segregation in individual's 27.1 family. Individual 27.1 (II.1), her brother (II.2) and mother (I.2) are heterozygous for the variant NM_005220.3(*DLX3*): c.561_562del; p.(Tyr188Glnfs*13). Her father's (I.1) DNA is not available.48. Variant segregation in individual's 27.2 family. Individual 27.2 (II.1) is heterozygous for the variant NM_005220.3(*DLX3*): c.561_562del; p.(Tyr188Glnfs*13). This variant is inherited from his affected heterozygous father (I.1).

SUPPLEMENTARY TABLE S1
List of gene sequenced in version 6.0 of the GenoDENT panel. Exons and 25 bp in flanking introns of these genes were sequenced using Next Generation Sequencing technics.

SUPPLEMENTARY TABLE S2
List of primer's sequences used for Sanger sequencing.

SUPPLEMENTARY TABLE S3
Variations found in individuals presenting with isolated amelogenesis imperfecta. Variations found in 17 different genes in 85 individuals presenting with isolated amelogenesis imperfecta. One hundred eleven variants were found, 19 variants are of uncertain significance. Variants known and previously published are reported in grey, variants previously reported by the team are represented in salmon, variants published thanks to GenoDENT panel are represented in blue or green, new variants reported for the first time are highlighted in green. Familial segregation is also reported when available and reported as: Family member code (Phenotype code, Genotype code): Fa: father; Mo: mother; S: sibling; D: daughter; So: son; Co: cousin; A: affected; U: unaffected; NA: not available; C: carrier; R: reference genotype.

SUPPLEMENTARY TABLE S4
Key diagnostic clinical signs associated to AI in syndromes.

References

Aaltonen, J., Horelli-Kuitunen, N., Fan, J.-B., Björses, P., Perheentupa, J., Myers, R., et al. (1997). High-resolution physical and transcriptional mapping of the autoimmune polyendocrinopathy–candidiasis–ectodermal dystrophy locus on chromosome 21q22.3 by FISH. *Genome Res.* 7, 820–829. doi:10.1101/gr.7.8.820

Acevedo, A. C., Poulter, J. A., Alves, P. G., de Lima, C. L., Castro, L. C., Yamaguti, P. M., et al. (2015). Variability of systemic and oro-dental phenotype in two families with non-lethal Raine syndrome with FAM20C mutations. *BMC Med. Genet.* 16, 8. doi:10.1186/s12881-015-0154-5

Aïoub, M., Lézot, F., Molla, M., Castaneda, B., Robert, B., Goubin, G., et al. (2007). Msx2 −/− transgenic mice develop compound amelogenesis imperfecta, dentinogenesis imperfecta and periodontal osteopetrosis. *Bone* 41, 851–859. doi:10.1016/j.bone.2007.07.023

Akyol, M. U., Alden, T. D., Amartino, H., Ashworth, J., Belani, K., Berger, K. I., et al. (2019). Recommendations for the management of MPS IVA: Systematic evidence- and consensus-based guidance. *Orphanet J. Rare Dis.* 14, 137. doi:10.1186/s13023-019-1074-9

Aldred, M. J., and Crawford, P. J. (1995). Amelogenesis imperfecta-towards a new classification. *Oral Dis.* 1, 2–5. doi:10.1111/j.1601-0825.1995.tb00148.x

Aldred, M. J., Savarirayan, R., and Crawford, P. J. M. (2003). Amelogenesis imperfecta: A classification and catalogue for the 21st century. *Oral Dis.* 9, 19–23. doi:10.1034/j.1601-0825.2003.00843.x

Alsharif, S., Hindi, S., and Khoja, F. (2018). Unilateral focal dermal hypoplasia (goltz syndrome): Case report and literature review. *Case Rep. Dermatol* 10, 101–109. doi:10.1159/000488521

Ashikov, A., Abu Bakar, N., Wen, X.-Y., Niemeijer, M., Rodrigues Pinto Osorio, G., Brand-Arzamendi, K., et al. (2018). Integrating glycomics and genomics uncovers SLC10A7 as essential factor for bone mineralization by regulating post-Golgi protein transport and glycosylation. *Hum. Mol. Genet.* 27, 3029–3045. doi:10.1093/hmg/ddy213

Aswath, N., Ramakrishnan, S. N., T'eresa, N., and Ramanathan, A. (2018). A novel ROGDI gene mutation is associated with Kohlschutter Tonz syndrome. *Oral Surg. Oral Med. Oral Pathol. Oral Radiol.* 125 (1), e8–e11. doi:10.1016/j.oooo.2017.09.016

Bardet, C., Courson, F., Wu, Y., Khaddam, M., Salmon, B., Ribes, S., et al. (2016). Claudin-16 deficiency impairs tight junction function in ameloblasts, leading to abnormal enamel formation. *J. Bone Min. Res.* 31, 498–513. doi:10.1002/jbmr.2726

Björses, P., Pelto-Huikko, M., Kaukonen, J., Aaltonen, J., Peltonen, L., and Ulmanen, I. (1999). Localization of the APECED protein in distinct nuclear structures. *Hum. Mol. Genet.* 8, 259–266. doi:10.1093/hmg/8.2.259

Bloch-Zupan, A., Bugueno, I. M., and Manière, M. C. (2021). Protocole National de Diagnostic et de Soins (PNDS): Amélogenèses imparfaites. Synthèse à destination du chirurgien-dentiste et du médecin traitant. https://www.has-sante.fr/jcms/p_3284538/fr/.

Bloch-Zupan, A., Sedano, H., and Scully, C. (2012). *Dento/oro/craniofacial anomalies and genetics*. 1st Ed. Amsterdam: Elsevier. 9780124160385.

Brookes, S. J., Barron, M. J., Smith, C. E. L., Poulter, J. A., Mighell, A. J., Inglehearn, C. F., et al. (2017). Amelogenesis imperfecta caused by N-terminal enamelin point mutations in mice and men is driven by endoplasmic reticulum stress. *Hum. Mol. Genet.* 26, 1863–1876. doi:10.1093/hmg/ddx090

Burgeson, R. E., Morris, N. P., Murray, L. W., Duncan, K. G., Keene, D. R., and Sakai, L. Y. (1985). The structure of type VII collagen. *Ann. N. Y. Acad. Sci.* 460, 47–57. doi:10.1111/j.1749-6632.1985.tb51156.x

Burzynski, N. J., Gonzalez, W. E., and Snawder, K. D. (1973). Autosomal dominant smooth hypoplastic amelogenesis imperfecta. Report of a case. *Oral Surg. Oral Med. Oral Pathol.* 36, 818–823. doi:10.1016/0030-4220(73)90333-2

Caciotti, A., Tonin, R., Mort, M., Cooper, D. N., Gasperini, S., Rigoldi, M., et al. (2018). Mis-splicing of the GALNS gene resulting from deep intronic mutations as a cause of Morquio a disease. *BMC Med. Genet.* 19, 183. doi:10.1186/s12881-018-0694-6

Caricasole, A., Ferraro, T., Rimland, J. M., and Terstappen, G. C. (2002). Molecular cloning and initial characterization of the MG61/PORC gene, the human homologue of the Drosophila segment polarity gene Porcupine. *Gene* 288, 147–157. doi:10.1016/S0378-1119(02)00467-5

Celli, J., Duijf, P., Hamel, B. C., Bamshad, M., Kramer, B., Smits, A. P., et al. (1999). Heterozygous germline mutations in the p53 homolog p63 are the cause of EEC syndrome. *Cell.* 99 (2), 143–153. doi:10.1016/s0092-8674(00)81646-3

Collier, P. M., Sauk, J. J., Rosenbloom, S. J., Yuan, Z. A., and Gibson, C. W. (1997). An amelogenin gene defect associated with human X-linked amelogenesis imperfecta. *Arch. Oral Biol.* 42 (3), 235–242. doi:10.1016/s0003-9969(96)00099-4

Crawford, P. J. M., Aldred, M., and Bloch-Zupan, A. (2007). Amelogenesis imperfecta. *Orphanet J. Rare Dis.* 2, 17. doi:10.1186/1750-1172-2-17

Daneshmandpour, Y., Darvish, H., Pashazadeh, F., and Emamalizadeh, B. (2019). Features, genetics and their correlation in Jalili syndrome: A systematic review. *J. Med. Genet.* 56, 358–369. doi:10.1136/jmedgenet-2018-105716

Darling, A. I. (1956). Some observations on amelogenesis imperfecta and calcification of the dental enamel. *Proc. R. Soc. Med.* 49, 759–765. doi:10.1177/003591575604901007

Daubert, D. M., Kelley, J. L., Udod, Y. G., Habor, C., Kleist, C. G., Furman, I. K., et al. (2016). Human enamel thickness and ENAM polymorphism. *Int. J. Oral Sci.* 8, 93–97. doi:10.1038/ijos.2016.1

de La Dure-Molla, M., Fournier, B. P., Manzanares, M. C., Acevedo, A. C., Hennekam, R. C., Friedlander, L., et al. (2019). Elements of morphology: Standard terminology for the teeth and classifying genetic dental disorders. *Am. J. Med. Genet. A* 179, 1913–1981. doi:10.1002/ajmg.a.61316

de la Dure-Molla, M., Quentric, M., Yamaguti, P. M., Acevedo, A.-C., Mighell, A. J., Vikkula, M., et al. (2014). Pathognomonic oral profile of Enamel Renal Syndrome (ERS) caused by recessive FAM20A mutations. *Orphanet J. Rare Dis.* 9, 84. doi:10.1186/1750-1172-9-84

Deidrick, K. K. M., Early, M., Constance, J., Stein, M., and Fete, T. J. (2016). Cognitive and psychological functioning in focal dermal hypoplasia. *Am. J. Med. Genet. C Semin. Med. Genet.* 172, 34–40. doi:10.1002/ajmg.c.31471

Dellow, E. L., Harley, K. E., Unwin, R. J., Wrong, O., Winter, G. B., and Parkins, B. J. (1998). Amelogenesis imperfecta, nephrocalcinosis, and hypocalciuria syndrome in two siblings from a large family with consanguineous parents. *Nephrol. Dial. Transpl.* 13 (12), 3193–3196. doi:10.1093/ndt/13.12.3193

DePristo, M. A., Banks, E., Poplin, R., Garimella, K. V., Maguire, J. R., Hartl, C., et al. (2011). A framework for variation discovery and genotyping using next-generation DNA sequencing data. *Nat. Genet.* 43, 491–498. doi:10.1038/ng.806

Dong, J., Amor, D., Aldred, M. J., Gu, T., Escamilla, M., and MacDougall, M. (2005). DLX3 mutation associated with autosomal dominant amelogenesis imperfecta with taurodontism. *Am. J. Med. Genet. A* 133A, 138–141. doi:10.1002/ajmg.a.30521

Dourado, M. R., Dos Santos, C. R. R., Dumitriu, S., Iancu, D., Albanyan, S., Kleta, R., et al. (2019). Enamel renal syndrome: A novel homozygous FAM20A founder mutation in 5 new Brazilian families. *Eur. J. Med. Genet.* 62 (11), 103561. doi:10.1016/j.ejmg.2018.10.013

Dubail, J., Huber, C., Chantepie, S., Sonntag, S., Tüysüz, B., Mihci, E., et al. (2018). SLC10A7 mutations cause a skeletal dysplasia with amelogenesis imperfecta mediated by GAG biosynthesis defects. *Nat. Commun.* 9, 3087. doi:10.1038/s41467-018-05191-8

Dugan, S. L., Temme, R. T., Olson, R. A., Mikhailov, A., Law, R., Mahmood, H., et al. (2015). New recessive truncating mutation in LTBP3 in a family with oligodontia, short stature, and mitral valve prolapse. *Am. J. Med. Genet. A* 167, 1396–1399. doi:10.1002/ajmg.a.37049

Durmaz, C. D., McGrath, J., Liu, L., and Karabulut, H. G. (2018). A novel PORCN frameshift mutation leading to focal dermal hypoplasia: A case report. *Cytogenet Genome Res.* 154, 119–121. doi:10.1159/000487580

Duverger, O., Ohara, T., Bible, P. W., Zah, A., and Morasso, M. I. (2017). DLX3-Dependent regulation of ion transporters and carbonic anhydrases is crucial for enamel mineralization. *J. Bone Min. Res.* 32, 641–653. doi:10.1002/jbmr.3022

El-Sayed, W., Parry, D. A., Shore, R. C., Ahmed, M., Jafri, H., Rashid, Y., et al. (2009). Mutations in the beta propeller WDR72 cause autosomal-recessive hypomaturation amelogenesis imperfecta. *Am. J. Hum. Genet.* 85, 699–705. doi:10.1016/j.ajhg.2009.09.014

Exome Aggregation ConsortiumLek, M., Karczewski, K. J., Minikel, E. V., Samocha, K. E., Banks, E., et al. (2016). Analysis of protein-coding genetic variation in 60,706 humans. *Nature* 536, 285–291. doi:10.1038/nature19057

Feldmeyer, L., Huber, M., Fellmann, F., Beckmann, J. S., Frenk, E., and Hohl, D. (2006). Confirmation of the origin of NISCH syndrome. *Hum. Mutat.* 27, 408–410. doi:10.1002/humu.20333

Feske, S., Müller, J. M., Graf, D., Kroczek, R. A., Dräger, R., Niemeyer, C., et al. (1996). Severe combined immunodeficiency due to defective binding of the nuclear factor of activated T cells in T lymphocytes of two male siblings. *Eur. J. Immunol.* 26 (9), 2119–2126. doi:10.1002/eji.1830260924

Feske, S. (2010). CRAC channelopathies. *Pflugers Arch.* 460, 417–435. doi:10.1007/s00424-009-0777-5

Flores, E. R., Tsai, K. Y., Crowley, D., Sengupta, S., Yang, A., McKeon, F., et al. (2002). p63 and p73 are required for p53-dependent apoptosis in response to DNA damage. *Nature* 416, 560–564. doi:10.1038/416560a

Fouillen, A., Dos Santos Neves, J., Mary, C., Castonguay, J.-D., Moffatt, P., Baron, C., et al. (2017). Interactions of AMTN, ODAM and SCPPPQ1 proteins of a specialized basal lamina that attaches epithelial cells to tooth mineral. *Sci. Rep.* 7, 46683. doi:10.1038/srep46683

Frick, K. K., Krieger, N. S., Nehrke, K., and Bushinsky, D. A. (2009). Metabolic acidosis increases intracellular calcium in bone cells through activation of the proton receptor OGR1. *J. Bone Min. Res.* 24, 305–313. doi:10.1359/jbmr.081015

Frisk, S., Grandpeix-Guyodo, C., Popovic Silwerfeldt, K., Hjartarson, H. T., Chatzianastassiou, D., Magnusson, I., et al. (2018). Goltz syndrome in males: A clinical report of a male patient carrying a novel PORCN variant and a review of the literature. *Clin. Case Rep.* 6, 2103–2110. doi:10.1002/ccr3.1783

Furukawa, Y., Haruyama, N., Nikaido, M., Nakanishi, M., Ryu, N., Oh-Hora, M., et al. (2017). Stim1 regulates enamel mineralization and ameloblast modulation. *J. Dent. Res.* 96, 1422–1429. doi:10.1177/0022034517719872

Gasse, B., Karayigit, E., Mathieu, E., Jung, S., Garret, A., Huckert, M., et al. (2013). Homozygous and compound heterozygous MMP20 mutations in amelogenesis imperfecta. *J. Dent. Res.* 92, 598–603. doi:10.1177/0022034513488393

Gasse, B., Prasad, M., Delgado, S., Huckert, M., Kawczynski, M., Garret-Bernardin, A., et al. (2017). Evolutionary analysis predicts sensitive positions of MMP20 and validates newly- and previously-identified MMP20 mutations causing amelogenesis imperfecta. *Front. Physiol.* 8, 398. doi:10.3389/fphys.2017.00398

Geoffroy, V., Herenger, Y., Kress, A., Stoetzel, C., Piton, A., Dollfus, H., et al. (2018). AnnotSV: An integrated tool for structural variations annotation. *Bioinformatics* 34, 3572–3574. doi:10.1093/bioinformatics/bty304

Geoffroy, V., Pizot, C., Redin, C., Piton, A., Vasli, N., Stoetzel, C., et al. (2015). VaRank: A simple and powerful tool for ranking genetic variants. *PeerJ* 3, e796. doi:10.7717/peerj.796

Gibson, C. W., Yuan, Z. A., Hall, B., Longenecker, G., Chen, E., Thyagarajan, T., et al. (2001). Amelogenin-deficient mice display an amelogenesis imperfecta phenotype. *J. Biol. Chem.* 276, 31871–31875. doi:10.1074/jbc.M104624200

Goodwin, A. F., Tidyman, W. E., Jheon, A. H., Sharir, A., Zheng, X., Charles, C., et al. (2014). Abnormal Ras signaling in Costello syndrome (CS) negatively regulates enamel formation. *Hum. Mol. Genet.* 23, 682–692. doi:10.1093/hmg/ddt455

Greene, S. R., Yuan, Z. A., Wright, J. T., Amjad, H., Abrams, W. R., Buchanan, J. A., et al. (2002). A new frameshift mutation encoding a truncated amelogenin leads to X-linked amelogenesis imperfecta. *Arch. Oral Biol.* 47, 211–217. doi:10.1016/s0003-9969(01)00111-x

Guerrini, R., Mei, D., Kerti-Szigeti, K., Pepe, S., Koenig, M. K., Von Allmen, G., et al. (2022). Phenotypic and genetic spectrum of ATP6V1A encephalopathy: A disorder of lysosomal homeostasis. *Brain* 145, 2687–2703. doi:10.1093/brain/awac145

Guo, D., Ling, J., Wang, M.-H., She, J.-X., Gu, J., and Wang, C.-Y. (2005). Physical interaction and functional coupling between ACDP4 and the intracellular ion chaperone COX11, an implication of the role of ACDP4 in essential metal ion transport and homeostasis. *Mol. Pain* 1, 15–8069. doi:10.1186/1744-8069-1-15

Guo, D., Regalado, E. S., Pinard, A., Chen, J., Lee, K., Rigelsky, C., et al. (2018). LTBP3 pathogenic variants predispose individuals to thoracic aortic aneurysms and dissections. *Am. J. Hum. Genet.* 102, 706–712. doi:10.1016/j.ajhg.2018.03.002

Happle, R., and Lenz, W. (1977). Striation of bones in focal dermal hypoplasia: Manifestation of functional mosaicism? *Br. J. Dermatol* 96, 133–135. doi:10.1111/j.1365-2133.1977.tb12534.x

Hardies, K., de Kovel, C. G. F., Weckhuysen, S., Asselbergh, B., Geuens, T., Deconinck, T., et al. (2015). Recessive mutations in SLC13A5 result in a loss of citrate transport and cause neonatal epilepsy, developmental delay and teeth hypoplasia. *Brain* 138, 3238–3250. doi:10.1093/brain/awv263

Harrison, S. M., Biesecker, L. G., and Rehm, H. L. (2019). Overview of specifications to the ACMG/AMP variant interpretation guidelines. *Curr. Protoc. Hum. Genet.* 103, e93. doi:10.1002/cphg.93

Hart, P. S., Aldred, M. J., Crawford, P. J. M., Wright, N. J., Hart, T. C., and Wright, J. T. (2002a). Amelogenesis imperfecta phenotype-genotype correlations with two amelogenin gene mutations. *Arch. Oral Biol.* 47, 261–265. doi:10.1016/s0003-9969(02)00003-1

Hart, P. S., Hart, T. C., Michalec, M. D., Ryu, O. H., Simmons, D., Hong, S., et al. (2004). Mutation in kallikrein 4 causes autosomal recessive hypomaturation amelogenesis imperfecta. *J. Med. Genet.* 41, 545–549. doi:10.1136/jmg.2003.017657

Hart, P. S., Hart, T. C., Simmer, J. P., and Wright, J. T. (2002b). A nomenclature for X-linked amelogenesis imperfecta. *Arch. Oral Biol.* 47, 255–260. doi:10.1016/s0003-9969(02)00005-5

Hart, T. C., Hart, P. S., Gorry, M. C., Michalec, M. D., Ryu, O. H., Uygur, C., et al. (2003). Novel ENAM mutation responsible for autosomal recessive amelogenesis imperfecta and localised enamel defects. *J. Med. Genet.* 40 (12), 900–906. doi:10.1136/jmg.40.12.900

Harutunian, K., Figueiredo, R., and Gay-Escoda, C. (2011). Tuberous sclerosis complex with oral manifestations: A case report and literature review. *Med. Oral Patol. Oral Cir. Bucal* 16, e478–e481. doi:10.4317/medoral.16.e478

Hassan, M. Q., Javed, A., Morasso, M. I., Karlin, J., Montecino, M., Wijnen, A. J. van, et al. (2004). Dlx3 transcriptional regulation of osteoblast differentiation: Temporal recruitment of Msx2, Dlx3, and Dlx5 homeodomain proteins to chromatin of the osteocalcin gene. *Mol. Cell. Biol.* 24, 9248–9261. doi:10.1128/MCB.24.20.9248-9261.2004

Heimler, A., Fox, J. E., Hershey, J. E., and Crespi, P. (1991). Sensorineural hearing loss, enamel hypoplasia, and nail abnormalities in sibs. *Am. J. Med. Genet.* 39, 192–195. doi:10.1002/ajmg.1320390214

Holcroft, J., and Ganss, B. (2011). Identification of amelotin- and ODAM-interacting enamel matrix proteins using the yeast two-hybrid system. *Eur. J. Oral Sci.* 119 (1), 301–306. doi:10.1111/j.1600-0722.2011.00870.x

Hollister, D. W., Klein, S. H., De Jager, H. J., Lachman, R. S., and Rimoin, D. L. (1973). The lacrimo-auriculo-dento-digital syndrome. *J. Pediatr.* 83, 438–444. doi:10.1016/s0022-3476(73)80268-9

Hu, J. C.-C., Chan, H.-C., Simmer, S. G., Seymen, F., Richardson, A. S., Hu, Y., et al. (2012a). Amelogenesis imperfecta in two families with defined AMELX deletions in ARHGAP6. *PLoS One* 7, e52052. doi:10.1371/journal.pone.0052052

Hu, J. C.-C., and Yamakoshi, Y. (2003). Enamelin and autosomal dominant amelogenesis imperfecta. *Crit. Rev. Oral Biol. Med.* 14, 387–398. doi:10.1177/154411130301400602

Hu, P., Lacruz, R. S., Smith, C. E., Smith, S. M., Kurtz, I., and Paine, M. L. (2012b). Expression of the sodium/calcium/potassium exchanger, NCKX4, in ameloblasts. *Cells Tissues Organs* 196, 501–509. doi:10.1159/000337493

Huckert, M., Mecili, H., Laugel-Haushalter, V., Stoetzel, C., Muller, J., Flori, E., et al. (2014). A novel mutation in the ROGDI gene in a patient with kohlschütter-tönz syndrome. *Mol. Syndromol.* 5, 293–298. doi:10.1159/000366252

Huckert, M., Stoetzel, C., Morkmued, S., Laugel-Haushalter, V., Geoffroy, V., Muller, J., et al. (2015). Mutations in the latent TGF-beta binding protein 3 (LTBP3) gene cause brachyolmia with amelogenesis imperfecta. *Hum. Mol. Genet.* 24, 3038–3049. doi:10.1093/hmg/ddv053

Inoki, K., Li, Y., Zhu, T., Wu, J., and Guan, K.-L. (2002). TSC2 is phosphorylated and inhibited by Akt and suppresses mTOR signalling. *Nat. Cell. Biol.* 4, 648–657. doi:10.1038/ncb839

Inoue, K., Zhuang, L., and Ganapathy, V. (2002). Human Na+-coupled citrate transporter: Primary structure, genomic organization, and transport function. *Biochem. Biophys. Res. Commun.* 299, 465–471. doi:10.1016/S0006-291X(02)02669-4

Intarak, N., Theerapanon, T., Thaweesapphithak, S., Suphapeetiporn, K., Porntaveetus, T., and Shotelersuk, V. (2019). Genotype-phenotype correlation and expansion of orodental anomalies in LTBP3-related disorders. *Mol. Genet. Genomics* 294, 773–787. doi:10.1007/s00438-019-01547-x

Iwase, M., Kaneko, S., Kim, H., Satta, Y., and Takahata, N. (2007). Evolutionary history of sex-linked mammalian amelogenin genes. *Cells Tissues Organs* 186, 49–59. doi:10.1159/000102680

Jabs, E. W., Müller, U., Li, X., Ma, L., Luo, W., Haworth, I. S., et al. (1993). A mutation in the homeodomain of the human MSX2 gene in a family affected with autosomal dominant craniosynostosis. *Cell.* 75, 443–450. doi:10.1016/0092-8674(93)90379-5

Jagtap, R., Alansari, R., Ruprecht, A., and Kashtwari, D. (2019). Trichodentoosseous syndrome: A case report and review of literature. *BJR Case Rep.* 5, 20190039. doi:10.1259/bjrcr.20190039

Jain, P., Kaul, R., Saha, S., and Sarkar, S. (2017). Tricho-dento-osseous syndrome and precocious eruption. *J. Clin. Exp. Dent.* 9, e494–e497. doi:10.4317/jced.53348

Jalili, I. K., and Smith, N. J. (1988). A progressive cone-rod dystrophy and amelogenesis imperfecta: A new syndrome. *J. Med. Genet.* 25, 738–740. doi:10.1136/jmg.25.11.738

Jani, P., Nguyen, Q. C., Almpani, K., Keyvanfar, C., Mishra, R., Liberton, D., et al. (2020). Severity of oro-dental anomalies in Loeys-Dietz syndrome segregates by gene mutation. *J. Med. Genet.* 57, 699–707. doi:10.1136/jmedgenet-2019-106678

Jaureguiberry, G., De la Dure-Molla, M., Parry, D., Quentric, M., Himmerkus, N., Koike, T., et al. (2012). Nephrocalcinosis (enamel renal syndrome) caused by autosomal recessive FAM20A mutations. *Nephron Physiol.* 122, 1–6. doi:10.1159/000349989

Ji, Y., Li, C., Tian, Y., Gao, Y., Dong, Z., Xiang, L., et al. (2021). Maturation stage enamel defects in Odontogenesis-associated phosphoprotein (Odaph) deficient mice. *Dev. Dyn.* 250, 1505–1517. doi:10.1002/dvdy.336

Kantaputra, P. N., Hamada, T., Kumchai, T., and McGrath, J. A. (2003). Heterozygous mutation in the SAM domain of p63 underlies rapp-hodgkin ectodermal dysplasia. *J. Dent. Res.* 82, 433–437. doi:10.1177/154405910308200606

Katsura, K. A., Horst, J. A., Chandra, D., Le, T. Q., Nakano, Y., Zhang, Y., et al. (2014). WDR72 models of structure and function: A stage-specific regulator of enamel mineralization. *Matrix Biol.* 38, 48–58. doi:10.1016/j.matbio.2014.06.005

Katsura, K., Nakano, Y., Zhang, Y., Shemirani, R., Li, W., and Den Besten, P. (2022). WDR72 regulates vesicle trafficking in ameloblasts. *Sci. Rep.* 12, 2820. doi:10.1038/s41598-022-06751-1

Kausalya, P. J., Amasheh, S., Günzel, D., Wurps, H., Müller, D., Fromm, M., et al. (2006). Disease-associated mutations affect intracellular traffic and paracellular Mg2+ transport function of Claudin-16. *J. Clin. Investig.* 116, 878–891. doi:10.1172/JCI26323

Khandelwal, P., Maheshnull, V., Mathur, V. P., Raut, S., Geetha, T. S., Nair, S., et al. (2021). Phenotypic variability in distal acidification defects associated with WDR72 mutations. *Pediatr. Nephrol.* 36, 881–887. doi:10.1007/s00467-020-04747-5

Kim, J. W., Lee, S. K., Lee, Z. H., Park, J. C., Lee, K. E., Lee, M. H., et al. (2008). FAM83H mutations in families with autosomal-dominant hypocalcified amelogenesis imperfecta. *Am. J. Hum. Genet.* 82, 489–494. doi:10.1016/j.ajhg.2007.09.020

Kim, J. W., Seymen, F., Lin, B. P. J., Kiziltan, B., Gencay, K., Simmer, J. P., et al. (2005a). ENAM mutations in autosomal-dominant amelogenesis imperfecta. *J. Dent. Res.* 84, 278–282. doi:10.1177/154405910508400314

Kim, J.-W., Simmer, J. P., Hart, T. C., Hart, P. S., Ramaswami, M. D., Bartlett, J. D., et al. (2005b). MMP-20 mutation in autosomal recessive pigmented hypomaturation amelogenesis imperfecta. *J. Med. Genet.* 42, 271–275. doi:10.1136/jmg.2004.024505

Kim, J.-W., Zhang, H., Seymen, F., Koruyucu, M., Hu, Y., Kang, J., et al. (2019). Mutations in RELT cause autosomal recessive amelogenesis imperfecta. *Clin. Genet.* 95, 375–383. doi:10.1111/cge.13487

Kim, J. W., Simmer, J. P., Hu, Y. Y., Lin, B. P., Boyd, C., Wright, J. T., et al. (2004). Amelogenin p.M1T and p.W4S mutations underlying hypoplastic X-linked amelogenesis imperfecta. *J. Dent. Res.* 83 (5), 378–383. doi:10.1177/154405910408300505

Kim, Y. J., Abe, Y., Kim, Y.-J., Fujiki, Y., and Kim, J.-W. (2021a). Identification of a homozygous PEX26 mutation in a heimler syndrome patient. *Genes. (Basel).* 12, 646. doi:10.3390/genes12050646

Kim, Y. J., Kang, J., Seymen, F., Koruyucu, M., Gencay, K., Shin, T. J., et al. (2017). Analyses of MMP20 missense mutations in two families with hypomaturation amelogenesis imperfecta. *Front. Physiol.* 8, 229. doi:10.3389/fphys.2017.00229

Kim, Y. J., Kang, J., Seymen, F., Koruyucu, M., Zhang, H., Kasimoglu, Y., et al. (2020). Alteration of exon definition causes amelogenesis imperfecta. *J. Dent. Res.* 99, 410–418. doi:10.1177/0022034520901708

Kim, Y. J., Lee, Y., Zhang, H., Song, J.-S., Hu, J. C.-C., Simmer, J. P., et al. (2021b). A novel de novo SP6 mutation causes severe hypoplastic amelogenesis imperfecta. *Genes. (Basel).* 12, 346. doi:10.3390/genes12030346

Kindelan, S. A., Brook, A. H., Gangemi, L., Lench, N., Wong, F. S., Fearne, J., et al. (2000). Detection of a novel mutation in X-linked amelogenesis imperfecta. *J. Dent. Res.* 79, 1978–1982. doi:10.1177/00220345000790120901

Kiritsi, D., Huilaja, L., Franzke, C.-W., Kokkonen, N., Pazzagli, C., Schwieger-Briel, A., et al. (2015). Junctional epidermolysis bullosa with LAMB3 splice-site mutations. *Acta Derm. Venereol.* 95, 849–851. doi:10.2340/00015555-2073

Kittler, R., Putz, G., Pelletier, L., Poser, I., Heninger, A.-K., Drechsel, D., et al. (2004). An endoribonuclease-prepared siRNA screen in human cells identifies genes essential for cell division. *Nature* 432, 1036–1040. doi:10.1038/nature03159

Kohlschütter, A., Chappuis, D., Meier, C., Tönz, O., Vassella, F., Herschkowitz, N., et al. (1974). Familial epilepsy and yellow teeth a disease of the CNS associated with enamel hypoplasia. *Helv. Paediatr. Acta* 29, 283–294.

Konrad, M., Schaller, A., Seelow, D., Pandey, A. V., Waldegger, S., Lesslauer, A., et al. (2006). Mutations in the tight-junction gene claudin 19 (CLDN19) are associated with renal magnesium wasting, renal failure, and severe ocular involvement. *Am. J. Hum. Genet.* 79, 949–957. doi:10.1086/508617

Kosaki, R., Naito, Y., Torii, C., Takahashi, T., Nakajima, T., and Kosaki, K. (2008). Split hand foot malformation with whorl-like pigmentary pattern: Phenotypic expression of somatic mosaicism for the p63 mutation. *Am. J. Med. Genet. A* 146A, 2574–2577. doi:10.1002/ajmg.a.32415

Kuga, T., Sasaki, M., Mikami, T., Miake, Y., Adachi, J., Shimizu, M., et al. (2016). FAM83H and casein kinase I regulate the organization of the keratin cytoskeleton and formation of desmosomes. *Sci. Rep.* 6, 26557. doi:10.1038/srep26557

Lacruz, R. S., and Feske, S. (2015). Diseases caused by mutations in ORAI1 and STIM1. *Ann. N. Y. Acad. Sci.* 1356, 45–79. doi:10.1111/nyas.12938

Lagerström, M., Dahl, N., Iselius, L., Bäckman, B., and Pettersson, U. (1990). Mapping of the gene for X-linked amelogenesis imperfecta by linkage analysis. *Am. J. Hum. Genet.* 46, 120–125.

Lagerström, M., Dahl, N., Nakahori, Y., Nakagome, Y., Bäckman, B., Landegren, U., et al. (1991). A deletion in the amelogenin gene (AMG) causes X-linked amelogenesis imperfecta (AIH1). *Genomics* 10, 971–975. doi:10.1016/0888-7543(91)90187-j

Landrum, M. J., Lee, J. M., Benson, M., Brown, G. R., Chao, C., Chitipiralla, S., et al. (2018). ClinVar: Improving access to variant interpretations and supporting evidence. *Nucleic Acids Res.* 46 (D1), D1062–D1067. doi:10.1093/nar/gkx1153

Larrègue, M., and Duterque, M. (1975). Letter: Striated osteopathy in focal dermal hypoplasia. *Arch. Dermatol* 111 (10), 1365. doi:10.1001/archderm.1975.01630220129019

Lau, E. C., Mohandas, T. K., Shapiro, L. J., Slavkin, H. C., and Snead, M. L. (1989). Human and mouse amelogenin gene loci are on the sex chromosomes. *Genomics* 4, 162–168. doi:10.1016/0888-7543(89)90295-4

Laugel-Haushalter, V., Bär, S., Schaefer, E., Stoetzel, C., Geoffroy, V., Alembik, Y., et al. (2019). A new SLC10A7 homozygous missense mutation responsible for a milder phenotype of skeletal dysplasia with amelogenesis imperfecta. *Front. Genet.* 10, 504. doi:10.3389/fgene.2019.00504

Lee, K.-E., Ko, J., Le, C. G. T., Shin, T. J., Hyun, H.-K., Lee, S.-H., et al. (2015). Novel LAMB3 mutations cause non-syndromic amelogenesis imperfecta with variable expressivity. *Clin. Genet.* 87, 90–92. doi:10.1111/cge.12340

Lee, N. P. Y., Tong, M. K., Leung, P. P., Chan, V. W., Leung, S., Tam, P.-C., et al. (2006). Kidney claudin-19: Localization in distal tubules and collecting ducts and dysregulation in polycystic renal disease. *FEBS Lett.* 580, 923–931. doi:10.1016/j.febslet.2006.01.019

Lee, S.-K., Seymen, F., Kang, H.-Y., Lee, K.-E., Gencay, K., Tuna, B., et al. (2010). MMP20 hemopexin domain mutation in amelogenesis imperfecta. *J. Dent. Res.* 89, 46–50. doi:10.1177/0022034509352844

Lee, S. K., Lee, K. E., Jeong, T. S., Hwang, Y. H., Kim, S., Hu, J. C., et al. (2011). FAM83H mutations cause ADHCAI and alter intracellular protein localization. *J. Dent. Res.* 90 (3), 377–381. doi:10.1177/0022034510389177

Lench, N. J., and Winter, G. B. (1995). Characterisation of molecular defects in X-linked amelogenesis imperfecta (AIH1). *Hum. Mutat.* 5, 251–259. doi:10.1002/humu.1380050310

Li, X., Yin, W., Pérez-Jurado, L., Bonadio, J., and Francke, U. (1995). Mapping of human and murine genes for latent TGF-β binding protein-2 (LTBP2). *Mamm. Genome* 6, 42–45. doi:10.1007/BF00350892

Liang, T., Hu, Y., Smith, C. E., Richardson, A. S., Zhang, H., Yang, J., et al. (2019). AMBN mutations causing hypoplastic amelogenesis imperfecta and Ambn knockout-

NLS-lacZ knockin mice exhibiting failed amelogenesis and Ambn tissue-specificity. *Mol. Genet. Genomic Med.* 7, e929. doi:10.1002/mgg3.929

Lindemeyer, R. G., Gibson, C. W., and Wright, T. J. (2010). Amelogenesis imperfecta due to a mutation of the enamelin gene: Clinical case with genotype-phenotype correlations. *Pediatr. Dent.* 32 (1), 56–60.

Lu, T., Li, M., Xu, X., Xiong, J., Huang, C., Zhang, X., et al. (2018). Whole exome sequencing identifies an AMBN missense mutation causing severe autosomal-dominant amelogenesis imperfecta and dentin disorders. *Int. J. Oral Sci.* 10, 26. doi:10.1038/s41368-018-0027-9

Ludwig, M.-G., Vanek, M., Guerini, D., Gasser, J. A., Jones, C. E., Junker, U., et al. (2003). Proton-sensing G-protein-coupled receptors. *Nature* 425, 93–98. doi:10.1038/nature01905

Maas, S. M., Jong, T. P. V. M. de, Buss, P., and Hennekam, R. C. M. (1996). EEC syndrome and genitourinary anomalies: An update. *Am. J. Med. Genet.* 63, 472–478. doi:10.1002/(SICI)1096-8628(19960614)63:3<472::AID-AJMG11>3.0

Mårdh, C. K., Bäckman, B., Holmgren, G., Hu, J. C., Simmer, J. P., and Forsman-Semb, K. (2002). A nonsense mutation in the enamelin gene causes local hypoplastic autosomal dominant amelogenesis imperfecta (AIH2). *Hum. Mol. Genet.* 11(9), 1069–1074. doi:10.1093/hmg/11.9.1069

Martelli Júnior, H., dos Santos Neto, P. E., de Aquino, S. N., de Oliveira Santos, C. C., Borges, S. P., Oliveira, E. A., et al. (2011). Amelogenesis imperfecta and nephrocalcinosis syndrome: A case report and review of the literature. *Nephron Physiol.* 118 (3), 62–65. doi:10.1159/000322828

Martino, F., D'Eufemia, P., Pergola, M. S., Finocchiaro, R., Celli, M., Giampà, G., et al. (1992). Child with manifestations of dermotrichic syndrome and ichthyosis follicularis-alopecia photophobia (IFAP) syndrome. *Am. J. Med. Genet.* 44, 233–236. doi:10.1002/ajmg.1320440222

Masunaga, T. (2006). Epidermal basement membrane: Its molecular organization and blistering disorders. *Connect. Tissue Res.* 47, 55–66. doi:10.1080/03008200600584157

Mátyás, G., Arnold, E., Carrel, T., Baumgartner, D., Boileau, C., Berger, W., et al. (2006). Identification and *in silico* analyses of novel TGFBR1 and TGFBR2 mutations in Marfan syndrome-related disorders. *Hum. Mutat.* 27, 760–769. doi:10.1002/humu.20353

McCarl, C. A., Picard, C., Khalil, S., Kawasaki, T., Röther, J., Papolos, A., et al. (2009). ORAI1 deficiency and lack of store-operated Ca2+ entry cause immunodeficiency, myopathy, and ectodermal dysplasia. *J. Allergy Clin. Immunol.* 124, 1311–1318. doi:10.1016/j.jaci.2009.10.007

McGrath, J. A., Li, K., Dunnill, M. G. S., McMillan, J. R., Christiano, A. M., Eady, R. A., et al. (1996). Compound heterozygosity for a dominant Glycine substitution and a recessive internal duplication mutation in the type XVII collagen gene results in junctional epidermolysis bullosa and abnormal dentition. Am. J. Pathol. 148 (6), 1787–1796.

McNally, B. A., Somasundaram, A., Yamashita, M., and Prakriya, M. (2012). Gated regulation of CRAC channel ion selectivity by STIM1. *Nature* 482, 241–245. doi:10.1038/nature10752

Mechaussier, S., Perrault, I., Dollfus, H., Bloch-Zupan, A., Loundon, N., Jonard, L., et al. (2020). Heimler syndrome. *Adv. Exp. Med. Biol.* 1299, 81–87. doi:10.1007/978-3-030-60204-8_7

Mendoza, G., Pemberton, T. J., Lee, K., Scarel-Caminaga, R., Mehrian-Shai, R., Gonzalez-Quevedo, C., et al. (2007). A new locus for autosomal dominant amelogenesis imperfecta on chromosome 8q24.3. *Hum. Genet.* 120, 653–662. doi:10.1007/s00439-006-0246-6

Molla, M., Descroix, V., Aïoub, M., Simon, S., Castañeda, B., Hotton, D., et al. (2010). Enamel protein regulation and dental and periodontal physiopathology in Msx2 mutant mice. *Am. J. Pathol.* 177, 2516–2526. doi:10.2353/ajpath.2010.091224

Montaño, A. M., Tomatsu, S., Brusius, A., Smith, M., and Orii, T. (2008). Growth charts for patients affected with Morquio A disease. *Am. J. Med. Genet. Part A* 146A, 1286–1295. doi:10.1002/ajmg.a.32281

Mory, A., Dagan, E., Illi, B., Duquesnoy, P., Mordechai, S., Shahor, I., et al. (2012). A nonsense mutation in the human homolog of Drosophila rogdi causes kohlschutter–tonz syndrome. *Am. J. Hum. Genet.* 90, 708–714. doi:10.1016/j.ajhg.2012.03.005

Müller, D., Kausalya, P. J., Meij, I. C., and Hunziker, W. (2006). Familial hypomagnesemia with hypercalciuria and nephrocalcinosis: Blocking endocytosis restores surface expression of a novel claudin-16 mutant that lacks the entire C terminal cytosolic tail. *Hum. Mol. Genet.* 15, 1049–1058. doi:10.1093/hmg/ddl020

Muto, T., Miyoshi, K., Horiguchi, T., and Noma, T. (2012). Dissection of morphological and metabolic differentiation of ameloblasts via ectopic SP6 expression. *J. Med. Investig.* 59, 59–68. doi:10.2152/jmi.59.59

Nagamine, K., Peterson, P., Scott, H. S., Kudoh, J., Minoshima, S., Heino, M., et al. (1997). Positional cloning of the APECED gene. *Nat. Genet.* 17, 393–398. doi:10.1038/ng1297-393

Nakamura, T., de Vega, S., Fukumoto, S., Jimenez, L., Unda, F., and Yamada, Y. (2008). Transcription factor epiprofin is essential for tooth morphogenesis by regulating epithelial cell fate and tooth number. *J. Biol. Chem.* 283, 4825–4833. doi:10.1074/jbc.M708388200

Nakamura, T., Unda, F., de-Vega, S., Vilaxa, A., Fukumoto, S., Yamada, K. M., et al. (2004). The Krüppel-like factor epiprofin is expressed by epithelium of developing teeth, hair follicles, and limb buds and promotes cell proliferation. *J. Biol. Chem.* 279, 626–634. doi:10.1074/jbc.M307502200

Nalbant, D., Youn, H., Nalbant, S. I., Sharma, S., Cobos, E., Beale, E. G., et al. (2005). FAM20: An evolutionarily conserved family of secreted proteins expressed in hematopoietic cells. *BMC Genomics* 6, 11. doi:10.1186/1471-2164-6-11

Neuhaus, C., Eisenberger, T., Decker, C., Nagl, S., Blank, C., Pfister, M., et al. (2017). Next-generation sequencing reveals the mutational landscape of clinically diagnosed usher syndrome: Copy number variations, phenocopies, a predominant target for translational read-through, and PEX26 mutated in heimler syndrome. *Mol. Genet. Genomic Med.* 5, 531–552. doi:10.1002/mgg3.312

Nikolopoulos, G., Smith, C. E. L., Brookes, S. J., El-Asrag, M. E., Brown, C. J., Patel, A., et al. (2020). New missense variants in RELT causing hypomineralised amelogenesis imperfecta. *Clin. Genet.* 97, 688–695. doi:10.1111/cge.13721

Nikolopoulos, G., Smith, C. E. L., Poulter, J. A., Murillo, G., Silva, S., Lamb, T., et al. (2021). Spectrum of pathogenic variants and founder effects in amelogenesis imperfecta associated with MMP20. *Hum. Mutat.* 42, 567–576. doi:10.1002/humu.24187

Noor, A., Windpassinger, C., Vitcu, I., Orlic, M., Rafiq, M. A., Khalid, M., et al. (2009). Oligodontia is caused by mutation in LTBP3, the gene encoding latent TGF-beta binding protein 3. *Am. J. Hum. Genet.* 84, 519–523. doi:10.1016/j.ajhg.2009.03.007

Nurbaeva, M. K., Eckstein, M., Concepcion, A. R., Smith, C. E., Srikanth, S., Paine, M. L., et al. (2015). Dental enamel cells express functional SOCE channels. *Sci. Rep.* 5, 15803. doi:10.1038/srep15803

Ogawa, T., Tomatsu, S., Fukuda, S., Yamagishi, A., Rezvi, G. M., Sukegawa, K., et al. (1995). Mucopolysaccharidosis IVA: Screening and identification of mutations of the N-acetylgalactosamine-6-sulfate sulfatase gene. *Hum. Mol. Genet.* 4, 341–349. doi:10.1093/hmg/4.3.341

O'Sullivan, J., Bitu, C. C., Daly, S. B., Urquhart, J. E., Barron, M. J., Bhaskar, S. S., et al. (2011). Whole-Exome sequencing identifies FAM20A mutations as a cause of amelogenesis imperfecta and gingival hyperplasia syndrome. *Am. J. Hum. Genet.* 88, 616–620. doi:10.1016/j.ajhg.2011.04.005

Ozdemir, D., Hart, P. S., Firatli, E., Aren, G., Ryu, O. H., and Hart, T. C. (2005a). Phenotype of ENAM mutations is dosage-dependent. *J. Dent. Res.* 84, 1036–1041. doi:10.1177/154405910508401113

Ozdemir, D., Hart, P. S., Ryu, O. H., Choi, S. J., Ozdemir-Karatas, M., Firatli, E., et al. (2005b). MMP20 active-site mutation in hypomaturation amelogenesis imperfecta. *J. Dent. Res.* 84, 1031–1035. doi:10.1177/154405910508401112

Papagerakis, P., Lin, H.-K., Lee, K. Y., Hu, Y., Simmer, J. P., Bartlett, J. D., et al. (2008). Premature stop codon in MMP20 causing amelogenesis imperfecta. *J. Dent. Res.* 87, 56–59. doi:10.1177/154405910808700109

Parker, N. J., Begley, C. G., Smith, P. J., and Fox, R. M. (1996). Molecular cloning of a novel human gene (D11S4896E) at chromosomal region 11p15.5. *Genomics* 37, 253–256. doi:10.1006/geno.1996.0553

Parry, D. A., Brookes, S. J., Logan, C. V., Poulter, J. A., El-Sayed, W., Al-Bahlani, S., et al. (2012). Mutations in C4orf26, encoding a peptide with *in vitro* hydroxyapatite crystal nucleation and growth activity, cause amelogenesis imperfecta. *Am. J. Hum. Genet.* 91, 565–571. doi:10.1016/j.ajhg.2012.07.020

Parry, D. A., Holmes, T. D., Gamper, N., El-Sayed, W., Hettiarachchi, N. T., Ahmed, M., et al. (2016a). A homozygous STIM1 mutation impairs store-operated calcium entry and natural killer cell effector function without clinical immunodeficiency. *J. Allergy Clin. Immunol.* 137, 955–957. doi:10.1016/j.jaci.2015.08.051

Parry, D. A., Mighell, A. J., El-Sayed, W., Shore, R. C., Jalili, I. K., Dollfus, H., et al. (2009). Mutations in CNNM4 cause Jalili syndrome, consisting of autosomal-recessive cone rod dystrophy and amelogenesis imperfecta. *Am. J. Hum. Genet.* 84, 266–273. doi:10.1016/j.ajhg.2009.01.009

Parry, D. A., Poulter, J. A., Logan, C. V., Brookes, S. J., Jafri, H., Ferguson, C. H., et al. (2013). Identification of mutations in SLC24A4, encoding a potassium-dependent sodium/calcium exchanger, as a cause of amelogenesis imperfecta. *Am. J. Hum. Genet.* 92, 307–312. doi:10.1016/j.ajhg.2013.01.003

Parry, D. A., Smith, C. E. L., El-Sayed, W., Poulter, J. A., Shore, R. C., Logan, C. V., et al. (2016b). Mutations in the pH-sensing G-protein-coupled receptor GPR68 cause amelogenesis imperfecta. *Am. J. Hum. Genet.* 99, 984–990. doi:10.1016/j.ajhg.2016.08.020

Pavlic, A., and Waltimo-Sirén, J. (2009). Clinical and microstructural aberrations of enamel of deciduous and permanent teeth in patients with autoimmune polyendocrinopathy-candidiasis-ectodermal dystrophy. *Arch. Oral Biol.* 54, 658–665. doi:10.1016/j.archoralbio.2009.03.009

Peracha, H., Sawamoto, K., Averill, L., Kecskemethy, H., Theroux, M., Thacker, M., et al. (2018). Molecular genetics and metabolism, special edition: Diagnosis, diagnosis and prognosis of Mucopolysaccharidosis IVA. *Mol. Genet. Metab.* 125, 18–37. doi:10.1016/j.ymgme.2018.05.004

Pereverzev, A., Komarova, S. V., Korcok, J., Armstrong, S., Tremblay, G. B., Dixon, S. J., et al. (2008). Extracellular acidification enhances osteoclast survival through an NFAT-independent, protein kinase C-dependent pathway. *Bone* 42, 150–161. doi:10.1016/j.bone.2007.08.044

Perniola, R. (2018). Twenty years of AIRE. *Front. Immunol.* 9, 98. doi:10.3389/fimmu.2018.00098

Picard, C., McCarl, C. A., Papolos, A., Khalil, S., Lüthy, K., Hivroz, C., et al. (2009). STIM1 mutation associated with a syndrome of immunodeficiency and autoimmunity. *N. Engl. J. Med.* 360, 1971–1980. doi:10.1056/NEJMoa0900082

Plaisancié, J., Collet, C., Pelletier, V., Perdomo, Y., Studer, F., Fradin, M., et al. (2015). MSX2 gene duplication in a patient with eye development defects. *Ophthalmic Genet.* 36, 353–358. doi:10.3109/13816810.2014.886270

Pollak, C., Floy, M., and Say, B. (2003). Sensorineural hearing loss and enamel hypoplasia with subtle nail findings: Another family with heimler's syndrome. *Clin. Dysmorphol.* 12, 55–58. doi:10.1097/00019605-200301000-00010

Polok, B., Escher, P., Ambresin, A., Chouery, E., Bolay, S., Meunier, I., et al. (2009). Mutations in CNNM4 cause recessive cone-rod dystrophy with amelogenesis imperfecta. *Am. J. Hum. Genet.* 84, 259–265. doi:10.1016/j.ajhg.2009.01.006

Portsteffen, H., Beyer, A., Becker, E., Epplen, C., Pawlak, A., Kunau, W.-H., et al. (1997). Human PEX1 is mutated in complementation group 1 of the peroxisome biogenesis disorders. *Nat. Genet.* 17, 449–452. doi:10.1038/ng1297-449

Poulter, J. A., Brookes, S. J., Shore, R. C., Smith, C. E. L., Abi Farraj, L., Kirkham, J., et al. (2014a). A missense mutation in ITGB6 causes pitted hypomineralized amelogenesis imperfecta. *Hum. Mol. Genet.* 23, 2189–2197. doi:10.1093/hmg/ddt616

Poulter, J. A., Murillo, G., Brookes, S. J., Smith, C. E. L., Parry, D. A., Silva, S., et al. (2014b). Deletion of ameloblastin exon 6 is associated with amelogenesis imperfecta. *Hum. Mol. Genet.* 23, 5317–5324. doi:10.1093/hmg/ddu247

Prasad, M. K., Geoffroy, V., Vicaire, S., Jost, B., Dumas, M., Le Gras, S., et al. (2016a). A targeted next-generation sequencing assay for the molecular diagnosis of genetic disorders with orodental involvement. *J. Med. Genet.* 53, 98–110. doi:10.1136/jmedgenet-2015-103302

Prasad, M. K., Laouina, S., El Alloussi, M., Dollfus, H., and Bloch-Zupan, A. (2016b). Amelogenesis imperfecta: 1 family, 2 phenotypes, and 2 mutated genes. *J. Dent. Res.* 95, 1457–1463. doi:10.1177/0022034516663200

Price, J. A., Bowden, D. W., Tim Wright, J., Pettenati, M. J., and Hart, T. C. (1998). Identification of a mutation in DLX3 associated with tricho-dento-osseous (TDO) syndrome. *Hum. Mol. Genet.* 7, 563–569. doi:10.1093/hmg/7.3.563

Raine, J., Winter, R. M., Davey, A., and Tucker, S. M. (1989). Unknown syndrome: Microcephaly, hypoplastic nose, exophthalmos, gum hyperplasia, cleft palate, low set ears, and osteosclerosis. *J. Med. Genet.* 26, 786–788. doi:10.1136/jmg.26.12.786

Rao, S., and Witkop, C. J. (1971). Inherited defects in tooth structure. *Birth Defects Orig. Artic. Ser.* 7, 153–184.

Rapp, R. S., and Hodgkin, W. E. (1968). Anhidrotic ectodermal dysplasia: Autosomal dominant inheritance with palate and lip anomalies. *J. Med. Genet.* 5, 269–272. doi:10.1136/jmg.5.4.269

Ratbi, I., Falkenberg, K. D., Sommen, M., Al Sheqaih, N., Guaoua, S., Vandeweyer, G., et al. (2015). Heimler syndrome is caused by hypomorphic mutations in the peroxisome-biogenesis genes PEX1 and PEX6. *Am. J. Hum. Genet.* 97, 535–545. doi:10.1016/j.ajhg.2015.08.011

Rathi, N., Mattoo, K., and Bhatnagar, S. (2014). Extending the use of a diagnostic occlusal splint to overcome existing lacunae of vertical dimension transfer in full mouth rehabilitation cases. *Am. J. Med. Case Rep.* 2, 291–297. doi:10.12691/ajmcr-2-12-9

Reese, M. G., Eeckman, F. H., Kulp, D., and Haussler, D. (1997). Improved splice site detection in Genie. *J. Comput. Biol.* 4, 311–323. doi:10.1089/cmb.1997.4.311

Reuber, B. E., Germain-Lee, E., Collins, C. S., Morrell, J. C., Ameritunga, R., Moser, H. W., et al. (1997). Mutations in PEX1 are the most common cause of peroxisome biogenesis disorders. *Nat. Genet.* 17, 445–448. doi:10.1038/ng1297-445

Rey, T., Tarabeux, J., Gerard, B., Delbarre, M., Le Béchec, A., Stoetzel, C., et al. (2019). Protocol GenoDENT: Implementation of a new NGS panel for molecular diagnosis of genetic disorders with orodental involvement. *Methods Mol. Biol.* 1922, 407–452. doi:10.1007/978-1-4939-9012-2_36

Richards, S., Aziz, N., Bale, S., Bick, D., Das, S., Gastier-Foster, J., et al. (2015). Standards and guidelines for the interpretation of sequence variants: A joint consensus recommendation of the American College of medical genetics and genomics and the association for molecular pathology. *Genet. Med.* 17, 405–424. doi:10.1038/gim.2015.30

Rinne, T., Hamel, B., van Bokhoven, H., and Brunner, H. G. (2006). Pattern of p63 mutations and their phenotypes-update. *Am. J. Med. Genet. A* 140, 1396–1406. doi:10.1002/ajmg.a.31271

Robinson, C. (2014). Enamel maturation: A brief background with implications for some enamel dysplasias. *Front. Physiol.* 5, 388. doi:10.3389/fphys.2014.00388

Rølling, I., Clausen, N., Nyvad, B., and Sindet-Pedersen, S. (1999). Dental findings in three siblings with Morquio's syndrome. *Int. J. Paediatr. Dent.* 9, 219–224. doi:10.1046/j.1365-263x.1999.00127.x

Ruspita, I., Das, P., Xia, Y., Kelangi, S., Miyoshi, K., Noma, T., et al. (2020). An msx2-sp6-follistatin pathway operates during late stages of tooth development to control amelogenesis. *Front. Physiol.* 11, 582610. doi:10.3389/fphys.2020.582610

Sabbioni, S., Veronese, A., Trubia, M., Taramelli, R., Barbanti-Brodano, G., Croce, C. M., et al. (1999). Exon structure and promoter identification of STIM1 (alias GOK), a human gene causing growth arrest of the human tumor cell lines G401 and RD. *Cytogenet Cellll Genet.* 86, 214–218. doi:10.1159/000015341

Sawamoto, K., Álvarez González, J. V., Piechnik, M., Otero, F. J., Couce, M. L., Suzuki, Y., et al. (2020). Mucopolysaccharidosis IVA: Diagnosis, treatment, and management. *Int. J. Mol. Sci.* 21, 1517. doi:10.3390/ijms21041517

Scherer, S. W., Heng, H. H. Q., Robinson, G. W., Mahon, K. A., Evans, J. P., and Tsui, L.-C. (1995). Assignment of the human homolog of mouse Dlx3 to Chromosome 17q21.3-q22 by analysis of somatic cell hybrids and fluorescence *in situ* hybridization. *Mamm. Genome* 6, 310–311. doi:10.1007/BF00352432

Schossig, A., Bloch-Zupan, A., Lussi, A., Wolf, N. I., Raskin, S., Cohen, M., et al. (2017). SLC13A5 is the second gene associated with Kohlschütter-Tönz syndrome. *J. Med. Genet.* 54, 54–62. doi:10.1136/jmedgenet-2016-103988

Schossig, A., Wolf, N. I., Fischer, C., Fischer, M., Stocker, G., Pabinger, S., et al. (2012). Mutations in ROGDI cause kohlschütter-tönz syndrome. *Am. J. Hum. Genet.* 90, 701–707. doi:10.1016/j.ajhg.2012.02.012

Schulze, C. (1970). "Developmental abnormalities of the teeth and jaws," in *Thoma's oral pathology*. Editors R. J. Gorlin and H. M. Goldman (St Louis: C. V. Mosby), 112–122.

Sewerin, S., Piontek, J., Schönauer, R., Grunewald, S., Rauch, A., Neuber, S., et al. (2022). Defective claudin-10 causes a novel variation of HELIX syndrome through compromised tight junction strand assembly. *Genes. Dis.* 9, 1301–1314. doi:10.1016/j.gendis.2021.06.006

Seymen, F., Kim, Y. J., Lee, Y. J., Kang, J., Kim, T. H., Choi, H., et al. (2016). Recessive mutations in ACPT, encoding testicular acid phosphatase, cause hypoplastic amelogenesis imperfecta. *Am. J. Hum. Genet.* 99, 1199–1205. doi:10.1016/j.ajhg.2016.09.018

Seymen, F., Lee, K.-E., Koruyucu, M., Gencay, K., Bayram, M., Tuna, E. B., et al. (2014a). ENAM mutations with incomplete penetrance. *J. Dent. Res.* 93, 988–992. doi:10.1177/0022034514548222

Seymen, F., Lee, K.-E., Koruyucu, M., Gencay, K., Bayram, M., Tuna, E. B., et al. (2015a). Novel ITGB6 mutation in autosomal recessive amelogenesis imperfecta. *Oral Dis.* 21, 456–461. doi:10.1111/odi.12303

Seymen, F., Lee, K.-E., Tran Le, C. G., Yildirim, M., Gencay, K., Lee, Z. H., et al. (2014b). Exonal deletion of SLC24A4 causes hypomaturation amelogenesis imperfecta. *J. Dent. Res.* 93, 366–370. doi:10.1177/0022034514523786

Seymen, F., Park, J.-C., Lee, K.-E., Lee, H.-K., Lee, D.-S., Koruyucu, M., et al. (2015b). Novel MMP20 and KLK4 mutations in amelogenesis imperfecta. *J. Dent. Res.* 94, 1063–1069. doi:10.1177/0022034515590569

Seymen, F., Zhang, H., Kasimoglu, Y., Koruyucu, M., Simmer, J. P., Hu, J. C.-C., et al. (2021). Novel mutations in GPR68 and SLC24A4 cause hypomaturation amelogenesis imperfecta. *J. Pers. Med.* 12, 13. doi:10.3390/jpm12010013

Shaheen, R., Ansari, S., Alshammari, M. J., Alkhalidi, H., Alrukban, H., Eyaid, W., et al. (2013). A novel syndrome of hypohidrosis and intellectual disability is linked to COG6 deficiency. *J. Med. Genet.* 50, 431–436. doi:10.1136/jmedgenet-2013-101527

Shapiro, M. B., and Senapathy, P. (1987). RNA splice junctions of different classes of eukaryotes: Sequence statistics and functional implications in gene expression. *Nucleic Acids Res.* 15, 7155–7174. doi:10.1093/nar/15.17.7155

Shore, R. C., Bäckman, B., Elcock, C., Brook, A. H., Brookes, S. J., and Kirkham, J. (2010). The structure and composition of deciduous enamel affected by local hypoplastic autosomal dominant amelogenesis imperfecta resulting from an ENAM mutation. *Cells Tissues Organs* 191, 301–306. doi:10.1159/000258703

Simmer, J. P., Hu, J. C.-C., Hu, Y., Zhang, S., Liang, T., Wang, S.-K., et al. (2021). A genetic model for the secretory stage of dental enamel formation. *J. Struct. Biol.* 213, 107805. doi:10.1016/j.jsb.2021.107805

Simmer, J. P., Hu, Y., Lertlam, R., Yamakoshi, Y., and Hu, J. C.-C. (2009). Hypomaturation enamel defects in Klk4 knockout/LacZ knockin mice. *J. Biol. Chem.* 284, 19110–19121. doi:10.1074/jbc.M109.013623

Simon, D. B., Lu, Y., Choate, K. A., Velazquez, H., Al-Sabban, E., Praga, M., et al. (1999). Paracellin-1, a renal tight junction protein required for paracellular Mg2+ resorption. *Science* 285, 103–106. doi:10.1126/science.285.5424.103

Simpson, M. A., Hsu, R., Keir, L. S., Hao, J., Sivapalan, G., Ernst, L. M., et al. (2007). Mutations in FAM20C are associated with lethal osteosclerotic bone dysplasia (Raine syndrome), highlighting a crucial molecule in bone development. *Am. J. Hum. Genet.* 81, 906–912. doi:10.1086/522240

Simpson, M. A., Scheuerle, A., Hurst, J., Patton, M. A., Stewart, H., and Crosby, A. H. (2009). Mutations in FAM20C also identified in non-lethal osteosclerotic bone dysplasia. *Clin. Genet.* 75, 271–276. doi:10.1111/j.1399-0004.2008.01118.x

Slegtenhorst, M. van, Hoogt, R. de, Hermans, C., Nellist, M., Janssen, B., Verhoef, S., et al. (1997). Identification of the tuberous sclerosis gene TSC1 on chromosome 9q34. *Science* 277, 805–808. doi:10.1126/science.277.5327.805

Smith, C. E. L., Kirkham, J., Day, P. F., Soldani, F., McDerra, E. J., Poulter, J. A., et al. (2017a). A fourth KLK4 mutation is associated with enamel hypomineralisation and structural abnormalities. *Front. Physiol.* 8, 333. doi:10.3389/fphys.2017.00333

Smith, C. E. L., Murillo, G., Brookes, S. J., Poulter, J. A., Silva, S., Kirkham, J., et al. (2016). Deletion of amelotin exons 3-6 is associated with amelogenesis imperfecta. *Hum. Mol. Genet.* 25, 3578–3587. doi:10.1093/hmg/ddw203

Smith, C. E. L., Poulter, J. A., Brookes, S. J., Murillo, G., Silva, S., Brown, C. J., et al. (2019). Phenotype and variant spectrum in the LAMB3 form of amelogenesis imperfecta. *J. Dent. Res.* 98, 698–704. doi:10.1177/0022034519835205

Smith, C. E. L., Whitehouse, L. L. E., Poulter, J. A., Wilkinson Hewitt, L., Nadat, F., Jackson, B. R., et al. (2020). A missense variant in specificity protein 6 (SP6) is associated with amelogenesis imperfecta. *Hum. Mol. Genet.* 29, 1417–1425. doi:10.1093/hmg/ddaa041

Smith, C. E., Whitehouse, L. L., Poulter, J. A., Brookes, S. J., Day, P. F., Soldani, F., et al. (2017b). Defects in the acid phosphatase ACPT cause recessive hypoplastic amelogenesis imperfecta. *Eur. J. Hum. Genet.* 25, 1015–1019. doi:10.1038/ejhg.2017.79

Spedicati, B., Cocca, M., Palmisano, R., Faletra, F., Barbieri, C., Francescatto, M., et al. (2021). Natural human knockouts and mendelian disorders: Deep phenotyping in Italian isolates. *Eur. J. Hum. Genet.* 29, 1272–1281. doi:10.1038/s41431-021-00850-9

Sripathomsawat, W., Tanpaiboon, P., Heering, J., Dötsch, V., Hennekam, R. C. M., and Kantaputra, P. (2011). Phenotypic analysis of Arg227 mutations of TP63 with emphasis on dental phenotype and micturition difficulties in EEC syndrome. *Am J M Genet A* 155, 228–232. doi:10.1002/ajmg.a.33768

Su, X., Chakravarti, D., Cho, M. S., Liu, L., Gi, Y. J., Lin, Y.-L., et al. (2010). TAp63 suppresses metastasis through coordinate regulation of Dicer and miRNAs. *Nature* 467, 986–990. doi:10.1038/nature09459

Suh, J., Choi, H. S., Kwon, A., Chae, H. W., Lee, J.-S., and Kim, H.-S. (2019). A novel compound heterozygous mutation of the AIRE gene in a patient with autoimmune polyendocrine syndrome type 1. *Ann. Pediatr. Endocrinol. Metab.* 24, 248–252. doi:10.6065/apem.2019.24.4.248

Sun, S., Yu, M., Fan, Z., Yeh, L.-T., Feng, H., Liu, H., et al. (2019). DLX3 regulates osteogenic differentiation of bone marrow mesenchymal stem cells via Wnt/β-catenin pathway mediated histone methylation of DKK4. *Biochem. Biophys. Res. Commun.* 516, 171–176. doi:10.1016/j.bbrc.2019.06.029

Sutton, V. R., and van Bokhoven, H. (2010). "TP63-Related disorders," in *GeneReviews® [Internet]*. Editors M. P. Adam, D. B. Everman, G. M. Mirzaa, R. A. Pagon, S. E. Wallace, L. J. H. Bean, et al. (Seattle (WA): University of Washington, Seattle), 1993–2022.

Tabata, M. J., Matsumura, T., Liu, J. G., Wakisaka, S., and Kurisu, K. (1996). Expression of cytokeratin 14 in ameloblast-lineage cells of the developing tooth of rat, both *in vivo* and *in vitro*. *Arch. Oral Biol.* 41, 1019–1027. doi:10.1016/s0003-9969(96)00087-8

Tanaka, A., Weinel, S., Nagy, N., O'Driscoll, M., Lai-Cheong, J. E., Kulp-Shorten, C. L., et al. (2012). Germline mutation in ATR in autosomal dominant oropharyngeal cancer syndrome. *Am. J. Hum. Genet.* 90, 511–517. doi:10.1016/j.ajhg.2012.01.007

Tanimoto, K., Le, T., Zhu, L., Witkowska, H. E., Robinson, S., Hall, S., et al. (2008). Reduced amelogenin-MMP20 interactions in amelogenesis imperfecta. *J. Dent. Res.* 87, 451–455. doi:10.1177/154405910808700516

The 1000 Geno; mes Project ConsortiumGibbs, R. A., Boerwinkle, E., Doddapaneni, H., Han, Y., Korchina, V., et al. (2015). A global reference for human genetic variation. *Nature* 526, 68–74. doi:10.1038/nature15393

Tomura, H., Wang, J. Q., Liu, J. P., Komachi, M., Damirin, A., Mogi, C., et al. (2008). Cyclooxygenase-2 expression and prostaglandin E2 production in response to acidic pH through OGR1 in a human osteoblastic cell line. *J. Bone Min. Res.* 23, 1129–1139. doi:10.1359/jbmr.080236

Torres, L. H. S., de-Azevedo-Vaz, S. L., Barroso, D. R. C., Silva, D. N., Velloso, T. R. G., and de Barros, L. A. P. (2018). Enamel-renal-syndrome: Case report. *Spec. Care Dent.* 38 (3), 172–175. doi:10.1111/scd.12288

Toyosawa, S., Fujiwara, T., Ooshima, T., Shintani, S., Sato, A., Ogawa, Y., et al. (2000). Cloning and characterization of the human ameloblastin gene. *Gene* 256, 1–11. doi:10.1016/S0378-1119(00)00379-6

Tucci, A., Kara, E., Schossig, A., Wolf, N. I., Plagnol, V., Fawcett, K., et al. (2013). Kohlschütter-Tönz syndrome: Mutations in ROGDI and evidence of genetic heterogeneity. *Hum. Mutat.* 34 (2), 296–300. doi:10.1002/humu.22241

Utami, T. W., Miyoshi, K., Hagita, H., Yanuaryska, R. D., Horiguchi, T., and Noma, T. (2011). Possible linkage of SP6 transcriptional activity with amelogenesis by protein stabilization. *J. Biomed. Biotechnol.* 2011, 320987. doi:10.1155/2011/320987

Vahidnezhad, H., Youssefian, L., Zeinali, S., Saeidian, A. H., Sotoudeh, S., Mozafari, N., et al. (2017). Dystrophic epidermolysis bullosa: COL7A1 mutation landscape in a multi-ethnic cohort of 152 extended families with high degree of customary consanguineous marriages. *J. Investig. Dermatol* 137, 660–669. doi:10.1016/j.jid.2016.10.023

van Bakel, I., Sepp, T., Ward, S., Yates, J. R. W., and Green, A. J. (1997). Mutations in the TSC2 gene: Analysis of the complete coding sequence using the protein truncation test (PTT). *Hum. Mol. Genet.* 6, 1409–1414. doi:10.1093/hmg/6.9.1409

Vieira, G. H., Rodriguez, J. D., Carmona-Mora, P., Cao, L., Gamba, B. F., Carvalho, D. R., et al. (2012). Detection of classical 17p11.2 deletions, an atypical deletion and RAI1 alterations in patients with features suggestive of Smith-Magenis syndrome. *Eur. J. Hum. Genet.* 20, 148–154. doi:10.1038/ejhg.2011.167

Vig, M., Peinelt, C., Beck, A., Koomoa, D. L., Rabah, D., Koblan-Huberson, M., et al. (2006). CRACM1 is a plasma membrane protein essential for store-operated Ca2+ entry. *Science* 312, 1220–1223. doi:10.1126/science.1127883

Wang, S. K., Choi, M., Richardson, A. S., Reid, B. M., Lin, B. P., Wang, S. J., et al. (2014b). ITGB6 loss-of-function mutations cause autosomal recessive amelogenesis imperfecta. *Hum. Mol. Genet.* 23, 2157–2163. doi:10.1093/hmg/ddt611

Wang, S.-K., Hu, Y., Simmer, J. P., Seymen, F., Estrella, N. M. R. P., Pal, S., et al. (2013). Novel KLK4 and MMP20 mutations discovered by whole-exome sequencing. *J. Dent. Res.* 92, 266–271. doi:10.1177/0022034513475626

Wang, S.-K., Zhang, H., Chavez, M. B., Hu, Y., Seymen, F., Koruyucu, M., et al. (2020). Dental malformations associated with biallelic MMP20 mutations. *Mol. Genet. Genomic Med.* 8, e1307. doi:10.1002/mgg3.1307

Wang, S., Choi, M., Richardson, A. S., Reid, B. M., Seymen, F., Yildirim, M., et al. (2014a). STIM1 and SLC24A4 are critical for enamel maturation. *J. Dent. Res.* 93, 94S-100S–100S. doi:10.1177/0022034514527971

Wang, X., Zhao, Y., Yang, Y., and Qin, M. (2015). Novel ENAM and LAMB3 mutations in Chinese families with hypoplastic amelogenesis imperfecta. *PLoS One* 10, e0116514. doi:10.1371/journal.pone.0116514

Wazen, R. M., Viegas-Costa, L. C., Fouillen, A., Moffatt, P., Adair-Kirk, T. L., Senior, R. M., et al. (2016). Laminin γ2 knockout mice rescued with the human protein exhibit enamel maturation defects. *Matrix Biol.* 52 (54), 207–218. doi:10.1016/j.matbio.2016.03.002

Weinmann, J. P., Svoboda, J. F., and Woods, R. W. (1945). Hereditary disturbances of enamel formation and Calcification**From the research department, loyola university, school of Dentistry, chicago College of dental surgery, and the department of health and welfare, bureau of health, division of dental health, augusta, Maine. *J. Am. Dent. Assoc.* 32, 397–418. doi:10.14219/jada.archive.1945.0063

Whitehouse, L. L. E., Smith, C. E. L., Poulter, J. A., Brown, C. J., Patel, A., Lamb, T., et al. (2019). Novel DLX3 variants in amelogenesis imperfecta with attenuated tricho-dento-osseous syndrome. *Oral Dis.* 25, 182–191. doi:10.1111/odi.12955

Wimalarathna, A., Abeyasinghe, U., Jayasooriya, P., and Herath, C. (2020). Amelogenesis imperfecta: A literature review based guide to diagnosis and management. *J. M. Dent.* 10, 94–101. doi:10.46875/jmd.v10i3.532

Witkop, C. J. (1988). Amelogenesis imperfecta, dentinogenesis imperfecta and dentin dysplasia revisited: Problems in classification. *J. Oral Pathol.* 17, 547–553. doi:10.1111/j.1600-0714.1988.tb01332.x

Witkop, C. J. (1957). Hereditary defects in enamel and dentin. *Acta Genet. Stat. Med.* 7, 236–239. doi:10.1159/000150974

Witkop, C. J. (1971). Manifestations of genetic diseases in the human pulp. *Oral Surg. Oral Med. Oral Pathol.* 32, 278–316. doi:10.1016/0030-4220(71)90232-5

Witkop, C. J., and Sauk, J. J. (1976). "Heritable defects of enamel," in *Oral facial genetics*. Editors R. Stewart and G. Prescott (St. Louis: C.V. Mosby Company), 151–226.

Wright, J. T., Carrion, I. A., and Morris, C. (2015). The molecular basis of hereditary enamel defects in humans. *J. Dent. Res.* 94, 52–61. doi:10.1177/0022034514556708

Wright, J. T. (2023). Enamel phenotypes: Genetic and environmental determinants. *Genes.* 14, 545. doi:10.3390/genes14030545

Wright, J. T., Puranik, C. P., and Farrington, F. (2016). Oral phenotype and variation in focal dermal hypoplasia. *Am. J. Med. Genet. C Semin. Med. Genet.* 172C, 52–58. doi:10.1002/ajmg.c.31478

Yamada, N., Fukuda, S., Tomatsu, S., Muller, V., Hopwood, J. J., Nelson, J., et al. (1998). Molecular heterogeneity in mucopolysaccharidosis IVA in Australia and Northern Ireland: Nine novel mutations including T312S, a common allele that confers a mild phenotype. *Hum. Mutat.* 11 (3), 202–208. doi:10.1002/(SICI)1098-1004(1998)11:3<202::AID-HUMU4>3.0.CO;2-J

Yamaguti, P. M., Neves, F. de A. R., Hotton, D., Bardet, C., Dure Molla, M. de L., Castro, L. C., et al. (2017). Amelogenesis imperfecta in familial hypomagnesaemia and hypercalciuria with nephrocalcinosis caused by CLDN19 gene mutations. *J. Med. Genet.* 54, 26–37. doi:10.1136/jmedgenet-2016-103956

Yamazaki, D., Funato, Y., Miura, J., Sato, S., Toyosawa, S., Furutani, K., et al. (2013). Basolateral Mg2+ extrusion via CNNM4 mediates transcellular Mg2+ transport across epithelia: A mouse model. *PLoS Genet.* 9, e1003983. doi:10.1371/journal.pgen.1003983

Yang, A., Schweitzer, R., Sun, D., Kaghad, M., Walker, N., Bronson, R. T., et al. (1999). p63 is essential for regenerative proliferation in limb, craniofacial and epithelial development. *Nature* 398, 714–718. doi:10.1038/19539

Yang, M., Mailhot, G., Birnbaum, M. J., MacKay, C. A., Mason-Savas, A., and Odgren, P. R. (2006). Expression of and role for ovarian cancer G protein-coupled receptor 1 (OGR1) during osteoclastogenesis. *J. Biol. Chem.* 281, 23598–23605. doi:10.1074/jbc.M602191200

Yenamandra, V. K., Vellarikkal, S. K., Chowdhury, M. R., Jayarajan, R., Verma, A., Scaria, V., et al. (2018). Genotype-phenotype correlations of dystrophic epidermolysis

bullosa in India: Experience from a tertiary care centre. *Acta Derm. Venereol.* 98, 873–879. doi:10.2340/00015555-2929

Yeo, G., and Burge, C. B. (2004). Maximum entropy modeling of short sequence motifs with applications to RNA splicing signals. *J. Comput. Biol.* 11, 377–394. doi:10.1089/1066527041410418

Yuan, J. P., Zeng, W., Huang, G. N., Worley, P. F., and Muallem, S. (2007). STIM1 heteromultimerizes TRPC channels to determine their function as store-operated channels. *Nat. Cell. Biol.* 9, 636–645. doi:10.1038/ncb1590

Yuen, W. Y., Pasmooij, A. M. G., Stellingsma, C., and Jonkman, M. F. (2012). Enamel defects in carriers of a novel LAMA3 mutation underlying epidermolysis bullosa. *Acta Derm. Venereol.* 92, 695–696. doi:10.2340/00015555-1341

Zanetti, A., D'Avanzo, F., AlSayed, M., Brusius-Facchin, A. C., Chien, Y. H., Giugliani, R., et al. (2021). Molecular basis of mucopolysaccharidosis IVA (Morquio A syndrome): A review and classification of GALNS gene variants and reporting of 68 novel variants. *Hum. Mutat.* 42 (11), 1384–1398. doi:10.1002/humu.24270

Zhang, H., Koruyucu, M., Seymen, F., Kasimoglu, Y., Kim, J. W., Tinawi, S., et al. (2019). WDR72 mutations associated with amelogenesis imperfecta and acidosis. *J. Dent. Res.* 98, 541–548. doi:10.1177/0022034518824571

Zhang, Z., Suzuki, Y., Shimozawa, N., Fukuda, S., Imamura, A., Tsukamoto, T., et al. (1999). Genomic structure and identification of 11 novel mutations of the PEX6 (peroxisome assembly factor-2) gene in patients with peroxisome biogenesis disorders. *Hum. Mutat.* 13, 487–496. doi:10.1002/(SICI)1098-1004(1999)13:6<487::AID-HUMU9>3.0.CO;2-T

Zoncu, R., Bar-Peled, L., Efeyan, A., Wang, S., Sancak, Y., and Sabatini, D. M. (2011). mTORC1 senses lysosomal amino acids through an inside-out mechanism that requires the vacuolar H(+)-ATPase. *Science* 334, 678–683. doi:10.1126/science.1207056

Supplementary material

Isolated

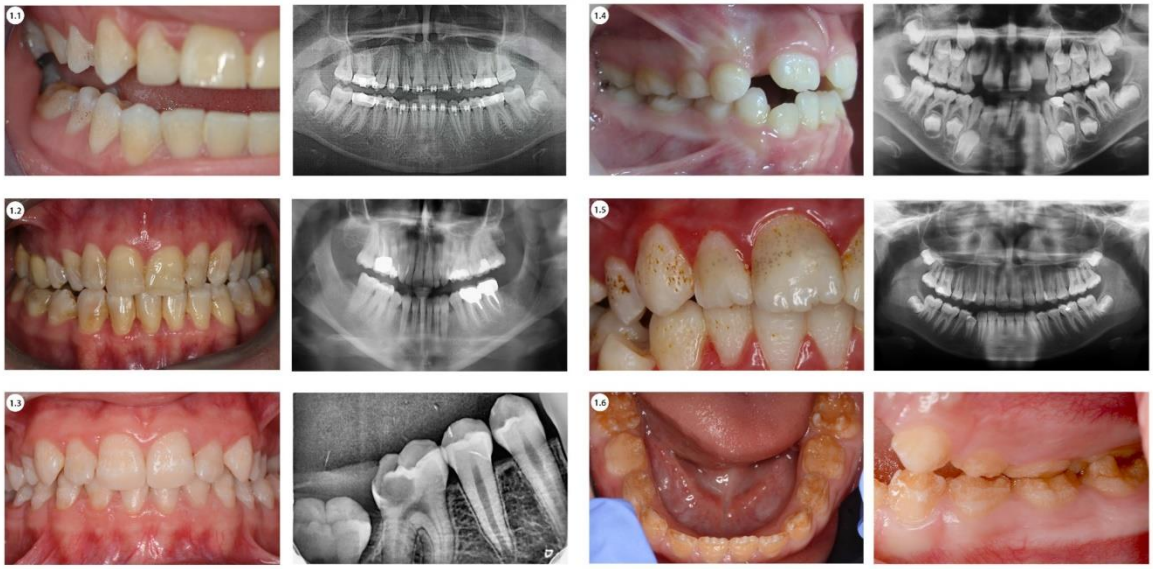

Supplementary Figure 1A *COL17A1*

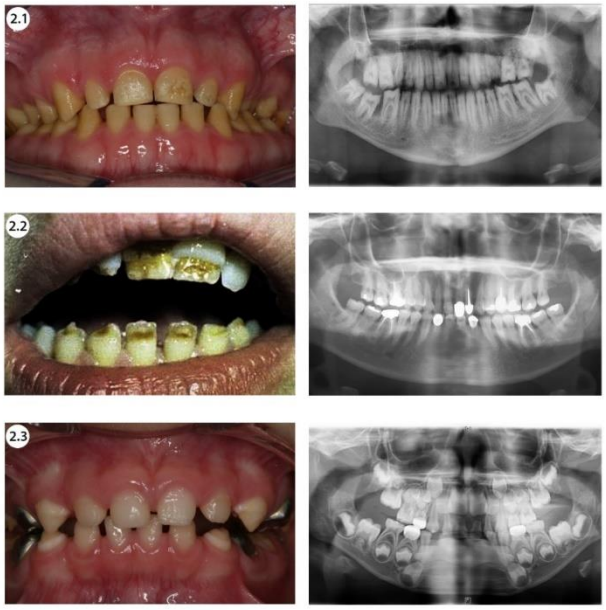

Supplementary Figure 1B *COL7A1*

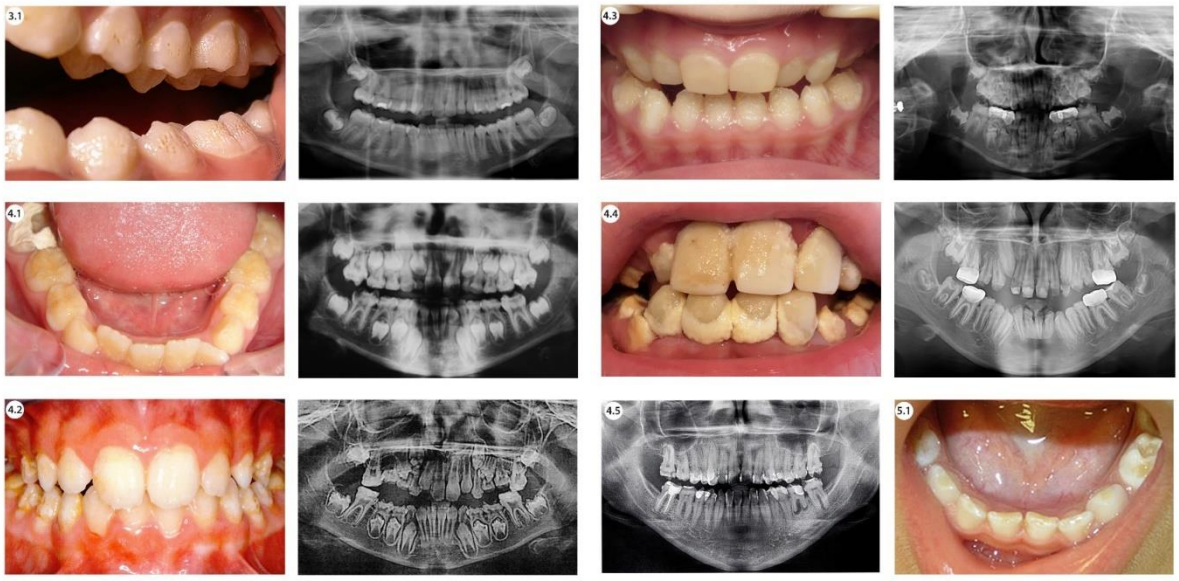

Supplementary Figure 1C *LAMA3, LAMB3 and LAMC2*

Supplementary Figure 1D *ENAM*

Supplementary Figure 1E *AMELX*

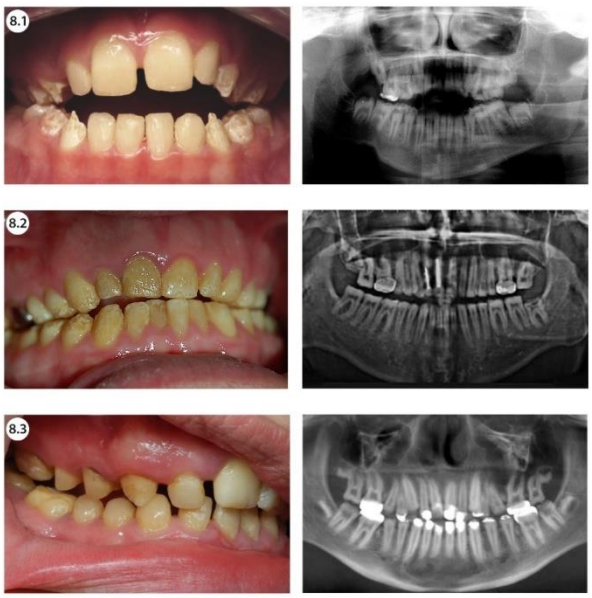

Supplementary Figure 1F *AMBN*

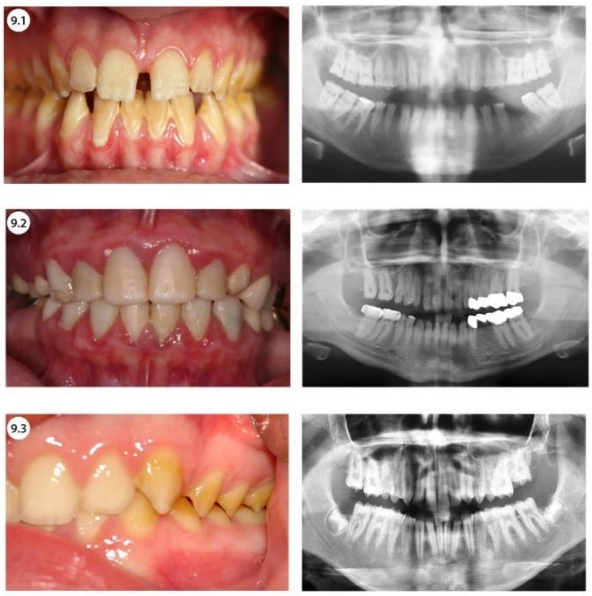

Supplementary Figure 1G *ACP4*

Supplementary Figure 1H ***KLK4 and MMP20***

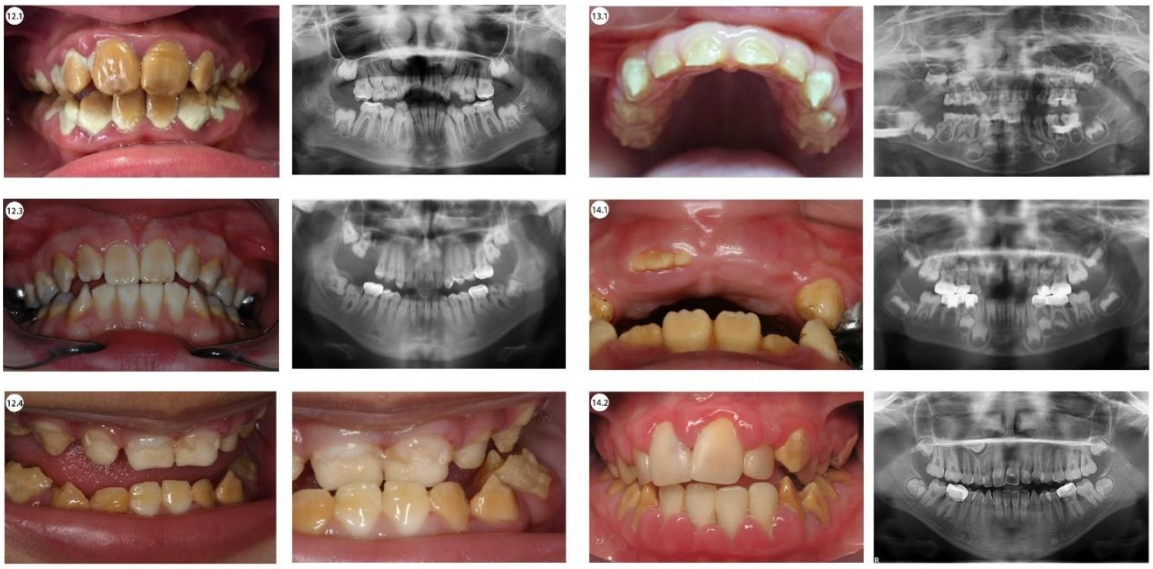

Supplementary Figure 1I ***WDR72, C4ORF26/ODAPH and SLC24A4***

Supplementary Figure 1J *FAM83H*

Supplementary Figure 1K *DLX3*

Syndromic

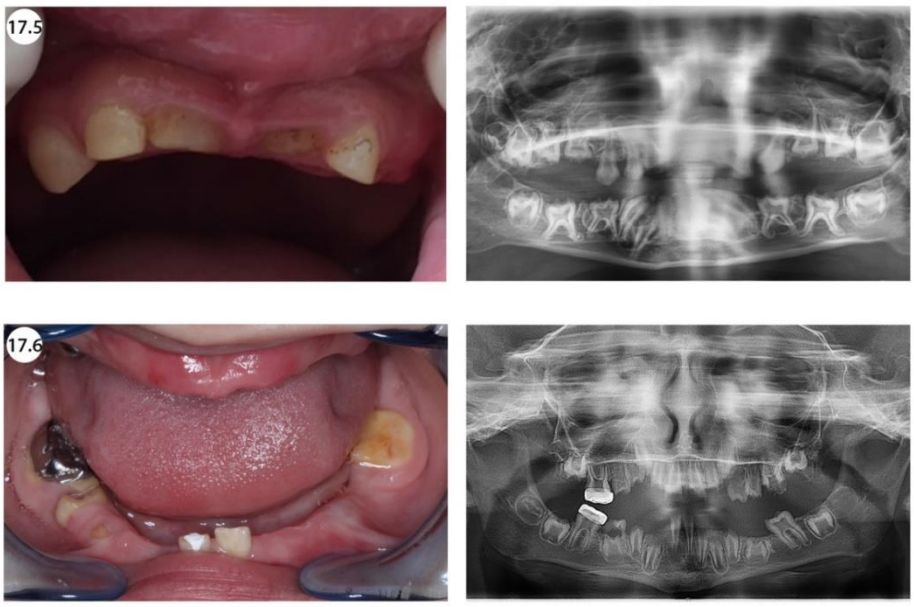

Supplementary Figure 1L *LTBP3*

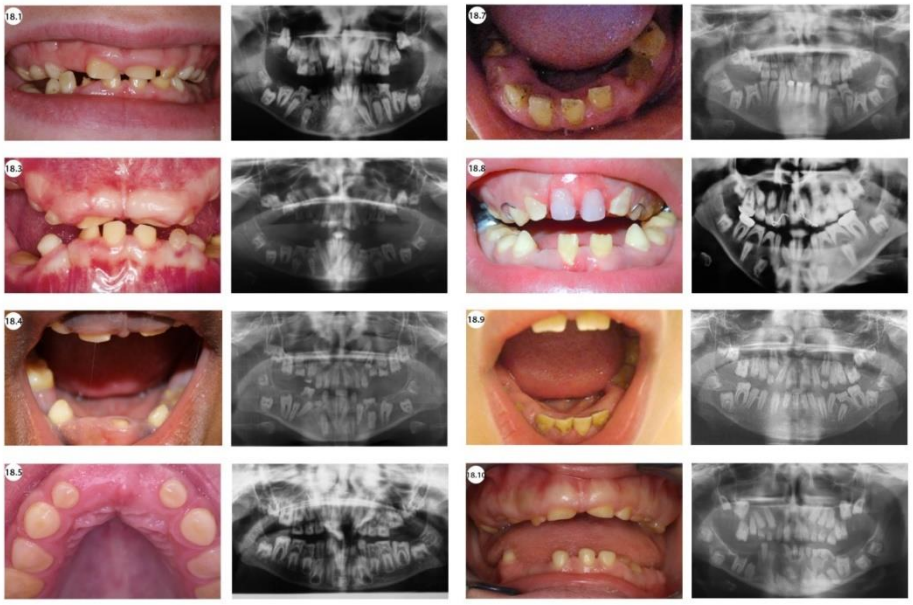

Supplementary Figure 1M *FAM20A*

Supplementary Figure 1N *GALNS and ARHGAP6*

Supplementary Figure 1O *TGFBR2* and *SLC13A5*

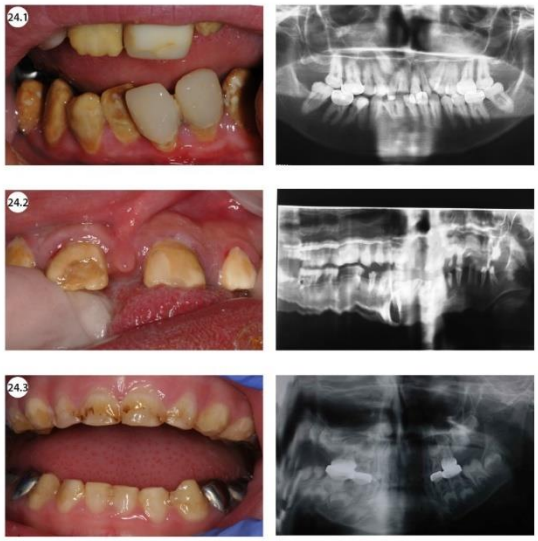

Supplementary Figure 1P *ROGDI*

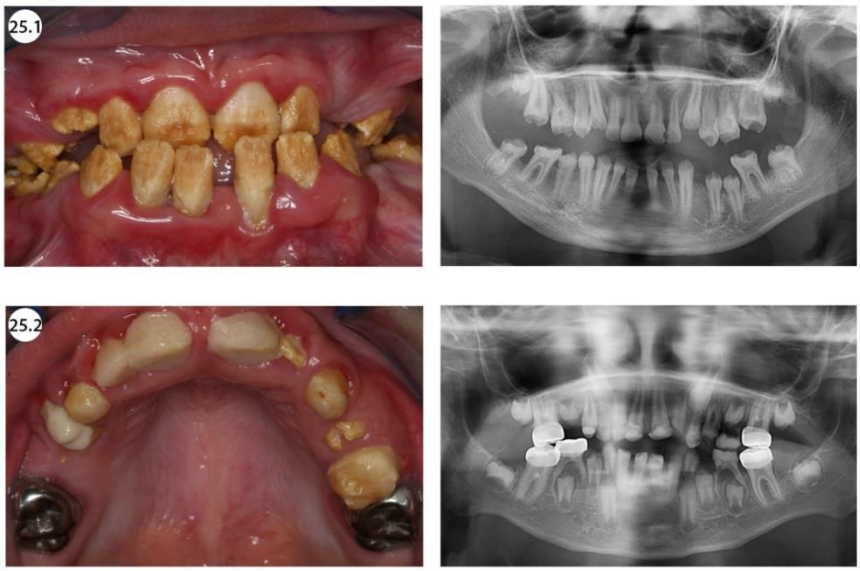

Supplementary Figure 1Q *SLC10A7*

Supplementary Figure 1R *CNNM4*

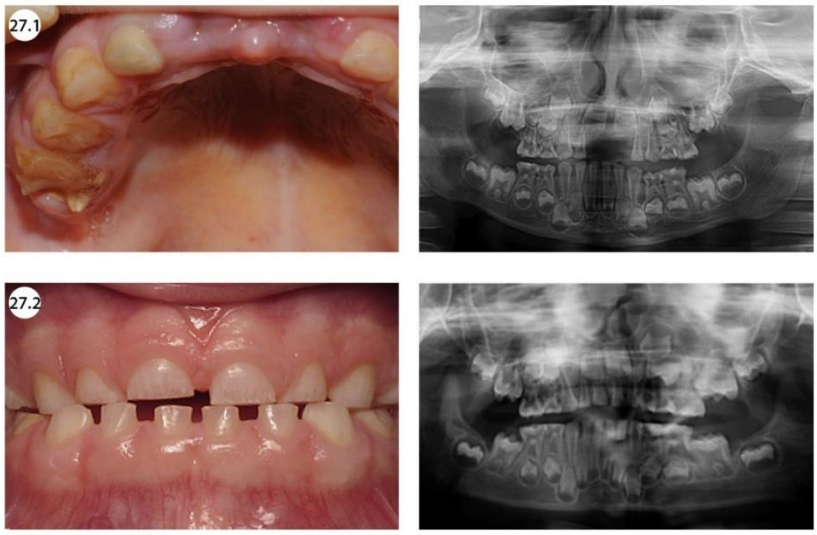

Supplementary Figure 1S *DLX3*

Isolated AI

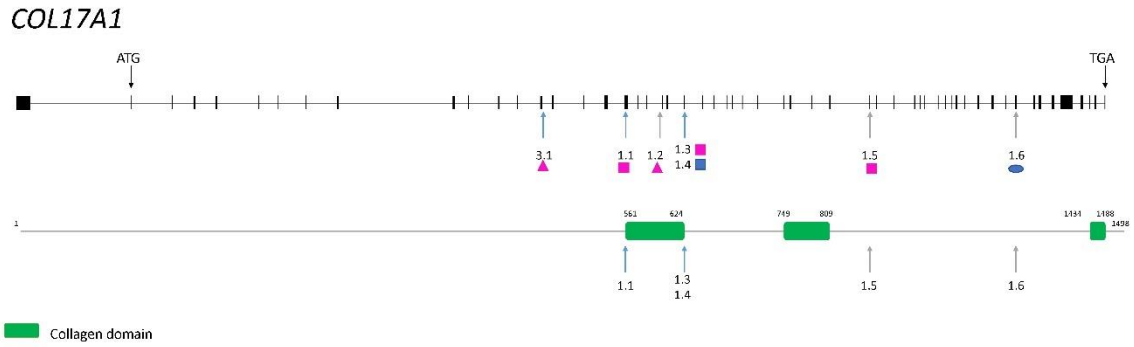

Supplementary Figure 2A

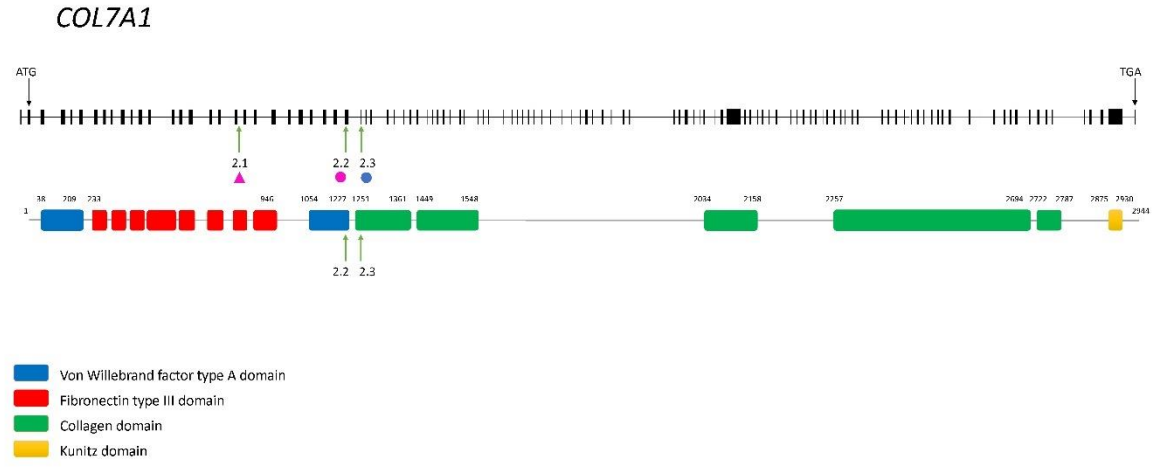

Supplementary Figure 2B

LAMA3

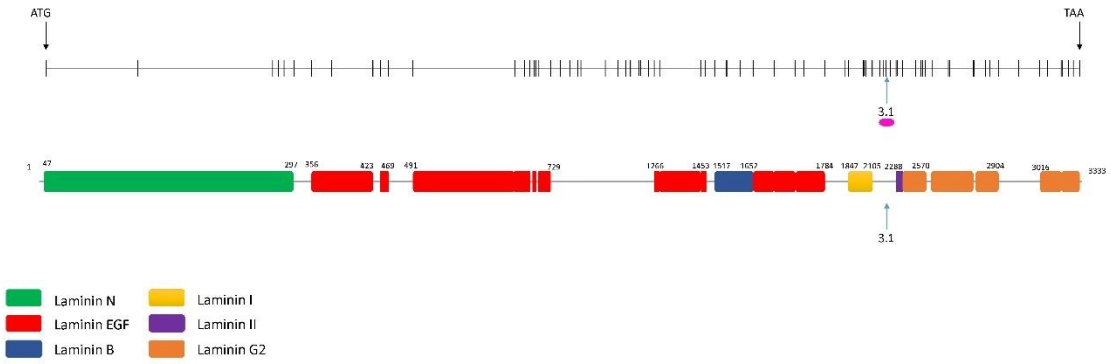

Supplementary Figure 2C

LAMB3

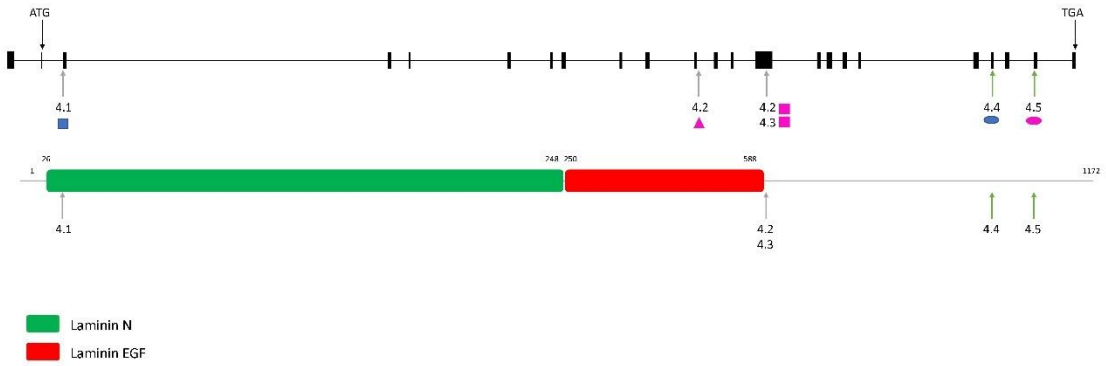

Supplementary Figure 2D

LAMC2

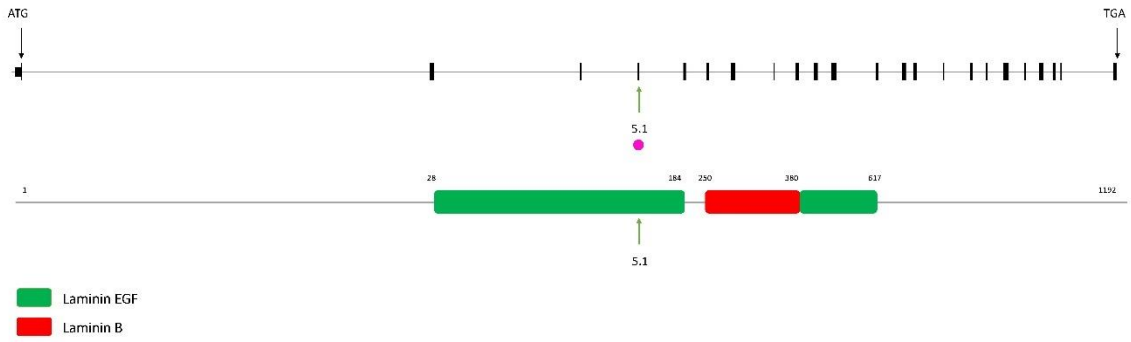

Supplementary Figure 2E

ENAM

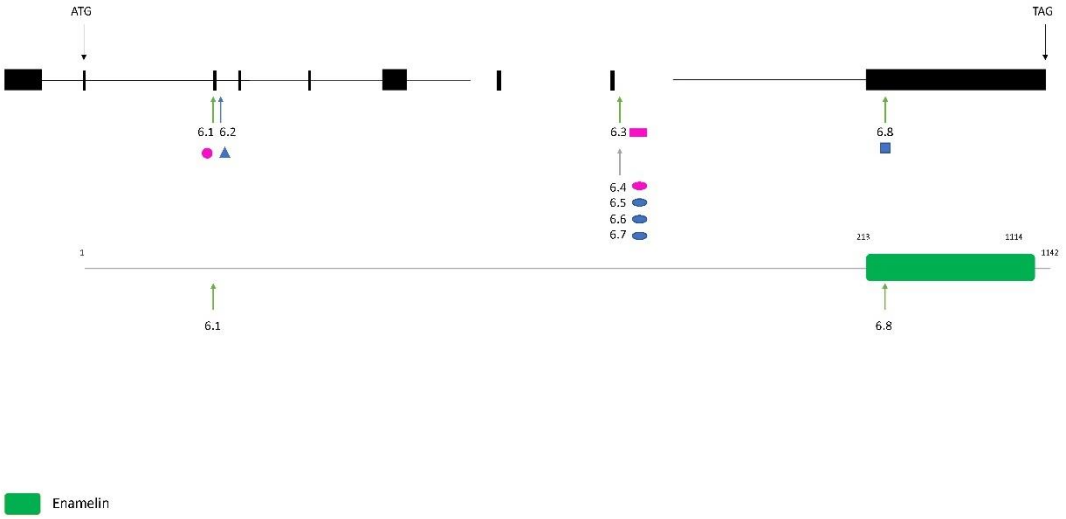

Supplementary Figure 2F

AMELX

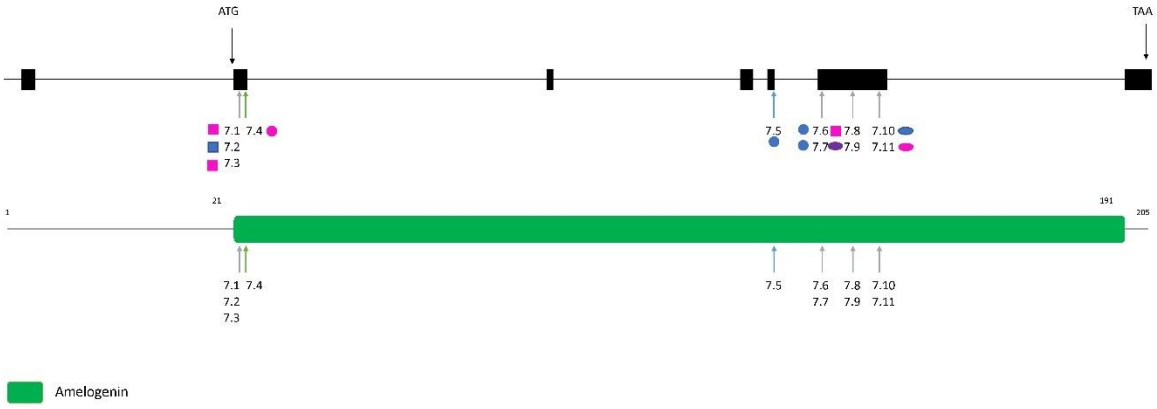

Supplementary Figure 2G

AMBN

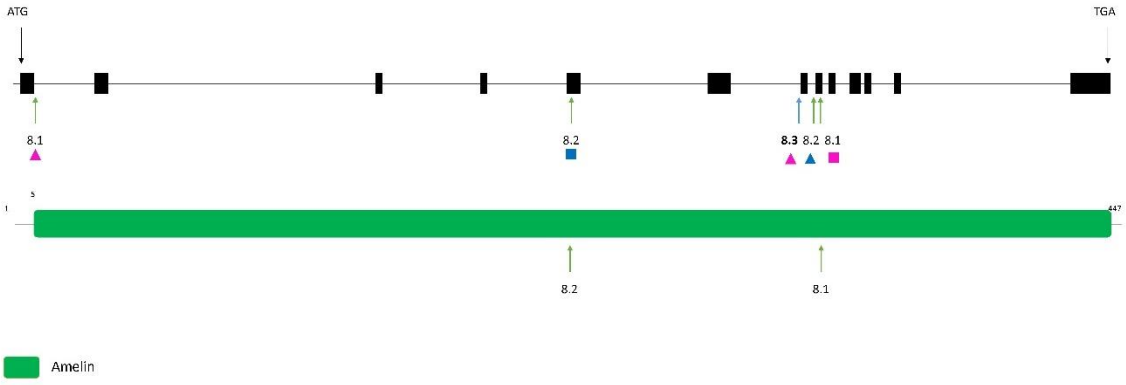

Supplementary Figure 2H

ACP4

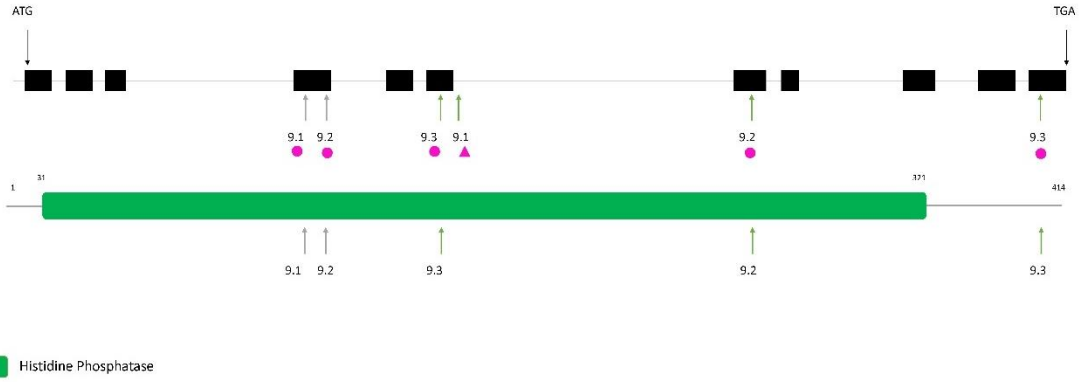

Supplementary Figure 2I

KLK4

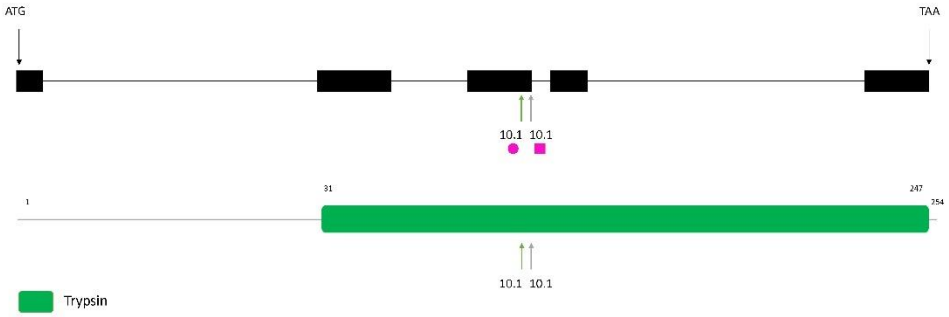

Supplementary Figure 2J

MMP20

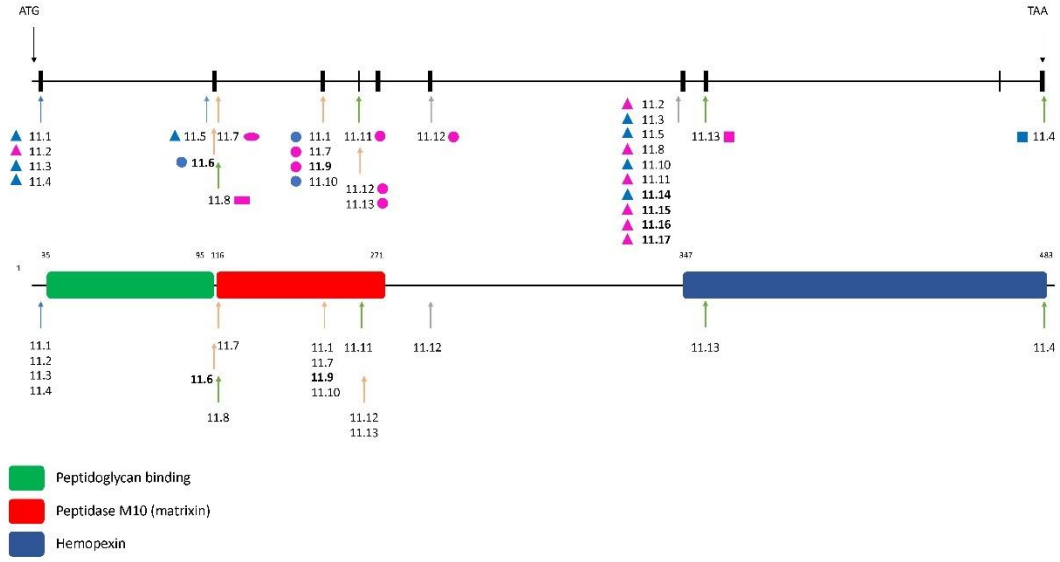

Supplementary Figure 2K

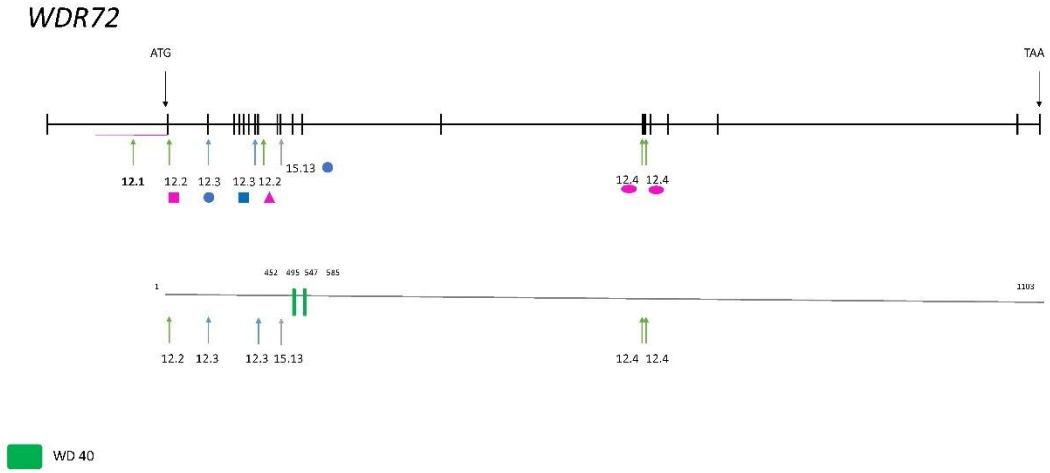

Supplementary Figure 2L

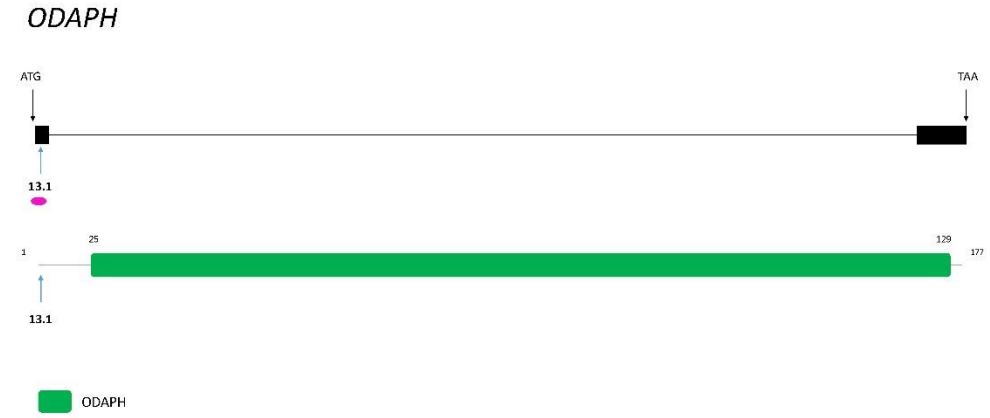

Supplementary Figure 2M

SLC24A4

Supplementary Figure 2N

FAM83H

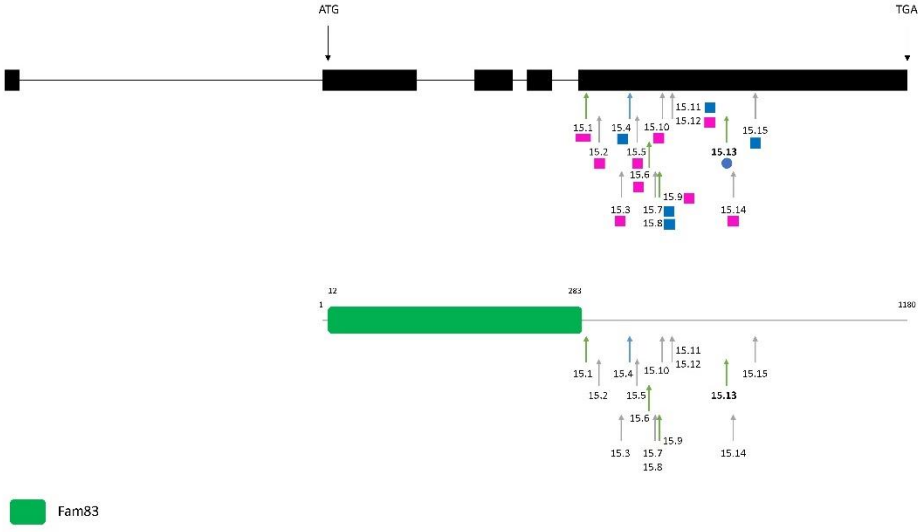

Supplementary Figure 2O

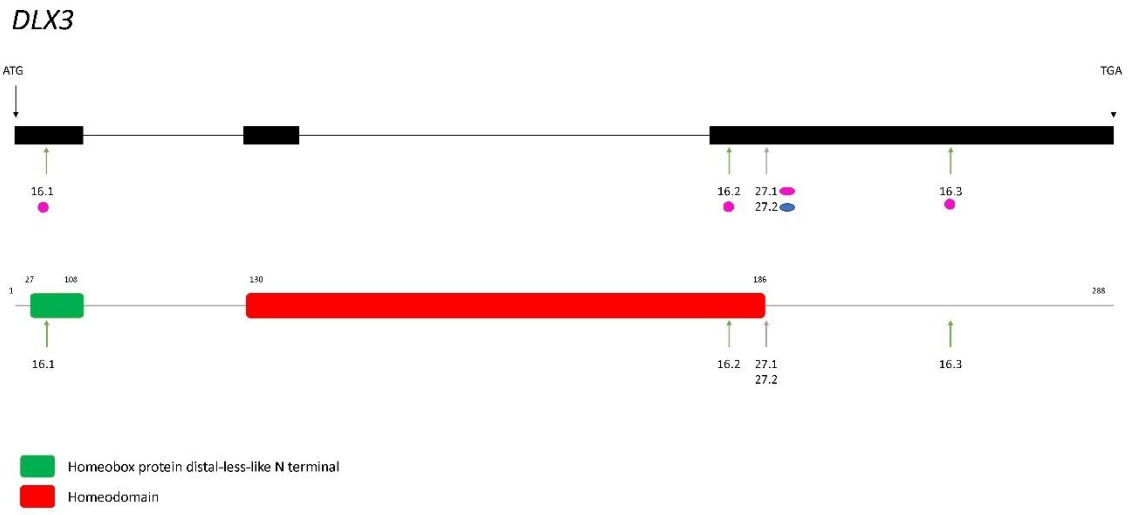

Supplementary Figure 2P

Syndromic AI

LTBP3

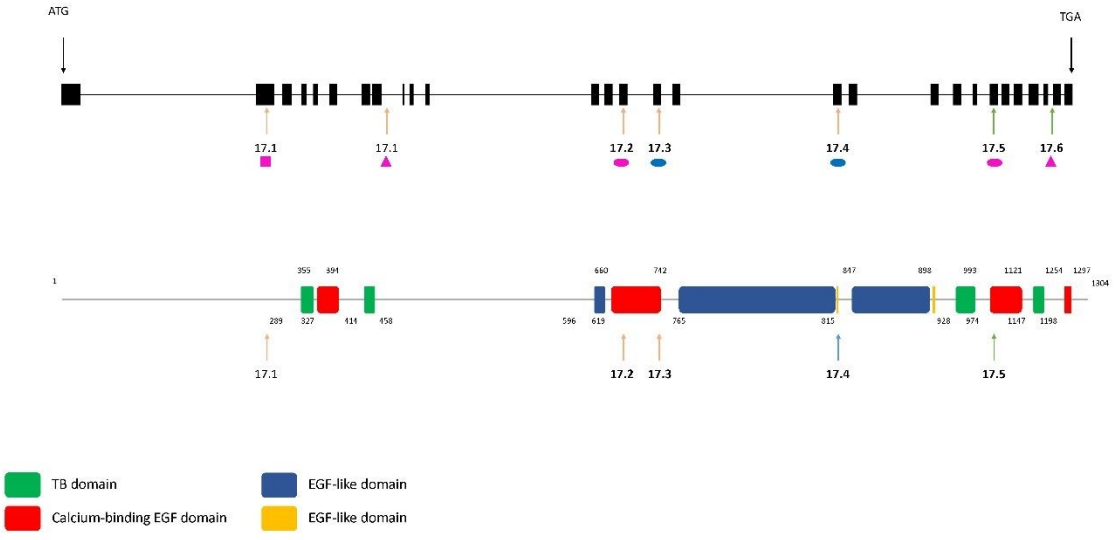

Supplementary Figure 2Q

FAM20A

Supplementary Figure 2R

GALNS

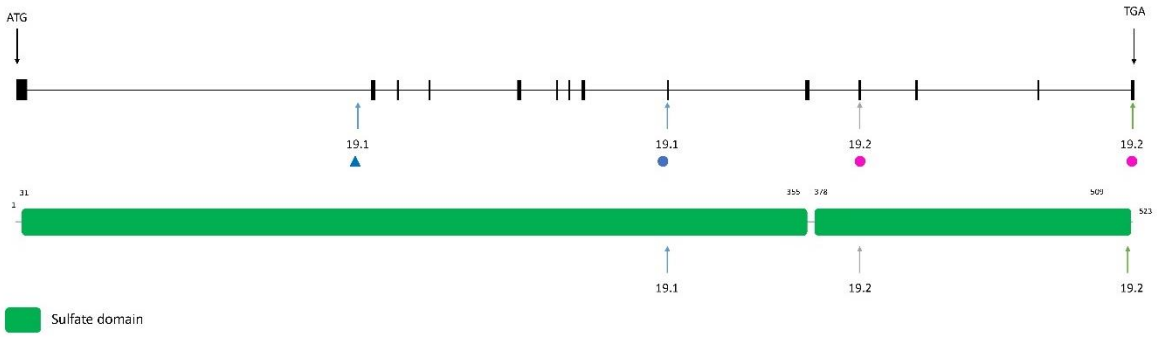

Supplementary Figure 2S

SLC13A5

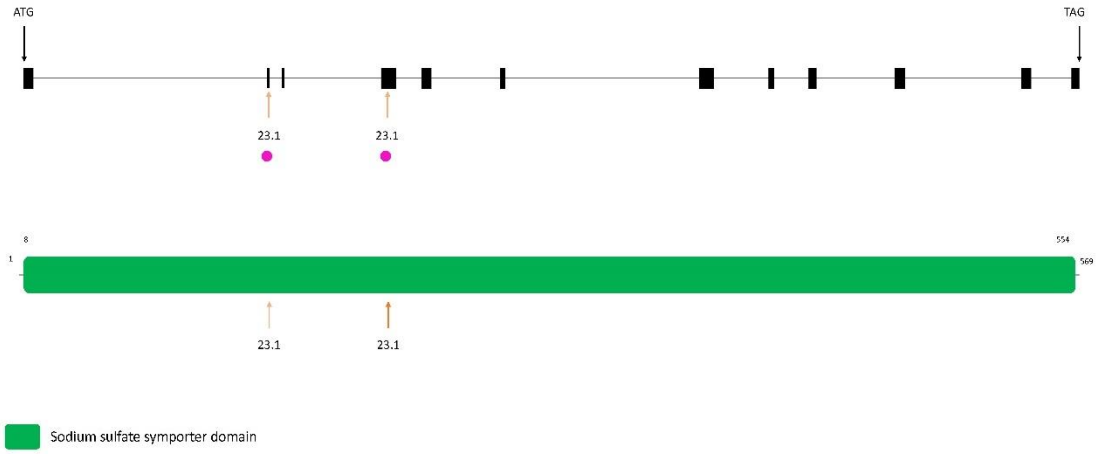

Supplementary Figure 2T

ROGDI

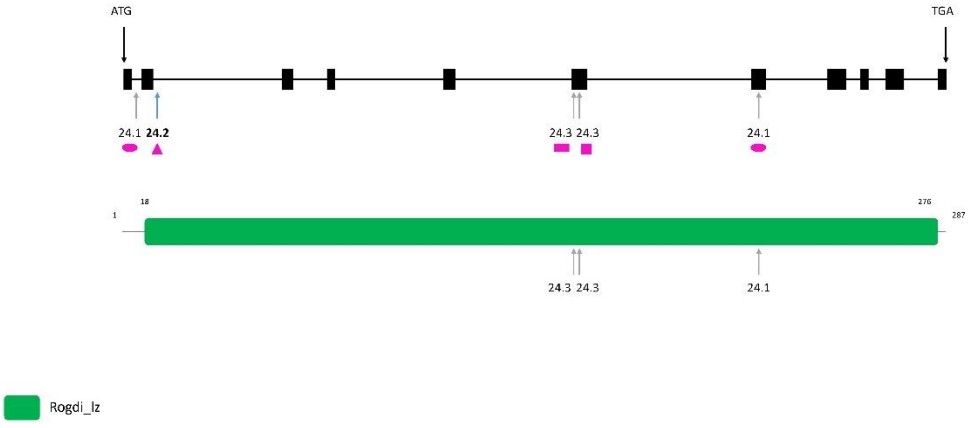

Supplementary Figure 2U

Supplementary Figure 2V

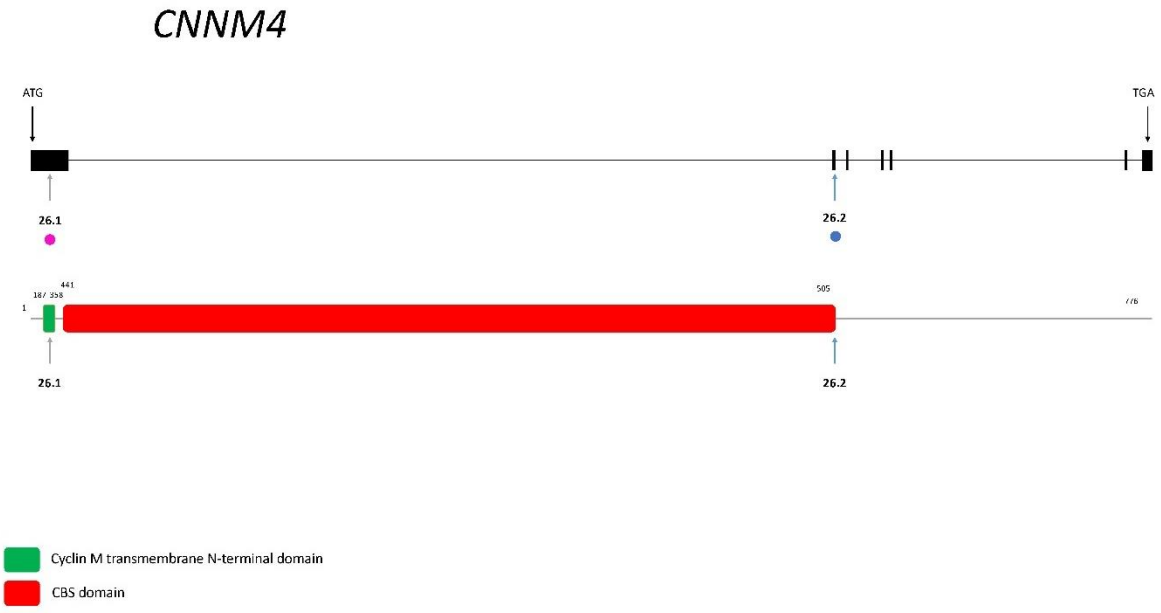

Supplementary Figure 2W

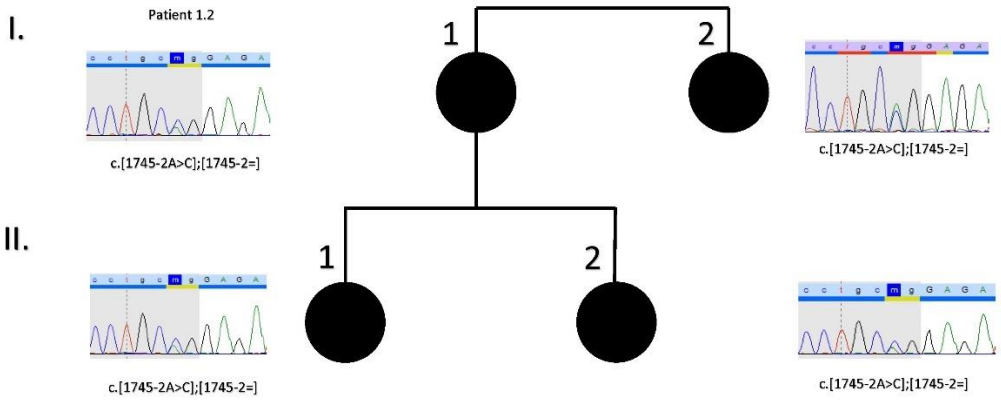

Supplementary Figure 3.1 *COL17A1*

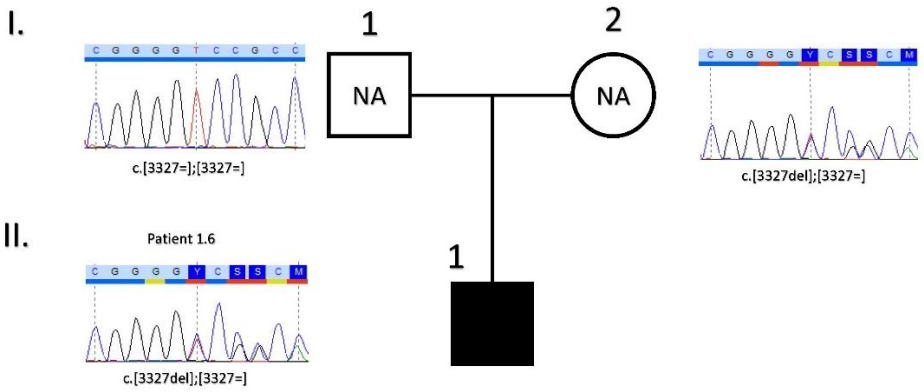

Supplementary Figure 3.2 *COL17A1*

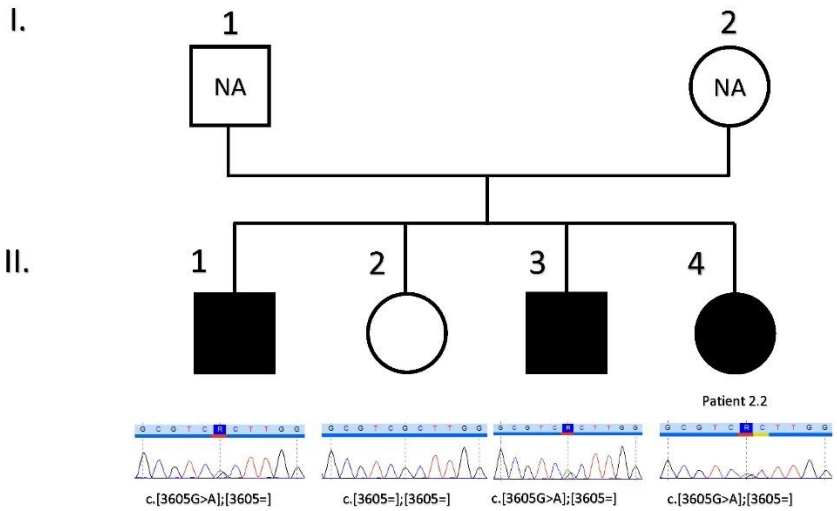

Supplementary Figure 3.3 *COL7A1*

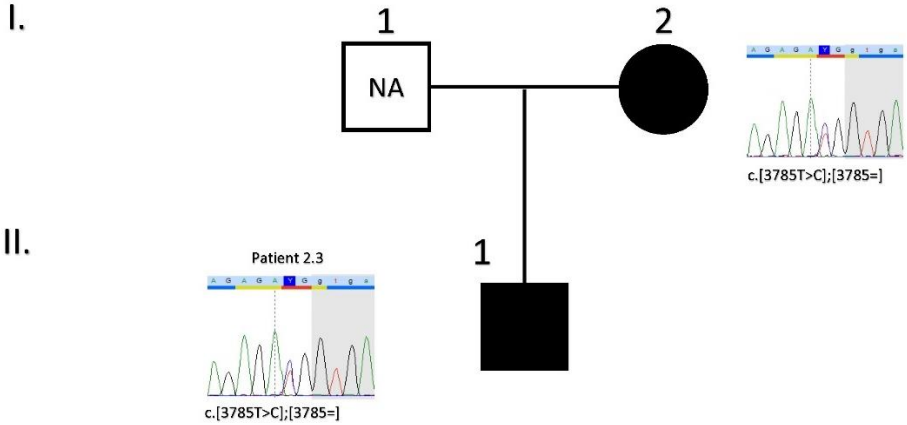

Supplementary Figure 3.4 *COL7A1*

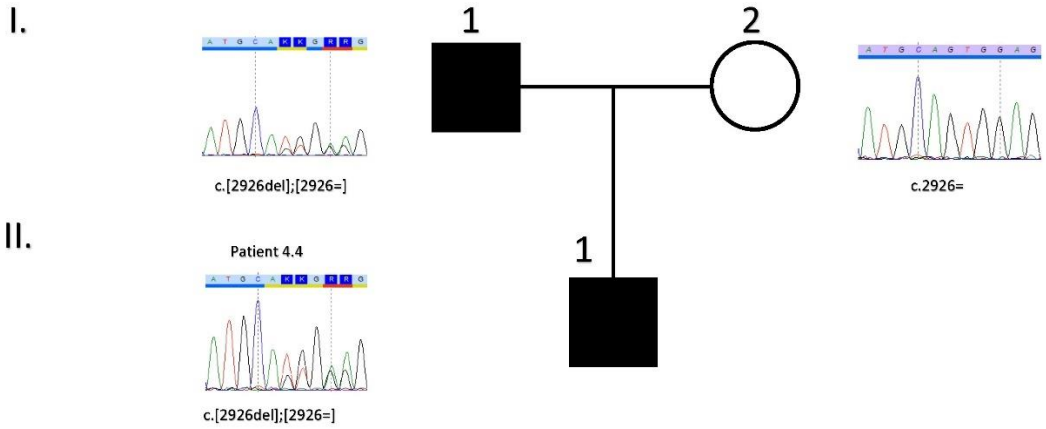

Supplementary Figure 3.5 *LAMB3*

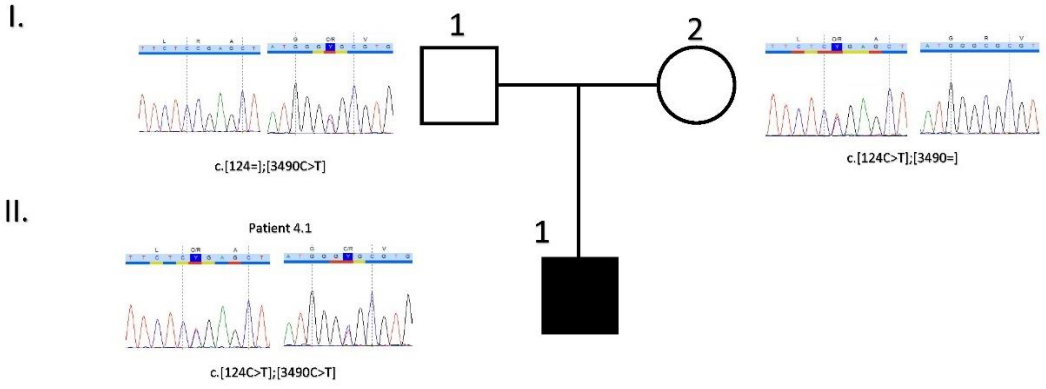

Supplementary Figure 3.6 *LAMB3*

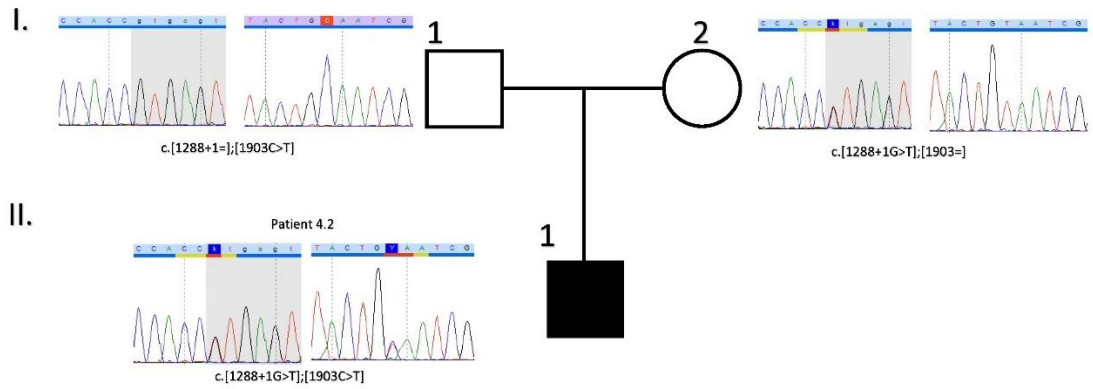

Supplementary Figure 3.7 *LAMB3*

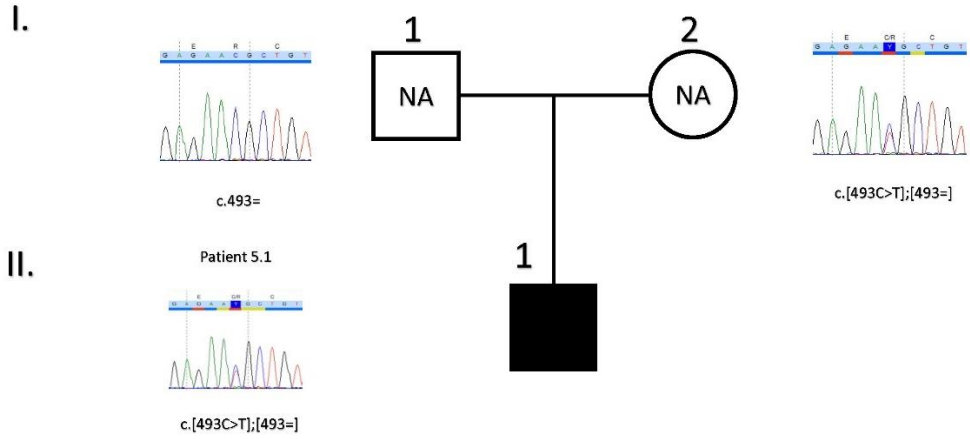

Supplementary Figure 3.8 *LAMC2*

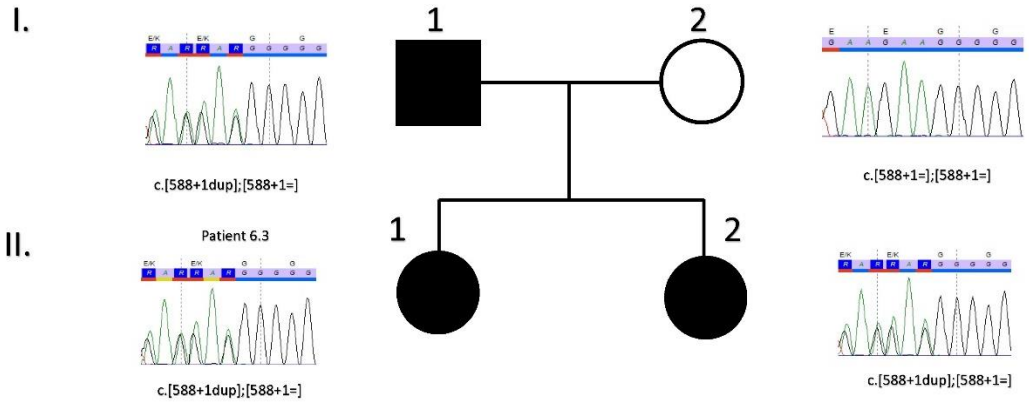

Supplementary Figure 3.9 *ENAM*

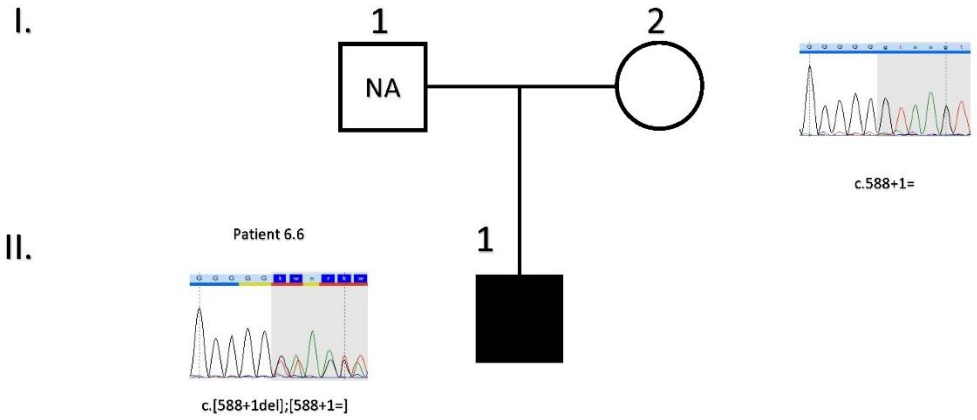

Supplementary Figure 3.10 *ENAM*

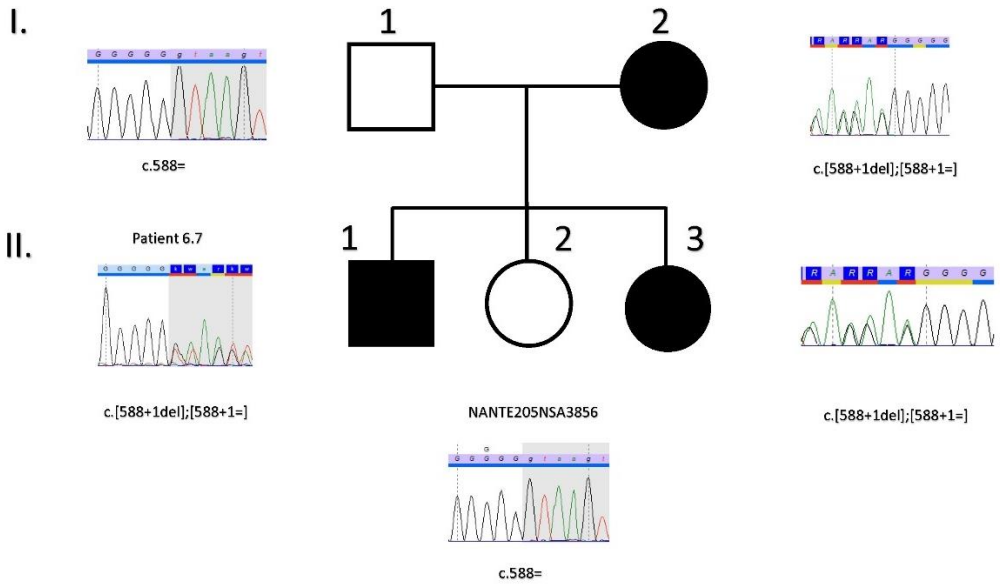

Supplementary Figure 3.11 *ENAM*

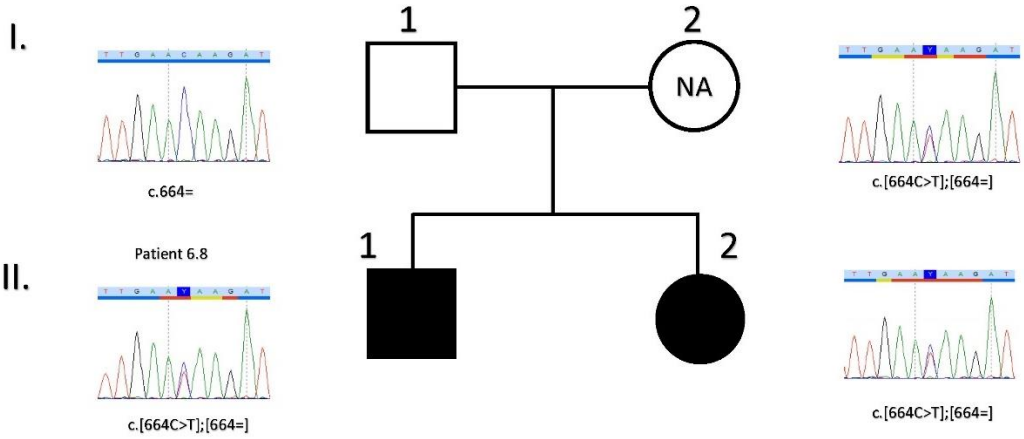

Supplementary Figure 3.12 *ENAM*

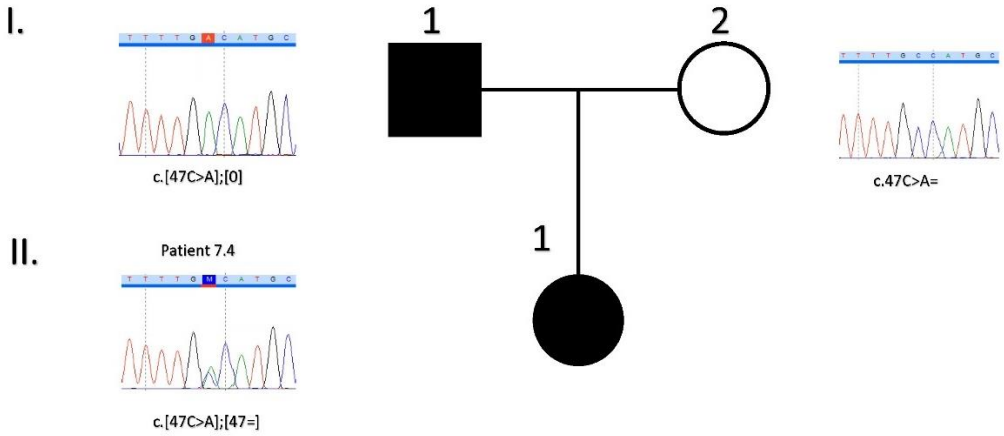

Supplementary Figure 3.13 *AMELX*

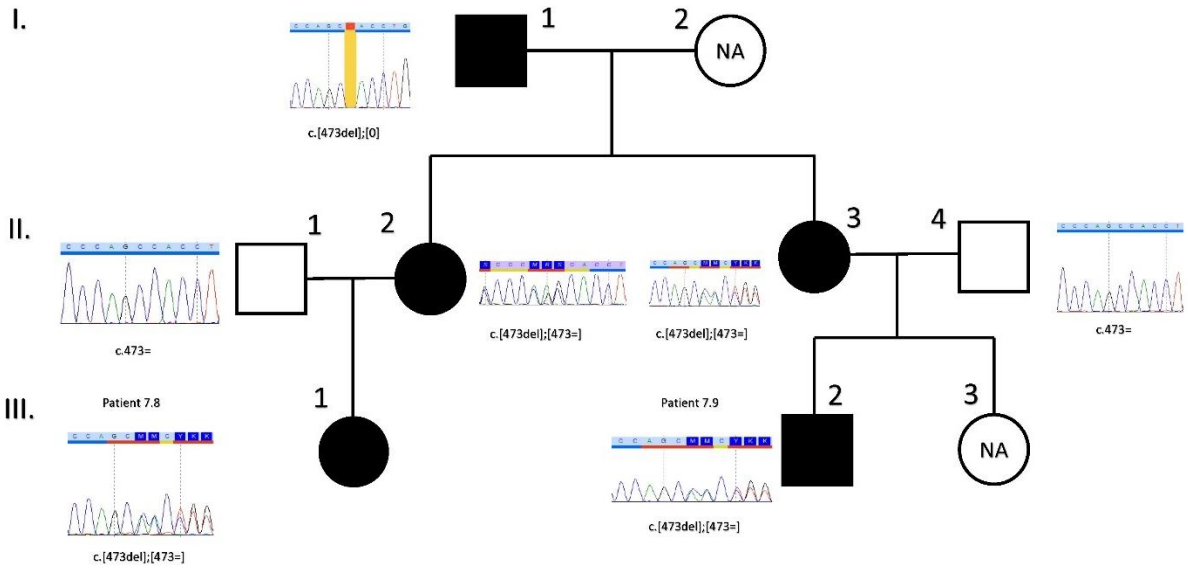

Supplementary Figure 3.14 *AMELX*

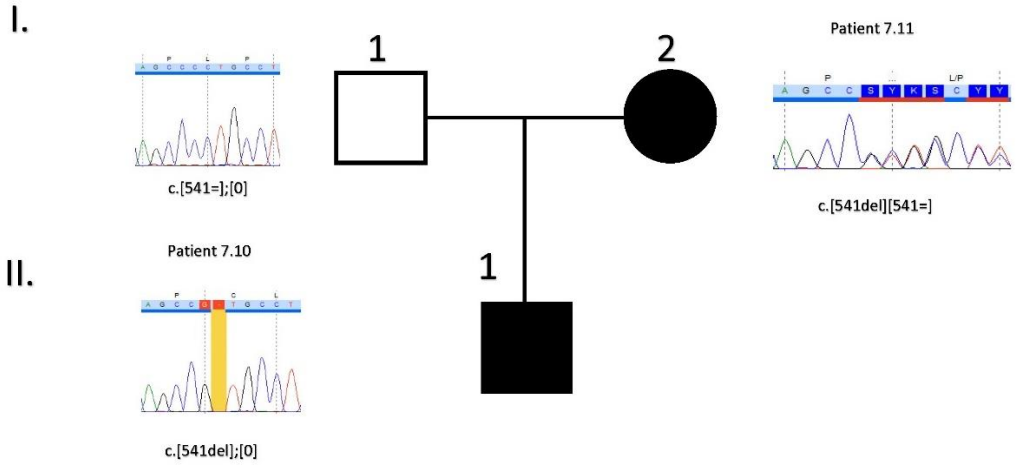

Supplementary Figure 3.15 *AMELX*

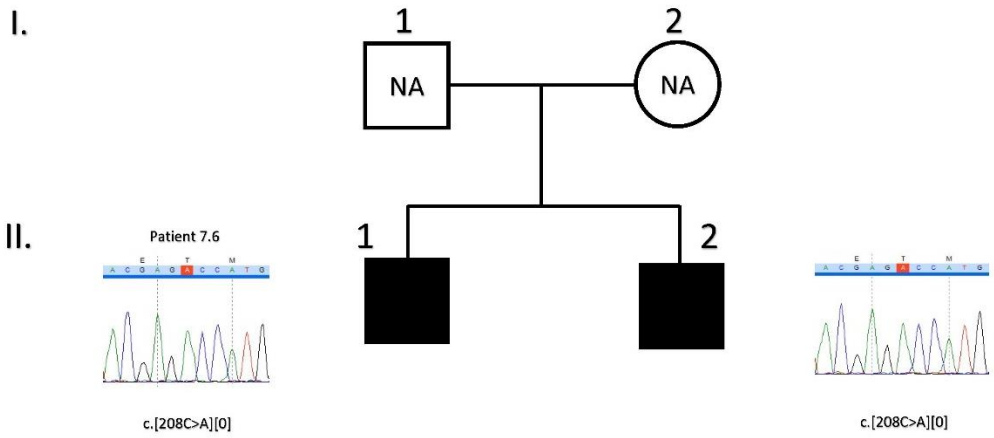

Supplementary Figure 3.16 *AMELX*

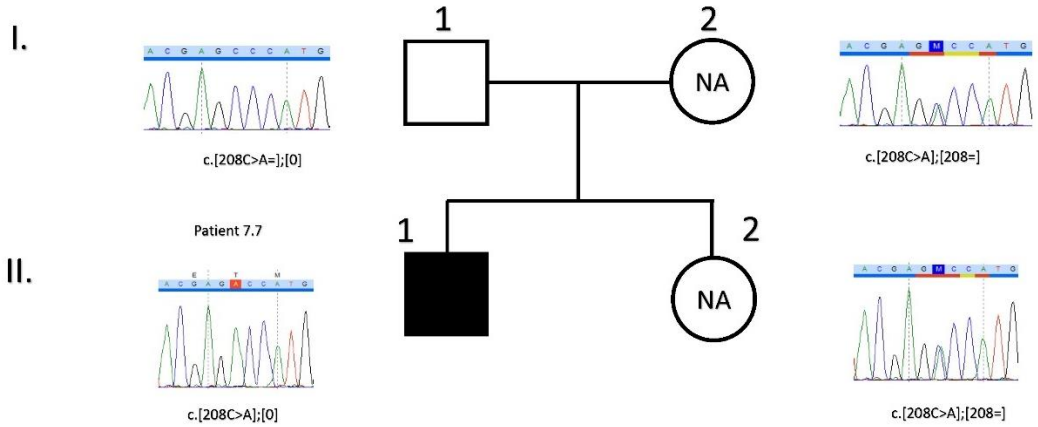

Supplementary Figure 3.17 *AMELX*

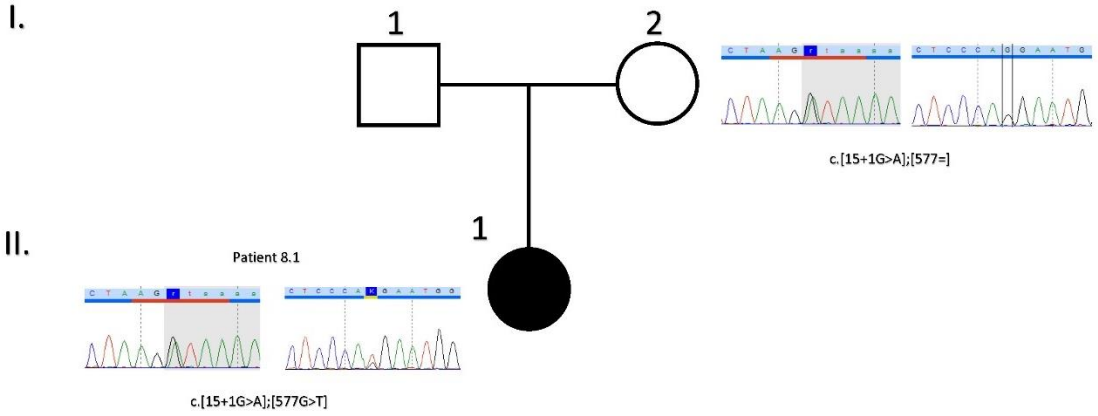

Supplementary Figure 3.18 *AMBN*

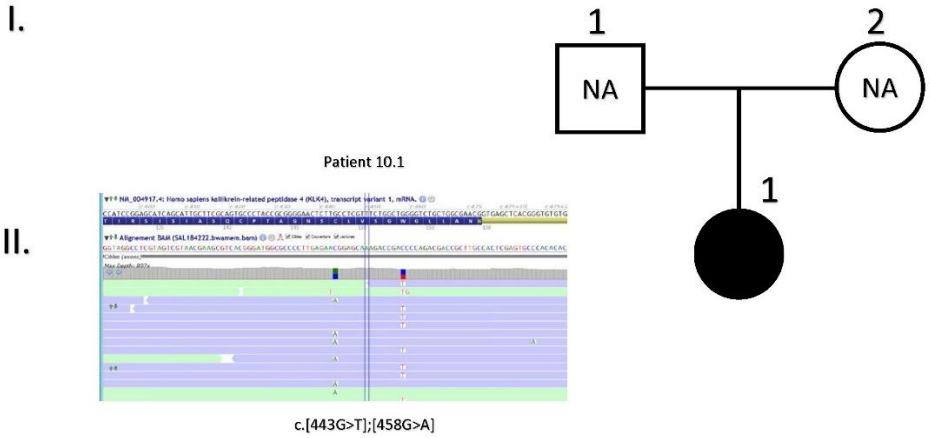

Supplementary Figure 3.19 *KLK4*

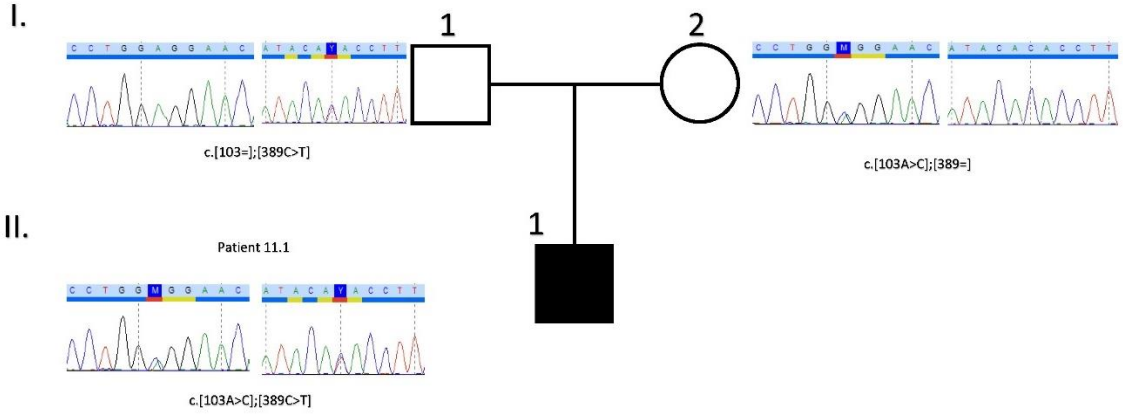

Supplementary Figure 3.20 *MMP20*

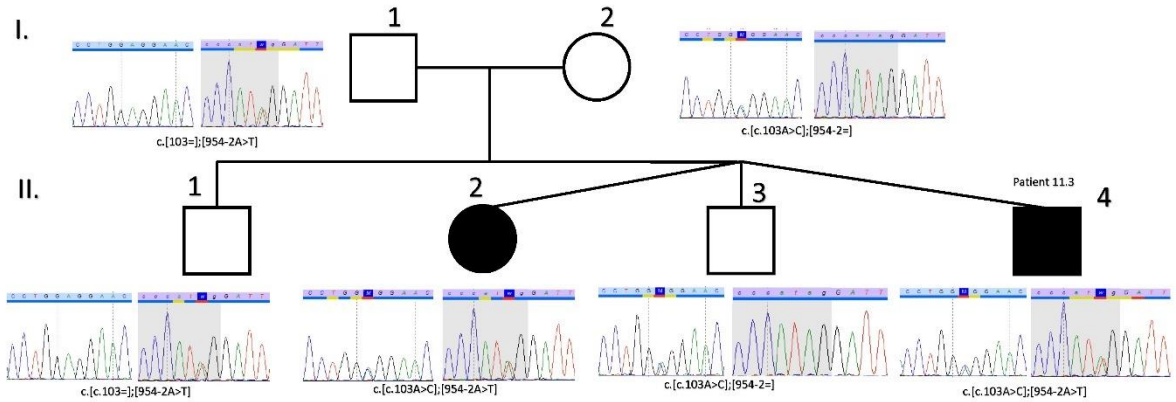

Supplementary Figure 3.21 *MMP20*

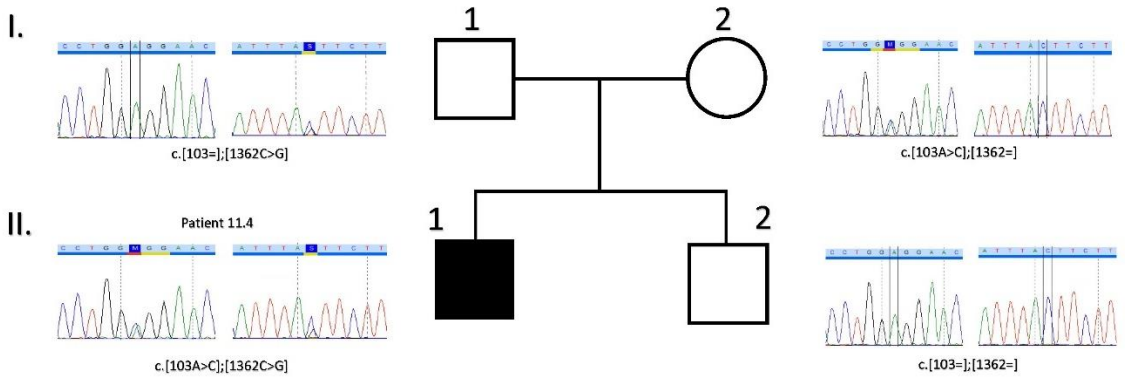

Supplementary Figure 3.22 *MMP20*

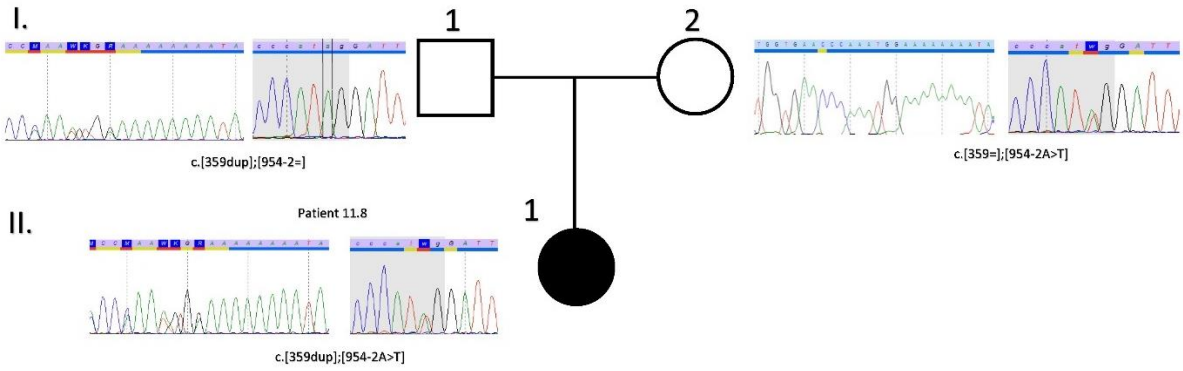

Supplementary Figure 3.23 *MMP20*

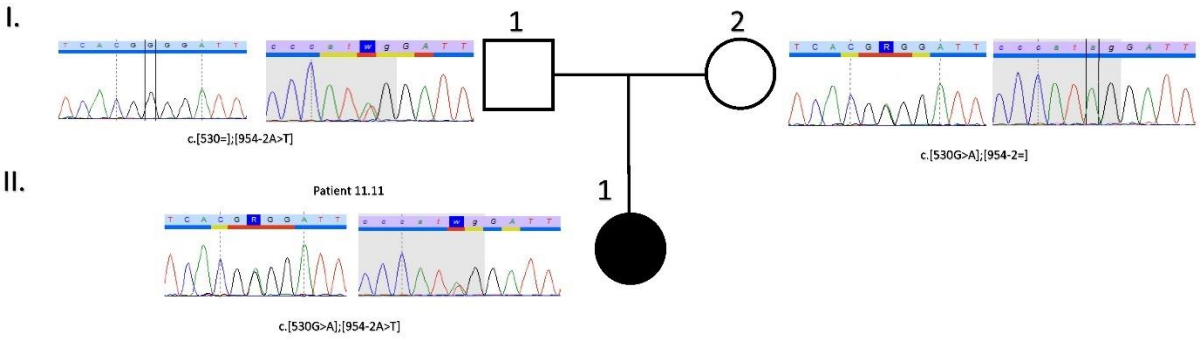

Supplementary Figure 3.24 *MMP20*

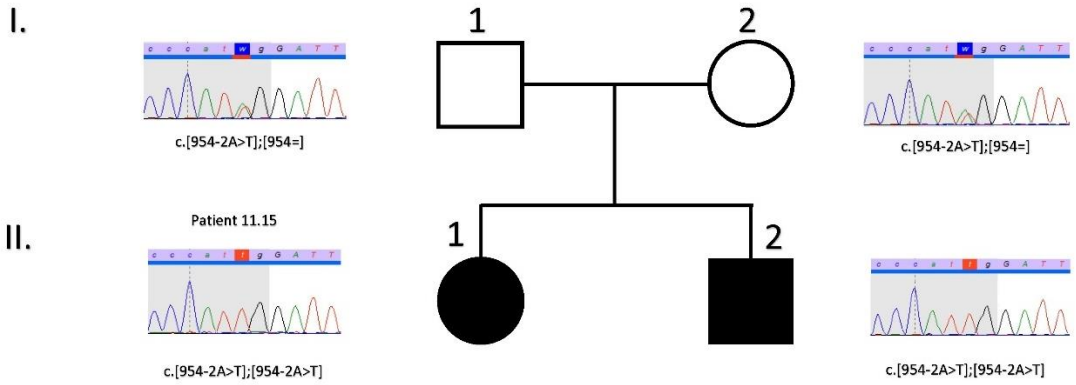

Supplementary Figure 3.25 *MMP20*

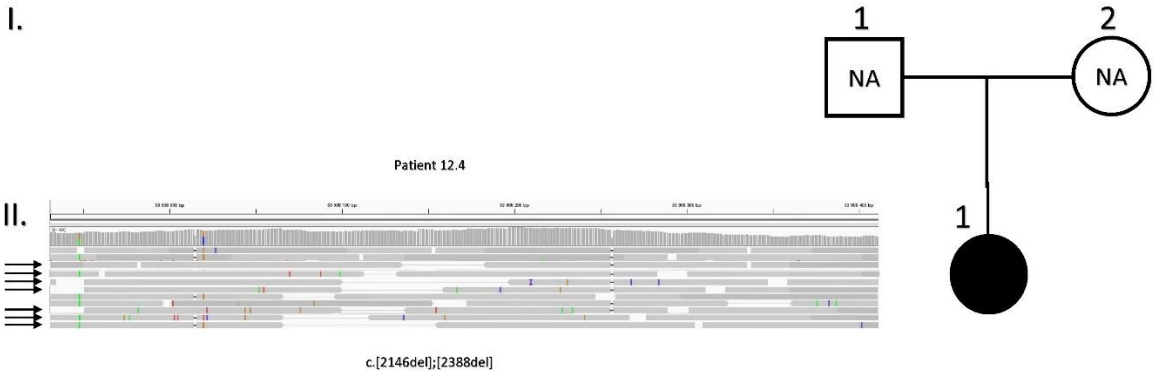

Supplementary Figure 3.26 *WDR72*

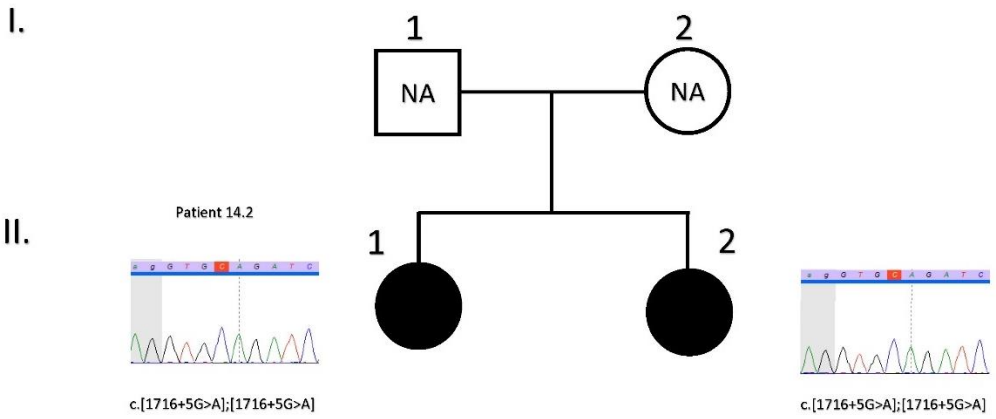

Supplementary Figure 3.27 *SLC24A4*

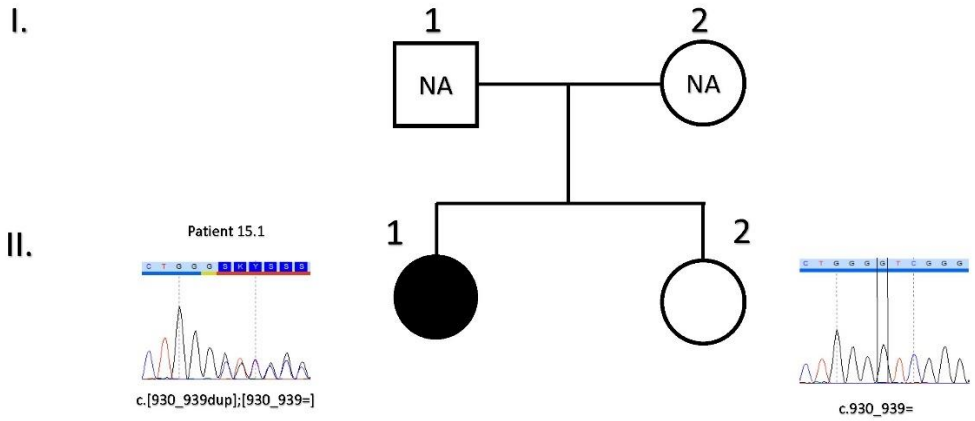

Supplementary Figure 3.28 *FAM83H*

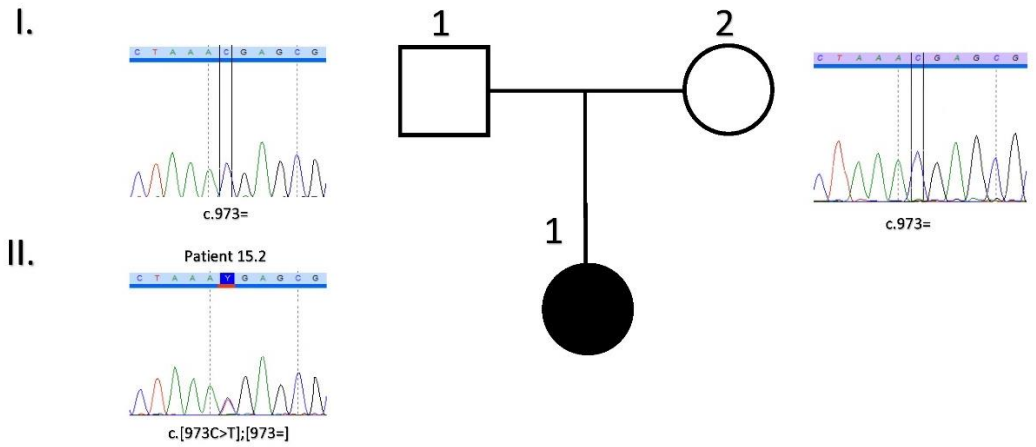

Supplementary Figure 3.29 *FAM83H*

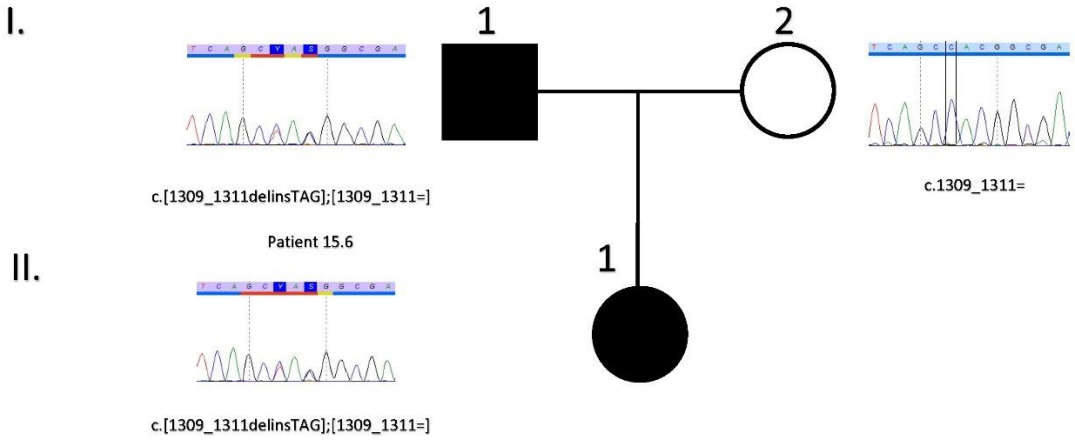

Supplementary Figure 3.30 *FAM83H*

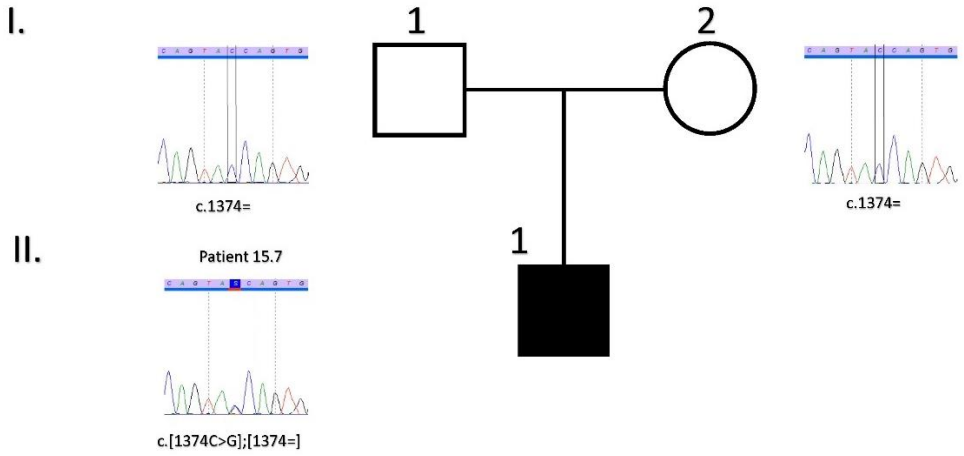

Supplementary Figure 3.31 *FAM83H*

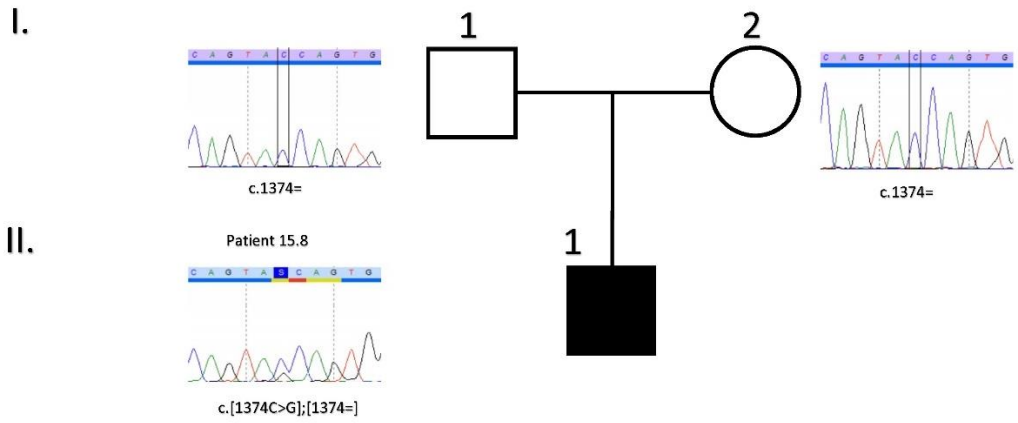

Supplementary Figure 3.32 *FAM83H*

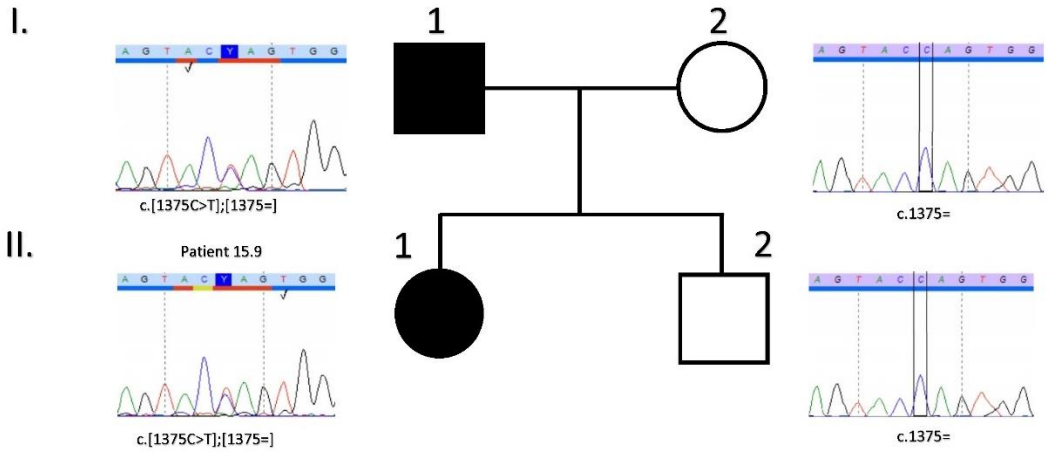

Supplementary Figure 3.33 *FAM83H*

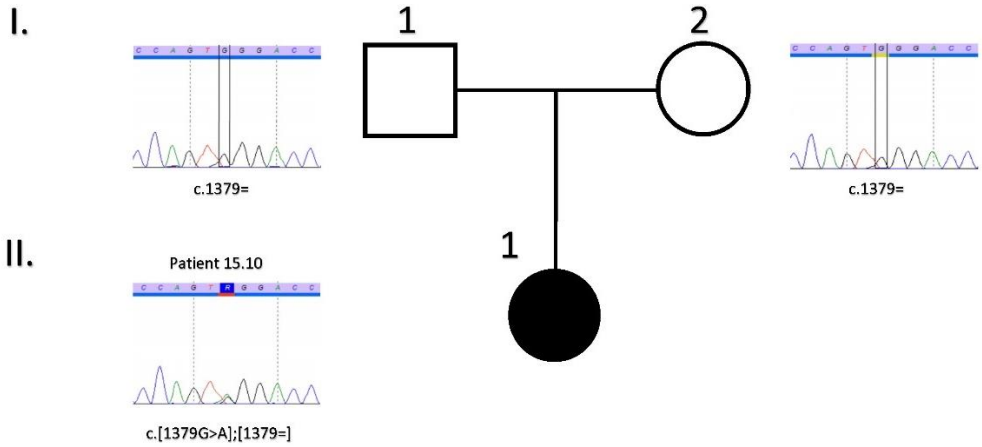

Supplementary Figure 3.34 *FAM83H*

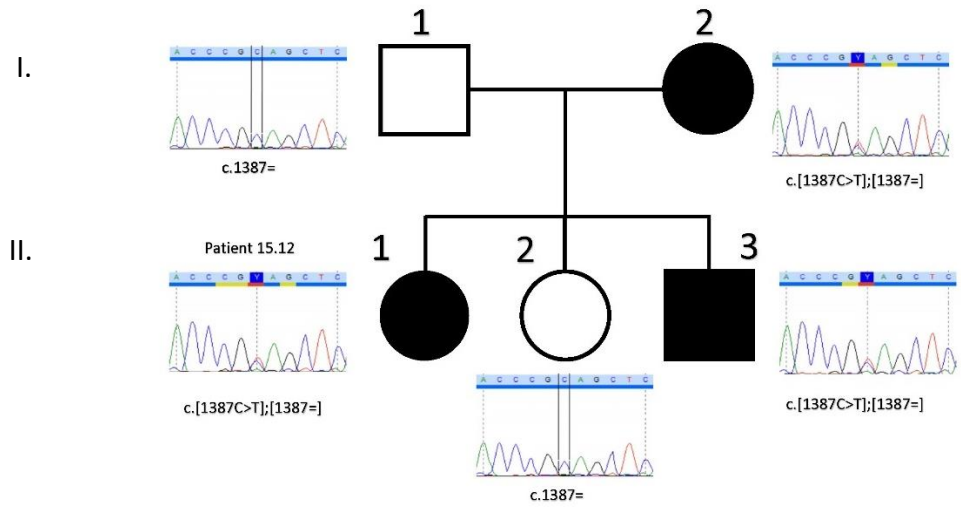

Supplementary Figure 3.35 *FAM83H*

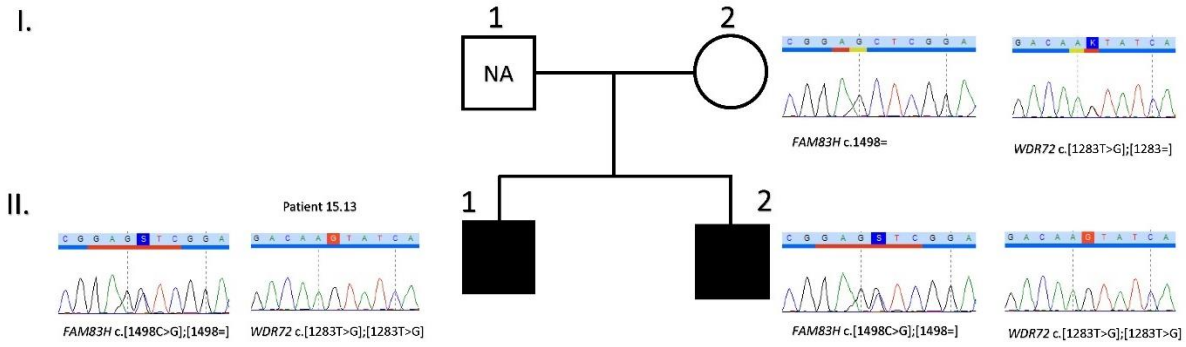

Supplementary Figure 3.36 *FAM83H*

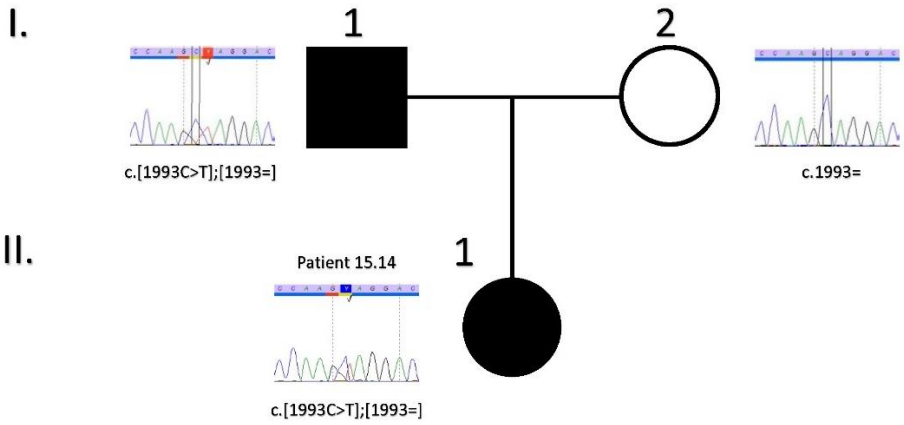

Supplementary Figure 3.37 *FAM83H*

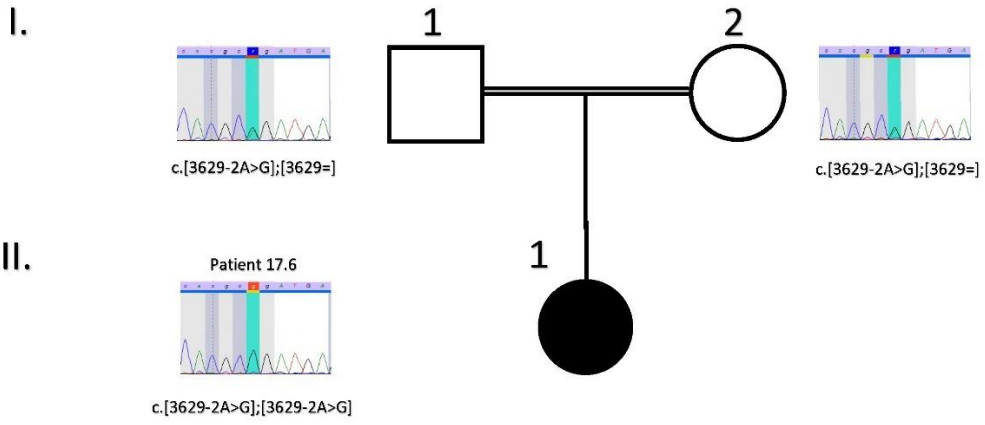

Supplementary Figure 3.38 *LTBP3*

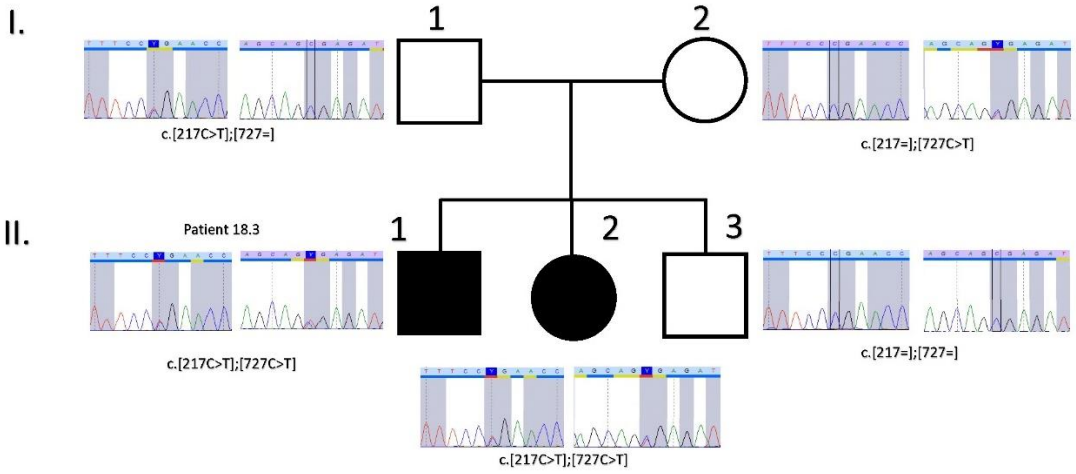

Supplementary Figure 3.39 *FAM20A*

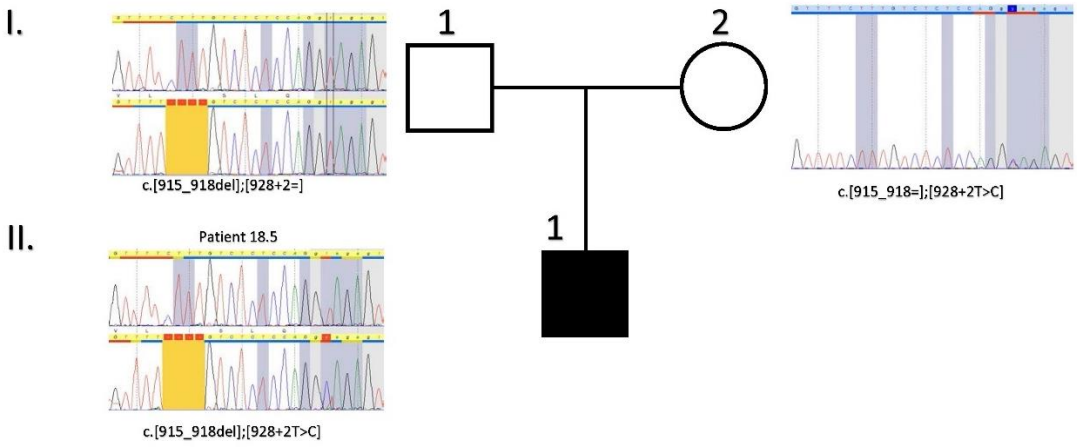

Supplementary Figure 3.40 *FAM20A*

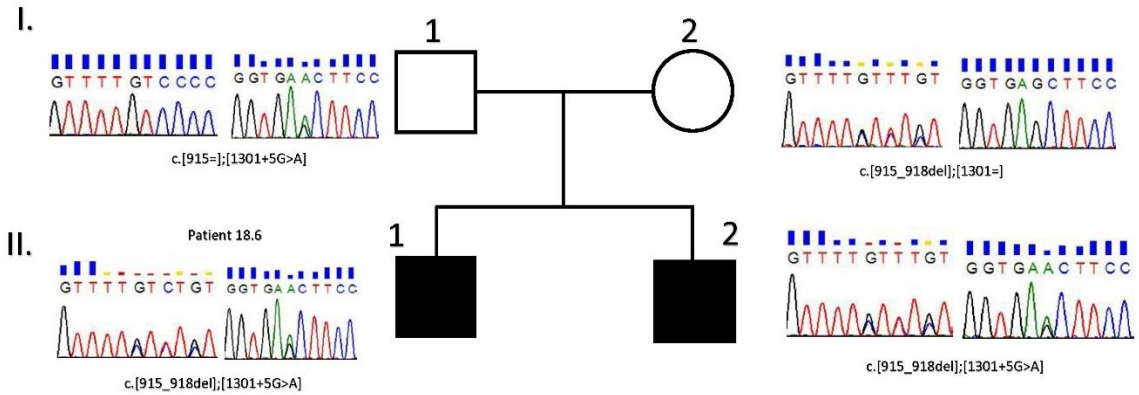

Supplementary Figure 3.41 *FAM20A*

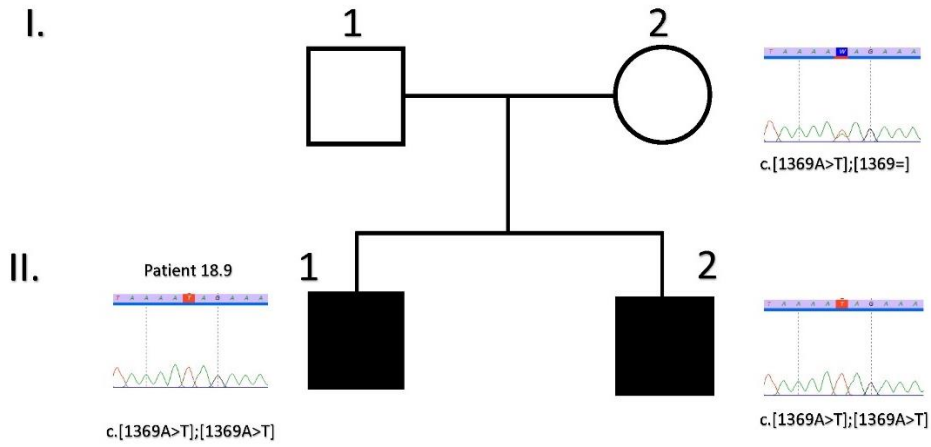

Supplementary Figure 3.42 *FAM20A*

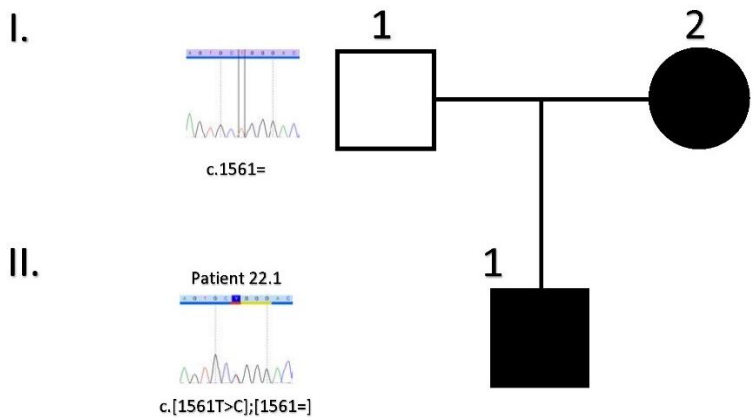

Supplementary Figure 3.43 *TGFBR2*

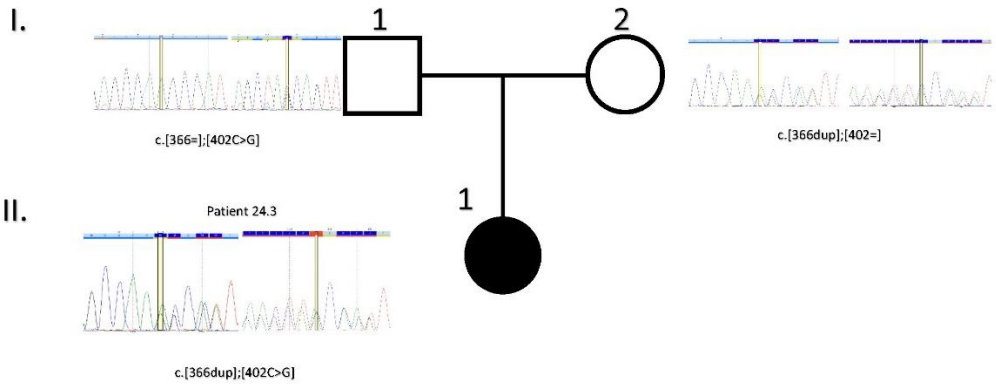

Supplementary Figure 3.44 *ROGDI*

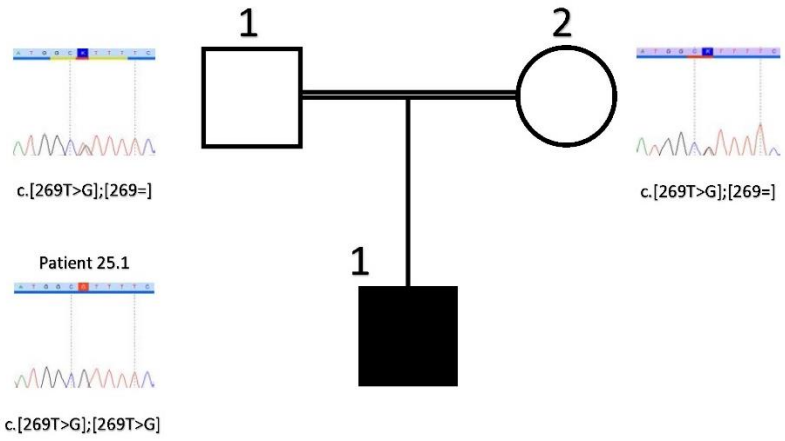

Supplementary Figure 3.45 SLC10A7

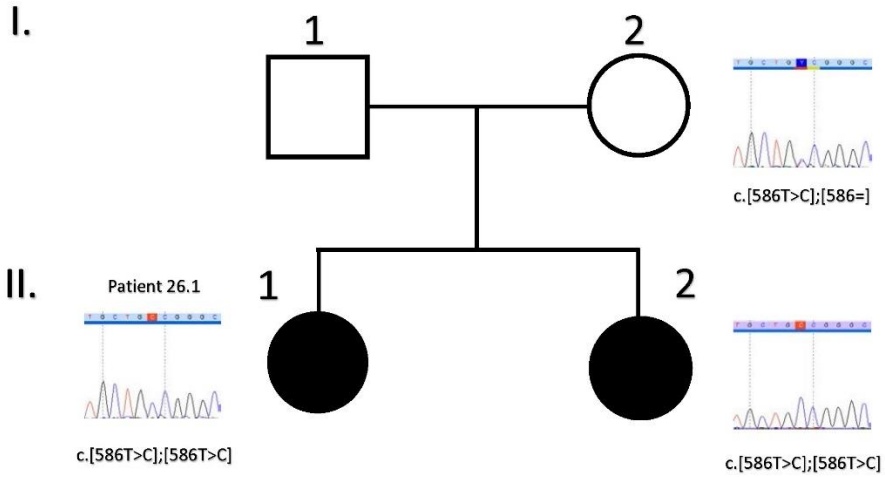

Supplementary Figure 3.46 CNNM4

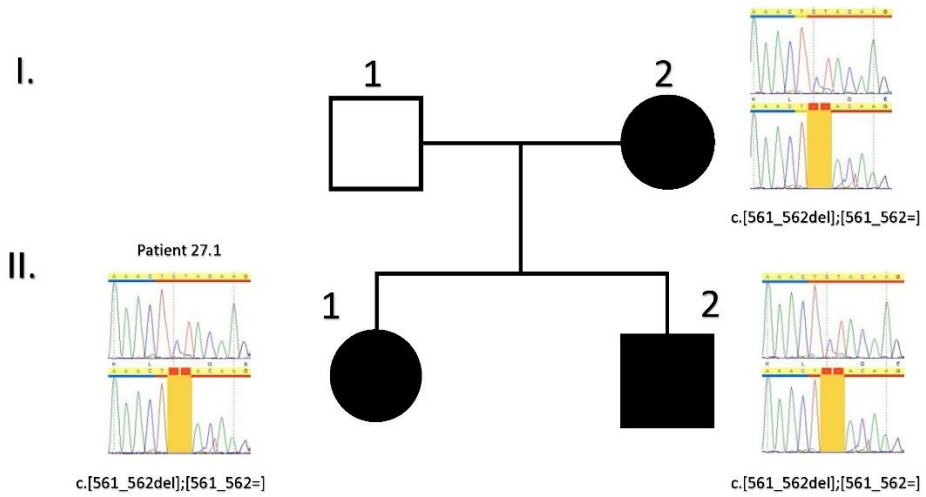

Supplementary Figure 3.47 DLX3

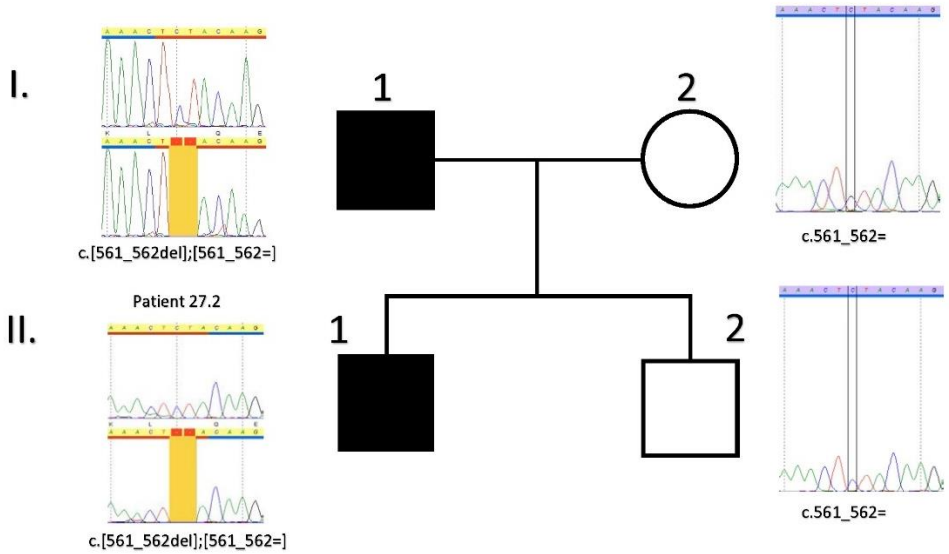

Supplementary Figure 3.48 DLX3

Supplementary Table S1. GenodentV6.0 567 genes

AAAS	ABCA5	ACP4	ACPT	ACVR1	ADAM10	ADAM15	ADAMTS1	ADAMTS10	ADAMTS2	ADGRV1	ADNP	AGL	AHCY	AIP
AIRE	AKAP13	AKT1	ALDH3A2	ALPL	ALX3	AMBN	AMELX	AMELY	AMER1	AMTN	ANKH	ANKRD11	ANTXR1	ANTXR2
AP1G2	AP3B1	APAF1	APC	AR	ARHGAP6	ARID1B	ATP6V0A2	ATP6V1B2	ATP6V1C2	ATR	ATRIP	ATRX	AXIN2	B3GAT3
B4GALT7	BANF1	BAZ1B	BCOR	BLM	BMP1	BMP2	BMP4	BRAF	C1R	C1S	C4ORF26	CA2	CACNA1S	CACNB2
CAMK4	CARD9	CASP14	CCBE1	CCDC134	CCDC8	CD96	CDC6	CDH1	CDH23	CDH3	CDKN1C	CDON	CELSR1	CELSR3
CENPJ	CEP152	CFDP1	CHD7	CHPF	CHST3	CHSY1	CHUK	CIAPIN1	CIB2	CKAP2L	CLCN7	CLDN1	CLDN10	CLDN15
CLDN16	CLDN19	CLDN3	CLEC7A	CLRN1	CNNM4	COG6	COL10A1	COL11A1	COL12A1	COL15A1	COL17A1	COL1A1	COL1A2	COL24A1
COL2A1	COL3A1	COL5A1	COL5A2	COL6A1	COL7A1	COL9A1	COL9A2	COX7B	CREB3L1	CREBBP	CROT	CRTAP	CRTC2	CSNK1A1
CSPP1	CTNNB1	CTNND1	CTSC	CTSK	CUL7	CYBA	CYBB	CYP27B1	DCAF17	DEPTOR	DFNB31	DGKG	DHCR24	DHCR7
DHODH	DKC1	DLL1	DLX3	DLX5	DMP1	DMTF1	DNM1	DOCK8	DOK2	DSG4	DSP	DSPP	DVL1	DVL3
EDA	EDAR	EDARADD	EFNB1	EHMT1	EIF2AK1	ELANE	ELN	EMR2	ENAM	ENPP1	EP300	ERCC3	ERCC4	ERCC8
EVC	EVC2	EXT1	EXT2	EYA1	EZR	FADD	FAM111B	FAM20A	FAM20B	FAM20C	FAM83H	FBN1	FERMT1	FERMT3
FGD1	FGF10	FGF13	FGF23	FGF3	FGF8	FGF9	FGFR1	FGFR2	FGFR3	FKBP10	FLNA	FLNB	FN1	FOXC1
FRAS1	FREM2	G6PC	GALC	GALNS	GALNT3	GAS1	GBP5	GDF5	GJA1	GJB3	GJB4	GJB6	GLA	GLB1
GLI2	GLI3	GNAS	GOLIM4	GORAB	GPC3	GPR68	GREM1	GREM2	GRHL2	GRHL3	GRIP1	GTF2I	GTF2IRD1	H19
H1FNT	HAX1	HCCS	HEMK1	HENMT1	HMBS	HMCN1	HNF1B	HOXB13	HOXD13	HRAS	HSPG2	IBSP	IDS	IDUA
IFIH1	IFITM5	IFT122	IFT140	IFT20	IFT43	IGF1R	IGSF3	IKBKG	IL11RA	IL17F	IL17RA	INSR	IPO4	IRF6
IRF8	IRX5	ITGA11	ITGA6	ITGB2	ITGB4	ITGB6	ITPR3	JAG1	KAL1	KANSL1	KAT6B	KATNB1	KAZN	KCNH1
KCNJ1	KCNJ2	KCTD1	KDF1	KDM6A	KIF7	KISS1	KISS1R	KL	KLK4	KMT2C	KMT2D	KRAS	KREMEN1	KRT14
KRT16	KRT17	KRT5	KRT6A	KRT6B	KRT6C	KRT83	LAMA3	LAMB2	LAMB3	LAMC2	LEF1	LEMD3	LEPRE1	LIFR
LIMK1	LMNA	LONP1	LRFN2	LRP4	LRP5	LRP6	LSS	LTBP2	LTBP3	LTF	LYSMD4	LYST	MAP2K1	MAP2K2
MASP1	MBTPS2	MED12	MED25	MEGF8	MEPE	MID1	MMP1	MMP14	MMP2	MMP20	MMP9	MPPE1	MSX1	MSX2
MTERF2	mTOR	MUTYH	MYCBP2	MYO1H	MYO7A	NAA10	NACC1	NCF1	NCF2	NCF4	NDN	NFKBIA	NHS	NIPBL
NKG7	NLRP1	NOD2	NOP10	NOTCH2	NOTCH3	NOTUM	NRAS	NSD1	NSUN2	NTRK1	OBSL1	OCRL	ODAM	OFD1
ORAI1	ORC1	OSTM1	PAX3	PAX9	PCDH15	PCNT	PDGFRB	PDZD7	PEX1	PEX26	PEX6	PHEX	PHKA2	PIGA
PIGL	PIK3CA	PIK3R1	PITX2	PKP1	PLEC	PLEKHM1	PLG	PLK4	PLOD1	PLXNB1	PLXNB2	PLXNB3	PLXND1	POC1A
POLD1	POLR1C	POLR1D	POLR3A	POLR3B	PORCN	PPIB	PRKAR1A	PROK2	PROKR2	PSAP	PTCH1	PTCH2	PTDSS1	PTH1R
PTHLH	PTPN11	PVRL1	PVRL4	RAB23	RAI1	RAPSN	RASGRP2	RBBP8	RBM28	RECQL4	RELT	REST	RFC2	RIMS4
RIN2	RMRP	RNF10	ROGDI	ROR2	RPS6KA3	RUNDC1	RUNX2	SALL4	SAMD12	SAT1	SATB2	SCARF2	SEC23A	SEC24D
SERPINF1	SERPING1	SERPINH1	SH3BP2	SH3PXD2B	SHH	SIX3	SLC10A7	SLC13A5	SLC20A1	SLC20A2	SLC24A4	SLC26A2	SLC29A3	SLC34A1
SLC34A2	SLC34A3	SLC35C1	SLC37A4	SLC39A13	SLC9A3R1	SMAD3	SMARCAL1	SMARCD2	SMG9	SMO	SMOC2	SNRPN	SNX33	SOS1
SOST	SOX10	SOX11	SOX18	SOX2	SOX21	SOX9	SP6	SP7	SPARC	SPARCL1	SPECC1L	SPP1	SPRED1	SPRY4
SQSTM1	SSUH2	STAT1	STAT3	STIM1	SUFU	SUMO1	SUOX	TACR3	TBCE	TBX1	TBX2	TBX22	TBX3	TCEAL7
TCIRG1	TCOF1	TCTEX1D2	TERC	TERT	TFAP2A	TFAP2B	TGFA	TGFB1	TGFB2	TGFB3	TGFBR1	TGFBR2	TGIF1	THRA
TINF2	TMCO1	TMEM165	TMEM38B	TNFRSF11A	TNFRSF11B	TNFSF11	TP63	TRAF6	TRIM37	TRIP10	TRIP11	TRPS1	TRPV3	TSC1
TSC2	TSPEAR	TUFT1	TWIST1	TWIST2	UBB	UBE3B	UBR1	UHRF1	USH1C	USH1G	USH2A	USP19	VAV1	VDR
VIPAS39	VPS13A	VPS13B	VPS33B	VPS4B	WDR19	WDR35	WDR6	WDR72	WDR83	WHSC1	WISP3	WNT1	WNT10A	WNT10B
WNT3	WNT5A	WRN	XPR1	ZEB1	ZEB2	ZFHX4	ZFPM1	ZIC2	ZMPSTE24	ZNF469	ZNF878			

Target gene	Target exon/intron	Transcript	Forward sequence	Reverse sequence
COL17A1	Intron 20	NM_000494.3	GATACTGCCAGAGTACCTGAA	CTCTCCAGAGCCTAAAACAAG
COL17A1	Exon 48	NM_000494.3	TGCTCTGATCTGCTTGCTGAGT	ACAGGTTTGAACGGCTCTGA
COL7A1	Exon 28	NM_000094.3	GAGAGGTGACATATTCAGCCCCAT	GTGGGGATAAGCCAGTCAG
COL7A1	Exon 30	NM_000094.3	GAGAGGTGACATATTCAGCCCCAT	GTGGGGATAAGCCAGTCAG
LAMB3	Exon 3	NM_000228.3	CCTCTTGCCCAACCAACAG	TGGAAGCTTGAGTGAGGGAAAGG
LAMB3	Exon 23	NM_000228.3	CCTCTACACATGCTACCTCCAGTTA	CATGAAAGTCTCCTGGAGATGGAA
LAMB3	Intron 11	NM_000228.3	TCCTACTGCGGTGGCTGCTGTT	TGACTCAGTCCCACCTTCCAA
LAMB3	Exon 14	NM_000228.3	TCTTGGCCCTAGCCTGTGACT	ACCAGCATGCCCGGTACTGGAA
LAMB3	Exon 20	NM_000228.3	TACAGAGGGCTGGGAGACAGGA	CACAAGACCAGAAAATCCAAG
LAMC2	Exon 4	NM_002336.2	AGTGAGTCCTTAAGTGTGTGAGA	GAAGGTCATCAACGTTTGTCAAGTA
ENAM	Intron 8	MN_031889.2	GGATTGCCAACAGATGCAGCCATA	CGGAAGCTTGAGCTACAGGTTCAT
ENAM	Intron 8	MN_031889.2	GGATTGCCAACAGATGCAGCCATA	CGGAAGCTTGAGCTACAGGTTCAT
ENAM	Intron 8	MN_031889.2	GGATTGCCAACAGATGCAGCCATA	CGGAAGCTTGAGCTACAGGTTCAT
ENAM	Exon 9	NM_031889.2	AAAGCTGAGCAGTGGTCAGAA	GCCCCATGACAGTACCAGTGAAAT
AMELX	Exon 2	NM_182680.1	CCCAACCTTTAGAGCCAACT	GGTCCCTTCCAAAAGCTTCCT
AMELX	Exon 6	NM_182680.1	GTCTACTCCACATGCAGACA	CTCTAGATCCTTGGTTGTCG
AMELX	Exon 6	NM_182680.1	GTCTACTCCACATGCAGACA	CTCTAGATCCTTGGTTGTCG
AMELX	Exon 6	NM_182680.1	GTCTACTCCACATGCAGACA	CTCTAGATCCTTGGTTGTCG
AMELX	Exon 6	NM_182680.1	GTCTACTCCACATGCAGACA	CTCTAGATCCTTGGTTGTCG
AMELX	Exon 6	NM_182680.1	GTCTACTCCACATGCAGACA	CTCTAGATCCTTGGTTGTCG
AMELX	Exon 6	NM_182680.1	GTCTACTCCACATGCAGACA	CTCTAGATCCTTGGTTGTCG
AMBN	Intron 1	NM_016519.5	TGTGGACTAATTGCAGGAGCAGAGA	GGATTACAACAAGCAATAATTCAGC
AMBN	Exon 8	NM_016519.5	GCAAACTCTTGGGTCATACCTC	GGAACCCATTATACTTCATATT
MMP20	Exon 1	NM_004771.3	ATCCTTGCTCGGAGGGTCCAGA	TTCACAAGCCACCTGGAATTCT
MMP20	Exon 3	NM_004771.3	GTACCGGATTATCCCAACTGTCTC	AGGTCATGTGGCTAACGGGAAA
MMP20	Exon 1	NM_004771.3	ATCCTTGCTCGGAGGGTCCAGA	TTCACAAGCCACCTGGAATTCT
MMP20	Intron 6	NM_004771.3	GGCAAGAGCAAAGGGCATTTAGTG	CAACCTGAGGACAAAGAGCAACTGA
MMP20	Exon 1	NM_004771.3	ATCCTTGCTCGGAGGGTCCAGA	TTCACAAGCCACCTGGAATTCT
MMP20	Exon 10	NM_004771.3	AACTGCCACCTGACAAATTCACAA	TTACAATATATGTCATGGAATCCAC
MMP20	Exon 2	NM_004771.3	CTTCAGTGACAAATAAGTGATCC	GTTCTTATTCTTATGGTTGTGAGG
MMP20	Intron 6	NM_004771.3	GGCAAGAGCAAAGGGCATTTAGTG	CAACCTGAGGACAAAGAGCAACTGA
MMP20	Exon 4	NM_004771.3	GTGGGGTAGGTTTTGCTATCGAAT	AGGGGATGACTGGTTCTTCAGATG
MMP20	Intron 6	NM_004771.3	GGCAAGAGCAAAGGGCATTTAGTG	CAACCTGAGGACAAAGAGCAACTGA
MMP20	Intron 6	NM_004771.3	GGCAAGAGCAAAGGGCATTTAGTG	CAACCTGAGGACAAAGAGCAACTGA
SLC24A4	Intron 16	NM_153647.3	TGCTGGGATTTCTGGATGGATTGG	TGCTCTTGGCAAAGACTGGACT
FAM83H	Exon 5	NM_198488.3	AGGAGTTCCGCATCCTCTTCG	AAGTCATCCGGGTCCGCGAAA
FAM83H	Exon 5	NM_198488.3	AGGAGTTCCGCATCCTCTTCG	AAGTCATCCGGGTCCGCGAAA
FAM83H	Exon 5	NM_198488.3	AGGAGTTCCGCATCCTCTTCG	AAGTCATCCGGGTCCGCGAAA
FAM83H	Exon 5	NM_198488.3	AGGAGTTCCGCATCCTCTTCG	AAGTCATCCGGGTCCGCGAAA
FAM83H	Exon 5	NM_198488.3	AGGAGTTCCGCATCCTCTTCG	AAGTCATCCGGGTCCGCGAAA
FAM83H	Exon 5	NM_198488.3	AGGAGTTCCGCATCCTCTTCG	AAGTCATCCGGGTCCGCGAAA
FAM83H	Exon 5	NM_198488.3	AGGAGTTCCGCATCCTCTTCG	AAGTCATCCGGGTCCGCGAAA
FAM83H	Exon 5	NM_198488.3	AGGAGTTCCGCATCCTCTTCG	AAGTCATCCGGGTCCGCGAAA
FAM83H	Exon 5	NM_198488.3	CTCTACCAGCAGCAGTACCA	GCCTGTGACGTGCTGAAGATG

WDR72	Exon 11	NM_182758.3	ATGCTGGCAATATGAATCTGG	AATCTTGTTTAGTGCAGTCT
FAM83H	Exon 5	NM_198488.3	CTCTACCAGCAGCAGTACCA	GCCTGTGACGTGCTGAAGATG
LTBP3	Intron 26	NM_001130144.3	AGCAATTCCTTCTGGGACACAAGC	ATATCTGAAGGTGAGGGCGACA
FAM20A	Exon 1	NM_017565.3	TTCCACCTCTGGCCCCAAGTA	GACTGGACTGTGAGGTCTGCAA
FAM20A	Exon 5	NM_017565.3	TTCCTTTCTCGCTGGTCATGCTCA	GGCGGGAAGCGTGTTCTTTGTA
FAM20A	Exon 6	NM_017565.3	CCTAGGTTTAAAGGCCCAGTGTTGA	TGCCCACACAGACTAGGTA
FAM20A	Intron 6	NM_017565.3	CCTAGGTTTAAAGGCCCAGTGTTGA	TGCCCACACAGACTAGGTA
FAM20A	Exon 6	NM_017565.3	CCTAGGTTTAAAGGCCCAGTGTTGA	TGCCCACACAGACTAGGTA
FAM20A	Intron 9	NM_017565.3	GAAAGCCTTAGACTTGAAGCCA	TTGTGAATCAGAGATTGGG
FAM20A	Exon 11	MN_017565.3	GCAAAGGACTGCAGGATACTGGAT	AGATTTCCCAGTGCACTCAGGAGA
DLX3	Exon 3	NM_005220.2	TGACAGAGCAGAATTTGGAC	CTGGAAGATGATGAGCCATTTA
DLX3	Exon 3	NM_005220.2	TGACAGAGCAGAATTTGGAC	CTGGAAGATGATGAGCCATTTA
TGFBR2	Exon 7	NM_003242.5	ACTCAGTCAGCACATGTTAAAT	TGACAATGTCAAAGGCATAGAAT
CNNM4	Exon 1	NM_020184.3	TCGAGCTCACCAAGGACCTG	TGTTGGCACCCACAGCCAG
SLC10A7	Exon 3	NM_001300842.3	TGACCAGTGCTTTGGTGCATCT	CACAGGATGAAGCATGAGGGTGTA
ROGDI	Exon 6	NM_024589.2	AACTCGCACAGACTCTTGTCTTGG	TGGTGAACAGTCACTCCAGCTT
ROGDI	Exon 6	NM_024589.2	AACTCGCACAGACTCTTGTCTTGG	TGGTGAACAGTCACTCCAGCTT

Supplementary Table 2: List of primer's sequences used for Sanger sequencing.

Supplementary Table S3: Variations found in individuals presenting with isolated amelogenesis imperfecta. Variations found in 17 different genes in 85 individuals presenting with isolated amelogenesis imperfecta. One hundred eleven variants were found, 19 variants are of uncertain significance. Variants known and previously published are reported in grey, variants previously reported by the team are represented in salmon, variants published thanks to GenoDENT panel are represented in blue or green, new variants reported for the first time are highlighted in green. Familial segregation is also reported when available and reported as: Family member code (Phenotype code, Genotype code): Fa: father; Mo: mother; S: sibling; D: daughter; So: son; Co: cousin; A: affected; U: unaffected; NA: not available; C: carrier; R: reference genotype.

Patient number	Diagnosis/AI	Gene	Variant and location	Zygosity	Mode of inheritance	rank	Effect of the mutation	Consistent with the known disease phenotype	Family segregation	Status	statut
1.1 (female)	Hypoplasic (pits)	***COL17A1*** Chr10(GRCh37) : NM_000494.4	**c.1646G>A** ; p.(Trp549*) Exon 18 (Prasad et al., 2016)	heterozygous	AD	5	nonsense	Yes	Mo5(A,C)	Panel	A1
1.2 (female)	Hypoplasic (pits)	***COL17A1*** Chr10(GRCh37) : NM_000494.4	**c.1745-2A>C**; p.? Intron 20 (Hérissé et al., 2021)	heterozygous	AD	4	splice	Yes	S2D(A,C)	Panel	D6S2
1.3 (female)	Hypoplasic (pits)	***COL17A1*** Chr10(GRCh37) : NM_000494.4	**c.1873C>T**; p.(Arg625*) Exon 23 (Prasad et al., 2016)	heterozygous	AD	5	nonsense	Yes	NA	Panel	A2
1.4 (male)	Hypoplasic (pits)	***COL17A1*** Chr10(GRCh37) : NM_000494.4	**c.1873C>T**; p.(Arg625*) Exon 23 (Prasad et al., JDR. 2016)	heterozygous	AD	5	nonsense	Yes	S2Co(A,C)	Panel	A1
1.5 (female)	Hypoplasic (pits)	***COL17A1*** Chr10(GRCh37) : NM_000494.4	**c.2407G>T**, p.(Gly803*) Exon 34 (Darling et al., 1999)	heterozygous	AD	5	nonsense	Yes	Mo(A,C)	Panel	A1
1.6 (male)	Hypoplasic (pits)	***COL17A1*** Chr10(GRCh37) : NM_000494.4	**c.3327del** ; p.(Pro1110Argfs*21) Exon 48 (Pasmooij et al., 2004)	heterozygous	AD	5	frameshift	Yes	Mo(NA,C)	Panel	A2
Patient number	**Diagnosis**	**Gene**	**Variant and location**	**Zygosity**		**rank**	**Effect of the mutation**	**Consistent with the known disease phenotype**	**Family segregation**	**Status**	**statut**
2.1 (female)	Hypoplastic (pits)	***COL7A1*** Chr3(GRCh37): NM_000094.4	**c.2440+3A>C** ; p.? Intron 19	heterozygous	AD	3	splice	Yes	NA	Panel	D6S2
2.2 (female)	Hypoplastic (pits)	***COL7A1*** Chr3(GRCh37): NM_000094.4	**c.3605G>A** ; p.(Arg1202His) Exon 28	heterozygous	AD	3	missense	Yes	2S(A,C)	Panel	A1
2.3 (male)	Hypoplastic (pits)	***COL7A1*** Chr3(GRCh37): NM_000094.4	**c.3785T>C** ; p.(Met1262Thr) Exon 30	heterozygous	AD	3	missense	Yes	Mo(A,C)	Panel	D1S2
Patient number	**Diagnosis**	**Gene**	**Variant and location**	**Zygosity**		**rank**	**Effect of the mutation**	**Consistent with the known disease phenotype**	**Family segregation**	**Status**	**statut**
3.1 (female)	Hypoplasic (pits)	***COL17A1*** Chr10(GRCh37): NM_000494.4	**c.1141+1G>A** ; p.? Intron 14 (Prasad et al., 2016)	heterozygous	AD	4	splice	Yes but more pitted	Mo(A,C)	Panel	A1
		LAMA3 Chr18(GRCh37): NM_198129.4	**c.6477_6486del** ; p.(Ile2159Metfs*16) Exon 51 (Prasad et al., 2016)	heterozygous	AD	4	frameshift		Mo(A,R)	Panel	A1
Patient number	**Diagnosis**	**Gene**	**Variant and location**	**Zygosity**		**rank**	**Effect of the mutation**	**Consistent with the known disease phenotype**	**Family segregation**	**Status**	**statut**
4.1 (male)	Hypoplasic (pits)	***LAMB3*** Chr1(GRCh37): NM_000228.3	**c.124C>T** ; p.(Arg42*) Exon 3 (McGrath et al., 1995)	compound heterozygous	AD	5	nonsense	Yes	Mo(U,C)	Panel	D1S2
			c.3490C>T ; p.(Arg1164Cys) Exon 23		AR	3	missense	Yes	Fa(U,C)	Panel	D1S2
4.2 (female)	Hypoplastic (pits) Agenesis 1s ot 2s history of recurrent corneal ulcers	***LAMB3*** Chr1(GRCh37): NM_000228.3	**c.1288+1G>T** ; p.? Intron 11 (Kiritsi et al., 2015)	compound heterozygous	AD	4	splice	Yes	Mo(U,C)	Panel	D9S2
			c.1903C>T ; p.(Arg635*) Exon 14 (Pulkkinen et al., 1994)		AD	5	nonsense	Yes	Fa(U,C)	Panel	D9S2
4.3 (female)	Hypoplastic (pits)	***LAMB3*** Chr1(GRCh37): NM_000228.3	**c.944-14C>G** ; p.? Intron 9	heterozygous	AD	3	splice	Yes	MoFa(U,NA)	Panel	A1
			c.1903C>T ; p.(Arg635*) Exon 14 (Pulkkinen et al., 1994)	heterozygous	AD	5	nonsense	Yes	MoFa(U,NA)	Panel	A1
4.4 (male)	Hypoplastic	***LAMB3*** Chr1(GRCh37): NM_000228.3	**c.2926del** ; p.(Val976Trpfs*51) Exon 20	heterozygous	AD	4	frameshift	Yes	Fa(A,C)	Panel	D3S1
4.5 (female)	Hypoplastic	***LAMB3*** Chr1(GRCh37): NM_000228.3	**c.3305del** ; p.(Gly1102Valfs*7) Exon 22	heterozygous	AD	4	frameshift	Yes	NA	Panel	D8S2
Patient number	**Diagnosis**	**Gene**	**Variant and location**	**Zygosity**		**rank**	**Effect of the mutation**	**Consistent with the known disease phenotype**	**Family segregation**	**Status**	**statut**
5.1 (female)	Hypoplastic	***LAMC2*** Chr1(GRCh37): NM_005562.3	**c.493C>T** ; p.(Arg165Cys) Exon 4	heterozygous	AD	3	missense	Never described phenotype	Mo(NA,C)	Panel	D2S1
Patient number	**Diagnosis**	**Gene**	**Variant and location**	**Zygosity**		**rank**	**Effect of the mutation**	**Consistent with the known disease phenotype**	**Family segregation**	**Status**	**statut**
6.1 (female)	Hypoplastic, long roots, delayed eruption	***ENAM*** Chr4(GRCh37): NM_031889.3	**c.101T>C** ; p.(Leu34Pro) Exon 3	heterozygous	AD	3	missense	Yes	NA	Panel	A1
6.2 (male)	Hypoplastic	***ENAM*** Chr4(GRCh37): NM_031889.3	**c.123+1G>A** ; p.? Intron 3 (Prasad et al., 2016)	heterozygous	AD	4	splice	Yes	S(A,C)	Panel	A2
6.3 (female)	Hypoplastic/hypomature	***ENAM*** Chr4(GRCh37): NM_031889.3	**c.588+1 dup** ; p.? Intron 8	heterozygous	AD	4	splice	Yes	FaS(A,C)	Panel	A?
6.4 (female)	Hypoplastic	***ENAM*** Chr4(GRCh37): NM_031889.3	**c.588+1 del** ; p.? Intron 8 (Kida et al., 2002)	heterozygous	AD	5	frameshift/splice	Yes	NA	Panel	D2S2
6.5 (male)	Hypoplastic	***ENAM*** Chr4(GRCh37): NM_031889.3	**c.588+1 del** ; p.? Intron 8 (Kida et al., 2002)	heterozygous	AD	5	frameshift/splice	Yes	NA	Panel	A
6.6 (male)	Hypoplastic	***ENAM*** Chr4(GRCh37): NM_031889.3	**c.588+1 del** ; p.? Intron 8 (Kida et al., 2002)	heterozygous	AD	5	frameshift/splice	Yes	Mo(U,R) Fa(NA,NA)	Panel	D12S1
6.7 (male)	Hypoplastic	***ENAM*** Chr4(GRCh37): NM_031889.3	**c.588+1 del** ; p.? Intron 8 (Kida et al., 2002)	heterozygous	AD	5	frameshift/splice	Yes	MoS(A,C)	Panel	D5S1
6.8 (male)	Hypoplastic	***ENAM*** Chr4(GRCh37): NM_031889.3	**c.664C>T** ; p.(Gln222*) Exon 9	heterozygous	AD	5	nonsense	Yes	S(A,C) Mo(NA,C)	Panel	D7S1
Patient number	**Diagnosis**	**Gene**	**Variant and location**	**Zygosity**		**rank**	**Effect of the mutation**	**Consistent with the known disease phenotype**	**Family segregation**	**Status**	**statut**
7.1 (female)	Hypoplastic, banding pattern, Lyonisation	***AMELX*** ChrX(GRCh37): NM_182680.1	**c.11G>A** ; p.(Trp4*) Exon 2 (Hart et al., 2002)	heterozygous	XL	5	nonsense	Yes	Fa(A,NA)	Panel	D1S2
7.2 (male, 7.3 father)	Hypoplastic	***AMELX*** ChrX(GRCh37): NM_182680.1	**c.11G>A** ; p.(Trp4*) Exon 2 (Hart et al., 2002)	hemizygous	XL	5	nonsense	Yes	D(A,C)	Panel +JY sire	A
7.3 (female, 7.2 daughter)	Hypoplastic, banding pattern, Lyonisation	***AMELX*** ChrX(GRCh37): NM_182680.1	**c.11G>A** ; p.(Trp4*) Exon 2 (Hart et al., 2002)	heterozygous	XL	5	nonsense	Yes	Fa(A,C)	Panel +JY sire	
7.4 (female)	Hypoplastic, banding pattern, Lyonisation	***AMELX*** ChrX(GRCh37): NM_182680.1	**c.47C>A** ; p.(Ala16Asp) Exon 2	heterozygous	XL	4	missense	Yes	Fa(A,C)	Panel	D5S1
7.5 (male)	Hypomature	***AMELX*** ChrX(GRCh37): NM_182680.1	**c.155C>T** ; p.(Pro52Leu) Exon 5 (Prasad et al., 2016)	hemizygous	XL	4	missense	No	Mo(U,R) Fa(U,R)	Panel	A1

7.6 (male)	Hypomature	***AMELX*** ChrX(GRCh37): NM_182680.1	**c.208C>A** ; p.(Pro70Thr) Exon 6 (Collier et al., 1997)	hemizygous	XI	5	missense	Yes	S(A,C)	Panel	D3S1
7.7 (male)	Hypomature Agenesis 12, 15, 22, 25, 28	***AMELX*** ChrX(GRCh37): NM_182680.1	**c.208C>A**; p.(Pro70Thr) Exon 6 (Collier PM et al., 1997)	hemizygous	XL	5	missense	Yes	MoS(NA,C)	Panel	A2
		WNT10A Chr12GRCh37): NM_025216.3	**c.682T>A**; p.(Phe228Ile) Exon 3 (Bohring et al., 2009)	heterozygous	XI	5	missense	Yes	NA	Panel	A2
7.8 (female, 7.9 cousin)	Hypoplastic, banding pattern, Lyonisation	***AMELX*** ChrX(GRCh37): NM_182680.1	**c.473del** ; p.(Pro158Hisfs*31) Exon 6 (Lench et al., 1995)	heterozygous	XL	5	frameshift	Yes	Mo(A,C)	Panel	D2S1
7.9 (male;XXY, 7.8 cousin)	Hypoplastic with banding pattern, behavioral disorders	***AMELX*** ChrX(GRCh37): NM_182680.1	**c.473del** ; p.(Pro158Hisfs*31) Exon 6 (Lench et al., 1995)	heterozygous	XI	5	frameshift	Yes	Mo(A,C)	Panel	Sanger
7.10 (male, 7.11 son)	Hypoplastic, no enamel, eruption delay, behavioral disorders	***AMELX*** ChrX(GRCh37): NM_182680.1	**c.541del** ; p.(Leu181Cysfs*8) Exon 6 (Kindelan et al., 2000)	hemizygous	XL	5	frameshift	Yes	Mo(A,C)	Exome	exome
7.11 (female, 7.10 mother)	Hypoplastic, banding pattern, Lyonisation	***AMELX*** ChrX(GRCh37): NM_182680.1	**c.541del** ; p.(Leu181Cysfs*8) Exon 6 (Kindelan et al., 2000)	heterozygous	XL	5	frameshift	Yes	D(A,C)	Exome	Exome
Patient number	**Diagnosis**	**Gene**	**Variant and location**	**Zygosity**		**rank**	**Effect of the mutation**	**Consistent with the known disease phenotype**	**Family segregation**	**Status**	**statut**
8.1 (female)	Hypoplastic	***AMBN*** Chr4(GRCh37): NM_016519.6	**c.15+1G>A** ; p.? Intron 1	putative compound heterozygous	AR	3	splice	No	Mo(U,C)	Panel	A1
			c.577G>T ; p.(Gly193*) Exon 8		AR	3	nonsense		NA		
8.2 (male)	Hypoplastic	***AMBN*** Chr4(GRCh37): NM_016519.6	**c.209C>G** ; p.(Ser70*) Exon 5	putative compound heterozygous	AR	3	nonsense	Yes	NA	Panel	D3S2
			c.571-1G>C ; p.? Intron 7		AR	3	splice		NA		
8.3 (female)	Hypoplastic	***AMBN*** Chr4(GRCh37): NM_016519.6	**c.532-1G>C** ; p.? Intron 6 (Prasad et al., 2016)	homozygous	AR	4	splice	Yes	S(A,C)	Panel	A
Patient number	**Diagnosis**	**Gene**	**Variant and location**	**Zygosity**		**rank**	**Effect of the mutation**	**Consistent with the known disease phenotype**	**Family segregation**	**Status**	**statut**
9.1 (female)	Hypoplastic, thin enamel	***ACP4*** Chr19(GRCh37): NM_033068.3	**c.331C>T** ; p.(Arg111Cys) Exon 4 (Seymen et al., 2016)	compound heterozygous	AR	4	missense	Yes	Mo(U,C)	exome	A
			c.645+1G>A ; p.? Intron 6		AR	4	splice		Fa(U,C)		
9.2 (female)	Hypoplastic	***ACP4*** Chr19(GRCh37): NM_033068.3	**c.428C>T** ; p.(Thr143Met) Exon 4 (Smith et al., 2017)	compound heterozygous	AR	4	missense	phenotype is not visible due to prosthodontic treatment (full mouth prosthodontic rehabilitation)	S(A,C) Fa(U,C)	exome	A2
			c.736G>A ; p.(Val246Met) Exon 7		AR	4	missense		S(A,C) Mo(U,C)		
9.3 (female)	Hypoplastic, thin enamel, Agenesis 18,28	***ACP4*** Chr19(GRCh37): NM_033068.3	**c.626T>C** ; p.(Leu209Pro) Exon 6	compound heterozygous	AR	3	missense	Yes	Mo(U,C)	exome	A1
			c.1199C>A ; p.(Ala400Asp) Exon 11		AR	3	missense		Fa(U,C)		
		WNT10A Chr12GRCh37): NM_025216.3	**c.682T>A**; p.(Phe228Ile) Exon 3 (Bohring et al., 2009)	heterozygous	AD	5	missense	Yes	FaS(NA,C)		A1
Patient number	**Diagnosis**	**Gene**	**Variant and location**	**Zygosity**		**rank**	**Effect of the mutation**	**Consistent with the known disease phenotype**	**Family segregation**	**Status**	**statut**
10.1 (female)	Hypomature (pigmented) soft, nail, dry skin	***KLK4*** Chr19(GRCh37): NM_004917.4	**c.443G>T** ; p.(Cys148Phe) Exon 3	compound heterozygous	AR	3	missense	Yes	NA	Panel	D3S2
			c.458G>A ; p.(Trp153*) Exon 3 (Hart et al., 2004)		AR	4	nonsense		NA		
Patient number	**Diagnosis**	**Gene**	**Variant and location**	**Zygosity**		**rank**	**Effect of the mutation**	**Consistent with the known disease phenotype**	**Family segregation**	**Status**	**statut**
11.1 (male)	Hypomature (pigmented)	***MMP20*** Chr11(GRCh37): NM_004771.4	**c.103A>C** ; p.(Arg35=) Exon 1 (Prasad et al., 2016)	compound heterozygous	AR	5	splice	Yes	Mo(U,C)	Panel	D5S1
			c.389C>T ; p.(Thr130Ile) Exon 3 (Gasse et al., 2013)		AR	4	missense		Fa(U,C)		
11.2 (female)	Hypomature (pigmented)	***MMP20*** Chr11(GRCh37): NM_004771.4	**c.103A>C** ; p.(Arg35=) Exon 1 (Prasad et al., 2016)	compound heterozygous	AR	5	splice	Yes	NA	JY sire	A1
			c.954-2A>T ; p.? Intron 6 (Kim et al., 2005)		AR	5	splice		NA		
11.3 (male)	Hypomature (pigmented)	***MMP20*** Chr11(GRCh37): NM_004771.4	**c.103A>C** ; p.(Arg35=) Exon 1 (Prasad et al., 2016)	compound heterozygous	AR	5	splice	Yes	Mo(U,C) S(A,C)	Panel	D6S1
			c.954-2A>T ; p.? Intron 6 (Kim et al., 2005)		AR	5	splice	Yes	Fa(U,C) S(A,C)	Panel	D6S1
11.4 (male)	Hypomature (pigmented)	***MMP20*** Chr11(GRCh37): NM_004771.4	**c.103A>C** ; p.(Arg35=) Exon 1 (Prasad et al., 2016)	compound heterozygous	AR	5	splice	Yes	Mo(U,C)	Panel	D5S1
			c.1362C>G ; p.(Tyr454*) Exon 10		AR	4	nonsense		Fa(U,C)		
11.5 (male)	Hypomature (pigmented)	***MMP20*** Chr11(GRCh37): NM_004771.4	**c.126+6T>G ; p.?** Intron 1 (Prasad et al., 2016)	compound heterozygous	AR	3	splice	Yes	NA	JY sire	A1
			c.954-2A>T ; p.? Intron 6 (Kim et al., 2005)		AR	5	splice		NA		
11.6 (male)	Hypomature (pigmented)	***MMP20*** Chr11(GRCh37): NM_004771.4	**c.323A>G** ; p.(Tyr108Cys) Exon 2 (Gasse et al., 2013)	homozygous	AR	4	missense	Yes	NA	Panel	A0
11.7 (female)	Hypomature (pigmented)	***MMP20*** Chr11(GRCh37): NM_004771.4	**c.359del** ; p.(Asn120Ilefs*3) Exon 2 (Gasse et al., 2013)	compound heterozygous	AR	4	frameshift	Yes	NA	JY sire	A0
			c.389C>T ; p.(Thr130Ile) Exon 3 (Gasse et al., 2013)		AR	4	missense		NA		
11.8 (female)	Hypomature (pigmented)	***MMP20*** Chr11(GRCh37): NM_004771.4	**c.359dup** ; p.(Asn120Lysfs*9) Exon 2	compound heterozygous	AR	4	frameshift	Yes	Fa(U,C)	Panel	D6S1
			c.954-2A>T ; p.? Intron 6 (Kim et al., 2005)		AR	5	splice		Mo(U,C)		

11.9 (female)	Hypomature (pigmented)	***MMP20*** Chr11(GRCh37): NM_004771.4	**c.389C>T** ; p.(Thr130Ile) Exon 3 (Gasse et al., 2013)	homozygous	AR	4	missense		NA	JY sirc	A0
11.10 (male)	Hypomature (pigmented)	***MMP20*** Chr11(GRCh37): NM_004771.4	**c.389C>T** ; p.(Thr130Ile) Exon 3 (Gasse et al., 2013)	compound heterozygous	AR	4	missense	Yes	NA	JY sirc	A0
			c.954-2A>T ; p.? Intron 6 (Kim et al., 2003)		AR	5	splice		NA		
11.11 (female)	Hypomature (pigmented)	***MMP20*** Chr11(GRCh37): NM_004771.4	**c.530G>A** ; p.(Gly177Glu) Exon 4	compound heterozygous	AR	3	missense	Yes	Mo(U,C)	Panel	D9S2
			c.954-2A>T ; p.? Intron 6 (Kim et al., 2003)		AR	5	splice		Fa(U,C)		
11.12 (female)	Hypomature (pigmented)	***MMP20*** Chr11(GRCh37): NM_004771.4	**c.566T>C** ; p.(Leu189Pro) Exon 4 (Gasse et al., 2017)	compound heterozygous	AR	4	missense	Yes	NA	JY sirc	A0
			c.910G>A ; p.(Ala304Thr) Exon 6 (Lee et al., 2010)		AR	4	missense		NA		
11.13 (female)	Hypomature (pigmented)	***MMP20*** Chr11(GRCh37): NM_004771.4	**c.566T>C** ; p.(Leu189Pro) Exon 4 (Gasse et al., 2017)	supposed compound heterozygous	AR	4	missense	Yes	NA	Panel	A2
			c.1126C>T ; p.(Gln376*) Exon 8		AR	4	nonsense		NA		
11.14 (male)	Hypomature (pigmented)	***MMP20*** Chr11(GRCh37): NM_004771.4	**c.954-2A>T** ; p.? Intron 6 (Kim et al., 2003)	homozygous	AR	5	splice	Yes	NA	Panel	D1S2
11.15 (female)	Hypomature (pigmented)	***MMP20*** Chr11(GRCh37): NM_004771.4	**c.954-2A>T** ; p.? Intron 6 (Kim et al., 2003)	homozygous	AR	5	splice	Yes	S(A,C)	Panel	D4S1
11.16 (female)	Hypomature (pigmented)	***MMP20*** Chr11(GRCh37): NM_004771.4	**c.954-2A>T** ; p.? Intron 6 (Kim et al., 2003)	homozygous	AR	5	splice	Yes	NA	JY sirc	A0
11.17 (female)	Hypomature (pigmented)	***MMP20*** Chr11(GRCh37): NM_004771.4	**c.954-2A>T** ; p.? Intron 6 (Kim et al., 2003)	homozygous	AR	5	splice	Yes	NA	JY sirc	A
Patient number	**Diagnosis**	**Gene**	**Variant and location**	**Zygosity**		**rank**	**Effect of the mutation**	**Consistent with the known disease phenotype**	**Family segregation**	**Status**	**statut**
12.1 (female)	Hypomature	***WDR72*** Chr15(GRCh37): NM_182758.4	**c.-13+889_7del** Intron 1-Exon2	homozygous	AR	4	deletion	Yes	NA	Panel	A2
12.2 (female)	Hypomature, small teeth, agenesis, nephrocalcinosis, mild deafness	***WDR72*** Chr15(GRCh37): NM_182758.4	**c.118C>T** : p.(Gln40*) Exon 2	putative compound heterozygous	AR	4	nonsense	Yes	NA	Panel	D1S2
			c.954+1_954+10del : p.? Intron 9		AR	4	splice		NA		
12.3 (male)	Hypomature	***WDR72*** Chr15(GRCh37): NM_182758.4	**c.182A>G** : p.(His61Arg) Exon 3 (Prasad et al., 2016)	compound heterozygous	AR	4	missense	Yes	Mo(U,C)	Panel	A
			c.815G>A ; p.(Trp272*) Exon 8 (Prasad et al., 2016)		AR	4	nonsense		Fa(U,C)		
12.4 (female)	Hypomature	***WDR72*** Chr15(GRCh37): NM_182758.4	**c.2146del** ; p.(Ala716Profs*10) Exon 15	compound heterozygous	AR	4	frameshift	Yes	NA	Panel	D6S2
			c.2388del ; p.(Lys796Asnfs*16) Exon 15		AR	4	frameshift		NA		
Patient number	**Diagnosis**	**Gene**	**Variant and location**	**Zygosity**		**rank**	**Effect of the mutation**	**Consistent with the known disease phenotype**	**Family segregation**	**Status**	**statut**
13.1 (female)	Hypomature	***ODAPH*** Chr4(GRCh37): NM_178497.5	**c.39_46del** ; p.(Cys14Glyfs*18) Exon 1 (Prasad et al. IDR, 2016)	homozygous	AR	4	frameshift	Yes	NA	Panel	A1*
Patient number	**Diagnosis**	**Gene**	**Variant and location**	**Zygosity**		**rank**	**Effect of the mutation**	**Consistent with the known disease phenotype**	**Family segregation**	**Status**	**statut**
14.1 (male)	Hypomature	***SLC24A4*** Chr14(GRCh37): NM_153646.4	**c.(1537+1_1538-1del)_*67** ; p.? Intron 14 (Prasad et al., 2016)	homozygous	AR	4	deletion	Yes	MoFa(U,C)	Panel	A1
14.2 (female)	Hypomature	***SLC24A4*** Chr14(GRCh37): NM_153646.4	**c.1716+5G>A** : p.? Intron 16	homozygous	AR	3	splice	Yes	S(A,C)	Panel	D1S2
Patient number	**Diagnosis**	**Gene**	**Variant and location**	**Zygosity**		**rank**	**Effect of the mutation**	**Consistent with the known disease phenotype**	**Family segregation**	**Status**	**statut**
15.1 (female)	Hypomineralized	***FAM83H*** Chr8(GRCh37): NM_198488.5	**c.930_939dup** ; p.(Val314Argfs*14) Exon 5	heterozygous	AD	5	frameshift	Yes	S(U,R)	Panel	D6S2
15.2 (female)	Hypomineralized	***FAM83H*** Chr8(GRCh37): NM_198488.5	**c.973C>T** : p.(Arg325*) Exon 5 (Kim et al., 2008)	heterozygous	AD	5	nonsense	Yes	MoFa(U,R)	Panel	D7S1
15.3 (female)	Hypomineralized	***FAM83H*** Chr8(GRCh37): NM_198488.5	**c.1261G>T** ; p.(Glu421*) Exon 5 (Nnwawaroe et al., 2018)	heterozygous	AD	5	nonsense	Yes	NA	Panel	A2
15.4 (male)	Hypomineralized	***FAM83H*** Chr8(GRCh37): NM_198488.5	**c.1282C>T** : p.(Gln428*) Exon 5 (Prasad et al., 2016)	heterozygous	AD	5	nonsense	Yes	Fa(A,C)	Panel	A1
15.5 (female)	Hypomineralized	***FAM83H*** Chr8(GRCh37): NM_198488.5	**c.1289C>A** ; p.(Ser430*) Exon 5 (Wright et al., 2011)	heterozygous	AD	5	nonsense	Yes	S(A,C)	Panel	A1
15.6 (female)	Hypomineralized	***FAM83H*** Chr8(GRCh37): NM_198488.5	**c.1309_1311delinsTAG** ; p.(His437*) Exon 5	heterozygous	AD	5	nonsense	Yes	Fa(A,C)	Panel	D1S1
15.7 (male)	Hypomineralized	***FAM83H*** Chr8(GRCh37): NM_198488.5	**c.1374C>G** ; p.(Tyr458*) Exon 5 (El Sayed et al., 2010)	heterozygous	AD	5	nonsense	Yes	MoFa(U,R)	Panel	A2
15.8 (male)	Hypomineralized	***FAM83H*** Chr8(GRCh37): NM_198488.5	**c.1374C>G** ; p.(Tyr458*) Exon 5 (El-Sayed et al., 2010)	heterozygous	AD	5	nonsense	Yes	MoFa(U,R)	Panel	A2
15.9 (female)	Hypomineralized	***FAM83H*** Chr8(GRCh37): NM_198488.5	**c.1375C>T** ; p.(Gln459*) Exon 5	heterozygous	AD	5	nonsense	Yes	Fa(A,C)	Panel	D8S1
15.10 (female)	Hypomineralized	***FAM83H*** Chr8(GRCh37): NM_198488.5	**c.1379G>A** ; p.(Trp460*) Exon 5 (Wright et al., 2009)	heterozygous	AD	5	nonsense	Yes	MoFa(U,R)	Panel	A2
15.11 (male)	Hypomineralized	***FAM83H*** Chr8(GRCh37): NM_198488.5	**c.1387C>T** ; p.(Gln463*) Exon 5 (Kantapura et al., 2016)	heterozygous	AD	5	nonsense	Yes	NA	Panel	D2S2
15.12 (female)	Hypomineralized	***FAM83H*** Chr8(GRCh37): NM_198488.5	**c.1387C>T** : p.(Gln463*) Exon 5 (Kantapura et al., 2016)	heterozygous	AD	5	nonsense	Yes	MoS(A,C)	Panel	D6S1
15.13 (male)	Hypomineralized	***WDR72*** Chr15(GRCh37): NM_182758.4	**c.1283T>G** : p.(Ile428Ser) Exon 11	homozygous	AR	3	missense	Yes	S(A,C)	Panel	D5S2
		FAM83H Chr8(GRCh37): NM_198488.5	**c.1498C>G** ; p.(Leu500Val) Exon 5	heterozygous	AD	3	missense		S(A,C)	Panel	D5S2
15.14 (female)	Hypomineralized	***FAM83H*** Chr8(GRCh37): NM_198488.5	**c.1993C>T** ; p.(Gln665*) Exon 5 (Lee et al., 2011)	heterozygous	AD	5	nonsense	Yes	Fa(A,C)	Panel	D7S1
15.15 (male)	Hypomineralized	***FAM83H*** Chr8(GRCh37): NM_198488.5	**c.2029C>T** ; p.(Gln677*) Exon 5 (Lee et al., 2008)	heterozygous	AD	5	nonsense	Yes	NA	Panel	A1
Patient number	**Diagnosis**	**Gene**	**Variant and location**	**Zygosity**		**rank**	**Effect of the mutation**	**Consistent with the known disease phenotype**	**Family segregation**	**Status**	**statut**
16.1 (female)	Hypoplastic	***DLX3*** Chr17(GRCh37): NM_005220.3	**c.92C>G** ; p.(Thr31Ser) Exon 1	heterozygous	AD	3	missense	Yes	S(NA,C) Mo(NA,R)	Panel	A1
16.2 (female)	Hypoplastic, taurodontism permanent molars	***DLX3*** Chr17(GRCh37): NM_005220.3	**c.537C>A** ; p.(Asn179Lys) Exon 3	heterozygous	AD	4	missense	Yes	NA	Panel	D7S2
16.3 (female)	Hypoplastic, taurodontism (16,26,36,46, primary molars)	***DLX3*** Chr17(GRCh37): NM_005220.3	**c.710A>G** ; p.(Tyr237Cys) Exon 3	heterozygous	AD	3	missense	Yes	S(A,C)	Panel	A1
		WNT10A Chr12GRCh37): NM_025216.3	**c.637G>A** ; p.(Gly213Ser) Exon 3 (Plaisancié et al., 2013)	heterozygous	AD	4	missense		S(NA,C)		

Supplementary Table S4: Key diagnostic clinical signs associated to AI in syndromes

Clinical signs	Associated to AI	Syndrome - mode of inheritance	Phenotype OMIM number	Gene	AI type
HEAD & NECK					
Head	Craniosynostosis	Craniosynostosis 2 - AD	604757	*MSX2*	Hypoplastic
	Micrognathia, Retrognathia	Loeys-Dietz syndrome 2 - AD	610168	*TGFBR2*	Hypoplastic
	Dysmorphic traits	Smith-Magenis syndrome - AD	182290	*RAI1*	Hypoplastic
		Short stature, and skeletal dysplasia with scoliosis - AR	618363	*SLC10A7*	Hypomineralized
Eye	Hypertelorism, Exotropia	Loeys-Dietz syndrome 2 - AD	610168	*TGFBR2*	Hypoplastic
	Severe visual impairment	Hypomagnesemia 5, renal, with ocular involvement - AR	248190	*CLDN19*	Hypoplastic
	Corneal opacities	Mucopolysaccharidosis IVA - AR	253000	*GALNS*	Hypoplastic
	Myopia	Craniosynostosis 2 - AD	604757	*MSX2*	Hypoplastic
	Cone-rod dystrophy, Nystagmus, Photophobia	Jalili syndrome - AR	217080	*CNNM4*	Hypomineralized
Ears	Sensorineural hearing loss	Heimler syndrome 1 – AR	234580	*PEX1*	Hypoplastic
		Heimler syndrome 2 - AR	616617	*PEX6*	Hypoplastic
		Heimler syndrome - AR	/	*PEX26*	Hypoplastic
	Moderate hearing impairment	Short stature, and skeletal dysplasia with scoliosis - AR	618363	*SLC10A7*	Hypomineralized
Orodental	Lip papillomas	Focal dermal hypoplasia - XLD	305600	*PORCN*	Hypoplastic
	Cleft lip	EEC syndrome-3 – AD	604292	*TP63*	Hypoplastic
		Raine syndrome - AR	259775	*FAM20C*	Hypoplastic
	Cleft palate	EEC syndrome-3 – AD	604292	*TP63*	Hypoplastic
		Raine syndrome – AR	259775	*FAM20C*	Hypoplastic
		Short stature, and skeletal dysplasia with scoliosis - AR	618363	*SLC10A7*	Hypomineralized
	Bifid uvula	Loeys-Dietz syndrome 2 - AD	610168	*TGFBR2*	Hypoplastic
	Gingival hyperplasia	Enamel-renal syndrome – AR	204690	*FAM20A*	Hypoplastic
		Raine syndrome - AR	259775	*FAM20C*	Hypoplastic
	Gingival fibroma	Tuberous sclerosis-1 – AD	191100	*TSC1*	Hypoplastic
		Tuberous sclerosis-2 - AD	613254	*TSC2*	Hypoplastic
	Tooth agenesis	Dental anomalies and short stature – AR	601216	*LTBP3*	Hypoplastic
		EEC syndrome-3 – AD	604292	*TP63*	Hypoplastic
		Developmental and epileptic encephalopathy 25 -AR	615905	*SLC13A5*	Hypoplastic
	Teeth eruption delay	Developmental and epileptic encephalopathy 25 -AR	615905	*SLC13A5*	Hypomature
	Microdontia	EEC syndrome-3 - AD	604292	*TP63*	Hypoplastic
	Taurodontism	Dental anomalies and short stature – AR	601216	*LTBP3*	Hypoplastic
		Trichodontoosseous syndrome - AD	190320	*DLX3*	Hypoplastic/ hypomature
	Widely spaced teeth	Mucopolysaccharidosis IVA - AR	253000	*GALNS*	Hypoplastic
	Caries	Mucopolysaccharidosis IVA – AR	253000	*GALNS*	Hypoplastic
		EEC syndrome-3 – AD	604292	*TP63*	Hypoplastic
		Jalili syndrome - AR	217080	*CNNM4*	Hypomineralized
SKIN, NAILS, & HAIR					
Skin	Melanotic macules, Facial angiofibromas	Tuberous sclerosis-1 – AD	191100	*TSC1*	Hypoplastic
		Tuberous sclerosis-2 - AD	613254	*TSC2*	Hypoplastic
	Ectodermal dysplasia	EEC syndrome-3 – AD	604292	*TP63*	Hypoplastic
		Focal dermal hypoplasia – XLD	305600	*PORCN*	Hypoplastic
		Immunodeficiency 9 – AR	612782	*ORAI1*	Hypomature
		Immunodeficiency 10 - AR	612783	*STIM1*	Hypomature
	Linear or reticular hyperpigmentation, Localized cutaneous deposits of superficial fat, Arborescent papillomas	Focal dermal hypoplasia - XLD	305600	*PORCN*	Hypoplastic
	Translucent skin	Loeys-Dietz syndrome 2 - AD	610168	*TGFBR2*	Hypoplastic
Nails	Nails abnormalities	Heimler syndrome 1 – AR	234580	*PEX1*	Hypoplastic
		Heimler syndrome 2 - AR	616617	*PEX6*	Hypoplastic
		Heimler syndrome – AR	/	*PEX26*	Hypoplastic
		Trichodontoosseous syndrome - AD	190320	*DLX3*	Hypoplastic/ hypomature
Hair	Kinky hair	Trichodontoosseous syndrome - AD	190320	*DLX3*	Hypoplastic/ hypomature
SKELETAL					
	Short stature	Dental anomalies and short stature – AR	601216	*LTBP3*	Hypoplastic
		Mucopolysaccharidosis IVA - AR	253000	*GALNS*	Hypoplastic

		Raine syndrome - AR	259775	*FAM20C*	Hypoplastic
		Focal dermal hypoplasia - XLD	305600	*PORCN*	Hypoplastic
		Short stature, and skeletal dysplasia with scoliosis - AR	618363	*SLC10A7*	Hypomineralized
	Osteosclerosis	Raine syndrome - AR	259775	*FAM20C*	Hypoplastic
	Brachyolmia	Dental anomalies and short stature – AR	601216	*LTBP3*	Hypoplastic
	Vertebral defects	Dental anomalies and short stature – AR	601216	*LTBP3*	Hypoplastic
	Skeletal dysplasia	Mucopolysaccharidosis IVA – AR	253000	*GALNS*	Hypoplastic
		Short stature, and skeletal dysplasia with scoliosis – AR	618363	*SLC10A7*	Hypomineralized
		Trichodontoosseous syndrome - AD	190320	*DLX3*	Hypoplastic
	Split-hand/foot malformation	EEC syndrome-3 – AD	604292	*TP63*	Hypoplastic
		Focal dermal hypoplasia - XLD	305600	*PORCN*	Hypoplastic
	Joint laxity	Loeys-Dietz syndrome 2 - AD	610168	*TGFBR2*	Hypoplastic
	Scoliosis	Short stature, and skeletal dysplasia with scoliosis - AR	618363	*SLC10A7*	Hypomineralized
	MUSCLE				
	Muscular hypotonia	Developmental and epileptic encephalopathy 25 -AR	615905	*SLC13A5*	Hypoplastic
		Immunodeficiency 9 – AR	612782	*ORAI1*	Hypomature
		Immunodeficiency 10 - AR	612783	*STIM1*	Hypomature
	NEUROLOGIC				
	Hamartomatous lesions of the brain, Learning difficulties, Autism	Tuberous sclerosis-1 – AD	191100	*TSC1*	Hypoplastic
		Tuberous sclerosis-2 - AD	613254	*TSC2*	Hypoplastic
	Ataxia, Lack of speech acquisition	Developmental and epileptic encephalopathy 25 -AR	615905	*SLC13A5*	Hypoplastic
		Kohlschutter-Tonz syndrome - AR	226750	*ROGDI*	Hypomature
	Abnormal involuntary movements	Developmental and epileptic encephalopathy 25 -AR	615905	*SLC13A5*	Hypoplastic
	Spasticity	Developmental and epileptic encephalopathy 25 -AR	615905	*SLC13A5*	Hypoplastic
		Kohlschutter-Tonz syndrome - AR	226750	*ROGDI*	Hypomature
	Seizures	Tuberous sclerosis-1 – AD	191100	*TSC1*	Hypoplastic
		Tuberous sclerosis-2 – AD	613254	*TSC2*	Hypoplastic
		Developmental and epileptic encephalopathy 93 – AD	618012	*ATP6V1A*	Hypoplastic
		Developmental and epileptic encephalopathy 25 –AR	615905	*SLC13A5*	Hypoplastic
		Kohlschutter-Tonz syndrome - AR	226750	*ROGDI*	Hypomature
	Intellectual disability	Smith-Magenis syndrome – AD	182290	*RAI1*	Hypoplastic
		Kohlschutter-Tonz syndrome - AR	226750	*ROGDI*	Hypomature
	Behaviour anomalies, Sleep	Smith-Magenis syndrome - AD	182290	*RAI1*	Hypoplastic
	disturbance				
	Delayed psychomotor development	Developmental and epileptic encephalopathy 93 – AD	618012	*ATP6V1*	Hypoplastic
		Developmental and epileptic encephalopathy 25 –AR	615905	*SLC13A5*	Hypoplastic
		Kohlschutter-Tonz syndrome - AR	226750	*ROGDI*	Hypomature
	Impaired intellectual development	Developmental and epileptic encephalopathy 93 – AD	618012	*ATP6V1A*	Hypoplastic
		Short stature, and skeletal dysplasia with scoliosis - AR	618363	*SLC10A7*	Hypomineralized
	CARDIOVASCULAR				
	Vascular defect	Dental anomalies and short stature – AR	601216	*LTBP3*	Hypoplastic
	Artery aneurysm, Arterial tortuosity	Loeys-Dietz syndrome 2 - AD	610168	*TGFBR2*	Hypoplastic
	GENITOURINARY				
	Nephrocalcinosis	Enamel-renal syndrome – AR	204690	*FAM20A*	Hypoplastic
		Raine syndrome – AR	259775	*FAM20C*	Hypoplastic
		Hypomagnesemia 3, renal – AR	248250	*CLDN16*	Hypoplastic
		Hypomagnesemia 5, renal, with ocular involvement – AR	248190	*CLDN19*	Hypoplastic
		Amelogenesis imperfecta, type IIA3 – AR	613211	*WDR72*	Hypomature
	Renal lesions	Tuberous sclerosis-1 – AD	191100	*TSC1*	Hypoplastic
		Tuberous sclerosis-2 – AD	613254	*TSC2*	Hypoplastic
		Hypomagnesemia 3, renal – AR	248250	*CLDN16*	Hypoplastic
		Hypomagnesemia 5, renal, with ocular involvement – AR	248190	*CLDN19*	Hypoplastic
		Smith Magenis	182290	*RAI1*	Hypoplastic
	ENDOCRINE FEATURES				
	Adrenal insufficiency, Hypoparathyroidism	Autoimmune polyendocrinopathy syndrome - AD/AR	240300	*AIRE*	Hypoplastic
	IMMUNOLOGY				
	Chronic mucocutaneous candidiasis	Autoimmune polyendocrinopathy syndrome - AD/AR	240300	*AIRE*	Hypoplastic
	Recurrent infections	Immunodeficiency 9 – AR	612782	*ORAI1*	Hypomature
		Immunodeficiency 10 - AR	612783	*STIM1*	Hypomature
	LABORATORY ABNORMALITIES				
	N-acetylgalactosamine-6-sulfatase deficiency	Mucopolysaccharidosis IVA - AR	253000	*GALNS*	Hypoplastic
	Hypomagnesemia, Hypercalciuria	Hypomagnesemia 3, renal - AR	248250	*CLDN16*	Hypoplastic

2. **A novel homozygous variant in *GJA1* causing a Hallermann-Streiff/Oculodentodigital Dysplasia overlapping Phenotype: a clinical report.**

A rare condition known as Hallermann-Streiff syndrome (HSS) causes developmental delays, short stature, and craniofacial characteristics. Despite most cases being isolated, the inheritance pattern of HSS remains a mystery. Clinical characteristics of HSS and oculodentodigital dysplasia (ODDD) coincide, making difficult to make a differential diagnosis. The transmembrane gap junction protein connexin 43 (CX43), which is encoded by the Gap Junction Protein Alpha 1 (*GJA1*) gene, is the causative gene of ODDD. These variants may reduce CX43 cell-to-cell communication, which exacerbates the symptoms of ODDD.

This case report shows the diagnosis of a 3-year-old girl presenting repeated dental abscesses. She was born to second-degree consanguineous parents and has two healthy siblings.

Specific craniofacial traits pathognomonic of HSS were revealed via extraoral examination. The teeth had a ghostly look due to very thin, under-mineralized hard tissues, short roots, and big pulp, which were confirmed by radiographic examination. First unerupted permanent molars also had hypomineralized dentin and enamel.

Whole-exome sequencing (WES) research was done to determine the genetic etiology producing the HSS phenotype and related dental abnormalities. Therefore, a unique homozygous variation of the *GJA1* gene was discovered that had a missense substitution in exon 2 [Chr6(GRCh37): g.121768554C>G NM_000165.4: c.561C>G p.Cys187Trp]. The variant was heterozygous in both parents.

Hallermann-Streiff syndrome and oculodentodigital dysplasia share a number of clinical traits. ODDD is primarily inherited in a dominant manner and is caused on by changes in the *GJA1* gene. It is still unclear what causes HSS at the molecular level. There is evidence of a recessive pattern of inheritance in people with ODDD or HSS/ODDD spectrum disorders.

The second extracellular loop of the CX43 protein is affected by the novel homozygous mutation in the *GJA1* gene, which results in clinical signs of the HSS and ODDD syndromes. Ion and small molecule exchange from cell to cell is made possible by the CX43 protein. CX43 is involved in the movement of ions from the papillary layer into the ameloblasts during enamel formation.

frontiers in Dental Medicine

ORIGINAL RESEARCH
published: 04 June 2021
doi: 10.3389/fdmed.2021.675130

A Novel Homozygous Variant in *GJA1* Causing a Hallermann-Streiff/Oculodentodigital Dysplasia Overlapping Phenotype: A Clinical Report

Alexandra Jimenez-Armijo[1†], Khadja Oumensour[2†], Bouchra Bousfiha[2], Tristan Rey[1,3], Virginie Laugel-Haushalter[1,4], Agnès Bloch-Zupan[1,4,5‡] and Samira El Arabi[2‡]*

[1] Université de Strasbourg, Institut de Génétique et de Biologie Moléculaire et Cellulaire, INSERM U1258, CNRS-UMR7104, Illkirch-Graffenstaden, France, [2] Faculté de médecine dentaire de l'Université Hassan II, Service de Pédodontie - Centre de Consultations et Traitements Dentaires, Casablanca, Morocco, [3] Hôpitaux Universitaires de Strasbourg, Laboratoires de diagnostic génétique, Institut de Génétique Médicale d'Alsace, Strasbourg, France, [4] Université de Strasbourg, Faculté de Chirurgie Dentaire, Strasbourg, France, [5] Hôpitaux Universitaires de Strasbourg, Pôle de Médecine et Chirurgie Bucco-Dentaires, Centre de référence des maladies rares orales et dentaires, CRMR O-Rares, Filière Santé Maladies rares TETE COU, European Reference Network ERN CRANIO, Strasbourg, France

OPEN ACCESS

Edited by:
Maisa Hanna-Maija Seppala,
King's College London,
United Kingdom

Reviewed by:
Dong Han,
Peking University Hospital of Stomatology, China
Dobrawa Napierala,
University of Pittsburgh, United States

***Correspondence:**
Agnès Bloch-Zupan
agnes.bloch-zupan@unistra.fr

[†]These authors share first authorship

[‡]These authors share senior authorship

Specialty section:
This article was submitted to Regenerative Dentistry, a section of the journal Frontiers in Dental Medicine

Received: 02 March 2021
Accepted: 28 April 2021
Published: 04 June 2021

Citation:
Jimenez-Armijo A, Oumensour K, Bousfiha B, Rey T, Laugel-Haushalter V, Bloch-Zupan A and El Arabi S (2021) A Novel Homozygous Variant in GJA1 Causing a Hallermann-Streiff/Oculodentodigital Dysplasia Overlapping Phenotype: A Clinical Report. Front. Dent. Med. 2:675130. doi: 10.3389/fdmed.2021.675130

This paper reports the case of a Moroccan girl with a phenotype within the clinical spectrum of both Hallermann-Streiff (HSS, OMIM 234100) and Oculodentodigital Dysplasia (ODDD, OMIM 164200) syndromes. The patient presented with repeated dental abscesses and severe early childhood caries. She had no learning deficit nor psychomotor regression; however, a language delay was noted. She also presented with obstructive sleep apnea syndrome and specific craniofacial features pathognomonic of HSS. Radiographic examination showed enamel and dentin defects, giving a ghost-like tooth appearance. Several clinical features of ODDD overlap those of HSS and may confuse diagnosis, considering that the inheritance of HSS is not described yet. The diagnostic odyssey of this patient ended with the identification by exome sequencing of a novel homozygous alteration in the *GJA1* gene. A missense substitution in exon 2 [Chr6(GRCh37): g.121768554C>G NM_000165.4: c.561C>G p.Cys187Trp] was identified by whole-exome sequencing (WES), suggesting a diagnosis of ODDD. This is the first report of a homozygous mutation affecting the second extracellular loop of the CX43 protein.

Keywords: case report, rare disease, oculodentodigital dysplasia, Hallermann Streiff, dental anomalies, connexin 43, syndrome

INTRODUCTION

Hallermann-Streiff syndrome (HSS, OMIM 234100) is a highly recognizable rare disease characterized by developmental delay, proportionate short stature, skeletal, chest, respiratory and skin defects, as well as distinct craniofacial features such as sparse hair, skin atrophy over scalp and nose, brachycephaly, frontal bossing, micrognathia, low set ears, microphthalmia, small pointed nose, microstomia, and developmental tooth anomalies. The inheritance pattern of this rare disease remains unsolved, with most cases having been described as isolated (1).

Several clinical features of HSS, such as microphthalmia, small nose, hypotrichosis and dental anomalies, overlap those found in oculodentodigital dysplasia (ODDD) confusing differential diagnosis. Alterations in Gap Junction protein Alpha 1 gene (*GJA1*) (OMIM 121014, HGNC ID: 4274, NM_000165.5), which is located on chromosome 6q22.31 and organized in two exons and one intron, have been reported as causative for ODDD. ODDD mode of inheritance has mostly been autosomal dominant (AD, OMIM 164200) but also occasionally autosomal recessive (AR, OMIM 257850) (2–4). With AD transmission, one affected parent transmits the variant to an affected child, and the variant may lead either to the complete spectrum of malformations or to milder manifestations. Only few individuals with recessive variants in *GJA1* have been reported (4–7), and a single one was described as presenting an overlapping HSS/ODDD spectrum associated to variant c.227G>A, p.R76H (8). In general, more severe clinical features are observed in AR ODDD (9).

GJA1 encodes the transmembrane, gap junction protein connexin 43 (CX43) that allows the exchange of ions and small molecules between cells (9, 10). This protein is composed of four α-helical transmembrane domains, two extracellular loops, and a cytoplasmic loop with the amino and carboxyl termini in the cytoplasm (11). Alterations in *GJA1* could produce protein products with a proper size but with different ways of assembling into functional gap junction plaques. A reduction in CX43 cell-to-cell communication caused by these variants contributes to the many symptoms associated with ODDD (12).

AD ODDD individuals present with a variable phenotype, including a characteristic facial appearance, and variable eye and digital anomalies (bilateral syndactyly, camptodactyly, and clinodactyly) (9). Other features such as hearing loss and neurologic abnormalities like seizures can occur as well (6). The craniofacial dysmorphic features (see **Table 1**) include microphthalmia, hypertelorism, thin nose, hypotrichosis, and dental anomalies like enamel dysplasia, tooth agenesis, and microdontia. A high prevalence of caries is also reported.

In this paper, we report the case of a Moroccan girl with a phenotype within the spectrum of both HSS and ODDD, whose diagnostic odyssey ended with the identification of a novel homozygous *GJA1* variant.

TABLE 1 | Clinical features in HSS, ODDD, and the proband.

Clinical features	ODDD	HSS	Proband
Brachycephaly with frontal and parietal bossing	+	+++	Yes
Microcephaly	+++		No
Prominent scalp veins		+++	No
Hypotrichosis	+++	+++	Yes
Low-set ears	+	+++	Yes
Deafness	+++		No
Microcornea	+++		No
Cataracts	++	+++	Yes
Bilateral microphthalmia	+++	+++	Yes
Ocular nystagmus	+	+++	Yes
Strabismus	+	+++	Yes
Sparse eyebrows	+++	+++	Yes
Long, thin and pointed nose	+++	+++	Yes
Maxillomandibular hypoplasia	++	+++	Yes
Small mouth with thin lips		+++	Yes
High arched and narrow palate	++	+++	Yes
Dental anomalies- enamel hypoplasia	+++	+++	Yes
Brachydactyly	+		Yes
Thin, gracile metacarpals		+++	No (medical records)
Cutaneous syndactyly	+++		No
Camptodactyly and clinodactyly	+++		Yes
Proportionate short stature		+++	Yes
Cognitive deficiencies	+++		Language delay
Seizures	++		No
Poor ossification		+++	No (medical records)
Obstructive sleep apnea		+/−	Yes
Skin atrophy	+++	+++	No

CASE PRESENTATION

This clinical case was conducted in compliance with the CARE guidelines.

Parents gave written informed consent for the transfer of clinical data in D4/phenodent database (www.phenodent.org), genetic testing (GenoDENT), DNA biobanking (https://clinicaltrials.gov: NCT01746121 et NCT02397824; DC-2012-1677 et DC-2012-1002), and the current publication.

A 3-year-old girl was examined in the pediatric dentistry unit because of repeated dental abscesses. She was born from second-degree consanguineous parents and has two siblings with no reported health problems. The medical history showed a normal pregnancy and a neonatal period without difficulties. The patient had no learning deficit nor psychomotor regression; however, a language delay was noted. She also presented obstructive sleep apnea syndrome.

Extraoral examination showed specific craniofacial features (**Table 1**, **Figure 1**) pathognomonic of HSS. Intraoral examination revealed poor oral hygiene with the presence of abundant dental plaque and gingival inflammation. Parents experienced great difficulties in brushing the child teeth.

All primary teeth presented brownish-yellow dyschromia, and a diagnosis of severe early childhood caries was proposed. However, significant fragility of dental structures suggested underlying mineralized tissue developmental anomalies (**Figures 1G–J**). Primary canines showed clearly hypoplastic enamel (**Figure 1G**).

Radiographic examination at 3 and 6 years of age confirmed the presence of enamel and dentin defects, with the teeth having a ghost-like appearance (very thin, under-mineralized hard tissues, short roots, and large pulps) (**Figures 1K,L**). Hypomineralized enamel and dentin were also clearly visible in first unerupted permanent molars (**Figure 1L**).

FIGURE 1 | Clinical features of the proband including intraoral examination and x-rays of primary and permanent dentitions. **(A,B)** First medical visit at 3-year-old. **(A)** Hypotrichosis, bilateral microphthalmia with nystagmus, hypertelorism. **(B)** A specific facial gestalt with convex nasal ridge, low set ears and mandibular retrognathia. **(C,D)** Patient at 6-year-old. Lack of lip support and accentuation of the nasolabial folds due to multiple teeth extractions. **(E,F)** The patient has brachydactyly, hand bilateral fifth finger clinodactyly, no signs of syndactyly. **(G,H)** Oral cavity at 3 years old. Primary teeth are affected by a severe form of early childhood caries. Teeth have a brownish yellow color and show significant brittleness of the dental structures. Temporary maxillary canines **(G)** are thin and conoid. **(I,J)** Intraoral images at 6-year-old. All primary teeth with dental abscess were extracted. A gingival recession was visible on 81 and 71. **(K,L)** Intraoral radiographs taken at 3 years of age confirmed hard tissue defects, thin dentin walls, short roots with gaping apices and large pulps giving the appearance of phantom teeth.

Before patient's oral management, hemostasis tests and a complete blood count were requested. Due to recurrent abscesses, primary tooth extractions were performed. Given the patient's anxiety, prosthetic rehabilitation was postponed until she was more cooperative. Regular follow-up was scheduled after 1 month and then every 3 months for preventive treatment to avoid appearance of new carious lesions on the remaining teeth. After 2 years, the child's cooperation allowed a prosthetic rehabilitation with removable denture, to be carried out.

To clarify the genetic etiology causing the HSS phenotype and associated dental anomalies, whole- exome sequencing (WES) analysis was carried out. Genomic DNA was isolated from the saliva of the proband and her parents, using the Oragene® DNA OG-250 commercial kits (DNA Genotek Inc., Ottawa, Ont, Canada) according to the manufacturer's protocol. WES was performed by Integragen (Evry, France). WES and bioinformatic analysis were done following the protocol described in (13). The variants were filtered excluding (1) variants represented with an allele frequency of more than 1% in public variation databases-including the 1,000 Genomes (14), the gnomAD database (15), (2) variants in the 5' or 3' UTR, (3) variants with intronic locations and no prediction of local splice effect, and (4) synonymous variants without prediction of local splice effect. The analysis was focused on homozygous and compound heterozygous variants consistant with a recessive mode of inheritance and/or on *de novo* variants. After variant filtration, 15 homozygous, 5 compound heterozygous and 2 *de novo* variants in 21 genes were left for investigation. None of them, excepting

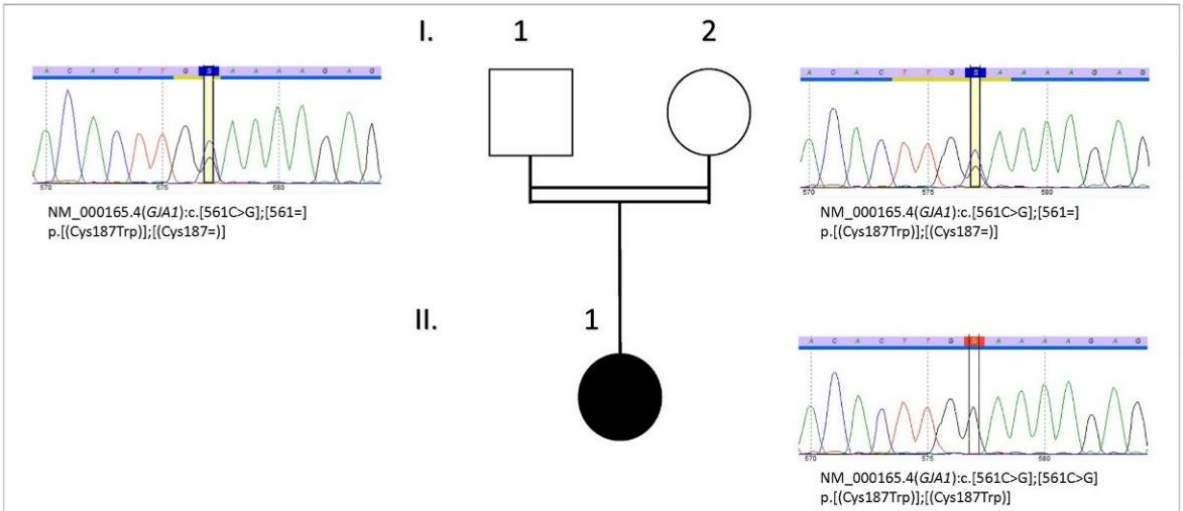

FIGURE 2 | Pedigree and DNA sequencing chromatograms of the family. Sanger sequencing was done to confirm familial segregation of the variant NM_000165.4 (*GJA1*):c.[561C>G] identified by exome sequencing. Parents (I.1 and I.2) were heterozygous and the index case (II.1) was homozygous for this variant.

variants in *GJA1* were consistent with the patient's phenotype see **Supplementary Tables 1**, **2**.

A novel homozygous variant in the *GJA1* gene, with a missense substitution in exon 2 [Chr6(GRCh37): g.121768554C>G NM_000165.4: c.561C>G p.Cys187Trp], was therefore identified. Parents were both heterozygous for the variant. Sanger sequencing was used to confirm WES data (**Figure 2**). Primer pair for exon 2 of *GJA1* was designed using AmplifX 1.5.4 (sense: TCTATCTTTGAGGTGGCCTTCT; antisense: CCACAATGGCTAGTGGCTGTAA). The amplification of the region of interest was performed on genomic DNA template, from both parents and proband, followed by bidirectional Sanger sequencing. This analysis comforted the exome sequencing results.

The variant (c.561C>G p.Cys187Trp) affected the second extracellular loop of the CX43 protein (**Figure 3**). The alignment of this domain sequence with sequences of other species showed that it was largely conserved between species, with the altered cysteine (Cys187) being highly conserved (**Figure 3C**). This variant was also predicted to be deleterious by SIFT (16) and by Polyphen2 (Polymorphism Phenotyping v2) (PPH2) (17). The variant is also not present in healthy people gnomAD database (15). Collectively, these findings suggested that this amino acid had an important function. This variant was therefore classified as class 4, likely pathogenic, according to ACMG criteria (18).

DISCUSSION

Oculodentodigital dysplasia (ODDD) and Hallermann-Streiff syndrome (HSS) share several clinical features. ODDD is caused by alterations in *GJA1* gene and mostly inherited in a dominant manner. The molecular etiology of HSS is not yet fully understood. Individuals diagnosed with ODDD or HSS/ODDD spectrum disorder, have been reported with a recessive pattern of inheritance (4, 8, 9).

Our patient initially diagnosed as suffering from HSS presented symptoms overlapping with both HSS and ODDD phenotypes (**Table 1**). In contrast to HSS, ODDD is characterized by specific digital anomalies (clinodactyly, camptodactyly, and syndactyly) (9). The girl presented brachydactyly in both hands and feet, and bilateral fifth finger clinodactyly in her hands, all pathognomonic signs of ODDD. She also had other symptoms matching both HSS and ODDD, such as hypotrichosis, and microphthalmia, as well as other traits more common in HSS like strabismus, high arched palate, and sleep apnea (**Table 1**). Whole-exome sequencing analysis excluded unlikely pathogenic alterations and pointed toward homozygous missense variants in *GJA1*. It provided a potential molecular diagnosis orienting toward a clinical diagnosis of ODDD. The proband's consanguineous parents, neither of whom reported clinical findings consistent with either syndromes, were both heterozygous for the selected *GJA1* variant.

The c.561C>G p.Cys187Trp detected variant affected a highly conserved amino acid (**Figure 3**) located in the second extracellular loop of CX43. Many modifications in the amino acid sequence of CX43 are disease causing, indicating that CX43 has a low tolerance for change to maintain its cellular function (19). Eighty-five percentage of ODDD causing genetic alterations are located within the first half of the protein, prior to amino acid 192. The extracellular cysteines are particularly important for the maintenance of the protein structure (9). This is the first reported variant affecting a cysteine residue of the extracellular loops. Functional studies of alterations, in the first and second extracellular loops, causing ODDD have shown that the protein product does not form homomeric junctional plaques, resulting

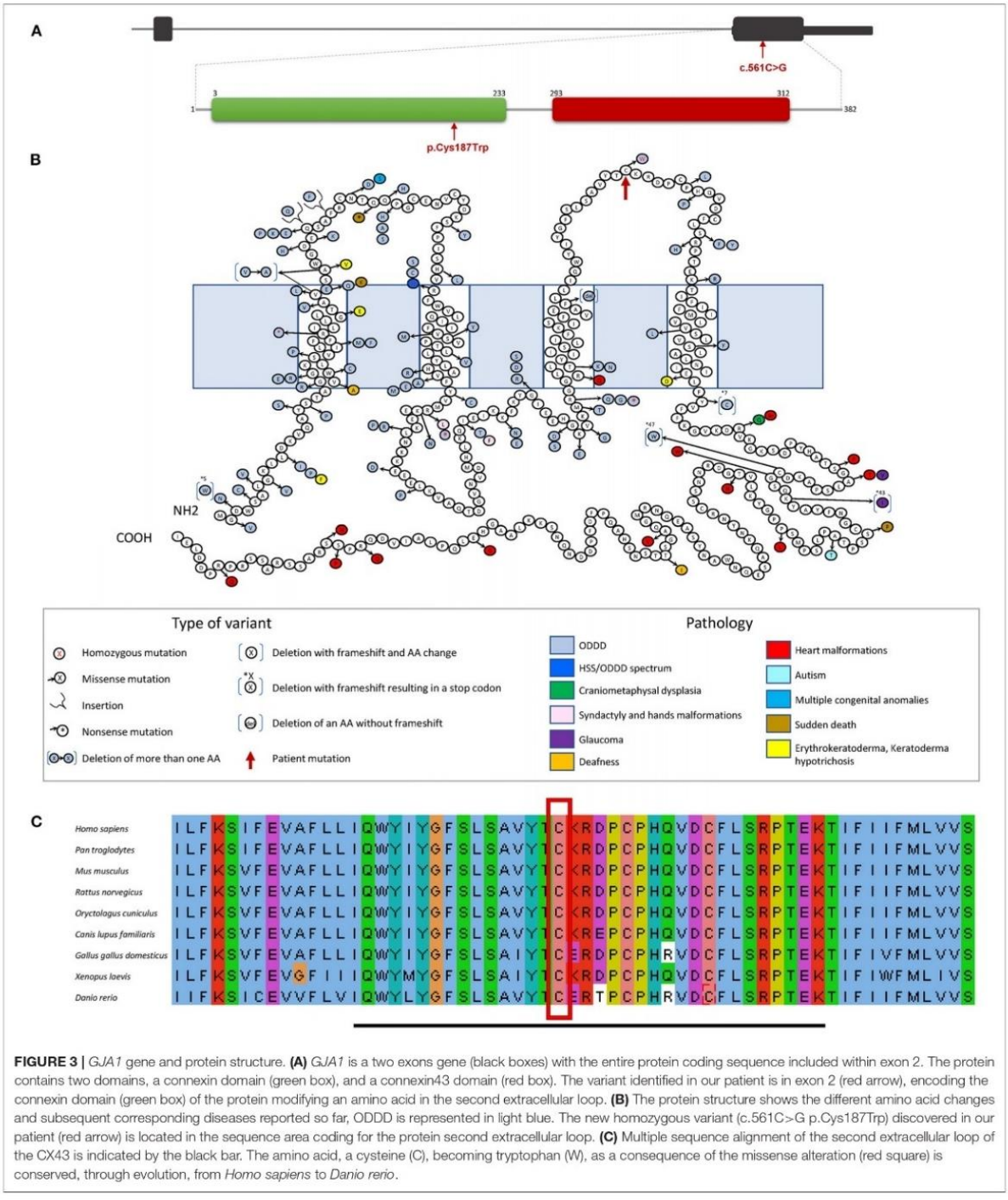

FIGURE 3 | *GJA1* gene and protein structure. **(A)** *GJA1* is a two exons gene (black boxes) with the entire protein coding sequence included within exon 2. The protein contains two domains, a connexin domain (green box), and a connexin43 domain (red box). The variant identified in our patient is in exon 2 (red arrow), encoding the connexin domain (green box) of the protein modifying an amino acid in the second extracellular loop. **(B)** The protein structure shows the different amino acid changes and subsequent corresponding diseases reported so far, ODDD is represented in light blue. The new homozygous variant (c.561C>G p.Cys187Trp) discovered in our patient (red arrow) is located in the sequence area coding for the protein second extracellular loop. **(C)** Multiple sequence alignment of the second extracellular loop of the CX43 is indicated by the black bar. The amino acid, a cysteine (C), becoming tryptophan (W), as a consequence of the missense alteration (red square) is conserved, through evolution, from *Homo sapiens* to *Danio rerio*.

in an abnormal intracellular space localization linked to the endoplasmic reticulum instead of a normal extracellular space localization (12).

We therefore considered the variant as disease causing and likely pathogenic and classified it as class 4, according to ACMG criteria (18). The proband's genotype was consistent with the

HSS/ODDD spectrum phenotype and homozygous variants had been reported once before in a patient presenting similar clinical traits i.e., a HSS/ODDD spectrum phenotype (8).

The enamel phenotype was however intriguing suggesting an important role of CX43 during amelogenesis. Indeed, CX43 contributes to ion transport enabling passage of ions directly from cells of the papillary layer into the ameloblast layer. Inactivation of *Cx43* in mouse induced distinct skeletal abnormalities and also affected amelogenesis, suggesting that gap junctions are required to fully mineralize enamel at maturation stage (20, 21).

Understanding the underlying disease pathophysiology, explaining the origin of the enamel defects, strengthened the need for special oral care. Multidisciplinary management is indispensable for these rare disease patients. For the pediatric dentist, the management of tooth mineralized tissues abnormalities, present in both HSS and ODDD, constitutes a challenge, especially in young children. It is recommended to protect, isolate (stainless steel crowns, glass ionomers, composite…) and maintain on the arch the dysplastic teeth until skeletal growth is complete. If infectious complications occur, tooth extraction, especially in the primary dentition, should be performed (22). This was the case for our patient. The use of general anesthesia was not recommended due to the deformation of the airways that could lead to fatal complications.

Recognizing orodental anomalies (i.e., enamel, dentin structural defects) as part of a rare disease is crucial to implement early preventive and appropriate management aiming at avoiding secondary burden such as infection and definite loss of teeth. These developmental anomalies could provide important clues facilitating rare disease diagnosis. Reaching an accurate diagnosis may require both precise phenotyping (clinical description) and genotyping.

Genetic testing is used to orientate, confirm a diagnosis. It can change the medical care. It also provides families with more information about long-term and health care needs, and future family planning. This may entitle patients to benefit from special multidisciplinary healthcare and management in dedicated rare diseases centers, to receive appropriate treatment according to international existing guidelines. In the family mentioned in this paper, searching for the gene responsible for an initial diagnosis of HSS pointed toward a related syndrome, ODDD. The molecular basis of HSS remains unknown, but this new discovered homozygous variant strengthens the hypothesis of an overlapping phenotype/genotype correlation in the intermingled HSS/ODDD spectrum. HSS/ODDD may actually be a single syndrome with clinical features spanning both HSS and ODDD and homozygous variants in specific locations of the *GJA1* gene sequence.

DATA AVAILABILITY STATEMENT

The datasets presented in this study can be found in online repositories. The names of the repository/repositories and accession number(s) can be found in the article/**Supplementary Material**.

ETHICS STATEMENT

Parents gave written informed consent for the transfer of clinical data in D4/phenodent database (www.phenodent.org), genetic testing (GenoDENT) and DNA biobanking (https://clinicaltrials.gov: NCT01746121 et NCT02397824; DC-2012-1677 et DC-2012-1002), and the current publication. Written informed consent to participate in this study was provided by the participants' legal guardian/next of kin. Written informed consent was obtained from the minor(s)' legal guardian/next of kin for the publication of any potentially identifiable images or data included in this article.

AUTHOR CONTRIBUTIONS

AB-Z and SE conceived the ideas. KO and BB collected the data. TR prepared the genetic material. VL-H analyzed the exome data. AJ-A and VL-H analyzed the clinical data. AJ-A, VL-H, and AB-Z led the writing. All authors contributed to the article and approved the submitted version.

FUNDING

This work was supported by the project No. 1.7 RARENET: a trinational network for education, research and management of complex and rare disorders in the Upper Rhine co-financed by the European Regional Development Fund (ERDF) of the European Union in the framework of the INTERREG V Upper Rhine program. AB-Z was a USIAS 2015 Fellow of the Institute of Advanced Studies (Institut d'Etudes Avancées) de l'Université de Strasbourg, France as well as a member of the ERN (European reference network) CRANIO initiative. This work was also supported by grants from the French Ministry of Health (National Program for Clinical Research, PHRC 2008 N°4266 Amelogenesis imperfecta), the University Hospital of Strasbourg (HUS, API, 2009–2012, Development of the oral cavity: from gene to clinical phenotype in Human) and the grant ANR-10-LABX-0030-INRT, a French State fund managed by the Agence Nationale de la Recherche under the frame programme Investissements d'Avenir labelled ANR-10-IDEX-0002-02. AJ-A received a CONYCIT/ANID, PhD Fellowship from Chile.

ACKNOWLEDGMENTS

We are grateful to the family for their participation and invaluable contribution. We thank Mrs. Marzena Kawczynski for continuous support and help with patient data management as well as Pr O. Klein (UCSF School of Dentistry) for critical reading of the manuscript.

SUPPLEMENTARY MATERIAL

The Supplementary Material for this article can be found online at: https://www.frontiersin.org/articles/10.3389/fdmed.2021.675130/full#supplementary-material

Supplementary Table 1 | Whole-exome sequencing data. https://doi.org/10.6084/m9.figshare.14387909.v4.

Supplementary Table 2 | Homozygous, compound heterozygous and *de novo* variants after filtration. https://doi.org/10.6084/m9.figshare.14387909.v4.

REFERENCES

1. Schmidt J, Wollnik B. Hallermann-Streiff syndrome: a missing molecular link for a highly recognizable syndrome. *Am J Med Genet Part C Semin Med Genet.* (2018) 178:398–406. doi: 10.1002/ajmg.c.31668
2. Abrams CK, Scherer SS. Gap junctions in inherited human disorders of the central nervous system. *Biochim Biophys Acta Biomembr.* (2012) 1818:2030–47. doi: 10.1016/j.bbamem.2011.08.015
3. Porntaveetus T, Srichomthong C, Ohazama A, Suphapeetiporn K, Shotelersuk V. A novel GJA1 mutation in oculodentodigital dysplasia with extensive loss of enamel. *Oral Dis.* (2017) 23:795–800. doi: 10.1111/odi.12663
4. Taşdelen E, Durmaz CD, Karabulut HG. Autosomal recessive oculodentodigital dysplasia: a case report and review of the literature. *Cytogenet Genome Res.* (2018) 154:181–6. doi: 10.1159/000489000
5. Hu Y, Chen, I.-P., de Almeida S, Tiziani V, Do Amaral CMR, et al. A novel autosomal recessive GJA1 missense mutation linked to craniometaphyseal dysplasia. *PLoS ONE.* (2013) 8:e73576. doi: 10.1371/journal.pone.0073576
6. Joss SK, Ghazawy S, Tomkins S, Ahmed M, Bradbury J, Sheridan E. Variable expression of neurological phenotype in autosomal recessive oculodentodigital dysplasia of two sibs and review of the literature. *Eur J Pediatr.* (2008) 167:341–5. doi: 10.1007/s00431-007-0468-1
7. Richardson RJ, Joss S, Tomkin S, Ahmed M, Sheridan E, Dixon MJ. A nonsense mutation in the first transmembrane domain of connexin 43 underlies autosomal recessive oculodentodigital syndrome. *J Med Genet.* (2006) 43:e37. doi: 10.1136/jmg.2005.037655
8. Pizzuti A, Flex E, Mingarelli R, Salpietro C, Zelante L, Dallapiccola B. A homozygous GJA1 gene mutation causes a Hallermann-Streiff/ODDD spectrum phenotype. *Hum Mutat.* (2004) 23:286. doi: 10.1002/humu.9220
9. Paznekas WA, Karczeski B, Vermeer S, Lowry RB, Delatycki M, Laurence F, et al. GJA1 mutations, variants, and connexin 43 dysfunction as it relates to the oculodentodigital dysplasia phenotype. *Hum Mutat.* (2009) 30:724–33. doi: 10.1002/humu.20958
10. Evans WH, Martin PEM. Gap junctions: structure and function (review). *Mol Membr Biol.* (2002) 19:121–36. doi: 10.1080/09687680210139839
11. Laird DW, Revel JP. Biochemical and immunochemical analysis of the arrangement of connexin43 in rat heart gap junction membranes. *J Cell Sci.* (1990) 97:109–17. doi: 10.1242/jcs.97.1.109
12. Shibayama J, Paznekas W, Seki A, Taffet S, Jabs EW, Delmar M, et al. Functional characterization of connexin43 mutations found in patients with oculodentodigital dysplasia. *Circ Res.* (2005) 96:e83–91. doi: 10.1161/01.RES.0000168369.79972.d2
13. Laugel-Haushalter V, Morkmued S, Stoetzel C, Geoffroy V, Muller J, Boland A, et al. Genetic evidence supporting the role of the calcium channel, CACNA1S, in tooth cusp and root patterning. *Front Physiol.* (2018) 9:1329. doi: 10.3389/fphys.2018.01329
14. The 1000 Genomes Project Consortium, Auton A, Brooks LD, Durbin RM, Garrison EP, Kang HM. A global reference for human genetic variation. *Nature.* (2015) 526:68–74. doi: 10.1038/nature15393
15. Exome Aggregation Consortium, Lek M, Karczewski KJ, Minikel EV, Samocha KE, Banks E, et al. Analysis of protein-coding genetic variation in 60,706 humans. *Nature.* (2016) 536:285–91. doi: 10.1038/nature19057
16. Vaser R, Adusumalli S, Leng SN, Sikic M, Ng PC. SIFT missense predictions for genomes. *Nat Protoc.* (2016) 11:1–9. doi: 10.1038/nprot.2015.123
17. Adzhubei IA, Schmidt S, Peshkin L, Ramensky VE, Gerasimova A, Bork P, et al. A method and server for predicting damaging missense mutations. *Nat Methods.* (2010) 7:248–9. doi: 10.1038/nmeth0410-248
18. Richards S, Aziz N, Bale S, Bick D, Das S, Gastier-Foster J, et al. Standards and guidelines for the interpretation of sequence variants: a joint consensus recommendation of the American College of Medical Genetics and Genomics and the Association for Molecular Pathology. *Genet Med.* (2015) 17:405–24. doi: 10.1038/gim.2015.30
19. Laird DW. Syndromic and non-syndromic disease-linked Cx43 mutations. *FEBS Lett.* (2014) 588:1339–48. doi: 10.1016/j.febslet.2013.12.022
20. Al-Ansari S, Jalali R, Plotkin LI, Bronckers, ALJJ, DenBesten P, Zhang Y, et al. The importance of connexin 43 in enamel development and mineralization. *Front Physiol.* (2018) 9:750. doi: 10.3389/fphys.2018.00750
21. Toth K, Shao Q, Lorentz R, Laird DW. Decreased levels of Cx43 gap junctions result in ameloblast dysregulation and enamel hypoplasia in Gja1Jrt/+ mice. *J Cell Physiol.* (2010) 223:601–9. doi: 10.1002/jcp.22046
22. Aminabadi NA, Pourkazemi M, Oskouei SG, Jamali Z. Dental management of oculodentodigital dysplasia: a case report. *J Oral Sci.* (2010) 52:337–42. doi: 10.2334/josnusd.52.337

Conflict of Interest: The authors declare that the research was conducted in the absence of any commercial or financial relationships that could be construed as a potential conflict of interest.

Copyright © 2021 Jimenez-Armijo, Oumensour, Bousfiha, Rey, Laugel-Haushalter, Bloch-Zupan and El Arabi. This is an open-access article distributed under the terms of the Creative Commons Attribution License (CC BY). The use, distribution or reproduction in other forums is permitted, provided the original author(s) and the copyright owner(s) are credited and that the original publication in this journal is cited, in accordance with accepted academic practice. No use, distribution or reproduction is permitted which does not comply with these terms.

3. Kohlschütter-Tönz syndrome

Kohlschütter-Tönz Syndrome (KTS, OMIM 226750, ORPHA: 1946) is a rare genetic disorder with autosomal recessive inheritance. It is characterized by early onset epilepsy, psychomotor regression, intellectual disability, and enamel defects. It is caused by mutations in *ROGDI* gene, encoding a protein of unknown function but highly conserved among species including *Danio rerio*, *Drosophila melanogaster*, *Xenopus laevis*, *Caenorhabditis elegans*, and *Mus musculus*, suggesting an important functional role [17,68,80,81]. After the first description of the syndrome in 1974 [82], several splice-site, non-sense, and frameshift mutations in *ROGDI* gene have been published delineating a similar phenotype in additional affected individuals (Figure 10) [13,17,77,81,83–85].

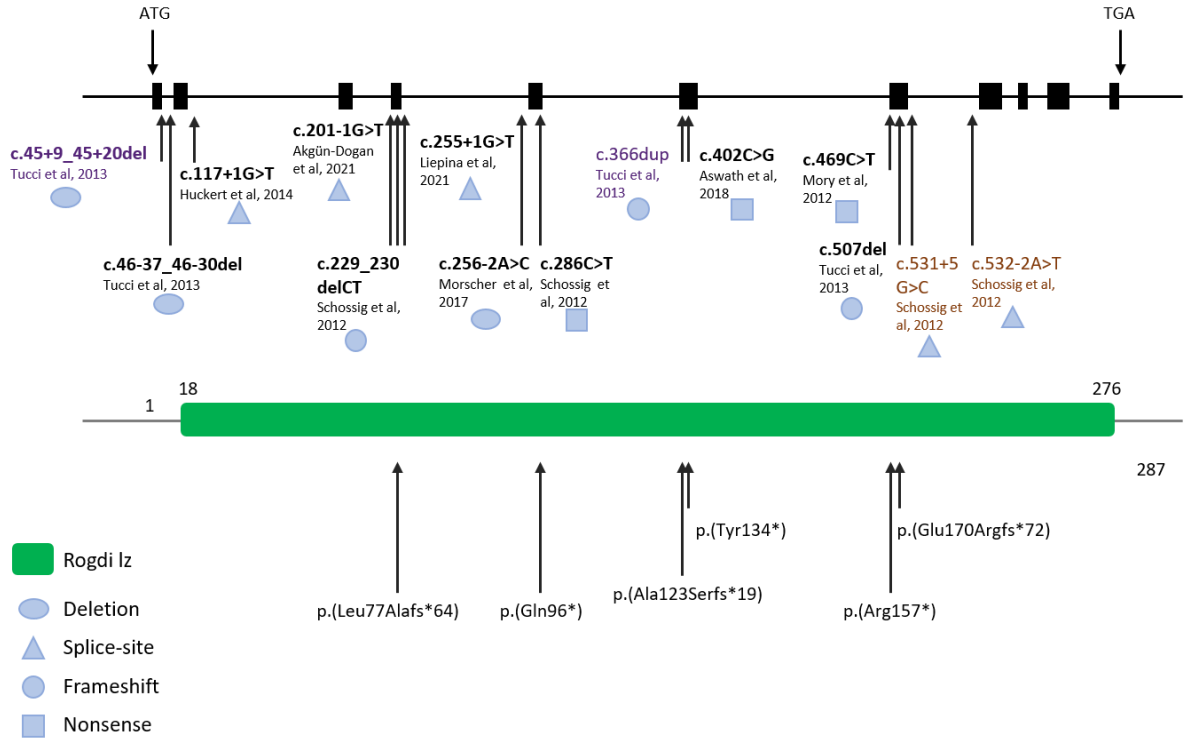

Figure 10. *ROGDI* variants and corresponding protein domain. The gene transcript NM_024589.3 is composed of 11 exons represented by vertical lines. The variations detected in this study are symbolized in bold if homozygous. Variants with purple color are compound heterozygous. Variants with brown color are compound heterozygous. The corresponding protein domains are represented according to the PFAM database. The arrows indicate the localization of the detected variant with predictable protein impact.

Linkage analyses followed by genomic sequencing have revealed that most, if not all, KTS patients have homozygous nonsense, frameshift, deletion, or splicing site mutations at the *ROGDI* locus 2–6 [83], but there are a number of families with an atypical phenotype which were negative for *ROGDI* mutations and failed to show homozygosity in the *ROGDI* region, suggesting genetic heterogeneity in atypical forms of the disease [85]. Huckert et al. (2014) [17] had reported a case of a 13-year-old Malian girl presenting with this rare disease. By genetic analysis, a novel *ROGDI* homozygous mutation was identified NM_024589.1:

c.117+1G>T [Chr16 (GRCh37): g.4852382C>A] which confirmed the diagnosis of KTS. The mutation abolishes the usual splice donor site of intron 2 which leads to the deletion of exon 2 and in-frame assembly of exon 3. Exon 2 encodes a highly conserved leucine-rich region that is essential for ROGDI protein function. Hence, this deletion may affect the function of the ROGDI protein.

ROGDI protein expression is not detectable in affected individuals, indicating that the loss of ROGDI function is likely responsible for the pathogenesis of KTS. In control human tissues, *ROGDI* transcripts are ubiquitously expressed, but elevated levels are observed in adult brain and spinal cord. This observation is consistent with the neurological phenotypes observed in KTS patients [81].

KTS epilepsy usually starts in the first year of life, and seizures are often resistant to treatment, even with newer antiepileptic drugs. Perampanel monotherapy, though, produced quite effective seizure control in a 6-year-old girl with unresponsive seizures to other drugs [2]. Detailed data on the characteristics of epilepsy in patients with KTS are still lacking showing a heterogeneity of the seizure type [84]. There have been reports of generalized tonic, tonic-clonic, myoclonic, atonic, and focal clonic seizures as well as seizures with secondary bilateral synchronization and consciousness [84,86,87].

In the majority of KTS cases, initial psychomotor development is normal and only 25% have a delayed psychomotor development. Usually, both coarse and fine motor skills are compromised. Others can be bedridden due to spastic tetraparesis, whereas some patients are ambulant (with or without help). In 23% of cases, severe progressive psychomotor regression with a fatal end was documented. Some children experience speech delays and slow language development. Learning difficulties, aggression, and attention deficit hyperactivity disorder have been also reported in some patients [17,80,88,89]. The most severely affected individuals display profound intellectual disability, never acquire speech, and become bedridden early in life (Table 2). Clinical and laboratory signs are not specific in the disease, except for dental findings. Therefore dental diagnosis is essential for the overall clinical diagnosis of KTS [77,84].

All affected individuals show variable yellow-to-brown discoloration of primary, as well as permanent teeth. These defects are observed upon the initial eruption of hypomineralized *amelogenesis imperfecta* (AI)-marked yellow/brownish teeth (Table 2). *ROGDI*-associated KTS AI has a characteristic hypomineralized, rough, colored type of maturation defect [77]. In KTS patients, enamel is soft, rough, and stained in various shades of brown. This enamel malformation has severe clinical consequences in the form of poor mechanical properties, high sensitivity to pain, high susceptibility to caries, and low esthetic quality. Clearly, the severity of these defects necessitate extensive dental treatment [84]. In the partially erupted first molar assessed from an individual with *ROGDI*-associated KTS, the hypomineralized enamel had normal thickness in non-erupted parts of the crown. When exposed to the oral cavity, the hypocalcified enamel was easily worn away or showed abfractions because it could not withstand the abrasive and occlusal forces during chewing (Figure 11). In both types of AI, exposed dentin may be temperature sensitive, and pits and cracks are predilection sites for caries. Hypersensitivity of teeth as well as high caries risk requires individual dental

prophylaxis and attentive dental monitoring and management [77]. The identification of the gene ROGDI role will hopefully help researchers and clinicians understand the intriguing combination of dental and neurological symptoms [84].

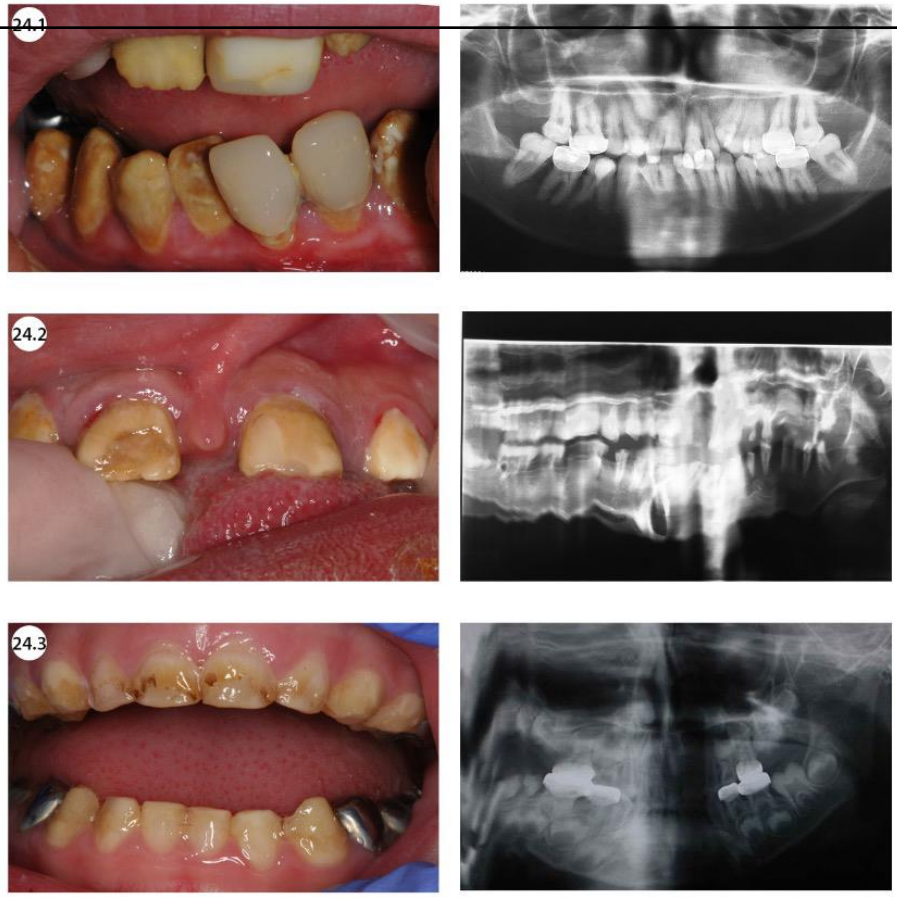

Figure 11. Clinical intraoral photographs and panoramic radiographs detailing the phenotype of amelogenesis imperfecta patient for each associated genotype. *ROGDI* (Kohlschütter-Tönz syndrome) Hypomature amelogenesis imperfecta. Individuals present a yellow-brownish discoloration of enamel affecting both primary and permanent dentitions. Stainless steel crowns are covering the molars in patients 24.1 and 24.3. Patient 24.2 was published in [17]. Source: Supplementary Figure 1P from article 2 [13]

The gathering of individuals suffering from KTS but not demonstrating any mutation in *ROGDI* gene allowed the identification of a second gene *SLC13A5*, (encoding a sodium-dependent citrate transporter) involved in KTS [77].

The pathogenic phenotypes commonly found in *ROGDI*- and *SLC13A5*- [77] associated KTS gives rise to the intriguing possibility that these two genes might work together to control the intracellular levels of citrate. This idea is further supported by the relevance of citrate metabolism to neurological phenotypes in KTS patients. Neurons are energetically dependent on astrocytes because neurons lack pyruvate carboxylase, an enzyme that converts pyruvate to oxaloacetate in the citric acid cycle [83].

Table 2. Clinical characteristics of Kohlschütter–Tönz syndrome with confirmed *ROGDI* pathogenic variants. Adapted from [2]

	Symptom and previously reported patients, n (%)
Neurological symptoms/findings	Epilepsy 43/43 (100%) Refractory epilepsy [17,84,85,89–91] 9/43 (21%) Cerebellar ataxia [17,88,89] 3/43 (7%) GDD or development regression [89] 43/43 (100%) Microcephaly [89,92–95] 6/43 (14%) Spasticity [82,88,89,91,96] 9/43 (21%) ADHD, hyperactivity [80,88,89] 7/43 (16%) Other behavioral disorders: aggressive and impulsive behavior [17,88] 2/43 (5%)
EEG	Hypsarrhythmia [89] 1/16 (6%) Other EEG abnormalities [86,88,90,91] 14/16 (88%)
MRI	Ventriculomegaly [82,89,96,97] 8/21 (38%) Cerebral atrophy [84,86,88–91,96,97] 9/21 (43%)
Others	Teeth anormalities: amelogenesis imperfecta 43/43 (100%) Eyes: loss of visual fixation, nystagmus, esotrophy [85,88] 3/43 (7%) Dysmorphic features: asymmetric skull, frontal bossing, short stature, scoliosis, broad or altered thumbs/toes, smooth philtrum, concave nasal bridge, short nose, hypoplastic ala nasi, small ears, deeply set eyes, bristly, coarse hair [17,85,88,90,96] 7/43 (16%)

Abbreviations: ADHD, attention deficit hyperactivity disorder; EEG, electroencephalogram; GDD, global developmental delay; MRI, magnetic resonance imaging.

Chapter 2: Mouse models

1. Pre-clinical animal models reproducing rare diseases of mineralized dental tissues

To better understand the etiology, progression, and potential therapy options for a variety of rare orodental diseases, mouse models have been extensively used in research.

Dental anomalies can be present alone or associated with extraoral symptoms of rare disorders. By definition, a rare disease impact fewer than one person worldwide in 2000.

Each dental abnormality is associated with a certain genetic and developmental issue. Here we present anomalies affecting the mineralized structures of the tooth. Numerous genetically altered mice used as models for rare diseases replicate the cranio-facial deformities, including dental anomalies, mimicking human's phenotypes. This enables a more in-depth examination of the effects of the underlying molecular dysfunctions. Additionally, there are rodent models available displaying dentin, enamel, and other dental defects in addition to gene mutations for which no human disease has yet been described.

The publication also discusses the differences in tooth conformation and dental composition between humans and mice. Despite these differences, both organisms exhibit the same pattern of tooth development and development, which makes the rodent a useful model for research on dental diseases and the mechanisms underlying their development.

The article recapitulates the various phenotypes that the models exhibit, replicating the defects present in humans, and describes the mouse models that have been described to explore enamel and dentin malformations (either isolated or associated with syndromes). Additionally, it shows rodent models with mutations that have never been described in humans but that also cause dental defects.

Vol. 30 • juin 2019 • n° 2

RC Réalités Cliniques

La revue thématique

Éditorial : **Les défis du clinicien…**

Anomalies des tissus durs de la dent

coordonné par
François Clauss

ISSN n°0969-5021
PRESSE EDITION MEDIA
indexée dans la base internationale ICMJE
60 €

NOUVEAU ! Prolongez votre lecture avec nos vidéos

Éditorial

François Clauss
Coordinateur scientifique

Anomalies des tissus durs de la dent

Les anomalies des tissus durs dentaires, qu'elles soient congénitales ou acquises, constituent un groupe hétérogène et large de pathologies nécessitant une approche multidisciplinaire. Les défis pour le clinicien se situent aussi bien sur le versant diagnostique que thérapeutique. Ces pathologies requièrent une importante transversalité et font l'objet de recherches cliniques, précliniques et fondamentales intenses, s'agissant de modèles d'étude pertinents de l'odontogenèse normale et pathologique.

La discussion du diagnostic différentiel entre formes isolées et syndromiques revêt une importance toute particulière, car elle conditionne une orientation éventuelle vers un bilan en génétique médicale visant à exclure toute anomalie systémique associée. Par exemple, face à un tableau clinique d'amélogenèse imparfaite, le clinicien pourra notamment proposer un bilan néphrologique, neurologique ou ophtalmologique.

La prévalence croissante d'une autre forme d'anomalie de structure amélaire, l'hypominéralisation molaire incisive (MIH), est un sujet d'étude et de préoccupation pour les cliniciens et épidémiologistes. La MIH est également un excellent modèle d'étude de l'impact des facteurs polluants environnementaux, des molécules antibiotiques et des perturbateurs endocriniens sur l'amélogenèse. De façon plus large, les mécanismes d'interactions génome-épigénome-environnement peuvent également être mieux appréhendés, notamment à travers la caractérisation des corrélations polymorphismes génétiques-phénotypes.

Sur le plan plus clinique, les réhabilitations conservatrices et prothétiques des anomalies amélaires et dentinaires sont complexes ; elles doivent être mises en place précocement et bénéficient grandement des techniques actuelles de CFAO, que ce soit en cours de croissance ou chez l'adulte. L'objectif de ce numéro spécial est de proposer un large panorama de ces différentes anomalies, et d'aider le clinicien à les diagnostiquer et les prendre en charge.

En vous souhaitant une excellente lecture.

Ont participé à ce numéro

José Tomas Ahumada
Docteur en chirurgie dentaire, Strasbourg

Isabelle Blanchet
MCU-PH associé,
O-Rares, Marseille

Agnès Bloch-Zupan
PU-PH
Docteur en biologie orale, Strasbourg

Ariane Camoin
MCU-PH
O-Rares, Marseille

François Clauss
PU-PH, odontologie pédiatrique
O-Rares, Strasbourg

Leonor Costa Mendes
AHU, Toulouse

Muriel de La Dure-Molla
O-Rares, Paris

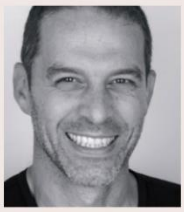

Olivier Etienne
MCU-PH temps partiel prothèses
O-Rares, Strasbourg

Benjamin P. Fournier
O-Rares, Paris

Alexandra Jimenez Armijo
Docteur en chirurgie dentaire, Strasbourg

Sophie Jung
MCU-PH
O-Rares, Strasbourg

Virginie Laugel-Haushalter
Docteur en biologie moléculaire, Strasbourg

Serena Lopez-Cazaux
MCU-PH
O-Rares, Nantes

Cyril Pérez
Ancien interne en odontologie, Strasbourg

Claire Pernier
MCU-PH, spécialiste qualifiée en orthopédie dento-faciale, Lyon

Élise Pilavyan
AHU en prothèse
Strasbourg

Zoé Prud'homme
O-Rares, Paris

Luc Raynaldy
Praticien hospitalier, Toulouse

Coline Simeoni
Spécialiste qualifiée en orthopédie dento-faciale, Lyon

Corinne Tardieu
PU-PH
O-Rares, Marseille

Frédéric Vaysse
PU-PH, Toulouse

Stéphane Viennot
MCU-PH, Lyon

Commission Paritaire N° 1119T82241 - Dépôt légal : à parution
© SAS L'Information Dentaire Tous droits de traduction, d'adaptation et de reproduction par tous procédés pour tous pays. Toute reproduction ou représentation intégrale ou partielle, par quelque procédé que ce soit, des pages publiées dans le présent ouvrage faite sans l'autorisation de l'éditeur, est illicite et constitue une contrefaçon. Seules sont autorisées, d'une part les reproductions strictement réservées à une utilisation collective et, d'autre part, les courtes citations justifiées par le caractère scientifique ou d'information de l'oeuvre dans laquelle elles sont incorporées (art. L 122-4 L. 122-5 et L. 335-2 du Code de la propriété intellectuelle).
Imprimé en France, par Corlet Imprimeur SA 14110 Condé-sur-Noireau

Conception fabrication 100% française

RC RÉALITÉS CLINIQUES

Présidente et Directrice de la Publication
Claudie Damour-Terrasson

Rédacteur en Chef
Olivier Etienne

Rédacteur en Chef Adjoint
Corinne Lallam

Comité éditorial
Romain Chéron, Marwan Daas, Emmanuel d'Incau
David Nisand, Fabienne Pérez

Directeur scientifique
Jean-Jacques Lasfargues

Conseil scientifique
Jean-Pierre Attal, Daniel Dot,
Michèle Muller Bolla

Comité de lecture
Sophie Bahi, Marcel Begin, Catherine Besnault, Eric Bonte, Denis Bouter, Frédric Bukiet, Jean-Luc Charrier, Catherine Chaussain, Florence Chemla, Jean-Marie Cheylan, Anne Claisse, François Clauss, Jean-Yves Cochet, Pierre Colon, Marc Danan, Pascal De March, Jacques Dejou, Jean-Marc Dersot, Raphaël Devillard, Sophie Domejean, Dominique Droz, Gérard Duminil, Nicolas Eid, Michel Fages, Céline Gaucher, Gérard Girot, Brigitte Grosgogeat, Dominique Guez, Martine Hennequin, Olivier Hue, Richard Kaleka, Gilles Laborde, Mike Lahmi, Alain Lautrou, Philippe Lesclous, Pierre Machtou, Paul Mariani, Dominique Martin, Didier Maurice, Brenda Mertens, Nathan Moreau, Christian Moussally, Cathy Nabet, Chantal Naulin-Ifi, Ludovic Pommel, Xavier Ravalec, Christophe Rignon-Bret, Jean-Louis Saffar, Hervé Tassery, Henri Tenenbaum, Gil Tirlet, Gauthier Weisrock, Maryse Wolikow, Gérard Zuck

Correspondants internationaux
Allemagne : J.F. Roulet
Angleterre : J. Webber, N.H.F. Wilson
Belgique : P. Lambrechts
Canada : D. Forest
États-Unis : D. Nathanson
Italie : M. Fuzzi, G. Goracci
Pays-Bas : JM. Ten Cate
Suisse : D. Dietschi, J. Samson

Secrétaire de rédaction
Géraldine Choquart

Premier rédacteur graphiste
David Dumand

Rédacteurs graphistes
Yannick Tiercy, Émilie Trani

Publicité/Communication/Fabrication
Sakina Zennache, Natacha Cabaret, Sophia Sabri
Souad Aschendorf

Traductions
Paul Riordan

Éditeur : L'Information Dentaire SAS
Siège Social : 44, rue de Prony - CS 80105 - 75017 Paris
Société détenue à 100% par la SAS PHILI@ MEDICAL EDITIONS
Représentant légal et Directrice des publications :
Madame Claudie Damour-Terrasson
Tél : 01 56 26 50 00 - Fax : 01 56 26 50 01
Mail : info@information-dentaire.fr
Internet : www.information-dentaire.fr

Répond aux critères qualité d'un document issu de la presse scientifique professionnelle (voir site de la HAS)

Volume 30 N° 2
Juin 2019
TRIMESTRIEL
Prix du n° : 60 €

Sommaire

Coordinateur scientifique : **François Clauss**

Anomalies des tissus durs de la dent

Ce numéro comporte un encart ID (offres abonnement et librairie, 8 p.) et une enveloppe T.

MOTS CLÉS : amélogenèse imparfaite, dentinogenèse imparfaite, modèles animaux, souris
KEYWORDS: amelogenesis imperfecta, dentinogenesis imperfecta, animal models, mouse

Modèles animaux : modélisations précliniques des maladies rares des tissus dentaires minéralisés

Virginie Laugel-Haushalter
Docteur en biologie moléculaire, attaché d'enseignement, Université de Strasbourg

Alexandra Jimenez Armijo
Docteur en chirurgie dentaire, assistant d'enseignement, Université de Strasbourg, Université du Chili

José Tomas Ahumada
Docteur en chirurgie dentaire, assistant d'enseignement, Université de Strasbourg, Université du Chili

Supawich Morkmued
Docteur en chirurgie dentaire, docteur en biologie des organismes : développement et physiologie, lecteur

Karen Niederreither
Docteur en biologie du développement MCU associé, Université de Strasbourg

Agnès Bloch-Zupan
PU-PH, docteur en chirurgie orale, Université de Strasbourg, Centre de référence des maladies rares orales et dentaires, O-Rares

RÉSUMÉ

Les anomalies dentaires peuvent exister de manière isolée ou être associées à des manifestations extra-orales dans le cadre des maladies rares. Les maladies rares, par définition, affectent moins d'une personne sur 2 000. Chaque anomalie dentaire correspond à des problématiques développementales et génétiques spécifiques. Nous nous intéresserons plus particulièrement aux anomalies affectant les tissus durs de la dent. De nombreuses souris génétiquement modifiées, modèles de maladies rares, reproduisent dans leurs phénotypes les anomalies cranio-faciales rencontrées chez l'Homme, y compris les anomalies dentaires, et autorisent ainsi une étude plus fine des conséquences des dysfonctionnements moléculaires associés. Par ailleurs, des modèles murins, mutés dans des gènes pour lesquels aucune maladie n'a, à ce jour, été décrite chez l'Homme, et présentant des anomalies de la dentine, de l'émail et des autres tissus dentaires, sont également disponibles. Ils constituent des preuves de l'implication de ces gènes dans la formation dentaire et mettent en lumière de nouveaux gènes-candidats potentiels dont la mutation doit être analysée chez les patients atteints d'anomalies des tissus durs de la dent.

ABSTRACT

Animal models: preclinical modeling of rare diseases of mineralised dental tissues

Dental abnormalities may exist in isolation or may be associated with extraoral manifestations of rare diseases. Rare diseases, by definition, affect fewer than one person in 2000. Each dental anomaly corresponds to specific developmental and genetic problems. We focus on abnormalities affecting the hard tissue of the tooth. Many genetically modified mice, models of rare diseases, reproduce in their phenotypes the cranio-facial abnormalities found in humans, including dental anomalies and thus allow a more detailed study of the consequences of the associated molecular dysfunctions. In addition, rodent models, with mutated genes for which no human disease has so far been described, and with abnormalities of dentine, enamel and other dental tissues, are also available. They provide evidence for the involvement of these genes in tooth formation and highlight potential new candidate genes whose mutation must be analysed in patients with hard tissue abnormalities of the tooth.

Les auteurs ne déclarent aucun lien d'intérêt.

Virginie Laugel-Haushalter et coll.

Les anomalies dentaires peuvent exister de manière isolée ou être associées à des manifestations extra-orales dans le cadre des maladies rares. Les maladies rares par définition affectent moins d'une personne sur 2000. À ce jour, on dénombre 8000 maladies rares dont 80 % sont d'origine génétique. De ce fait, elles concernent au total trois à quatre millions de personnes en France, et près de vingt-cinq millions en Europe. Les anomalies dentaires, qu'elles soient de nombre, forme, taille, structure ou d'éruption/résorption, sont une des manifestations phénotypiques des maladies rares ou syndromes témoignant ainsi dans leur chronologie, grâce au caractère minéralisé des tissus dentaires, des troubles issus du développement. Parmi ces maladies rares, 900 présentent des manifestations cliniques phénotypiques bucco-dentaires et 750 des fentes labio-palatines.

L'odontogenèse, classiquement divisée en cinq stades (la lame, le bourgeon, le capuchon, la cloche, l'édification radiculaire avec l'éruption dentaire), est contrôlée par des interactions entre les compartiments ectomésenchymateux et épithéliaux ; elle est régulée par des voies de signalisation conservées du développement bien connues aujourd'hui (FGF, BMP, SHH, WNT, TGFbeta, NOTCH, TNF), identifiées dans les travaux de recherche sur les souris transgéniques.

Chez l'Homme, la formule dentaire s'exprime au sein de deux dentures (temporaire et permanente) et est composée de dents de morphologies différentes avec, en avant, les incisives suivies des canines, puis des prémolaires et des molaires. La souris, quant à elle, ne possède qu'un jeu de dents (monophyodontie) et sa formule dentaire, contrairement à celle de l'Homme, n'est composée que de deux types de dents (trois molaires et une incisive par hémi-arcade) séparées par un espace sans dent appelé diastème. De plus, la souris possède des incisives à croissance continue ayant un développement asymétrique avec dépôt de l'émail uniquement sur la partie labiale et une partie linguale analogue de la racine. Les incisives de rongeur ont un émail de couleur orangée.

Malgré ces différences, les processus de formation et de développement dentaire chez l'Homme et la souris sont similaires. En effet, le même code de communication cellulaire a été conservé au cours de l'évolution, ce qui permet de considérer la souris comme un modèle pertinent de l'odontogenèse humaine. En effet, de nombreuses souris génétiquement modifiées, modèles de maladies rares, reproduisent dans leurs phénotypes les anomalies cranio-faciales rencontrées chez l'homme, y compris les anomalies dentaires, et autorisent ainsi une étude plus précise des conséquences des dysfonctionnements moléculaires associés ***(fig. 1 et 2)***.

Chaque anomalie dentaire correspond à des problématiques génétiques et de développement et spécifiques comme l'origine embryologique des cellules dentaires, l'établissement du patron de la dentition, la régionalisation du développement dentaire, l'acquisition de l'identité et la morphogenèse, la mise en place des différents tissus, l'histogenèse, les cytodifférenciations terminales des odontoblastes, des améloblastes et des autres cellules dentaires, la synthèse de matrices extracellulaires de la dentine et de l'émail, du cément suivie de leur minéralisation, l'édification radiculaire et ensuite la mise en place de la dent sur l'arcade en lien direct avec le remodelage osseux.

Du fait de la grande conservation des processus développementaux, la dent embryonnaire de souris, et en particulier celle des différents modèles mimant les anomalies dentaires rencontrées chez l'Homme, constitue un modèle privilégié pour l'investigation de ces mécanismes développementaux.

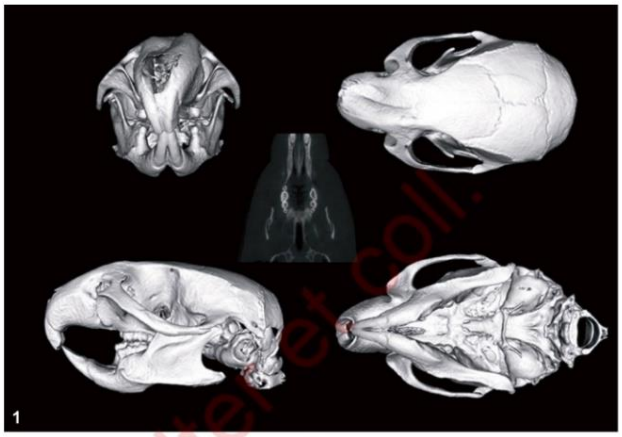

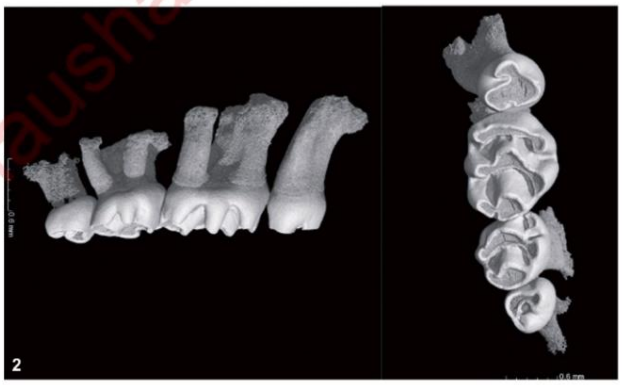

Fig. 1 - Anomalies cranio-faciales rencontrées dans un modèle murin inactivé pour le gène Rsk2 *reproduisant le phénotype clinique rencontré dans le syndrome de Coffin-Lowry, un trouble neurologique rare lié à l'X. Vue tridimensionnelle du crâne reconstituée après une acquisition en microCT (scanner haute résolution).*

Fig. 2 - Anomalies de la formule dentaire dans la souris modèle inactivée pour Rsk2 *avec la présence d'une molaire surnuméraire en avant de la première molaire (quadrant maxillaire droit). La formule dentaire normale chez la souris compte une incisive et trois molaires par quadrant. Vue tridimensionnelle (face vestibulaire, face occlusale) des molaires maxillaires droites après une acquisition en microCT (scanner haute résolution, courtoisie Pr L. Viriot).*

Tous droits réservés Elsevier Haushalter et coll.

Les anomalies de formation de l'émail

Chez l'Homme, les amélogenèses imparfaites (AI) constituent un groupe hétérogène de maladies rares héréditaires. Elles peuvent être présentes de manière isolée ou associées à d'autres manifestations cliniques dans le cadre de syndromes. Elles ont été associées à plus de trente gènes, et de nouveaux gènes sont continuellement découverts. Leur prévalence est de 1 pour 4000 à 1 pour 15000. Elles ont été classées selon leurs manifestations cliniques et le stade du développement dentaire auquel elles interviennent.

Si l'altération survient pendant la formation de la matrice protéique, maquette tridimensionnelle de l'émail en devenir, cela donne lieu à une hypoplasie (défaut quantitatif) ; si elle a lieu durant les étapes de minéralisation, cela se traduit par une hypominéralisation (défaut qualitatif, émail plus mou et dyschromique) ; enfin, si elle a lieu durant la seconde étape du processus de minéralisation c'est-à-dire la maturation qui permet l'élimination de la matrice protéique et la croissance des cristaux d'hydroxyapatite, cela se traduit par une hypomaturation de l'émail (défaut qualitatif avec un émail relativement dur mais ayant perdu sa translucidité, présentant souvent des taches).

Les modèles murins d'anomalies de l'émail dites isolées

Dans cette première partie, nous nous attacherons à décrire les modèles murins existant pour les formes d'AI non syndromiques. Les caractéristiques phénotypiques sont reprises dans le ***tableau I***.

Les premières mutations dans des gènes responsables d'AI qui ont été rapportées étaient impliquées dans des anomalies de l'émail dites isolées dès 1996. En effet, des mutations dans les gènes codant pour les protéines de la matrice extracellulaire de l'émail comme l'amélogénine *AMELX*, l'énaméline *ENAM*, l'améloblastine *AMBN* ou l'amélotine *AMTN*, et pour les protéases comme la métalloprotéinase *MMP20*, et la kallicréine *KLK4* ont été associées à des formes d'AI non syndromiques. Suite à ces premières découvertes, d'autres gènes ont continuellement été associés aux AI et ce, notamment grâce à l'analyse phénotypique et moléculaire de modèles murins qui miment le phénotype clinique rencontré chez l'Homme. Ainsi, de nouveaux gènes jouant un rôle dans la formation ou la maturation de l'émail ont été rapportés comme étant associés à des AI non syndromiques. Les gènes pour lesquels à la fois des mutations chez l'Homme et un phénotype murin ont été décrits codent pour des protéines aux fonctions cellulaires diverses. En effet, ITGB6 est une protéine d'adhésion cellulaire, WDR72 est associée au transporteur de calcium SLC24A4, FAM20A est une pseudokinase qui contrôle l'expression d'autres gènes, notamment FAM20C, et GPR68 est une protéine dont la fonction est encore inconnue.

• **AMELX** est une protéine de la matrice amélaire riche en proline et en histidine. Chez l'Homme, des mutations dans le gène *AMELX* sont majoritairement responsables d'une AI de type hypoplasique liée à l'X (OMIM #301200). Plus de vingt mutations différentes ont été décrites dans ce gène, et l'effet de ces mutations résulterait d'une perte de fonction de la protéine. Les souris *Amelx-/-* présentent également des défauts de l'émail avec un émail hypoplasique de couleur blanc crayeux et une usure excessive des molaires [1].

• **ENAM** est la plus grosse protéine de la matrice amélaire, à laquelle elle contribue à hauteur de 5 %. Les premières mutations à avoir été décrites dans ce gène chez l'Homme étaient transmises selon le mode autosomique dominant. Une première mutation affectant l'épissage avait été identifiée à l'origine d'une AI avec un émail mou et très sévèrement hypoplasique (OMIM#104500). Un phénotype plus léger serait quant à lui lié à des mutations faux sens (OMIM #204650). Par la suite, plusieurs mutations autosomiques récessives ont également été décrites avec une sévérité dépendante du statut (homozygote ou hétérozygote). Les souris mutantes *Enam-/-* (homozygotes inactivées pour les deux copies du gène) présentent également une hypoplasie de l'émail avec un émail irrégulier et des incisives de couleur blanc crayeux [2] et un détachement des améloblastes avec l'émail en production conduisant à une transformation de l'organe de l'émail.

• **AMTN** est une protéine riche en proline, leucine, thréonine et glutamine sécrétée au cours de la maturation des améloblastes. Chez l'Homme, une délétion donnant une protéine de plus petite taille a été décrite comme responsable d'une AI hypominéralisée autosomique dominante (OMIM #610912). Les souris mutantes *Amtn-/-* ont des incisives mandibulaires avec un aspect crayeux et un émail plus mou présentant un retard de minéralisation [3].

• **AMBN** est une protéine riche en glycine et leucine. Elle est exprimée tout au long de l'amélogenèse mais atteint un pic au stade de la sécrétion. Deux mutations seulement ont été rapportées dans le gène *AMBN* chez des patients atteints d'AI hypoplasique récessive de transmission autosomique (OMIM#616270). Les souris *Amtn-/-* ont un émail hypoplasique et hypocalcifié. Les améloblastes se détachent progressivement de l'émail et perdent leur polarité [4].

• **MMP20** est sécrétée par les améloblastes et est nécessaire au contrôle de la morphologie des cristaux d'hydroxyapatite. Chez l'Homme, des mutations dans le gène causent une AI hypomature autosomique dominante (OMIM#612529). De nombreuses mutations faux sens, stop, de décalage du cadre de lecture et affectant des sites d'épissage dans ce gène ont été décrites. La souris *Mmp20-/-* présente elle aussi des défauts amélaires incluant un émail hypoplasique et hypominéralisé [5].

• ***KLK4*** code pour une sérine protéase qui est exprimée et sécrétée par les améloblastes lors du stade de maturation. Elle joue un rôle dans la croissance des cristaux d'hydroxyapatite grâce à son action de dégradation des protéines de l'émail. Des mutations dans le gène sont associées à des AI hypomatures à transmission autosomique récessive (OMIM #204700). Les souris *Klk4-/-* présentent également un émail hypomature, sensible à l'abrasion lors de l'alimentation conduisant à une forte mortalité si les souris ne sont pas nourries avec une nourriture molle adaptée [6].

• **ITGB6** est impliquée dans l'adhésion cellulaire et elle est exprimée principalement lors du stade de maturation des améloblastes. Les patients avec des mutations autosomiques récessives dans ce gène ont soit un émail hypominéralisé avec des puits, soit un émail hypoplasique avec une surface rugueuse (OMIM #616221). Les souris *Itgb6-/-* ont un émail hypominéralisé avec des puits et des prismes désorganisés [7].

• **RELT** est une protéine à domaine riche en cystéines qui induit la voie de signalisation *NF-KB* et qui est exprimée aux stades pré-sécrétoires et sécrétoires. Chez l'Homme, des mutations homozygotes ont été décrites

Tableau I - Modèles murins d'amélogenèse imparfaite pour lesquels des mutations ont été décrites chez l'Homme

Syndrome	Caractéristiques	Gène	Transmission	Modèle murin	Phénotype souris
AI Type IE, #300391	Hypoplasie, hypominéralisation, hypomaturation	*AMELX*	X	*Amelx-/-*	Défaut de l'émail : couleur blanc crayeux, usure excessive des molaires, hypoplasie de l'émail
AI, Type IB, AI1B = AIH2 #104500 AD Type IC, AI1C #204650 AR	Émail hypoplasique, lisse, puits, béance antérieure	*ENAM*	AD AR	*Enam -/-*	Hypoplasie de l'émail, incisives de couleur blanc crayeux
AI, type IF, #616270	AI hypoplasique	*AMBN*	AR	*Ambn-/-*	Émail hypoplasique, hypocalcifié
AI, type IH, #616221	Émail hypominéralisé avec des puits ou émail hypoplasique avec une surface rugueuse	*ITGB6*	AR	*Itgb6-/-*	Émail hypominéralisé avec des puits
AI, hypoplasique, #611211	Émail hypoplasique avec une usure rapide	*RELT*	AR	*Relt-/-*	Malformations dentaires avec émail rugueux qui s'use rapidement
AI, Type IIA1, AI2A1, #204700	Hypomaturation de l'émail	*KLK4*	AR	*Klk4-/-*	Émail hypomature, sensible à l'abrasion
AI, Type IIA2, AI2A2, #612529	Hypomaturation de l'émail	*MMP20*	AR	*Mmp20 -/-*	Hypoplasie et hypominéralisation de l'émail
AI, Type IIA3, AI2A3, #613211	Hypomaturation de l'émail	*WDR72*	AR	*Wdr72-/-*	AI hypomature avec un émail opaque
AI, Type IIA5	AI hypomature, hypominéralisée	*SLC24A4*	AR	*Slc24a4-/-*	Hypominéralisé, abrasion rapide
AI, hypomaturation type IIA6, #601404	AI hypominéralisée	*GPR68*	AR	*Gpr68-/-*	Retard de formation de l'émail et défaut structuraux mineurs
AI, type IIIB, #617607	AI hypominéralisée	*AMTN*	AD	*Amtn-/-*	Émail mou avec un retard de minéralisation, aspect crayeux
Épidermolyse bulleuse jonctionnelle EBJ #226700 Et type non Herlitz (#226650) AR	Puits de l'émail, cloques sur la peau et dans la bouche	*LAMA3, LAMB3, LAMC2, COL17A1*	AR	*Col17a1-/-* *Lama3-/-*	Moins d'hémidesmosome, minéralisation de l'émail retardée, phénotype plus sévère chez les souris *Lama3-/-* que chez les *Col17a1-/-*
AI hypoplasique AI type IA (LAMB3)	Puits dans l'émail	*LAMB3, COL17A1*	AD		
AI et dysplasie squelettique #611459	AI hypominéralisée, petite taille, dysplasie squelettique	*SLC10A7*	AR	*Slc10a7-/-*	Anomalies squelettiques et AI
AI et brachyolmie #601216	AI hypoplasique, retard de croissance, brachyolmie, prédisposition aux dissections aortiques	*LTBP3*	AR	*Ltbp3-/-*	AI hypoplasique sévère, ostéosclérose, ostéoarthrite, élargissement vasculaire aortique
Syndrome émail-rein #204690	Agénésie de l'émail Hyperplasie gingivale Néphrocalcinose	*FAM20A*	AR	*Fam20a-/-*	Émail avec des puits
Syndrome de Raine #259775	AI hypoplasique, dysplasie squelettique, dysmorphie faciale	*FAM20C*	AR	*Fam20c-/-*	Hypominéralisation du squelette, anomalies métaboliques et osseuses, hypophosphatémie
Hypomagnésémie, hypercalciurie, néphrocalcinose #248250, #248190	Hypomagnésémie, hypercalciurie, néphrocalcinose	*CLDN16* *CLDN19*	AR	*Cldn16*	Perte sévère d'émail, émail cassant

Virginie Lesage-Haushalter

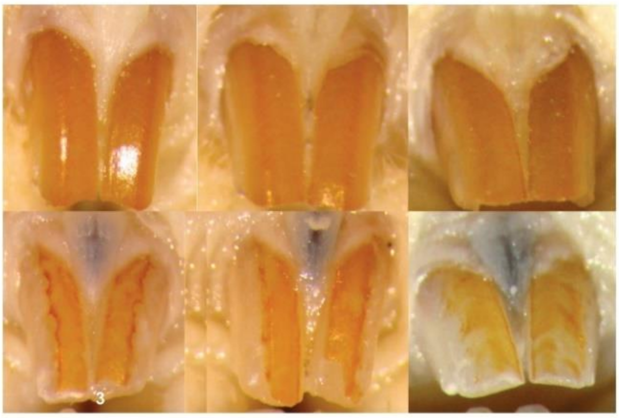

Fig. 3 - Anomalies de l'émail (amélogenèse imparfaite) observables chez trois souris inactivées pour le gène Ltbp3-/- au niveau des incisives maxillaires (partie inférieure de la figure). Les incisives de souris, à croissance continue ont normalement un aspect orangé (partie supérieure de la figure).

comme impliquées dans une AI hypoplasique avec une usure rapide de l'émail [8]. Les souris *Relt-/-* ont des malformations dentaires et un émail avec une surface rugueuse qui s'use rapidement. Les zones normalement non minéralisées à la jonction dentino-amélaire sont très minéralisées, ce qui altère probablement les propriétés mécaniques de cette zone de jonction [8].

• **SLC24A4** est un canal potassium sodium/calcium dépendant. Il est exprimé au stade de maturation des améloblastes au niveau de la membrane au contact de l'émail. Des mutations dans le gène sont à l'origine d'une AI hypomature, hypominéralisée à transmission autosomique récessive (OMIM#609840). Chez la souris *Slc24a4-/-*, l'émail est hypominéralisé et a tendance à s'abraser laissant apparaître la dentine [9].

• **GPR68** est une protéine détectrice de protons qui est exprimée tout au long de l'amélogenèse, avec une expression plus forte au pôle de l'améloblaste en contact avec la matrice amélaire. Des mutations autosomiques récessives chez l'Homme sont à l'origine d'une AI hypominéralisée (OMIM#617217) due à une perte de fonction de la protéine. Le phénotype chez la souris *Gpr68-/-* est plus léger, avec un retard de formation de l'émail et des défauts structuraux mineurs [10].

• **WDR72** est une protéine intracellulaire exprimée plus fortement lors du stade de maturation des améloblastes. Chez l'Homme, des mutations autosomiques récessives tronquant la protéine sont responsables d'une AI hypomature (OMIM#613211). Chez certains patients, des hypodonties et un retard d'éruption dentaire sont aussi notés, ainsi qu'une petite taille parfois associée. *WDR72* est aussi impliquée dans l'acidose tubulaire rénale. Les souris mutantes *Wdr72-/-* ont une AI hypomature avec un émail opaque [11].

Les modèles murins d'AI syndromiques

Des modèles souris ont également été décrits comme mimant les cas d'AI associées à d'autres signes cliniques dans le cadre de syndromes. Les caractéristiques phénotypiques de ces modèles que nous décrirons dans cette deuxième partie sont répertoriées dans le ***tableau I***. Les protéines impliquées dans ces AI syndromiques appartiennent elles aussi à différents groupes de protéines tels que les protéines d'adhésion cellulaire (LAMA3, LAMB3 et LAMC2, COL17A1), les transporteurs calciques (SLC10A7), les protéines de la voie TGFbeta (LTBP3) ou encore au groupe des kinases (FAM20A, FAM20C).

Les gènes *LAMA3, LAMB3* et *LAMC2* codent pour les trois sous-unités de la protéine Laminine (LM332) qui a un rôle dans l'adhésion des améloblastes à la surface de l'émail et dont COL17A1 est un des ligands. Des mutations à l'état autosomique récessif dans ces laminines ou dans leur ligand causent le syndrome d'épidermolyse bulleuse (OMIM#226700, #226650) associant des anomalies cutanées à une AI hypoplasique avec un émail présentant des puits. Lorsqu'il existe seulement une mutation sur l'un des allèles de ces gènes, la mutation est autosomique dominante et cause une AI similaire mais isolée sans autres anomalies associées (OMIM#104530). Les souris mutantes *Col17-/-* ont moins d'hémidesmosomes que les sauvages et ont une minéralisation de l'émail retardée avec un émail aprismatique [12], tandis que les souris *Lama3-/-* ont un phénotype similaire mais plus sévère avec des améloblastes de plus petite taille et un émail très désorganisé [13].

• ***SLC10A7*** code pour une protéine qui forme un canal transporteur de calcium. Son expression est retrouvée aux niveaux des améloblastes mais aussi des os en cours de formation. Chez l'Homme, des mutations dans ce gène associent une AI hypominéalisée à une dysplasie squelettique dont la sévérité est variable. Le modèle murin *Slc10a7-/-* présente un phénotype similaire associant des anomalies squelettiques à une AI [14].

• ***LTBP3*** est exprimé au niveau des améloblastes en cours de différenciation ainsi qu'au niveau cardiaque, pulmonaire et vertébral. Chez l'Homme, des mutations sont responsables d'une AI hypoplasique syndromique associée à un retard de croissance et une brachyolmie (tronc court) et une prédisposition aux dissections aortiques (OMIM#601216). La souris *Ltbp3-/-* reproduit le phénotype clinique et présente une AI hypoplasique sévère avec un émail fin et désorganisé, ainsi qu'un élargissement vasculaire aortique ***(fig. 3)***. Elle développe également une ostéosclérose et une ostéoarthrite [15].

• **FAM20A** est une pseudokinase qui contrôlerait la localisation et l'activation de FAM20C qui est en charge de la phosphorylation de la majorité des peptides matriciels de l'émail. Des mutations dans *FAM20A* sont à l'origine du syndrome émail-rein (ERS) à transmission autosomique récessive (OMIM#204690). Les patients ont une AI hypoplasique avec parfois une absence quasi totale d'émail. Les anomalies associées sont un retard, voire une absence d'éruption dentaire, des follicules dentaires hyperplasiques et des calcifications ectopiques au niveau de la gencive, de la pulpe, du ligament et de l'organe de l'émail [16]. Des néphrocalcinoses ont aussi été rapportées. Les souris *Fam20a-/-* ont une couche améloblastique désorganisée qui se détache, donnant un émail avec des puits [17]. Des mutations autosomiques récessives dans le gène *FAM20C* sont quant à elle impliquées dans le syndrome de Raine

(OMIM#259775). Le syndrome associe une AI hypoplasique sévère à une dysplasie squelettique et une dysmorphie faciale. Chez la souris *Fam20c-/-*, on observe outre l'AI, une hypominéralisation du squelette, des anomalies métaboliques et osseuses et une hypophosphatémie [17].

Les anomalies de formation de la dentine

Les dysplasies de la dentine sont caractérisées par des dents à courtes racines, coniques, avec croissance aberrante de la dentine dans la chambre pulpaire et présentant parfois des anomalies de teinte (dents ambrées). Il en existe plusieurs types et leur prévalence est de 1 pour 100 000. Dans cette partie, nous décrirons les modèles murins mimant les pathologies associées à des anomalies de la dentine. Le ***tableau II*** récapitule les modèles disponibles pour les anomalies dentinaires isolées et syndromiques.

Les modèles murins d'anomalies de la dentine dites isolées

Les anomalies de la dentine dites isolées sont associées à des mutations dans un seul gène codant pour une protéine fortement anionique par ses phosphorylations qui constitue le composant majoritaire (mis à part le collagène) de la dentine, *DSPP* (sialophosphoprotéine dentinaire).

DSPP code pour trois protéines dont DPP et DSP qui constituent les composants majoritaires (mis à part le collagène) de la dentine. Des mutations dans ce gène chez l'Homme ont été associées à quatre maladies rares affectant la dentine : la dentinogenèse imparfaite avec surdité (OMIM#60594), la dentinogenèse imparfaite de type II et III (OMIM#125420, #125490) et la dysplasie dentinaire de type II (OMIM#125500). Les souris *Dspp-/-* ont des défauts de la dentine correspondant à ceux rencontrés dans la dentinogenèse de type III chez l'Homme. Les chambres pulpaires sont élargies et une hypominéralisation aboutissant à l'exposition de la pulpe dentaire [18].

Les modèles murins d'anomalies de la dentine syndromiques

Une dentine anormale est aussi présente dans des syndromes pour lesquels des modèles murins mimant les anomalies ont été décrits. Leurs caractéristiques phénotypiques sont présentées dans le ***tableau II***.

Les ostéogenèses imparfaites sont caractérisées par des anomalies de la formation des os, avec une masse osseuse faible et des tendances aux fractures. Parfois, il y a des anomalies associées de formation de la dentine. Elles sont divisées en plusieurs types et sous-types. L'ostéogenèse imparfaite de type IV (OMIM#166220) est associée à une dentinogenèse imparfaite et est liée, chez l'Homme, à des mutations dans les gènes *COL1A1* et *COL1A2* qui codent pour les chaînes pro-alpha1 et pro-alpha3 du collagène de type I. Les souris mutantes *Col1a1(Jrt)/+* reproduisent le phénotype d'ostéogenèse imparfaite et présentent également une dentinogenèse imparfaite [19].

L'hypophosphatasie (OMIM#171760) est caractérisée par un large spectre de défauts des tissus minéralisés (os, dents) et est causée par des déficiences dans le gène *ALPL* codant par la phosphatase alcaline

Tableau II - Modèles murins de dentinogenèse imparfaite pour lesquels des mutations ont été décrites chez l'Homme

Syndrome	Caractéristiques	Gène	Transmission	Modèle murin	Phénotype souris
Surdité avec dentinogenèse #605594	Défauts de la dentine anormale, perte d'audition progressive	*DSPP*	AD	*Dspp-/-*	Reproduction du phénotype de la dentinogenèse de type III, élargissement de la chambre dentaire et hypominéralisation de la dentine
Dentinogenèse imparfaite, type II #125490, type III #125500	Défauts de la dentine	*DSPP*	AD		
Dysplasie de la dentine II, #125420	Dysplasie coronale de la dentine, dents opalescentes, racines courtes	*DSPP*	AD		
Ostéogenèse imparfaite avec ou sans dentinogenèse type I	Défauts de la dentine et des os	*COL1A1, COL1A2*	AD, AR	*Col1a1(Jrt)/+*	Ostéogenèse avec dentinogenèse imparfaite
Hypophosphatasie infantile, #241500, 241510, 146300	Anomalies squelettiques, petite taille, absences, perte prématurée des dents , cranio-synostose, hypercalcémie	*ALPL*	AR, AD	*Ak2p-/-*	Hypominéralisation de la dentine et du cément de l'os alvéolaire, petite taille, craniosynostose, hypercalcémie

Virginie Laugel-Haushalter et coll.

Tableau III - Modèles murins avec défauts de l'émail ou de la dentine sans mutations répertoriées chez l'Homme		
Gène	**Modèle murin**	**Phénotype souris**
Nfi-c/ctf	*Nfic -/-*	Absence des racines des molaires, incisives mandibulaires fines et cassantes, incisives maxillaire fragiles, dents surnuméraires
Periostin (Postn)	*Periostin -/-*	Défaut d'émail sur les incisives : émail plus fin, petite taille
Smoothened (Smo)	*K14 transgénique*	Hypoplasie de l'émail
Sp3	*Sp3 -/-*	Hypoplasie de l'émail
Sp6	*Sp6 -/-*	Dents surnuméraires, hypoplasie de l'émail, structure dentinaire anormale, trouble de la formation des racines
Trpm7	*Trpm7 KR*	Volume de l'émail réduit avec un émail opaque et blanc
Cdc42	*K5-Cre*	Dents blanches, usure rapide, émail hypomature
Bmp2, Bmp4	*K14-Cre*	Émail hypoplasique
Foxo1, Smad3	*Foxo1 RX-Cre*	Hypomaturation de l'émail
Tbx1	*Tbx1-/-*	Pas d'émail
Sppl2a	*Sppl2a-/-*	Émail non homogène, détachement des couches supérieures
Slc26a1, Slc26a7	*Slc26a1, SLc26a7-/-*	Densité de l'émail diminuée, maturation retardée
Tgfbr2	*Tgfbr2-/-*	Dentine dysplasique, oblitération de la pulpe similaire à la dentinogenèse de type II
Mmp9	*Mmp9-/-*	Dentinogenèse imparfaite, diminution de la densité de la dentine
Notum	*Notum-/-*	Dentine défectueuse, se casse facilement, fracture dentaire, agénésie rénale

Vivianne Laugel-Haushalter et coll.

non tissu-spécifique *(TNSALP)*. Différents modes de transmission ont été mis en évidence (AR et AD). Les souris *Akp2-/-* présentent une hypominéralisation de la dentine, du cément et de l'os alvéolaire [20].

Les modèles murins sans maladies rares associées identifiées chez l'Homme

Des modèles de souris présentant des anomalies dentaires au niveau des tissus minéralisés sont également décrits dans la littérature, sans que des mutations dans les gènes incriminés aient pu à ce jour être associées à des maladies rares et des anomalies dentaires chez l'Homme. Les caractéristiques phénotypiques de ces modèles sont présentées dans le ***tableau III***.

Les modèles présentant des anomalies de l'émail concernent des souris mutées pour des gènes ayant des fonctions diverses. En effet, cela inclut des souris mutées dans des gènes codant pour des transporteurs comme *Slc26a1* ou *Slc26a7* [21], une protéase intramembranaire *Sppl2a* [22], des gtapses comme *Cdc42* [23], des kinases comme *Trpm7* [24], des protéines de la famille des *Tgfbeta* comme *Bmp2, Bmp4, FoxO1* ou *Smad4* [25,26], des facteurs de transcription comme *Tbx1, Sp3,Sp6* ou *Nfic* [27-29], et une protéine impliquée dans le développement des ostéoclastes *Postn* [30].

Les modèles présentant des anomalies de la dentine sont également répertoriés dans le ***tableau III***. Ils concernent un gène impliqué dans la voie *Tgfbeta, Tgfbr2* [31], une protéase, *Mmp9* [32] et une enzyme qui régule la voie *Wnt, Notum* [33]. Des travaux récents identifient les maladies rares associées à certains de ces modèles murins comme celui inactivant les protéines *Claudine – Clnd16* [34] et *Clnd19* [35] un composant des jonctions cellulaires, dont les phénotypes dentaires ont été identifiés chez l'Homme.

Conclusion

Les souris mutées dans les gènes associés à des mutations causant des pathologies des tissus minéralisés dentaires miment le phénotype clinique rencontré chez l'Homme. Ainsi, le modèle murin constitue un modèle de choix pour l'étude des mécanismes moléculaires à l'origine de ces anomalies. Des modèles de souris présentant des anomalies de la dentine et de l'émail pour lesquels aucune mutation n'a, à ce jour été décrite chez l'Homme, sont également disponibles. Ils constituent des preuves de l'implication de ces gènes dans la formation de l'émail et de la dentine et mettent en lumière de nouveaux candidats potentiels à analyser chez les patients atteints d'anomalies des tissus durs de la dent.

Les travaux sur les modèles de maladies rares ont été développés grâce aux financements apportés par le Fonds Européen de Développement Régional (Feder) dans le cadre des programmes Interreg IV et V Rarenet. Ces travaux sont soutenus par l'Agence Nationale de la Recherche ANR-10-LABX-0030-INRT, et le programme Investissements d'Avenir ANR-10-IDEX-0002-02.

Bibliographie

1. Barron MJ, Brookes SJ, Kirkham J, Shore RC, Hunt C, Mironov A et al. A mutation in the mouse Amelx tri-tyrosyl domain results in impaired secretion of amelogenin and phenocopies human X-linked amelogenesis imperfecta. Hum Mol Genet. 2010 Apr 1;19(7):1230-47.
2. Hu JC-C, Hu Y, Smith CE, McKee MD, Wright JT, Yamakoshi Y et al. Enamel defects and ameloblast-specific expression in Enam knock-out/lacz knock-in mice. J Biol Chem. 2008 Apr;283(16):10858-71.
3. Nakayama Y, Holcroft J, Ganss B. Enamel hypomineralization and structural defects in amelotin-deficient mice. J Dent Res. 2015 May;94(5):697-705.
4. Fukumoto S, Kiba T, Hall B, Iehara N, Nakamura T, Longenecker G et al. Ameloblastin is a cell adhesion molecule required for maintaining the differentiation state of ameloblasts. J Cell Biol. 2004 Dec 6;167(5):973-83.
5. Bartlett JD, Beniash E, Lee DH, Smith CE. Decreased mineral content in MMP-20 null mouse enamel is prominent during the maturation stage. J Dent Res. 2004 Dec;83(12):909-13.
6. Simmer JP, Hu Y, Lertlam R, Yamakoshi Y, Hu JC-C. Hypomaturation enamel defects in Klk4 knockout/LacZ knockin mice. J Biol Chem. 2009 Jul 10;284(28):19110-21.
7. Mohazab L, Koivisto L, Jiang G, Kytömäki L, Haapasalo M, Owen GR et al. Critical role for αvβ6 integrin in enamel biomineralization. J Cell Sci. 2013;126:732-44.
8. Kim JW, Zhang H, Seymen F, Koruyucu M, Hu Y, Kang J et al. Mutations in RELT cause autosomal recessive amelogenesis imperfecta. Clin Genet. 2019 Mar;95(3):375-83.
9. Parry DA, Poulter JA, Logan CV, Brookes SJ, Jafri H, Ferguson CH et al. Identification of mutations in SLC24A4, encoding a potassium-dependent sodium/calcium exchanger, as a cause of amelogenesis imperfecta. Am J Hum Genet. 2013 Feb 7;92(2):307-12.
10. Parry DA, Smith CEL, El-Sayed W, Poulter JA, Shore RC, Logan CV et al. Mutations in the pH-Sensing G-protein-coupled receptor GPR68 cause amelogenesis imperfecta. Am J Hum Genet. 2016 Oct 6;99(4):984-90.
11. Katsura KA, Horst JA, Chandra D, Le TQ, Nakano Y, Zhang Y et al. WDR72 models of structure and function: a stage-specific regulator of enamel mineralization. Matrix Biol. 2014 Sep;38:48-58.
12. Asaka T, Akiyama M, Domon T, Nishie W, Natsuga K, Fujita Y et al. Type XVII collagen is a key player in tooth enamel formation. Am J Patho. 2009 Jan;174(1):91-100.
13. Ryan MC, Lee K, Miyashita Y, Carter WG. Targeted disruption of the LAMA3 gene in mice reveals abnormalities in survival and late stage differentiation of epithelial cells. J Cell Biol. 1999 Jun 14;145(6):1309-24.
14. Dubail J, Huber C, Chantepie S, Sonntag S, Tüysüz B, Mihci E et al. SLC10A7 mutations cause a skeletal dysplasia with amelogenesis imperfecta mediated by GAG biosynthesis defects. Nat Comm. 2018 Aug 6;9(1):3087.
15. Huckert M, Stoetzel C, Morkmued S, Laugel-Haushalter V, Geoffroy V, Muller J et al. Mutations in the latent TGF-beta binding protein 3 (LTBP3) gene cause brachyolmia with amelogenesis imperfecta. Hum Mol Genet. 2015 Jun;24(11):3038-49.
16. Lignon G, Beres F, Quentric M, Rouzière S, Weil R, De La Dure-Molla M et al. FAM20A gene mutation: amelogenesis or ectopic mineralization? Front Physiol. 2017 May 3;8:267.
17. Vogel P, Hansen GM, Read RW, Vance RB, Thiel M, Liu J et al. Amelogenesis imperfecta and other biomineralization defects in Fam20a and Fam20c null mice. Vet Pathol. 2012 Nov;49(6):998-1017.
18. Sreenath T, Thyagarajan T, Hall B, Longenecker G, D'Souza R, Hong S et al. Dentin sialophosphoprotein knockout mouse teeth display widened predentin zone and develop defective dentin mineralization similar to human dentinogenesis imperfecta type III. J Biol Chem. 2003 Jul 4;278(27):24874-80.
19. Eimar H, Tamimi F, Retrouvey M, Rauch F, Aubin JE, McKee MD. Craniofacial and dental defects in the Col1a1Jrt/+ mouse model of osteogenesis imperfecta. J Dent Res. 2016;95:761-8.
20. McKee MD, Yadav MC, Foster BL, Somerman MJ, Farquharson C, Millán JL. Compounded PHOSPHO1/ALPL deficiencies reduce dentin mineralization. J Dent Res. 2013 Aug;92(8):721-7.
21. Yin K, Guo J, Lin W, Robertson SYT, Soleimani M, Paine ML. Deletion of Slc26a1 and Slc26a7 delays enamel mineralization in mice. Front Physiol. 2017 May 16;8:307.
22. Bronckers AL, Gueneli N, Lüllmann-Rauch R, Schneppenheim , Moraru AP, Himmerkus N et al. The intramembrane protease SPPL2A is critical for tooth enamel formation. J Bone Miner Res. 2013 Jul;28(7):1622-30.
23. Tian X, Liang WC, Feng Y, Wang J, Zhang VW, Chou CH et al. Expanding genotype/phenotype of neuromuscular diseases by comprehensive target capture/NGS. Neurol Genet. 2015 Aug 13;1(2):e14.
24. Ogata K, Tsumuraya T, Oka K, Shin M, Okamoto F, Kajiya H et al. The crucial role of the TRPM7 kinase domain in the early stage of amelogenesis. Sci Rep. 2017;7:18099.
25. Poché RA, Sharma R, Garcia MD, Wada AM, Nolte MJ, Udan RS et al. Transcription factor FoxO1 is essential for enamel biomineralization. PLoS One. 2012;7(1):e30357.
26. Xie X, Liu C, Zhang H, Jani PH, Lu Y, Wang X et al. Abrogation of epithelial BMP2 and BMP4 causes Amelogenesis mperfecta by reducing MMP20 and KLK4 expression. Sci Rep. 2016;6:25364.
27. Catón J, Luder HU, Zoupa M, Bradman M, Bluteau G, Tucker AS et al. Enamel-free teeth: Tbx1 deletion affects amelogenesis in rodent incisors. Dev Biol. 2009 Apr 15;328(2):493-505.
28. Nakamura T, de Vega S, Fukumoto S, Jimenez L, Unda F, Yamada Y. Transcription factor epiprofin is essential for tooth morphogenesis by regulating epithelial cell fate and tooth number. J Biol Chem. 2008 Feb 22;283(8):4825-33.
29. Steele-Perkins G, Butz KG, Lyons GE, Zeichner-David M, Kim HJ, Cho MI et al. Essential role for NFI-C/CTF transcription-replication factor in tooth root development. Mol Cell Biol. 2003 Feb;23(3):1075-84.
30. Rios H, Koushik SV, Wang H, Wang J, Zhou HM, Lindsley A et al. Periostin null mice exhibit dwarfism, incisor enamel defects, and an early-onset periodontal disease-like phenotype. Mol Cell Biol. 2005 Dec;25(24):11131-44.
31. Ahn YH, Kim TH, Choi H, Bae CH, Yang YM, Baek JA et al. Disruption of Tgfbr2 in odontoblasts leads to aberrant pulp calcification. J Dent Res. 2015 Jun;94(6):828-35.
32. Yuan G, Chen L, Feng J, Yang G, Ni Q, Xu X et al. Dentin Sialoprotein is a novel substrate of matrix metalloproteinase 9 *in vitro* and *in vivo*. Sci Rep. 2017 Feb;7:42449.
33. Vogel P, Read RW, Hansen GM, Powell DR, Kantaputra PN, Zambrowicz B et al. Dentin dysplasia in notum knockout mice. Vet Pathol. 2016 Jul;53(4):853-62.
34. Bardet C, Courson F, Wu Y, Khaddam M, Salmon B, Ribes S et al. Claudin-16 deficiency impairs tight junction function in ameloblasts, leading to abnormal enamel formation. J Bone Miner Res. 2016 Mar;31(3):498-513.
35. Yamaguti PM, Neves FA, Hotton D, Bardet C, De La Dure-Molla M, Castro LC et al. Amelogenesis imperfecta in familial hypomagnesaemia and hypercalciuria with nephrocalcinosis caused by CLDN19 gene mutations. J Med Genet. 2017 Jan;54(1):26-37.

Correspondance :
agnes.bloch-zupan@unistra.fr, v.haushalter@unistra.fr

Virginia Laugel-Haushalter

2. The *Rogdi* Knockout Mouse is a Model for Kohlschütter–Tönz Syndrome

This study is about a novel knockout mouse model that inactivates *Rogdi*, a gene and corresponding protein with yet unknown functions. *ROGDI* variants are also responsible in humans for Kohlschütter-Tönz Syndrome (KTS, OMIM 226750, ORPHA: 1946), a rare genetic disorder with autosomal recessive inheritance. This disease is characterized by early-onset epilepsy, psychomotor regression, intellectual disability, and enamel defects.

Little is known about the pathophysiology leading to the KTS phenotype when *ROGDI* is altered. *ROGDI* transcripts are present in organs/tissues affected during mouse and human brain development. The localization of transcripts to neuronal presynaptic sites in rats suggests that *Rogdi* may regulate protein exocytosis. Rogdi is present in two important types of synapses in the hippocampus: the mossy fiber and hilar synapses [95]. *Rogdi* is also expressed during odontogenesis from the cup stage in E14.5 mouse embryos [17]. Regarding cellular localization, the ROGDI protein is localized in the nuclear envelope of cultured human cells [81]. The pathophysiology of epilepsy involves defects in gamma-aminobutyric acid (GABA)ergic transmission known to induce sleep disorders. A *Rogdi* homolog in Drosophila has been consistently shown to act as a novel sleep-promoting factor by supporting a specific subset of GABAergic transmissions. As a result, *Rogdi* mutant flies exhibit insomnia-like behaviors accompanied by sleep fragmentation and delay in sleep initiation [83].

The crystal structure of the ROGDI protein (287 amino acids, 32kD) in humans comprises an alpha domain with four leucine-zipper helices, and a beta-sheet domain. The ZIP-like motif in the alpha domain appears to mediate their intramolecular interactions, contributing to the overall structure and stability of a monomeric ROGDI protein. Disruption of the four-helix bundle following mutations leads to significant destabilization of the protein structure [68].

Despite the information and data published on ROGDI, its function remains unknown to date.

Here, we report that *Rogdi* expression is enriched since early stages, during both tooth and neurological development. *Rogdi* homozygous mutant mice recapitulate patient's phenotype. Micro-CT and scanning electron microscopy imaging analysis show a less dense and low mineral content of the enamel layer, mimicking the amelogenesis imperfecta phenotype displayed in KTS patients. They also exhibit epilepsy susceptibility, memory impairment, and hyperactivity. To understand neurodegenerative and enamel deficits, comparative genomic studies were conducted. Whole genome RNA-sequencing, combined with bioinformatic approaches, helped uncover a *Rogdi* transcriptional network. We propose a new role for Rogdi through the identification of partners as members of the V-ATPase complex and demonstrate the impairment of acidification and pH cycling both during amelogenesis and in stomach function. These results could lead to the development of new therapeutic avenues.

This article has an important translational significance, providing a mouse model that displays the clinical characteristics found in patients and the discover of new phenotypes such as gastrointestinal difficulties that could also be part of the KTS syndrome.

Here we present the *Rogdi*$^{-/-}$ mutant as a novel model deciphering partially KTS pathophysiology. *Rogdi*$^{-/-}$ mutant defects in acidification might explain the unusual combination of enamel and neurological rare disease symptoms.

Article submitted to Scientific Reports (*Sci Rep*)

The *Rogdi* Knockout Mouse is a Model for Kohlschütter–Tönz Syndrome

Alexandra Jimenez-Armijo[1], Supawich Morkmued[2], José Tomás Ahumada[1], Naji Kharouf[3], Yvan de Feraudy[1,4], Gergo Gogl[1], Fabrice Riet[5], Karen Niederreither[1], Jocelyn Laporte[1], Marie Christine Birling[5], Mohammed Selloum[5], Yann Herault[1,5], Magali Hernandez[6], Agnès Bloch-Zupan*[1,7,8,9,10]

Affiliations

[1] Université de Strasbourg, Institut de Génétique et de Biologie Moléculaire et Cellulaire (IGBMC), INSERM U1258, CNRS- UMR7104, Illkirch, France.

[2] Faculty of Dentistry, Pediatrics Division, Department of Preventive Dentistry, Khon Kaen University, Khon Kaen, Thailand

[3] Université de Strasbourg, Laboratoire de Biomatériaux et Bioingénierie, Inserm UMR_S 1121, Strasbourg, France.

[4] Department of Neuropediatrics, Strasbourg University Hospital, Strasbourg, France.

[5] Université de Strasbourg, CNRS, INSERM, CELPHEDIA, PHENOMIN, Institut Clinique de la Souris (ICS), Illkirch, France.

[6] Centre Hospitalier Régional Universitaire de Nancy, Université de Lorraine, Competence Center for Rare Oral and Dental Diseases, Nancy, France.

[7] Université de Strasbourg, Faculté de Chirurgie Dentaire, Strasbourg, France.

[8] Université de Strasbourg, Institut d'études avancées (USIAS), Strasbourg, France.

[9] Hôpitaux Universitaires de Strasbourg (HUS), Pôle de Médecine et Chirurgie Bucco-dentaires, Hôpital Civil, Centre de référence des maladies rares orales et dentaires, O-Rares, Filière Santé Maladies rares TETE COU, European Reference Network ERN CRANIO, Strasbourg, France.

[10] Eastman Dental Institute, University College London, London, United Kingdom.

***Corresponding author**

Agnès Bloch-Zupan

agnes.bloch-zupan@unistra.fr

Abstract

Kohlschütter–Tönz syndrome (KTS) is a rare autosomal recessive disorder characterized by severe intellectual disability, early-onset epileptic seizures, and amelogenesis imperfecta. Loss of *ROGDI* expression likely produces these severe patient defects. Here, we present a novel *Rogdi* mutant mouse demonstrating that *Rogdi*$^{-/-}$ loss of function recapitulates most KTS patient symptoms. Mutants displayed pronounced pentylenetetrazol-induced seizures, confirming epilepsy susceptibility. Spontaneous locomotion and circadian activity tests demonstrate *Rogdi* mutant hyperactivity mirroring patient spasticity. Object recognition impairment indicates memory deficits. *Rogdi*$^{-/-}$ mutant enamel was markedly less mature. Scanning electron microscopy confirmed its hypomineralized/hypomature crystallization, as well as its low mineral content. Transcriptomic RNA sequencing of postnatal day 5 lower incisors showed downregulated enamel matrix proteins *Enam, Amelx,* and *Ambn*. Enamel crystallization is highly pH-dependent, as an acidic pH is required to accelerate matrix protein degradation and to promote mineralization. *Rogdi*$^{-/-}$ teeth exhibit no signs of cyclic dental acidification. Additionally, expression changes in *Wdr72*, *Slc9a3r2*, and *Atp6v0c* were identified as potential contributors to these tooth acidification abnormalities. These proteins interact through the acidifying V-ATPase complex. Here, we present the *Rogdi*$^{-/-}$ mutant as a novel model to partially decipher KTS pathophysiology. *Rogdi*$^{-/-}$ mutant defects in acidification might explain the unusual combination of enamel and rare neurological disease symptoms.

Introduction

Kohlschütter-Tönz syndrome (KTS, OMIM 226750, ORPHA: 1946) is a rare genetic disorder with autosomal recessive inheritance. It is caused by mutations in the *ROGDI* gene, encoding a protein of unknown function but whose high conservation among diverse species, including Caenorhabditis elegans, Drosophila melanogaster, Danio rerio, Xenopus laevis, and Mus musculus, suggests its critical role [1–4]. After the first description of the syndrome in 1974 [5], several additional affected individuals with splice-site, nonsense, and frameshift mutations in *ROGDI* have been reported [1,2,6–8].

KTS patients always display debilitating neurological deficits, including early childhood-onset epilepsy, spasticity, intellectual disability, and psychomotor regression. Likewise, dental defects, a dysplastic brown to yellow enamel marking amelogenesis imperfecta (AI) [2,6], are always seen. Nephrocalcinosis has also been described recently as a new clinical feature in patients with KTS [9].

Epilepsy often manifests within the first year of life, with seizures frequently resistant to diverse antiepileptic treatments. While monotherapy with perampanel has provided seizure control in some patients [9], the most severely affected individuals have profound intellectual disability, never acquire speech, and become bedridden early in life [1,2,10]. Clinical diagnosis of KTS is usually not made using neurological deficits (as these are found in numerous disorders). Hence, enamel discoloration is typically a first indicator of a KTS diagnosis [6,11].

Amelogenesis imperfecta (AI) is a heterogeneous group of diseases affecting enamel formation [12]. While AI can present as an isolated disease, it can also coexist with other abnormalities, as observed in KTS [13]. AI is classified into four main categories (hypoplastic, hypomature, hypocalcified, hypomature hypoplastic with taurodontism) according to clinical defects and inheritance mode [14]. In *ROGDI*-associated KTS, AI is of the hypomineralization type (less mineralized, porous, rough, and brown stained in both primary and permanent teeth) with maturation defects and associated rough colored dental surfaces [11]. Disturbances during the maturation stage of amelogenesis result in pathologically softer-hypomature enamel of normal thickness. Enamel defects result in frequent caries and sensitive and esthetically disfigured teeth.

Quantitative PCR shows enriched expression of *ROGDI* in the human brain, spinal cord, blood, heart, and bone marrow [1]. Presynaptic *ROGDI* localization in rat hippocampal neurons suggests functions in protein exocytosis [13]. ROGDI is also localized in the nuclear envelope of cultured human cells [1,8], suggesting that it functions as a transcription factor. Structural analysis of this protein, however, shows the lack of basic amino acid residues typically located at the N-terminus of the ZIP domain transcription factors, which are required for DNA binding and nuclear localization [8]. *Rogdi* is expressed early in the E14.5 cap stage tooth in mouse [2], suggesting developmental roles.

A mouse mutant model of *Rogdi* inactivation was created at the Institut Clinique de la Souris (ICS), Illkirch, France. We report here the phenotypic manifestations observed in this mouse

model to further understand KTS disease and the pathophysiology behind *Rogdi* loss of function.

Results

Rogdi expression analysis

To explore a possible correspondence between clinical features encountered in humans and mouse models, we performed a detailed *Rogdi* transcript location analysis in wild-type (WT) mice.

In situ hybridization experiments at embryonic (E) 8.5-10.5-stage of post coitus development-indicated no early differential domains of *Rogdi* expression. Starting at E12.5, we detected enriched *Rogdi* transcripts in neuroepithelium tissues, including the brain, spinal cord, and spinal ganglion (Figure 1A). Differential expression in the liver and vascular endothelium was also apparent at this stage. At E14.5 (Figure 1B), central nervous system expression, including in the trigeminal and spinal ganglia, persisted. Liver and kidney enrichments were also observed (Figure 1B).

With *ROGDI* patients displaying clear alterations in brain function - intellectual disability, psychomotor regression, epileptic seizures, and ataxia [2,6] - we examined *Rogdi* transcript levels in wild-type adult mice. In the 7-week-old adult brain, enriched expression in both the hippocampus (HPC) and cerebellum (CE) (Figure 1I, 1J) suggested a persistent role of *Rogdi* in neurological development. In addition, reanalysis of single-cell transcriptomics of twenty-four cell populations in five regions of the central nervous system [15] demonstrated strong expression of *Rogdi* transcripts in neurons from the cortex and cerebellum, such as corticostriatal neurons, corticospinal neurons, neurons (CCK), stellate and basket cells, unipolar brush cells, and granule cells, whose functions correlate to the phenotype in patients and in our mouse mutant (see Supplementary Table S1).

During tooth development, transcripts were localized from the dental lamina at E12.5 (Figure 1A, 1C), to the cap stage at E14.5 (Figure 1B, 1D), to the bell stage at E16.5 (Figure 1E, 1F), and at postnatal PN1 (Figure 1G) in both the ectodermal and ectomesenchymal compartments. *Rogdi* displayed differential enrichment in both ameloblasts and odontoblasts. At PN5 (Figure 1H), a strong signal was observed in ameloblasts only, likely correlating with a critical role of *Rogdi* in amelogenesis. According to the dataset consulted in https://kleintools.hms.harvard.edu/tools/springViewer_1_6_dev.html?datasets/Sharir_et_al_2019/control_epithelial [16] *Rogdi* transcripts are enriched in the incisor epithelium, specifically in the preameloblast and ameloblast classes. Cycling cells and non-ameloblast epithelial cells also have expression, but at lower levels. *Rogdi* transcript levels are 100 times lower than those of the enamel matrix proteins *Ambn* and *Enam* but are comparable to the levels of *Orai1* and *Stim1*, which are responsible for syndromic hypomature AI [17–19].

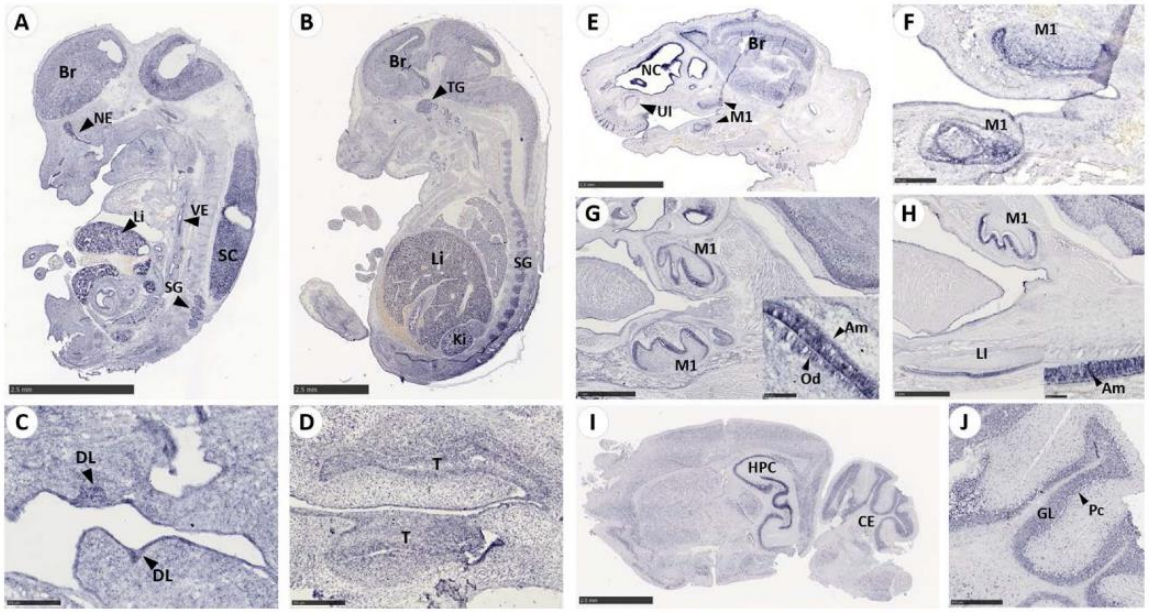

Figure 1. *Rogdi* expression. (A) Rogdi mRNA is expressed in the brain (Br), nasal epithelium (NE), spinal cord (SC), spinal ganglion (SG), and liver (Li) at E12.5. (B) At E14.5, continued enriched expression in the brain and liver is observed, and trigeminal ganglion (TG), spinal ganglion (SG), and kidney (Ki) *Rogdi* enrichment is observed. *Rogdi* molar odontogenic expression begins at (C) E12.5 in the dental lamina (DL), (D) continues in the E14.5 cap stage and in (F) E16.5 bell stage molars. (E) Expression of *Rogdi* mRNA at E16.5 in the brain, nasal cavity (NC), vibrissae (VB), upper incisor (UI) and first molar (M1) at the bell stage. (G) At postnatal day P1, *Rogdi* mRNA is present in ameloblasts and odontoblasts of the lower molar. (H) At P5, enriched expression in ameloblasts appears (compare insert panels in G [P1] vs. H [P5] showing P5 ameloblast enrichment. (I) Adult mouse brain. Pronounced expression of Rogdi in the hippocampus (HPC) and in the cerebellum (CE) is observed. (J) In the cerebellum, *Rogdi* appears to be enriched in the granular layer (GL) and Purkinje cells (Pc).

Specifically, the ROGDI protein was enriched in the ameloblast Tomes's process during the secretory stage of amelogenesis (Figure 2A, 2B, 2C), during transition (Figure 2D) and in the apical part of mature ameloblasts (Figure 2E, 2F).

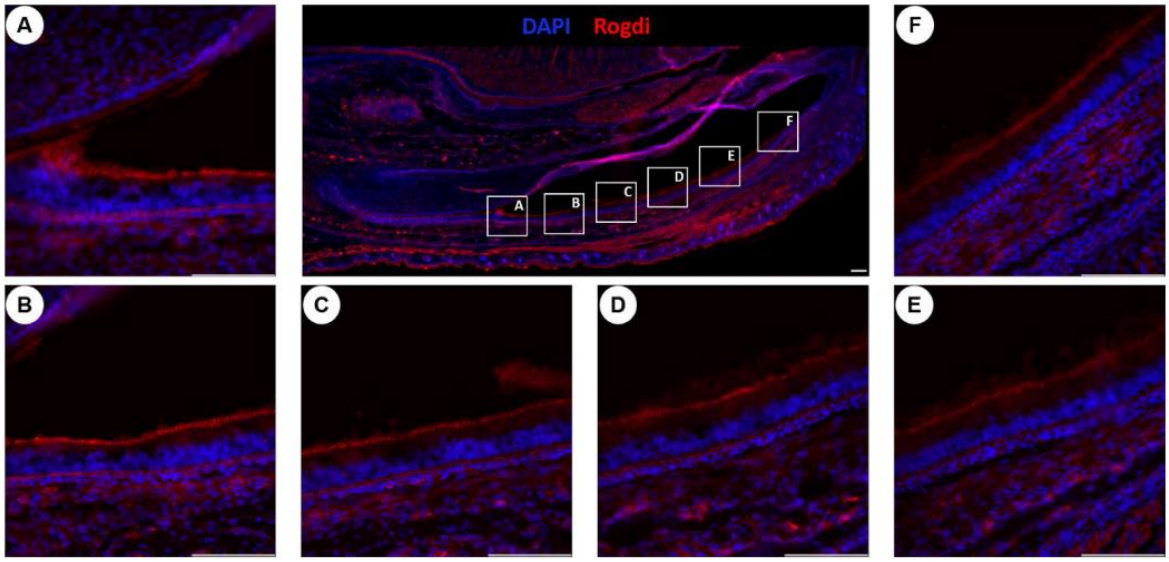

Figure 2. Rogdi protein localization in the postnatal 1-day lower incisor. Immunodetection of Rogdi in lower incisor ameloblasts showed **(A, B, C)** transition between secretory and early maturation-stage ameloblasts with positive staining at the apical border in Tomes's processes. **(D, E, F)** Maturation-stage ameloblasts present a more diffuse signal of Rogdi at the apical pole. Boxes A-F show the respective location in the lower incisor of images A to F. From a less differentiated ameloblast (box A) to a more differentiated ameloblast (box F). Notice that the cervical loop appears on the left side of the image. Am, ameloblasts. Scale bar: 100 µm.

Creating a *Rogdi* mouse loss-of-function model

To investigate the role of Rogdi in development and disease, we created a mouse loss-of-function model targeting exons 6 to 11 by homologous recombination (see Figure 3A for the *Rogdi* knockout construct and Supplementary Figure S1 for the genotyping strategy). *Rogdi* mouse mutants were found to be viable at early stages. Nevertheless, they did not follow a normal Mendelian birth ratio, as in heterozygous crosses, only 1/5 of the offspring were *Rogdi*$^{-/-}$ (Supplementary Table S2). No gross embryonic (E9.5, E12.5) or fetal (E14.5–18.5) malformations were observed in *Rogdi*$^{-/-}$ mutants. However, there was early lethality at postnatal stages, with more than 64% of *Rogdi*$^{-/-}$ mutants not surviving after 12 weeks of age. After weaning, the *Rogdi*$^{-/-}$ mutants had a significantly lower weight than the WT (Figure 3B). This impaired growth and weight discrepancy in mutant mice was observed during the whole life of the animal. The other parameters – body temperature (°C), body position, tremor, palpebral closure, coat appearance, whiskers, lacrimation, and defecation - were comparable between genotypes. The oldest living *Rogdi*$^{-/-}$ mouse was 49 weeks old.

To understand the early lethality of mutants, a necropsy examination was performed using the protocol described in Scudamore, Busk and Vowell (2014). Examination of 26 *Rogdi*$^{-/-}$ *mice* showed a distended stomach full of undigested food in 80% of the *Rogdi*$^{-/-}$ mice. The stomach content in *Rogdi*$^{-/-}$ mice had a pH of 6 instead of a normal acidic pH. The appearance of the

bowel was normal with fecal matter along its structure (Figure 3C compare WT and *Rogdi KO*). One *Rogdi*$^{-/-}$ mouse presented hepatomegaly with an abnormal pale color in both kidneys. Another *Rogdi*$^{-/-}$ had a similar defect in its kidneys. 3 *Rogdi*$^{-/-}$ had a urinary bladder full of urine and with a viscous liquid inside. The other organs did not show any particularities.

Dysmorphic features such as microcephaly, asymmetric skull, frontal bossing, short stature, scoliosis, and short nose have been reported in the literature [2,21]. Micro-CT imaging (μ-CT) was performed for morphometric analysis of 8-week-old *Rogdi*$^{-/-}$ mutant and WT mouse skulls. The form (size and shape) of both males and females in *Rogdi*$^{-/-}$ mice was significantly different from that in WT mice. An overall reduction in head dimensions was found, with a significant decrease in dimensions in the nasal bone, premaxillary bone, maxillary bone, temporal bone (with the squamosal portion), and occipital bone. Additionally, increased dimensions were found in the parietal bone and frontal bone, mimicking the frontal and parietal bossing of the human phenotype (Figure 3D).

Blood chemistry parameters measured on the plasma showed significantly lower levels of calcium in *Rogdi*$^{-/-}$ males and higher levels of alkaline phosphatase only in *Rogdi*$^{-/-}$ females. No differences between groups were found in blood cell count.

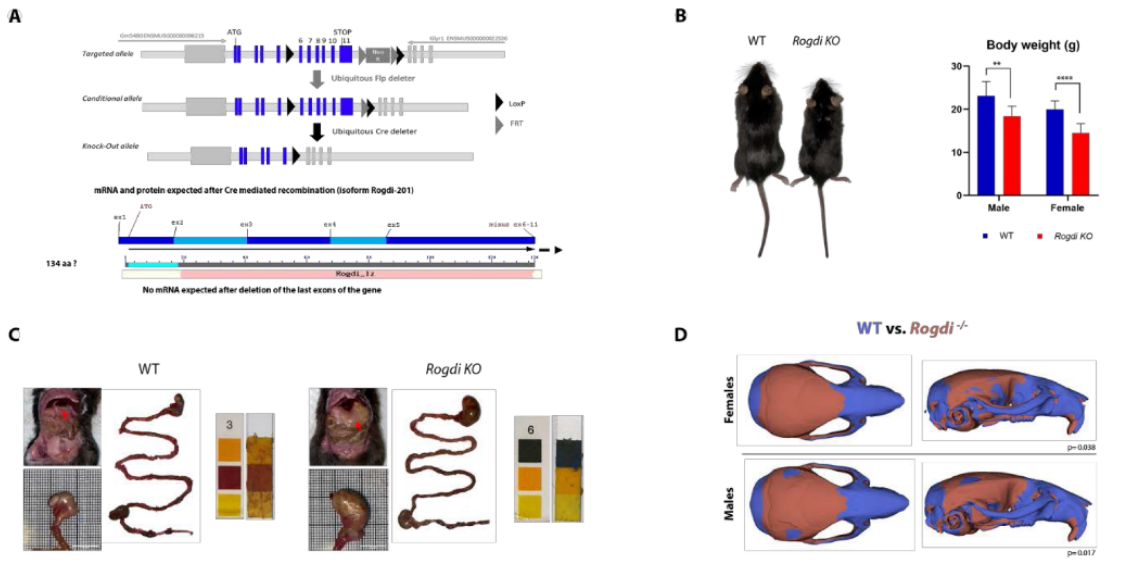

Figure 3. *Rogdi*$^{-/-}$ mouse model. (A) Illustrates the mutation strategy and the protein expected after Cre-mediated recombination consisting of a truncated 134 amino acid protein. (B) Representative picture of an 8-week-old *Rogdi* knockout mouse (left) and a control littermate (right). The column graph on the right shows the body weights of *Rogdi* knockout female and male mice and control littermates between 8 and 12 weeks old. (C) Representative picture of the abdominal area of a WT and *Rogdi KO* mouse (red arrow illustrates stomach) reveals impairment in stomach emptying in *Rogdi KO* mouse. *Rogdi KO* presents an enlarged stomach compared to WT. Measurement of the pH (Merck Acilit® pH Indicator Strips; 0 - 6 pH Range) of stomach contents indicates an almost neutral pH (6) in *Rogdi KO*, whereas WT has a normal acidic pH (3). No other abnormalities were found in the gastrointestinal tract. (D) Form

differences between WT and *Rogdi* $^{-/-}$. WT are displayed in blue and *Rogdi*$^{-/-}$ in red. In the figure WT vs *Rogdi*$^{-/-}$ form difference rigid alignment, in blue is possible to observe the bones with decreased dimensions in *Rogdi*$^{-/-}$. In red, the bones with increased dimensions (frontal and parietal bone) in *Rogdi*$^{-/-}$. *Rogdi*$^{-/-}$ males and females present a similar form.
Scale bar: 10 mm. ** $p < 0.01$ **** $p < 0.0001$.

Locomotory/grip defects, hyperactivity, memory impairment and epilepsy in *Rogdi* knockout mice

Behavioral tests evaluating motor and memory impairment in *Rogdi*$^{-/-}$ and respective controls showed significant increases in locomotor activity during the first hour of the circadian activity test and during habituation (Hab), acquisition (Acq), and retention (Ret) sessions of the novel object recognition test (NOR) (Figure 4A-B), which could be interpreted as hyperactivity disorder in the mutant mice, a feature already described in KTS [4]. Cognitive impairment assayed by NOR showed that *Rogdi*$^{-/-}$ mutants exhibited memory impairment (Figure 4C). Object exploration time was significantly increased in *Rogdi*$^{-/-}$ mutants during the acquisition session, probably a consequence of hyperactivity here too. Nevertheless, a significantly decreased recognition index in *Rogdi*$^{-/-}$ mutants was found with no difference from chance (Figure 4C). These behavioral tests indeed suggest that *Rogdi*$^{-/-}$ memory defects reflected intellectual impairments found in KTS [1,2,6].
Motor function was tested using grip strength and rotarod tests. Sex and batch effects were observed in the grip strength test (Supplementary Figure S2), where in the second group of *Rogdi*$^{-/-}$ females, muscle strength was significantly decreased (Supplementary Figure S2B). The rotarod test indicated no differences between groups (Supplementary Figure S2C). These data suggest that there is no motor impairment in our line, except for some females. Finally, the elevated plus maze (EPM) test was used to assess anxiety-related behavior and showed no differences between the genotypes (Supplementary Figure S2D). In addition, histological analyses in the tibialis anterior (TA), gastrocnemius (Gas) and quadriceps (Qua) muscles revealed no significant variation in the muscle/body weight ratio between *Rogdi*$^{-/-}$ and WT mice (Supplementary Figure S3A). MinFeret and small fiber percentages were similar between both groups (Supplementary Figure S3B and S3C). Histological cross sections of TA, Gas and Qua muscles from both groups showed no morphological differences (Supplementary Figure S3D). SEM of the tibialis anterior, gastrocnemius, and quadriceps muscles showed no differences between the groups.
Early onset, generalized myoclonic seizures and focal and generalized seizures have been reported in KTS [6]. We did not detect spontaneous seizures in young or older *Rogdi*$^{-/-}$ mice. Thus, we decided to induce seizures using a timed pentylenetetrazol infusion test (PTZ). The test was performed to assess the susceptibility of *Rogdi*$^{-/-}$ versus WT mice to develop induced epilepsy. Compared to WT mice, the *Rogdi*$^{-/-}$ mutant animals exhibited higher susceptibility and faster seizure onset. All mice manifested myoclonic seizures, although only *Rogdi*$^{-/-}$ mutants developed clonic seizures. At the end of the convulsion, less than 40% of the WT

mice (3 of 8) presented a tonic seizure, whereas more than 90% of the *Rogdi*$^{-/-}$ mutant mice (6 of 7) had one (Figure 4D).

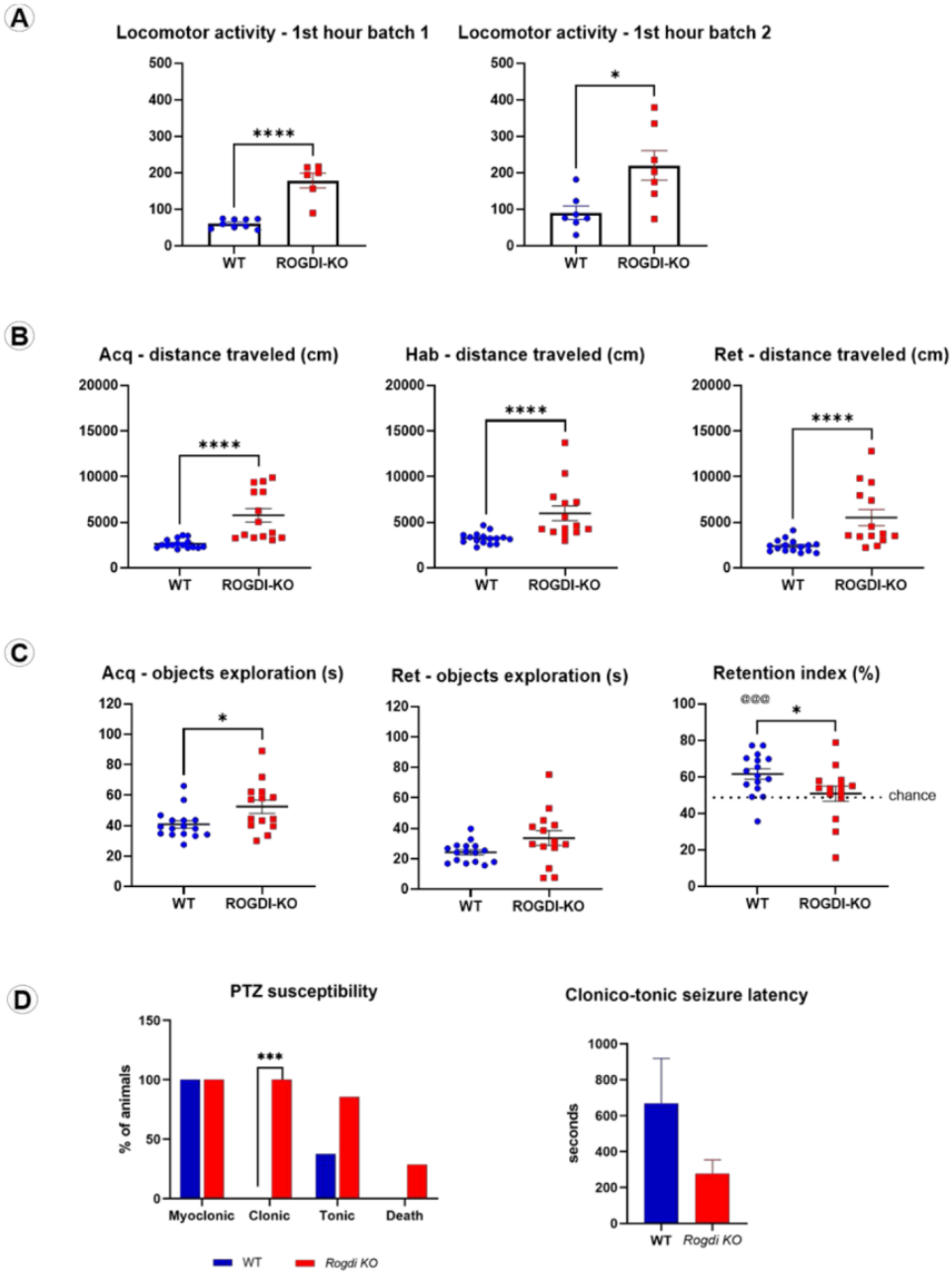

Figure 4. Locomotor activity, memory assessment and epilepsy susceptibility of adult WT vs. *Rogdi* $^{-/-}$. (A) Locomotor activity during the first hour of the circadian activity test. A batch effect was observed, with a higher significance in the first batch. (B) Locomotor activity (distance) in the whole arena during the habituation, acquisition and retention sessions of the novel object recognition test (NOR). (C) NOR: Exploration time (s) of the objects during the acquisition (Acq) that was significantly increased in *Rogdi* $^{-/-}$ mice and retention (Ret) sessions with no difference between groups. The recognition index (%) was significantly decreased in *Rogdi* $^{-/-}$ mice. It was higher than by chance for the WT mice, whereas it was not

significantly different for *Rogdi* $^{-/-}$ mice. (D) PTZ test results show that a higher percentage of *Rogdi* knockout mice developed clonic and tonic convulsive seizures compared to the control group (WT). WT did not present clonic seizures. *Rogdi KO* mice had a shorter latency for clonic-tonic seizures. Data are expressed as the mean ± SEM. * $p < 0.05$; *** $p < 0.001$, **** $p < 0.0001$, @@@ $p < 0.001$ vs chance.

Altered cerebellar and hippocampal morphology

We observed cerebellar and hippocampal histology during development at PN15. Several regional alterations in cerebellar morphometry were observed in *Rogdi*$^{-/-}$ mice compared with WT mice (Table 1). *Rogdi* mutants displayed a decrease in the thickness of the simplex molecular layer (Mol) ($p<0.01$) and crus II internal granular layer (IGL) ($p<0.0001$), while the external granular layer (EGL) of simplex ($p<0.05$) and paramedian ($p<0.001$) lobules was thicker than that of WT. No alteration was observed in the vermal lobule IV/V and crus I lobule.

Table 1. Thickness variations for granular and molecular layers of cerebellar cortex lobules in PN15 WT vs. *Rogdi*$^{-/-}$ mice. The Purkinje cell layer is included in the molecular layer measure. IGL: internal granular layer; Mol: molecular layer; EGL: external granular layer.

CEREBELLUM					
	Vermal lobule IV/V	Simplex	Crus I	Crus II	Paramedian
IGL	-11.9 %	-4.3 %	2.5 %	-23.4 %****	0.8 %
Mol	-1.7 %	-6.8 %**	-1.9 %	21.2 %*	3.4 %
EGL	3.6 %	23.1 %*	30 %$^{\#}$	21.2 %*	69 %***

$^{\#}p = 0.05$; *$p < 0.05$; **$p < 0.01$; ***$p < 0.001$; ****$p < 0.0001$ (unpaired Student's t Test)

In the hippocampus, the thickness of the Oriens layer of the CA1 region was decreased in *Rogdi*$^{-/-}$ mice ($p < 0.001$), while the granular layer of the dentate gyrus was thicker ($p < 0.01$) compared to control mice (Table 2).

Table 2. Percentage of thickness variation measured in subregions of the hippocampal formation of PN15 *Rogdi*$^{-/-}$ mice relative to wild-type mice.

HIPPOCAMPAL FORMATION

CA1			Dentate Gyrus	
Oriens	Pyramidal	Molecular and radiatum	Granular	Molecular
-24.1%***	6.1%	-3.4%	25.7%**	2.4%

**p < 0.01; ***p < 0.001 (unpaired Student's t Test)

Amelogenesis Imperfecta-like dental defects

At adult stages, when comparing WT vs. *Rogdi*$^{-/-}$ mutants macroscopically, clear tooth malformations were observed. Phenotypically, the *Rogdi* mutant mouse presented a severe enamel AI-like defect. The labial surface of the rodent incisor (the crown analog covered by enamel) normally has a yellow/orange color pigmentation, as iron is present at approximately 0.03% in enamel [22]. Hence, mouse teeth have this characteristic color, seen as dark orange upper incisors. Incisors of control mice are yellow, reflecting enamel pigmentation, always darker in the upper incisors. The incisors of *Rogdi*$^{-/-}$ mutant mice had a chalky white color (Figure 5A, compare WT vs. *Rogdi*$^{-/-}$). The whiter aspect and reduced surface shine correspond to reduced enamel thickness and undermineralized enamel (compare red arrowheads in Figure 5A WT and *Rogdi*$^{-/-}$), a typical enamel phenotype encountered in AI-like mouse models [23,24]. Whiteness also indicates reduced enamel-specific iron accumulation typical of other murine AI-like models. All male and female *Rogdi*$^{-/-}$mutants displayed these enamel defects. *Rogdi*$^{-/-}$ mutants (compared to WT, Figure 5A) had pronounced chalky lightening with white patches showing fragmentation or "chipping" more pronounced at the bases of the lower incisors, and molars were abraded and more rounded with enamel loss in the occlusal side exposing the dentin. This attrition points towards structural defects in enamel integrity.

µCT imaging showed a reduction in optical density (darker appearance of mutant enamel), revealing reduced enamel mineral density in both incisors and molars (Figure 5B). *Rogdi* mutation produced a near complete absence of opaque mineralized enamel matrix, showing a phenotype similar to the observed defects in affected patients.

Histological analysis showed a difference in the ameloblast layer between WT and *Rogdi*$^{-/-}$ (Supplementary Figure S4), with a disorganized layer where both secretory and mature ameloblasts were slightly shorter and seemed less polarized with a rounder nucleus in *Rogdi*$^{-/-}$ mutants (compare panels Supplementary Figure S4B, S4C [WT] to Supplementary Figure S4E, S4F [*Rogdi*$^{-/-}$]). The underlying stratum intermedium and stellated reticulum were collapsed, and the outer dental epithelium was also disorganized. Fewer blood vessels were seen. These histological alterations further attest to a critical role of *Rogdi* during amelogenesis.

To assay overall structural changes, *Rogdi*$^{-/-}$ mutant samples were analyzed using scanning electron microscopy (SEM) imaging. Enamel thickness in both the upper incisors and lower

molars was normal in *Rogdi*$^{-/-}$ mutants (Figure 5C), suggesting that EMP secretion was intact. The prismatic organization and the intermingled decussation pattern were conserved in *Rogdi*$^{-/-}$ enamel (compare WT and *Rogdi*$^{-/-}$ in Figure 5C). In mice, all rods are parallel to one another in each layer, but layers alternate so that rods are at 60° from one another [25]. Enamel rods were devoid of crystals, similar to reports of other AI mouse models [26,27]. Enamel of wild-type incisors showed normal crystallization, whereas *Rogdi* null incisors were undermineralized (Figure 5C), demonstrating a severe enamel hypomineralization-type phenotype. X-ray energy dispersion spectrometry (to determine overall mineral content) indicated that the enamel matrix indeed had a reduced mineral content in *Rogdi*$^{-/-}$ mutants. Calcium levels in maturation stage and fully mineralized stage enamel were reduced by more than 80% and 70%, respectively, compared to controls. Phosphorus levels were also diminished at both stages, with approximately 80% in maturation and 50% in final mineralized enamel. Carbon levels indicative of organic content were higher in mutants and did not differ between maturation stage and mineralized enamel in *Rogdi*$^{-/-}$ mutants (Table in Figure 5C), suggesting a lack of enamel matrix degradation during the maturation stage of amelogenesis. SEM analysis was also performed in teeth from one of the patients with KTZ from the Reference Center for Rare Orodental Diseases, CRMR O-Rares. Canine (23) did not present enamel. Enamel in premolar (45) was present but hypoplastic. The calcium-phosphate ratio was 1.65 (Supplementary Figure S5), while normal values are approximately 2.17 ± 0.1 [28]. These data showed that the mineral content in KTS teeth is diminished, which is consistent with the observed phenotype in *Rogdi* null mice.

Defective incisor acidification in *Rogdi* mutants

pH modulation is extremely important during enamel formation, especially at the maturation stage where ameloblasts modulate and alternate between a smooth end and a ruffle border, involving repetitive pH changes in the forming enamel seen as acid (pH 6.0) and neutral (pH 7.2) bands. To explore these steps, methyl red staining was performed in 12-week-old lower incisors for pH analysis. Methyl red stains red at acidic pH (~5.0 – 5.8) and yellow at neutral pH (~6.6 – 8.6). The results revealed a clear red acidic band at the maturation stage in WT mice (Figure 5D). However, in *Rogdi*$^{-/-}$ mutant enamel, no acid bands appeared, staining all the enamel yellow (Figure 5D), showing no changes in pH during amelogenesis. When pH modulation is delayed or disrupted, enamel mineralization is known to be reduced [29,30]. This defect in acidification is observed in *Rogdi*$^{-/-}$ mutants (Figure 5D).

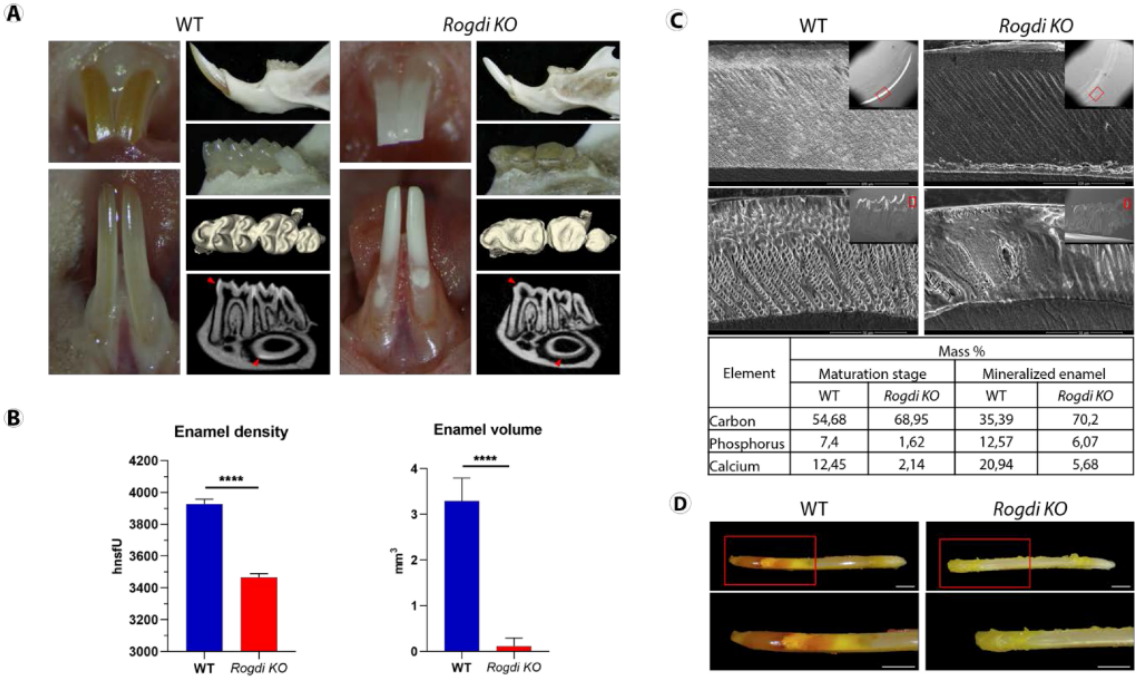

Element	Mass %			
	Maturation stage		Mineralized enamel	
	WT	*Rogdi KO*	WT	*Rogdi KO*
Carbon	54,68	68,95	35,39	70,2
Phosphorus	7,4	1,62	12,57	6,07
Calcium	12,45	2,14	20,94	5,68

Figure 5. *Rogdi* tooth phenotype. (A) Comparison of incisors of WT 8-week-old mice, with darker yellow/orange pigmentation in the upper incisor, to incisors of 8-week-old *Rogdi*$^{-/-}$ mutant mice, which have a chalky white color. *Rogdi*$^{-/-}$ mutant lower incisors show chalky lightening with white patches in the cervical tooth zone. The *Rogdi KO* mouse presented abraded cusps in the molars that were severely worn, losing enamel at occlusal surfaces and exposing the dentin that remained relatively intact, confirming the enamel phenotype. Optical sections in a sagittal plane show reduced enamel mineral density in the lower molars and incisor (red arrowheads). (B) Analysis of enamel volume and density shows that *Rogdi KO* enamel is highly diminished and less dense than that of WT mice. (C) Scanning electron microscopy (SEM) imaging of 8-week-old WT and *Rogdi*$^{-/-}$ teeth shows a reduced mineral density of enamel in both incisors and molars in *Rogdi* KO. Red boxed regions in insert panels show regions in which higher magnification of SEM images were obtained. The enamel of *WT* presents a constant thickness and a clear decussating prism pattern, while the *Rogdi*$^{-/-}$ variant produces a near complete absence of opaque mineralized enamel matrix. Table of energy dispersive X-ray spectrometry (EDX) data for quantification of element composition of enamel in maturation stage of amelogenesis and mineralized enamel. The calcium and phosphate concentrations in the enamel layer of the wild-type mouse are normal, but both concentrations are highly diminished in the *Rogdi* mutant. Carbon levels are higher in *Rogdi* KO, suggesting a lack of enamel matrix protein degradation during the maturation stage of amelogenesis. (D) Methyl-red staining in 12-week-old lower incisors. In wild-type mice, secretory-stage enamel stained neutral (yellow) with methyl-red. In maturation-stage enamel, methyl-red staining revealed 2 broad acidic bands in control mice, the first intensely deep-red and the second (incisal) weaker. No red bands (acidic) were noted in the enamel of *Rogdi KO* mice. **** $p < 0.0001$. Scale bar: 1 mm.

RNA sequencing analysis of postnatal 5 (PN5) incisors

To track global gene expression alterations, independent lower incisors of PN5 male *Rogdi* mutants and WT controls were analyzed by high-throughput RNA sequencing (RNA-seq). Principal component analysis (PCA plot, Supplementary Figure S6A) revealed a clear separation between *WT* and *Rogdi*$^{-/-}$ mutant samples. Bioinformatic analysis was performed by selecting significant genes using a p-value < 0.05 and an absolute value of log2 fold-change > 0.3, providing volcano plots (Supplementary Figure S6B) plotting log2 fold-change on the X-axis versus statistical significance. RNA-seq data confirmed the downregulation of *Rogdi* transcripts, affecting neurodegeneration and synapse pathways, calcium signaling, tight junctions, Wnt, Notch and Hedgehog signaling networks, among others (Supplementary Figure S6C).

Enamel formation or amelogenesis is a strictly controlled process in which ameloblasts secrete enamel in a two-stage process. During the secretion stage, ameloblasts secrete enamel matrix proteins (EMPs), including amelogenin (AMEL), ameloblastin (AMBN), and enamelin (ENAM), which are regulatory targets that are all reduced in *Rogdi* mutants (Table 3) and are important to ameloblast differentiation, enamel crystallite formation and orientation, and prismatic architecture [31–33]. In the maturation stage, enzymes such as matrix metalloproteinase 20 (MMP20) and kallikrein 4 (KLK4) cleave newly secreted EMPs into various derivative fragments [34], allowing full mineralization (98% hydroxyapatite mineral content).

Downregulated genes at PN5 included *Lama3, Itgb6, Acp4, Lamb3* and *Col17a1*, all known as well as causative of amelogenesis imperfecta [33,35]. Genes involved in amelogenesis, such as *Car12, Cnnm4, Amtn, Ltbp3, Slc24a4, Lamb2, Gpr68* and *Orai1,* were upregulated. *Slc9a3r2* and *Atp6v0c* were upregulated in our RNA-seq data, and both proteins are part of the V-ATPase complex [36,37]. *Wdr72,* described as a homologue of WDR7 [38], was also upregulated (Table 3).

Table 3. RNA-seq. Data are presented as log2-fold changes in *Rogdi*$^{-/-}$ vs. WT samples. For instance, a FC log2 value of -1.00 will correspond to a 50% reduction in mRNA level in the *Rogdi*$^{-/-}$ samples. Genes encoding regulators of tooth development and amelogenesis, cell-cell adhesion and cell-matrix adhesion, proteins involved in ion transport such as calcium and transmembrane transport are either reduced or increased in mutant samples.

Gene name	Description	Log2 FC (*Rogdi*$^{-/-}$ vs WT)	*p*-value
Tooth development			
Tspear	thrombospondin type laminin G domain and EAR repeats	-0.55	4.4E-04
Trp63	transformation related protein 63	-0.53	8.6E-06
Nkx2-3	NK2 homeobox 3	-0.50	1.8E-03

Edar	ectodysplasin-A receptor	-0.43	1.7E-02
Perp	PERP. TP53 apoptosis effector	-0.41	1.0E-06
Shh	sonic hedgehog	-0.37	3.2E-02
Apc	APC. WNT signaling pathway regulator	-0.35	1.7E-05
Acvr2a	activin receptor IIA	-0.31	1.1E-03
Wnt10a	wingless-type MMTV integration site family. member 10A	0.32	5.8E-03
Foxc1	forkhead box C1	0.34	2.1E-02
Dll1	delta like canonical Notch ligand 1	0.36	1.4E-02
Twist1	twist basic helix-loop-helix transcription factor 1	0.38	1.7E-03
Phex	phosphate regulating endopeptidase homolog. X-linked	0.38	6.2E-05
Dspp	dentin sialophosphoprotein	0.39	2.1E-04
Tgfb1	transforming growth factor. beta 1	0.44	1.6E-04
Gas1	growth arrest specific 1	0.44	7.6E-04
Wnt6	wingless-type MMTV integration site family. member 6	0.44	3.8E-04
Hand2	heart and neural crest derivatives expressed 2	0.53	1.2E-06
Osr1	odd-skipped related transcription factor 1	0.54	2.2E-03
Id3	inhibitor of DNA binding 3	0.56	1.8E-05
Msx1	msh homeobox 1	0.56	1.5E-07
Col1a1	collagen. type I. alpha 1	0.62	5.3E-11
Amelogenesis			
Lama3	laminin. alpha 3	-1.01	8.8E-12
Itgb6	integrin beta 6	-0.89	5.1E-09
Enam	enamelin	-0.66	1.0E-04
Acp4	acid phosphatase 4	-0.65	1.9E-04
Amelx	amelogenin. X-linked	-0.63	4.2E-04
Ambn	ameloblastin	-0.62	2.9E-04
Lamb3	laminin. beta 3	-0.60	1.4E-05
Shh	sonic hedgehog	-0.37	3.2E-02
Col17a1	collagen. type XVII. alpha 1	-0.36	7.3E-06
Itgb4	integrin beta 4	-0.33	8.0E-04
Car12	carbonic anhydrase 12	0.30	3.3E-02
Cnnm4	cyclin M4	0.30	4.3E-03
Amtn	amelotin	0.35	2.4E-02
Ltbp3	latent transforming growth factor beta binding protein 3	0.37	3.6E-04
Slc24a4	solute carrier family 24 (sodium/potassium/calcium exchanger). member 4	0.38	2.8E-02
Lamb2	laminin. beta 2	0.39	5.5E-04
Wdr72	WD repeat domain 72	0.40	2.6E-02
Gpr68	G protein-coupled receptor 68	0.44	6.6E-05
Orai1	ORAI calcium release-activated calcium modulator 1	0.47	4.6E-05

Cell-cell adhesion			
Ctnna2	catenin (cadherin associated protein). alpha 2	-1.18	5.8E-09
Nfasc	neurofascin	-1.08	2.2E-07
Lama3	laminin. alpha 3	-1.01	4.2E-09
Kirrel2	kirre like nephrin family adhesion molecule 2	-0.71	2.0E-03
Rap1gap	Rap1 GTPase-activating protein	-0.66	6.6E-08
Cdh1	cadherin 1	-0.64	1.3E-05
Nectin4	nectin cell adhesion molecule 4	-0.59	3.9E-04
Celsr2	cadherin. EGF LAG seven-pass G-type receptor 2	-0.57	2.7E-04
Dsg1b	desmoglein 1 beta	-0.52	4.1E-02
Celsr1	cadherin. EGF LAG seven-pass G-type receptor 1	-0.51	5.0E-04
Itga3	integrin alpha 3	-0.50	3.6E-04
Pkp1	plakophilin 1	-0.48	7.4E-03
Cdh6	cadherin 6	-0.47	4.3E-05
Jag1	jagged 1	-0.47	1.4E-03
Perp	PERP. TP53 apoptosis effector	-0.41	8.9E-05
Dsc3	desmocollin 3	-0.41	1.8E-03
Cdh3	cadherin 3	-0.38	1.8E-02
Prickle1	prickle planar cell polarity protein 1	-0.36	3.9E-06
Abl2	v-abl Abelson murine leukemia viral oncogene 2 (arg. Abelson-related gene)	-0.34	1.6E-04
Srf	serum response factor	0.30	4.5E-02
Cx3cl1	chemokine (C-X3-C motif) ligand 1	0.39	8.9E-03
Cldn5	claudin 5	0.40	3.7E-02
Tgfb1	transforming growth factor. beta 1	0.44	4.8E-03
Lims2	LIM and senescent cell antigen like domains 2	0.46	3.7E-02
Col13a1	collagen. type XIII. alpha 1	0.53	1.9E-02
Cell-matrix adhesion			
Itgb6	integrin beta 6	-0.89	9.9E-07
Fermt1	fermitin family member 1	-0.58	5.2E-03
Itga3	integrin alpha 3	-0.50	3.6E-04
Sirpa	signal-regulatory protein alpha	-0.42	3.1E-04
Npnt	nephronectin	-0.42	7.1E-05
Emp2	epithelial membrane protein 2	-0.41	9.3E-03
Itgb4	integrin beta 4	-0.33	1.5E-02
Srf	serum response factor	0.30	4.5E-02
Col5a3	collagen. type V. alpha 3	0.40	4.9E-02
Emilin1	elastin microfibril interfacer 1	0.47	1.3E-03
Col13a1	collagen. type XIII. alpha 1	0.53	1.9E-02
Bcan	brevican	0.63	1.0E-08
Hemidesmosome assembly			

Lama3	laminin. alpha 3	-1.01	4.2E-09
Col17a1	collagen. type XVII. alpha 1	-0.36	4.1E-04
Itgb4	integrin beta 4	-0.33	1.5E-02
Plec	plectin	0.33	3.3E-02
Ion transport			
Slc38a3	solute carrier family 38. member 3	-1.09	2.5E-09
Slc39a4	solute carrier family 39 (zinc transporter). member 4	-1.05	1.1E-07
Slc24a2	solute carrier family 24 (sodium/potassium/calcium exchanger). member 2	-0.89	8.7E-11
Otop2	otopetrin 2	-0.88	6.4E-05
Kcnh3	potassium voltage-gated channel. subfamily H (eag-related). member 3	-0.86	5.7E-05
Slco4a1	solute carrier organic anion transporter family. member 4a1	-0.85	5.9E-05
Lrrc8d	leucine rich repeat containing 8D	-0.77	2.8E-10
Steap1	six transmembrane epithelial antigen of the prostate 1	-0.69	3.4E-04
Cacna2d2	calcium channel. voltage-dependent. alpha 2/delta subunit 2	-0.65	5.7E-03
Slc24a3	solute carrier family 24 (sodium/potassium/calcium exchanger). member 3	-0.63	1.1E-03
Fxyd3	FXYD domain-containing ion transport regulator 3	-0.58	6.3E-07
Kcnip2	Kv channel-interacting protein 2	-0.58	1.1E-02
Kcnk3	potassium channel. subfamily K. member 3	-0.57	6.5E-03
Cldn17	claudin 17	-0.56	2.2E-02
Kcnb2	potassium voltage gated channel. Shab-related subfamily. member 2	-0.55	5.4E-03
Grik3	glutamate receptor. ionotropic. kainate 3	-0.54	2.4E-02
Fxyd4	FXYD domain-containing ion transport regulator 4	-0.53	2.2E-03
Itpr1	inositol 1.4.5-trisphosphate receptor 1	-0.53	2.6E-03
Tmc7	transmembrane channel-like gene family 7	-0.50	2.8E-02
Slc39a8	solute carrier family 39 (metal ion transporter). member 8	-0.50	6.8E-03
Scnn1b	sodium channel. nonvoltage-gated 1 beta	-0.48	3.2E-02
Kcna3	potassium voltage-gated channel. shaker-related subfamily. member 3	-0.47	4.9E-02
Slc41a3	solute carrier family 41. member 3	-0.45	1.7E-03
Nipa2	non-imprinted in Prader-Willi/Angelman syndrome 2 homolog (human)	-0.45	8.0E-03
Kcnk1	potassium channel. subfamily K. member 1	-0.43	2.5E-04
Nalcn	sodium leak channel. non-selective	-0.37	3.8E-02
Tmc4	transmembrane channel-like gene family 4	-0.34	2.4E-02
Tmem38a	transmembrane protein 38A	-0.33	4.7E-03

Kcnh1	potassium voltage-gated channel. subfamily H (eag-related). member 1	-0.32	4.5E-02
Lrrc8c	leucine rich repeat containing 8 family. member C	-0.31	1.2E-03
Slc39a11	solute carrier family 39 (metal ion transporter). member 11	-0.31	3.4E-04
Slc12a4	solute carrier family 12. member 4	-0.31	9.5E-04
Cacna1d	calcium channel. voltage-dependent. L type. alpha 1D subunit	-0.30	2.6E-02
Cnnm4	cyclin M4	0.30	4.9E-02
Calhm2	calcium homeostasis modulator family member 2	0.31	4.6E-02
Kcnn1	potassium intermediate/small conductance calcium-activated channel. subfamily N. member 1	0.34	3.7E-02
Kcnq4	potassium voltage-gated channel. subfamily Q. member 4	0.35	3.2E-02
Kcnc3	potassium voltage gated channel. Shaw-related subfamily. member 3	0.35	4.5E-02
Glrb	glycine receptor. beta subunit	0.37	1.8E-02
Grin2d	glutamate receptor. ionotropic. NMDA2D (epsilon 4)	0.39	2.8E-02
Best1	bestrophin 1	0.40	4.2E-02
Otop1	otopetrin 1	0.40	4.4E-02
Slc39a7	solute carrier family 39 (zinc transporter). member 7	0.41	3.3E-02
Kcnk2	potassium channel. subfamily K. member 2	0.44	6.5E-04
Scn1a	sodium channel. voltage-gated. type I. alpha	0.46	4.3E-02
Slc38a11	solute carrier family 38. member 11	0.47	4.9E-04
Scn1b	sodium channel. voltage-gated. type I. beta	0.47	7.7E-03
Orai1	ORAI calcium release-activated calcium modulator 1	0.47	1.8E-03
Kcnh2	potassium voltage-gated channel. subfamily H (eag-related). member 2	0.47	2.5E-03
Atp7b	ATPase. Cu++ transporting. beta polypeptide	0.49	3.7E-02
Kcnj4	potassium inwardly-rectifying channel. subfamily J. member 4	0.51	2.4E-02
Kcnn4	potassium intermediate/small conductance calcium-activated channel. subfamily N. member 4	0.56	1.1E-03
Atp6v0c	ATPase. H+ transporting. lysosomal V0 subunit C	0.60	3.4E-04
Calcium ion transport			
Slc24a2	solute carrier family 24 (sodium/potassium/calcium exchanger). member 2	-0.89	8.7E-11
F2r	coagulation factor II (thrombin) receptor	-0.78	8.1E-12
Cacna2d2	calcium channel. voltage-dependent. alpha 2/delta subunit 2	-0.65	5.7E-03
Slc24a3	solute carrier family 24 (sodium/potassium/calcium exchanger). member 3	-0.63	1.1E-03
Oprd1	opioid receptor. delta 1	-0.54	9.2E-03
Wnk3	WNK lysine deficient protein kinase 3	-0.54	1.4E-03

Itpr1	inositol 1.4.5-trisphosphate receptor 1	-0.53	2.6E-03
Nalcn	sodium leak channel. non-selective	-0.37	3.8E-02
Cacna1d	calcium channel. voltage-dependent. L type. alpha 1D subunit	-0.30	2.6E-02
Rgs4	regulator of G-protein signaling 4	0.35	3.7E-03
Nos3	nitric oxide synthase 3. endothelial cell	0.35	2.1E-02
Wfs1	wolframin ER transmembrane glycoprotein	0.38	3.7E-04
Jak3	Janus kinase 3	0.39	4.6E-02
Best1	bestrophin 1	0.40	4.2E-02
Orai1	ORAI calcium release-activated calcium modulator 1	0.47	1.8E-03
Cdh23	cadherin 23 (otocadherin)	0.50	5.5E-05
Kcnn4	potassium intermediate/small conductance calcium-activated channel. subfamily N. member 4	0.56	1.1E-03
Transmembrane transport			
Slc39a4	solute carrier family 39 (zinc transporter). member 4	-1.05	1.1E-07
Slc24a2	solute carrier family 24 (sodium/potassium/calcium exchanger). member 2	-0.89	8.7E-11
Slc4a9	solute carrier family 4. sodium bicarbonate cotransporter. member 9	-0.87	8.9E-05
Kcnh3	potassium voltage-gated channel. subfamily H (eag-related). member 3	-0.86	5.7E-05
Slco4a1	solute carrier organic anion transporter family. member 4a1	-0.85	5.9E-05
Sv2b	synaptic vesicle glycoprotein 2 b	-0.67	2.7E-03
Abcg5	ATP binding cassette subfamily G member 5	-0.67	5.4E-05
Slc24a3	solute carrier family 24 (sodium/potassium/calcium exchanger). member 3	-0.63	1.1E-03
Kcnb2	potassium voltage gated channel. Shab-related subfamily. member 2	-0.55	5.4E-03
Itpr1	inositol 1.4.5-trisphosphate receptor 1	-0.53	2.6E-03
Slc39a8	solute carrier family 39 (metal ion transporter). member 8	-0.50	6.8E-03
Ano9	anoctamin 9	-0.49	4.9E-02
Slc25a13	solute carrier family 25 (mitochondrial carrier. adenine nucleotide translocator). member 13	-0.47	6.4E-03
Kcna3	potassium voltage-gated channel. shaker-related subfamily. member 3	-0.47	4.9E-02
Abca4	ATP-binding cassette. sub-family A (ABC1). member 4	-0.40	2.9E-02
Slc7a2	solute carrier family 7 (cationic amino acid transporter. y+ system). member 2	-0.37	2.1E-02
Nalcn	sodium leak channel. non-selective	-0.37	3.8E-02
Mfsd14a	major facilitator superfamily domain containing 14A	-0.36	7.5E-03
Slc7a5	solute carrier family 7 (cationic amino acid transporter. y+ system). member 5	-0.34	3.5E-04

Kcnh1	potassium voltage-gated channel. subfamily H (eag-related). member 1	-0.32	4.5E-02
Slc39a11	solute carrier family 39 (metal ion transporter). member 11	-0.31	3.4E-04
Slc12a4	solute carrier family 12. member 4	-0.31	9.5E-04
Cacna1d	calcium channel. voltage-dependent. L type. alpha 1D subunit	-0.30	2.6E-02
Slc2a10	solute carrier family 2 (facilitated glucose transporter). member 10	0.30	2.3E-02
Slc25a19	solute carrier family 25 (mitochondrial thiamine pyrophosphate carrier). member 19	0.32	4.2E-02
Spns1	spinster homolog 1	0.32	1.9E-02
Abcg1	ATP binding cassette subfamily G member 1	0.33	1.5E-02
Kcnq4	potassium voltage-gated channel. subfamily Q. member 4	0.35	3.2E-02
Kcnc3	potassium voltage gated channel. Shaw-related subfamily. member 3	0.35	4.5E-02
Slc39a7	solute carrier family 39 (zinc transporter). member 7	0.41	3.3E-02
Scn1a	sodium channel. voltage-gated. type I. alpha	0.46	4.3E-02
Kcnh2	potassium voltage-gated channel. subfamily H (eag-related). member 2	0.47	2.5E-03
Ano8	anoctamin 8	0.54	1.9E-04
Slc16a12	solute carrier family 16 (monocarboxylic acid transporters). member 12	0.54	6.4E-03

Rogdi transcripts were also analyzed by qPCR, showing a 4.5-fold lower expression fold change of exons 1-4 in the *Rogdi*$^{-/-}$ group than in the WT group, and a 1500-fold lower expression fold change of exons 6-11 in the *Rogdi*$^{-/-}$ group (Supplementary Figure S6D). This result was confirmed by RNA-seq data showing an 8-fold reduction (log2 FC -2.97). The *Rogdi* null mutant would be predicted based on crystallographic analysis to produce a 134 amino acid nonfunctional degraded protein, disrupting the alpha domain of Rogdi, which could impair protein stability, causing loss of function [3].

ROGDI protein interactions (Bioplex and OpenCell interactomes [39,40]) indicated that ROGDI interacts with ATPase proteins (ATP1A2, ATP2A1), myosin heavy chain (MYH7, MYH8), TUBA3C, NUDT3, and 3 proteins of the Rabconnectin-3 complex - WDR7, DMXL1 and DMXL2- (Figure 6) associated with V-ATPase assembly, which is essential for acidification [36,38]. In humans, it has been reported (BioGRID, https://thebiogrid.org/) that ROGDI interacts with the same proteins described above and subunits of the V1 complex of V-ATPases (ATP6V1G1, ATP6V1E2, ATP6V1H, ATP6V1C1, ATP6V1E1, ATP6V1F and ATP6V1B2). ROGDI also interacts with DISC1 (implicated in schizophrenia and neuronal migration [41]), CEP63 (linked to

microcephaly and dyslexia [42,43]), CIT and KIF14 (linked to microcephaly [44]), PLEKHA4 (involved in autism [45]), and KIAA1377 (associated with amyotrophy [46]) (see Supplementary Figure S7).

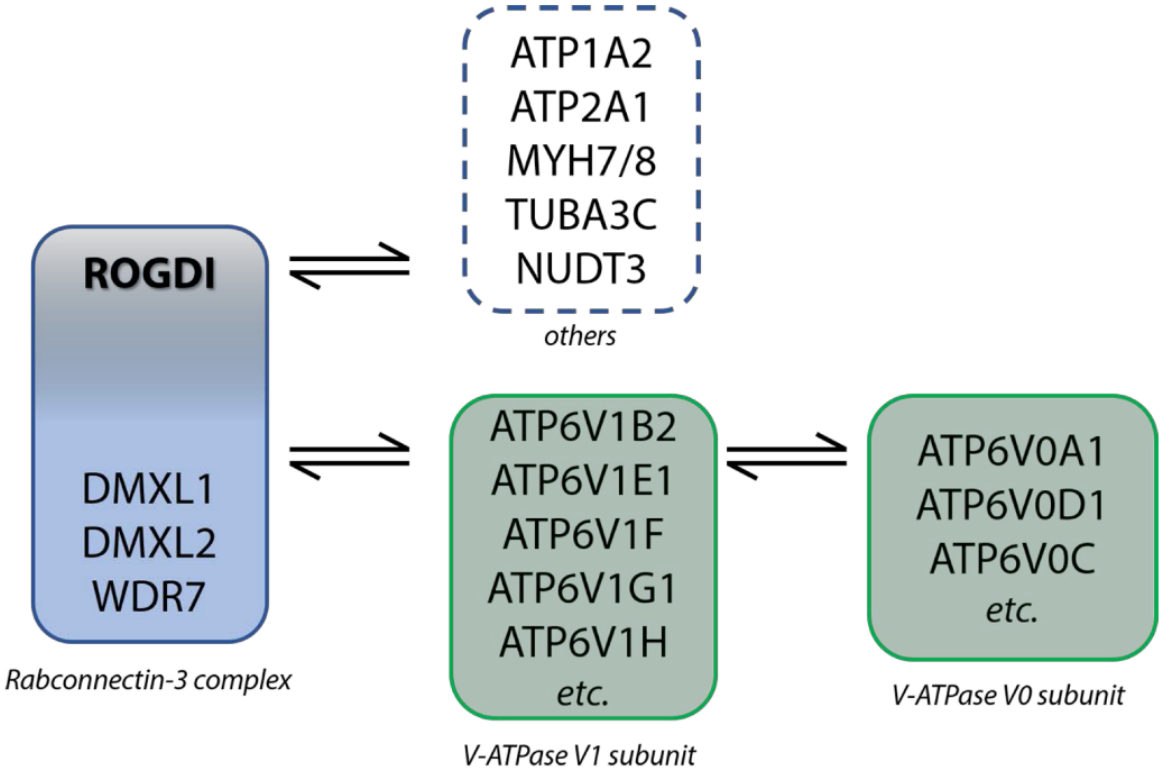

Figure 6. ROGDI protein interaction network. The protein-protein interaction network of ROGDI was assembled based on the results of the OpenCell and BioPlex interactomic projects. ROGDI was found to be part of the Rabconnectin-3 complex, which interacts with the V1 subunit but not with the V0 subunit of the V-ATPase complex. In addition, ROGDI was also found to interact with other partners: ATPase proteins (Atp1a2, Atp2a1), myosin heavy chain (Myh7, Myh8), Tuba3c, and Nudt3.

Discussion

The mouse loss of function of *Rogdi* recapitulates major clinical KTS changes.

Understanding and finding treatments for extremely rare genetic disorders such as Kohlschütter-Tönz syndrome (of which, to date, only 43 cases have been reported worldwide) requires novel tools and data mining. To date, there is no defined molecular function of the ROGDI protein explaining the unique combination of KTS patient defects. Functions have been hypothesized based on ROGDI presynaptic localization, potentially regulating exocytosis in the developing brain [13]. Crystallographic modeling revealed that ROGDI has α domains adapting leucine ZIPPER-like structures and β domains resembling a claudin-like tight junction protein [3]. Tight junction proteins form selective barriers regulating the epithelial permeability of solutes [47]. There is even debate as to whether some patient mutations indeed produce a degraded protein [6]. Here, we clearly demonstrate that the murine loss-of-function of *Rogdi* reproduces the full range of KTS phenotypes observed in humans.

Rogdi mouse mutants are susceptible to developing epilepsy and memory impairment, recapitulating KTS patient clinical findings. The cerebellum plays a leading role in coordination, cognition, and language function [48]. *Rogdi*$^{-/-}$ mice display various stage-specific increases in the thickness of the external granular layer (EGL). Early increases in EGL thickness (via augmented EGL proliferation) can produce impaired motor coordination in other models [49]. We observed increases in EGL thickness in both the simplex and paramedian lobules of PN15 *Rogdi*$^{-/-}$ mice, whereas no modification was observed in the IGL, suggesting that the migration of granule cells from the external layer to the internal layer was preserved but that postmigration apoptosis was delayed or defective. *Rogdi*$^{-/-}$ mice also presented a decreased molecular layer in the simplex lobule, possibly reflecting a growth defect in Purkinje dendritic arborization. In the crus II lobule, the reduction in IGL thickness associated with an increase in EGL thickness indicates a delayed organization characterized by an accumulation of premigratory cells in the EGL and a migration defect to the IGL. The hypertrophy of the molecular layer of the crus II lobule could be explained by postmigratory apoptosis and/or synaptic selection defects. Cerebral CT scans and MRI on selected KTS patients show brain atrophy, including a smaller hippocampus and hypoplasia of the cerebellar vermis [1,6,10,21]. The observed architectural defects could explain the clinical signs of KTS patients. Indeed, simplex and paramedian lobules are involved in sensory-motor functions, while the crus II lobule participates in cognitive functions [50]. Dysregulated growth in both *Rogdi*$^{-/-}$ mice and KTS patients suggests a central role in disease etiology. Likewise, *Rogdi*$^{-/-}$ mice display decreased hippocampal CA1 stratum oriens thickness, suggesting a growth defect in the basal dendritic arbors of pyramidal cells, potentially impairing memory. RNA-seq supported the dysregulation of genes regulating hippocampal development, synapse organization, and neurotransmitter transport (see Supplementary Table S3).

The mouse model also presents amelogenesis imperfecta with a severe hypomineralization-type enamel phenotype, which presents as white teeth instead of the normal yellow color found in control mice. Mineral content analysis displayed a lack of mineralization in both incisors and molars in the *Rogdi*$^{-/-}$ mice with low calcium and phosphate concentrations. Mutants also display higher carbon levels (indicating the presence of organic content) [51]. Normally, organic reductions occur between the maturation stage and mineralized enamel, and the absence of this reduction in *Rogdi*$^{-/-}$ mutants indicates impaired enamel matrix protein degradation and/or removal, which is required during the maturation stage of amelogenesis [52]. Thus, these results confirmed that most mutations affecting *ROGDI* found in individuals with Kohlschütter-Tönz syndrome are loss-of function mutations.

Alterations in several enamel-regulating genes contribute to the dental phenotype in the *Rogdi*$^{-/-}$mutant

During tooth development, enamel may be modified in its width, microstructure, or mineralization degree, causing amelogenesis imperfecta (AI) [53]. To date, variants in over 95 genes are associated with nonsyndromic or syndromic AI [12]. In KTS, enamel is soft, rough, and stained in various shades of brown, presenting AI of the hypomature/hypomineralized type [1,2,6–8]. *Rogdi*$^{-/-}$ mouse enamel mirrors the most severe human KTS patient's clinical feature (hypomineralized enamel). In mice, this manifests as a chalky, easily chipping white enamel compared to the normal strong yellow/orange enamel found in wild type. Morphologically, both secretory and mature ameloblasts were disorganized, slightly shorter and lacked polarization. *Rogdi*$^{-/-}$ defects appear during enamel maturation, showing a lack of mineralization quantified by the reduction of calcium (~80%) and phosphorus (~50%) in a normally organized nondegraded enamel matrix. Rogdi protein localization in the apical pole of ameloblasts (see Figure 2) suggests roles in EMP degradation to allow mineralization [33,52]. This severe hypomineralization accompanies defective crystallization. These defects are similar to phenotypes seen in mouse mutants for *Klk4* and *Wdr72* [27,54,55].

Whole-transcriptome analysis of PN5 *Rogdi*$^{-/-}$ mutant incisors showed reductions in the transcripts coding for enamel matrix proteins *Enam, Amelx*, and *Ambn* (see Table 3). These genes are all expressed during early stages of amelogenesis [56] and are essential for controlled enamel crystallite growth and prismatic architecture [32,33,57].

We found other downregulated genes whose mutations produce amelogenesis imperfecta. These include *Lama3, Lamb3, Lamc2* and *Col17a1* (Table 3). These proteins participate in cell-to-cell or cell-to-extracellular matrix adhesion. Ameloblasts must tightly contact the extracellular matrix [35]. RNA-seq analysis revealed that the *Rogdi* mutation reduced several components of the cell adhesion pathway (see Table 3). LAMA3, LAMB3 and LAMC2 form the heterotrimeric protein laminin 332 (LM332), located in mature ameloblasts and Tomes' processes hemidesmosomes, the latter structure mediating cell adhesion [58,59]. COL17A1 is

another component of hemidesmosomes and a ligand for LM332, participating in epithelial-mesenchymal interactions required for ameloblast differentiation and adhesion and enamel formation [35]. *Col17 -/-* mice, similar to *Rogdi*$^{-/-}$ mice, exhibit reduced expression of the enamel proteins Amelx, Ambn, and Enam, further indicating incomplete ameloblast differentiation [60].

Genes involved in Tomes' process regulation, vesicle/ion transport, cell adhesion, and pH sensing during enamel maturation are often increased in PN5 *Rogdi* mutant incisors. These include *Amtn, Wdr72, Slc24a4, Cnnm4, Orai1,* and *Gpr68,* which are overexpressed in PN5 incisors. Amelotin (AMTN) may regulate cell-matrix adhesion, promoting enamel crystallization [61]. The enamel of *Amtn*-overexpressing mice has disorganized enamel crystals, which are thin, fragile, and lack Tomes' processes – a structure marking secretory ameloblasts [62]. WDR72 appears to be required for endocytic vesicle trafficking [54]. Endocytosis is needed to remove degraded enamel protein debris, supporting enamel crystallite growth [35]. Excess WDR72 (found in maturation stage ameloblasts [63,64]) might dysregulate enamel matrix protein processing. Excess WDR72 may contribute to *Rogdi* mutant *Enam, Amelx*, and *Ambn* reductions. The $Na^+/Ca^{2+}+K^+$-Exchanger SLC24A4 is also increased. It has been hypothesized that SLC24A4 is responsible for actively transporting Ca^{2+} ions from ameloblasts into the enamel matrix during maturation [65]. SLC24A4 excess may correlate with reduced enamel Ca^{2+} levels, changes observed in *Rogdi* mutant enamel. CNNM4 protein is localized in ameloblasts and mediates transcellular Mg^{2+} transport [66]. *Orai1* forms the pore of the calcium release-activated calcium channel. It has strong expression during the secretory stage, which fades at the end of the maturation stage of amelogenesis [67]. GPR68 is also expressed in ameloblasts through all stages of amelogenesis, with strong expression at the ameloblast apical pole serving as a pH sensor and directing ameloblasts to switch between conformations - ruffle-ended and smooth-ended - at the maturation stage [68].
While no enormous reductions in gene expression were observed in *Rogdi*$^{-/-}$ mutant incisors, cumulative alterations could be synergistic. In humans, *ENAM* variants exhibit dosage-dependent phenotypes [69]. In the case of *AMBN* variants, only biallelic defects will cause amelogenesis imperfecta [70]. Mice lacking a single copy of two enamel-regulating genes, such as *Mmp20/Klk4,* demonstrating smaller reductions in two matrix proteases, can indeed synergize during dental enamel formation [55,57,71].

Collectively, these results indicate that most downregulated genes are expressed during the secretory stage of amelogenesis, controlling ameloblast differentiation and/or adhesion. In contrast, upregulated genes play a more significant role in vesicle/ion transport, cell adhesion, and/or pH sensing during enamel maturation.

Rogdi mutants can be used to understand many KTS-associated features

According to our data, the *Rogdi* mutant mouse model presents a susceptibility to epilepsy. Behavioral test results showed hyperactivity and memory impairment. Some *Rogdi*$^{-/-}$ female

mice also displayed decreased muscle strength. These data correlate with KTS patient phenotypes. The *Rogdi* mutant mouse exhibits severe enamel defects in both incisor and molar teeth. *Rogdi* mutants form less mineralized enamel, producing an "amelogenesis imperfecta"-like phenotype, perfectly mimicking severe KTS patient defects.

In addition to the typical KTS features, *Rogdi* mutants also present problems associated with the digestive system, which is potentially linked to pH regulation. ROGDI is expressed in the digestive organs [72]. Investigating whether digestive disorders are present is indeed relevant for overall patient quality of life. This model could help to decipher new symptoms and improve patient treatment.

Concerning the antiepileptic treatments used in patients, described that therapy with perampanel gives good results [9]. Perampanel (PER) is a first-in-class orally active, selective, noncompetitive alpha-amino-3-hydroxy-5-methyl-4-isoxazolepropionic acid (AMPA) receptor agonist [73]. AMPA receptors are hypothesized to be involved in the synchronization of excitatory glutamatergic transmission, which leads to the production of seizures. Perampanel had a small but discernible impact on NMDA receptors when tested *in vitro*. PER was found to be more effective at preventing seizures in mouse models of tonic-clonic generalized seizures and absence seizures than carbamazepine and sodium valproate [74]. Other treatments have been used in KTS patients without much success [2,10,75]. As *Rogdi*$^{-/-}$ has epilepsy susceptibility, it could serve as a model to test new antiepileptic drugs for KTS patients and their mechanism of action.

RODGI bridges with the V-ATPase pathway, a link between enamel formation and other functions

Loss of *ROGDI* might produce enamel and brain defects by perturbing the vacuolar type (V)-ATPase-dependent lysosomal acidification pathway [76]. V-ATPases (H^+- ATPases) are multisubunit, ATP-dependent proton pumps made up of an integral membrane V0 subcomplex that creates the transmembrane proton pore and a peripheral V1 subcomplex that contains the sites of ATP hydrolysis. They control pH homeostasis, participate in vesicle transport and membrane fusion, and play crucial roles in synaptic transmission [36]. Defects in V-ATPase action impair the ATP-driven proton pump, disrupting lysosomal acidification. This contributes to lysosomal storage disorders, a family of disorders marked by severe neurodegeneration, epilepsy, alterations found in Alzheimer's disease and Parkinson's disease [77], and to other neurodevelopmental/neurodegenerative diseases [78]. V-ATPase function is indispensable for viable adults [79]. V-ATPase function is essentially required to maintain lysosomal pH gradients, a process also required in tooth formation. To generate highly mineralized enamel, ameloblasts must have an acidic pH, generating a ruffled border [80]. Missense mutation of the V-ATPase component *ATP6V1A* produces enamel dysplasia in patients, along with epilepsy and brain atrophy [81]. V-ATPase a3 subunit disruption in mice

produces hypoplastic, hypomineralized enamel due to disruptions in the secretory stage of amelogenesis [82].

We hypothesized that the unique combination of neurological and enamel phenotypes characterizing KTS patients could result from defective V-ATPase-driven acidification. The V1 subcomplex can be released from the V0 subcomplex in response to signals such as glucose deprivation, inhibiting ATPase activity and proton transport. The disassembly of V-ATPase is a mechanism that regulates ATPase activity. Assembly of V1 with V0 (required for ATP-driven proton transport) requires assistance of the yeast RAVE (Regulator of H^+-ATPase of Vacuolar and Endosomal membranes) or its functional equivalent in higher eukaryotes - the Rabconnectin-3 complexes [38]. The aldolase enzyme also participates in V-ATPase assembly. Aldolase mutant cells have a phenotype comparable to the Rav1 – a RAVE component-mutant. It has been reported that the RAVE complex and aldolase may work together to control V-ATPase assembly [83].

The crystal structure of one of the RAVE complex components, Rav2, is strikingly similar in its domains to the human ROGDI protein [38]. The interactome of human ROGDI was explored in OpenCell [40]. Several endogenously tagged proteins from the V1 subunit of the V-ATPase complex were able to identify ROGDI as an interaction partner. It was also found that ROGDI shares an interactomic community with DMXL1, DMXL2, and WDR7, components of the V-ATPase chaperone Rabconnectin-3 complex. Despite their high interactomic similarity, no direct interactions could be detected between them, possibly because all these proteins displayed very low cellular abundance, making their endogenous complexes challenging to capture. However, by overexpressing DMXL1 or WDR7, it was possible to detect their interaction with ROGDI. A similar conclusion was observed in the BioPlex interactome project (Supplementary Figure S7A), where overexpressed ROGDI was found to interact with other components of the Rabconnectin-3 complex (DMXL1, DMXL2, and WDR7), among others [84]. In addition, all Rabconnectin-3 complex components (Rogdi, Dmxl1, Dmxl2 and Wdr7) were identified as interaction partners of the V-ATPase B1 subunit based on immunoprecipitation in mouse kidney lysates [36].

Our results solidify the ROGDI-V-ATPase connection. *Rogdi*$^{-/-}$ mutants exhibit severe reductions in enamel acidification (see Figure 5D), likely accounting for morphological deterioration in enamel structure. RNA-seq data from *Rogdi* mutant incisors shows increased *Slc9a3r2*, *Atp6v0c* and *Wdr72* (a WDR7 homologue) levels -known to interact with the acidifying V-ATPase complex and with DMXL1 and DMXL2 -proteins interacting with Rabconnectin-3 complex (also required for acidification). These changes likely affect pH regulation, disrupting acidification [63]. Given the similarity to WDR7 and links to pH control, it is important to investigate the possibility that WDR72 may participate in Rabconnectin-3 complexes, at least in some specific locations such as teeth. *Rogdi*$^{-/-}$ mutants can indeed be used to explore whether a reduction in lysosomal acidification in brain sites such as the hippocampus explains defects in learning in *Rogdi*$^{-/-}$ mutants in future studies. Along with lysosomal defects, reduced glutamate uptake due to pH imbalance can also lead to

neurodegenerative diseases [85]. Indeed, V-ATPase pumps regulate pH in the hippocampus and have been implicated in Alzheimer's and Parkinson's disease [86]. Here, V-ATPase and *DMXL2* reductions can also produce epilepsy [37,87,88]. V-ATPases have a role in the filling and exocytosis of glutamate, helping in the acidification of the vesicle and facilitating membrane binding of the vesicle followed by glutamate exocytosis by detachment of the V1 and V1C1 domains from the V0 domain [85].

In the stomach, V-ATPase may serve as an additional pathway for acid secretion or as an internal proton-buffering mechanism. It has been reported that mice lacking functional V-ATPase (ATP6v0a3) in the stomach have an elevated gastric pH [89,90], which may also help to explain the stomach phenotype found in *Rogdi*$^{-/-}$ mutants, where pH also appears to be higher in *Rogdi*$^{-/-}$ compared to WT (Figure 3C).

V-ATPase significantly increases during the maturation stage at the apical membrane of ameloblasts compared to the secretory stage [91]. Enamel grows in a pH-sensitive protein matrix that is related to enamel protein self-assembly and enamel crystal development [92]. We show an absence of acidification in mutant incisors (Figure 5D), suggesting that the absent pH reductions in *Rogdi* mutants blocked the ameloblast maturation stage by hindering the stepwise removal of EMPs such as amelogenins from the crystal surface of enamel [52]. Defects in ameloblast organelle acidification that limit the degradation of enamel proteins can indeed cause amelogenesis imperfecta [52,93].

V-ATPase alterations can also aggravate or produce cancer, neurodegenerative diseases, and diabetes and disrupt energy and nutrient-sensing functions within cells [94]. People with KTS present epilepsy, psychomotor regression, intellectual disability (ID), nephrocalcinosis, and enamel defects [9]. Distal renal tubular acidosis is also linked to mutations in V-ATPase subunit isoforms and could lead to nephrocalcinosis [38,95]. Neurons similarly use energy from proton-pumping V-ATPases to load neurotransmitters into synaptic vesicles. Synaptic signal propagation requires neurotransmitter release [96]; hence, V-ATPase or other acidification disruptions could produce a range of ID, epilepsy, or hyperactivity symptoms [78]. Considering ROGDI as a regulator of V-ATPase assembly, it could be interesting to study treatments targeting the reassembly of the proton pump to help in its function.

The *Rogdi* mutant will be a useful new model for analyzing treatment outcomes, according to all the findings provided here. Hence, these findings point to new perspectives on the function of ROGDI in cell biology and pathophysiology.

Material and Methods

Animals

The *Rogdi* cKO mutant mouse line was established at the Mouse Clinical Institute (Institut Clinique de la Souris, MCI/ICS) - PHENOMIN (http://www.phenomin.fr) in the Genetic Engineering and Model Validation Department.
The targeting vector was constructed as follows. A 2.8 kb fragment encompassing exons 6 (ENSMUSE00000128063) to 11 (ENSMUSE00000427909) comprising the whole interLoxP genomic sequence was amplified by PCR (from BAC RP24-424L20 genomic DNA) and subcloned in an MCI proprietary vector. This ICS vector includes a neomycin resistance cassette surrounded by FRT sites, as well as 2 loxP sites. Two PCR fragments corresponding to the 5' and 3' homology arms (1.8 and 1.7 kb, respectively) were subsequently cloned into the plasmid obtained in the first cloning step to obtain the final targeting construct. The linearized construct was electroporated into C57BL/6N mouse embryonic stem cells (ESCs; S3 in house developed line). After G418 selection, targeted clones were identified by PCR using external primers and further confirmed by Southern blotting with a Neo probe (5' and 3' digests) as well as a 3' external probe. Four positive ES clones were injected into BALB/cN blastocysts. The resulting male chimeras were bred with Flp deleter females that show maternal contribution [97]. Germline transmission of the cKO allele with direct excision of the flipped selection cassette was obtained. The resulting line was mated with ROSA26-deleter CRE mice to delete exon 6 to exon 11. Offspring mice were backcrossed on a C57BL/6N background.
Rogdi $^{-/-}$ mice were genotyped with oligonucleotides and PCR amplification as described in Supplementary Figure S1.

In situ hybridization

A full-length *Rogdi* probe (Dharmacon) was used to generate an antisense probe. *In situ* hybridization (ISH) was performed using digoxigenin-labeled RNA probes on 10 µm frozen sections. The samples were fixed in 4% paraformaldehyde for 10 min at 4°C, rinsed with PBS, dehydrated in graded ethanol (70%, 95%, 100%, and 95%) for 5 min each, and dried for 1 hour. The probe was diluted to 1 µg/ml in prewarmed hybridization buffer (65°C) and denatured for 10 min at 70°C. The slides with the probe and coverslip were placed in a humidified chamber at 65°C overnight. 5x SSC prewarmed (70°C) was used to allow coverslips to detach. The samples were washed for 1 h at 70°C in 0.2x SSC and transferred to 0.2x SSC room temperature (RT) for 15 min. Washing for 2 x 30 min at RT with slow agitation in 1x maleic acid buffer Tween (MABT) was followed by blocking in MABT with 2% blocking reagent and 20% heat-inactivated normal goat serum (NGS) for 1 h at RT, and a 1/2000 anti-digoxigenin antibody in blocking solution was added for 2 h at RT. Washing 5 x 20 min at RT

in MABT 1x, rinsing 2 x 10 min in alkaline phosphatase buffer (NTMT) 1x was performed. Hybridized probes were visualized with NTMT, BCIP and NBT in PBT.

Immunohistochemistry

Embryos (E12.5 to E18.5) and postnatal day (PN) 1, 3, 5, 7 and 14 heads were freshly fixed in 4% paraformaldehyde for 24 hours, demineralized with 10% EDTA (postnatal stages), cryoprotected with 20% sucrose, and embedded in Shandon Cryomatrix Frozen Embedding Medium (Thermo Scientific™). Frozen sagittal sections (10 µm) were cut using a Leica CM3050 S cryostat and placed on Superfrost Plus™ slides for immunohistochemistry. Antigen retrieval was performed according to the manufacturer's antibody protocol. The samples were blocked with 5% normal donkey serum (NDS) or normal goat serum (NGS) in 0,05% TBS Tween 20 (TBSTw). Sections were incubated with anti-Rogdi (Proteintech® 17047-1-AP) in blocking solution (1:100). After washing with TBSTw, samples were incubated with secondary Ab labeled with fluorophore in TBS (1:500) and DAPI (5 mg/ml) to a final dilution of 1:5000-10000. Sections were mounted with FluoroMount-G Mounting medium (FP-483331, Interchim). Images were acquired with an upright motorized microscope (Leica DM 4000 B) equipped with a Photometrics CoolSNAP HQ2 camera and analyzed in Leica Application Suite X software.

Data analysis of single-cell sequencing of the central nervous system

Single-cell transcriptomics of twenty-four cell populations in five regions of the central nervous system produced by [15] were analyzed for *Rogdi* expression. Reads were grouped into low (50 RPKM to 500 RPKM), moderate (500 RPMK to 2000 RPKM), or high expression (>2000 RPKM).

Data analysis of single-cell sequencing of the incisor epithelium

Rogdi expression in incisor epithelium was analyzed in https://kleintools.hms.harvard.edu/tools/springViewer_1_6_dev.html?datasets/Sharir_et_al_2019/control_epithelial. This tool identifies distinct cell types by single-cell transcriptomic analysis and delineates their spatial organization in the incisor epithelium. SPRING representation of the incisor epithelium dataset described in [16] presents 15 spectral clusters, grouped into 3 main classes: cycling cells, pre-ameloblasts and ameloblasts, and non-ameloblast epithelial cells.

Behavioral tests

WT (n=16 [first cohort= 6 males and 3 females/second cohort= 3 males and 4 females]) and *Rogdi*$^{-/-}$ (n=14 [first cohort= 3 males and 3 females/second cohort= 3 males and 5 females]) mice at 10 weeks of age at the beginning of the study were tested. Different tests to check activity, memory and locomotor activity were performed (circadian activity, elevated plus maze, novel object recognition, gross neurological examination, grip, rotarod). Data from 2 independent batches and from both sexes were pooled when no batch effect or sex effect was detected.

Gross neurological examination (SHIRPA)

General health and basic sensory motor functions were evaluated using a modified SHIRPA protocol. This analysis provided an overview of physical appearance, body weight, neurological reflexes, and sensory-motor abilities. Data were analyzed using unpaired Student's t-test.

Circadian activity

Spontaneous locomotor activity and rearing activity were measured using individual cages (20 x 10 x 8 cm) equipped with infrared captors (Imetronic, Pessac, France). Mice were tested for 32 hours to measure habituation to the apparatus as well as nocturnal and diurnal activities. The results were expressed per 1 h period and/or as a total of the different activities. Statistical analyses were performed using two-way ANOVA, Sidak's multiple comparisons and unpaired Student's t-test.

Novel Object Recognition

Mice were evaluated in a circular closed arena (30 cm diameter and 50 cm height basin). An EthoVision XT video tracking system (Noldus, Wageningen, Netherlands) was used to record locomotor activity. The arena was homogeneously illuminated at 20 Lux. Animals spent 10 minutes habituating to the arena. Each mouse was placed in the periphery of the arena and given full reign to freely explore the apparatus. The distance travelled was recorded over the test session. The following day, mice were tested for object recognition in the same arena. They underwent a 10-minute acquisition trial during which they were positioned in the arena in the presence of two test objects (A and A'). The time the animal spent exploring the samples (sniffing) was manually recorded. One hour later, a 10-minute retention trial was conducted. The animal was placed in the arena with one of the samples A and an additional object B, and the times tA and tB it took to investigate each item were noted. A recognition index (RI) was determined as (tB / (tA + tB)) x100. Animals were isolated during the retention interval. Data were analyzed using unpaired Student's t-test for retention of object exploration and retention index. The Mann-Whitney test was used for the distance travelled during habituation, acquisition and retention sessions and for acquisition object exploration.

Grip test

This test measures the maximal muscle strength using an isometric dynamometer connected to a grid. Once the animal is holding the grid with its four paws, it is slowly moved backwards until it releases it. Mice were given three testing trials separated by approximately 10 sec intervals. The strength developed by the animal was measured in grams and adjusted to the body weight of the animal. Data were analyzed using unpaired Student's t-test.

Rotarod test

This test evaluates an animal's ability to stay balanced on a rotating rod (Bioseb, Chaville, France). Mice were given three testing trials during which the rotation speed accelerated from 4 to 40 rotations per minute in 5 minutes. Trials were separated by 15 min intervals. Endurance and motor coordination performance were measured using the average latency. Data were analyzed using unpaired Student's t-test.

Elevated plus maze

The apparatus used is automated and made of PVC (Imetronic, Pessac, France). It consists of two open arms (30 X 5 cm) opposite one to the other and crossed by two enclosed arms (30 x 5 x 15 cm). The apparatus is equipped with infrared captors allowing the detection of the mouse in the enclosed arms and different areas of the open arms. Mice were tested for 5 min, during which the number of entries into and time spent in the open arms were measured and used as an index of anxiety. Closed arm entries and total arm entries were used as measures of general motor activity. Data were analyzed using unpaired Student's t-test.

Muscle analysis

The tibialis anterior, gastrocnemius and quadriceps muscles were dissected from 8-week-old WT (n=3) and *Rogdi*$^{-/-}$ (n=3) mice and used for light microscopy and scanning electron microscopy (SEM). Muscle weight was measured and normalized to body weight. For light microscopy, 10 µm cross-sections of snap-frozen muscle were stained with hematoxylin and eosin and Gomori trichrome. Stained sections were digitalized with a NanoZoomer 2.0-HT (Hamamatsu Photonics). Histological analysis was performed using NDP.view2 software. For SEM, ultrathin serial sections were picked up on grids and contrasted with uranyl acetate and lead citrate. The grids were examined for morphology analysis with a Morgagni 268D electron microscope (FEI Electron Optics, Eindhoven, the Netherlands) equipped with a Mega View III camera (Soft Imaging System). Muscle fiber size analysis was performed in the tibialis anterior, including an average of 1986 (range 1380-3499) muscle fibers per individual. Data from 6 mice with a total of 11914 fibers were acquired and analyzed. Fiji and Cellpose 2.0 software were employed for the study. The fibers' smallest diameter i.e. The minimum diameter of Feret (MinFeret) was determined (fibers located at the periphery of the sections not fully captured in the photographs were excluded from the analysis). Normally distributed continuous data for muscle ratio/body weight and small fiber percentages were summarized

as the means ± standard deviation. Prism 9 (GraphPad Software, San Diego, CA) was used for data analysis using unpaired Student's t-test and Welch's correction when unequal standard deviations were found.

Pentylenetetrazol induced seizure (PTZ)

WT (n=8) and *Rogdi*$^{-/-}$ (n=7) males, aged between 10 ± 1 weeks, were used to test epilepsy susceptibility. Pentylenetetrazol is a noncompetitive GABA-A receptor antagonist that induces seizures and is used to determine the seizure threshold. The animal was intraperitoneally injected with 40 mg/kg pentylenetetrazol and placed in a translucent cage. The different stages of the seizure that the animal exhibited were observed during the 20 minutes after injection.

Cerebellum and hippocampal formation analysis

Postnatal day (PN) 15 brains (n=6 for *Rogdi*$^{-/-}$ and n=6 for WT) were rapidly removed after decapitation and snap-frozen in cooled (-35°C to -45°C) 2-methylbutane. Brain samples were stored at -80°C. Frozen coronal sections (20 µm) were fixed with 4% formaldehyde solution for 24 hours and stained with 0.5% cresyl violet (Sigma-Aldrich, France) solution following the protocol proposed by Bolam (1992) [98]. Slides were mounted with mounting medium (Eukitt®). Cerebellum and hippocampus images were digitalized with NanoZoomer 2.0-HT (Hamamatsu Photonics). Structures of interest were identified using the Franklin and Paxinos mouse brain stereotaxic atlas (third edition, Elsevier 2007) [99]. The thicknesses of the internal and external granular layers (IGL and EGL, respectively) and the molecular layer (Mol) were measured using NDP.view2 (Hamamatsu) software. Planimetry of the cerebellar cortex on the sections was verified by observing that Purkinje cells formed a continuous line parallel to the lobule fissure [100,101]. In a central segment of each lobule, six measurements per section from two sections per mouse were performed. The Purkinje cell layer made up of perikaryal was included in the molecular layer. All selected lobules were measured posterior to the bregma point, at a level of 6.12 mm for simplex and vermis IV-V, at a level of 6.64 to 6.84 mm for paramedian and at a level of 6.36 to 6.72 for crus I and crus II. The CA1 and dentate gyrus granular and molecular layers of the hippocampal formation were measured in a similar manner at 1.7 to 1.82 mm posterior to the bregma point. Statistical analysis was performed using Student's t-test.

Blood analysis

Blood was collected at the temporal vein on unfasted conscious WT (n=9, 6 males and 3 females) and *Rogdi*$^{-/-}$ (n=5, 3 males and 2 females) mice at the age of 14 weeks. Blood chemistry was performed on an OLYMPUS AU-480 automated laboratory workstation (Beckmann Coulter, US) with kits and controls supplied by Beckmann Coulter. Internal quality

control materials (Olympus) were analyzed daily to monitor precision throughout the experiment. Blood chemistry parameters were measured on the plasma samples: calcium, phosphorus, and alkaline phosphatase (ALP). A complete blood cell count was performed on total blood using the Veterinary hematology analyzer Element HT5 (Scil Animal Care, France). Statistical analysis was performed using Student's t-test.

Microtomography (µ-CT) imaging

The heads of 20 8-week-old adult (10 females and 10 males) *Rogdi-/-* mutant and wild-type (WT) mice were analyzed. All samples were scanned using the Quantum FX micro-CT imaging system (Caliper Life Sciences, Hopkinton, MA, USA), which operates at 80 kV and 160 µA, with high resolution (pixel size of 10-80 µm), to evaluate the morphology and density of the skull and tooth. A 3-D model was created using the software Slicer 4.10.2. Dento-cranio-facial bone anatomy was sorted into coronal, transverse, and sagittal planes at the levels of the skull, mandible, and teeth. The images were analyzed using FIJI (ImageJ2), winEDMA, MorphoJ 1.07.a and Stratovan Checkpoint (Stratovan Corporation. Version 2018.08.07).

Scanning electron microscopy (SEM)

Mandibles of 8-week-old control and *Rogdi*$^{-/-}$ mice were dissected and stored in 70% ethanol at 4°C. Samples were embedded in Epon 812 (Euromedex, Souffelweyeresheim, France) and then sectioned along the sagittal plane using a diamond saw mounted on a microtome (Walter EBNER, Le Locle, Switzerland). The sample surface was polished with 1200, 2400, and 4000 SiC abrasive papers under continuous water irrigation [102]. Then, the polished sections were etched using 20% citric acid for 2 min, rinsed for 10 s with distilled water, and dehydrated in a graded series of ethanol solutions. Mounting was performed on aluminum SEM stubs and sputter-coated with a gold–palladium alloy (20/80 weight %) employing a Hummer JR sputtering device (Technics, CA, USA). The morphological and chemical characteristics were determined using a Quanta 250 FEG scanning electron microscope (FEI Com- 190 pany, Eindhoven, The Netherlands) at 7.5 kV acceleration voltage of electrons. EDX analysis was performed with a working distance of 10 mm and an acquisition period of 30 s [103]. The weight percentages of chemical elements of the surfaces of the different dental tissues were attained.

Histology

Heads of postnatal (PN) -1, 3, 5, 7 and 14 - days WT (n=3 per stage) and *Rogdi*$^{-/-}$ (n=3 per stage) mice were fixed in 4% formaldehyde for 24 hours, washed in PBS, and demineralized in 10% ethylenediaminetetraacetic acid (EDTA pH 7.3) at room temperature until hard tissues were soft enough to cut (the demineralizing solution was changed every 3 days). After washing in

water two times for 30 minutes on a rocking platform, the heads were dehydrated in graded ethanol (70%, 95%, and 100%), cleared in Histosol®, and embedded in paraffin at 60°C under vacuum (Leica TP1050 Vacuum Tissue Processor). The heads were oriented to produce sagittal cuts and embedded in paraffin. Ten micrometer sections were stained with hematoxylin and eosin (H&E) according to standard procedures.

Methyl red staining

Twelve-week-old hemimandibles from *Rogdi*$^{-/-}$ and WT mice were dissected. Bone and enamel organs covering the lower incisors were removed, and cellular debris was cleaned from the enamel surfaces. Fresh filtered methyl red solution (Methyl red-C.I. 13020- 50 mg, 0.1 M sodium hydroxide 1.86 mL, 95% ethanol 50 mL, distilled H_2O q.s. 100 mL) was prepared before dissection. Incisors were dipped into the pH indicator methyl red for at least 10 min. Incisors were placed on filter paper, and pictures were taken immediately after incubation using a Leica M80 stereo microscope equipped with a Motic Moticam 580 camera.

RNA sequencing

Total RNA was extracted from 6 males per genotype, control and *Rogdi*$^{-/-}$ at PN5, and final analyses were performed with 4 control and 5 *Rogdi*$^{-/-}$ samples according to the principal component analysis. Both lower incisors were pulled for RNA extraction using an RNeasy Plus Micro Kit (Qiagen). Gene expression quantification was performed from uniquely aligned reads using htseq-count [104] version 0.6.1p1, with annotations from Ensembl version 93 genome browser and "union" mode explained in http://htseq.readthedocs.io/en/master/. Only nonambiguously assigned reads were retained for further analyses. Comparisons of interest (WT *vs* *Rogdi*$^{-/-}$) were performed using the test for differential expression proposed by Love et al. (2014) [105] and implemented in the Bioconductor package DESeq2 version 1.16.1. Genes with high Cook's distance were filtered out. Independent filtering based on the mean of normalized counts was performed to filter out those genes that had no or little chance of showing significant evidence of differential expression (without looking at their statistic). P-values were adjusted using the Benjamini and Hochberg (1995) [106] method for multiple testing. Significant genes were selected using an adjusted p-value <0.05 and an absolute value of log2 fold-change >0.3. Data were analyzed using Cytoscape 3.9.1 [107] and DAVID [108].

Quantitative real-time PCR (RT-qPCR)

First-strand cDNA synthesis from WT and *Rogdi*$^{-/-}$ male lower incisor mRNA was performed with SuperScript® IV Reverse Transcriptase (Invitrogen). LightCycler® 480 SYBR Green I Master (Roche Life Science) incorporation into amplified PCR products was detected using a RealPlex 2 qPCR Real Time PCR ThermoCycler. Primer sequences (listed in Supplementary Table S4)

were designed using the Primer3web program. Expression was normalized to glyceraldehyde-3-phosphate dehydrogenase (*Gapdh*) levels. Six mice of each genotype were used to check *Rogdi* exon expression. Tests were performed in triplicate to confirm variations. Statistical analysis was performed by Student's t test.

Rogdi protein interactions network

Three databases were consulted to look for Rogdi protein interactions:
BioPlex Interactome is a catalog of human protein-protein interactions that BioPlex v3 contains interactomes of 10,128 human proteins from 293T cells and the interactomes of 5,522 proteins from HCT116 cells [39,84].
OpenCell is a proteome-scale collection of protein localization and interaction measurements in human cells. It contains the interactomes of 1310 endogenous proteins [40].
A repository for biomedical interactions known as BioGRID (version 4.4.218) [109] contains data that have been gathered through intensive curation efforts. From 81,725 publications from important model organism species, the data set contains interactions, chemical associations, and post-translational modifications (PTMs). All information was freely accessible for download.
All information was freely accessible for download.

Ethics statement

All animals were maintained and manipulated under animal protocols in accordance with the French Ministry of Agriculture guidelines for the use of laboratory animals (C67-218-37-IGBMC « Mécanismes responsables de malformations osseuses et bucco dentaires: analyse de modèles murins » n° APAFIS#3957-2016020516359388v1) and with NIH guidelines provided in the Guide for the Care and Use of Laboratory Animals. All methods and experimental procedures were reviewed and approved by the IGBMC institutional safety committee. This study is reported in accordance with ARRIVE guidelines.
The mice were fed *ad libitum* with humidified pellets placed at the bottom of the cage. *The Rogdi* gene targeting strategy, as well as the characterization of mice with a disrupted *Rogdi* gene, are illustrated in Figure 3 and Supplementary Figure S1.

Data availability

The analyzed RNA sequencing data that support the findings of this study is available in Gene Expression Omnibus with the accession number GSE239863 https://www.ncbi.nlm.nih.gov/geo/query/acc.cgi?acc=GSE239863.

References

1. Mory, A. *et al.* A Nonsense Mutation in the Human Homolog of Drosophila rogdi Causes Kohlschutter–Tonz Syndrome. *The American Journal of Human Genetics* **90**, 708–714 (2012).
2. Huckert, M. *et al.* A Novel Mutation in the *ROGDI* Gene in a Patient with Kohlschütter-Tönz Syndrome. *Mol Syndromol* **5**, 293–298 (2014).
3. Lee, H. *et al.* The crystal structure of human Rogdi provides insight into the causes of Kohlschutter-Tönz Syndrome. *Sci Rep* **7**, 3972 (2017).
4. Aswath, N., Ramakrishnan, S. N., Teresa, N. & Ramanathan, A. A novel ROGDI gene mutation is associated with Kohlschutter-Tonz syndrome. *Oral Surgery, Oral Medicine, Oral Pathology and Oral Radiology* **125**, e8–e11 (2018).
5. Kohlschütter, A. *et al.* Familial epilepsy and yellow teeth--a disease of the CNS associated with enamel hypoplasia. *Helv Paediatr Acta* **29**, 283–294 (1974).
6. Schossig, A. *et al.* Mutations in ROGDI Cause Kohlschütter-Tönz Syndrome. *The American Journal of Human Genetics* **90**, 701–707 (2012).
7. Tucci, A. *et al.* Kohlschütter-Tönz Syndrome: Mutations in *ROGDI* and Evidence of Genetic Heterogeneity. *Human Mutation* **34**, 296–300 (2013).
8. Kim, M. *et al.* Rogdi Defines GABAergic Control of a Wake-promoting Dopaminergic Pathway to Sustain Sleep in Drosophila. *Sci Rep* **7**, 11368 (2017).
9. Liepina, L. *et al.* Kohlschütter–Tönz syndrome: Case report with novel feature and detailed review of features associated with ROGDI variants. *American Journal of Medical Genetics Part A* **188**, 1263–1279 (2022).
10. Akgün-Doğan, Ö. *et al.* Kohlschütter-Tönz Syndrome With a Novel ROGD1 Variant in 3 Individuals: A Rare Clinical Entity. *J Child Neurol* **36**, 816–822 (2021).

11. Schossig, A. *et al.* SLC13A5 is the second gene associated with Kohlschütter–Tönz syndrome. *Journal of Medical Genetics* **54**, 54–62 (2017).

12. Bloch-Zupan, A. *et al.* Amelogenesis imperfecta: Next Generation Sequencing sheds light on Witkop's classification. *Frontiers in Physiology* **14**, (2023).

13. Riemann, D., Wallrafen, R. & Dresbach, T. The Kohlschütter-Tönz syndrome associated gene Rogdi encodes a novel presynaptic protein. *Sci Rep* **7**, 15791 (2017).

14. Witkop, C. J. Amelogenesis imperfecta, dentinogenesis imperfecta and dentin dysplasia revisited: problems in classification. *J Oral Pathol* **17**, 547–553 (1988).

15. Doyle, J. P. *et al.* Application of a Translational Profiling Approach for the Comparative Analysis of CNS Cell Types. *Cell* **135**, 749–762 (2008).

16. Sharir, A. *et al.* A large pool of actively cycling progenitors orchestrates self-renewal and injury repair of an ectodermal appendage. *Nat Cell Biol* **21**, 1102–1112 (2019).

17. McCarl, C.-A. *et al.* ORAI1 deficiency and lack of store-operated Ca2+ entry cause immunodeficiency, myopathy and ectodermal dysplasia. *J Allergy Clin Immunol* **124**, 1311-1318.e7 (2009).

18. Picard, C. *et al.* STIM1 mutation associated with a syndrome of immunodeficiency and autoimmunity. *N Engl J Med* **360**, 1971–1980 (2009).

19. Parry, D. A. *et al.* A homozygous STIM1 mutation impairs store-operated calcium entry and natural killer cell effector function without clinical immunodeficiency. *J Allergy Clin Immunol* **137**, 955-957.e8 (2016).

20. Scudamore, C. L., Busk, N. & Vowell, K. A simplified necropsy technique for mice: making the most of unscheduled deaths. *Lab Anim* **48**, 342–344 (2014).

21. Haberlandt, E. *et al.* Yellow teeth, seizures, and mental retardation: A less severe case of Kohlschütter–Tönz syndrome. *American Journal of Medical Genetics Part A* **140A**, 281–283 (2006).

22. Pindborg, J. J. The pigmentation of the rat incisor as an index of metabolic disturbances. *Oral Surg Oral Med Oral Pathol* **6**, 780–789 (1953).

23. Hu, J. C.-C. *et al.* Enamelin Is Critical for Ameloblast Integrity and Enamel Ultrastructure Formation. *PLoS One* **9**, e89303 (2014).

24. Masuya, H. *et al.* Enamelin (Enam) is essential for amelogenesis: ENU-induced mouse mutants as models for different clinical subtypes of human amelogenesis imperfecta (AI). *Human Molecular Genetics* **14**, 575–583 (2005).

25. Beniash, E. *et al.* The hidden structure of human enamel. *Nat Commun* **10**, 4383 (2019).

26. Katsura, K. A. *et al.* WDR72 models of structure and function: A stage-specific regulator of enamel mineralization. *Matrix Biology* **38**, 48–58 (2014).

27. Wang, S.-K. *et al.* Critical roles for WDR72 in calcium transport and matrix protein removal during enamel maturation. *Mol Genet Genomic Med* **3**, 302–319 (2015).

28. Arnold, W. H. & Gaengler, P. Quantitative analysis of the calcium and phosphorus content of developing and permanent human teeth. *Annals of Anatomy - Anatomischer Anzeiger* **189**, 183–190 (2007).

29. Denbesten, P. K., Crenshaw, M. A. & Wilson, M. H. Changes in the Fluoride-induced Modulation of Maturation Stage Ameloblasts of Rats. *J Dent Res* **64**, 1365–1370 (1985).

30. Smith, C. E., Nanci, A. & Denbesten, P. K. Effects of chronic fluoride exposure on morphometric parameters defining the stages of amelogenesis and ameloblast modulation in rat incisors. *The Anatomical Record* **237**, 243–258 (1993).

31. Fukumoto, S. *et al.* Ameloblastin is a cell adhesion molecule required for maintaining the differentiation state of ameloblasts. *Journal of Cell Biology* **167**, 973–983 (2004).

32. Wright, J. T. *et al.* The role of amelogenin during enamel-crystallite growth and organization in vivo. *European Journal of Oral Sciences* **119**, 65–69 (2011).

33. Lacruz, R. S., Habelitz, S., Wright, J. T. & Paine, M. L. Dental Enamel Formation and Implications for Oral Health and Disease. *Physiological Reviews* **97**, 939–993 (2017).

34. Lu, T. *et al.* Whole exome sequencing identifies an AMBN missense mutation causing severe autosomal-dominant amelogenesis imperfecta and dentin disorders. *Int J Oral Sci* **10**, 26 (2018).

35. Smith, C. E. L. *et al.* Amelogenesis Imperfecta; Genes, Proteins, and Pathways. *Frontiers in Physiology* **8**, (2017).

36. Merkulova, M. *et al.* Mapping the H+ (V)-ATPase interactome: identification of proteins involved in trafficking, folding, assembly and phosphorylation. *Sci Rep* **5**, 14827 (2015).

37. Mattison, K. A. *et al.* ATP6V0C variants impair V-ATPase function causing a neurodevelopmental disorder often associated with epilepsy. *Brain* awac330 (2022) doi:10.1093/brain/awac330.

38. Jaskolka, M. C., Winkley, S. R. & Kane, P. M. RAVE and Rabconnectin-3 Complexes as Signal Dependent Regulators of Organelle Acidification. *Front. Cell Dev. Biol.* **9**, 698190 (2021).

39. Schweppe, D. K., Huttlin, E. L., Harper, J. W. & Gygi, S. P. BioPlex Display: An Interactive Suite for Large-Scale AP–MS Protein–Protein Interaction Data. *J. Proteome Res.* **17**, 722–726 (2018).

40. Cho, N. H. *et al.* OpenCell: Endogenous tagging for the cartography of human cellular organization. *Science* **375**, eabi6983 (2022).

41. Camargo, L. M. *et al.* Disrupted in Schizophrenia 1 Interactome: evidence for the close connectivity of risk genes and a potential synaptic basis for schizophrenia. *Mol Psychiatry* **12**, 74–86 (2007).

42. Einarsdottir, E. *et al.* Mutation in CEP63 co-segregating with developmental dyslexia in a Swedish family. *Hum Genet* **134**, 1239–1248 (2015).

43. Marjanović, M. *et al.* CEP63 deficiency promotes p53-dependent microcephaly and reveals a role for the centrosome in meiotic recombination. *Nat Commun* **6**, 7676 (2015).

44. Pervaiz, N., Kang, H., Bao, Y. & Abbasi, A. A. Molecular evolutionary analysis of human primary microcephaly genes. *BMC Ecol Evol* **21**, 76 (2021).

45. Hashimoto, R. *et al.* Whole-exome sequencing and neurite outgrowth analysis in autism spectrum disorder. *J Hum Genet* **61**, 199–206 (2016).

46. Lim, Y.-M. *et al.* Exome sequencing identifies KIAA1377 and C5orf42 as susceptibility genes for monomelic amyotrophy. *Neuromuscular Disorders* **22**, 394–400 (2012).

47. Anderson, J. M. & Van Itallie, C. M. Physiology and function of the tight junction. *Cold Spring Harb Perspect Biol* **1**, a002584 (2009).

48. Koziol, L. F. *et al.* Consensus Paper: The Cerebellum's Role in Movement and Cognition. *Cerebellum* **13**, 151–177 (2014).

49. Ceccarelli, M. *et al.* Altered cerebellum development and impaired motor coordination in mice lacking the Btg1 gene: Involvement of cyclin D1. *Developmental Biology* **408**, 109–125 (2015).

50. Stoodley, C. J. & Schmahmann, J. D. Evidence for topographic organization in the cerebellum of motor control versus cognitive and affective processing. *Cortex* **46**, 831–844 (2010).

51. Scimeca, M., Bischetti, S., Lamsira, H. K., Bonfiglio, R. & Bonanno, E. Energy Dispersive X-ray (EDX) microanalysis: A powerful tool in biomedical research and diagnosis. *Eur J Histochem* **62**, 2841 (2018).

52. Bronckers, A. L. J. J. Ion Transport by Ameloblasts during Amelogenesis. *J Dent Res* **96**, 243–253 (2017).

53. Crawford, P. J., Aldred, M. & Bloch-Zupan, A. Amelogenesis imperfecta. *Orphanet J Rare Dis* **2**, 17 (2007).

54. Katsura, K. A. *et al.* WDR72 models of structure and function: A stage-specific regulator of enamel mineralization. *Matrix Biol* **0**, 48–58 (2014).

55. Hu, Y. *et al.* MMP20, KLK4, and MMP20/KLK4 double null mice define roles for matrix proteases during dental enamel formation. *Mol Genet Genomic Med* **4**, 178–196 (2015).

56. Kawasaki, K., Suzuki, T. & Weiss, K. M. Genetic basis for the evolution of vertebrate mineralized tissue. *Proc Natl Acad Sci U S A* **101**, 11356–11361 (2004).

57. Zhang, H. *et al.* ENAM mutations and digenic inheritance. *Mol Genet Genomic Med* **7**, e00928 (2019).

58. Yoshiba, N. *et al.* Expression and localization of laminin-5 subunits in the mouse incisor. *Cell Tissue Res* **292**, 143–149 (1998).

59. Nievers, M. G., Schaapveld, R. Q. J. & Sonnenberg, A. Biology and function of hemidesmosomes. *Matrix Biology* **18**, 5–17 (1999).

60. Asaka, T. *et al.* Type XVII Collagen is a Key Player in Tooth Enamel Formation. *The American Journal of Pathology* **174**, 91–100 (2009).

61. Abbarin, N., San Miguel, S., Holcroft, J., Iwasaki, K. & Ganss, B. The Enamel Protein Amelotin Is a Promoter of Hydroxyapatite Mineralization. *Journal of Bone and Mineral Research* **30**, 775–785 (2015).

62. Lacruz, R. S. *et al.* Targeted Overexpression of Amelotin Disrupts the Microstructure of Dental Enamel. *PLOS ONE* **7**, e35200 (2012).

63. El-Sayed, W. *et al.* Mutations in the Beta Propeller WDR72 Cause Autosomal-Recessive Hypomaturation Amelogenesis Imperfecta. *Am J Hum Genet* **85**, 699–705 (2009).

64. Hu, P. *et al.* Expression of the Sodium/Calcium/Potassium Exchanger, NCKX4, in Ameloblasts. *CTO* **196**, 501–509 (2012).

65. Wang, S. *et al.* STIM1 and SLC24A4 Are Critical for Enamel Maturation. *J Dent Res* **93**, 94S-100S (2014).

66. Yamazaki, D. *et al.* Basolateral Mg2+ Extrusion via CNNM4 Mediates Transcellular Mg2+ Transport across Epithelia: A Mouse Model. *PLoS Genetics* **9**, (2013).

67. Zheng, L. *et al.* Orai1 expression pattern in tooth and craniofacial ectodermal tissues and potential functions during ameloblast differentiation. *Developmental Dynamics* **244**, 1249–1258 (2015).

68. Parry, D. A. *et al.* Mutations in the pH-Sensing G-protein-Coupled Receptor GPR68 Cause Amelogenesis Imperfecta. *The American Journal of Human Genetics* **99**, 984–990 (2016).

69. Seymen, F. *et al.* ENAM Mutations with Incomplete Penetrance. *J Dent Res* **93**, 988–992 (2014).

70. Liang, T. *et al.* AMBN mutations causing hypoplastic amelogenesis imperfecta and Ambn knockout-NLS-lacZ knockin mice exhibiting failed amelogenesis and Ambn tissue-specificity. *Mol Genet Genomic Med* **7**, e929 (2019).

71. Xie, X. *et al.* Abrogation of epithelial BMP2 and BMP4 causes Amelogenesis Imperfecta by reducing MMP20 and KLK4 expression. *Sci Rep* **6**, 25364 (2016).

72. Uhlén, M. *et al.* Tissue-based map of the human proteome. *Science* **347**, 1260419 (2015).

73. Hanada, T. *et al.* Perampanel: A novel, orally active, noncompetitive AMPA-receptor antagonist that reduces seizure activity in rodent models of epilepsy. *Epilepsia* **52**, 1331–1340 (2011).

74. Krauss, G. L. *et al.* Randomized phase III study 306: Adjunctive perampanel for refractory partial-onset seizures. *Neurology* **78**, 1408–1415 (2012).

75. Mory, A. *et al.* Kohlschutter-Tonz Syndrome: Clinical and Genetic Insights Gained From 16 Cases Deriving From a Close-Knit Village in Northern Israel. *Pediatric Neurology* **50**, 421–426 (2014).

76. Colacurcio, D. J. & Nixon, R. A. Disorders of lysosomal acidification - the emerging role of v-ATPase in aging and neurodegenerative disease. *Ageing Res Rev* **32**, 75–88 (2016).

77. Song, Q., Meng, B., Xu, H. & Mao, Z. The emerging roles of vacuolar-type ATPase-dependent Lysosomal acidification in neurodegenerative diseases. *Transl Neurodegener* **9**, 17 (2020).

78. Dubos, A. *et al.* Conditional depletion of intellectual disability and Parkinsonism candidate gene ATP6AP2 in fly and mouse induces cognitive impairment and neurodegeneration. *Hum Mol Genet* **24**, 6736–6755 (2015).

79. Wendling, O. *et al.* Atp6ap2 ablation in adult mice impairs viability through multiple organ deficiencies. *Sci Rep* **7**, 9618 (2017).

80. Lacruz, R. S. *et al.* Adaptor Protein Complex 2 (AP-2) Mediated, Clathrin Dependent Endocytosis, And Related Gene Activities, Are A Prominent Feature During Maturation Stage Amelogenesis. *J Bone Miner Res* **28**, 672–687 (2013).

81. Guerrini, R. *et al.* Phenotypic and genetic spectrum of ATP6V1A encephalopathy: a disorder of lysosomal homeostasis. *Brain* **145**, 2687–2703 (2022).

82. Johnson, L. *et al.* V-ATPases Containing a3 Subunit Play a Direct Role in Enamel Development in Mice. *J Cell Biochem* **118**, 3328–3340 (2017).

83. Lu, M., Sautin, Y. Y., Holliday, L. S. & Gluck, S. L. The glycolytic enzyme aldolase mediates assembly, expression, and activity of vacuolar H+-ATPase. *J Biol Chem* **279**, 8732–8739 (2004).

84. Huttlin, E. L. *et al.* Dual Proteome-scale Networks Reveal Cell-specific Remodeling of the Human Interactome. *Cell* **184**, 3022-3040.e28 (2021).

85. Satarker, S. *et al.* Astrocytic Glutamatergic Transmission and Its Implications in Neurodegenerative Disorders. *Cells* **11**, (2022).

86. Pappas, C. A. & Ransom, B. R. A depolarization-stimulated, bafilomycin-inhibitable H+ pump in hippocampal astrocytes. *Glia* **9**, 280–291 (1993).

87. Fassio, A. *et al.* De novo mutations of the ATP6V1A gene cause developmental encephalopathy with epilepsy. *Brain* **141**, 1703–1718 (2018).

88. Esposito, A. *et al.* Biallelic DMXL2 mutations impair autophagy and cause Ohtahara syndrome with progressive course. *Brain* **142**, 3876–3891 (2019).

89. Schinke, T. *et al.* Impaired gastric acidification negatively affects calcium homeostasis and bone mass. *Nat Med* **15**, 674–681 (2009).

90. Kopic, S. *et al.* Vacuolar-type H+-ATPase-mediated proton transport in the rat parietal cell. *Pflugers Arch - Eur J Physiol* **463**, 419–427 (2012).

91. Sarkar, J., Wen, X., Simanian, E. J. & Paine, M. L. V-type ATPase proton pump expression during enamel formation. *Matrix Biology* **52–54**, 234–245 (2016).

92. Zhang, Y. *et al.* Highly acidic pH facilitates enamel protein self-assembly, apatite crystal growth and enamel protein interactions in the early enamel matrix. *Front Physiol* **13**, 1019364 (2022).

93. Lacruz, R. S. *et al.* Requirements for Ion and Solute Transport, and pH Regulation During Enamel Maturation. *J Cell Physiol* **227**, 1776–1785 (2012).

94. Eaton, A. F., Merkulova, M. & Brown, D. The H^+-ATPase (V-ATPase): from proton pump to signaling complex in health and disease. *American Journal of Physiology-Cell Physiology* **320**, C392–C414 (2021).

95. Choi, J. S. *et al.* Incomplete Distal Renal Tubular Acidosis with Nephrocalcinosis. *Chonnam Med J* **47**, 170–172 (2011).

96. Abbas, Y. M., Wu, D., Bueler, S. A., Robinson, C. V. & Rubinstein, J. L. Structure of V-ATPase from mammalian brain. *Science* **367**, 1240–1246 (2020).

97. Birling, M.-C., Dierich, A., Jacquot, S., Hérault, Y. & Pavlovic, G. Highly-efficient, fluorescent, locus directed cre and FlpO deleter mice on a pure C57BL/6N genetic background. *genesis* **50**, 482–489 (2012).

98. Bolam, J. P. *Experimental Neuroanatomy: A Practical Approach*. (Oxford University Press, 1992).

99. Paxinos, G. & Franklin, K. B. J. *The Mouse Brain in Stereotaxic Coordinates*. (Elsevier Science, 2007).

100. Yamasaki, S., Ohmori, H., Yamashita, K. & Yasuda, M. A morphometric study on postnatal development of the external granular layer of mice cerebella, focusing on local difference. *Hiroshima J Med Sci* **50**, 53–60 (2001).

101. Zhang, C., Hua, T., Zhu, Z. & Luo, X. Age-related changes of structures in cerebellar cortex of cat. *J Biosci* **31**, 55–60 (2006).

102. Kharouf, N. *et al.* Physicochemical and Antibacterial Properties of Novel, Premixed Calcium Silicate-Based Sealer Compared to Powder–Liquid Bioceramic Sealer. *J Clin Med* **9**, 3096 (2020).

103. Kharouf, N. *et al.* Tannic acid speeds up the setting of mineral trioxide aggregate cements and improves its surface and bulk properties. *Journal of Colloid and Interface Science* **589**, 318 (2021).

104. Anders, S., Pyl, P. T. & Huber, W. HTSeq--a Python framework to work with high-throughput sequencing data. *Bioinformatics* **31**, 166–169 (2015).

105. Love, M. I., Huber, W. & Anders, S. Moderated estimation of fold change and dispersion for RNA-seq data with DESeq2. *Genome Biology* **15**, 550 (2014).

106. Benjamini, Y. & Hochberg, Y. Controlling the False Discovery Rate: A Practical and Powerful Approach to Multiple Testing. *Journal of the Royal Statistical Society. Series B (Methodological)* **57**, 289–300 (1995).

107. Reimand, J. *et al.* Pathway enrichment analysis and visualization of omics data using g:Profiler, GSEA, Cytoscape and EnrichmentMap. *Nat Protoc* **14**, 482–517 (2019).

108. Sherman, B. T. *et al.* DAVID: a web server for functional enrichment analysis and functional annotation of gene lists (2021 update). *Nucleic Acids Res* **50**, W216–W221 (2022).

109. Oughtred, R. *et al.* The BioGRID database: A comprehensive biomedical resource of curated protein, genetic, and chemical interactions. *Protein Sci* **30**, 187–200 (2021).

Acknowledgments

This work was supported by grants from the French Ministry of Health (National Program for Clinical Research, PHRC 2008 N°4266 Amelogenesis imperfecta), the University Hospital of Strasbourg (HUS, API, 2009–2012, 'Development of the oral cavity: from gene to clinical phenotype in Human'), the European Regional Development Fund (ERDF) of the European Union in the framework of the INTERREG IV and V Upper Rhine program RARENET (2016-2019), Agence Nationale de la Recherche, "programme Investissements d'Avenir" (ANR-10-INBS-07 PHENOMIN), Recherche Filière TETECOU 2021, and AFM Téléthon (23933).
This work of the Interdisciplinary Thematic Institute IMCBio, as part of the ITI 2021-2028 program of the University of Strasbourg, CNRS and Inserm, was supported by IdEx Unistra (ANR-10-IDEX-0002), and by SFRI-STRAT'US project (ANR 20-SFRI-0012) and EUR IMCBio (ANR-17-EURE-0023) under the framework of the French Investments for the Future Program.
We thank the patients' support group Pierre-Henri et ses amis for its support.
YDF is a fellow for poste d'accueil Inserm. AJ-A received funding from the National Agency for Research and Development (ANID)/Scholarship Program/ DOCTORADO BECAS CHILE/2019-72200405. JTA received funding from the National Agency for Research and Development (ANID)/Scholarship Program/ DOCTORADO BECAS CHILE/2020- 72210028.
We thank Matthieu Jung and Christelle Thibault-Carpentier from the IGBMC-GenomEast platform. We are also thankful to Yves Lutz and Elvire Guiot from the Imaging Center of IGBMC (ici.igbmc.fr) for their assistance in microscopy imaging. We are grateful to Claire Chevalier, Sophie Brignon and Milan Herrmann for outstanding help with animal care and to the Histopathology and Embryology facilities- IGBMC for their expertise.
We appreciate the patients' and families' participation and priceless support. We thank Mrs. Marzena Kawczynski for her ongoing assistance and support managing the patient's data.

Author contribution

Conception and design: AJ-A and AB-Z. Acquisition of data: AJ-A, JTA, SM, NK, YDF, FB, MS, MH. Analysis and interpretation of data: AJ-A, JTA, NK, YDF, FB, MS, MH, AB-Z. Manuscript draft: AJ-A, KN, AB-Z. Revising the article: AJ-A, SM, JTA, NK, YDF, GG, FR, KN, JL, M-CB, MS, YH, MH, AB-Z.

Conflict of interest statement

The authors declare no competing interests.

Supplementary material

The *Rogdi* Knockout Mouse is a Model for Kohlschütter–Tönz Syndrome

Alexandra Jimenez-Armijo[1], Supawich Morkmued[2], José Tomás Ahumada[1], Naji Kharouf[3], Yvan de Feraudy[1,4], Gergo Gogl[1], Fabrice Riet[5], Karen Niederreither[1], Jocelyn Laporte[1], Marie Christine Birling[5], Mohammed Selloum[5], Yann Herault[1,5], Magali Hernandez[6], Agnès Bloch-Zupan*[1,7,8,9,10]

Affiliations

[1] Université de Strasbourg, Institut de Génétique et de Biologie Moléculaire et Cellulaire (IGBMC), INSERM U1258, CNRS- UMR7104, Illkirch, France.

[2] Faculty of Dentistry, Pediatrics Division, Department of Preventive Dentistry, Khon Kaen University, Khon Kaen, Thailand

[3] Université de Strasbourg, Laboratoire de Biomatériaux et Bioingénierie, Inserm UMR_S 1121, Strasbourg, France.

[4] Department of Neuropediatrics, Strasbourg University Hospital, Strasbourg, France.

[5] Université de Strasbourg, CNRS, INSERM, CELPHEDIA, PHENOMIN, Institut Clinique de la Souris (ICS), Illkirch, France.

[6] Centre Hospitalier Régional Universitaire de Nancy, Université de Lorraine, Competence Center for Rare Oral and Dental Diseases, Nancy, France.

[7] Université de Strasbourg, Faculté de Chirurgie Dentaire, Strasbourg, France.

[8] Université de Strasbourg, Institut d'études avancées (USIAS), Strasbourg, France.

[9] Hôpitaux Universitaires de Strasbourg (HUS), Pôle de Médecine et Chirurgie Bucco-dentaires, Hôpital Civil, Centre de référence des maladies rares orales et dentaires, O-Rares, Filière Santé Maladies rares TETE COU, European Reference Network ERN CRANIO, Strasbourg, France.

[10] Eastman Dental Institute, University College London, London, United Kingdom.

***Corresponding author**

Agnès Bloch-Zupan

agnes.bloch-zupan@unistra.fr

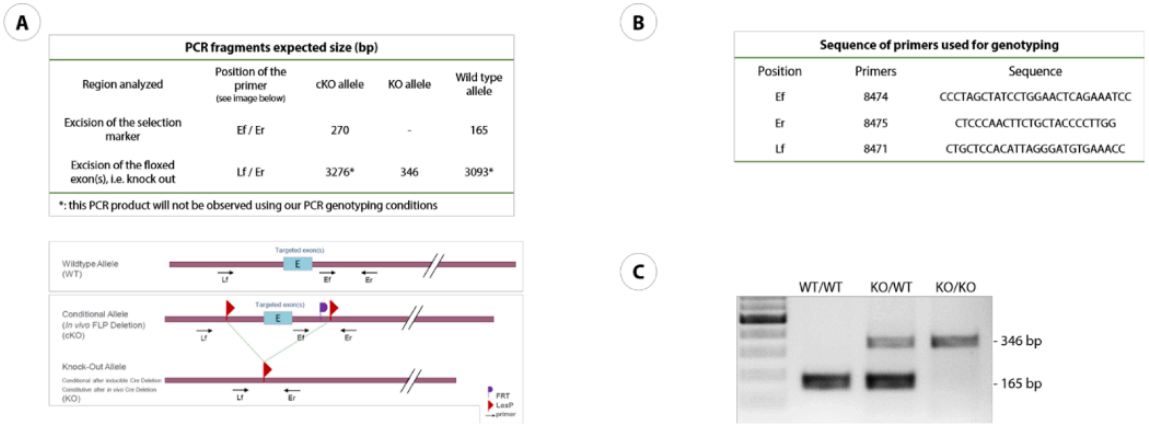

Supplementary Figure S1. Rogdi knockout genotyping strategy. (A) Table shows PCR fragments expected size of the different regions analyzed. Knock out strategy for deletion of exons 6 to 11 prior to and after homologous recombination is illustrated. Arrows identify primer annealing sites for RT-PCR. (B) Primers sequence used for genotyping. (C) Shows an example of PCR genotyping of littermates from heterozygous breeding. The lower bands (165 bp) are the wild-type amplification products; the higher bands (346 bp) are the same products lacking exon 6 to 11.

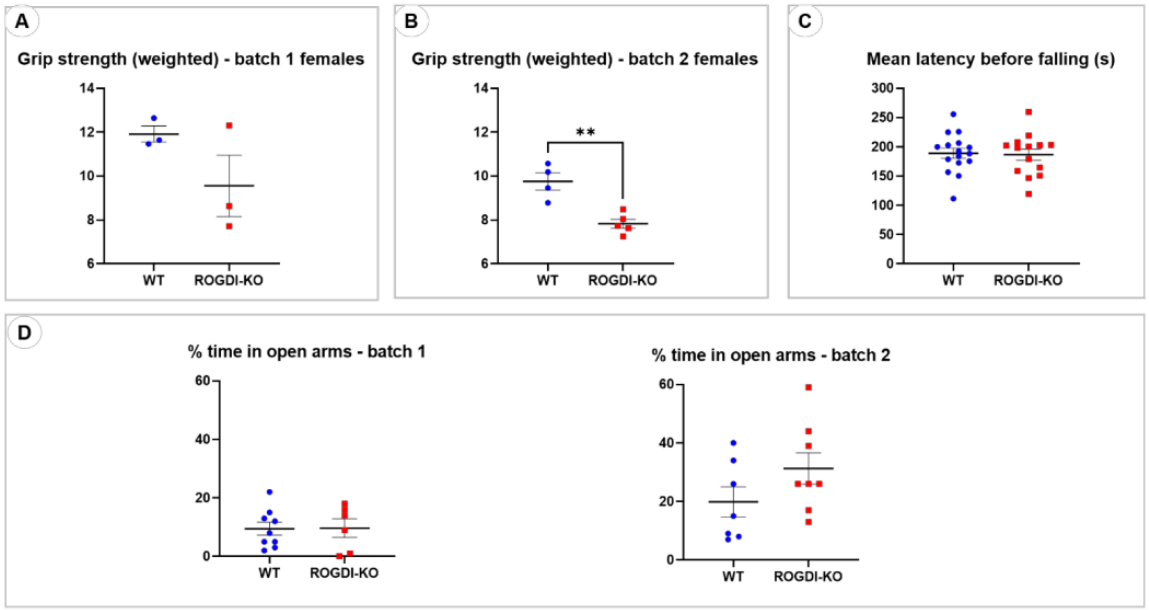

Supplementary Figure S2. Skeletal muscle function, motor coordination and balance, and anxiety-related behavior in *Rogdi*$^{-/-}$ mice. (A, B) Raw grip strength (4 paws) and grip strength adjusted to body weight (mean of 3 trials), second batch (B) of females show a significant decrease in muscle strength compared to WT. (C) Latency before falling from the rotarod accelerating from 4 to 40 rpm in 5 min (mean of the 3 trials) shows no difference between

genotypes. (D) Percentage of time spent in the open arms for batch 1 and batch 2 show no difference between groups. Data are expressed as mean ± SEM. ** p < 0.01.

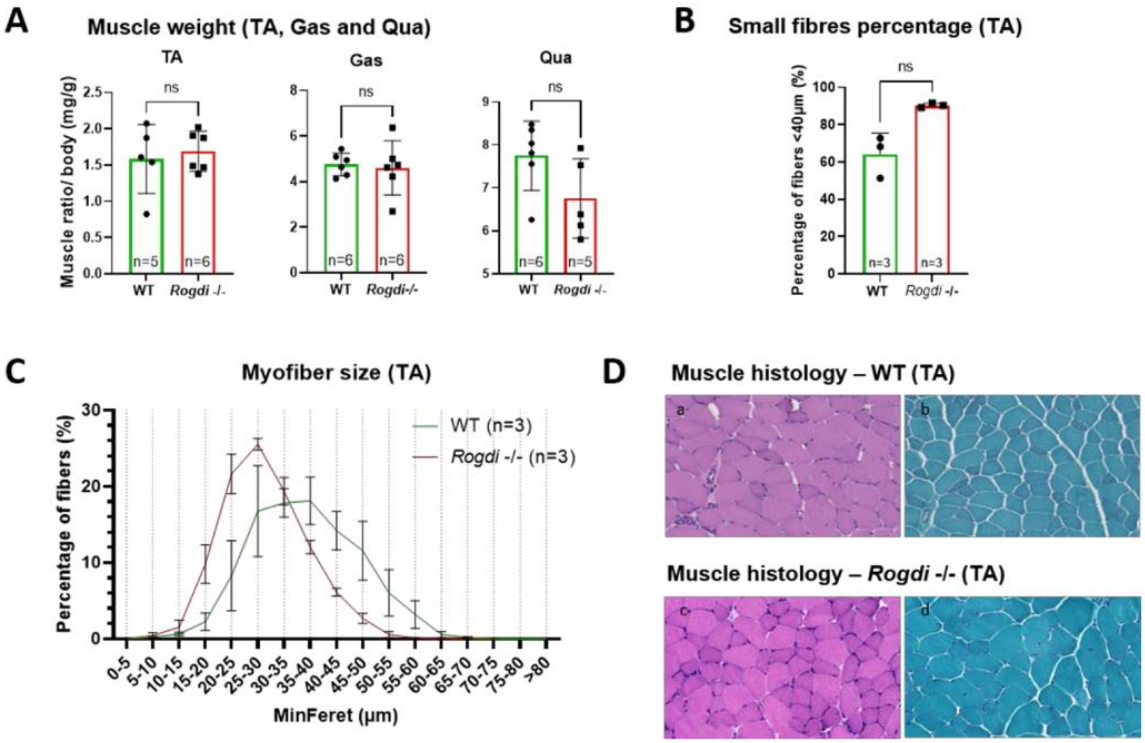

Supplementary Figure S3. Muscle analysis. Muscle/ body weight (A), percentage of small muscle fibers (B) and global MinFeret distributions (C) within control and *Rogdi* $^{-/-}$ mice showed no difference at 8 weeks of age. Results are expressed as mean values ± SD. No difference in term of muscle histology was observed between a control and a *Rogdi* $^{-/-}$ mouse (D) at 8 weeks of age [a: hematoxilin and eosin staining; b: gomori trichrome staining]. ns: not significant. TA: tibialis anterior; Gas: gastrocnemiens; Qua: quadriceps.

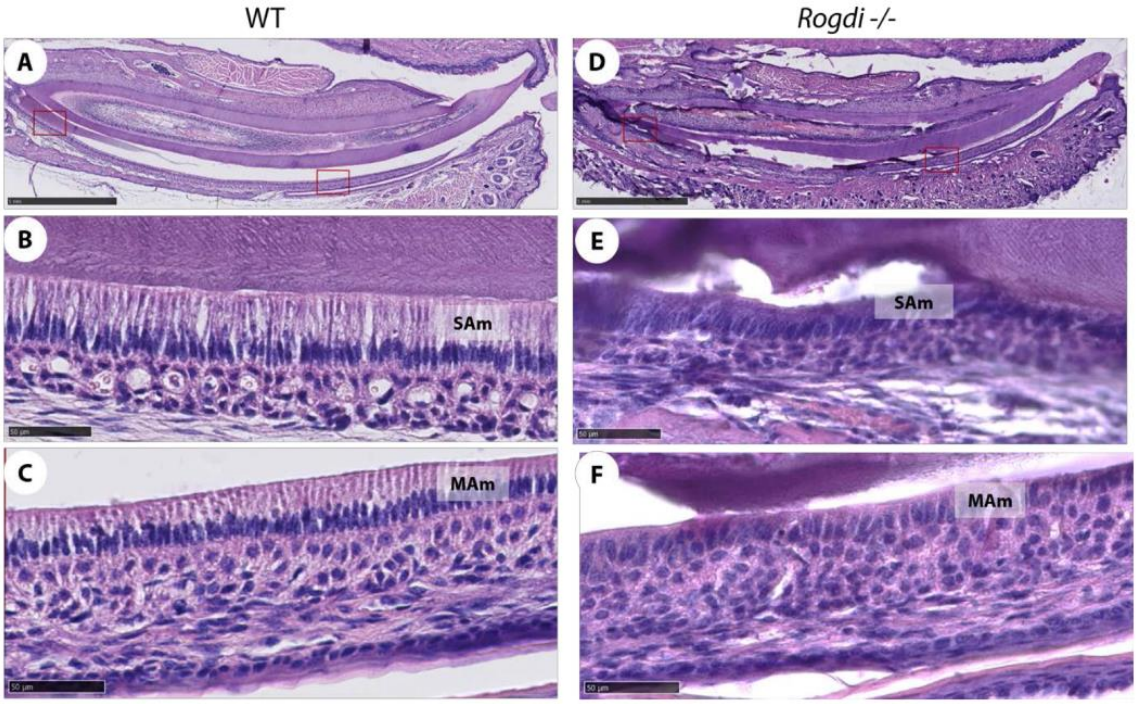

Supplementary Figure S4. Histological analysis of 2-week-old incisor of control and *Rogdi*$^{-/-}$ mice after hematoxylin-eosin staining. Respective boxed regions in A and D are magnified to show the secretory stage (left) and maturation stage (right) ameloblasts layer of the lower incisors. Secretory (E) and maturation-stage (F) ameloblasts are smaller and the nuclei are rounded in *Rogdi*$^{-/-}$ compared to WT samples (B, C). SAm: secretory ameloblasts; MAm: maturation-stage ameloblasts.

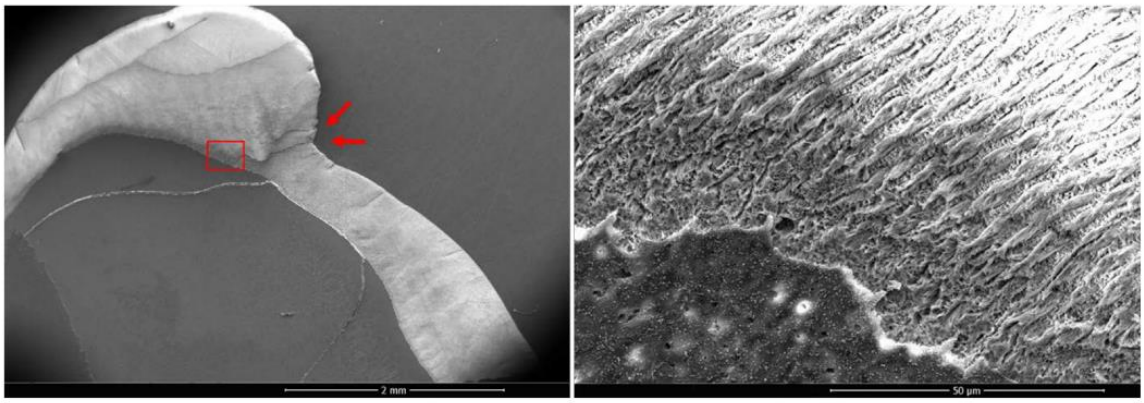

Element	Mass %	Atomic %
Carbon	4.06	9.17
Phosphorus	17.33	15.18
Calcium	37.02	25.05

Supplementary Figure S5. Scanning electron microscopy (SEM) of *ROGDI*-associated KTS patient Premolar (45). Enamel was present, but this was hypoplastic (red arrows). Red boxed region show region in which SEM image was obtained. The enamel presents a clear decussating prism pattern. Table of energy dispersive X-ray spectrometry data for quantification of element display levels of element content in enamel. Calcium-phosphate ratio (Ca/P) was of 1.65.

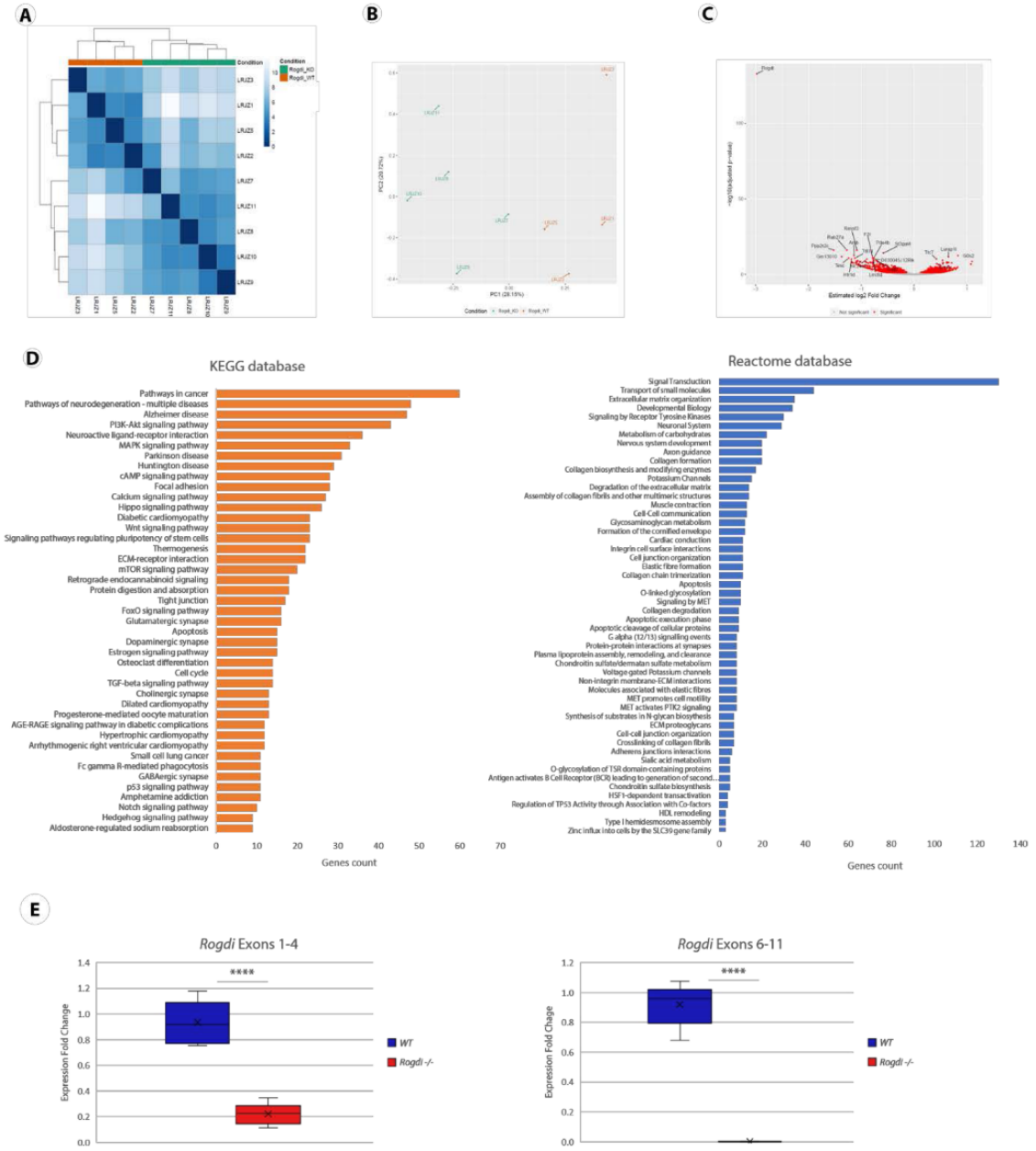

Supplementary Figure S6. *Rogdi KO* vs WT comparison. (A) Heatmap of sample-to-sample distances. Values correspond to the SERE [1] coefficient. The distances were computed from the raw counts. Hierarchical clustering was performed using the Unweighted Pair Group Method with Arithmetic mean (UPGMA) algorithm. (B) Principal component analysis. PCi axis represents the principal component i and the number into brackets indicates the percentage of explained variance associated with this axis. Principal Component Analysis was computed on variance stabilizing transformed data calculated with the method proposed in [2]. (C) *Rogdi KO* vs WT volcano-plot representing -log10 (adjusted p-value) as a function of the estimated log2 Fold-Change. Significant genes were selected using the following threshold: adjusted p-value lower than 0.05. For significant genes, a selection of first gene names according to the

adjusted p-value is displayed. (D) Kyoto Encyclopedia of Genes and Genomes (KEGG) and Reactome pathway enrichment analysis for up- and down-regulated genes between control vs *Rogdi*$^{-/-}$ samples. Analysis shows pathways of neurodegeneration, calcium signaling, synapse, transport of small molecules, and degradation of extracellular matrix, among others, were affected in *Rogdi*$^{-/-}$ mice. (E) RNA expression Fold change of *Rogdi*. RT-qPCR was performed on RNA extracted from postnatal 5-day lower incisors. Results were plotted on a graph with the expression of exons 1-4 (left) and 6-11 (right) of *Rogdi*. Fold-change was calculated based on mRNA relative expression of control group and normalized to *Gapdh* expression. ****p<0.0001.

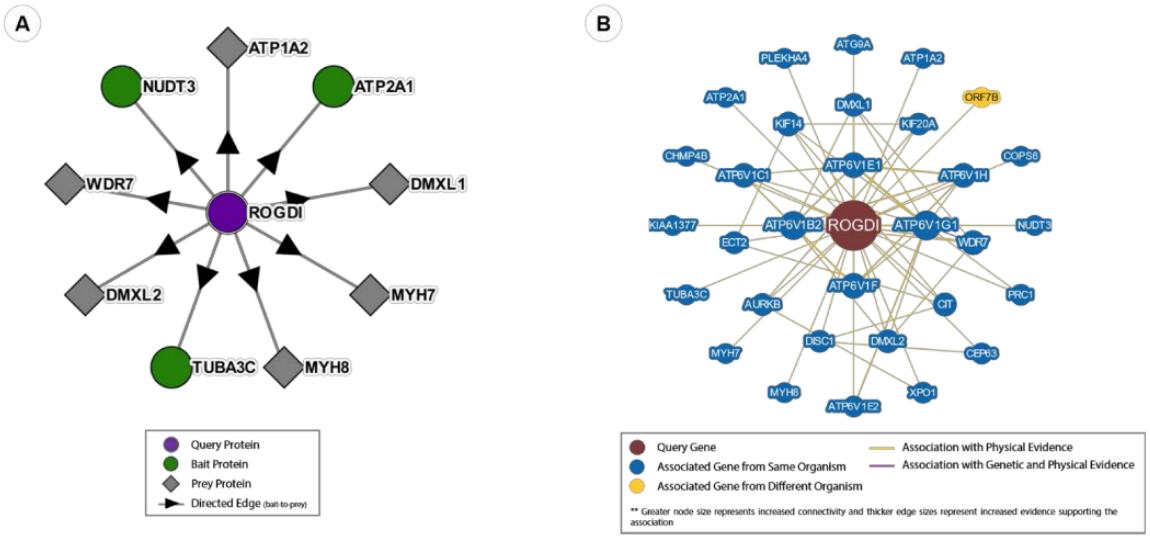

Supplementary Figure S7. ROGDI protein interactions network. (A) Rogdi interaction network in human cell lines HEK293T and HCT116 (Bioplex) [3]. (B) Interaction protein network of ROGDI revealed by the BioGRID database (https://thebiogrid.org).

Supplementary Table S1. *Rogdi* expression in 24 cell populations of the central nervous system [4] displayed from the highest expression to the lowest expression.

Cell Type	Region	*Rogdi* expression (RPKM)	Cell function
Corticostriatal Neurons	Cortex	3168.8	Motivated behavior [5]
Cholinergic Neurons	Basal Ganglion	2388.9	Regulate attention, memory, reward pathways, and motor activity [6]
Corticospinal, Corticopontine Neurons	Cortex	2379.9	Principal motor system for controlling movements that require the greatest skill and flexibility [7]
Neurons (CCK)	Cortex	2065.9	To regulate emotion and sculpt the network oscillations associated with cognition [8]
Corticothalamic Neurons	Cortex	2022.0	Involved in high-cognitive functions, such as decision-making and working memory [9]
Cholinergic Neurons	Forebrain	1734.2	Attentive functions [10]
Stellate & Basket Cells	Cerebellum	1591.6	Inhibitory GABAergic interneurons of the brain [11]
Motor Neurons	Brain Stem	1583.1	Alternative route to convey the information to the muscle targets in the periphery [12]
Drd1 Medium Spiny Neurons	Striatum	1532.4	GABAergic inhibitory cell [13]
Unipolar Brush Cell	Cerebellum	1218.3	Glutamatergic interneuron involved in the sensorimotor processes that regulate body, head and eye position, as well as in regions of the cochlear nucleus that process sensorimotor information [14]
Granule Cells	Cerebellum	1030.9	Involved in functions ranging from processing visual and motor information to learning and memory [15]
Interneurons (Cort)	Cortex	993.6	Ability to induce slow-wave sleep activity and regulated synaptic integration by augmenting the hyperpolarization-activated current IH [16]
Drd2 Medium Spiny Neurons	Striatum	895.9	GABAergic inhibitory cell [13]
Purkinje Cells	Cerebellum	779.9	Role in coordination, control, and learning of movements [17]
Interneurons (Pnoc)	Cortex	697.7	May be crucial for the maturation and neurogenesis of adult granule cells, as newly generated granule cells initially only receive GABAergic input from local interneurons [18]
Motor Neurons	Spinal Cord	526.8	Responsible for transmitting a movement-inducing signal from the upper motor neuron to the effector muscle [12]
Mature Oligodendrocytes & Progenitors	Cortex	467.9	Myelinating cells of the central nervous system (CNS) [19]
Golgi Cells	Cerebellum	444.2	Control on spatio-temporal signal organization and information storage in the granular layer playing a critical role for cerebellar computation [20]

Astrocytes	Cortex	441.3	Role in glutamate, ion (i.e., Ca^{2+}, K^{+}) and water homeostasis, defense against oxidative/nitrosative stress, energy storage, mitochondria biogenesis, scar formation, tissue repair via angiogenesis and neurogenesis, and synapse modulation [21]
Mature Oligodendrocytes	Cortex	401.7	Myelinating cells of the central nervous system (CNS) [19]
Mature Oligodendrocytes	Cerebellum	327.9	Myelinating cells of the central nervous system (CNS) [19]
Mature Oligodendrocytes & Progenitors	Cerebellum	290.1	Myelinating cells of the central nervous system (CNS) [19]
Bergmann Glia	Cerebellum	185.3	Role in controlling the membrane potential and thereby the activity of adjacent Purkinje cells [22]
Astrocytes	Cerebellum	150.0	Role in glutamate, ion (i.e., Ca^{2+}, K^{+}) and water homeostasis, defense against oxidative/nitrosative stress, energy storage, mitochondria biogenesis, scar formation, tissue repair via angiogenesis and neurogenesis, and synapse modulation [21]

Supplementary Table S2. Punnett square with WT, heterozygous and *Rogdi KO* ratio found and expected from heterozygous breeding.

	WT	**KO**
WT	**234 (24.7%; exp 25%)**	**517 (54.5%; exp 50%)**
KO	**517 (54.5%; exp 50%)**	**198 (20.9%; exp 25%)**

Supplementary Table S3. RNA sequencing. Data are presented as log2 fold changes in *Rogdi*$^{-/-}$ vs. WT samples. For instance, a FC log2 value of −1.00 will correspond to a 50% reduction in mRNA level in the *Rogdi*$^{-/-}$ samples. Genes encoding regulators of nervous system development including hippocampus, synapse organization, synaptic transmission, learning, memory and locomotor behavior are often dysregulated in *Rogdi*$^{-/-}$ PN5 lower incisors.

Gene name	**Description**	**Log2 FC** (*Rogdi*$^{-/-}$ vs WT)	***p*-value**
Nervous system development			
Plxna4	plexin A4	-1.05	7.6E-07
Gpm6a	glycoprotein m6a	-0.93	3.0E-09
Rassf10	Ras association (RalGDS/AF-6) domain family (N-terminal) member 10	-0.70	1.0E-05

Tox	thymocyte selection-associated high mobility group box	-0.55	8.6E-05
Alk	anaplastic lymphoma kinase	-0.54	3.1E-02
Igf2bp3	insulin-like growth factor 2 mRNA binding protein 3	-0.46	1.0E-04
Nav2	neuron navigator 2	-0.41	4.9E-02
Rtn4ip1	reticulon 4 interacting protein 1	-0.39	2.0E-02
Ntrk2	neurotrophic tyrosine kinase. receptor. type 2	-0.37	2.7E-02
Fzd6	frizzled class receptor 6	-0.36	1.4E-02
Apc	APC. WNT signaling pathway regulator	-0.35	8.0E-04
Lmtk2	lemur tyrosine kinase 2	-0.34	2.9E-02
Ophn1	oligophrenin 1	-0.33	3.5E-03
Slit3	slit guidance ligand 3	0.30	3.1E-02
Dab1	disabled 1	0.32	9.4E-04
Zbtb45	zinc finger and BTB domain containing 45	0.32	3.1E-02
Insc	INSC spindle orientation adaptor protein	0.32	4.9E-03
Bicdl1	BICD family like cargo adaptor 1	0.32	4.4E-02
Tfap2a	transcription factor AP-2. alpha	0.33	2.3E-02
Sema7a	sema domain. immunoglobulin domain (Ig). and GPI membrane anchor. (semaphorin) 7A	0.35	4.4E-04
Numbl	numb-like	0.36	1.9E-02
Glrb	glycine receptor. beta subunit	0.37	1.8E-02
Metrn	meteorin. glial cell differentiation regulator	0.39	4.2E-02
Chac1	ChaC. cation transport regulator 1	0.48	7.2E-03
Sh2b2	SH2B adaptor protein 2	0.48	6.5E-03
Atoh8	atonal bHLH transcription factor 8	0.51	1.6E-03
Sema6b	sema domain. transmembrane domain (TM). and cytoplasmic domain. (semaphorin) 6B	0.57	3.2E-04
Cer1	cerberus 1. DAN family BMP antagonist	0.57	9.7E-03
Synapse organization			
Nfasc	neurofascin	-1.08	2.2E-07
Gpm6a	glycoprotein m6a	-0.93	3.0E-09
Wnt3a	wingless-type MMTV integration site family. member 3A	-0.71	2.3E-03
Rims3	regulating synaptic membrane exocytosis 3	-0.64	3.9E-04
Wnt7a	wingless-type MMTV integration site family. member 7A	-0.59	8.8E-04
Klk8	kallikrein related-peptidase 8	-0.54	1.5E-02
Klk8	kallikrein related-peptidase 8	-0.54	1.5E-02
Tuba1a	tubulin. alpha 1A	-0.30	4.6E-05
Tuba1a	tubulin. alpha 1A	-0.30	4.6E-05
Ptprs	protein tyrosine phosphatase. receptor type. S	0.33	1.1E-02
Chrd	chordin	0.39	2.8E-02
Lamb2	laminin. beta 2	0.39	1.1E-02

Mapt	microtubule-associated protein tau	0.41	2.2E-02
Dvl1	dishevelled segment polarity protein 1	0.41	4.6E-05
Shank3	SH3 and multiple ankyrin repeat domains 3	0.45	4.5E-03
C1ql3	C1q-like 3	0.48	5.9E-03
Shank2	SH3 and multiple ankyrin repeat domains 2	0.49	1.1E-05
Apoe	apolipoprotein E	0.59	1.8E-04
Bsn	bassoon	0.61	8.1E-03
Chemical synaptic transmission			
Htr1d	5-hydroxytryptamine (serotonin) receptor 1D	-1.18	8.5E-11
Cntnap2	contactin associated protein-like 2	-0.93	9.9E-07
Sv2b	synaptic vesicle glycoprotein 2 b	-0.67	2.7E-03
Ston2	stonin 2	-0.65	1.0E-04
Slc12a4	solute carrier family 12. member 4	-0.31	9.5E-04
Glrb	glycine receptor. beta subunit	0.37	1.8E-02
Htr1b	5-hydroxytryptamine (serotonin) receptor 1B	0.59	4.2E-03
Tpgs1	tubulin polyglutamylase complex subunit 1	0.62	9.1E-03
Glutamatergic synaptic transmission			
Ntrk2	neurotrophic tyrosine kinase. receptor. type 2	-0.37	2.7E-02
Grin2d	glutamate receptor. ionotropic. NMDA2D (epsilon 4)	0.39	2.8E-02
Shank3	SH3 and multiple ankyrin repeat domains 3	0.45	4.5E-03
Shank2	SH3 and multiple ankyrin repeat domains 2	0.49	1.1E-05
Synaptic vesicle endocytosis			
Cd24a	CD24a antigen	-0.87	5.5E-05
Sh3gl2	SH3-domain GRB2-like 2	-0.67	1.5E-06
Ston2	stonin 2	-0.65	1.0E-04
Amph	amphiphysin	-0.46	2.6E-03
Ophn1	oligophrenin 1	-0.33	3.5E-03
Regulation of synaptic vesicle exocytosis			
Htr1d	5-hydroxytryptamine (serotonin) receptor 1D	-1.18	8.5E-11
Sv2b	synaptic vesicle glycoprotein 2 b	-0.67	2.7E-03
Htr1b	5-hydroxytryptamine (serotonin) receptor 1B	0.59	4.2E-03
Rims3	regulating synaptic membrane exocytosis 3	-0.64	3.9E-04
Wnt7a	wingless-type MMTV integration site family. member 7A	-0.59	8.8E-04
Pfn2	profilin 2	-0.38	3.8E-06
Kcnh1	potassium voltage-gated channel. subfamily H (eag-related). member 1	-0.32	4.5E-02
Rab3a	RAB3A. member RAS oncogene family	0.38	6.0E-03
Dvl1	dishevelled segment polarity protein 1	0.41	4.6E-05
Rims1	regulating synaptic membrane exocytosis 1	0.69	1.3E-05

Hippocampus development			
Wnt3a	wingless-type MMTV integration site family. member 3A	-0.71	2.3E-03
Alk	anaplastic lymphoma kinase	-0.54	3.1E-02
Trp73	transformation related protein 73	-0.38	1.9E-02
Tuba1a	tubulin. alpha 1A	-0.30	4.6E-05
Srf	serum response factor	0.30	4.5E-02
Dab1	disabled 1	0.32	9.4E-04
Ptprs	protein tyrosine phosphatase. receptor type. S	0.33	1.1E-02
Anxa3	annexin A3	0.34	1.1E-02
Uqcrq	ubiquinol-cytochrome c reductase. complex III subunit VII	0.51	2.1E-02
Sema6b	sema domain. transmembrane domain (TM). and cytoplasmic domain. (semaphorin) 6B	0.57	3.2E-04
Sct	secretin	0.61	5.4E-04
Bcan	brevican	0.63	1.0E-08
Learning or memory			
Cntnap2	contactin associated protein-like 2	-0.93	9.9E-07
Slc24a2	solute carrier family 24 (sodium/potassium/calcium exchanger). member 2	-0.89	8.7E-11
Crhr1	corticotropin releasing hormone receptor 1	-0.89	5.7E-05
Th	tyrosine hydroxylase	-0.86	3.0E-05
Pak6	p21 (RAC1) activated kinase 6	-0.84	1.5E-06
Jph4	junctophilin 4	-0.83	2.5E-08
Klk8	kallikrein related-peptidase 8	-0.54	1.5E-02
Itga3	integrin alpha 3	-0.50	3.6E-04
Amph	amphiphysin	-0.46	2.6E-03
Stra6	stimulated by retinoic acid gene 6	-0.40	1.8E-02
Zfp385a	zinc finger protein 385A	-0.38	1.6E-02
Ntrk2	neurotrophic tyrosine kinase. receptor. type 2	-0.37	2.7E-02
Nedd9	neural precursor cell expressed. developmentally down-regulated gene 9	-0.35	5.3E-06
Abl2	v-abl Abelson murine leukemia viral oncogene 2 (arg. Abelson-related gene)	-0.34	1.6E-04
Prnp	prion protein	-0.34	2.4E-03
Tuba1a	tubulin. alpha 1A	-0.30	4.6E-05
Igf2	insulin-like growth factor 2	0.35	9.5E-03
Mapt	microtubule-associated protein tau	0.41	2.2E-02
Kcnk2	potassium channel. subfamily K. member 2	0.44	6.5E-04
Ptprz1	protein tyrosine phosphatase. receptor type Z. polypeptide 1	0.45	1.6E-03
Shank3	SH3 and multiple ankyrin repeat domains 3	0.45	4.5E-03

Shank2	SH3 and multiple ankyrin repeat domains 2	0.49	1.1E-05
Foxo6	forkhead box O6	0.53	2.7E-02
Jun	jun proto-oncogene	0.63	6.4E-05
Jph3	junctophilin 3	0.65	5.8E-03
Nog	noggin	0.76	3.1E-05
Locomotory behavior			
Cntnap2	contactin associated protein-like 2	-0.93	9.9E-07
Th	tyrosine hydroxylase	-0.86	3.0E-05
Pak6	p21 (RAC1) activated kinase 6	-0.84	1.5E-06
Slc6a3	solute carrier family 6 (neurotransmitter transporter. dopamine). member 3	-0.59	1.3E-02
Celsr1	cadherin. EGF LAG seven-pass G-type receptor 1	-0.51	5.0E-04
Nav2	neuron navigator 2	-0.41	4.9E-02
Zfp385a	zinc finger protein 385A	-0.38	1.6E-02
Zdhhc8	zinc finger. DHHC domain containing 8	0.30	3.3E-03
Shank3	SH3 and multiple ankyrin repeat domains 3	0.45	4.5E-03
Cdh23	cadherin 23 (otocadherin)	0.50	5.5E-05
Wnt signaling			
Wnt3a	wingless-type MMTV integration site family. member 3A	-0.71	2.3E-03
Wnt7a	wingless-type MMTV integration site family. member 7A	-0.59	8.8E-04
Celsr2	cadherin. EGF LAG seven-pass G-type receptor 2	-0.57	2.7E-04
Apcdd1	adenomatosis polyposis coli down-regulated 1	-0.48	5.4E-04
Cxxc4	CXXC finger 4	-0.47	2.3E-02
Tle4	transducin-like enhancer of split 4	-0.37	3.2E-03
Prickle1	prickle planar cell polarity protein 1	-0.36	3.9E-06
Fzd6	frizzled class receptor 6	-0.36	1.4E-02
Apc	APC. WNT signaling pathway regulator	-0.35	8.0E-04
Myc	myelocytomatosis oncogene	0.32	1.4E-02
Pias4	protein inhibitor of activated STAT 4	0.32	2.3E-02
Cpz	carboxypeptidase Z	0.35	3.7E-02
Fzd8	frizzled class receptor 8	0.39	1.1E-02
Dvl1	dishevelled segment polarity protein 1	0.41	4.6E-05
Wnt6	wingless-type MMTV integration site family. member 6	0.44	8.7E-03
Lzts2	leucine zipper. putative tumor suppressor 2	0.49	4.0E-03
Hic1	hypermethylated in cancer 1	0.50	2.4E-02
Wnt10b	wingless-type MMTV integration site family. member 10B	0.50	1.8E-02
Gsc	goosecoid homeobox	0.57	1.8E-02
Notch signaling			

Tspear	thrombospondin type laminin G domain and EAR repeats	-0.55	9.7E-03
Trp63	transformation related protein 63	-0.53	4.6E-04
Jag1	jagged 1	-0.47	1.4E-03
Cdh6	cadherin 6	-0.47	4.3E-05
Perp	PERP. TP53 apoptosis effector	-0.41	8.9E-05
Arrb1	arrestin. beta 1	-0.39	1.4E-02
Ptp4a3	protein tyrosine phosphatase 4a3	0.32	4.0E-02
Notch4	notch 4	0.39	1.4E-02
Zbtb7a	zinc finger and BTB domain containing 7a	0.39	2.9E-02
Mib2	mindbomb E3 ubiquitin protein ligase 2	0.39	1.2E-02
Tcim	transcriptional and immune response regulator	0.43	7.4E-08
Tgfb1	transforming growth factor. beta 1	0.44	4.8E-03
Akt1s1	AKT1 substrate 1 (proline-rich)	0.46	3.3E-02
Chac1	ChaC. cation transport regulator 1	0.48	7.2E-03
Dtx1	deltex 1. E3 ubiquitin ligase	0.54	8.8E-03

Supplementary Table S4. Primers sequence used for RT-qPCR

Genes	Forward primer	Reverse primer
Rogdi exons 1-4	5’ - GGAGGAGGAGTTTCGCTGGT	5’ - CCTGGGAGAGTGAAGCGGAG
Rogdi exons 6-11	5’ - GCAACCCACCTCCACCAAGA	5’ - AGAGTTGCAGGGAGACGGTG
Gapdh	5’ - CCACCCATGGCAAATTCCATGGCA	5’ - TCTAGACGGCAGGTCAGGTCCACC

References

1. Schulze, S. K., Kanwar, R., Gölzenleuchter, M., Therneau, T. M. & Beutler, A. S. SERE: Single-parameter quality control and sample comparison for RNA-Seq. *BMC Genomics* **13**, 524 (2012).
2. Love, M. I., Huber, W. & Anders, S. Moderated estimation of fold change and dispersion for RNA-seq data with DESeq2. *Genome Biology* **15**, 550 (2014).
3. Schweppe, D. K., Huttlin, E. L., Harper, J. W. & Gygi, S. P. BioPlex Display: An Interactive Suite for Large-Scale AP–MS Protein–Protein Interaction Data. *J. Proteome Res.* **17**, 722–726 (2018).
4. Doyle, J. P. *et al.* Application of a Translational Profiling Approach for the Comparative Analysis of CNS Cell Types. *Cell* **135**, 749–762 (2008).
5. Shepherd, G. M. G. Corticostriatal connectivity and its role in disease. *Nat Rev Neurosci* **14**, 278–291 (2013).
6. Allaway, K. C. & Machold, R. Developmental specification of forebrain cholinergic neurons. *Developmental Biology* **421**, 1–7 (2017).
7. Martin, J. H. The corticospinal system: from development to motor control. *Neuroscientist* **11**, 161–173 (2005).
8. Whissell, P. D. *et al.* Selective Activation of Cholecystokinin-Expressing GABA (CCK-GABA) Neurons Enhances Memory and Cognition. *eNeuro* **6**, (2019).
9. Vaasjo, L. O. *et al.* Characterization and manipulation of Corticothalamic neurons in associative cortices using Syt6-Cre transgenic mice. *J Comp Neurol* **530**, 1020–1048 (2022).
10. Villano, I. *et al.* Basal Forebrain Cholinergic System and Orexin Neurons: Effects on Attention. *Front Behav Neurosci* **11**, 10 (2017).
11. Li, W. *et al.* Dendritic Inhibition by Shh Signaling-Dependent Stellate Cell Pool Is Critical for Motor Learning. *J Neurosci* **42**, 5130–5143 (2022).
12. Stifani, N. Motor neurons and the generation of spinal motor neuron diversity. *Front Cell Neurosci* **8**, 293 (2014).
13. Gangarossa, G. *et al.* Distribution and compartmental organization of GABAergic medium-sized spiny neurons in the mouse nucleus accumbens. *Front Neural Circuits* **7**, 22 (2013).
14. Mugnaini, E., Sekerková, G. & Martina, M. The unipolar brush cell: a remarkable neuron finally receiving deserved attention. *Brain Res Rev* **66**, 220–245 (2011).
15. Giovannucci, A. *et al.* Cerebellar granule cells acquire a widespread predictive feedback signal during motor learning. *Nat Neurosci* **20**, 727–734 (2017).
16. Maynard, K. R. *et al.* TrkB Signaling Influences Gene Expression in Cortistatin-Expressing Interneurons. *eNeuro* **7**, ENEURO.0310-19.2019 (2020).
17. Kano, M. & Watanabe, M. Chapter 4 - Cerebellar circuits. in *Neural Circuit and Cognitive Development (Second Edition)* (eds. Rubenstein, J., Rakic, P., Chen, B. & Kwan, K. Y.) 79–102 (Academic Press, 2020). doi:10.1016/B978-0-12-814411-4.00004-4.

18. Miller, J. A. *et al.* Conserved molecular signatures of neurogenesis in the hippocampal subgranular zone of rodents and primates. *Development* **140**, 4633–4644 (2013).
19. Kuhn, S., Gritti, L., Crooks, D. & Dombrowski, Y. Oligodendrocytes in Development, Myelin Generation and Beyond. *Cells* **8**, 1424 (2019).
20. D'Angelo, E. The critical role of Golgi cells in regulating spatio-temporal integration and plasticity at the cerebellum input stage. *Front Neurosci* **2**, 35–46 (2008).
21. Kim, Y., Park, J. & Choi, Y. K. The Role of Astrocytes in the Central Nervous System Focused on BK Channel and Heme Oxygenase Metabolites: A Review. *Antioxidants (Basel)* **8**, 121 (2019).
22. Wang, F., Xu, Q., Wang, W., Takano, T. & Nedergaard, M. Bergmann glia modulate cerebellar Purkinje cell bistability via Ca2+-dependent K+ uptake. *Proc Natl Acad Sci U S A* **109**, 7911–7916 (2012).

3. Impaired vitamin D signaling in *VDR$_{gem}$* mutants reveals novel targets in tooth and alveolar bone

Vitamin D is an essential endocrine regulator of mineral absorption, increasing inorganic calcium and phosphate uptake, which are crucial for proper skeletal and dental formation. Vitamin D insufficiency affects up to 70% of the general population, with severe hypovitaminosis D causing symptoms like rickets and stunted growth in children. Vitamin D signaling can be ligand-dependent or ligand-independent, depending on the target gene.

Critical vitamin D receptor (VDR) targets are homeostatic regulators of mineral uptake, ensuring bone growth in a structurally integrated manner. Both tooth and surrounding alveolar bone are highly mineralized, and human vitamin D/VDR deficiency produces hypocalcified, fragile intramembranous bones. In rodents, vitamin-D deficient mineralization permanently alters dentin and enamel composition and can alter tooth morphology.

VDR mutants have been used to understand how molecular targets of vitamin D signaling regulate skeletal and dental mineralization. VDR inactivation in mice reproduces human vitamin D resistant type II rickets, displaying severe hypocalcemia and hypophosphatemia, with teeth showing skeletal and dental defects.

Here, we report the mouse expression of the VDR during tooth, skeletal and intestinal development. Two models with deficient VDR signaling – *VDR-null* and *VDR$_{gem}$* – were studied to understand VDR signaling and its unliganded and liganded role during tooth and bone development. *VDR$_{gem}$* mice present a VDR unresponsive to endogenous 1,25(OH)2D3, which can be used to selectively dissect which VDR defects are ligand-dependent (such as bone mineralization) and which phenotypes like alopecia are due to the absence of unliganded VDR in promoting hair follicle proliferation.

Overall, dental and skeletal defects are more severe in *VDR$_{gem}$* mice than in *VDR-null* mice. *VDR$_{gem}$* inactivation produces severe reductions in alveolar bone and dentin mineralization. *VDR-null* and *VDR$_{gem}$* were both hypocalcemic and hypophosphatemic, maintaining a normal Ca/P ratio.

The *VDR$_{gem}$* mutant serves as a powerful tool to understand how vitamin D receptor and its derivatives regulate dental development and may promote alveolar bone regeneration or offset periodontal disease.

Global transcriptomic analysis revealed an impairment in developmental pathways conferring vitamin D actions in tooth and bone normal growth. While the vitamin D receptor is disrupted in both VDR mutants, *VDR-null* and *VDR$_{gem}$* models present different affected pathways.

Impaired vitamin D signaling in *VDR$_{gem}$* mutants reveals novel targets in tooth and alveolar bone

Alexandra Jimenez-Armijo[1], Naji Kharouf[2], Supawich Morkmued[3], Valérie Fraulob[1], Daniel Metzger[1], Karen Niederreither[1], Gilles Laverny[1], Agnès Bloch-Zupan*[1,4,5,6,7]

Affiliations

[1] Université de Strasbourg, Institut de Génétique et de Biologie Moléculaire et Cellulaire (IGBMC), INSERM U1258, CNRS- UMR7104, Illkirch, France.

[2] Université de Strasbourg, Laboratoire de Biomatériaux et Bioingénierie, Inserm UMR_S 1121, Strasbourg, France.

[3] Faculty of Dentistry, Pediatrics Division, Department of Preventive Dentistry, Khon Kaen University, Khon Kaen, Thailand

[4] Université de Strasbourg, Faculté de Chirurgie Dentaire, Strasbourg, France.

[5] Université de Strasbourg, Institut d'études avancées (USIAS), Strasbourg, France.

[6] Hôpitaux Universitaires de Strasbourg (HUS), Pôle de Médecine et Chirurgie Bucco-dentaires, Hôpital Civil, Centre de référence des maladies rares orales et dentaires, O-Rares, Filière Santé Maladies rares TETE COU, European Reference Network ERN CRANIO, Strasbourg, France.

[7] Eastman Dental Institute, University College London, London, United Kingdom.

***Corresponding author**
Agnès Bloch-Zupan
agnes.bloch-zupan@unistra.fr

Abstract

Deficiencies in vitamin D induce hypocalcemia and hypophosphatemia, events which compromise normal tooth and alveolar bone development. Here we report that *VDR*$_{gem}$ mice, which bear a point-mutated vitamin D receptor unresponsive to the endogenous vitamin D ligand, have a greater severity of tooth and alveolar bone defects than *VDR*-null (VDR$^{-/-}$) mice. Micro computed tomography (μCT) and histological analysis of adult *VDR*$_{gem}$ mice indicates/unravels severely reduced alveolar bone density, with abnormal root and pulp morphology. *VDR*$_{gem}$ mutants had severely hypocalcified alveolar bone and dentin- comparatively worse than *VDR*$^{-/-}$ mice- as confirmed by scanning electron microscopy and mineral analysis. This genetically confirmed that vitamin D acting through its receptor enabled bone and tooth to accumulate enough calcium and phosphorous for structural integrity. In addition, enamel structure was defective in *VDR*$_{gem}$ mice, which displayed hypomineralized areas. Transcriptional profiling of postnatal day 5 *VDR*$_{gem}$ and *VDR*$^{-/-}$ mutant incisors revealed vitamin D ligand signaling targets which promote mineralization, induce alveolar bone growth, assure dentin integrity, and regulate ribosomal protein synthesis (ribosomal protein deficiencies marking COVID-19 infection). RNA sequencing analysis of more severely affected *VDR*$_{gem}$ mutants uniquely showed defects in developmental targets- notably fibroblast growth factor and sonic hedgehog signaling reductions. Collectively, the severe defects in *VDR*$_{gem}$ tooth and alveolar bone demonstrates the importance of vitamin D actions during odontogenesis.

Introduction

Vitamin D is an endocrine regulator of mineral absorption, increasing inorganic calcium and phosphate uptake - actions which are indispensably required for proper skeletal and dental formation (Christakos et al., 2016). Frequent and sometimes severe vitamin D deficiencies can manifest, as generation of bioactive vitamin D requires synthesis of its precursor cholecalciferol in response to sufficient levels of sun generated UVB radiation in skin. Vitamin D insufficiency is a common worldwide problem, occurring in upwards of 60% of the general population (Holick, 2017). In children a severe hypovitaminosis D manifests as typical rickets symptoms, including bowed legs and stunted growth (Elder & Bishop, 2014). A large number of pathologies– immune deficiencies, cancer incidence, metabolic disease, and neurological pathologies correlate with low serum vitamin D levels (Hoel et al., 2016), highlighting the importance of vitamin D extra-skeletal activities.

The activities of the major metabolite of vitamin D -1,25 dihydroxyvitamin D_3 [$1,25(OH)_2D_3$]- are mediated through binding to the vitamin D receptor (VDR), a member of the nuclear receptor superfamily. Upon ligand binding, VDR heterodimerizes with its retinoid X receptor (RXR) partner allowing it to bind to vitamin D response elements (VDRE) in the regulatory region of its target gene. VDR induces the expression of pro-mineralization genes such as osteopontin, BGLAP (osteocalcin), and regulates osteoclast activity (Christakos et al., 2016). VDR signaling can be ligand-dependent, as when it binds to 1,25(OH)2D3, or ligand-independent, in which VDR does not require vitamin D binding (Bikle, 2021).

Critical VDR targets are homeostatic regulators of mineral (inorganic calcium and phosphate) uptake, whose intricate control assures bone growth in a structurally integrated manner (Christakos et al., 2016). Both tooth and surrounding alveolar bone are highly mineralized. Human vitamin D/VDR deficiency produces hypocalcified, fragile intramembranous bones (Li et al., 1997; Yoshizawa et al., 1997), similar to nutritional and genetic rodent models (X. Zhang et al., 2011). In rodents, hypoplastic or hypomineralized enamel (Lézot et al., 2006; Ranggård & Norén, 1994; X. Zhang, Rahemtulla, et al., 2009), hypocalcified dentin (X. Zhang, Beck, et al., 2009), hyperplastic/enlarged pulp chambers, shortened roots, malocclusion, and periodontal decay have been reported (Foster et al., 2014). Likewise, patients with vitamin D receptor activation defects display hypoplastic enamel (Gjørup et al., 2018). Tooth eruption can also be delayed (X. Zhang, Beck, et al., 2009), with reduced dentin tubule density in erupted incisors (X. Zhang et al., 2007). Hence vitamin-D deficient mineralization permanently alters dentin and enamel composition and additionally can modify tooth morphology (reviewed in Foster et al., 2014).

VDR mutants have been employed to understand how molecular targets of vitamin D signaling regulate skeletal and dental mineralization (Bouillon et al., 2008; Foster et al., 2014). VDR inactivation in mice (*VDR*$^{-/-}$ null mice) reproduces human vitamin D resistant type II rickets (HVDRR) (Li et al., 1997; Yoshizawa et al., 1997) displaying severe hypocalcemia and hypophosphatemia, with mice showing skeletal and dental defects. Interestingly, while this model is vitamin D resistant, ossification defects can be restored by normalizing mineral levels

through dietary elevations or re-expression of VDR in the intestine (Kaufmann et al., 2015; Van Cromphaut et al., 2001). Skin alopecia, though, cannot be dietarily rescued (Li et al., 1998). To understand VDR signaling and its unliganded and liganded role during tooth and bone development, two models with deficient VDR signaling were studied. Mice with a point-mutated VDR (termed *VDR$_{gem}$*) and *VDR-null* mice. *VDR$_{gem}$* mice present a VDR unresponsive to endogenous 1,25$(OH)_2D_3$ (Huet et al., 2015). These mouse mutants can be employed to selectively dissect which VDR defects are ligand dependent (such as bone mineralization), as opposed to phenotypes like alopecia which are due to the absence of unliganded VDR in promoting hair follicle proliferation (Christakos et al., 2016). Initial reports on *VDR$_{gem}$* mice showed that mineral ion and bone homeostasis are more impaired in VDR$_{gem}$ mice versus *VDR-null* mice (Huet et al., 2015). Here we report dental defects in *VDR$_{gem}$* mouse mutant. This *VDR$_{gem}$* ligand blocking mutant produces more severe hypocalcified alveolar bone defects than *VDR-null* mutant mice. Other dental defects include hypocalcemia and hypophosphatemia in dentin and alveolar bone. Enamel structure is altered in *VDR$_{gem}$* mice, with an impaired organization of the enamel crystals and hypomineralized areas. The *VDR$_{gem}$* mutant serves as a powerful tool to understand how vitamin D receptor and its derivatives regulate dental development and might serve to promote alveolar bone regeneration or offset periodontal disease.

Material and Methods

Animal models

VDR-null mice were generated by substitution of exon 2 containing the initiation codon by a neo cassette (Yoshizawa et al., 1997).
VDR_{gem} mice were generated using a targeting vector, encompassing VDR exons (E) 8 to 10 in which the CTG codon encoding mouse VDR Leu304 was mutated to CAG encoding a His, and containing a LoxP flanked cassette encoding the neomycin resistance gene located in the intron between E9 and E10. The protocol and genotyping strategy for both models has been described in (Huet et al., 2015).
Animals were kept in a temperature- and humidity-controlled environment with a 12-hour cycle of light and darkness, unrestricted access to water, and a standard rodent diet (ref D04; 2800 kcal/kg, 9,000 mg/kg calcium and 1,000 UI/kg vitamin D3, Usine d'Alimentation Rationelle). All experimental protocols were approved by the IGBMC's Animal Care and Use Committee and the French ministry of Higher Education and Research (APAFIS#15589-201806191874970v4). Mice were bred and maintained in accordance with institutional guidelines.

In situ hybridization

A full-length *Vitamin D receptor* probe (Dharmacon) was used to generate an antisense probe. *In situ* hybridization (ISH) was performed using digoxigenin-labeled RNA probes (diluted to 1 ug/ml) on 10 µm frozen sections. Blocking was performed with 2% Blocking Reagent and 20% heat inactivated normal goat serum (NGS). Anti-Digoxigenin antibody (1/2000, Roche) in blocking solution was added. Hybridized probes were visualized with NTMT (0.1 M NaCl, 0.1 M Tris-HCl pH 9.5, 50 mM MgCl2, 0.1% Tween 20), BCIP (5-bromo-4-chloro-3-indolyl-phosphate, Roche) and NBT (Nitroblue tetrazolium chloride, Roche) in PBT (PBS + 0.1% Tween-20).

Histology

Wild-type (WT), *VDR-null* and VDR_{gem} PN5 days and adult heads were fixed in 4% formaldehyde and demineralized in 10% ethylenediaminetetraacetic acid (EDTA pH 7.3) at room temperature until tissue was soft. Heads were dehydrated in graded ethanol (70%, 95%, and 100%), cleared in Histosol®, and embedded in paraffin at 60°C under vacuum (Leica TP1050 Vacuum Tissue Processor). Ten µm sagittal sections were stained with hematoxylin and eosin (H&E) according to standard protocols.

Microtomography (Micro-CT) imaging

Heads of adult *VDR-null* and VDR_{gem} mutant and wild-type (WT) mice were analyzed. All samples were scanned using the Quantum FX micro-CT imaging system (Caliper Life Sciences,

Hopkinton, MA, USA), which operates at 80 kV and 160 µA, with high resolution (pixel size of 10-80 µm), to evaluate the morphology and density of the skull and tooth. A 3-D model was created using the software Slicer 4.10.2. Dento-cranio-facial bone anatomy was sorted in coronal, transverse, and sagittal planes at the levels of the skull, mandible, and teeth. The images were analyzed using FIJI (ImageJ) and Slicer 4.10.2.

Scanning electron microscopy

Mandibular teeth of WT, *VDR-null* and VDR_{gem} adult mice were dissected, rinsed, and stored in 70% ethanol at 4°C until analysis. Embedding was done in Epon 812 (Euromedex, Souffelweyersheim, France). Sagittal sections were acquired according to the protocol (Kharouf et al., 2020). The embedded half incisors and molars were etched with a 20% (m/v) citric acid solution for 2 min, rinsed with distilled water, dehydrated in a graded series of ethanol. They were then mounted on aluminum SEM stubs, and sputter-coated with a gold–palladium alloy (20/80 weight %) using a HUMMER JR sputtering device (Technics, CA, USA). Scanning electron microscopy was performed using a Quanta 250 FEG scanning electron microscope (FEI Company- 190 pany, Eindhoven, the Netherlands) functioning with an accelerating voltage of electrons of 7.5 kV. EDX analysis was performed with a working distance of 10 mm and an acquisition time of 30 s (Kharouf et al., 2021). The weight percentages of chemical elements of the surfaces of the different dental tissues were attained.

RNA sequencing

Postnatal 5 (PN5) stage male lower incisors from WT, *VDR-null* and VDR_{gem} were dissected for RNA extraction using RNeasy Plus Micro Kit (Qiagen). Library preparation was performed at the GenomEast platform at the Institute of Genetics and Molecular and Cellular Biology using TruSeq Stranded mRNA Reference Guide - PN 1000000040498. RNA-Seq libraries were generated from 300 ng of total RNA using TruSeq Stranded mRNA Library Prep Kit and IDT for Illumina - TruSeq RNA UD Indexes (96 Indexes, 96 Samples) (Illumina, San Diego, USA), according to manufacturer's instructions. Libraries were sequenced on an Illumina HiSeq 4000 sequencer as single read 50 base reads. Image analysis and base calling were performed using RTA version 2.7.7 and bcl2fastq version 2.20.0.422. Genes with high Cook's distance were filtered out. Independent filtering based on the mean of normalized counts was performed to filter out those genes that have no or little chance of showing significance evidence of differential expression (without looking at their statistic). P-values were adjusted for multiple testing using the Benjamini and Hochberg (1995) method. Significant genes were selected using adjusted p-value < 0.05 and absolute value of log2 fold-change of > than 0.3. Data analysis was performed with Cytoscape 3.9.1 (Assenov et al., 2008; Merico et al., 2010; Morris et al., 2011; Reimand et al., 2019; Shannon et al., 2003) and the Database for Annotation, Visualization and Integrated Discovery-DAVID (Huang et al., 2009; Sherman et al., 2022).

Results

Vitamin D Receptor expression

Enriched expression of vitamin D receptor at embryonic and postnatal stages comprise hair follicles of the vibrissae (whiskers), skin, and sites of endochondral ossification including the mandible and maxillary jaw bones (Figure 1 A-I), as well as intramembranous ossification regions such as ribs and vertebrate axial skeleton (AS) (Figure 1A, 1C).

Bone and dentin in adult mice are primary targets of 1,25-dihydroxyvitamin D_3, which has an anabolic function in the development of both structures in the mandible (Liu et al., 2009). In adult mineralized tissues, VDR has been reported in osteoblasts, osteoclasts, ameloblasts and odontoblasts (X. Zhang, Beck, et al., 2009). We observed enriched VDR mRNA in fetal-stage bone and tooth mesenchyme (Figure 1). At embryonic day (E)14.5-16.5 cap-stage odontogenesis *VDR* is expressed in the dental papilla (DP), with more pronounced levels in surrounding bone (Figure 1B, 1D). At postnatal (PN)1 and PN7 stage, *VDR* is enriched in alveolar bone, odontoblasts, and pulp (Figure 1E-1I).

VDR_{gem} induces severe reductions in alveolar bone and dentin mineralization

We performed morphological analysis of *VDR_{gem}* to assess when and where vitamin D carried out its actions on bone and tooth. In neonatal mice at postnatal day 5 (PN5) no significative differences in bone development or tooth structures were found between groups (Figure 2), suggesting gross structural changes appear at later stages.

µCT imaging was done for morphological analysis to investigate how an absence of VDR activation adversely affected adult alveolar bone and tooth morphogenesis. Comparing WT, *VDR-null*, and *VDR_{gem}* for enamel, dentin, and alveolar bone mineralization, ablation of ligand-activating vitamin D actions (*VDR_{gem}* mutants Figure 3G-I) causes more severe reductions in cranial bone density compared with *VDR-null* (Figure 3D-F). Optical sections (µCT imaging) revealed severe alveolar bone loss at the level of the molars and incisors in *VDR_{gem}* (Figure 3H, 3I). Throughout alveolar bone, intertrabecular space became progressively larger in *VDR-null* and *VDR_{gem}* mice (Figure 3 - compare ★ marked regions in C, F, I).

Gross morphological dissection of the jaws showed bone fragility (coronoid process was fractured during dissection) and more rounded in the angular and condylar mandibular processes in *VDR_{gem}* (Figure 4C arrowheads). Bone appears immature without cortical bone confirming µCT images in intact samples (Figure 4G★). The greater porosity of remaining bone was reflected in a darker appearance – likely resulting from reduced calcium and phosphorous mineral deposition (see Table 1). The boxed region 2 in Figure 4 (D-F) show alveolar bone reductions in histological samples. Masson's trichrome staining revealed an abundance of collagen fibers (blue) and a completely normal architecture of alveolar bone with a normal number of osteocytes and mature bone (red) in WT mice (Supplementary figure S1A-B). *VDR-null* showed a similar staining to the WT, with a smaller number of osteocytes and larger

trabeculae (Supplementary figure S1C-D), whereas, *VDR$_{gem}$* presented an abnormal architecture of alveolar bone, with very few trabeculae (Supplementary figure S1E-F).
In addition, histological analysis showed enlarged predentin and progressively thinner dentin in *VDR-null* and *VDR$_{gem}$* compared with WT samples (Figure 4G-I). Entrapped odontoblasts were found in *VDR$_{gem}$* (Figure 4I, black arrowheads), similar to defects found in *VDR-null* previously described in Lezot et al (2002).
Regarding tooth and alveolar bone ultrastructure, SEM measurements showed less dentin tubules with an abnormal mineralization pattern in *VDR$_{gem}$* mainly affecting the peritubular dentin. In addition, mineral content quantification analysis in WT, *VDR-null* and *VDR$_{gem}$* mice, showed that *VDR-null* and *VDR$_{gem}$* were both hypocalcemic and hypophosphatemic maintaining a normal Ca/P ratio, and having about 60% of reduction in *VDR$_{gem}$* calcium mass compared to WT (Figure 5, Table 1). On the other side, the enamel in *VDR-null* and *VDR$_{gem}$* had smaller prisms and interprismatic space. Enamel thickness is not constant in *VDR$_{gem}$* with thinner enamel areas. The outer prismatic enamel appeared abnormal, presenting a more parallel crystal organization, possibly due to a loss of movement in ameloblasts, or maybe cells in secretory and maturation stages are affected. Some regions in *VDR$_{gem}$* enamel were hypomineralized with about 20% less calcium mass (black arrowheads Figure 5F, Supplementary Figure S2).
Ultrastructural analysis in alveolar bone revealed less quantity of osteocytes in *VDR-null* and *VDR$_{gem}$* (Figure 5H-I) compared to WT (Figure 5G), with a trabecular bone highly disorganized in *VDR$_{gem}$* mice, having an appearance of immature bone (Figure 5I). Mineral composition analysis indicated about 50% of calcium mass reduction in *VDR-null* and more than 90% in *VDR$_{gem}$* compared to WT mice. Both groups were hypocalcemic and hypophosphatemic, though there was a maintenance in Ca/P ratio (Table 1).

Global transcriptional profiling indicates developmental pathways confer vitamin D actions in tooth

We performed a global transcriptomic analysis (RNA sequencing [RNA-seq]) to survey what mRNA alterations manifested in postnatal day 5 (PN5) lower incisors of *VDR-null* vs. *VDR$_{gem}$* teeth. At this stage (PN5), it is possible to observe all amelogenesis stages, giving the perfect time to study tooth mineralization (Pugach & Gibson, 2014) and is before gross morphological alterations are observed in *VDR$_{gem}$* and *VDR-null* mutants.
While the vitamin D receptor is disrupted in both VDR mutants, *VDR-null* and *VDR$_{gem}$* models present different affected pathways (Figure 6). The absence of VDR impairs mitochondrial integrity, increased reactive oxygen species production, and ultimately produced cell death (Ricca et al., 2018). Besides oxidative phosphorylation pathway, other pathways found altered in *VDR-null* samples include regulation of pluripotency of stem cells, Notch signaling, salivary secretion and mineral absorption (Figure 6A).
In the case of *VDR$_{gem}$*, there were 30% more dysregulated genes compared to *VDR-null.* Furthermore, *VDR$_{gem}$* results display different deregulated KEGG pathways with an enrichment in pathways regulating embryonic and fetal development. These included

fibroblast growth factor reductions, Hedgehog signaling deficits, altered Wnt and calcium signaling, and perturbations in MAPK and mTOR signaling (Figure 6B).
Interestingly, among the 2,528 dysregulated genes in *VDR-null* mice and the 3,346 dysregulated genes found in VDR_{gem}, only 559 genes were dysregulated in both groups (Figure 6C). Moreover, only 366 genes had a similar expression pattern (see Heatmap Figure 6D). Examining our targets for target genes described as causatives for oro-dental diseases (Rey et al., 2019), we found 70 dysregulated genes in *VDR-null* mice and 144 genes in VDR_{gem} mice (Supplementary Table S1, Supplementary Figure S3).

VDR_{gem} analysis suggests fibroblast growth factor and sonic hedgehog signaling require VDR activation

Some of the most downregulated genes in *VDR-null* PN5 mice were *Col2a1, Ltf, Pold1, Twist2, Tbx1, Dlx5, Zfpm1, Kdf1, Scarf2, Map2k2*. *Tbx1* reductions, marking DiGeorge syndrome chromosome 22 microdeletion, induce tooth proliferation defects (Cao et al., 2010). Upregulated genes include *Clec7a, Cldn19, Ibsp, Ctsc, Adgrv1, Cldn1, Tmem165, Insr, Adamts1, Antxr2* (Supplementary Table S1). These genes have all been identified in the GenoDENT NGS panel for tooth development anomalies found in rare diseases (Rey et al., 2019).

In the case of VDR_{gem} - the most downregulated genes were fibroblast growth factors *Fgf3*, *Fgf10*, and *Fgf9,* the sonic hedgehog (*Shh*) receptor *Ptch1* and its transcriptional activator *Gli1*. Other VDR_{gem} reductions are *Sox11, Grem2, Cacnb2, Uhrf1, Camk4, Orc1*. Upregulated genes found include *Krt6a, Gjb4, Casp14, Gjb6, Pax3, Krt14, Gjb3, Krt6b, Krt16, Wnt10b* (Table 3).

Comparing RNA-seq results with a clinical bone disorder gene panel (Mortier et al., 2019) *VDR-null* mice had 27 dysregulated genes involved in bone diseases, with 13 of them being involved in Constitutional Disorders of Bone linked to skeletal abnormalities. Notably *Sox9* null mutants display spondyloepimetaphyseal dysplasia as cranial neural crest cannot differentiate to osteoblasts (Mori-Akiyama et al., 2003) (Supplementary Table S2). *Kif22* mutations also produce the inherited bone disorder spondyloepimetaphyseal dysplasia (Min et al., 2011). In VDR_{gem}, 56 genes were related to bone diseases; 25 of these genes are causative of Constitutional Disorders of Bone and 12 other genes have been found in the Lyse-Condensation-Proliferation gene panel (Supplementary Table S2).

Discussion

Severe defects in *VDR$_{gem}$* tooth and alveolar bone show the importance of vitamin D actions during odontogenesis

Basic developmental processes are regulated by $1,25(OH)_2D_3$. Vitamin D affects cell division and proliferation in a variety of cell types such as in the immune system, skin, and in tissues that participate in phospho-calcium metabolism, notably the intestine and bone (Berdal et al., 1995). Target cells for $1,25(OH)_2D_3$ also include ameloblasts and odontoblasts, substantiating these cell types as targets for dental defects observed during vitamin D deficiency or during hereditary vitamin D-resistant rickets (Berdal et al., 1993). VDR and RXR are the most highly expressed nuclear receptors in mesenchymal cells, including odontoblasts, at postnatal stages (Houari et al., 2016). Here, we observed that VDR transcripts are expressed at embryonic stages of tooth development, specifically in the mesenchyme, reflecting the strong effects of VDR mutation on dentin, with even stronger impairments observed in the pointed mutation *VDR$_{gem}$*. In addition, we demonstrate VDR expression in early developing stages of gut, tooth, and bone organogenesis. Other studies have indicated the presence of VDR mRNA in ameloblasts and striatum intermedium cells during the presecretion and secretion stages of enamel formation (Davideau et al., 1996; Lézot et al., 2006). In mature ameloblasts, VDR and RXR control ameloblast differentiation and the expression of genes involved in amelogenesis such as amelogenin and calbindin D 28k (Berdal et al., 1993; Houari et al., 2016; Papagerakis et al., 1999). VDR mutation leads to areas of enamel hypomineralization with a reduction of calcium and phosphorus in *VDR$_{gem}$* mice, although the overall amounts of calcium and phosphate were found to be normal.

In this study we have used *VDR$_{gem}$* and *VDR-null* mice as a tool to understand how complete absence of endogenous vitamin D ligand or VDR signaling during the entire developmental process can adversely affect cranium and tooth formation. As the *VDR$_{gem}$* cannot respond to endogenous vitamin D, these mutants display the most severe phenotypes marking complete vitamin D deficiency. *VDR$_{gem}$* defects are thus more severe than *VDR-null* mutants. This is consistent with prior research on the physiological effects of unliganded VDR (Huet et al., 2015). Bone mineral homeostasis is more impaired in *VDR$_{gem}$* mutants vs. *VDR* null mice. Previous genomic analysis of the intestine of *VDR$_{gem}$* samples showed of the top 100 downregulated genes, 38% were involved in ion mineral homeostasis (Huet et al., 2015). We likewise observed mineralization and bone homeostasis targets show greater impairment comparing RNA-seq analysis of *VDR$_{gem}$* vs. *VDR-null* mutant incisors. Reductions of alveolar bone density reflect severe reductions in calcium and phosphorus deposition in *VDR$_{gem}$* mice. This indicates increasingly altered molecular targets likely produce greater morphogenic consequences.

Alteration in developmental pathways may contribute to dental defects in *VDR$_{gem}$*

To use the tooth as a model to track organ maturation, we analyzed the gene expression of PN5 lower incisors of both VDR mutant models – *VDR-null* and *VDR$_{gem}$*- as at this stage we can follow tooth mineralization (Pugach & Gibson, 2014).

RNA-seq analysis of *VDR-null* indicated that the Notch signaling pathway is altered with several target genes downregulated such as *Jag2, Notch3, Spen, Ctbp1, Numbl, Dtx1, Dtx3, Rbpjl, and Tle2* (Table 3). Although it is expressed beginning at early stages of tooth development, *Jag2* is only found in the inner enamel epithelial cells from which ameloblasts emerge. *Jag2 -/-* mice develop teeth with abnormal shape (Mitsiadis et al., 2005, 2010). Mineral absorption is also dysregulated in *VDR-null* mutants with alterations in important genes involved in calcium transport and ions homeostasis such as *Atp2b1, Trpm7, Mt2, Slc9a3, Slc40a1* (Table 3). Reduced bone mineral density, hypocalcemia, and an altered response to 1,25(OH)2D3 have been identified in *Atp2b1* mutations in mice (Ehara et al., 2018; Ryan et al., 2015). Also, *Slc9a3* appears to be important for calcium absorption in the gut and kidneys (Pan et al., 2012). TRPM7 is also necessary for mineral absorption in the intestine (Mittermeier et al., 2019). *Slc40A1* seems to have a role in osteoclast differentiation (Xie et al., 2016), while MT2 is involved in osteoblast differentiation (Maria et al., 2018).

In addition, oxidative phosphorylation was also altered (Figure 6A). This pathway is essential for Ca^{2+} homeostasis, which controls the enamel matrix synthesis and triggers the differentiation of ectomesenchymal cells into odontoblasts (Imhof et al., 2020).

VDR$_{gem}$ mutant incisors showed the highest reductions in the expression of several fibroblast growth factors -*Fgf3*, *Fgf10*, and *Fgf9*. In addition, sonic hedgehog (*Shh*) receptor *Ptch1* and its transcriptional activator *Gli1* (Cohen et al., 2015) were reduced. Fibroblast growth factors (FGFs) regulate cell proliferation and differentiation in bone and are important for tooth development. Fgf3 and Fgf10 act synergistically to regulate molar size (X.-P. Wang et al., 2007). They aide in the formation of enamel and dentin. FGF impregnated matrices increase alveolar bone regeneration because of effects promoting osteogenic differentiation (R. Wang et al., 2021). *Fgf3* and *Fgf10* are expressed in the mesenchyme of cap and bell stage fetal tooth. Fgf inhibition at E12.5 also produces smaller tooth buds (Du et al., 2018). Moreover, Shh also plays a role in early tooth formation with a critical role in cell growth and differentiation. Shh has a strong expression in the bud and cap stages of odontogenesis (Cobourne & Sharpe, 2013; Seppala et al., 2017; Shahi et al., 2010). Disrupted SHH signaling alters molar and cusp morphology, along with root development (Dassule et al., 2000). Fgfs also function alongside SHH in the continuously growing cervical loop of the incisor (Jussila & Thesleff, 2012). Potentially FGFs could synergistically interact with SHH to regulate alveolar bone -SHH/FGF interactions could be analogous to growth regulatory loops observed in developing limb (Delgado & Torres, 2017), and during murine incisor regenerative growth (Jussila & Thesleff, 2012). Structural genes that were highly upregulated in *VDR$_{gem}$* but not in *VDR-null*, included *Krt10, Krt76, Krt2, Krt19, Krt15, Krt6a, Krt1, Krt7,* amongst others (Table 3).

Igf2 appeared upregulated in *VDR$_{gem}$* (Table 3). The insulin-like growth factor 2 (Igf2) expression has been shown to be active at prenatal stages, but its expression decreases after

birth (Khan et al., 2012). When IGF binds to receptors, pathways including the MAPK and AKT pathways are activated, coordinating proliferation and differentiation and dentin mineralization (He et al., 2022; F. Zhang et al., 2020). Both MAPK and PI3K-Akt pathways were altered in the VDR_{gem}. mTOR pathway was also dysregulated in VDR_{gem}. mTOR is strongly expressed since the beginning of odontogenesis in oral epithelia and bud stage, in the dental epithelium and mesenchyme (Figure 2B). Its expression continues in both ameloblasts and odontoblasts (Liu et al., 2023; Nie et al., 2020).

Our RNA-seq data indicate that early development-related genes are dysregulated in VDR mutants, demonstrating that VDR functions as an active repressor - especially in VDR_{gem}. Whereas *VDR-null* shows a strong impairment in calcium and mineralization regulation. Although the vitamin D receptor is altered in both models, the two distinct molecular profiles indicating unliganded repressive effects in VDR_{gem} at PN5 could account for more severe structural alterations found at adult stages.

Numerous reductions in ribosomal protein expression in *VDR* mutant incisors

Ribosomal proteins expression can be reduced in COVID-19 (Jiao et al., 2023). Interestingly we observed 1 to 2.3 -fold reductions in the levels of 32 ribosomal proteins in *VDR-null* incisors (Table 2). Epidemiological studies indicate vitamin D deficiency might contributes to COVID infection rates and disease severity (Gibbons et al., 2022). The basis of this protective effect is rooted in immune system targets of vitamin D regulating the severity of the COVID-19 induced cytokine storm- whose pulmonary vasoconstrictive and scaring actions affect patient survival/lung oxygenation (Chauss et al., 2022). Interestingly, three patient groups showing greatest COVID-19 morbidity are (1) persons of greater skin pigmentation (skin melanin inhibiting vitamin D biosynthesis), (2) the elderly (aged skin showing reduced vitamin D synthesis, and (3) the obese (fat serving to store serum vitamin D-reducing overall levels (Bae et al., 2022). Another pathway in which COVID-19 can evade the immune detection is by targeting/reducing ribosome biogenesis. This would lead to immune evasion allowing for increased viral replication (Bianco & Mohr, 2019). The numerous reductions in ribosomal protein synthesis in *VDR* mutants could reflect a global action of vitamin D in preventing viral infections.

Acknowledgments

This work was supported by grants from - the French Ministry of Health (National Program for Clinical Research, PHRC 2008 N°4266 Amelogenesis imperfecta) - the University Hospital of Strasbourg (HUS, API, 2009–2012, 'Development of the oral cavity: from gene to clinical phenotype in Human')- the European Regional Development Fund (ERDF) of the European Union in the framework of the INTERREG IV and V Upper Rhine program RARENET (2016-2019) - Recherche Filière TETECOU 2021- Agence Nationale de la Recherche (ANR-21-CE17-0009).
This work of the Interdisciplinary Thematic Institute IMCBio, as part of the ITI 2021-2028 program of the University of Strasbourg, CNRS and Inserm, was supported by IdEx Unistra (ANR-10-IDEX-0002), and by SFRI-STRAT'US project (ANR 20-SFRI-0012) and EUR IMCBio (ANR-17-EURE-0023) under the framework of the French Investments for the Future Program.
AJ-A received funding from the National Agency for Research and Development (ANID)/Scholarship Program/ DOCTORADO BECAS CHILE/2019- 72200405.
We thank Matthieu Jung and Christelle Thibault-Carpentier from IGBMC-GenomEast platform, and Regis Lutzing for his technical assistance. We are also thankful to the Histopathology and Embryology facilities and the animal facility from IGBMC for their help and expertise.

Author contribution

Conception and design: GL and AB-Z. Acquisition of data: AJ-A, SM, NK, VF. Analysis and interpretation of data: AJ-A, NK, KN, AB-Z. Drafting manuscript: AJ-A, KN, GL, AB-Z. Revising the article: AJ-A, NK, SM, DM, KN, GL, AB-Z.

Conflict of interest statement

The authors declare no competing interests

References

1. Assenov, Y., Ramírez, F., Schelhorn, S.-E., Lengauer, T., & Albrecht, M. (2008). Computing topological parameters of biological networks. *Bioinformatics*, *24*(2), 282–284. https://doi.org/10.1093/bioinformatics/btm554
2. Bae, J. H., Choe, H. J., Holick, M. F., & Lim, S. (2022). Association of vitamin D status with COVID-19 and its severity: Vitamin D and COVID-19: a narrative review. *Reviews in Endocrine & Metabolic Disorders*, *23*(3), 579–599. https://doi.org/10.1007/s11154-021-09705-6
3. Berdal, A., Hotton, D., Pike, J. W., Mathieu, H., & Dupret, J.-M. (1993). Cell- and Stage-Specific Expression of Vitamin D Receptor and Calbindin Genes in Rat Incisor: Regulation by 1,25-Dihydroxyvitamin D3. *Developmental Biology*, *155*(1), 172–179. https://doi.org/10.1006/dbio.1993.1016
4. Berdal, A., Papagerakis, P., Hotton, D., Bailleul-Forestier, I., & Davideau, J. L. (1995). Ameloblasts and odontoblasts, target-cells for 1,25-dihydroxyvitamin D3: A review. *The International Journal of Developmental Biology*, *39*(1), 1. https://doi.org/10.1387/ijdb.7626415
5. Bianco, C., & Mohr, I. (2019). Ribosome biogenesis restricts innate immune responses to virus infection and DNA. *ELife*, *8*, e49551. https://doi.org/10.7554/eLife.49551
6. Bikle, D. D. (2021). Ligand-Independent Actions of the Vitamin D Receptor: More Questions Than Answers. *JBMR Plus*, *5*(12), e10578. https://doi.org/10.1002/jbm4.10578
7. Bouillon, R., Carmeliet, G., Verlinden, L., van Etten, E., Verstuyf, A., Luderer, H. F., Lieben, L., Mathieu, C., & Demay, M. (2008). Vitamin D and Human Health: Lessons from Vitamin D Receptor Null Mice. *Endocrine Reviews*, *29*(6), 726–776. https://doi.org/10.1210/er.2008-0004
8. Cao, H., Florez, S., Amen, M., Huynh, T., Skobe, Z., Baldini, A., & Amendt, B. A. (2010). Tbx1 Regulates Progenitor Cell Proliferation in the Dental Epithelium by Modulating PITX2 Activation of p21. *Developmental Biology*, *347*(2), 289–300. https://doi.org/10.1016/j.ydbio.2010.08.031
9. Chauss, D., Freiwald, T., McGregor, R., Yan, B., Wang, L., Nova-Lamperti, E., Kumar, D., Zhang, Z., Teague, H., West, E. E., Vannella, K. M., Ramos-Benitez, M. J., Bibby, J., Kelly, A., Malik, A., Freeman, A. F., Schwartz, D. M., Portilla, D., Chertow, D. S., … Afzali, B. (2022). Autocrine Vitamin D-signaling switches off pro-inflammatory programs of Th1 cells. *Nature Immunology*, *23*(1), 62–74. https://doi.org/10.1038/s41590-021-01080-3
10. Christakos, S., Dhawan, P., Verstuyf, A., Verlinden, L., & Carmeliet, G. (2016). Vitamin D: Metabolism, Molecular Mechanism of Action, and Pleiotropic Effects. *Physiological Reviews*, *96*(1), 365–408. https://doi.org/10.1152/physrev.00014.2015
11. Cobourne, M. T., & Sharpe, P. T. (2013). Diseases of the tooth: The genetic and molecular basis of inherited anomalies affecting the dentition. *WIREs Developmental Biology*, *2*(2), 183–212. https://doi.org/10.1002/wdev.66
12. Cohen, M., Kicheva, A., Ribeiro, A., Blassberg, R., Page, K. M., Barnes, C. P., & Briscoe, J. (2015). Ptch1 and Gli regulate Shh signalling dynamics via multiple mechanisms. *Nature Communications*, *6*(1), 1. https://doi.org/10.1038/ncomms7709
13. Dassule, H. R., Lewis, P., Bei, M., Maas, R., & McMahon, A. P. (2000). Sonic hedgehog regulates growth and morphogenesis of the tooth. *Development*, *127*(22), 4775–4785. https://doi.org/10.1242/dev.127.22.4775

14. Davideau, J. L., Papagerakis, P., Hotton, D., Lezot, F., & Berdal, A. (1996). In situ investigation of vitamin D receptor, alkaline phosphatase, and osteocalcin gene expression in oro-facial mineralized tissues. *Endocrinology*, *137*(8), 3577–3585. https://doi.org/10.1210/endo.137.8.8754789
15. Delgado, I., & Torres, M. (2017). Coordination of limb development by crosstalk among axial patterning pathways. *Developmental Biology*, *429*(2), 382–386. https://doi.org/10.1016/j.ydbio.2017.03.006
16. Du, W., Du, W., & Yu, H. (2018). The Role of Fibroblast Growth Factors in Tooth Development and Incisor Renewal. *Stem Cells International*, *2018*, 7549160. https://doi.org/10.1155/2018/7549160
17. Ehara, Y., Hirawa, N., Sumida, K., Fujiwara, A., Kagimoto, M., Ooki-Okuyama, Y., Fujita, M., Katsumata, M., Kobayashi, Y., Saka, S., Katou, I., Yatsu, K., Umemura, S., & Tamura, K. (2018). Reduced secretion of parathyroid hormone and hypocalcemia in systemic heterozygous ATP2B1-null hypertensive mice. *Hypertension Research*, *41*(9), 699–707. https://doi.org/10.1038/s41440-018-0067-8
18. Elder, C. J., & Bishop, N. J. (2014). Rickets. *Lancet*, *383*(9929), 9929.
19. Foster, B. L., Nociti, F. H., & Somerman, M. J. (2014). The Rachitic Tooth. *Endocrine Reviews*, *35*(1), 1–34. https://doi.org/10.1210/er.2013-1009
20. Gibbons, J. B., Norton, E. C., McCullough, J. S., Meltzer, D. O., Lavigne, J., Fiedler, V. C., & Gibbons, R. D. (2022). Association between vitamin D supplementation and COVID-19 infection and mortality. *Scientific Reports*, *12*, 19397. https://doi.org/10.1038/s41598-022-24053-4
21. Gjørup, H., Beck-Nielsen, S. S., & Haubek, D. (2018). Craniofacial and dental characteristics of patients with vitamin-D-dependent rickets type 1A compared to controls and patients with X-linked hypophosphatemia. *Clinical Oral Investigations*, *22*(2), 745–755. https://doi.org/10.1007/s00784-017-2149-4
22. He, P., Zheng, L., & Zhou, X. (2022). IGFs in Dentin Formation and Regeneration: Progress and Remaining Challenges. *Stem Cells International*, *2022*, 3737346. https://doi.org/10.1155/2022/3737346
23. Hoel, D. G., Berwick, M., de Gruijl, F. R., & Holick, M. F. (2016). The risks and benefits of sun exposure 2016. *Dermato-Endocrinology*, *8*(1), e1248325. https://doi.org/10.1080/19381980.2016.1248325
24. Holick, M. F. (2017). The vitamin D deficiency pandemic: Approaches for diagnosis, treatment and prevention. *Reviews in Endocrine and Metabolic Disorders*, *18*(2), 153–165. https://doi.org/10.1007/s11154-017-9424-1
25. Houari, S., Loiodice, S., Jedeon, K., Berdal, A., & Babajko, S. (2016). Expression of Steroid Receptors in Ameloblasts during Amelogenesis in Rat Incisors. *Frontiers in Physiology*, *7*, 503. https://doi.org/10.3389/fphys.2016.00503
26. Huang, D. W., Sherman, B. T., & Lempicki, R. A. (2009). Systematic and integrative analysis of large gene lists using DAVID bioinformatics resources. *Nature Protocols*, *4*(1), 44–57. https://doi.org/10.1038/nprot.2008.211
27. Huet, T., Laverny, G., Ciesielski, F., Molnár, F., Ramamoorthy, T. G., Belorusova, A. Y., Antony, P., Potier, N., Metzger, D., Moras, D., & Rochel, N. (2015). A Vitamin D Receptor Selectively Activated by Gemini Analogs Reveals Ligand Dependent and Independent Effects. *Cell Reports*, *10*(4), 516–526. https://doi.org/10.1016/j.celrep.2014.12.045

28. Imhof, T., Rosenblatt, K., Pryymachuk, G., Weiland, D., Noetzel, N., Deschner, J., Baris, O. R., Kimoloi, S., Koch, M., Wiesner, R. J., & Korkmaz, Y. (2020). Epithelial loss of mitochondrial oxidative phosphorylation leads to disturbed enamel and impaired dentin matrix formation in postnatal developed mouse incisor. *Scientific Reports*, *10*(1), 1. https://doi.org/10.1038/s41598-020-77954-7
29. Jiao, L., Liu, Y., Yu, X.-Y., Pan, X., Zhang, Y., Tu, J., Song, Y.-H., & Li, Y. (2023). Ribosome biogenesis in disease: New players and therapeutic targets. *Signal Transduction and Targeted Therapy*, *8*, 15. https://doi.org/10.1038/s41392-022-01285-4
30. Jussila, M., & Thesleff, I. (2012). Signaling networks regulating tooth organogenesis and regeneration, and the specification of dental mesenchymal and epithelial cell lineages. *Cold Spring Harbor Perspectives in Biology*, *4*(4), a008425. https://doi.org/10.1101/cshperspect.a008425
31. Kaufmann, M., Lee, S. M., Pike, J. W., & Jones, G. (2015). A High-Calcium and Phosphate Rescue Diet and VDR-Expressing Transgenes Normalize Serum Vitamin D Metabolite Profiles and Renal Cyp27b1 and Cyp24a1 Expression in VDR Null Mice. *Endocrinology*, *156*(12), 4388–4397. https://doi.org/10.1210/en.2015-1664
32. Khan, Q.-E.-S., Sehic, A., Skalleberg, N., Landin, M. A., Khuu, C., Risnes, S., & Osmundsen, H. (2012). Expression of delta-like 1 homologue and insulin-like growth factor 2 through epigenetic regulation of the genes during development of mouse molar. *European Journal of Oral Sciences*, *120*(4), 292–302. https://doi.org/10.1111/j.1600-0722.2012.00976.x
33. Kharouf, N., Arntz, Y., Eid, A., Zghal, J., Sauro, S., Haikel, Y., & Mancino, D. (2020). Physicochemical and Antibacterial Properties of Novel, Premixed Calcium Silicate-Based Sealer Compared to Powder–Liquid Bioceramic Sealer. *Journal of Clinical Medicine*, *9*(10), 3096. https://doi.org/10.3390/jcm9103096
34. Kharouf, N., Zghal, J., Addiego, F., Gabelout, M., Jmal, H., Haïkel, Y., Bahlouli, N., & Ball, V. (2021). Tannic acid speeds up the setting of mineral trioxide aggregate cements and improves its surface and bulk properties. *Journal of Colloid and Interface Science*, *589*, 318. https://doi.org/10.1016/j.jcis.2020.12.115
35. Lézot, F., Descroix, V., Hotton, D., Mauro, N., Kato, S., & Berdal, A. (2006). Vitamin D and tissue non-specific alkaline phosphatase in dental cells. *European Journal of Oral Sciences*, *114*(s1), 178–182. https://doi.org/10.1111/j.1600-0722.2006.00338.x
36. Lézot, F., Descroix, V., Mesbah, M., Hotton, D., Blin, C., Papagerakis, P., Mauro, N., Kato, S., MacDougall, M., Sharpe, P., & Berdal, A. (2002). Cross-Talk Between Msx/Dlx Homeobox Genes and Vitamin D During Tooth Mineralization. *Connective Tissue Research*, *43*(2–3), 509–514. https://doi.org/10.1080/03008200290000583
37. Li, Y. C., Amling, M., Pirro, A. E., Priemel, M., Meuse, J., Baron, R., Delling, G., & Demay, M. B. (1998). Normalization of Mineral Ion Homeostasis by Dietary Means Prevents Hyperparathyroidism, Rickets, and Osteomalacia, But Not Alopecia in Vitamin D Receptor-Ablated Mice**This work was supported by NIH Grants DK-46974 (to M.B.D.) and DE-04724 (to R.B.) and a NIH National Research Service Award (to Y.C.L.). *Endocrinology*, *139*(10), 4391–4396. https://doi.org/10.1210/endo.139.10.6262
38. Li, Y. C., Pirro, A. E., Amling, M., Delling, G., Baron, R., Bronson, R., & Demay, M. B. (1997). Targeted ablation of the vitamin D receptor: An animal model of vitamin D-dependent rickets type II with alopecia. *Proceedings of the National Academy of Sciences of the United States of America*, *94*(18), 9831–9835.

39. Liu, H., Guo, J., Wang, L., Chen, N., Karaplis, A., Goltzman, D., & Miao, D. (2009). Distinctive anabolic roles of 1,25-dihydroxyvitamin D3 and parathyroid hormone in teeth and mandible versus long bones. *Journal of Endocrinology*, *203*(2), 203–213. https://doi.org/10.1677/JOE-09-0247
40. Liu, H., Yue, Y., Xu, Z., Guo, L., Wu, C., Zhang, D., Luo, L., Huang, W., Chen, H., & Yang, D. (2023). MTORC1 signaling pathway regulates tooth repair. *International Journal of Oral Science*, *15*(1), 1. https://doi.org/10.1038/s41368-023-00218-3
41. Maria, S., Samsonraj, R. M., Munmun, F., Glas, J., Silvestros, M., Kotlarczyk, M. P., Rylands, R., Dudakovic, A., van Wijnen, A. J., Enderby, L. T., Lassila, H., Dodda, B., Davis, V. L., Balk, J., Burow, M., Bunnell, B. A., & Witt-Enderby, P. A. (2018). Biological effects of melatonin on osteoblast/osteoclast cocultures, bone, and quality of life: Implications of a role for MT2 melatonin receptors, MEK1/2, and MEK5 in melatonin-mediated osteoblastogenesis. *Journal of Pineal Research*, *64*(3), 10.1111/jpi.12465. https://doi.org/10.1111/jpi.12465
42. Merico, D., Isserlin, R., Stueker, O., Emili, A., & Bader, G. D. (2010). Enrichment Map: A Network-Based Method for Gene-Set Enrichment Visualization and Interpretation. *PLoS ONE*, *5*(11), e13984. https://doi.org/10.1371/journal.pone.0013984
43. Min, B.-J., Kim, N., Chung, T., Kim, O.-H., Nishimura, G., Chung, C. Y., Song, H. R., Kim, H. W., Lee, H. R., Kim, J., Kang, T.-H., Seo, M.-E., Yang, S.-D., Kim, D.-H., Lee, S.-B., Kim, J.-I., Seo, J.-S., Choi, J.-Y., Kang, D., … Cho, T.-J. (2011). Whole-Exome Sequencing Identifies Mutations of KIF22 in Spondyloepimetaphyseal Dysplasia with Joint Laxity, Leptodactylic Type. *American Journal of Human Genetics*, *89*(6), 760–766. https://doi.org/10.1016/j.ajhg.2011.10.015
44. Mitsiadis, T. A., Graf, D., Luder, H., Gridley, T., & Bluteau, G. (2010). BMPs and FGFs target Notch signalling via jagged 2 to regulate tooth morphogenesis and cytodifferentiation. *Development (Cambridge, England)*, *137*(18), 3025–3035. https://doi.org/10.1242/dev.049528
45. Mitsiadis, T. A., Regaudiat, L., & Gridley, T. (2005). Role of the Notch signalling pathway in tooth morphogenesis. *Archives of Oral Biology*, *50*(2), 137–140. https://doi.org/10.1016/j.archoralbio.2004.10.006
46. Mittermeier, L., Demirkhanyan, L., Stadlbauer, B., Breit, A., Recordati, C., Hilgendorff, A., Matsushita, M., Braun, A., Simmons, D. G., Zakharian, E., Gudermann, T., & Chubanov, V. (2019). TRPM7 is the central gatekeeper of intestinal mineral absorption essential for postnatal survival. *Proceedings of the National Academy of Sciences of the United States of America*, *116*(10), 4706–4715. https://doi.org/10.1073/pnas.1810633116
47. Mori-Akiyama, Y., Akiyama, H., Rowitch, D. H., & de Crombrugghe, B. (2003). Sox9 is required for determination of the chondrogenic cell lineage in the cranial neural crest. *Proceedings of the National Academy of Sciences of the United States of America*, *100*(16), 9360–9365. https://doi.org/10.1073/pnas.1631288100
48. Morris, J. H., Apeltsin, L., Newman, A. M., Baumbach, J., Wittkop, T., Su, G., Bader, G. D., & Ferrin, T. E. (2011). clusterMaker: A multi-algorithm clustering plugin for Cytoscape. *BMC Bioinformatics*, *12*, 436. https://doi.org/10.1186/1471-2105-12-436
49. Mortier, G. R., Cohn, D. H., Cormier-Daire, V., Hall, C., Krakow, D., Mundlos, S., Nishimura, G., Robertson, S., Sangiorgi, L., Savarirayan, R., Sillence, D., Superti-Furga, A., Unger, S., & Warman, M. L. (2019). Nosology and classification of genetic skeletal

disorders: 2019 revision. *American Journal of Medical Genetics Part A*, *179*(12), 2393–2419. https://doi.org/10.1002/ajmg.a.61366

50. Nie, X., Zheng, J., Cruciger, M., Yang, P., & Mao, J. J. (2020). MTOR plays a pivotal role in multiple processes of enamel organ development principally through the mTORC1 pathway and in part via regulating cytoskeleton dynamics. *Developmental Biology*, *467*(1), 77–87. https://doi.org/10.1016/j.ydbio.2020.08.010
51. Pan, W., Borovac, J., Spicer, Z., Hoenderop, J. G., Bindels, R. J., Shull, G. E., Doschak, M. R., Cordat, E., & Alexander, R. T. (2012). The epithelial sodium/proton exchanger, NHE3, is necessary for renal and intestinal calcium (re)absorption. *American Journal of Physiology - Renal Physiology*, *302*(8), F943–F956. https://doi.org/10.1152/ajprenal.00504.2010
52. Papagerakis, P., Hotton, D., Lezot, F., Brookes, S., Bonass, W., Robinson, C., Forest, N., & Berdal, A. (1999). Evidence for regulation of amelogenin gene expression by 1,25-dihydroxyvitamin D3 in vivo. *Journal of Cellular Biochemistry*, *76*(2), 194–205. https://doi.org/10.1002/(SICI)1097-4644(20000201)76:2<194::AID-JCB4>3.0.CO;2-U
53. Pugach, M. K., & Gibson, C. W. (2014). Analysis of enamel development using murine model systems: Approaches and limitations. *Frontiers in Physiology*, *5*. https://doi.org/10.3389/fphys.2014.00313
54. Ranggård, L., & Norén, J. G. (1994). Effect of hypocalcemic state on enamel formation in rat maxillary incisors. *Scandinavian Journal of Dental Research*, *102*(5), 249–253. https://doi.org/10.1111/j.1600-0722.1994.tb01464.x
55. Reimand, J., Isser, R., Voisin, V., Kucera, M., Tannus-Lopes, C., Rostamianfar, A., Wadi, L., Meyer, M., Wong, J., Xu, C., Merico, D., & Bader, G. D. (2019). Pathway enrichment analysis and visualization of omics data using g:Profiler, GSEA, Cytoscape and EnrichmentMap. *Nature Protocols*, *14*(2), 482–517. https://doi.org/10.1038/s41596-018-0103-9
56. Rey, T., Tarabeux, J., Gerard, B., Delbarre, M., Le Béchec, A., Stoetzel, C., Prasad, M., Laugel-Haushalter, V., Kawczynski, M., Muller, J., Chelly, J., Dollfus, H., Manière, M.-C., & Bloch-Zupan, A. (2019). Protocol GenoDENT: Implementation of a New NGS Panel for Molecular Diagnosis of Genetic Disorders with Orodental Involvement. In P. Papagerakis (Ed.), *Odontogenesis: Methods and Protocols* (pp. 407–452). Springer. https://doi.org/10.1007/978-1-4939-9012-2_36
57. Ricca, C., Aillon, A., Bergandi, L., Alotto, D., Castagnoli, C., & Silvagno, F. (2018). Vitamin D Receptor Is Necessary for Mitochondrial Function and Cell Health. *International Journal of Molecular Sciences*, *19*(6), 1672. https://doi.org/10.3390/ijms19061672
58. Ryan, Z. C., Craig, T. A., Filoteo, A. G., Westendorf, J. J., Cartwright, E. J., Neyses, L., Strehler, E. E., & Kumar, R. (2015). Deletion of the Intestinal Plasma Membrane Calcium Pump, Isoform 1, Atp2b1, in Mice is Associated with Decreased Bone Mineral Density and Impaired Responsiveness to 1, 25-Dihydroxyvitamin D3. *Biochemical and Biophysical Research Communications*, *467*(1), 152–156. https://doi.org/10.1016/j.bbrc.2015.09.087
59. Seppala, M., Fraser, G. J., Birjandi, A. A., Xavier, G. M., & Cobourne, M. T. (2017). Sonic Hedgehog Signaling and Development of the Dentition. *Journal of Developmental Biology*, *5*(2), 6. https://doi.org/10.3390/jdb5020006
60. Shahi, M. H., Afzal, M., Sinha, S., Eberhart, C. G., Rey, J. A., Fan, X., & Castresana, J. S. (2010). Regulation of sonic hedgehog-GLI1 downstream target genes PTCH1, Cyclin D2,

Plakoglobin, PAX6 and NKX2.2 and their epigenetic status in medulloblastoma and astrocytoma. *BMC Cancer*, *10*, 614. https://doi.org/10.1186/1471-2407-10-614

61. Shannon, P., Markiel, A., Ozier, O., Baliga, N. S., Wang, J. T., Ramage, D., Amin, N., Schwikowski, B., & Ideker, T. (2003). Cytoscape: A Software Environment for Integrated Models of Biomolecular Interaction Networks. *Genome Research*, *13*(11), 2498. https://doi.org/10.1101/gr.1239303
62. Sherman, B. T., Hao, M., Qiu, J., Jiao, X., Baseler, M. W., Lane, H. C., Imamichi, T., & Chang, W. (2022). DAVID: A web server for functional enrichment analysis and functional annotation of gene lists (2021 update). *Nucleic Acids Research*, *50*(W1), W216–W221. https://doi.org/10.1093/nar/gkac194
63. Van Cromphaut, S. J., Dewerchin, M., Hoenderop, J. G. J., Stockmans, I., Van Herck, E., Kato, S., Bindels, R. J. M., Collen, D., Carmeliet, P., Bouillon, R., & Carmeliet, G. (2001). Duodenal calcium absorption in vitamin D receptor–knockout mice: Functional and molecular aspects. *Proceedings of the National Academy of Sciences of the United States of America*, *98*(23), 13324–13329. https://doi.org/10.1073/pnas.231474698
64. Wang, R., Liu, W., Guo, H., Ge, S., Huang, H., & Yang, P. (2021). Alveolar ridge preservation with fibroblast growth factor-2 modified acellular dermal matrix membrane and a bovine-derived xenograft: An experimental in vivo study. *Clinical Oral Implants Research*, *32*(7), 808–817. https://doi.org/10.1111/clr.13749
65. Wang, X.-P., Suomalainen, M., Felszeghy, S., Zelarayan, L. C., Alonso, M. T., Plikus, M. V., Maas, R. L., Chuong, C.-M., Schimmang, T., & Thesleff, I. (2007). An Integrated Gene Regulatory Network Controls Stem Cell Proliferation in Teeth. *PLoS Biology*, *5*(6), e159. https://doi.org/10.1371/journal.pbio.0050159
66. Xie, W., Lorenz, S., Dolder, S., & Hofstetter, W. (2016). Extracellular Iron is a Modulator of the Differentiation of Osteoclast Lineage Cells. *Calcified Tissue International*, *98*(3), 275–283. https://doi.org/10.1007/s00223-015-0087-1
67. Yoshizawa, T., Handa, Y., Uematsu, Y., Takeda, S., Sekine, K., Yoshihara, Y., Kawakami, T., Arioka, K., Sato, H., Uchiyama, Y., Masushige, S., Fukamizu, A., Matsumoto, T., & Kato, S. (1997). Mice lacking the vitamin D receptor exhibit impaired bone formation, uterine hypoplasia and growth retardation after weaning. *Nature Genetics*, *16*(4), 4. https://doi.org/10.1038/ng0897-391
68. Zhang, F., Zhang, S., Hu, Y., Wang, N., Wu, L., & Ding, M. (2020). Role of PI3K/AKT Signaling Pathway in Proliferation, Migration and Odontogenic Differentiation of Human Dental Pulp Stem Cells. *Journal of Hard Tissue Biology*, *29*(2), 99–104. https://doi.org/10.2485/jhtb.29.99
69. Zhang, X., Beck, P., Rahemtulla, F., & Thomas, H. F. (2009). Regulation of Enamel and Dentin Mineralization by Vitamin D Receptor. *Comparative Dental Morphology*, *13*, 102–109. https://doi.org/10.1159/000242400
70. Zhang, X., Rahemtulla, F. G., MacDougall, M. J., & Thomas, H. F. (2007). Vitamin D receptor deficiency affects dentin maturation in mice. *Archives of Oral Biology*, *52*(12), 1172–1179. https://doi.org/10.1016/j.archoralbio.2007.06.010
71. Zhang, X., Rahemtulla, F., Zhang, P., Beck, P., & Thomas, H. F. (2009). Different enamel and dentin mineralization observed in VDR deficient mouse model. *Archives of Oral Biology*, *54*(4), 299–305. https://doi.org/10.1016/j.archoralbio.2009.01.002
72. Zhang, X., Rahemtulla, F., Zhang, P., & Thomas, H. F. (2011). VDR deficiency affects alveolar bone and cementum apposition in mice. *Archives of Oral Biology*, *56*(7), 672–677. https://doi.org/10.1016/j.archoralbio.2010.12.004

Figures

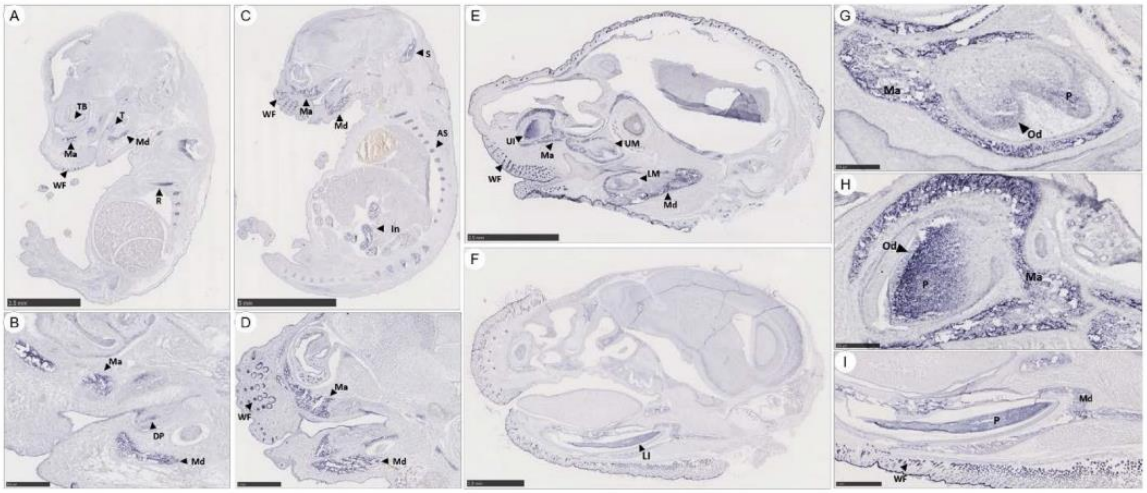

Figure 1. *VDR* expression. (A, B) VDR mRNA at E14.5 is present in whisker follicles (WF), maxillary (Ma) and mandibular (Md) bone development, turbinate bones (TB), tooth development (T), and ribs (R). (C, D) At E16.5, similar expression in bone development is observed, with expression in skull (S), axial skeleton (AS), and intestine (In). At post-natal stages PN1 (E, G, H) and PN7 (F, I), enriched expression is observed in tooth development, specifically in mesenchymal cells from the pulp (P) and odontoblasts (Od). VDR transcripts are also enriched in maxillary (Ma) and mandibular (Md) bone at these stages. UM: upper molar; LM: lower molar; LI: lower incisor.

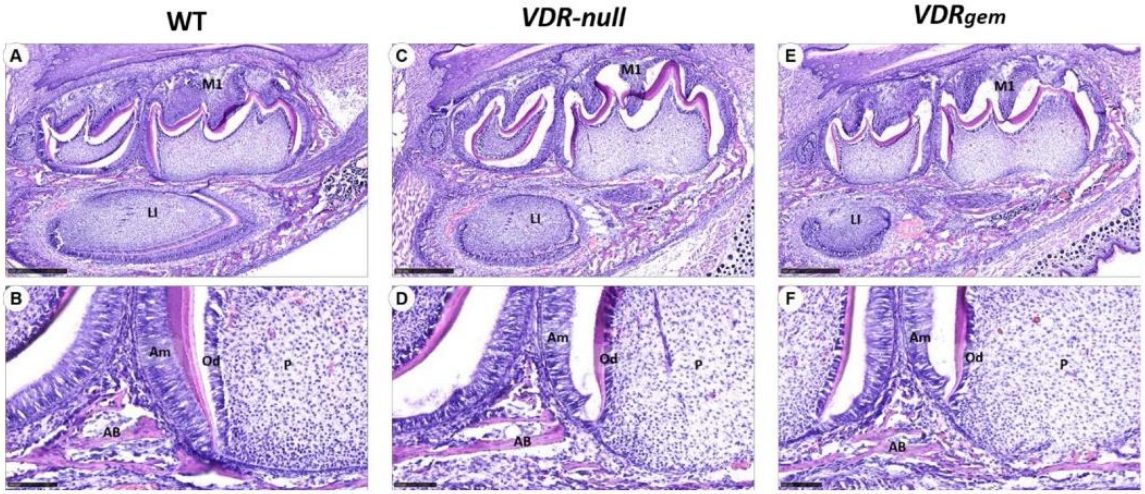

Figure 2. Hematoxylin-eosin staining of postnatal PN5 WT, *VDR-null* and VDR_{gem} mice. Histological analysis in WT (A, B), *VDR-null* (C, D) and VDR_{gem} (E, F) shows no differences in bone or tooth structures between groups. M1: 1st molar; LI: lower incisor; Am: ameloblasts; Od: odontoblasts; P: pulp; AB: alveolar bone

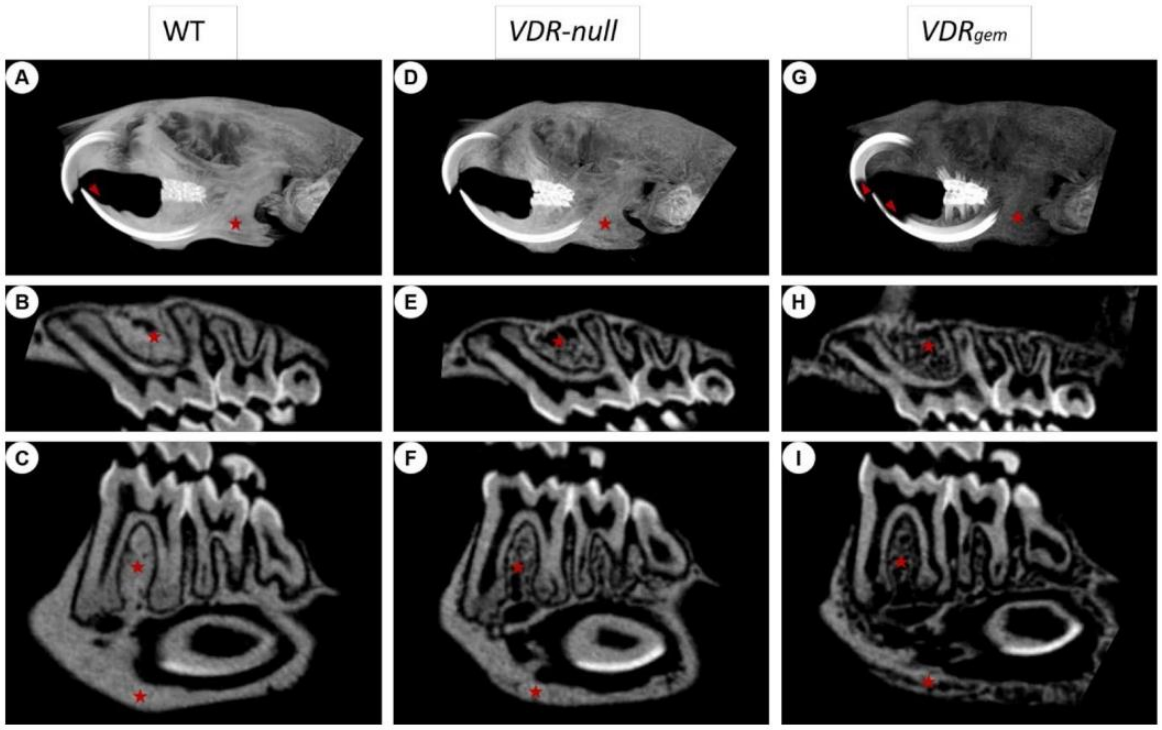

Figure 3. Micro-CT (µCT) imaging of adult WT, *VDR-null* and *VDR$_{gem}$* head and teeth. (A, B, C) Comparison of WT mice, with normal bone density and dental tissues to (D, E, F) *VDR-null* mutants which have a less dense bone with more trabecular space and a thinner dentin; and to (G, H, I) *VDR$_{gem}$* mice showing a more impaired phenotype with no exposed dentin in lower and upper incisors (red arrowheads) and bone with larger trabecular spaces and no cortical (compare ★ marks).

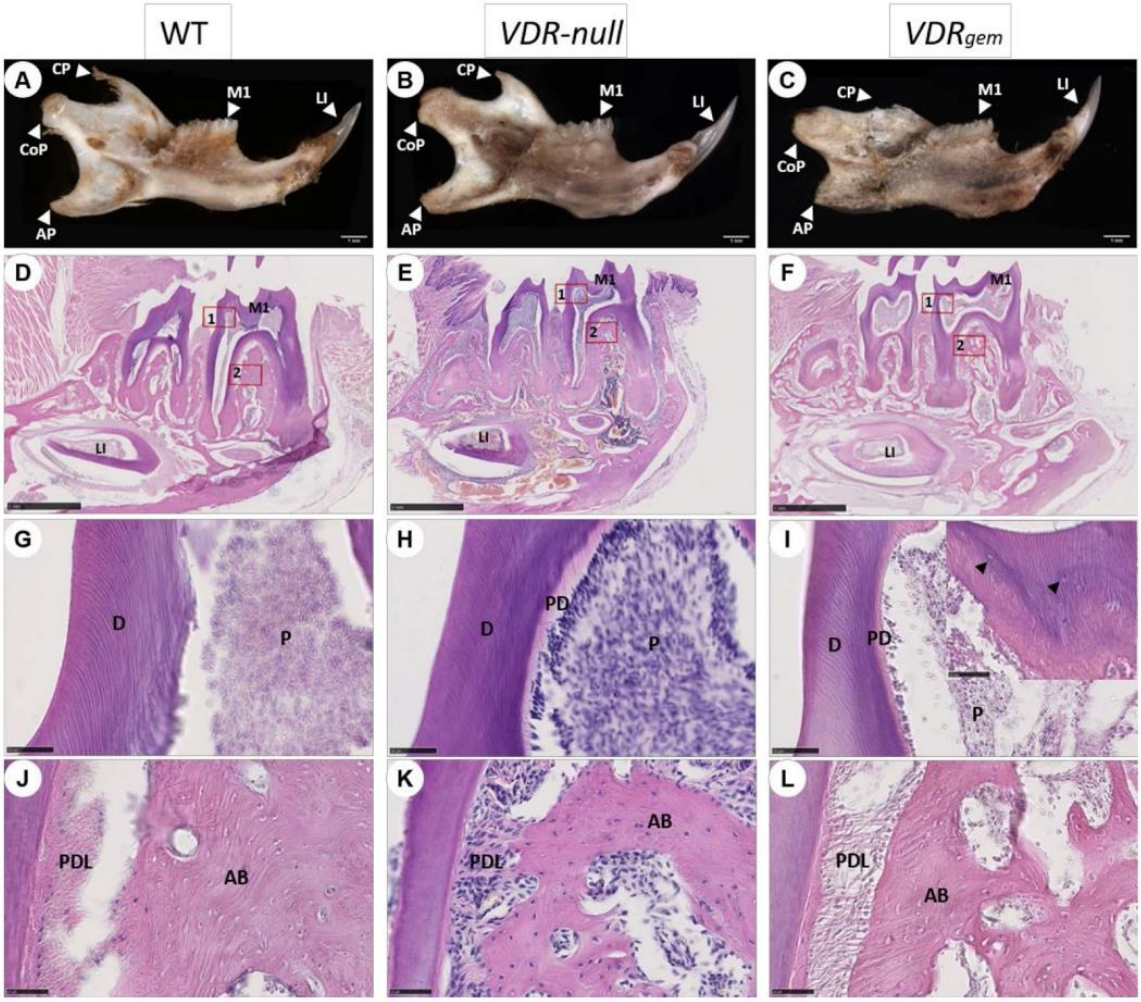

Figure 4. Bone and dental phenotype of adult WT, *VDR-null* and *VDR$_{gem}$* mice after hematoxylin-eosin staining. Gross morphology of adult mandibles in (A) WT, (B) *VDR-null* and (C) *VDR$_{gem}$*. *VDR-null* and *VDR$_{gem}$* bone has a darker appearance lacking cortical bone in *VDR$_{gem}$*. *VDR$_{gem}$* mandible is smaller with angular and condylar processes less defined. Coronoid process was fractured due to the bone fragility. (D-E) Histological features of dentin (box 1) and alveolar bone (box 2). (G-I) High magnification images of box 1 show a thinner dentin with an extended predentin in both mutant models. (I) In *VDR$_{gem}$*, entrapped odontoblasts were visible in dentin (black arrowheads). (J-L) High magnification images of box 2 show alveolar bone reductions with larger trabecular spaces in both mutants with a more pronounced phenotype in *VDR$_{gem}$*. AP: Angular process; CoP: condylar process; CP: coronoid process; M1: 1st molar; LI: lower incisor; D: dentin; PD: predentin; P: pulp; PDL: periodontal ligament; AB: alveolar bone

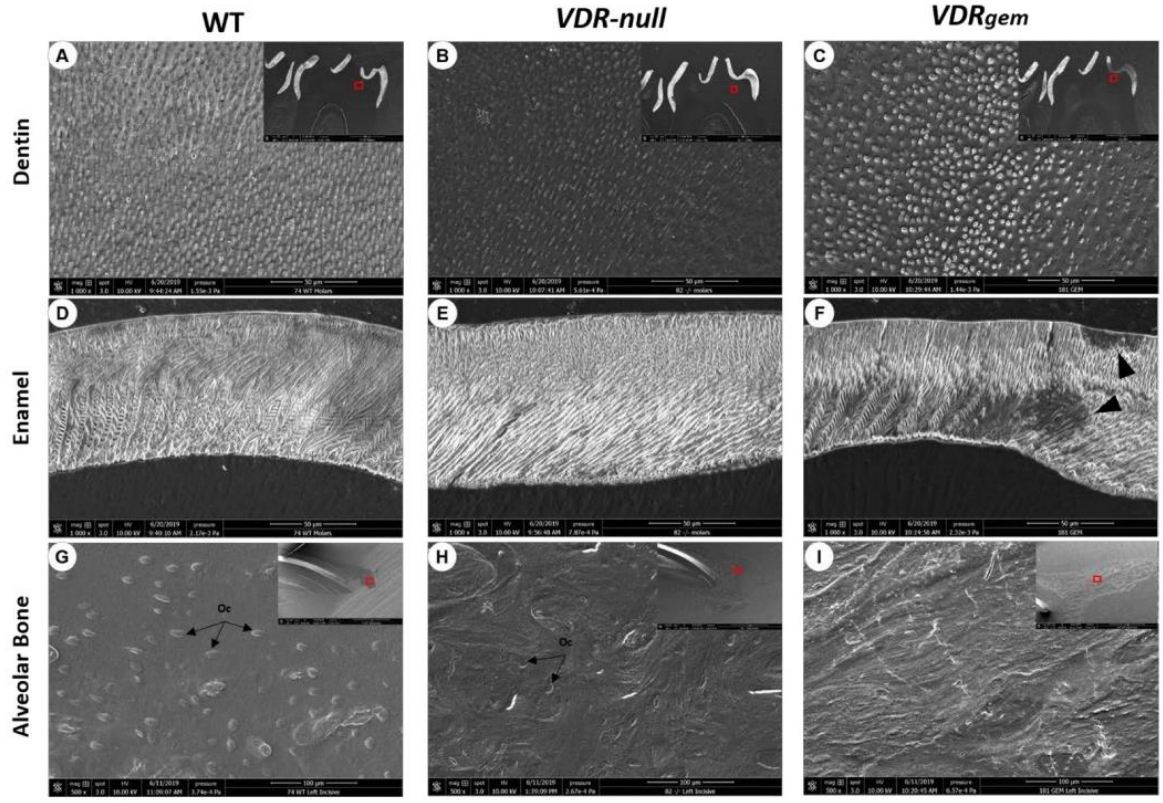

Figure 5. Scanning electron microscopy (SEM) imaging of WT, *VDR-null* and VDR_{gem} teeth and alveolar bone. (A-C) SEM in dentin showed less dentin tubules with an abnormal mineralization pattern in VDR_{gem} mainly affecting the peritubular dentin. (D-F) In enamel, *VDR-null* and VDR_{gem} ultrastructure is altered compared to WT sample with smaller crystal prisms and interprismatic space. (F) In VDR_{gem}, enamel thickness is not constant with a thinner enamel layer in some areas and hypomineralized spots (black arrowheads). Outer prismatic enamel has a more parallel crystal organization. (G-I) Alveolar bone analysis in WT, *VDR-null* and VDR_{gem} shows a highly disorganized bone in both mutants with more impairment in VDR_{gem} mice. Osteocytes (Oc) are diminished in *VDR-null* and VDR_{gem} (H, I) compared to WT (G).

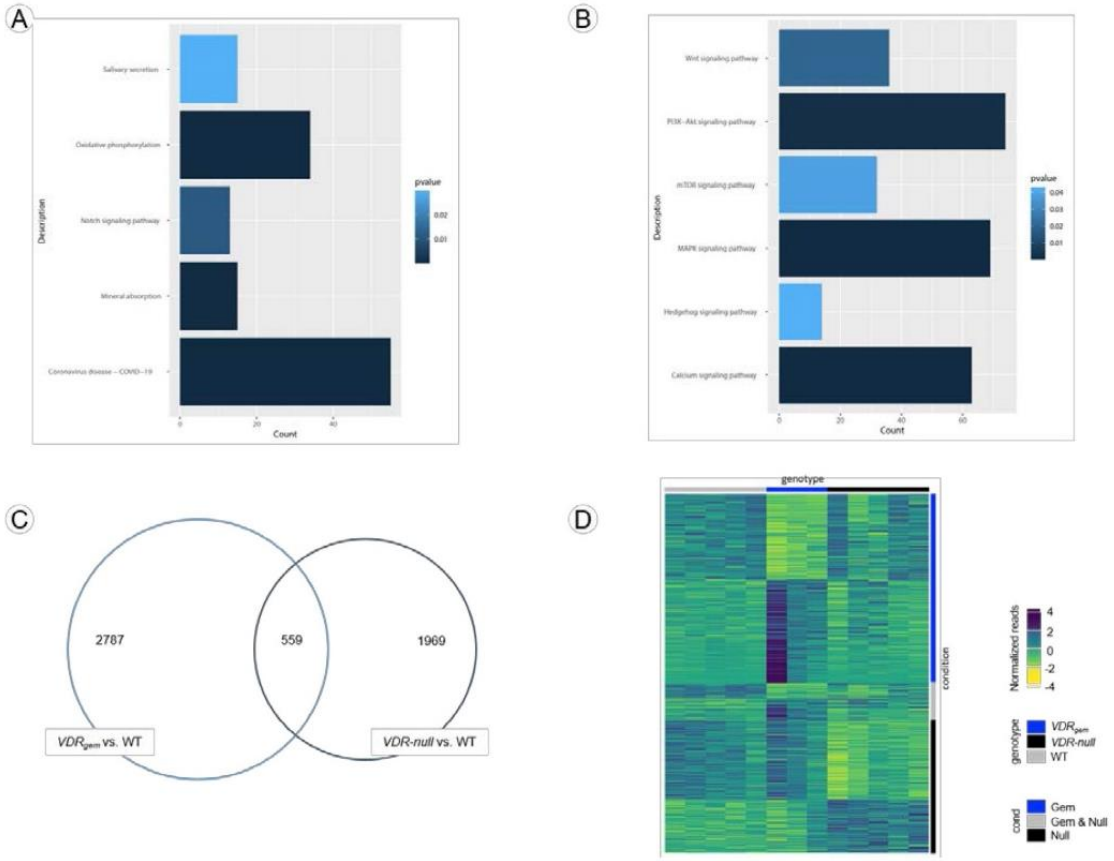

Figure 6. Kyoto Encyclopedia of Genes and Genomes (KEGG) pathway and genes dysregulated in *VDR-null* and *VDR$_{gem}$*. KEGG pathway enrichment analysis for up- and down-regulated genes of (A) *VDR-null* and (B) *VDR$_{gem}$* samples. (C) Venn diagram shows deregulated genes comparing WT with *VDR-null* and *VDR$_{gem}$* samples, 341 genes are dysregulated in both *VDR-null* and *VDR$_{gem}$*. (D) Heatmap shows the difference in pattern expression between groups.

Supplementary material

Impaired vitamin D signaling in *VDR$_{gem}$* mutants reveals novel targets in tooth and alveolar bone

Alexandra Jimenez-Armijo[1], Naji Kharouf[2], Supawich Morkmued[3], Valérie Fraulob[1], Daniel Metzger[1], Karen Niederreither[1], Gilles Laverny[1], Agnès Bloch-Zupan*[1,4,5,6,7]

Affiliations

[1] Université de Strasbourg, Institut de Génétique et de Biologie Moléculaire et Cellulaire (IGBMC), INSERM U1258, CNRS- UMR7104, Illkirch, France.

[2] Université de Strasbourg, Laboratoire de Biomatériaux et Bioingénierie, Inserm UMR_S 1121, Strasbourg, France.

[3] Faculty of Dentistry, Pediatrics Division, Department of Preventive Dentistry, Khon Kaen University, Khon Kaen, Thailand

[4] Université de Strasbourg, Faculté de Chirurgie Dentaire, Strasbourg, France.

[5] Université de Strasbourg, Institut d'études avancées (USIAS), Strasbourg, France.

[6] Hôpitaux Universitaires de Strasbourg (HUS), Pôle de Médecine et Chirurgie Bucco-dentaires, Hôpital Civil, Centre de référence des maladies rares orales et dentaires, O-Rares, Filière Santé Maladies rares TETE COU, European Reference Network ERN CRANIO, Strasbourg, France.

[7] Eastman Dental Institute, University College London, London, United Kingdom.

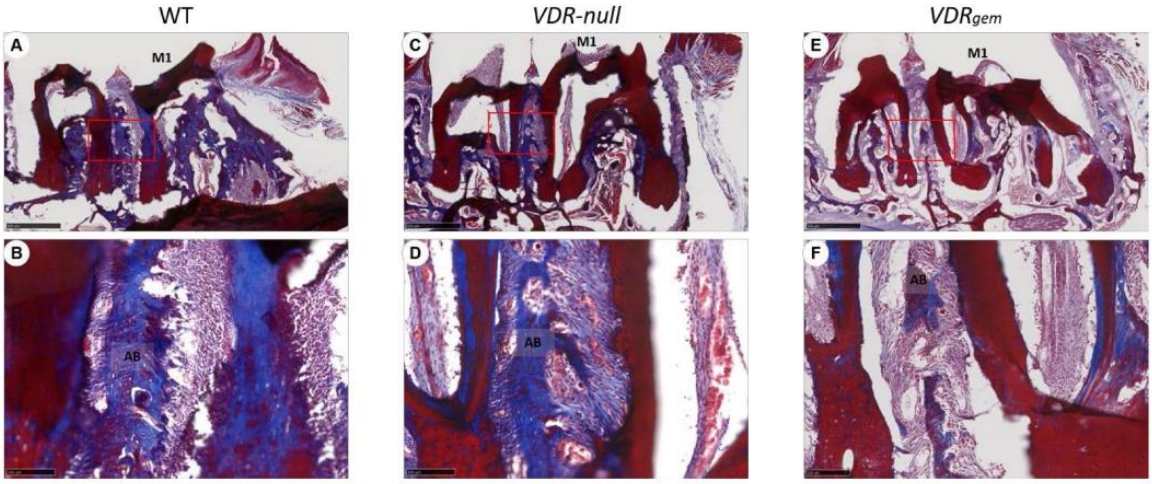

Supplementary Figure S1. Masson's trichrome staining of WT, *VDR-null* and *VDR$_{gem}$* adult alveolar bone. Histological analysis revealed a normal architecture of alveolar bone (Collagen fibers stain blue and mature bone stain red) in WT (A, B) and *VDR-null* (C, D) samples. (D) *VDR-null* alveolar bone has a reduced number of osteocytes and larger trabecular space. (E, F) *VDR$_{gem}$* has an abnormal alveolar bone architecture compared to the control, with very few trabeculae.

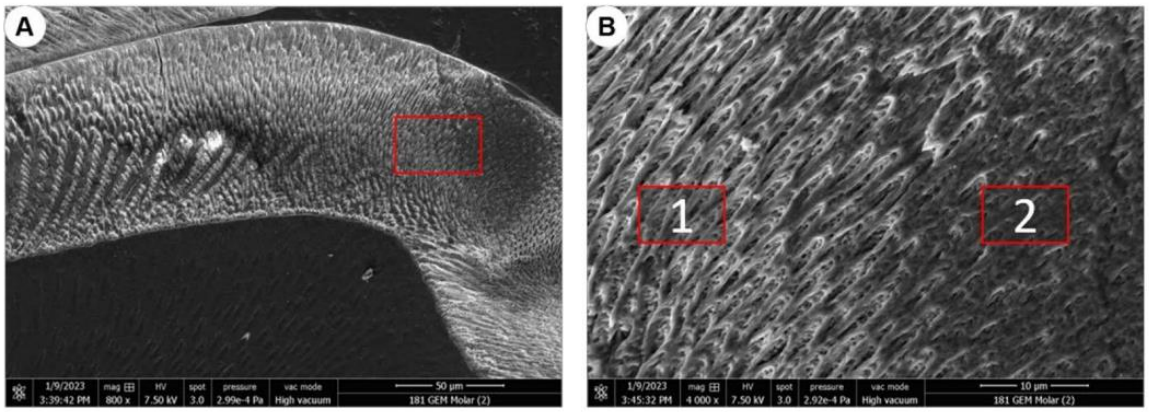

	Calcium mass	Phosphate mass	Ca/P
1	33,41	18,07	1,85
2	26,37	15,65	1,68

Supplementary Figure S2. Scanning electron microscopy (SEM) imaging of *VDR$_{gem}$* enamel and mineral content. (A) *VDR$_{gem}$* enamel show hypomineralized areas. (B) High magnification images of red box from (A) show the difference between a normal enamel (box 1) and a hypomineralized enamel (box 2). Mineral quantification analysis from box 1 and 2 are described in the table below, showing that hypomineralized enamel (box 2) has around 20% less calcium mass, affecting the Ca/P ratio.

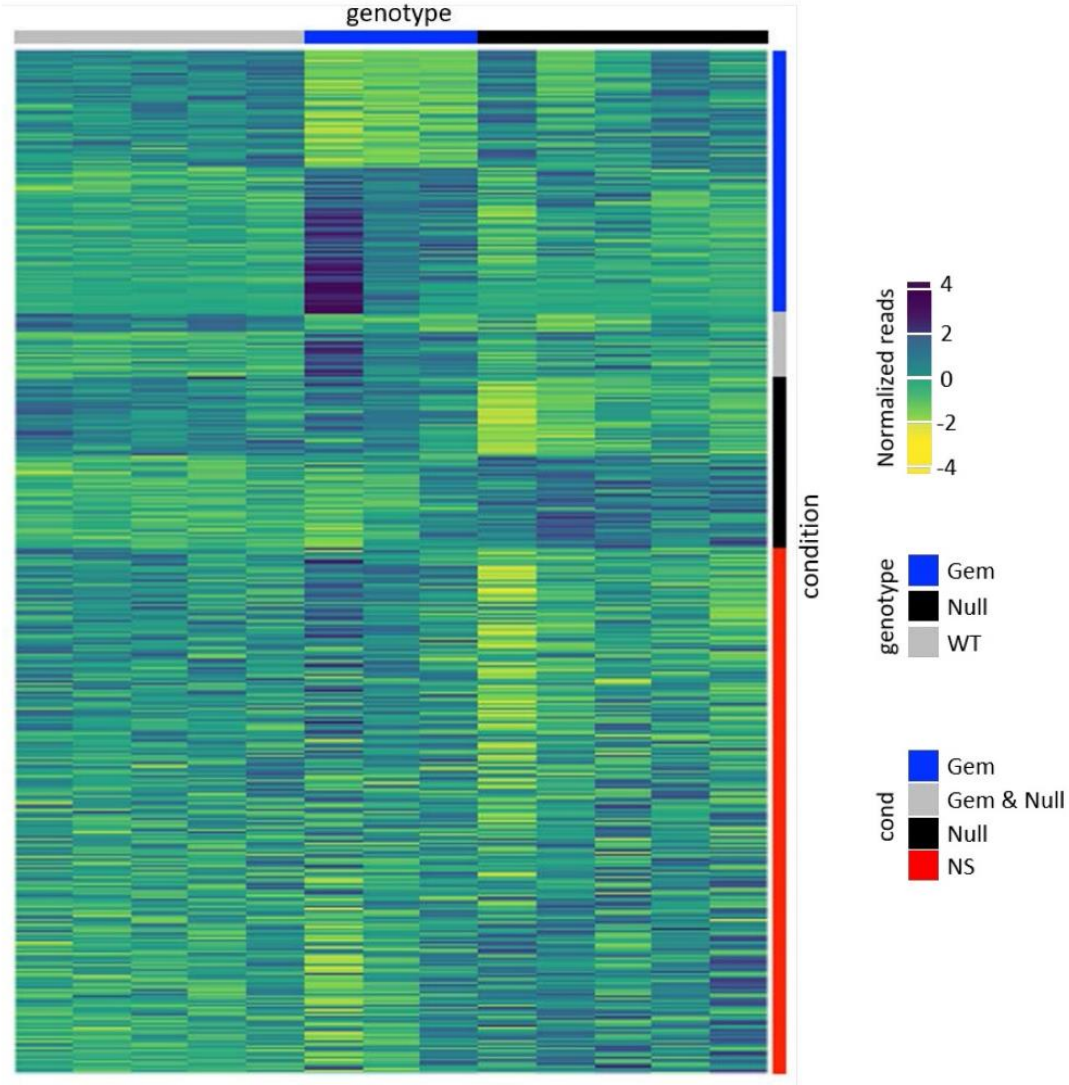

Supplementary Figure S3. Heatmap of tooth development genes and its regulation in different conditions. Heatmap shows a unique pattern expression for each condition. Each column represents a sample, and each row represents a gene as well as the fold change and the q-value associated with the comparison.

Table 1. Energy dispersive X-ray spectrometry (EDX) data for quantification of element composition of enamel, dentin and alveolar bone in WT, *VDR-null* and VDR_{gem} adult mice samples.

Calcium Mass % ± SD			Calcium atomic %			Phosphate atomic %			Ca/P ± SD		
Enamel											
WT	*VDR-null*	VDR_{gem}	WT	*VDR-null*	VDR_{gem}	WT	*VDR-null*	VDR_{gem}	WT	*VDR-null*	VDR_{gem}
37.78 ± 1.5	35.46 ± 1.9	37.35 ± 4.2	23.29	20.88	21.26	13.82	13.11	12.21	1.69 ± 0.07	1.59 ± 0.06	1.83 ± 0.07
Dentin											
WT	*VDR-null*	VDR_{gem}	WT	*VDR-null*	VDR_{gem}	WT	*VDR-null*	VDR_{gem}	WT	*VDR-null*	VDR_{gem}
6.36 ± 2.6	4.66 ± 1.4	2.65 ± 0.7	2.38	1.66	0.96	1.96	1.39	1.13	1.23 ± 0.5	1.45 ± 0.8	0.85 ± 0.08
Alveolar bone											
WT	*VDR-null*	VDR_{gem}	WT	*VDR-null*	VDR_{gem}	WT	*VDR-null*	VDR_{gem}	WT	*VDR-null*	VDR_{gem}
10.30 ± 2.5	5.59 ± 2.9	0.81 ± 0.3	3.93	2.06	0.27	3.19	1.68	0.29	1.22 ± 0.1	1.19 ±0.1	1.22 ± 0.6

Table 2. RNA-seq *VDR-null* vs. WT. Data are presented as log2 fold changes in VDR_{gem} vs. WT samples. For instance, a FC log2 value of −1.00 will correspond to a 50% reduction in mRNA level in the VDR_{gem} samples. Genes encoding regulators of oxidative phosphorylation, mineral absorption, Notch signaling, structural genes or ribosomes (COVID-19) are either reduced or increased in mutant samples.

Gene name	Description	Log2 FC	P-value
	Oxidative phosphorylation		
Uqcrq	ubiquinol-cytochrome c reductase. complex III subunit VII	-0.75	2.34E-05
Uqcr11	ubiquinol-cytochrome c reductase. complex III subunit XI	-0.71	1.83E-05
Uqcr10	ubiquinol-cytochrome c reductase. complex III subunit X	-0.62	4.57E-06
Ndufb7	NADH:ubiquinone oxidoreductase subunit B7	-0.58	1.74E-04
Atp6v0c	ATPase. H+ transporting. lysosomal V0 subunit C	-0.56	9.76E-04
Cox5b	cytochrome c oxidase subunit 5B	-0.51	1.20E-04
Ndufs7	NADH:ubiquinone oxidoreductase core subunit S7	-0.51	1.19E-03
Ndufa7	NADH:ubiquinone oxidoreductase subunit A7	-0.49	3.75E-05
Atp5e	ATP synthase. H+ transporting. mitochondrial F1 complex. epsilon subunit	-0.49	2.66E-06
Atp5d	ATP synthase. H+ transporting. mitochondrial F1 complex. delta subunit	-0.48	2.07E-04
Cox6b2	cytochrome c oxidase subunit 6B2	-0.47	1.68E-05
Ndufa2	NADH:ubiquinone oxidoreductase subunit A2	-0.46	6.00E-04
Ndufa13	NADH:ubiquinone oxidoreductase subunit A13	-0.46	1.34E-03
Ndufb6	NADH:ubiquinone oxidoreductase subunit B6	-0.44	1.68E-05
Cox6a1	cytochrome c oxidase subunit 6A1	-0.42	2.92E-03

Ndufc2	NADH:ubiquinone oxidoreductase subunit C2	-0.39	4.63E-03
Ndufs8	NADH:ubiquinone oxidoreductase core subunit S8	-0.37	7.41E-04
Atp6v1g1	ATPase. H+ transporting. lysosomal V1 subunit G1	-0.37	1.02E-02
Ndufs6	NADH:ubiquinone oxidoreductase core subunit S6	-0.35	2.82E-03
Ndufa11	NADH:ubiquinone oxidoreductase subunit A11	-0.35	3.24E-03
Ndufb10	NADH:ubiquinone oxidoreductase subunit B10	-0.33	4.37E-04
Cox17	cytochrome c oxidase assembly protein 17. copper chaperone	-0.33	3.70E-02
Ndufa8	NADH:ubiquinone oxidoreductase subunit A8	-0.29	3.14E-04
Ndufb11	NADH:ubiquinone oxidoreductase subunit B11	-0.29	7.32E-03
Atp6v1f	ATPase. H+ transporting. lysosomal V1 subunit F	-0.27	2.74E-02
Cox8a	cytochrome c oxidase subunit 8A	-0.27	2.07E-02
Ndufb8	NADH:ubiquinone oxidoreductase subunit B8	-0.26	8.32E-03
Ndufab1	NADH:ubiquinone oxidoreductase subunit AB1	0.27	3.04E-02
Atp5g1	ATP synthase. H+ transporting. mitochondrial F0 complex. subunit C1 (subunit 9)	0.31	5.21E-03
Cycs	cytochrome c. somatic	0.42	3.48E-02
Atp5g2	ATP synthase. H+ transporting. mitochondrial F0 complex. subunit C2 (subunit 9)	0.71	3.64E-04
	Mineral absorption		
Mt1	metallothionein 1	-0.66	1.37E-03
Fxyd2	FXYD domain-containing ion transport regulator 2	-0.64	9.85E-05
Mt2	metallothionein 2	-0.63	2.05E-02
Fth1	ferritin heavy polypeptide 1	-0.50	1.11E-04
Ftl1	ferritin light polypeptide 1	-0.40	3.94E-04
Atp1a3	ATPase. Na+/K+ transporting. alpha 3 polypeptide	-0.39	3.27E-02
Atox1	antioxidant 1 copper chaperone	-0.27	1.36E-02
Atp2b1	ATPase. Ca++ transporting. plasma membrane 1	0.27	2.56E-02
Atp1b3	ATPase. Na+/K+ transporting. beta 3 polypeptide	0.28	8.94E-03
Trpm7	transient receptor potential cation channel. subfamily M. member 7	0.31	2.23E-02
Atp1b2	ATPase. Na+/K+ transporting. beta 2 polypeptide	0.36	1.62E-02
Slc40a1	solute carrier family 40 (iron-regulated transporter). member 1	0.55	3.28E-04
Atp1a2	ATPase. Na+/K+ transporting. alpha 2 polypeptide	0.55	1.69E-02
Slc9a3	solute carrier family 9 (sodium/hydrogen exchanger). member 3	0.67	2.32E-02
	Notch signaling pathway		
Ncor2	nuclear receptor co-repressor 2	-0.63	5.01E-05
Tle2	transducin-like enhancer of split 2	-0.61	4.01E-04
Jag2	jagged 2	-0.50	1.21E-03
Dtx1	deltex 1. E3 ubiquitin ligase	-0.41	2.77E-02
Rbpjl	recombination signal binding protein for immunoglobulin kappa J region-like	-0.40	2.07E-02
Dtx3	deltex 3. E3 ubiquitin ligase	-0.34	5.49E-04
Numbl	numb-like	-0.34	7.24E-03
Dvl2	dishevelled segment polarity protein 2	-0.33	4.86E-03
Ctbp1	C-terminal binding protein 1	-0.30	3.09E-03
Dvl1	dishevelled segment polarity protein 1	-0.30	2.57E-02

Spen	spen family transcription repressor	-0.28	1.75E-02
Notch3	notch 3	-0.26	4.41E-02
Rbpj	recombination signal binding protein for immunoglobulin kappa J region	0.29	8.51E-03
	Structural genes		
Krt8	keratin 8	-0.84	1.41E-04
Krt18	keratin 18	-0.78	8.34E-03
Krt71	keratin 71	-0.67	1.50E-02
Krt82	keratin 82	-0.55	4.92E-02
Krt8-ps	keratin 8. pseudogene	0.40	4.97E-02
Krtap24-1	keratin associated protein 24-1	0.57	4.57E-02
	Coronavirus disease – COVID-19		
Rpl36	ribosomal protein L36	-1.34	4.00E-10
Il12a	interleukin 12a	-0.96	1.10E-03
Rps7	ribosomal protein S7	-0.92	5.00E-07
Rplp1	ribosomal protein. large. P1	-0.89	5.80E-05
Rplp2	ribosomal protein. large P2	-0.84	1.10E-06
Rpl38	ribosomal protein L38	-0.8	1.90E-03
Rpl29	ribosomal protein L29	-0.71	2.90E-04
Rps21	ribosomal protein S21	-0.63	5.10E-05
Rpl27	ribosomal protein L27	-0.55	2.70E-03
Rps2	ribosomal protein S2	-0.54	1.50E-06
Fau	Finkel-Biskis-Reilly murine sarcoma virus (FBR-MuSV) ubiquitously expressed (fox derived)	-0.53	9.40E-03
Rpl28	ribosomal protein L28	-0.52	9.60E-04
Rpl35	ribosomal protein L35	-0.5	9.20E-03
Rps19	ribosomal protein S19	-0.49	2.00E-03
Rps25	ribosomal protein S25	-0.48	8.90E-03
Rps15	ribosomal protein S15	-0.48	4.20E-04
Pik3r2	phosphoinositide-3-kinase regulatory subunit 2	-0.47	2.20E-04
Nfkbib	nuclear factor of kappa light polypeptide gene enhancer in B cells inhibitor. beta	-0.46	4.20E-03
Rps9	ribosomal protein S9	-0.45	1.30E-04
Rps10	ribosomal protein S10	-0.43	2.20E-02
Rpl8	ribosomal protein L8	-0.43	1.10E-03
Rpl18a	ribosomal protein L18A	-0.42	1.20E-04
Rps5	ribosomal protein S5	-0.42	1.70E-03
Ace	angiotensin I converting enzyme (peptidyl-dipeptidase A) 1	-0.41	9.60E-04
Mapk13	mitogen-activated protein kinase 13	-0.4	1.80E-02
Rpl7a	ribosomal protein L7A	-0.39	3.60E-03
Rpl39	ribosomal protein L39	-0.39	7.20E-03
Rpl37a	ribosomal protein L37a	-0.38	8.10E-03
Rplp0	ribosomal protein. large. P0	-0.38	4.80E-03
Rpl37	ribosomal protein L37	-0.37	2.20E-03
Rpl6	ribosomal protein L6	-0.36	8.70E-04

C8b	complement component 8. beta polypeptide	-0.36	4.60E-02
Rps8	ribosomal protein S8	-0.35	4.40E-03
Rpl41	ribosomal protein L41	-0.34	3.80E-02
Rpl18	ribosomal protein L18	-0.33	1.80E-03
Rpl32	ribosomal protein L32	-0.31	1.60E-02
Rps14	ribosomal protein S14	-0.31	4.40E-03
Rpl10a	ribosomal protein L10A	-0.31	1.10E-02
Rps11	ribosomal protein S11	-0.3	3.70E-03
Fcgr3	Fc receptor. IgG. low affinity III	0.37	1.70E-02
Cybb	cytochrome b-245. beta polypeptide	0.38	1.80E-02
Pik3r3	phosphoinositide-3-kinase regulatory subunit 3	0.38	3.20E-03
Tlr3	toll-like receptor 3	0.42	1.20E-02
F13a1	coagulation factor XIII. A1 subunit	0.42	6.90E-03
Rpl37rt	ribosomal protein L37. retrotransposed	0.45	2.10E-04
Oas1a	2'-5' oligoadenylate synthetase 1A	0.47	1.40E-02
Agtr1a	angiotensin II receptor. type 1a	0.49	1.00E-04
Tlr8	toll-like receptor 8	0.59	1.80E-02
C3ar1	complement component 3a receptor 1	0.63	1.90E-05
C8a	complement component 8. alpha polypeptide	0.67	1.00E-02
Rpl3l	ribosomal protein L3-like	0.69	1.80E-02
Gm15501	predicted pseudogene 15501	0.73	1.20E-06
Tlr7	toll-like receptor 7	0.81	5.90E-05
Il2	interleukin 2	0.84	3.70E-03
Rps27rt	ribosomal protein S27. retrogene	0.95	1.40E-09

Table 3. RNA-seq *VDR_{gem}* vs. WT. Data are presented as log2 fold changes in *VDR_{gem}* vs. WT samples. For instance, a FC log2 value of −1.00 will correspond to a 50% reduction in mRNA level in the *VDR_{gem}* samples. Genes encoding regulators of calcium signaling, MAPK, PI3K-Akt, Wnt, mTOR and Hedgehog signaling, are either reduced or increased in mutant samples.

Gene name	Description	Log2 FC	p-value
	Calcium signaling pathway		
Fgf3	fibroblast growth factor 3	-1.69	2.39E-09
Fgf10	fibroblast growth factor 10	-1.16	2.92E-05
Camk4	calcium/calmodulin-dependent protein kinase IV	-1.02	2.46E-05
Egf	epidermal growth factor	-0.72	3.51E-04
Gnal	guanine nucleotide binding protein. alpha stimulating. olfactory type	-0.71	1.35E-03
Grin2b	glutamate receptor. ionotropic. NMDA2B (epsilon 2)	-0.62	3.68E-03
Camk1g	calcium/calmodulin-dependent protein kinase I gamma	-0.59	3.62E-05
Prkcb	protein kinase C. beta	-0.55	2.99E-03
Cacna1h	calcium channel. voltage-dependent. T type. alpha 1H subunit	-0.47	4.14E-02
Fgf9	fibroblast growth factor 9	-0.44	2.38E-02
Cacna1d	calcium channel. voltage-dependent. L type. alpha 1D subunit	-0.41	1.45E-02
Slc8a2	solute carrier family 8 (sodium/calcium exchanger). member 2	-0.33	3.72E-02
P2rx4	purinergic receptor P2X. ligand-gated ion channel 4	0.27	7.85E-03

Pdgfrb	platelet derived growth factor receptor. beta polypeptide	0.30	5.39E-03
Cacna1a	calcium channel. voltage-dependent. P/Q type. alpha 1A subunit	0.30	1.36E-02
Itpkb	inositol 1.4.5-trisphosphate 3-kinase B	0.30	5.54E-04
Slc8a1	solute carrier family 8 (sodium/calcium exchanger). member 1	0.31	1.89E-02
Adcy4	adenylate cyclase 4	0.33	6.80E-03
Sphk1	sphingosine kinase 1	0.34	2.47E-02
Slc8a3	solute carrier family 8 (sodium/calcium exchanger). member 3	0.38	4.39E-02
Nfatc1	nuclear factor of activated T cells. cytoplasmic. calcineurin dependent 1	0.38	9.91E-03
Orai1	ORAI calcium release-activated calcium modulator 1	0.40	4.10E-02
Met	met proto-oncogene	0.41	1.26E-02
Tgfa	transforming growth factor alpha	0.41	2.32E-02
Chrna7	cholinergic receptor. nicotinic. alpha polypeptide 7	0.41	3.12E-02
Atp2a3	ATPase. Ca++ transporting. ubiquitous	0.42	1.20E-02
Atp2b4	ATPase. Ca++ transporting. plasma membrane 4	0.43	2.80E-03
Ptger3	prostaglandin E receptor 3 (subtype EP3)	0.45	3.51E-03
Plcg2	phospholipase C. gamma 2	0.45	4.01E-04
Stim2	stromal interaction molecule 2	0.45	3.22E-04
Tacr1	tachykinin receptor 1	0.46	1.75E-02
Adcy7	adenylate cyclase 7	0.47	3.07E-04
P2rx6	purinergic receptor P2X. ligand-gated ion channel. 6	0.48	1.89E-03
Ptk2b	PTK2 protein tyrosine kinase 2 beta	0.50	4.31E-03
Pdgfb	platelet derived growth factor. B polypeptide	0.50	2.55E-03
Mylk	myosin. light polypeptide kinase	0.52	2.01E-04
Tfeb	transcription factor EB	0.53	9.91E-03
Hrc	histidine rich calcium binding protein	0.53	4.54E-02
Bdkrb2	bradykinin receptor. beta 2	0.54	1.27E-03
Itpr2	inositol 1.4.5-triphosphate receptor 2	0.56	1.45E-04
Pde1b	phosphodiesterase 1B. Ca2+-calmodulin dependent	0.56	4.56E-04
Tnnc1	troponin C. cardiac/slow skeletal	0.59	4.27E-02
Erbb3	erb-b2 receptor tyrosine kinase 3	0.60	4.32E-03
Tbxa2r	thromboxane A2 receptor	0.61	3.89E-03
Mst1r	macrophage stimulating 1 receptor (c-met-related tyrosine kinase)	0.69	1.49E-03
Mst1	macrophage stimulating 1 (hepatocyte growth factor-like)	0.69	1.85E-02
Casq2	calsequestrin 2	0.70	1.11E-02
Ltb4r2	leukotriene B4 receptor 2	0.72	4.18E-03
Adora2b	adenosine A2b receptor	0.73	6.64E-03
Ptgfr	prostaglandin F receptor	0.75	2.06E-07
Fgf18	fibroblast growth factor 18	0.76	7.73E-03
Egfr	epidermal growth factor receptor	0.77	2.53E-06
Agtr1a	angiotensin II receptor. type 1a	0.78	1.24E-08
Ptger1	prostaglandin E receptor 1 (subtype EP1)	0.80	2.00E-05
Itpkc	inositol 1.4.5-trisphosphate 3-kinase C	0.81	6.00E-04
P2rx2	purinergic receptor P2X. ligand-gated ion channel. 2	0.82	9.64E-04
Gna15	guanine nucleotide binding protein. alpha 15	0.95	8.86E-05
Fgf7	fibroblast growth factor 7	0.99	2.20E-05
Adrb2	adrenergic receptor. beta 2	1.13	1.45E-06

Calm4	calmodulin 4	1.17	2.15E-07
Oxtr	oxytocin receptor	1.25	5.55E-06
Calml3	calmodulin-like 3	1.56	1.83E-09
	MAPK signaling pathway		
Fgf3	fibroblast growth factor 3	-1.69	2.39E-09
Fgf10	fibroblast growth factor 10	-1.16	2.92E-05
Cacnb2	calcium channel. voltage-dependent. beta 2 subunit	-1.05	8.81E-06
Dusp9	dual specificity phosphatase 9	-0.89	7.98E-05
Cacna2d2	calcium channel. voltage-dependent. alpha 2/delta subunit 2	-0.77	5.37E-04
Stmn1	stathmin 1	-0.74	4.35E-07
Egf	epidermal growth factor	-0.72	3.51E-04
Ngfr	nerve growth factor receptor (TNFR superfamily. member 16)	-0.68	1.00E-04
Angpt1	angiopoietin 1	-0.64	9.79E-04
Map3k13	mitogen-activated protein kinase kinase kinase 13	-0.59	1.66E-03
Arrb1	arrestin. beta 1	-0.57	5.24E-06
Pla2g4b	phospholipase A2. group IVB (cytosolic)	-0.57	2.09E-02
Rasgrf2	RAS protein-specific guanine nucleotide-releasing factor 2	-0.55	6.22E-03
Prkcb	protein kinase C. beta	-0.55	2.99E-03
Cacna1h	calcium channel. voltage-dependent. T type. alpha 1H subunit	-0.47	4.14E-02
Fgf9	fibroblast growth factor 9	-0.44	2.38E-02
Map4k1	mitogen-activated protein kinase kinase kinase kinase 1	-0.41	3.16E-02
Rasa2	RAS p21 protein activator 2	-0.41	4.75E-03
Cacna1d	calcium channel. voltage-dependent. L type. alpha 1D subunit	-0.41	1.45E-02
Tab1	TGF-beta activated kinase 1/MAP3K7 binding protein 1	-0.36	1.21E-03
Map3k5	mitogen-activated protein kinase kinase kinase 5	-0.34	4.00E-02
Dusp5	dual specificity phosphatase 5	-0.33	2.80E-02
Traf2	TNF receptor-associated factor 2	-0.28	5.26E-04
Dusp3	dual specificity phosphatase 3 (vaccinia virus phosphatase VH1-related)	0.26	1.70E-02
Efna1	ephrin A1	0.27	3.19E-02
Il1rap	interleukin 1 receptor accessory protein	0.28	2.30E-02
Cacna2d3	calcium channel. voltage-dependent. alpha2/delta subunit 3	0.28	6.21E-03
Map4k3	mitogen-activated protein kinase kinase kinase kinase 3	0.28	1.42E-03
Tnfrsf1a	tumor necrosis factor receptor superfamily. member 1a	0.29	7.14E-03
Pdgfrb	platelet derived growth factor receptor. beta polypeptide	0.30	5.39E-03
Cacna1a	calcium channel. voltage-dependent. P/Q type. alpha 1A subunit	0.30	1.36E-02
Relb	avian reticuloendotheliosis viral (v-rel) oncogene related B	0.30	2.50E-02
Igf2	insulin-like growth factor 2	0.34	3.67E-02
Rras2	related RAS viral (r-ras) oncogene 2	0.35	2.78E-02
Dusp16	dual specificity phosphatase 16	0.35	3.22E-02
Cd14	CD14 antigen	0.36	3.54E-02
Nfatc1	nuclear factor of activated T cells. cytoplasmic. calcineurin dependent 1	0.38	9.91E-03
Gadd45b	growth arrest and DNA-damage-inducible 45 beta	0.39	9.76E-03
Dusp8	dual specificity phosphatase 8	0.39	3.01E-02
Met	met proto-oncogene	0.41	1.26E-02

Tgfa	transforming growth factor alpha	0.41	2.32E-02
Mapk12	mitogen-activated protein kinase 12	0.46	5.44E-03
Nr4a1	nuclear receptor subfamily 4. group A. member 1	0.48	1.20E-02
Pdgfb	platelet derived growth factor. B polypeptide	0.50	2.55E-03
Mapk13	mitogen-activated protein kinase 13	0.53	4.73E-03
Dusp10	dual specificity phosphatase 10	0.54	1.34E-03
Mapkapk3	mitogen-activated protein kinase-activated protein kinase 3	0.56	8.49E-05
Jun	jun proto-oncogene	0.57	4.56E-03
Map3k6	mitogen-activated protein kinase kinase kinase 6	0.58	6.34E-03
Erbb3	erb-b2 receptor tyrosine kinase 3	0.60	4.32E-03
Rras	related RAS viral (r-ras) oncogene	0.61	2.32E-04
Jund	jun D proto-oncogene	0.64	5.54E-03
Artn	artemin	0.64	3.29E-03
Dusp2	dual specificity phosphatase 2	0.69	2.75E-03
Flnc	filamin C. gamma	0.70	2.23E-05
Cacng5	calcium channel. voltage-dependent. gamma subunit 5	0.71	3.17E-03
Fgf18	fibroblast growth factor 18	0.76	7.73E-03
Egfr	epidermal growth factor receptor	0.77	2.53E-06
Il1b	interleukin 1 beta	0.83	4.46E-03
Dusp1	dual specificity phosphatase 1	0.86	1.01E-05
Flt3l	FMS-like tyrosine kinase 3 ligand	0.94	1.01E-05
Fgf7	fibroblast growth factor 7	0.99	2.20E-05
Hspb1	heat shock protein 1	1.02	4.90E-04
Rasgrp1	RAS guanyl releasing protein 1	1.10	9.35E-06
Efna3	ephrin A3	1.11	1.45E-06
Pla2g4f	phospholipase A2. group IVF	1.12	3.40E-05
Hspa1a	heat shock protein 1A	1.33	1.35E-07
Hspa1b	heat shock protein 1B	1.45	1.59E-07
Fos	FBJ osteosarcoma oncogene	1.51	4.99E-09
	PI3K-Akt signaling pathway		
Fgf3	fibroblast growth factor 3	-1.69	2.39E-09
Fgf10	fibroblast growth factor 10	-1.16	2.92E-05
Ccnd1	cyclin D1	-0.86	7.41E-07
Brca1	breast cancer 1. early onset	-0.74	1.21E-04
Egf	epidermal growth factor	-0.72	3.51E-04
Ccne2	cyclin E2	-0.72	7.22E-05
Ngfr	nerve growth factor receptor (TNFR superfamily. member 16)	-0.68	1.00E-04
Angpt1	angiopoietin 1	-0.64	9.79E-04
Bcl2	B cell leukemia/lymphoma 2	-0.61	2.55E-06
Itga4	integrin alpha 4	-0.51	1.76E-02
Lama1	laminin. alpha 1	-0.48	2.39E-02
Ccne1	cyclin E1	-0.47	3.98E-03
Fgf9	fibroblast growth factor 9	-0.44	2.38E-02
Sgk3	serum/glucocorticoid regulated kinase 3	-0.42	3.41E-03
Irs1	insulin receptor substrate 1	-0.40	6.66E-03

Tsc1	TSC complex subunit 1	-0.37	6.33E-04
Mlst8	MTOR associated protein. LST8 homolog (S. cerevisiae)	-0.35	7.21E-05
Epor	erythropoietin receptor	-0.35	3.40E-02
Gng7	guanine nucleotide binding protein (G protein). gamma 7	-0.33	1.70E-03
Phlpp2	PH domain and leucine rich repeat protein phosphatase 2	-0.33	1.64E-02
Magi1	membrane associated guanylate kinase. WW and PDZ domain containing 1	-0.29	2.03E-02
Cdk2	cyclin-dependent kinase 2	-0.26	4.49E-03
Lama4	laminin. alpha 4	0.26	1.31E-02
Efna1	ephrin A1	0.27	3.19E-02
Creb3	cAMP responsive element binding protein 3	0.28	3.75E-02
Itga9	integrin alpha 9	0.29	4.60E-03
Itga6	integrin alpha 6	0.29	1.48E-02
Pdgfrb	platelet derived growth factor receptor. beta polypeptide	0.30	5.39E-03
Pten	phosphatase and tensin homolog	0.30	2.40E-02
Jak3	Janus kinase 3	0.30	4.46E-02
Lamc3	laminin gamma 3	0.32	3.99E-02
Itga1	integrin alpha 1	0.32	2.39E-02
Ppp2r3a	protein phosphatase 2. regulatory subunit B''. alpha	0.33	1.59E-03
Col4a2	collagen. type IV. alpha 2	0.33	4.91E-03
Bad	BCL2-associated agonist of cell death	0.33	3.51E-02
Itga8	integrin alpha 8	0.33	1.02E-02
Igf2	insulin-like growth factor 2	0.34	3.67E-02
Il4ra	interleukin 4 receptor. alpha	0.36	3.05E-02
Col4a1	collagen. type IV. alpha 1	0.37	2.59E-03
Eif4ebp1	eukaryotic translation initiation factor 4E binding protein 1	0.37	2.51E-02
Thbs2	thrombospondin 2	0.38	1.17E-02
Itga11	integrin alpha 11	0.40	9.34E-04
Met	met proto-oncogene	0.41	1.26E-02
Tgfa	transforming growth factor alpha	0.41	2.32E-02
Col6a1	collagen. type VI. alpha 1	0.46	3.77E-05
Col6a2	collagen. type VI. alpha 2	0.46	4.88E-04
Osmr	oncostatin M receptor	0.46	6.43E-03
Nr4a1	nuclear receptor subfamily 4. group A. member 1	0.48	1.20E-02
Ppp2r5b	protein phosphatase 2. regulatory subunit B'. beta	0.48	9.68E-04
Pdgfb	platelet derived growth factor. B polypeptide	0.50	2.55E-03
Spp1	secreted phosphoprotein 1	0.53	2.69E-02
Tnn	tenascin N	0.53	1.79E-03
Itgb5	integrin beta 5	0.55	3.23E-05
Col1a2	collagen. type I. alpha 2	0.56	1.63E-03
Il6ra	interleukin 6 receptor. alpha	0.56	1.55E-03
Comp	cartilage oligomeric matrix protein	0.59	2.70E-02
Prkaa2	protein kinase. AMP-activated. alpha 2 catalytic subunit	0.60	4.36E-03
Erbb3	erb-b2 receptor tyrosine kinase 3	0.60	4.32E-03
Reln	reelin	0.61	3.09E-04
Sgk1	serum/glucocorticoid regulated kinase 1	0.62	9.18E-07
Ibsp	integrin binding sialoprotein	0.64	8.79E-04

Col2a1	collagen. type II. alpha 1	0.67	2.19E-02
Itgb3	integrin beta 3	0.67	1.15E-04
Thbs3	thrombospondin 3	0.70	4.52E-07
Itga7	integrin alpha 7	0.71	5.61E-05
Fgf18	fibroblast growth factor 18	0.76	7.73E-03
Lpar5	lysophosphatidic acid receptor 5	0.76	9.63E-03
Egfr	epidermal growth factor receptor	0.77	2.53E-06
Flt3l	FMS-like tyrosine kinase 3 ligand	0.94	1.01E-05
Itga2b	integrin alpha 2b	0.96	2.43E-04
Tnxb	tenascin XB	0.98	5.03E-05
Fgf7	fibroblast growth factor 7	0.99	2.20E-05
Efna3	ephrin A3	1.11	1.45E-06
Thbs4	thrombospondin 4	1.17	3.50E-09
	Wnt signaling pathway		
Sfrp5	secreted frizzled-related sequence protein 5	-1.60	5.08E-08
Sfrp2	secreted frizzled-related protein 2	-1.35	2.36E-09
Tcf7	transcription factor 7. T cell specific	-0.90	1.23E-06
Ccnd1	cyclin D1	-0.86	7.41E-07
Rspo1	R-spondin 1	-0.66	9.82E-04
Lef1	lymphoid enhancer binding factor 1	-0.66	3.27E-05
Rspo2	R-spondin 2	-0.65	2.43E-02
Fzd7	frizzled class receptor 7	-0.59	3.83E-08
Axin2	axin 2	-0.58	4.88E-07
Frzb	frizzled-related protein	-0.57	1.75E-03
Prkcb	protein kinase C. beta	-0.55	2.99E-03
Bambi	BMP and activin membrane-bound inhibitor	-0.55	2.64E-06
Notum	notum palmitoleoyl-protein carboxylesterase	-0.53	1.51E-02
Cxxc4	CXXC finger 4	-0.37	3.20E-02
Fzd3	frizzled class receptor 3	-0.35	4.95E-03
Ruvbl1	RuvB-like protein 1	-0.32	1.21E-02
Siah1b	siah E3 ubiquitin protein ligase 1B	-0.31	3.98E-02
Fzd5	frizzled class receptor 5	-0.27	4.94E-02
Tle4	transducin-like enhancer of split 4	0.31	1.61E-02
Wnt11	wingless-type MMTV integration site family. member 11	0.33	4.44E-02
Lgr4	leucine-rich repeat-containing G protein-coupled receptor 4	0.37	7.03E-04
Cer1	cerberus 1. DAN family BMP antagonist	0.37	4.90E-02
Nfatc1	nuclear factor of activated T cells. cytoplasmic. calcineurin dependent 1	0.38	9.91E-03
Daam1	dishevelled associated activator of morphogenesis 1	0.39	4.83E-03
Wnt5b	wingless-type MMTV integration site family. member 5B	0.42	7.36E-03
Sfrp1	secreted frizzled-related protein 1	0.45	2.04E-03
Wnt2b	wingless-type MMTV integration site family. member 2B	0.45	3.12E-02
Tle1	transducin-like enhancer of split 1	0.46	2.19E-04
Sfrp4	secreted frizzled-related protein 4	0.48	1.17E-04
Dkk2	dickkopf WNT signaling pathway inhibitor 2	0.54	2.44E-04
Jun	jun proto-oncogene	0.57	4.56E-03

Wnt16	wingless-type MMTV integration site family. member 16	0.57	2.90E-02
Wnt4	wingless-type MMTV integration site family. member 4	0.61	9.66E-04
Lgr5	leucine rich repeat containing G protein coupled receptor 5	0.67	2.26E-02
Wnt10b	wingless-type MMTV integration site family. member 10B	1.03	2.81E-09
Wnt7b	wingless-type MMTV integration site family. member 7B	1.34	1.05E-07
	mTOR signaling pathway		
Skp2	S-phase kinase-associated protein 2 (p45)	-0.89	1.07E-07
Atp6v1b1	ATPase. H+ transporting. lysosomal V1 subunit B1	-0.67	6.05E-03
Fzd7	frizzled class receptor 7	-0.59	3.83E-08
Prkcb	protein kinase C. beta	-0.55	2.99E-03
Rragd	Ras-related GTP binding D	-0.52	8.15E-03
Irs1	insulin receptor substrate 1	-0.40	6.66E-03
Tsc1	TSC complex subunit 1	-0.37	6.33E-04
Fzd3	frizzled class receptor 3	-0.35	4.95E-03
Mlst8	MTOR associated protein. LST8 homolog (S. cerevisiae)	-0.35	7.21E-05
Lpin1	lipin 1	-0.29	2.93E-02
Prr5l	proline rich 5 like	-0.27	1.46E-02
Fzd5	frizzled class receptor 5	-0.27	4.94E-02
Atp6v1h	ATPase. H+ transporting. lysosomal V1 subunit H	0.28	1.40E-02
Tnfrsf1a	tumor necrosis factor receptor superfamily. member 1a	0.29	7.14E-03
Pten	phosphatase and tensin homolog	0.30	2.40E-02
Atp6v1b2	ATPase. H+ transporting. lysosomal V1 subunit B2	0.30	2.85E-02
Wnt11	wingless-type MMTV integration site family. member 11	0.33	4.44E-02
Atp6v1a	ATPase. H+ transporting. lysosomal V1 subunit A	0.35	3.75E-03
Atp6v1e1	ATPase. H+ transporting. lysosomal V1 subunit E1	0.35	1.45E-02
Eif4ebp1	eukaryotic translation initiation factor 4E binding protein 1	0.37	2.51E-02
Slc3a2	solute carrier family 3 (activators of dibasic and neutral amino acid transport). member 2	0.37	2.85E-03
Wnt5b	wingless-type MMTV integration site family. member 5B	0.42	7.36E-03
Rnf152	ring finger protein 152	0.44	5.40E-03
Wnt2b	wingless-type MMTV integration site family. member 2B	0.45	3.12E-02
Wnt16	wingless-type MMTV integration site family. member 16	0.57	2.90E-02
Prkaa2	protein kinase. AMP-activated. alpha 2 catalytic subunit	0.60	4.36E-03
Wnt4	wingless-type MMTV integration site family. member 4	0.61	9.66E-04
Sgk1	serum/glucocorticoid regulated kinase 1	0.62	9.18E-07
Clip1	CAP-GLY domain containing linker protein 1	0.63	3.00E-04
Atp6v1c2	ATPase. H+ transporting. lysosomal V1 subunit C2	0.75	2.26E-03
Wnt10b	wingless-type MMTV integration site family. member 10B	1.03	2.81E-09
Wnt7b	wingless-type MMTV integration site family. member 7B	1.34	1.05E-07
	Hedgehog signaling pathway		
Ptch1	patched 1	-1.22	1.51E-08
Gli1	GLI-Kruppel family member GLI1	-1.16	8.94E-08
Shh	sonic hedgehog	-1.04	4.01E-04
Ptch2	patched 2	-0.97	7.21E-04
Hhip	Hedgehog-interacting protein	-0.88	2.09E-03

Ccnd1	cyclin D1	-0.86	7.41E-07
Bcl2	B cell leukemia/lymphoma 2	-0.61	2.55E-06
Arrb1	arrestin. beta 1	-0.57	5.24E-06
Csnk1g1	casein kinase 1. gamma 1	-0.53	3.69E-04
Evc	EvC ciliary complex subunit 1	-0.33	1.17E-03
Gpr161	G protein-coupled receptor 161	-0.31	4.55E-03
Gas1	growth arrest specific 1	0.34	4.43E-02
Cdon	cell adhesion molecule-related/down-regulated by oncogenes	0.42	3.33E-03
Boc	biregional cell adhesion molecule-related/down-regulated by oncogenes (Cdon) binding protein	0.61	5.25E-05
	Structural genes		
Krt10	keratin 10	2.428767	9.70E-19
Krt76	keratin 76	1.881164	5.86E-12
Krt2	keratin 2	1.679981	1.22E-10
Krt19	keratin 19	1.622124	2.22E-09
Krt15	keratin 15	1.594074	5.37E-08
Krt6a	keratin 6A	1.535615	1.52E-08
Krt1	keratin 1	1.423761	2.14E-09
Krt7	keratin 7	1.385129	2.20E-06
Krt24	keratin 24	1.331517	4.02E-07
Krt14	keratin 14	1.249257	1.40E-05
Krt6b	keratin 6B	1.150228	6.87E-07
Krt16	keratin 16	1.053443	4.98E-06
Krt9	keratin 9	1.044944	2.03E-06
Krt5	keratin 5	0.975178	0.000746
Krt78	keratin 78	0.823654	9.07E-05
Krt42	keratin 42	0.755794	0.00625
Krt23	keratin 23	0.738123	0.000312
Krt13	keratin 13	0.729104	0.00019
Krt84	keratin 84	0.700875	0.017114
Krt12	keratin 12	0.698802	0.002493
Krt4	keratin 4	0.657306	0.000477
Krt75	keratin 75	0.601409	0.032302
Krt32	keratin 32	0.467055	0.003407
Krt77	keratin 77	0.404151	0.022505
Krt82	keratin 82	-0.60082	0.036566
Krt28	keratin 28	-0.74114	0.008684
Krt18	keratin 18	-1.06858	0.000263
Krt8	keratin 8	-1.4661	1.25E-09

Supplementary Table S1. RNA-seq. Tooth development genes. Data are presented as log2 fold changes in *VDR-null* vs. WT and VDR_{gem} vs. WT samples. For instance, a FC log2 value of −1.00 will correspond to a 50% reduction in mRNA level in the mutant (*VDR-null* and/or VDR_{gem}) samples. Genes encoding regulators of tooth development described in GenoDENT panel (Rey et al., 2019) are either reduced or increased in mutant samples. Rows in yellow indicate genes downregulated in *VDR-null* and upregulated in VDR_{gem}. Light blue indicates genes downregulated in both *VDR-null* and VDR_{gem}. Green indicates genes upregulated in both *VDR-null* and VDR_{gem}.

Gene name	Description	Log2 FC	P-value
	VDR-null vs. WT		
Col2a1	collagen. type II. alpha 1	-0.78	6.50E-03
Ltf	lactotransferrin	-0.70	1.45E-02
Pold1	polymerase (DNA directed). delta 1. catalytic subunit	-0.64	2.77E-04
Twist2	twist basic helix-loop-helix transcription factor 2	-0.64	1.42E-03
Tbx1	T-box 1	-0.63	7.45E-04
Dlx5	distal-less homeobox 5	-0.60	1.26E-05
Zfpm1	zinc finger protein. multitype 1	-0.59	7.37E-04
Kdf1	keratinocyte differentiation factor 1	-0.56	1.77E-02
Scarf2	scavenger receptor class F. member 2	-0.55	2.73E-04
Map2k2	mitogen-activated protein kinase kinase 2	-0.55	1.27E-04
Rai1	retinoic acid induced 1	-0.53	4.13E-04
Ntrk1	neurotrophic tyrosine kinase. receptor. type 1	-0.51	2.43E-02
Chpf	chondroitin polymerizing factor	-0.51	2.98E-03
Recql4	RecQ protein-like 4	-0.50	3.38E-03
Lmna	lamin A	-0.49	4.64E-03
Med25	mediator complex subunit 25	-0.47	2.56E-05
Ifitm5	interferon induced transmembrane protein 5	-0.46	2.86E-02
Spp1	secreted phosphoprotein 1	-0.46	3.69E-02
Ror2	receptor tyrosine kinase-like orphan receptor 2	-0.41	2.39E-04
Smg9	smg-9 homolog. nonsense mediated mRNA decay factor (C. elegans)	-0.40	4.42E-04
Pex6	peroxisomal biogenesis factor 6	-0.39	1.34E-02
Smoc2	SPARC related modular calcium binding 2	-0.38	3.66E-02
Naa10	N(alpha)-acetyltransferase 10. NatA catalytic subunit	-0.38	9.36E-04
Axin2	axin 2	-0.37	1.95E-04
Slc9a3r1	solute carrier family 9 (sodium/hydrogen exchanger). member 3 regulator 1	-0.37	3.24E-02
Kif7	kinesin family member 7	-0.37	3.87E-03
Katnb1	katanin p80 (WD40-containing) subunit B 1	-0.34	1.24E-03
Adamts10	a disintegrin-like and metallopeptidase (reprolysin type) with thrombospondin type 1 motif. 10	-0.34	4.06E-02
Tuft1	tuftelin 1	-0.33	4.74E-02
Megf8	multiple EGF-like-domains 8	-0.33	5.47E-03
Fermt3	fermitin family member 3	-0.32	2.17E-02
Plec	plectin	-0.31	3.12E-02

Slc24a4	solute carrier family 24 (sodium/potassium/calcium exchanger). member 4	-0.31	4.73E-02
Arhgap6	Rho GTPase activating protein 6	-0.30	4.67E-02
Dvl1	dishevelled segment polarity protein 1	-0.30	2.57E-02
Tcof1	treacle ribosome biogenesis factor 1	-0.29	2.21E-02
Akt1	thymoma viral proto-oncogene 1	-0.28	2.37E-03
Pth1r	parathyroid hormone 1 receptor	-0.28	3.02E-02
Dnm1	dynamin 1	-0.28	8.31E-03
Gtf2ird1	general transcription factor II I repeat domain-containing 1	-0.26	4.42E-03
Notch3	notch 3	-0.26	4.41E-02
Atr	ataxia telangiectasia and Rad3 related	0.26	3.50E-02
Cdon	cell adhesion molecule-related/down-regulated by oncogenes	0.27	3.43E-02
Tmco1	transmembrane and coiled-coil domains 1	0.28	7.08E-05
Masp1	mannan-binding lectin serine peptidase 1	0.28	4.62E-02
Cog6	component of oligomeric golgi complex 6	0.28	9.45E-04
Gja1	gap junction protein. alpha 1	0.29	1.60E-03
Mmp20	matrix metallopeptidase 20 (enamelysin)	0.29	4.47E-02
Slc10a7	solute carrier family 10 (sodium/bile acid cotransporter family). member 7	0.30	2.17E-04
Slc13a5	solute carrier family 13 (sodium-dependent citrate transporter). member 5	0.30	2.61E-02
Dmtf1	cyclin D binding myb-like transcription factor 1	0.30	7.60E-04
Sat1	spermidine/spermine N1-acetyl transferase 1	0.30	1.67E-02
Trps1	transcriptional repressor GATA binding 1	0.33	1.75E-03
Sparcl1	SPARC-like 1	0.34	7.77E-03
Mbtps2	membrane-bound transcription factor peptidase. site 2	0.35	7.54E-03
Zeb2	zinc finger E-box binding homeobox 2	0.35	4.31E-03
Adam10	a disintegrin and metallopeptidase domain 10	0.35	9.14E-04
Tgfbr1	transforming growth factor. beta receptor I	0.36	2.67E-03
Cybb	cytochrome b-245. beta polypeptide	0.38	1.82E-02
Antxr2	anthrax toxin receptor 2	0.40	1.80E-06
Adamts1	a disintegrin-like and metallopeptidase (reprolysin type) with thrombospondin type 1 motif. 1	0.44	3.58E-03
Insr	insulin receptor	0.45	1.42E-03
Tmem165	transmembrane protein 165	0.45	1.45E-05
Cldn1	claudin 1	0.46	4.29E-02
Adgrv1	adhesion G protein-coupled receptor V1	0.47	1.03E-02
Vdr	vitamin D (1.25-dihydroxyvitamin D3) receptor	0.52	3.83E-04
Ctsc	cathepsin C	0.53	5.04E-07
Ibsp	integrin binding sialoprotein	0.63	2.50E-04
Cldn19	claudin 19	0.67	2.23E-02
Clec7a	C-type lectin domain family 7. member a	0.96	9.35E-05

	VDR_{gem} *vs. WT*		
Fgf3	fibroblast growth factor 3	-1.69	2.39E-09
Ptch1	patched 1	-1.22	1.51E-08
Sox11	SRY (sex determining region Y)-box 11	-1.21	9.45E-09
Fgf10	fibroblast growth factor 10	-1.16	2.92E-05
Grem2	gremlin 2. DAN family BMP antagonist	-1.07	2.68E-04
Cacnb2	calcium channel. voltage-dependent. beta 2 subunit	-1.05	8.81E-06
Shh	sonic hedgehog	-1.04	4.01E-04
Uhrf1	ubiquitin-like. containing PHD and RING finger domains. 1	-1.02	1.13E-06
Camk4	calcium/calmodulin-dependent protein kinase IV	-1.02	2.46E-05
Orc1	origin recognition complex. subunit 1	-1.01	1.34E-05
Cdc6	cell division cycle 6	-0.98	2.34E-06
Ptch2	patched 2	-0.97	7.21E-04
Prokr2	prokineticin receptor 2	-0.95	2.66E-04
Edaradd	EDAR (ectodysplasin-A receptor)-associated death domain	-0.91	3.09E-04
Tspear	thrombospondin type laminin G domain and EAR repeats	-0.91	2.14E-04
Twist2	twist basic helix-loop-helix transcription factor 2	-0.86	9.33E-05
Sox9	SRY (sex determining region Y)-box 9	-0.86	1.38E-06
Recql4	RecQ protein-like 4	-0.75	8.79E-05
Blm	Bloom syndrome. RecQ like helicase	-0.71	8.99E-05
Plk4	polo like kinase 4	-0.70	1.52E-04
Sall4	spalt like transcription factor 4	-0.69	3.07E-03
Ckap2l	cytoskeleton associated protein 2-like	-0.68	8.99E-04
Lef1	lymphoid enhancer binding factor 1	-0.66	3.27E-05
Dhcr24	24-dehydrocholesterol reductase	-0.64	6.49E-04
Frem2	Fras1 related extracellular matrix protein 2	-0.59	4.03E-03
Axin2	axin 2	-0.58	4.88E-07
Ahcy	S-adenosylhomocysteine hydrolase	-0.57	5.04E-06
Dlx5	distal-less homeobox 5	-0.53	5.89E-04
Notum	notum palmitoleoyl-protein carboxylesterase	-0.53	1.51E-02
Smoc2	SPARC related modular calcium binding 2	-0.52	1.08E-02
Sp6	trans-acting transcription factor 6	-0.50	2.63E-05
Zfp799	zinc finger protein 799	-0.48	2.57E-03
Pold1	polymerase (DNA directed). delta 1. catalytic subunit	-0.47	1.74E-02
Snrpn	small nuclear ribonucleoprotein N	-0.45	2.68E-02
Fgf9	fibroblast growth factor 9	-0.44	2.38E-02
Lss	lanosterol synthase	-0.43	1.05E-02
Wdr6	WD repeat domain 6	-0.42	4.87E-04
Dlx3	distal-less homeobox 3	-0.41	2.05E-03
Zfp563	zinc finger protein 563	-0.40	1.30E-02
Zfp955b	zinc finger protein 955B	-0.38	9.14E-03
Chst3	carbohydrate sulfotransferase 3	-0.38	2.27E-02

Dkc1	dyskeratosis congenita 1. dyskerin	-0.38	4.78E-03
Tsc1	TSC complex subunit 1	-0.37	6.33E-04
Aaas	achalasia. adrenocortical insufficiency. alacrimia	-0.36	2.47E-04
Tcof1	treacle ribosome biogenesis factor 1	-0.35	1.46E-02
Cep152	centrosomal protein 152	-0.35	2.46E-03
Evc	EvC ciliary complex subunit 1	-0.33	1.17E-03
Msx2	msh homeobox 2	-0.32	4.34E-03
Kcnj2	potassium inwardly-rectifying channel. subfamily J. member 2	-0.32	4.22E-02
Cib2	calcium and integrin binding family member 2	-0.32	3.24E-03
Zfp617	zinc finger protein 617	-0.31	3.31E-02
Fras1	Fraser extracellular matrix complex subunit 1	-0.31	3.23E-02
Zfp952	zinc finger protein 952	-0.31	1.29E-02
Ccdc134	coiled-coil domain containing 134	-0.31	4.76E-03
Naa10	N(alpha)-acetyltransferase 10. NatA catalytic subunit	-0.29	2.64E-02
Rfc2	replication factor C (activator 1) 2	-0.29	4.70E-03
Bmp4	bone morphogenetic protein 4	-0.29	3.23E-03
Ercc8	excision repaiross-complementing rodent repair deficiency. complementation group 8	-0.27	1.85E-02
Vps33b	vacuolar protein sorting 33B	0.26	6.60E-04
Kcnh1	potassium voltage-gated channel. subfamily H (eag-related). member 1	0.28	4.76E-02
Itga6	integrin alpha 6	0.29	1.48E-02
Pdgfrb	platelet derived growth factor receptor. beta polypeptide	0.30	5.39E-03
Car2	carbonic anhydrase 2	0.30	1.85E-02
Enpp1	ectonucleotide pyrophosphatase/phosphodiesterase 1	0.30	3.29E-02
Atp6v1b2	ATPase. H+ transporting. lysosomal V1 subunit B2	0.30	2.85E-02
Stat3	signal transducer and activator of transcription 3	0.32	1.46E-03
Crot	carnitine O-octanoyltransferase	0.33	8.46E-04
Gas1	growth arrest specific 1	0.34	4.43E-02
C1ra	complement component 1. r subcomponent A	0.35	1.50E-02
Antxr1	anthrax toxin receptor 1	0.35	4.43E-05
Serping1	serine (or cysteine) peptidase inhibitor. clade G. member 1	0.36	4.23E-03
Zeb2	zinc finger E-box binding homeobox 2	0.36	8.64E-03
Col5a2	collagen. type V. alpha 2	0.37	9.12E-03
Nfkbia	nuclear factor of kappa light polypeptide gene enhancer in B cells inhibitor. alpha	0.38	4.14E-03
Arhgap6	Rho GTPase activating protein 6	0.39	1.97E-02
Trip10	thyroid hormone receptor interactor 10	0.39	1.61E-03
Adamts2	a disintegrin-like and metallopeptidase (reprolysin type) with thrombospondin type 1 motif. 2	0.39	3.72E-04
Orai1	ORAI calcium release-activated calcium modulator 1	0.40	4.10E-02
Antxr2	anthrax toxin receptor 2	0.40	2.61E-05
Itga11	integrin alpha 11	0.40	9.34E-04

Tuft1	tuftelin 1	0.40	3.22E-02
Mmp9	matrix metallopeptidase 9	0.41	4.94E-02
Tgfa	transforming growth factor alpha	0.41	2.32E-02
Mmp14	matrix metallopeptidase 14 (membrane-inserted)	0.41	2.96E-04
Cdon	cell adhesion molecule-related/down-regulated by oncogenes	0.42	3.33E-03
Ltbp2	latent transforming growth factor beta binding protein 2	0.42	4.12E-02
Polr1d	polymerase (RNA) I polypeptide D	0.42	2.24E-02
Eda	ectodysplasin-A	0.43	6.42E-04
Sparc	secreted acidic cysteine rich glycoprotein	0.43	9.07E-03
Cdkn1c	cyclin-dependent kinase inhibitor 1C (P57)	0.44	2.44E-02
Dock8	dedicator of cytokinesis 8	0.44	7.42E-03
Plec	plectin	0.44	7.55E-03
Tfap2a	transcription factor AP-2. alpha	0.45	1.47E-02
Amtn	amelotin	0.45	7.60E-03
Col6a1	collagen. type VI. alpha 1	0.46	3.77E-05
Notch3	notch 3	0.46	1.89E-03
Tnfsf11	tumor necrosis factor (ligand) superfamily. member 11	0.47	1.52E-02
Sparcl1	SPARC-like 1	0.47	1.07E-03
Ctsk	cathepsin K	0.48	9.41E-03
Pth1r	parathyroid hormone 1 receptor	0.49	9.88E-04
Xpr1	xenotropic and polytropic retrovirus receptor 1	0.50	1.64E-03
Adam15	a disintegrin and metallopeptidase domain 15 (metargidin)	0.50	1.57E-03
Col12a1	collagen. type XII. alpha 1	0.51	6.86E-05
Trps1	transcriptional repressor GATA binding 1	0.52	1.86E-05
Mmp2	matrix metallopeptidase 2	0.53	1.33E-07
Spp1	secreted phosphoprotein 1	0.53	2.69E-02
Col17a1	collagen. type XVII. alpha 1	0.55	2.16E-02
Clrn1	clarin 1	0.56	4.44E-02
Col1a2	collagen. type I. alpha 2	0.56	1.63E-03
Slc24a4	solute carrier family 24 (sodium/potassium/calcium exchanger). member 4	0.56	1.14E-03
Samd12	sterile alpha motif domain containing 12	0.57	3.77E-02
Col5a1	collagen. type V. alpha 1	0.61	2.13E-05
Ibsp	integrin binding sialoprotein	0.64	8.79E-04
Eya1	EYA transcriptional coactivator and phosphatase 1	0.64	3.68E-04
Ctsc	cathepsin C	0.65	8.80E-08
Ezr	ezrin	0.66	1.89E-03
Col2a1	collagen. type II. alpha 1	0.67	2.19E-02
Klk4	kallikrein related-peptidase 4 (prostase. enamel matrix. prostate)	0.70	7.36E-04
Lmna	lamin A	0.73	1.77E-04
Atp6v1c2	ATPase. H+ transporting. lysosomal V1 subunit C2	0.75	2.26E-03

Fam83h	family with sequence similarity 83. member H	0.76	7.33E-03
Col15a1	collagen. type XV. alpha 1	0.76	3.46E-08
Grhl3	grainyhead like transcription factor 3	0.77	7.93E-03
Cldn1	claudin 1	0.78	1.44E-03
Col3a1	collagen. type III. alpha 1	0.79	4.15E-07
Slc34a2	solute carrier family 34 (sodium phosphate). member 2	0.81	5.79E-03
Odam	odontogenic. ameloblast asssociated	0.81	6.97E-06
Masp1	mannan-binding lectin serine peptidase 1	0.84	1.01E-07
Eln	elastin	0.93	9.81E-06
Pkp1	plakophilin 1	0.94	1.22E-03
Sox2	SRY (sex determining region Y)-box 2	0.95	4.71E-04
Tfap2b	transcription factor AP-2 beta	0.97	2.21E-04
Krt5	keratin 5	0.98	7.46E-04
Dsp	desmoplakin	0.99	4.84E-04
Wnt10b	wingless-type MMTV integration site family. member 10B	1.03	2.81E-09
Krt16	keratin 16	1.05	4.98E-06
Krt6b	keratin 6B	1.15	6.87E-07
Gjb3	gap junction protein. beta 3	1.16	1.87E-05
Krt14	keratin 14	1.25	1.40E-05
Pax3	paired box 3	1.34	3.94E-08
Gjb6	gap junction protein. beta 6	1.41	1.70E-06
Casp14	caspase 14	1.42	7.36E-08
Gjb4	gap junction protein. beta 4	1.51	3.62E-08
Krt6a	keratin 6A	1.54	1.52E-08

Supplementary Table 2. RNA-seq. Bone development genes. Data are presented as log2 fold changes in *VDR-null* vs. WT and VDR_{gem} vs. WT samples. For instance, a FC log2 value of −1.00 will correspond to a 50% reduction in mRNA level in the mutant (*VDR-null* and/or VDR_{gem}) samples. Genes encoding regulators of tooth development described in Bone markers panel (Mortier et al., 2019) are either reduced or increased in mutant samples. Rows in yellow indicate genes downregulated in *VDR-null* and upregulated in VDR_{gem}. Light blue indicates genes downregulated in both *VDR-null* and VDR_{gem}. Green indicates genes upregulated in both *VDR-null* and VDR_{gem}.

Gene name	**Description**	**Log2 FC**	**P-value**
	***VDR-null vs.* WT**		
	Constitutional Disorders of Bone		
Col2a1	collagen type II alpha 1	-0.78	6.5E-03
Srcap	Snf2-related CREBBP activator protein	-0.59	7.9E-04
Comp	cartilage oligomeric matrix protein	-0.54	3.1E-02
Col9a3	collagen type IX alpha 3	-0.46	1.8E-02
Acan	aggrecan	-0.45	1.7E-02
Ror2	receptor tyrosine kinase-like orphan receptor 2	-0.41	2.4E-04
Tonsl	tonsoku-like. DNA repair protein	-0.35	2.9E-02
Adamts10	a disintegrin-like and metallopeptidase (reprolysin type) with thrombospondin type 1 motif. 10	-0.34	4.1E-02
Trps1	transcriptional repressor GATA binding 1	0.33	1.7E-03
Wac	WW domain containing adaptor with coiled-coil	0.39	7.4E-05
Pappa2	pappalysin 2	0.43	4.5E-03
Slco5a1	solute carrier organic anion transporter family. member 5A1	0.45	2.6E-02
Tmem165	transmembrane protein 165	0.45	1.4E-05
	Bone Fragility		
Xylt2	xylosyltransferase II	-0.31	6.4E-03
Mbtps2	membrane-bound transcription factor peptidase. site 2	0.35	7.5E-03
	Lyse-Condensation-Proliferation		
Col2a1	collagen type II alpha 1	-0.78	6.5E-03
Lmna	lamin A	-0.49	4.6E-03
Fermt3	fermitin family member 3	-0.32	2.2E-02
Antxr2	anthrax toxin receptor 2	0.40	1.8E-06
Hpgd	hydroxyprostaglandin dehydrogenase 15 (NAD)	0.42	5.3E-03
Ano5	anoctamin 5	0.77	9.2E-03
	Statural Growth		
Tonsl	tonsoku-like. DNA repair protein	-0.35	2.9E-02
Apc2	APC regulator of WNT signaling pathway 2	-0.35	3.6E-02
Tgfbr1	transforming growth factor. beta receptor I	0.36	2.7E-03
Npr3	natriuretic peptide receptor 3	0.55	1.7E-03

	Spondylocostal dysostosis		
Tbx6	T-box 6	-0.44	4.4E-02
Myo18b	myosin XVIIIb	0.66	2.6E-02
	***VDR_{gem} vs.* WT**		
	Constitutional Disorders of Bone		
Kif22	kinesin family member 22	-1.00	5.4E-07
Sox9	SRY (sex determining region Y)-box 9	-0.86	1.4E-06
Gdf6	growth differentiation factor 6	-0.73	7.1E-03
Nppc	natriuretic peptide type C	-0.61	2.2E-02
Tonsl	tonsoku-like. DNA repair protein	-0.57	1.7E-03
Fgf9	fibroblast growth factor 9	-0.44	2.4E-02
Chst3	carbohydrate sulfotransferase 3	-0.38	2.3E-02
Mcm9	minichromosome maintenance 9 homologous recombination repair factor	-0.30	8.2E-03
Csgalnact1	chondroitin sulfate N-acetylgalactosaminyltransferase 1	0.35	2.8E-02
Mmp9	matrix metallopeptidase 9	0.41	4.9E-02
Ltbp2	latent transforming growth factor beta binding protein 2	0.42	4.1E-02
Bgn	biglycan	0.43	4.5E-03
Mmp13	matrix metallopeptidase 13	0.44	6.1E-03
Pth1r	parathyroid hormone 1 receptor	0.49	9.9E-04
Trps1	transcriptional repressor GATA binding 1	0.52	1.9E-05
Lmx1b	LIM homeobox transcription factor 1 beta	0.56	2.2E-02
Comp	cartilage oligomeric matrix protein	0.59	2.7E-02
Pappa2	pappalysin 2	0.62	2.2E-04
Col2a1	collagen type II alpha 1	0.67	2.2E-02
Adamtsl4	ADAMTS-like 4	0.69	3.8E-05
Ihh	Indian hedgehog	0.70	1.8E-02
Acan	aggrecan	0.78	2.0E-04
Prg4	proteoglycan 4 (megakaryocyte stimulating factor articular superficial zone protein)	0.81	4.9E-03
Tnxb	tenascin XB	0.98	5.0E-05
Bmpr1b	bone morphogenetic protein receptor. type 1B	1.20	1.2E-05
	Bone Fragility		
Sox9	SRY (sex determining region Y)-box 9	-0.86	1.4E-06
Dlx3	distal-less homeobox 3	-0.41	2.1E-03
Fam111a	family with sequence similarity 111. member A	-0.35	2.6E-02
Ccdc134	coiled-coil domain containing 134	-0.31	4.8E-03
Pls3	plastin 3 (T-isoform)	0.26	1.3E-02
Sparc	secreted acidic cysteine rich glycoprotein	0.43	9.1E-03
Sfrp4	secreted frizzled-related protein 4	0.48	1.2E-04

	Lyse-Condensation-Proliferation		
Dhcr24	24-dehydrocholesterol reductase	-0.64	6.5E-04
Dlx3	distal-less homeobox 3	-0.41	2.1E-03
Antxr2	anthrax toxin receptor 2	0.40	2.6E-05
Met	met proto-oncogene	0.41	1.3E-02
Mmp14	matrix metallopeptidase 14 (membrane-inserted)	0.41	3.0E-04
Tnfsf11	tumor necrosis factor (ligand) superfamily. member 11	0.47	1.5E-02
Ctsk	cathepsin K	0.48	9.4E-03
Mmp2	matrix metallopeptidase 2	0.53	1.3E-07
Hpgd	hydroxyprostaglandin dehydrogenase 15 (NAD)	0.53	1.9E-03
Col2a1	collagen type II alpha 1	0.67	2.2E-02
Lmna	lamin A	0.73	1.8E-04
Il1rn	interleukin 1 receptor antagonist	1.66	1.7E-09
	Statural Growth		
Ptch1	patched 1	-1.22	1.5E-08
Tonsl	tonsoku-like. DNA repair protein	-0.57	1.7E-03
Ezh2	enhancer of zeste 2 polycomb repressive complex 2 subunit	-0.37	1.2E-02
Pdgfrb	platelet derived growth factor receptor. beta polypeptide	0.30	5.4E-03
Pten	phosphatase and tensin homolog	0.30	2.4E-02
Ppp2r5b	protein phosphatase 2. regulatory subunit B'. beta	0.48	9.7E-04
Npr3	natriuretic peptide receptor 3	0.60	2.2E-03
Cbs	cystathionine beta-synthase	0.95	5.8E-04
	Spondylocostal dysostosis		
Bmper	BMP-binding endothelial regulator	-0.44	1.9E-03
Meox1	mesenchyme homeobox 1	0.56	1.3E-05
Mesp2	mesoderm posterior 2	1.10	2.8E-05
	Adams-Oliver		
Notch1	notch 1	0.3	2.70E-02

Discussion, conclusions and perspectives

Rare diseases and translational research

Each week, new rare diseases are discovered, adding to the list of more than 7,000 described rare disorders. 80% of these disorders are genetically based. In France 3–4 million people are afflicted with rare diseases, compared with a total of 30 million people found in the rest of Europe. Given the lack of information and awareness about these developmental anomalies, clinical identification and management of individuals with rare disorders and their accompanying orodental malformations is quite difficult. Indeed, medical experts and dentists take between 5 and 30 years to provide an accurate diagnosis. For an earlier, faster, and more accurate identification of these uncommon disorders, a thorough examination of the oral cavity may yield crucial information.

A continuous range of research, from fundamental biomedical study discoveries into clinical practice, is necessary for the development of new disease treatments and preventative strategies. To close the gap between applying laboratory discoveries to human clinical trials, numerous techniques and tactics have been created. Translational research in the field of rare diseases is crucial to improving patient's health. One important investigative tool in molecular genetics involves the generation of mouse models that mimic the diseases' clinical features. This obviously will aide our understanding the physiological role and molecular mechanism of action of these to date orphan disease genes. The studies performed in animal models may also help identify novel symptoms that may be present in humans, but have not yet been linked to the syndrome. Mouse models can also be used to test innovative new therapeutics.

The reference center for rare oral and dental diseases (CRMR O-Rares) combines clinical, preclinical, bioinformatics, genetic, and biological approaches to understand oral and dental defects present in rare diseases. The team has generated mouse models of uncommon disorders including for the *Smoc2* and *Rogdi* genes.

The objectives of this PhD were to investigate through translational research the etiology of a rare disease, and to understand the molecular genetics of the basic biological processes that affect human health, with a focus on bench-to-bedside research.

Briefly, the first article is focused on the molecular classification of amelogenesis *imperfecta*. Depending on the enamel defects and the inheritance mode, amelogenesis *imperfecta* can be divided into different categories. The main types are: hypoplastic (type I); hypomaturation (type II); hypocalcified (type III); and hypomaturation/hypoplasia/taurodontism (type IV). Depending on the inheritance we can have AI X-linked, autosomal dominant, or autosomal recessive. We were able to further refine this classification to a molecular level as a result of the phenotype and genetic data following Witkop's classification from 1988 [78]. We categorized the AI types in the context of a full phenotype study supported by clinical characteristics and imaging, as well as their linkage with genes and identified pathogenic variants. Genetic data was obtained from the GenoDENT NGS panel or exome sequencing from a cohort of 115 individuals. We identified 151 different variants, with 47 newly reported and classified in classes 4 or 5, defined as likely pathogenic or pathogenic, respectively. From these 151 variants, 42 were identified in syndromic AI, with 10 variants reported for the first time in this publication (7 class 4, 3 VUS). *FAM20A* (enamel-

kidney syndrome), *LTBP3* (Verloes Bourguignon syndrome), and *ROGDI* (Kohlschütter-Tönz syndrome) were the most commonly discovered genes for syndromic AI [98].

This publication will aide practitioners to assess and diagnose AI more precisely, enabling the identification of syndromic variations when AI is associated with other symptoms.

The second published article described the diagnosis of a patient who shared clinical traits with two distinct syndromes: Hallermann-Streiff and oculodentodigital dysplasia [99]. The genomic analysis assisted in identifying a new variant that might be responsible for this phenotype. Hallermann-Streiff syndrome (HSS) is a rare condition causing developmental delays, short stature, and craniofacial characteristics with an unknown inheritance pattern. Clinical characteristics of HSS and oculodentodigital dysplasia (ODDD) coincide, making it difficult to differentiate between the two. ODDD is caused by variants in the transmembrane gap junction protein connexin 43 (CX43), which is encoded by the Gap Junction Protein Alpha 1 gene (*GJA1*).

Genetic testing is essential for validating diagnoses, enhancing medical care, and informing families about future medical requirements. Hence, genetic testing enables patients to get a more specialized, multidisciplinary healthcare and management specific to their illness, while also adhering to global standards.

Although the exact molecular cause of HSS is unknown, the identification of the homozygous variant in *GJA1* gene shows that the HSS/ODDD spectrum shares a common phenotype and genotype. Clinical traits from both HSS and ODDD may be combined into a single syndrome known as HSS/ODDD if homozygous mutations are found in particular regions of the *GJA1* gene.

Variants in CX43 may reduce cell-to-cell communication, exacerbating ODDD symptoms. CX43 channels have been found in tooth papillary cells and ameloblasts [11]. Both syndromes present dental anomalies, specifically amelogenesis *imperfecta*.

It is therefore important to recognize, characterize, and precisely record dental anomalies and phenotypes, so that they may be integrated within the familial, medical and dental histories of each patient. Such detailed recording will reveal developmental origins and go some way towards providing additional clues for understanding underlying etiopathogenic mechanisms and unravelling e.g. a syndrome diagnosis. Moreover, developing new tools like computer-assisted facial recognition programs may enhance the detection and diagnosis of some disorders [100].

While patient DNA can be sequenced to find potential genes causing clinical malformations, the molecular basis can neither be elucidated nor novel treatment approaches could be design by basing our approach solely in humans.

To go further into understanding the fundamental molecular basis of orodental patterning and morphogenesis, it is of great importance to study rare diseases in *in-vivo* models, such as mice or *in-vitro* using cellular approaches. The mouse dentition is a powerful model to study the genesis of human orodental anomalies. A number of genetically modified mice generated so far display dental defects that mimic the pathology encountered in humans.

This doctoral work aims at better understanding the molecular basis of rare diseases, and overcoming the inherent limitations of patient-based research. Essential to this goal was the involvement in the creation and investigation of novel mouse models of human rare diseases.

Pr. Bloch-Zupan, specialist in odontogenetics at the Reference Center for Rare Diseases, identified patients with loss of function mutations in the *ROGDI* gene causing Kolschutter Tonz syndrome (KTS). This syndrome presents neurodegenerative disorders (intellectual disability, epilepsy, psychomotor regression) and a generalized enamel malformation called amelogenesis *imperfecta*. My research objectives included elucidating function(s) of this novel signaling pathway using a mouse model with a *Rogdi* inactivation. To understand the functional properties of the *ROGDI* gene that produces both neurodegenerative and dental enamel defects, we compared the knockout mouse to KTS patient defects.

Molecular, cellular, and structural analyses were performed to validate the *Rogdi* $^{-/-}$ mouse model as a model for KTS and to establish the role of Rogdi during development of neuroepithelial and biomineralized tissues with relevance in the development and pathophysiology of the rare disease known as Kolschütter-Tönz Syndrome.

A striking characteristic of KTS-affected children is their global developmental delay (KTS individuals displaying intellectual disability, spasticity, and seizures). The progressive nature of their neurological decline might be attributed to epileptic seizures inducing epileptic encephalopathy [80,81,84]. Our data showed *Rogdi* displays enriched central nervous system expression, with higher levels in the fetal and adult brain (hippocampus and cerebellum) and spinal cord. This suggests that ROGDI has critical roles during brain formation, potentially continuing during organ homeostasis.

Tooth enamel in patients is soft, rough, and stained in various shades of brown - a diagnosis of amelogenesis *imperfecta* with a hypomature/hypomineralized type [17,77,81,83–85]. Tooth mineral content analyses show a reduction in calcium and phosphate levels, consistent with the observed phenotype (article #4 The *Rogdi* Knockout Mouse is a Model for Kohlschütter–Tönz Syndrome).

Rogdi transcripts are enriched in the incisor epithelium, specifically in the pre-ameloblasts and ameloblasts classes. Cycling cells and non-ameloblasts epithelial cells also have expression, but at lower levels. *Rogdi* transcripts are 100 times lower than those of enamel matrix proteins (*Ambn* and *Enam*), but are comparable to levels of *Orai1* and *Stim1*, which are responsible for syndromic hypomature AI (https://kleintools.hms.harvard.edu/tools/springViewer_1_6_dev.html?datasets/Sharir_et_al_2019/control_epithelial) [101]. Our results also found expression of *Rogdi* beginning at early stages of tooth development (E12.5). *Rogdi* levels are enriched during tooth morphogenesis during the formation of the dental lamina throughout all stages of fetal tooth growth. At postnatal stages this expression switches and appears localized in ameloblasts- cells involved in enamel formation. Besides, we found Rogdi protein is localized in the apical pole of the ameloblasts. This data correlates with the phenotype of AI found in our mouse model and in humans, indicating a role of Rogdi during amelogenesis.

This data confirms the significant role that *Rogdi* plays in the onset of the disease, as evidenced by the fact that it is expressed throughout early stages of tooth and brain development. Our results also demonstrate expression in the liver and kidney, noteworthy because nephrocalcinosis was recently reported as a new clinical feature [2].

The research project involved the analysis of the *Rogdi* knockout mouse. To understand neurodegenerative and enamel deficits, behavioral tests, imaging analyses, and comparative genomic studies were conducted.

Rogdi homozygous mutant mice recapitulate patient's phenotype

We thoroughly analyzed the mouse morphological aspects in order to investigate potential correspondences with the Kohlschütter-Tönz phenotype. *Rogdi* mouse mutants were found to be viable at early stages, although they did not exhibit the expected Mendelian ratio (1/5). Mouse mutants were smaller than wildtype (WT) mice and had an early lethality rate, typically dying around 12 weeks of age.

One of the clinical characteristics seen in KTS patients is epilepsy. Depending on the patient, it has been found that they can develop myoclonic, focal, and generalized seizures, as well as generalized tonic-clonic seizures [84]. A timed pentylenetetrazol infusion test (PTZ) (40 mg/kg, i.p.) was carried out to analyze if the *Rogdi* mice were more prone to seizures. The *Rogdi*$^{-/-}$ mutant animals showed greater susceptibility and faster seizure onset when compared to control mice. These findings indicate that the *Rogdi KO* mice had a higher probability of developing epilepsy.

The study also found significant increases in locomotor activity in *Rogdi*$^{-/-}$ mice during circadian activity and novel object recognition (NOR) tests, indicating a hyperactivity disorder. Memory impairment was also observed, with increased object exploration time during the NOR. Both findings correlate with phenotypes found in KTS patients. To better understand Rogdi function in brain development, we analyzed histological sections of the hippocampus and cerebellum. These analyses revealed an altered cerebellar and hippocampal morphology related with motor coordination, cognition, and language function [102,103], correlating the findings from the behavioral tests. Besides, cerebral CT scans and MRI on KTS patients show brain atrophy, including smaller hippocampus and hypoplasia of the cerebellar vermis [81,84,86,88]. The observed architectural defects could explain the clinical signs of KTS patients. Dysregulated brain growth in both *Rogdi*$^{-/-}$ mice and KTS patients suggest a central role in disease etiology with a potential role in memory establishment.

Teeth of the *Rogdi* mutant mice have extensive enamel abnormalities related to an amelogenesis *imperfecta*-like phenotype. These defects are a result of a lack of mineral accumulation and enamel maturation. Calcium and phosphorus levels are significantly decreased in the *Rogdi KO*. Carbon levels, indicative of organic content, were higher in mutants and did not differ between maturation stage of amelogenesis and mineralized enamel in *Rogdi*$^{-/-}$ mutants. pH analyses performed in adult lower incisors revealed altered pH regulation. *Rogdi*$^{-/-}$ mutants display neutral pH during the maturation stage of enamel formation, whereas an

acidic pH is required for enamel maturation. Hence precisely at the maturation stage of enamel formation, a pH reduction is necessary for enamel crystal growth and protein degradation. The neutral pH in *Rogdi*$^{-/-}$ mutants could most likely explain the high carbon levels found during mineral content analyses.

Examination of other organs showed a distended stomach full of undigested food in the *Rogdi*$^{-/-}$ mice. The stomach content in *Rogdi*$^{-/-}$ had a pH of 6 instead of a normal acidic pH of 3 for fed mice [104]. In addition, 10% of the *Rogdi*$^{-/-}$ had a urinary bladder full of urine and with a viscous liquid inside of it. Renal defects (nephrocalcinosis) have been reported in KTS patients [2]. Interestingly, we discovered that at least one of the patients was receiving medical therapy because of persistent constipation after asking the family if they had digestive issues. Irritable bowel syndrome patients (at times displaying persistent constipation) have altered (less acidic) gastrointestinal pH [105]. In order to improve the quality of life for those who have the disease, this *Rogdi* mutant model may also aid in the elucidation of novel clinical aspects to be considered in the diagnosis and treatment of KTS.

Whole genome RNA-sequencing, combined with bioinformatic approaches helped to uncover *Rogdi* transcriptional network. It was confirmed the downregulation of *Rogdi* transcripts, affecting neurodegeneration and synapses pathways, calcium signaling, tight junction, Wnt, Notch and Hedgehog signaling networks, among others. Genes known to be causative of amelogenesis imperfecta, such as *Lama3*, *Itgb6*, *Acp4*, *Lamb3*, *Col17a1*, *Cnnm4*, *Ltbp3*, *Slc24a4*, *Gpr68,* and *Orai1*, were either down or upregulated [9,43]. *Slc9a3r2* and *Atp6v0c* were upregulated in our RNA-seq data, both proteins are part of the V-ATPase complex, involved in acidification [106,107]. *Wdr72*, described as a homologue of WDR7 [64], was also upregulate.

Understanding dysregulated pathways in rare diseases is crucial for therapeutic development. Research is currently focused on molecular and pathophysiologic pathways shared by numerous illnesses, revealing potential targets for small-molecule intervention, even if the mutated gene is not a druggable target [108].

Rogdi and the role of V-ATPase in acidification

Loss of ROGDI function may cause enamel and brain defects by disrupting the vacuolar type (V)-ATPase dependent lysosomal acidification pathway [109]. V-ATPases are crucial for pH homeostasis, vesicle transport, membrane fusion, and synaptic transmission. Defects in V-ATPase action lead to lysosomal disorders like Alzheimer's and Parkinson's disease. V-ATPase function is essential for adult development and maintaining lysosomal pH gradients, also required in tooth formation [67,110–112]. V-ATPases pump H^+ ions into the endosomes causing an acidification of 5.5–6.0. For many receptors, this pH causes a conformational shift that frequently leads in the release of bound ligands from receptors [113]. The process of endocytosis and the targeting of receptors and ligands are increasingly used in drug delivery methods. Potential therapies for cancer, Alzheimer's, Parkinson's, and lysosomal storage diseases use nanoscale drug carriers that target endolysosomes [114].

Signals like glucose deprivation, will cause a decrease in ATPase activity, and proton transfer, where the V1 subcomplex will be detached from the V0 subcomplex. The yeast RAVE (Regulator of H^+-ATPase of Vacuolar and Endosomal membranes) or its functional equivalent in higher eukaryotes, the Rabconnectin-3 complexes [64], are necessary for the assembly of V1 with V0 [115]. The crystal structure of one of RAVE complex components, Rav2, is strikingly similar to the human ROGDI protein [64]. In addition, ROGDI protein shares an interactome community with DMXL1, DMXL2, and WDR7, components of the V-ATPase chaperone Rabconnectin-3 complex [64,116].

The results found in this PhD work solidify the ROGDI-V-ATPase connection. *Rogdi*$^{-/-}$ mutants exhibit severe reductions in enamel acidification, likely accounting for morphological deterioration in enamel structure. RNA-seq data from *Rogdi* mutant incisors shows increased *Slc9a3r2, Atp6v0c,* and *Wdr72* levels, which interact with the acidifying V-ATPase complex and DMXL1 and DMXL2 proteins. These changes likely affect pH regulation, disrupting acidification [117]. Defects in ameloblast organelle acidification that limit the degradation of enamel proteins can cause amelogenesis imperfecta [8,47].

In the stomach, V-ATPase may serve as an additional pathway for acid secretion or as an internal proton-buffering mechanism [118,119]. V-ATPase alterations can also aggravate or produce cancer, neurodegenerative diseases, diabetes, and disrupting energy and nutrient-sensing functions within cells [120].

Considering ROGDI as a regulator of V-ATPase assembly, it could be interesting to study treatments targeting the reassembly of the proton pump to help in its functioning. In addition, a better understanding of the altered pathways in the mouse mutant model may aide in more effectively focusing patient care.

The *Rogdi* mutant is a useful new model for analyzing treatment outcomes and points to new perspectives on the function of ROGDI in cell biology and pathophysiology, and to test functional hypothesis about its potential role in the V-ATPase assembly.

Considering the pathways that are altered in our model, one of interest is calcium signaling. Numerous signaling pathways are controlled by intracellular calcium levels, which are also subject to intricate spatial and temporal control. For example, in Alzheimer's disease, altered calcium signaling and the involvement of intracellular calcium reserves have long been recognized [121,122]. Endolysosomes and endoplasmic reticulum (ER) are the two main intracellular calcium reserves [123]. Endolysosome de-acidification causes the release of calcium from endolysosomes, and the accompanying rise in cytoplasmic calcium levels can activate related pathways and calcium export from ER [124]. Furthermore, long-term depression has been related to Ca^{2+} signaling modification, which may also contribute to memory impairment [122,125,126].

Using high affinity ligands that are specific to receptors to target macromolecular complexes can help to control, not only the cellular identification of these carriers, but also the trafficking pathway and their activity within the cell. Therapies focused along these routes might considerably help disorders connected with the endosomes and lysosomes [114].

In addition, endolysosome de-acidification has been associated with elevated levels of circulating cholesterol, a risk factor for developing sporadic Alzheimer's disease [127].

It has been described that ML-SA1, an agonist of TRPML1, significantly decreased endolysosome pH in rat primary cultured neurons. In addition, when TRPML1 knockdown does not affect endolysosome pH, it blocks the magnitude of ML-SA1-induced acidification. The mechanisms by which TRPML1 activation affects endolysosome pH remain unclear. These findings indicate that ML-SA1 induced endolysosome acidification is, at least, in part by activating TRPML1 [128].

It is possible that calcium released from TRPML1 activates calcium-activated potassium channels, increasing the exchange of potassium and hydrogen ions, or that calcium released from TRPML1 affects the activity of V-ATPase, which maintains the acidic environment of endolysosomes [128]. Treatments that increase V-ATPase activity and acidify endolysosomes may prevent the onset of symptoms associated with lysosomal disorders [125].

Vitamin D receptor gemini mouse model used to study craniofacial and tooth abnormalities

Due to our interest in craniofacial development, we also collaborated with Dr. Gilles Laverny (Team Pathophysiological role of nuclear receptor signaling – Dr. Daniel Metzger) in a project characterizing dental and bone alterations in a mouse with a point mutation in the ligand binding domain of the vitamin D receptor (VDR). This highly specific vitamin D ligand (gemini) can exert potent anti-inflammatory and antiproliferative actions. Gemini mice can be used to elucidate the importance of the vitamin D ligand in tissue mineralization and define vitamin D targets. VDR_{gem} mice, which have a point-mutated vitamin D receptor, have a greater severity of tooth and alveolar bone defects than *VDR-null* mice. These mice have reduced alveolar bone density, abnormal root and pulp morphology, and severely hypocalcified alveolar bone and dentin. Additionally, VDR_{gem} mice display hypomineralized enamel structures. The importance of this study is we show mutants with the complete absence of VDR display less severe defects bone/dental defects than VDR_{gem} mice. We can thus conclude that an unliganded vitamin D receptor has a worse physiological consequence for bone and tooth formation (compared to a total absence of the VDR receptor). Vitamin D indeed acts through its receptor allowing bone and tooth to accumulate sufficient calcium and phosphorous required for structural integrity. Low vitamin D3 levels afflicts more than 1 billion children and adults worldwide [129]. Increasing vitamin D3 intake or its skin photosynthesis will likely improve bone and tooth integrity in humans. This can be further concluded from results on VDR_{gem} mice- the most severe example of how the unliganded VDR receptor can have possible detrimental effects.

Therapeutic treatments in rare diseases: a global view

When it comes to rare diseases and the unique issues they present, having an effective animal model that exhibits a phenotype that is equivalent to the human disease allows for the testing of functional hypotheses and the creation of bioengineering tools that could be advantageous to the entire population. On the other hand, a rare disease's molecular foundation might be considered while attempting a treatment already employed for other well-known disorders with comparable altered pathways.

Researchers can utilize the outcomes of animal models to guide the design of human therapeutic trials if they show promising results. However, it is important to proceed cautiously and understand that human responses could vary from those seen in animals.

Overall, animal models are essential for developing both medical and scientific understanding. To study and treat human diseases and biological processes, however, there are many steps that must be taken. Results are more thorough and dependable when data is combined from several sources, such as animal models, *in vitro* experiments, and clinical research.

Using our expertise in orodental development, we were able to extensively characterize orofacial defects in all the mouse models that we studied. With the assistance and knowledge of specialists who study brain development, it was feasible to take a first step toward understanding the neurological impairments in the *Rogdi* mutant mouse.

The fact that our *Rogdi* mutant mouse model presents all the known clinical features in KTS creates a novel model to investigate the origins of this disease and the unknown function of this protein.

Testing the hypothesis that the Rogdi protein directs exocytosis and/or serves as a transcription factor that regulates the formation of enamel and the function of neurons, will develop a range of useful conceptual and practical tools for regenerative medicine. Our goal is to test for phenotypic rescue using pharmacological and gene therapy approaches.

Molecule screening, for example, of proteins known to be part of the Rabconnectin-3 complex, such as DMXL1, DMXL2, and WDR7 [64,106] could be worth testing to prove their connection with ROGDI function.

Despite significant advancements in research to comprehend the molecular foundation and the development of specialized therapeutics, the majority of rare diseases still do not have recognized treatments.

Antisense oligonucleotides (ASOs), small interfering RNAs (siRNAs), gene and cell therapies, as well as protein-based treatments are possible experimental treatment strategies in *Rodgi* mouse mutants (along with other rare disease mouse models). For example, RNA seq analysis has revealed potentially critical protein targets in *Rodgi* mouse mutants. In these cases, protein-based targeted re-expression can serve to modulate these targets and replace the dysfunctional or missing proteins. ASOs, siRNAs and gene and cell therapy are more relevant to transcription factor targets and/or compensation for dysfunctional intracellular proteins.

Together, these treatment modalities enable an extensive coverage of targets and mechanisms, which can be expanded by combining different approaches [108].

Currently, there is a great interest in using cellular disease models including pluripotent stem cells, organoids, along with technologies for more rapid gene editing such as CRISPR-Cas9 [130,131]. Collectively, such advances in technology will be relevant at the translational research level.

In addition to the aforementioned experimental strategies, we can consider repurposing medications that have already been demonstrated to be safe and well tolerated in other conditions. Here, the logic is to adapt rare disease symptomatic treatment(s) in shared pathway for intervention strategies. The specificity of such an approach will improve as rare disease phenotype screening advances [108].

We must also work together to address common obstacles. Some of the issues include access to data from electronic medical records and patient-specific clinical outcomes [108].

Today, much research done in rare diseases is abandoned well before it even reaches the clinic and even the preclinical stage. Despite the fact that the number of orphan drug designations is continuously rising worldwide, approved orphan medications only treat a small percentage of rare diseases [14].

Finally, it should be noted that, despite the fact that a rare disease affects only a small number of people, collectively there are more than 400 million patients suffering from a rare disease worldwide.

This doctoral thesis work was possible thanks to the following grants: the French Ministry of Health (National Program for Clinical Research, PHRC 2008 N°4266 Amelogenesis imperfecta), the University Hospital of Strasbourg (HUS, API, 2009–2012, ‘Development of the oral cavity: from gene to clinical phenotype in Human’), the European Regional Development Fund (ERDF) of the European Union in the framework of the INTERREG IV and V Upper Rhine program RARENET (2016-2019), Agence Nationale de la Recherche, “programme Investissements d'Avenir” (ANR-10-INBS-07 PHENOMIN), Recherche Filière TETECOU 2021. Patients’ support group Pierre-Henri et ses amis.

This work of the Interdisciplinary Thematic Institute IMCBio, as part of the ITI 2021-2028 program of the University of Strasbourg, CNRS and Inserm, was supported by IdEx Unistra (ANR-10-IDEX-0002), and by SFRI-STRAT’US project (ANR 20-SFRI-0012) and EUR IMCBio (ANR-17-EURE-0023) under the framework of the French Investments for the Future Program.

I received funding from the National Agency for Research and Development (ANID)/Scholarship Program/DOCTORADO BECAS CHILE/2019- 72200405.

Future work will be based on continuous collaborations between the Institute of Genetics and Cellular and Molecular Biology, CNRS- UMR7104, INSERM U1258 (IGBMC), the Faculté de Chirurgie Dentaire de l’Université de Strasbourg, the Centre de Référence Maladies

Rares O-Rares, Pôle de Médecine et Chirurgie Bucco-Dentaires, Hôpitaux Universitaires de Strasbourg, France, and University of Chile. This work will focus on the genetics of rare disorders and attempt to uncover potential therapeutic solutions by exploring the genotypes behind families and patients showing exceptional rare orodental phenotypes.

Résumé de la thèse en français

Intitulé de la thèse : **ROGDI- une nouvelle protéine avec un motif leucine-zipper-régulant le développement neurologique et orofacial**

Introduction

Au sein de l'Union Européenne, une maladie est dite rare lorsqu'elle touche moins d'une personne sur 2000. Plus de 7000 maladies rares sont décrites et chaque semaine de nouvelles maladies rares sont identifiées. 80 % des maladies rares ont une origine génétique. Les maladies rares touchent 3 à 4 millions de personnes en France et près de 25 millions en Europe [14]. Pour de nombreuses maladies rares, en raison d'un déficit de connaissances tant médicales que scientifiques, de nombreux patients ne sont pas diagnostiqués et leur maladie reste non identifiée. Un examen attentif de la cavité buccale peut fournir des informations précieuses pour un diagnostic plus précoce, plus rapide et plus précis des telles maladies [16,17].

Depuis 2004, la France est un des principaux acteurs mondiaux dans le domaine des maladies rares grâce à des stratégies nationales, notamment la mise en place de 23 réseaux de santé et du Centre de référence pour les maladies bucco-dentaires rares (CRMR O-Rares). Ce réseau contribue au diagnostic des maladies rares, à la mise en œuvre des thérapies et à l'organisation de la prise en charge des patients.

Les recherches menées par le CRMR O-Rares intègrent des approches cliniques, précliniques, bio-informatiques, génétiques et biologiques, y compris des approches développementales. Les principaux objectifs du CRMR O-Rares comprennent l'étude des anomalies bucco-dentaires d'un point de vue phénotypique, génotypique et fondamental. Des équipes scientifiques et cliniques multidisciplinaires ont collaboré au développement d'outils de diagnostic performants et de nouvelles méthodes thérapeutiques. De plus, en collaboration avec l'Institut Clinique de la Souris (ICS), il a été possible de générer de nouveaux modèles murins de maladies rares, permettant l'exploration phénotypique à l'aide de techniques d'imagerie. La compréhension des mécanismes développementaux et physiopathologiques peut conduire à des thérapies innovantes telles que la régénération de l'os maxillaire et l'ostéo-intégration des implants dentaires.

La caractérisation d'anomalies dentaires et buccales s'est avérée être un outil essentiel pour la détection précoce de certaines maladies rares. Plus de 950 maladies rares présentent des anomalies du développement bucco-dentaire, souvent causées par des mutations génétiques. Les anomalies peuvent affecter la forme, la structure interne et la topographie des dents et peuvent être isolées (sans autres symptômes ou anomalies associées) ou faire partie d'un syndrome. Les modèles murins porteurs de mutations ciblées de gènes jouent un rôle déterminant dans la compréhension des mécanismes moléculaires qui déterminent la morphogenèse dentaire [26].

Les dents sont des organes d'origine ectodermique qui se développent selon une série de stades morphologiques distincts, impliquant des interactions entre l'épithélium buccal et l'ectomésenchyme. L'odontogenèse est un processus complexe impliquant des interactions génétiques, moléculaires et cellulaires. Elle comprend la formation de la lamina dentaire, le

stade des placodes dentaires, le stade du bourgeon, de la cupule et de la cloche, suivis de la cytodifférenciation terminale des odontoblastes et des améloblastes. La formation des racines et l'éruption des dents ont alors lieu [26,27]. Outre son intérêt propre, l'étude de l'odontogenèse est un bon modèle pour comprendre les principes moléculaires généraux de l'organogenèse.

L'émail est une structure d'origine ectodermique, constituée à 96-98% de minéral sous la forme de cristaux d'hydroxyapatite. Sa formation implique les améloblastes, cellules post-mitotiques issues de l'ectoderme oral, qui sécrètent une matrice extracellulaire organique spécifique, hautement organisée, d'épaisseur définie. Chez les mammifères, l'amélogenèse peut être divisée en trois étapes : pré-sécrétion, sécrétion et maturation [42]. Concomitamment à l'étape de minéralisation de cette matrice, des enzymes spécifiques éliminent le contenu protéique pour permettre la minéralisation complète pendant cette phase de maturation.

Au cours de la phase de sécrétion, les améloblastes libèrent des protéines (EMP, Enamel Matrix Proteins) qui contribuent à la matrice de l'émail. Ces EMP comprennent l'amélogénine (AMEL), l'améloblastine (AMBN) et l'énaméline (ENAM). Au cours de la phase de maturation, des enzymes comme la métalloprotéinase matricielle 20 (MMP20) et la kallikrein 4 (KLK4 une peptidase dépendante du calcium), clivent les EMP nouvellement sécrétées en divers fragments dérivés, essentiels pour la minéralisation [7]. Tout au long de la phase de sécrétion, les cristaux d'émail augmentent principalement en longueur, et la couche d'émail s'épaissit. Des perturbations au cours de la phase de sécrétion entraînent un amincissement ou une hypoplasie de la couche d'émail finale. À un certain stade du programme de développement, la phase de maturation commence et les améloblastes subissent une transition qui non seulement réduit leur activité de sécrétion de protéines de l'émail, mais initie également la sécrétion de la kallikréine 4 (KLK4), une sérine protéase qui dégrade la matrice organique, facilitant ainsi son élimination du compartiment extracellulaire [7,44]. À la fin de cette étape, l'émail a terminé sa minéralisation. Des perturbations au cours de la phase de maturation de l'amélogenèse se traduisent par un émail anormalement mou (hypomaturation) alors qu'il est d'épaisseur normale. Ce stade de l'amélogenèse est caractérisé par une modulation (ou cycle) de l'homéostasie du pH dans l'environnement de la matrice de l'émail en voie de minéralisation [46]. Le cycle du pH implique la transformation cyclique des améloblastes à bordure plissée (RE, ruffled-ended) face à un émail légèrement acide, en améloblastes à bordure lisse (SE, smooth-ended) à proximité d'un émail au pH neutre [8,47,54] .

Les amélogenèses imparfaites (Amelogenesis *Imperfecta*, AI) constituent un groupe hétérogène de maladies affectant la formation de l'émail dentaire [68,69]. L'AI peut se présenter comme une maladie isolée ou coexister avec d'autres anomalies et symptômes dans le cadre de troubles syndromiques tels que le syndrome de Kohlschütter-Tönz [95].

Le syndrome de Kohlschütter-Tönz (KTS, OMIM #226750, ORPHA : 1946) est une maladie génétique rare à transmission autosomique récessive. Il se caractérise par une épilepsie d'apparition précoce, une régression psychomotrice, une déficience intellectuelle et des défauts de l'émail. Il est causé par des mutations dans le gène *ROGDI*, codant pour une protéine de fonction encore inconnue mais hautement conservée au cours de l'évolution parmi les espèces, notamment chez *Caenorhabditis elegans, Drosophila melanogaster, Danio rerio, Xenopus laevis* et *Mus musculus*, ce qui suggère un rôle fonctionnel important [17,68,80,81]. Après la

première description du syndrome en 1974 [82], et la découverte d'une mutation du gène *ROGDI* (localisé en 16p13.3, et constitué de 11 exons, 5.98 kb) en 2012, plusieurs types de mutations non-sens, affectant un site d'épissage, et/ou provoquant un décalage du cadre de lecture ont été publiées, délimitant un phénotype similaire chez d'autres individus affectés par ce syndrome [17,77,81,83–85].

L'épilepsie débute généralement au cours de la première année de vie et les crises sont souvent résistantes au traitement, même avec les nouveaux médicaments antiépileptiques. Les signes cliniques et biologiques ne sont pas spécifiques de la maladie, à l'exception du phénotype bucco-dentaire ; ce dernier est donc essentiel pour le diagnostic clinique du KTS [84]. Tous les individus affectés présentent une coloration variable jaune à brune des dents temporaires et permanentes dès leur éruption, pathognomonique d'une amélogenèse imparfaite (AI) hypominéralisée.

Dans les KTS associés aux mutations du gène *ROGDI*, l'AI est caractérisée par une hypominéralisation et des défauts de maturation avec des surfaces dentaires rugueuses de couleur brun orangé [77]. Des perturbations au cours de l'étape de maturation engendrent un émail moins minéralisé, anormalement riche en protéines, cliniquement coloré, mou et poreux, mais d'épaisseur normale. Comme mentionné plus haut, cette étape de l'amélogenèse est modulée par le contrôle de l'homéostasie du pH dans l'environnement de la matrice de l'émail. Cette modulation (ou cycle du pH) est importante pour permettre une fonction optimisée des enzymes dégradant la matrice extracellulaire [8].

Il existe peu d'informations pour comprendre la pathophysiologie conduisant au phénotype du KTS lorsque *ROGDI* est muté. L'analyse de l'expression de *ROGDI* humain par PCR quantitative (détection des ARNm) indique une expression dans le cerveau, la moelle épinière, le sang, le cœur et la moelle osseuse [81]. Chez le rat, la localisation des transcrits aux sites présynaptiques neuronaux suggère que *Rogdi* pourrait réguler l'exocytose des protéines. Les transcrits sont présents dans deux types importants de synapses dans l'hippocampe : celles des fibres moussues et les synapses hilaires [95]. La physiopathologie de l'épilepsie implique des défauts de transmission de l'acide gamma-aminobutyrique (signalisation GABAergique) connus pour induire des troubles du sommeil. Il a été démontré qu'un homologue de *Rogdi* chez la drosophile agit comme un facteur favorisant le sommeil en soutenant un sous-ensemble spécifique de transmissions GABAergiques. De manière intéressante, les mouches mutantes pour *Rogdi* présentent des troubles du comportement semblables à ceux de l'insomnie, caractérisés par une fragmentation du sommeil et des retards dans l'initiation du sommeil [83]. Chez la souris, *Rogdi* est exprimé pendant l'odontogenèse depuis le stade de la cupule au stade embryonnaire E14.5 [17]. Concernant la localisation cellulaire, la protéine ROGDI est localisée dans l'enveloppe nucléaire des cellules humaines en culture [81].

La structure cristalline de la protéine ROGDI (287 acides aminés, 32 kD) humaine permet de définir 2 domaines, un domaine alpha, avec un faisceau de quatre hélices de type leucine-zipper (ZIP), et un domaine de feuillets bêta. Le motif de type ZIP dans le domaine alpha semble médier les interactions intramoléculaires, contribuant à la structure globale et à la stabilité d'une protéine ROGDI monomère. La perturbation du faisceau des quatre hélices suite

à des mutations semble entraîner une déstabilisation significative de la structure de la protéine [68].

Malgré les informations et les données publiées sur ROGDI, sa fonction reste inconnue à ce jour.

Des patients atteints du syndrome de Kolschütter-Tönz ont été diagnostiqués et pris en charge au Centre de référence des maladies rares orales et dentaires (CRMR O-Rares) des Hôpitaux Universitaires de Strasbourg. Le diagnostic clinique a été confirmé au niveau moléculaire par séquençage d'ADN via le panel NGS GenoDENT [19] identifiant des mutations pathogènes dans *ROGDI*. Afin d'avoir un meilleur aperçu de la compréhension de la maladie et de la fonction de *ROGDI*, et pour explorer les options de traitement, un modèle murin portant une mutation de perte de fonction dans *Rogdi* a été créé à l'Institut Clinique de la Souris (grâce à des financements via les programmes Interreg IV et V RARENET). La stratégie choisie a conduit à supprimer les exons 6 à 11 afin de mimer le génotype de certains patients KTS traités au sein du CRMR O-Rares de Strasbourg.

Les objectifs de mon travail de thèse ont été d'analyser ce mutant de souris *Rogdi*$^{-/-}$ pour comprendre le rôle de Rogdi pendant le développement et les mécanismes pathophysiologiques sous-tendant les anomalies et symptômes rencontrés dans le KTS. La caractérisation du rôle de Rogdi facilitera la compréhension du phénotype rencontré dans cette maladie, notamment en ce qui concerne les anomalies dentaires et neurologiques, et permettra de proposer des pistes pour améliorer la prise en charge des patients.

Dans une première partie, cette thèse décrit les amélogenèses imparfaites [98,99] et les phénotypes spécifiques de l'émail rencontrés dans les maladies rares chez l'homme, qu'elles soient isolées ou syndromiques, ainsi que dans les modèles murins de ces maladies [132]. Elle détaille ensuite les travaux menés sur le modèle murin inactivé pour le gène *Rogdi* et récapitulant le phénotype rencontré dans le KTS grâce à des approches comportementales, histologiques et moléculaires.

Les résultats sont ici résumés :

Chapitre 1 : Maladies oro-dentaires rares

Le premier chapitre de ma thèse donne un aperçu des maladies orodentaires rares et de la recherche clinique corrélant le phénotype et la génétique.

L'amélogenèse imparfaite (AI) est l'objet principal de cette thèse. L'amélogenèse imparfaite est observée dans un groupe hétérogène de maladies caractérisées par une perturbation du développement de l'émail. Nous proposons une évolution dans la classification des phénotypes de l'AI. Pour cela nous avons utilisé les outils du séquençage de nouvelle génération (NGS) pour classer ce groupe de maladies au niveau moléculaire et au niveau clinique. La classification utilisée jusqu'à présent a été décrite par Witkop en 1988 [78], divisant les AI en 4 types selon la nature des défauts de l'émail et le mode de transmission (Type I hypoplasique,

Type II hypomature, Type III hypominéralisé, et Type IV hypomature/hypoplasique avec taurodontisme). Il existe actuellement plus de 100 gènes connus pour être à l'origine d'AI. Au centre de référence des maladies rares bucco-dentaires (CRMR O-Rares, Strasbourg), les patients présentant une AI ont été recrutés et évalués selon le protocole D4/phenodent (www.phenodent.org).

Nous avons utilisé un panel spécialisé de séquençage de nouvelle génération (NGS) appelé GenoDENT [19], pour étudier un groupe de patients atteints d'AI afin d'identifier la cause génétique de la maladie et d'améliorer le diagnostic et le traitement. Une cohorte de 115 patients présentant une AI isolée (73 %) ou syndromique (27 %) a été recrutée et évaluée. Le panel GenoDENT, qui étudie 567 gènes à la fois, a été utilisé pour l'analyse moléculaire. Les résultats ont été mis en corrélation avec le phénotype du patient pour parvenir à un diagnostic final. Dans l'AI isolée et syndromique, l'AI la plus fréquente est le type hypoplasique, suivi du type hypomature et du type hypominéralisé. Ces analyses ont permis de clarifier la base moléculaire de la classification de l'AI de Witkop [98].

Un deuxième article sur un rapport de cas intitulé "A novel homozygous variant in *GJA1* causing a Hallermann-Streiff/Oculodentodigital Dysplasia overlapping Phenotype: a clinical report" montre que grâce au séquençage d'exome (WES), il a été possible d'identifier un variant homozygote dans le gène *GJA1* qui affecte la protéine connexine (CX) 43, provoquant un phénotype qui combine les caractéristiques cliniques du syndrome de Hallermann-Streiff (HSS, OMIM 234100) et de la dysplasie oculodentodigitale (ODD, OMIM 164200). L'une des caractéristiques cliniques des patients atteints de ces syndromes est le défaut d'émail. La protéine CX43 permet l'échange d'ions et de petites molécules d'une cellule à l'autre. Au cours du développement de l'émail, CX43 est impliquée dans le transport d'ions de la couche papillaire vers les améloblastes.

Chapitre 2 : Les modèles murins

De nombreuses lignées de souris génétiquement modifiées utilisées comme modèles pour des maladies rares reproduisent les anomalies crâniofaciales et dentaires observées chez l'homme. L'étude de ces modèles permet un examen plus approfondi des effets des dysfonctionnements moléculaires sous-jacents. Dans le cadre du réseau O-Rares, nous identifions, traitons et réalisons des criblages génomiques de patients présentant des anomalies crâniofaciales dentaires inhabituelles afin d'identifier les gènes candidats. En outre, il existe des modèles de rongeurs présentant des défauts de la dentine, de l'émail et d'autres tissus dentaires, ainsi que des mutations génétiques pour lesquelles aucune maladie humaine n'a encore été décrite. Ils apportent la preuve que les gènes mutés jouent un rôle dans le développement des dents et identifient de nouveaux gènes candidats potentiels chez l'homme.

Caractéristiques du modèle de souris inactivé pour *Rogdi*

Les mutants de souris *Rogdi* (*Rogdi*$^{-/-}$) sont viables ; néanmoins, les naissances ne sont pas observées à la fréquence attendue selon les lois de Mendel, car dans les croisements hétérozygotes, seulement 1/5 de la progéniture est *Rogdi*$^{-/-}$. Aucune malformation aux stades embryonnaires (E9.5, E12.5) ou fœtaux (E14.5-18.5) n'a été observée chez les mutants *Rogdi*$^{-/-}$. Cependant, les animaux montrent une létalité précoce avec plus de 60% des mutants *Rogdi*$^{-/-}$ ne survivant pas après l'âge de 12 semaines post-natales (PN). Après le sevrage, les mutants *Rogdi*$^{-/-}$ ont un poids significativement inférieur à celui des souris sauvages (WT). Cette différence de poids se maintient tout au long de la vie de l'animal.

***Rogdi* et son rôle dans le neurodéveloppement**

Des crises tonico-cloniques généralisées d'apparition précoce, des crises myocloniques et des crises focales et généralisées ont été rapportées dans le KTS [84]. Concernant notre modèle murin, les souris *Rogdi*$^{-/-}$ n'ont pas présenté de crises épileptiques spontanées ou leur détection a échoué. Un test d'infusion de pentylènetétrazol (PTZ) a été effectué pour évaluer la susceptibilité des souris *Rogdi*$^{-/-}$ à développer une épilepsie induite. Les animaux mutants ont montré une plus grande susceptibilité que les souris témoin (WT), avec une apparition plus rapide des crises.

Les personnes atteintes de KTS présentent des déficiences motrices et cognitives évidentes [17,68]. Les tests comportementaux évaluant ces caractéristiques chez les souris *Rogdi*$^{-/-}$ et les contrôles respectifs ont montré, chez les mutants, une activité locomotrice accrue pendant la première heure du test d'activité circadienne ainsi que pendant le test de reconnaissance de nouveaux objets, ce qui pourrait refléter un trouble d'hyperactivité chez les souris mutantes, caractéristique déjà décrite dans le KTS [80]. De plus, nous avons observé que les souris *Rogdi*$^{-/-}$ présentent des troubles de la mémoire lors du test de reconnaissance de nouveaux objets. Ces résultats suggèrent que les souris *Rogdi*$^{-/-}$ présentent une déficience de la mémoire qui pourrait s'apparenter à la déficience intellectuelle sévère trouvée dans le KTS [17,81,84]. La fonction motrice des mutants a été testée à l'aide de tests de force de préhension (Grip strength) et de cylindre tournant (Rotarod). La force de préhension est significativement diminuée chez les souris femelles *Rogdi*$^{-/-}$. Le test du Rotarod n'a indiqué aucune différence entre les groupes. Ces données indiquent qu'il n'y a pas de déficience motrice dans notre lignée, sauf chez certaines femelles. Les analyses histologiques des muscles tibial antérieur, gastrocnémien et quadriceps, faites en collaboration avec l'équipe de Jocelyn Laporte (IGBMC), n'ont révélé aucune variation significative entre les souris *Rogdi*$^{-/-}$ et WT.

Concernant l'expression de *Rogdi*, nous avons détecté par hybridation *in situ* ses transcrits à partir de E12.5, dans les tissus du neuroépithélium, y compris le cerveau, la moelle épinière et les ganglions spinaux. Une expression dans le foie et l'endothélium vasculaire est également apparente à ce stade. À E14.5, l'expression persiste dans le système nerveux central, y compris dans les ganglions trigéminés et spinaux. Un signal positif a également été observé dans le foie et les reins. Dans le cerveau adulte de 7 semaines, l'expression enrichie dans l'hippocampe et le cervelet suggère un rôle persistant de *Rogdi* dans le développement de ces structures.

Les analyses histologiques des cerveaux au jour post-natal (PN)15 ont montré une organisation altérée de certains lobules cérébelleux (simplex, crus II, paramédian) des souris *Rogdi*$^{-/-}$. Ces altérations traduisent un retard de développement. De plus, les souris mutantes présentent des défauts d'organisation des composants de l'hippocampe, notamment un défaut de croissance de l'arborisation dendritique basale des cellules pyramidales de la corne d'Ammon 1 (CA1).

Rogdi et son rôle dans le développement crâniofacial et l'amélogenèse

L'analyse morphométrique des souris *Rogdi*$^{-/-}$ et WT âgées de 8 semaines, réalisée à partir de l'imagerie micro-CT (μ-CT), n'a révélé aucun changement significatif chez les femelles, alors que chez les mâles, on a constaté la présence de bosses pariétales et des variations dans la partie antérieure du crâne, montrant une tête plus courte et plus large chez les mutants *Rogdi*$^{-/-}$ que chez les contrôles (WT).

À l'âge adulte, des anomalies dentaires ont été observées chez les souris mutantes. D'un point de vue phénotypique, les souris mutantes *Rogdi*$^{-/-}$ présentent des défauts sévères de l'émail. Normalement, la surface labiale des incisives de rongeurs présente une pigmentation de couleur jaune/orange, en raison de la présence d'environ 0,03 % de fer dans l'émail [133]. Les mutants *Rogdi*$^{-/-}$ montrent un éclaircissement crayeux prononcé de l'émail, avec des taches blanches suggérant une fragmentation ou un "effritement" plus prononcé à la base des incisives inférieures ; les molaires étaient abrasées et plus arrondies avec une perte d'émail du côté occlusal exposant la dentine. Cette attrition indique des défauts structurels dans l'intégrité de l'émail. L'aspect plus blanc et la brillance réduite de la surface correspondent à une épaisseur d'émail réduite et à un émail sous-minéralisé, un phénotype typique rencontré dans les modèles de souris avec une AI [134,135].

En ce qui concerne les changements de densité et de volume de l'émail, il a été possible de montrer une différence significative de densité chez les mutants *Rogdi*$^{-/-}$ par rapport aux souris de type sauvage. La microscopie électronique à balayage (MEB) a montré que l'organisation prismatique et le modèle de croisement de ces prismes d'émail étaient conservés dans l'émail des souris *Rogdi*$^{-/-}$. Les prismes d'émail étaient cependant dépourvus de cristaux, comme dans d'autres modèles de souris AI [57,135]. L'émail des incisives de souris témoin présentait une structure cristalline normale, tandis que les incisives de souris *Rogdi*$^{-/-}$ étaient hypo-minéralisées, démontrant un phénotype sévère de l'émail. Les niveaux de calcium et de phosphore étaient réduits par rapport aux souris témoins. Les niveaux de carbone indiquant la teneur en protéines étaient plus élevés chez les mutants et ne différaient pas entre le stade de maturation et d'émail minéralisé, ce qui suggère une absence de dégradation de la matrice protéique de l'émail pendant le stade de maturation de l'amélogenèse chez les mutants.

Il est possible que les souris *Rogdi*$^{-/-}$ présentent une altération du cycle du pH, contribuant aux défauts de maturation de l'émail. L'altération du pH a été testée chez les souris mutantes avec la solution indicatrice de pH rouge de méthyle qui colore l'émail. Chez les souris *Rogdi*$^{-/-}$, aucune bande rouge donc acide n'a été observée, contrairement aux souris WT, ce qui suggère qu'il n'y a pas de changement de pH pendant l'amélogenèse, une anomalie qui pourrait fortement perturber la minéralisation de l'émail.

L'analyse histologique de souris WT et *Rogdi*$^{-/-}$ a montré des différences à l'échelle cellulaire et tissulaire dans la couche améloblastique, qui chez les mutants est désorganisée et dans laquelle les améloblastes sécrétoires et de maturation sont légèrement plus courts et semblent moins polarisés, avec un noyau plus rond que chez les souris témoin. Le stratum intermedium sous-jacent et le réticulum stellaire collapsé à l'épithélium dentaire externe étaient également désorganisés. Ces altérations histologiques attestent du rôle critique de Rogdi pendant l'amélogenèse.

Notre analyse par hybridation *in situ* a montré que pendant le développement de la dent, *Rogdi* était exprimé depuis le stade de la lame dentaire à E12.5, au stade de la cupule à E14.5, au stade de la cloche à E16.5, et au stade postnatal (PN)1 tant dans les compartiments ectodermiques qu'ectomésenchymateux. Les transcrits de *Rogdi* montrent un enrichissement dans les améloblastes et les odontoblastes. A PN5, un signal fort a été observé dans les améloblastes uniquement, ce qui pourrait refléter un rôle critique de *Rogdi* dans l'amélogenèse.

En ce qui concerne l'expression de la protéine Rogdi, l'immunohistochimie n'a pas montré d'expression significative de Rogdi pendant le développement de la dent aux stades embryonnaires (peut-être en raison de limites dans la sensibilité de détection). Aux stades postnataux, elle semble être enrichie dans la partie apicale des améloblastes.

En recherchant l'interactome de Rogdi avec d'autres protéines, nous avons trouvé grâce à l'aide de Gergo Gogl (IGBMC) dans Bioplex Explorer [136] que Rogdi interagit avec Atp1a2, Atp2a1, Myh7, Myh8, Tuba3c, Nudt3, Wdr7, Dmxl1 et Dmxl2. Ces trois dernières protéines - Wdr7, Dmxl1 et Dmxl2 - sont associées à la V-ATPase [64,106]. Les V-ATPases sont des pompes à protons, essentielles pour l'acidification des endosomes, des lysosomes et du réseau trans-Golgi, ainsi que pour la sécrétion d'acide par les ostéoclastes, les cellules intercalaires du rein et certaines cellules tumorales [64]. Rogdi serait la protéine Rav2 du complexe RAVE favorisant la réassociation du complexe V-ATPase.

Dans notre modèle de souris *Rogdi*$^{-/-}$, nous avons trouvé des résultats qui confirment le lien entre ROGDI et V-ATPase. Les mutants *Rogdi*$^{-/-}$ présentent de fortes réductions de l'acidification de l'émail, ce qui explique probablement la détérioration morphologique de la structure de l'émail. Les données de séquençage d'ARN des incisives des mutants PN5 montrent une augmentation des niveaux de *Slc9a3r2*, *Atp6v0c* et *Wdr72*, qui interagissent avec le complexe acidifiant V-ATPase et les protéines DMXL1 et DMXL2. Ces changements affectent probablement la régulation du pH, perturbant l'acidification pendant l'amélogenèse [117].

Les souris *Rogdi*$^{-/-}$ ont par ailleurs un estomac distendu et rempli de nourriture non digérée. Le contenu de l'estomac des souris *Rogdi*$^{-/-}$ avait un pH de 6 au lieu d'un pH acide entre 3 et 4. Dans l'estomac, la V-ATPase peut servir de voie supplémentaire pour la sécrétion d'acide ou de mécanisme interne de tamponnement des protons [118,119]. Des défauts dans l'acidification des organites de l'améloblaste qui limitent la dégradation des protéines de l'émail peuvent causer l'amélogenèse imparfaite [8,47]. Les altérations de la V-ATPase peuvent également aggraver ou produire des cancers, des maladies neurodégénératives, des diabètes et perturber les fonctions de détection de l'énergie et des nutriments au sein des cellules [120].

Pour confirmer et détailler ces données, nous avons réalisé un séquençage de l'ARN dans les incisives inférieures postnatales de 5 jours (PN5) de souris WT et *Rogdi*$^{-/-}$. Les données ont confirmé la diminution de l'expression de divers gènes, pouvant affecter les voies de la neurodégénérescence et des synapses, la signalisation calcique, les jonctions serrées et les réseaux de signalisation de la voie Wnt. Les gènes dont l'expression est réduite à PN5 comprennent *Lama3, Itgb6, Enam, Acp4, Amelx, Ambn, Lamb3 et Col17a1*, qui sont tous des gènes connus pour être impliqués dans les amélogénèses imparfaites. D'autres gènes impliqués dans les amélogenèses imparfaites tels que *Car12, Cnnm4, Amtn, Ltbp3, Slc24a4, Lamb2, Wdr72, Gpr68 et Orai1* étaient régulés à la hausse. *Slc9a3r2* et *Atp6v0c* sont régulés à la hausse dans nos données, et ces deux protéines font partie du complexe V-ATPase. *Wdr72* est également régulé à la hausse, et ce gène a été décrit comme un homologue de *WDR7* (codant pour une protéine du complexe V-ATPase*).*

Un modèle de souris avec une mutation du récepteur de la vitamine D (VDR gemini) utilisé pour étudier les anomalies craniofaciales et dentaires

Dans le cadre d'une collaboration avec l'équipe de Daniel Metzger et Gilles Laverny (IGBMC), j'ai également eu l'occasion d'étudier un nouveau mutant de souris pour le gène du récepteur de la vitamine D (VDR). La vitamine D est un régulateur endocrinien essentiel de l'absorption des minéraux. Elle est cruciale pour la formation correcte du squelette et des dents [137], et la signalisation par la vitamine D peut être ligand-dépendante ou ligand-indépendante en fonction du gène-cible [138]. Les cibles essentielles du récepteur de la vitamine D sont des régulateurs homéostatiques de l'absorption des minéraux, assurant la croissance des os d'une manière structurellement intégrée [137]. Chez les rongeurs, la minéralisation anormale due à une déficience en vitamine D modifie de façon permanente la composition de la dentine et de l'émail et peut altérer la morphologie de la dent [139–141]. Les mutants "conventionnels" *VDR*$^{-/-}$ (*VDR-null*) ont été utilisés pour comprendre comment les cibles moléculaires de la signalisation par la vitamine D régulent la minéralisation du squelette et des dents [142,143].

Pendant mon travail de thèse, j'ai pu analyser deux modèles de signalisation VDR-déficiente, à savoir les lignées de souris mutantes *VDR-null* et VDR_{gem}, pour mieux comprendre la signalisation VDR et son rôle pendant le développement des dents et des os. Les souris VDR_{gem} expriment un VDR muté (VDR_{gem} pour *gemini*) qui ne répond pas à la vitamine D [1,25(OH)2D3] endogène. Ce mutant peut donc être utilisé pour distinguer sélectivement les défauts du VDR qui dépendent du ligand (comme la minéralisation osseuse) et les phénotypes dus à l'absence de VDR non "ligandé", comme l'alopécie due à une anomalie des follicules pileux. Dans l'ensemble, les défauts dentaires et squelettiques sont plus graves chez les souris VDR_{gem} que chez les souris *VDR-null*. Ces souris présentent une densité osseuse alvéolaire réduite, une morphologie anormale de la racine et de la pulpe, et une hypocalcification sévère de l'os alvéolaire et de la dentine. La vitamine D, agissant par l'intermédiaire de son récepteur, permet à l'os et à la dent d'accumuler suffisamment de calcium et de phosphore pour assurer leur intégrité structurelle. L'analyse transcriptomique globale a révélé une altération des voies de développement conférant à la vitamine D une action sur la croissance normale des dents et des os.

Conclusion

En conclusion, les modèles animaux sont essentiels pour la compréhension médicale et scientifique des maladies rares et de leurs anomalies spécifiques. En utilisant des modèles murins présentant des phénotypes similaires à ceux de l'homme, les chercheurs peuvent tester des hypothèses fonctionnelles et développer de nouveaux traitements qui bénéficieront à l'ensemble de la population. La combinaison de données provenant de modèles animaux, d'expériences in vitro et de la recherche clinique permet d'obtenir des résultats plus complets et plus fiables.

Le modèle de souris mutant inactivé pour *Rogdi* présente un phénotype superposable à celui retrouvé dans le KTS chez l'homme. Les défauts d'émail récapitulent une amélogenèse imparfaite. Les résultats d'immunohistochimie montrent une expression de Rogdi dans les améloblastes aux stades postnataux. Ce modèle montre également une susceptibilité à l'épilepsie, ainsi que des troubles de la mémoire et une hyperactivité.

La génération de ce mutant a permis d'obtenir un nouveau modèle pour étudier la physiopathologie du KTS et explorer la fonction de cette protéine. Il est nécessaire de poursuivre les recherches sur le rôle de *ROGDI* au cours du développement du cerveau et des dents, afin d'envisager des stratégies thérapeutiques. En outre, le criblage de molécules et l'analyse fonctionnelle de protéines connues pour faire partie du complexe Rabconnectin-3, telles que DMXL1, DMXL2 et WDR7 pourrait permettre de les relier à la fonction de ROGDI et aux processus biologiques dont elles font partie.

References

1. Salerno C, D'Avola V, Oberti L, Almonte E, Bazzini EM, Tartaglia GM, et al. Rare Genetic Syndromes and Oral Anomalies: A Review of the Literature and Case Series with a New Classification Proposal. Children (Basel). 2021 Dec 26;9(1):12.

2. Liepina L, Kalnina ML, Micule I, Gailite L, Rots D, Kalnina J, et al. Kohlschütter–Tönz syndrome: Case report with novel feature and detailed review of features associated with ROGDI variants. American Journal of Medical Genetics Part A. 2022;188(4):1263–79.

3. Duijf PHG, van Bokhoven H. Ectodermal dysplasia: Skinny models on the catwalk. Drug Discovery Today: Disease Models. 2005 Jun 1;2(2):111–8.

4. Yamada S, Lav R, Li J, Tucker AS, Green JBA. Molar Bud-to-Cap Transition Is Proliferation Independent. J Dent Res. 2019 Oct;98(11):1253–61.

5. Wang J, Feng JQ. Signaling Pathways Critical for Tooth Root Formation. J Dent Res. 2017 Oct;96(11):1221–8.

6. Nanci A, editor. Chapter 5 - Development of the Tooth and Its Supporting Tissues. In: Ten Cate's Oral Histology (Eighth Edition) [Internet]. St. Louis (MO): Mosby; 2013 [cited 2023 Jun 27]. p. 70–94. Available from: https://www.sciencedirect.com/science/article/pii/B9780323078467000057

7. Nurbaeva MK, Eckstein M, Feske S, Lacruz RS. Ca2+ transport and signalling in enamel cells. J Physiol. 2017 May 15;595(10):3015–39.

8. Bronckers ALJJ. Ion Transport by Ameloblasts during Amelogenesis. J Dent Res. 2017 Mar;96(3):243–53.

9. Smith CEL, Poulter JA, Antanaviciute A, Kirkham J, Brookes SJ, Inglehearn CF, et al. Amelogenesis Imperfecta; Genes, Proteins, and Pathways. Frontiers in Physiology [Internet]. 2017 [cited 2023 Mar 28];8. Available from: https://www.frontiersin.org/articles/10.3389/fphys.2017.00435

10. Varga G, DenBesten P, Rácz R, Zsembery Á. Importance of bicarbonate transport in pH control during amelogenesis - need for functional studies. Oral Dis. 2018 Sep;24(6):879–90.

11. Josephsen K, Takano Y, Frische S, Praetorius J, Nielsen S, Aoba T, et al. Ion transporters in secretory and cyclically modulating ameloblasts: a new hypothesis for cellular control of preeruptive enamel maturation. American Journal of Physiology-Cell Physiology. 2010 Dec;299(6):C1299–307.

12. Hermans F, Hemeryck L, Lambrichts I, Bronckaers A, Vankelecom H. Intertwined Signaling Pathways Governing Tooth Development: A Give-and-Take Between Canonical Wnt and Shh. Front Cell Dev Biol. 2021 Oct 29;9:758203.

13. Bloch-Zupan A, Rey T, Jimenez-Armijo A, Kawczynski M, Kharouf N, O-Rare consortium, et al. Amelogenesis imperfecta: Next-generation sequencing sheds light on Witkop's classification. Frontiers in Physiology [Internet]. 2023 [cited 2023 May 9];14. Available from: https://www.frontiersin.org/articles/10.3389/fphys.2023.1130175

14. European Commission [Internet]. 2023 [cited 2023 Jul 19]. European Commission. Rare diseases. Available from: https://health.ec.europa.eu/non-communicable-diseases/expert-group-public-health/rare-diseases_en

15. Goldstein B. E. El desafío de las enfermedades raras y de alto costo en Chile. Prevalencia y protección financiera según normativa vigente [Internet]. Biblioteca del Congreso Nacional de Chile/BCN; 2021. Available from: https://obtienearchivo.bcn.cl/obtienearchivo?id=repositorio/10221/32791/2/BCN_Desafio_de_Enfermedades_Raras_en_Chile_para_reposit.pdf

16. de La Dure-Molla M de L, Fournier BP, Manzanares MC, Acevedo AC, Hennekam RC, Friedlander L, et al. Elements of morphology: Standard terminology for the teeth and classifying genetic dental disorders. American Journal of Medical Genetics Part A. 2019;179(10):1913–81.

17. Huckert M, Mecili H, Laugel-Haushalter V, Stoetzel C, Muller J, Flori E, et al. A Novel Mutation in the *ROGDI* Gene in a Patient with Kohlschütter-Tönz Syndrome. Mol Syndromol. 2014;5(6):293–8.

18. French Ministry for Solidarity and Health, French Ministry for Higher Education, Research and Innovation, editors. French national plan for Rare Diseases 2018-2022 [Internet]. 2018. Available from: https://sante.gouv.fr/IMG/pdf/pnmr3_-_en.pdf

19. Rey T, Tarabeux J, Gerard B, Delbarre M, Le Béchec A, Stoetzel C, et al. Protocol GenoDENT: Implementation of a New NGS Panel for Molecular Diagnosis of Genetic Disorders with Orodental Involvement. In: Papagerakis P, editor. Odontogenesis: Methods and Protocols [Internet]. New York, NY: Springer; 2019 [cited 2021 May 24]. p. 407–52. (Methods in Molecular Biology). Available from: https://doi.org/10.1007/978-1-4939-9012-2_36

20. Prasad MK, Geoffroy V, Vicaire S, Jost B, Dumas M, Le Gras S, et al. A targeted next-generation sequencing assay for the molecular diagnosis of genetic disorders with orodental involvement. J Med Genet. 2016 Feb;53(2):98–110.

21. Huckert M, Stoetzel C, Morkmued S, Laugel-Haushalter V, Geoffroy V, Muller J, et al. Mutations in the latent TGF-beta binding protein 3 (LTBP3) gene cause brachyolmia with amelogenesis imperfecta. Hum Mol Genet. 2015 Jun 1;24(11):3038–49.

22. Wehrle A, Witkos TM, Unger S, Schneider J, Follit JA, Hermann J, et al. Hypomorphic mutations of TRIP11 cause odontochondrodysplasia. JCI Insight. 2019 Feb 7;4(3):e124701.

23. Bloch-Zupan A, Jamet X, Etard C, Laugel V, Muller J, Geoffroy V, et al. Homozygosity mapping and candidate prioritization identify mutations, missed by whole-exome sequencing, in SMOC2, causing major dental developmental defects. Am J Hum Genet. 2011 Dec 9;89(6):773–81.

24. Laugel-Haushalter V, Bär S, Schaefer E, Stoetzel C, Geoffroy V, Alembik Y, et al. A New SLC10A7 Homozygous Missense Mutation Responsible for a Milder Phenotype of Skeletal Dysplasia With Amelogenesis Imperfecta. Front Genet. 2019 May 28;10:504.

25. Laugel-Haushalter V, Morkmued S, Stoetzel C, Geoffroy V, Muller J, Boland A, et al. Genetic Evidence Supporting the Role of the Calcium Channel, CACNA1S, in Tooth Cusp and Root Patterning. Front Physiol. 2018;9:1329.

26. Mitsiadis TA, Graf D. Cell fate determination during tooth development and regeneration. Birth Defect Res C. 2009 Sep;87(3):199–211.

27. Cobourne MT, Sharpe PT. Tooth and jaw: molecular mechanisms of patterning in the first branchial arch. Archives of Oral Biology. 2003 Jan 1;48(1):1–14.

28. Cobourne MT, Sharpe PT. Diseases of the tooth: the genetic and molecular basis of inherited anomalies affecting the dentition. WIREs Developmental Biology. 2013;2(2):183–212.

29. Lu T, Li M, Xu X, Xiong J, Huang C, Zhang X, et al. Whole exome sequencing identifies an AMBN missense mutation causing severe autosomal-dominant amelogenesis imperfecta and dentin disorders. Int J Oral Sci. 2018 Sep;10(3):26.

30. Thesleff I, Åberg T. Molecular regulation of tooth development. Bone. 1999 Jul 1;25(1):123–5.

31. Chai Y, Jiang X, Ito Y, Bringas P, Han J, Rowitch DH, et al. Fate of the mammalian cranial neural crest during tooth and mandibular morphogenesis. Development. 2000 Apr;127(8):1671–9.

32. Miletich I, Sharpe PT. Neural crest contribution to mammalian tooth formation. Birth Defects Res C Embryo Today. 2004 Jun;72(2):200–12.

33. Jiménez-Rojo L, Granchi Z, Graf D, Mitsiadis TA. Stem Cell Fate Determination during Development and Regeneration of Ectodermal Organs. Front Physiol. 2012 Apr 25;3:107.

34. Li J, Parada C, Chai Y. Cellular and molecular mechanisms of tooth root development. Development. 2017 Feb 1;144(3):374–84.

35. Kumakami-Sakano M, Otsu K, Fujiwara N, Harada H. Regulatory mechanisms of Hertwig′s epithelial root sheath formation and anomaly correlated with root length. Experimental Cell Research. 2014 Jul 15;325(2):78–82.

36. Puthiyaveetil JSV, Kota K, Chakkarayan R, Chakkarayan J, Thodiyil AKP. Epithelial – Mesenchymal Interactions in Tooth Development and the Significant Role of Growth Factors and Genes with Emphasis on Mesenchyme – A Review. J Clin Diagn Res. 2016 Sep;10(9):ZE05–9.

37. Santosh ABR, Jones TJ. The Epithelial-Mesenchymal Interactions: Insights into Physiological and Pathological Aspects of Oral Tissues. Oncol Rev. 2014 Mar 17;8(1):239.

38. Tucker A, Sharpe P. The cutting-edge of mammalian development; how the embryo makes teeth. Nat Rev Genet. 2004 Jul;5(7):499–508.

39. Lu X, Yu F, Liu J, Cai W, Zhao Y, Zhao S, et al. The epidemiology of supernumerary teeth and the associated molecular mechanism. Organogenesis. 2017 Jun 9;13(3):71–82.

40. Hosoya A, Shalehin N, Takebe H, Shimo T, Irie K. Sonic Hedgehog Signaling and Tooth Development. Int J Mol Sci. 2020 Feb 26;21(5):1587.

41. Yu M, Wong SW, Han D, Cai T. Genetic analysis: Wnt and other pathways in non-syndromic tooth agenesis. Oral Dis. 2019 Apr;25(3):646–51.

42. Hu JCC, Hu Y, Smith CE, McKee MD, Wright JT, Yamakoshi Y, et al. Enamel Defects and Ameloblast-specific Expression in Enam Knock-out/lacZ Knock-in Mice. Journal of Biological Chemistry. 2008 Apr;283(16):10858–71.

43. Lacruz RS, Habelitz S, Wright JT, Paine ML. Dental Enamel Formation and Implications for Oral Health and Disease. Physiological Reviews. 2017 Jul 1;97(3):939–93.

44. Hu JCC, Chun YHP, Al Hazzazzi T, Simmer JP. Enamel Formation and Amelogenesis Imperfecta. Cells Tissues Organs. 2007;186(1):78–85.

45. Bronckers ALJJ, Lyaruu D, Jalali R, Medina JF, Zandieh-Doulabi B, DenBesten PK. Ameloblast Modulation and Transport of Cl−, Na+, and K+ during Amelogenesis. J Dent Res. 2015 Dec 1;94(12):1740–7.

46. Yin K, Guo J, Lin W, Robertson SYT, Soleimani M, Paine ML. Deletion of Slc26a1 and Slc26a7 Delays Enamel Mineralization in Mice. Front Physiol. 2017;8:307.

47. Lacruz RS, Smith CE, Moffatt P, Chang EH, Bromage TG, Bringas P, et al. Requirements for Ion and Solute Transport, and pH Regulation During Enamel Maturation. J Cell Physiol. 2012 Apr;227(4):1776–85.

48. Hu Y, Smith CE, Cai Z, Donnelly LA -J., Yang J, Hu JC -C., et al. Enamel ribbons, surface nodules, and octacalcium phosphate in C57 BL /6 *Amelx* $^{-/-}$ mice and *Amelx* $^{+/-}$ lyonization. Mol Genet Genomic Med. 2016 Nov;4(6):641–61.

49. Gutiérrez-Cantú FJ, Feria-Velasco A, Palacios-Arenas LN, Alvarado-Estrada KN, Avelar-González FJ, Flores-Reyes H, et al. Amelogenin and enamelysin localization in human dental germs. In Vitro CellDevBiol-Animal. 2011 Jun 1;47(5):355–60.

50. Núñez SM, Chun YHP, Ganss B, Hu Y, Richardson AS, Schmitz JE, et al. Maturation stage enamel malformations in Amtn and Klk4 null mice. Matrix Biol. 2016;52–54:219–33.

51. Lu Y, Papagerakis P, Yamakoshi Y, Hu JCC, Bartlett JD, Simmer JP. Functions of KLK4 and MMP-20 in dental enamel formation. Biol Chem. 2008 Jun;389(6):695–700.

52. Abbarin N, San Miguel S, Holcroft J, Iwasaki K, Ganss B. The Enamel Protein Amelotin Is a Promoter of Hydroxyapatite Mineralization. Journal of Bone and Mineral Research. 2015;30(5):775–85.

53. Markovich D. Slc13a1 and Slc26a1 KO models reveal physiological roles of anion transporters. Physiology (Bethesda). 2012 Feb;27(1):7–14.

54. Yin K, Lei Y, Wen X, Lacruz RS, Soleimani M, Kurtz I, et al. SLC26A Gene Family Participate in pH Regulation during Enamel Maturation. PLoS One. 2015;10(12):e0144703.

55. Tye CE, Sharma R, Smith CE, Bartlett JD. Altered Ion-responsive Gene Expression in Mmp20 Null Mice. J Dent Res. 2010 Dec;89(12):1421–6.

56. Chang EH, Lacruz RS, Bromage TG, Bringas P, Welsh MJ, Zabner J, et al. Enamel pathology resulting from loss of function in the cystic fibrosis transmembrane conductance regulator in a porcine animal model. Cells Tissues Organs. 2011;194(2–4):249–54.

57. Katsura KA, Horst JA, Chandra D, Le TQ, Nakano Y, Zhang Y, et al. WDR72 models of structure and function: A stage-specific regulator of enamel mineralization. Matrix Biology. 2014 Sep;38:48–58.

58. Smith CE, Issid M, Margolis HC, Moreno EC. Developmental changes in the pH of enamel fluid and its effects on matrix-resident proteinases. Adv Dent Res. 1996 Nov;10(2):159–69.

59. Lacruz RS, Smith CE, Kurtz I, Hubbard MJ, Paine ML. New Paradigms on the Transport Functions of Maturation-stage Ameloblasts. J Dent Res. 2013 Feb;92(2):122–9.

60. Jalali R, Guo J, Zandieh-Doulabi B, Bervoets T, Paine M, Boron W, et al. NBCe1 (SLC4A4) a potential pH Regulator in Enamel Organ Cells during Enamel Development in the Mouse. Cell Tissue Res. 2014 Nov;358(2):433–42.

61. Kawasaki-Nishi S, Nishi T, Forgac M. Arg-735 of the 100-kDa subunit a of the yeast V-ATPase is essential for proton translocation. Proc Natl Acad Sci U S A. 2001 Oct 23;98(22):12397–402.

62. Manolson MF, Yu H, Chen W, Yao Y, Li K, Lees RL, et al. The a3 isoform of the 100-kDa V-ATPase subunit is highly but differentially expressed in large (>or=10 nuclei) and small (<or= nuclei) osteoclasts. J Biol Chem. 2003 Dec 5;278(49):49271–8.

63. Sun-Wada GH, Tabata H, Kawamura N, Futai M, Wada Y. Differential expression of a subunit isoforms of the vacuolar-type proton pump ATPase in mouse endocrine tissues. Cell Tissue Res. 2007 Aug;329(2):239–48.

64. Jaskolka MC, Winkley SR, Kane PM. RAVE and Rabconnectin-3 Complexes as Signal Dependent Regulators of Organelle Acidification. Front Cell Dev Biol. 2021 Jun 24;9:698190.

65. Bronckers AL, Lyaruu DM, Bervoets TJ, Medina JF, DenBesten P, Richter J, et al. Murine ameloblasts are immunonegative for Tcirg1, the V-H-ATPase subunit essential for the osteoclast plasma membrane proton pump. Bone. 2012 Apr;50(4):901–8.

66. Guerrini R, Mei D, Kerti-Szigeti K, Pepe S, Koenig MK, Von Allmen G, et al. Phenotypic and genetic spectrum of ATP6V1A encephalopathy: a disorder of lysosomal homeostasis. Brain. 2022 Aug 27;145(8):2687–703.

67. Johnson L, Ganss B, Wang A, Zirngibl RA, Johnson DE, Owen C, et al. V-ATPases Containing a3 Subunit Play a Direct Role in Enamel Development in Mice. J Cell Biochem. 2017 Oct;118(10):3328–40.

68. Lee H, Jeong H, Choe J, Jun Y, Lim C, Lee C. The crystal structure of human Rogdi provides insight into the causes of Kohlschutter-Tönz Syndrome. Sci Rep. 2017 Dec;7(1):3972.

69. Toupenay S, Fournier BP, Manière MC, Ifi-Naulin C, Berdal A, de La Dure– Molla M. Amelogenesis imperfecta: therapeutic strategy from primary to permanent dentition across case reports. BMC Oral Health. 2018 Dec;18(1):108.

70. Lundgren GP, Vestlund GIM, Dahllöf G. Crown therapy in young individuals with amelogenesis imperfecta: Long term follow-up of a randomized controlled trial. J Dent. 2018 Sep;76:102–8.

71. Protocole National de Diagnostic et de Soins (PNDS) Amélogenèses imparfaites [Internet]. Centre de référence des maladies rares orales et dentaires O-Rares, Hôpitaux Universitaires de Strasbourg et Filière de Santé des Malformations de la tête, du cou et des dents (TETECOU); 2021. Available from: https://www.has-sante.fr/plugins/ModuleXitiKLEE/types/FileDocument/doXiti.jsp?id=p_3284537

72. Morkmued S, Hemmerle J, Mathieu E, Laugel-Haushalter V, Dabovic B, Rifkin DB, et al. Enamel and dental anomalies in latent-transforming growth factor beta-binding protein 3 mutant mice. Eur J Oral Sci. 2017 Feb;125(1):8–17.

73. Morkmued S, Clauss F, Schuhbaur B, Fraulob V, Mathieu E, Hemmerlé J, et al. Deficiency of the SMOC2 matricellular protein impairs bone healing and produces age-dependent bone loss. Sci Rep. 2020 Sep 9;10(1):14817.

74. Yamakoshi Y, Richardson AS, Nunez SM, Yamakoshi F, Milkovich RN, Hu JCC, et al. Enamel proteins and proteases in Mmp20 and Klk4 null and double-null mice. Eur J Oral Sci. 2011 Dec;119 Suppl 1(Suppl 1):206–16.

75. Brookes SJ, Barron MJ, Smith CEL, Poulter JA, Mighell AJ, Inglehearn CF, et al. Amelogenesis imperfecta caused by N-terminal enamelin point mutations in mice and men is driven by endoplasmic reticulum stress. Hum Mol Genet. 2017 May 15;26(10):1863–76.

76. Ji Y, Li C, Tian Y, Gao Y, Dong Z, Xiang L, et al. Maturation stage enamel defects in Odontogenesis-associated phosphoprotein (Odaph) deficient mice. Dev Dyn. 2021 Oct;250(10):1505–17.

77. Schossig A, Bloch-Zupan A, Lussi A, Wolf NI, Raskin S, Cohen M, et al. SLC13A5 is the second gene associated with Kohlschütter–Tönz syndrome. Journal of Medical Genetics. 2017 Jan 1;54(1):54–62.

78. Witkop CJ. Amelogenesis imperfecta, dentinogenesis imperfecta and dentin dysplasia revisited: problems in classification. J Oral Pathol. 1988 Nov;17(9–10):547–53.

79. Crawford PJ, Aldred M, Bloch-Zupan A. Amelogenesis imperfecta. Orphanet J Rare Dis. 2007 Dec;2(1):17.

80. Aswath N, Ramakrishnan SN, Teresa N, Ramanathan A. A novel ROGDI gene mutation is associated with Kohlschutter-Tonz syndrome. Oral Surgery, Oral Medicine, Oral Pathology and Oral Radiology. 2018 Jan;125(1):e8–11.

81. Mory A, Dagan E, Illi B, Duquesnoy P, Mordechai S, Shahor I, et al. A Nonsense Mutation in the Human Homolog of Drosophila rogdi Causes Kohlschutter–Tonz Syndrome. The American Journal of Human Genetics. 2012 Apr;90(4):708–14.

82. Kohlschütter A, Chappuis D, Meier C, Tönz O, Vassella F, Herschkowitz N. Familial epilepsy and yellow teeth--a disease of the CNS associated with enamel hypoplasia. Helv Paediatr Acta. 1974 Oct;29(4):283–94.

83. Kim M, Jang D, Yoo E, Oh Y, Sonn JY, Lee J, et al. Rogdi Defines GABAergic Control of a Wake-promoting Dopaminergic Pathway to Sustain Sleep in Drosophila. Sci Rep. 2017 Dec;7(1):11368.

84. Schossig A, Wolf NI, Fischer C, Fischer M, Stocker G, Pabinger S, et al. Mutations in ROGDI Cause Kohlschütter-Tönz Syndrome. The American Journal of Human Genetics. 2012 Apr;90(4):701–7.

85. Tucci A, Kara E, Schossig A, Wolf NI, Plagnol V, Fawcett K, et al. Kohlschütter-Tönz Syndrome: Mutations in *ROGDI* and Evidence of Genetic Heterogeneity. Human Mutation. 2013 Feb;34(2):296–300.

86. Haberlandt E, Svejda C, Felber S, Baumgartner S, Günther B, Utermann G, et al. Yellow teeth, seizures, and mental retardation: A less severe case of Kohlschütter–Tönz syndrome. American Journal of Medical Genetics Part A. 2006;140A(3):281–3.

87. Morscher RJ, Rauscher C, Sperl W, Rittinger O. Seizures, enamel defects and psychomotor developmental delay: The first patient with Kohlschütter-Tönz syndrome caused by a ROGDI-gene deletion. Seizure. 2017 Aug;50:118–20.

88. Akgün-Doğan Ö, Simsek-Kiper PO, Taşkıran E, Schossig A, Utine GE, Zschocke J, et al. Kohlschütter-Tönz Syndrome With a Novel ROGD1 Variant in 3 Individuals: A Rare Clinical Entity. J Child Neurol. 2021 Sep 1;36(10):816–22.

89. Mory A, Dagan E, Shahor I, Mandel H, Illi B, Zolotushko J, et al. Kohlschutter-Tonz Syndrome: Clinical and Genetic Insights Gained From 16 Cases Deriving From a Close-Knit Village in Northern Israel. Pediatric Neurology. 2014 Apr 1;50(4):421–6.

90. Schossig A, Wolf N, Koch MJ, Bast T, Hoffmann GF, Zschocke J, et al. Epileptische Enzephalopathie und Zahnschmelzdefekt (Kohlschütter-Tönz-Syndrom): Drei Fallberichte und Literaturübersicht. Medizinische Genetik. 2007 Nov 10;19(4):422–6.

91. Schossig A, Wolf NI, Kapferer I, Kohlschütter A, Zschocke J. Epileptic encephalopathy and amelogenesis imperfecta: Kohlschütter–Tönz syndrome. European Journal of Medical Genetics. 2012 May 1;55(5):319–22.

92. Bailleul-Forestier I, Berdal A, Vinckier F, de Ravel T, Fryns JP, Verloes A. The genetic basis of inherited anomalies of the teeth. Part 2: Syndromes with significant dental involvement. European Journal of Medical Genetics. 2008 Sep 1;51(5):383–408.

93. Irvine AD. Towards a unified classification of the ectodermal dysplasias: Opportunities outweigh challenges. American Journal of Medical Genetics Part A. 2009;149A(9):1970–2.

94. Lamartine J. Towards a new classification of ectodermal dysplasias. Clinical and Experimental Dermatology. 2003 Jul 1;28(4):351–5.

95. Riemann D, Wallrafen R, Dresbach T. The Kohlschütter-Tönz syndrome associated gene Rogdi encodes a novel presynaptic protein. Sci Rep. 2017 Dec;7(1):15791.

96. Musumeci SA, Ella M, Ferri R, Romano C. A further family with epilepsy, dementia and yellow teeth: the Kohlschütter syndrome. 1995;6.

97. Petermöller M, Kunze J, Groß-Selbeck G. Kohlschütter Syndrome: Syndrome of Epilepsy - Dementia - Amelogenesis Imperfecta. Neuropediatrics. 1993 Dec;24(06):337–8.

98. Bloch-Zupan A, Rey T, Jiménez Armijo A, Kawczynski M, Kharouf N, Consortium OR, et al. Amelogenesis imperfecta: Next Generation Sequencing sheds light on Witkop's classification. Frontiers in Physiology [Internet]. 2023 [cited 2023 Apr 3];14. Available from: https://www.frontiersin.org/articles/10.3389/fphys.2023.1130175

99. Jimenez-Armijo A, Oumensour K, Bousfiha B, Rey T, Laugel-Haushalter V, Bloch-Zupan A, et al. A Novel Homozygous Variant in GJA1 Causing a Hallermann-Streiff/Oculodentodigital Dysplasia Overlapping Phenotype: A Clinical Report. Frontiers in Dental Medicine [Internet]. 2021 [cited 2023 May 3];2. Available from: https://www.frontiersin.org/articles/10.3389/fdmed.2021.675130

100. Gurovich Y, Hanani Y, Bar O, Nadav G, Fleischer N, Gelbman D, et al. Identifying facial phenotypes of genetic disorders using deep learning. Nat Med. 2019 Jan;25(1):60–4.

101. Sharir A, Marangoni P, Zilionis R, Wan M, Wald T, Hu JK, et al. A large pool of actively cycling progenitors orchestrates self-renewal and injury repair of an ectodermal appendage. Nat Cell Biol. 2019 Sep;21(9):1102–12.

102. Koziol LF, Budding D, Andreasen N, D'Arrigo S, Bulgheroni S, Imamizu H, et al. Consensus Paper: The Cerebellum's Role in Movement and Cognition. Cerebellum. 2014 Feb;13(1):151–77.

103. Ceccarelli M, Micheli L, D'Andrea G, De Bardi M, Scheijen B, Ciotti M, et al. Altered cerebellum development and impaired motor coordination in mice lacking the Btg1 gene: Involvement of cyclin D1. Developmental Biology. 2015 Dec 1;408(1):109–25.

104. McConnell EL, Basit AW, Murdan S. Measurements of rat and mouse gastrointestinal pH, fluid and lymphoid tissue, and implications for in-vivo experiments. Journal of Pharmacy and Pharmacology. 2008 Jan 1;60(1):63–70.

105. Lalezari D. Gastrointestinal pH profile in subjects with irritable bowel syndrome. Ann Gastroenterol. 2012;25(4):333–7.

106. Merkulova M, Păunescu TG, Azroyan A, Marshansky V, Breton S, Brown D. Mapping the H+ (V)-ATPase interactome: identification of proteins involved in trafficking, folding, assembly and phosphorylation. Sci Rep. 2015 Dec;5(1):14827.

107. Mattison KA, Tossing G, Mulroe F, Simmons C, Butler KM, Schreiber A, et al. ATP6V0C variants impair V-ATPase function causing a neurodevelopmental disorder often associated with epilepsy. Brain. 2022 Sep 8;awac330.

108. Tambuyzer E, Vandendriessche B, Austin CP, Brooks PJ, Larsson K, Miller Needleman KI, et al. Therapies for rare diseases: therapeutic modalities, progress and challenges ahead. Nat Rev Drug Discov. 2020 Feb;19(2):93–111.

109. Colacurcio DJ, Nixon RA. Disorders of lysosomal acidification - the emerging role of v-ATPase in aging and neurodegenerative disease. Ageing Res Rev. 2016 Dec;32:75–88.

110. Song Q, Meng B, Xu H, Mao Z. The emerging roles of vacuolar-type ATPase-dependent Lysosomal acidification in neurodegenerative diseases. Transl Neurodegener. 2020 May 11;9(1):17.

111. Dubos A, Castells-Nobau A, Meziane H, Oortveld MAW, Houbaert X, Iacono G, et al. Conditional depletion of intellectual disability and Parkinsonism candidate gene ATP6AP2 in fly and mouse induces cognitive impairment and neurodegeneration. Hum Mol Genet. 2015 Dec 1;24(23):6736–55.

112. Wendling O, Champy MF, Jaubert S, Pavlovic G, Dubos A, Lindner L, et al. Atp6ap2 ablation in adult mice impairs viability through multiple organ deficiencies. Sci Rep. 2017 Aug 29;7:9618.

113. Rudenko G, Henry L, Henderson K, Ichtchenko K, Brown MS, Goldstein JL, et al. Structure of the LDL Receptor Extracellular Domain at Endosomal pH. Science. 2002 Dec 20;298(5602):2353–8.

114. Bareford LM, Swaan PW. ENDOCYTIC MECHANISMS FOR TARGETED DRUG DELIVERY. Adv Drug Deliv Rev. 2007 Aug 10;59(8):748–58.

115. Lu M, Sautin YY, Holliday LS, Gluck SL. The glycolytic enzyme aldolase mediates assembly, expression, and activity of vacuolar H+-ATPase. J Biol Chem. 2004 Mar 5;279(10):8732–9.

116. Cho NH, Cheveralls KC, Brunner AD, Kim K, Michaelis AC, Raghavan P, et al. OpenCell: Endogenous tagging for the cartography of human cellular organization. Science. 2022 Mar 11;375(6585):eabi6983.

117. El-Sayed W, Parry DA, Shore RC, Ahmed M, Jafri H, Rashid Y, et al. Mutations in the Beta Propeller WDR72 Cause Autosomal-Recessive Hypomaturation Amelogenesis Imperfecta. Am J Hum Genet. 2009 Nov 13;85(5):699–705.

118. Schinke T, Schilling AF, Baranowsky A, Seitz S, Marshall RP, Linn T, et al. Impaired gastric acidification negatively affects calcium homeostasis and bone mass. Nat Med. 2009 Jun;15(6):674–81.

119. Kopic S, Wagner MEH, Griessenauer C, Socrates T, Ritter M, Geibel JP. Vacuolar-type H+-ATPase-mediated proton transport in the rat parietal cell. Pflugers Arch - Eur J Physiol. 2012 Mar 1;463(3):419–27.

120. Eaton AF, Merkulova M, Brown D. The H^+-ATPase (V-ATPase): from proton pump to signaling complex in health and disease. American Journal of Physiology-Cell Physiology. 2021 Mar 1;320(3):C392–414.

121. Magi S, Castaldo P, Macrì ML, Maiolino M, Matteucci A, Bastioli G, et al. Intracellular Calcium Dysregulation: Implications for Alzheimer's Disease. Biomed Res Int. 2016;2016:6701324.

122. Supnet C, Bezprozvanny I. The dysregulation of intracellular calcium in Alzheimer disease. Cell Calcium. 2010 Feb;47(2):183–9.

123. Christensen KA, Myers JT, Swanson JA. pH-dependent regulation of lysosomal calcium in macrophages. Journal of Cell Science. 2002 Feb 1;115(3):599–607.

124. Penny CJ, Kilpatrick BS, Eden ER, Patel S. Coupling acidic organelles with the ER through Ca^{2+} microdomains at membrane contact sites. Cell Calcium. 2015 Oct;58(4):387–96.

125. Afghah Z, Chen X, Geiger JD. Role of endolysosomes and inter-organellar signaling in brain disease. Neurobiol Dis. 2020 Feb;134:104670.

126. Berridge MJ. Calcium hypothesis of Alzheimer's disease. Pflugers Arch - Eur J Physiol. 2010 Feb 1;459(3):441–9.

127. Hui L, Chen X, Geiger JD. Endolysosome involvement in LDL cholesterol-induced Alzheimer's disease-like pathology in primary cultured neurons. Life Sci. 2012 Dec 10;91(23–24):1159–68.

128. Hui L, Soliman ML, Geiger NH, Miller NM, Afghah Z, Lakpa KL, et al. Acidifying endolysosomes prevented LDL-induced amyloidogenesis. J Alzheimers Dis. 2019;67(1):393–410.

129. Holick MF. The vitamin D deficiency pandemic: Approaches for diagnosis, treatment and prevention. Rev Endocr Metab Disord. 2017 Jun 1;18(2):153–65.

130. Scott A. How CRISPR is transforming drug discovery. Nature. 2018 Mar 7;555(7695):S10–1.

131. Takahashi T. Organoids for Drug Discovery and Personalized Medicine. Annu Rev Pharmacol Toxicol. 2019 Jan 6;59(1):447–62.

132. Laugel-Haushalter V, Jimenez-Armijo A, Ahumada JT, Morkmued S, Niederreither K, Bloch-Zupan A. Modèles animaux : modélisations précliniques des maladies rares des tissus dentaires minéralisés. Realités Cliniques. 2019 Jun;30:96–103.

133. Pindborg JJ. The pigmentation of the rat incisor as an index of metabolic disturbances. Oral Surg Oral Med Oral Pathol. 1953 Jun;6(6):780–9.

134. Hu Y, Smith CE, Richardson AS, Bartlett JD, Hu JCC, Simmer JP. MMP20, KLK4, and MMP20/KLK4 double null mice define roles for matrix proteases during dental enamel formation. Mol Genet Genomic Med. 2015 Dec 20;4(2):178–96.

135. Wang SK, Hu Y, Yang J, Smith CE, Nunez SM, Richardson AS, et al. Critical roles for WDR72 in calcium transport and matrix protein removal during enamel maturation. Mol Genet Genomic Med. 2015 Jul;3(4):302–19.

136. Schweppe DK, Huttlin EL, Harper JW, Gygi SP. BioPlex Display: An Interactive Suite for Large-Scale AP–MS Protein–Protein Interaction Data. J Proteome Res. 2018 Jan 5;17(1):722–6.

137. Christakos S, Dhawan P, Verstuyf A, Verlinden L, Carmeliet G. Vitamin D: Metabolism, Molecular Mechanism of Action, and Pleiotropic Effects. Physiol Rev. 2016 Jan;96(1):365–408.

138. Bikle DD. Ligand-Independent Actions of the Vitamin D Receptor: More Questions Than Answers. JBMR Plus. 2021 Nov 23;5(12):e10578.

139. Lézot F, Descroix V, Hotton D, Mauro N, Kato S, Berdal A. Vitamin D and tissue non-specific alkaline phosphatase in dental cells. European Journal of Oral Sciences. 2006;114(s1):178–82.

140. Ranggård L, Norén JG. Effect of hypocalcemic state on enamel formation in rat maxillary incisors. Scand J Dent Res. 1994 Oct;102(5):249–53.

141. Zhang X, Rahemtulla F, Zhang P, Beck P, Thomas HF. Different enamel and dentin mineralization observed in VDR deficient mouse model. Archives of Oral Biology. 2009 Apr 1;54(4):299–305.

142. Bouillon R, Carmeliet G, Verlinden L, van Etten E, Verstuyf A, Luderer HF, et al. Vitamin D and Human Health: Lessons from Vitamin D Receptor Null Mice. Endocr Rev. 2008 Oct;29(6):726–76.

143. Foster BL, Nociti FH, Somerman MJ. The Rachitic Tooth. Endocr Rev. 2014 Feb;35(1):1–34.

Alexandra JIMENEZ-ARMIJO

ROGDI- une nouvelle protéine avec un motif leucine-zipper-régulant le développement neurologique et orofacial

Résumé

Une maladie est dite rare lorsqu'elle touche moins d'une personne sur 2000. Environ 900 maladies rares sont associées à des anomalies bucco-dentaires et crâniofaciales. Les objectifs de cette thèse comprennent l'étude des anomalies orales, en particulier l'amélogenèse imparfaite, et la génération de modèles murins qui reproduisent les signes cliniques de ces maladies. Le syndrome de Kohlschütter-Tönz (KTS) est une maladie autosomique récessive rare causée par des variants du gène *ROGDI*. Les patients atteints du KTS souffrent de crises d'épilepsie, et présentent une déficience intellectuelle et une amélogenèse imparfaite. La protéine ROGDI est conservée chez les métazoaires, cependant, sa fonction reste inconnue. Nous présentons ici un nouveau modèle de souris knock-out *Rogdi*$^{-/-}$ qui récapitule la plupart des symptômes des patients atteints de KTS. Les souris *Rogdi*$^{-/-}$ ont des anomalies sévères de l'émail, avec un phénotype de type amélogenèse imparfaite. Ce mutant fournit un nouveau modèle pour étudier les origines du KTS et la fonction du gène *Rogdi*.

Mots-clés : *maladies rares, émail, amélogenèse imparfaite, modèles murins, syndrome de Kohlschütter-Tönz.*

Résumé en anglais

A disease is defined as rare when it affects less than one in 2,000 people. Around 900 rare diseases are associated with oral and craniofacial anomalies. The main objectives of this thesis include the study of oral anomalies, specifically amelogenesis *imperfecta*, and the generation of mouse models that mimic the clinical features of these diseases. Kohlschütter-Tönz syndrome (KTS) is a rare autosomal recessive disorder caused by *ROGDI* variants. Patients with KTS display epileptic seizures, intellectual disability, and amelogenesis *imperfecta*. ROGDI is highly conserved across metazoans, however, its function remains unknown. Here, we describe a novel *Rogdi*$^{-/-}$ knockout mouse model that recapitulates most KTS patient symptoms. In particular, *Rogdi*$^{-/-}$ mutants display severe enamel defects, showing an amelogenesis *imperfecta*-like phenotype. This mouse mutant provides a novel model to investigate the origins of KTS and the function of the *Rogdi* gene.

Keywords: *rare diseases, enamel, amelogenesis imperfecta, mouse models, Kohlschütter-Tönz syndrome.*